MEMBRANE LIPID CHANGES IN *ARABIDOPSIS THALIANA* IN RESPONSE TO ENVIRONMENTAL STRESSES

by

HIEU SY VU

B.A., Vietnam National University-Ho Chi Minh City, 2005

AN ABSTRACT OF A DISSERTATION

submitted in partial fulfillment of the requirements for the degree

DOCTOR OF PHILOSOPHY

Division of Biology
College of Arts and Sciences

KANSAS STATE UNIVERSITY
Manhattan, Kansas

2014

Abstract

The molecular mechanisms by which plants respond to environmental stresses to sustain growth and yield have great importance to agriculture. Lipid metabolites are a major element of plant stress responses. The model plant *Arabidopsis thaliana* is well-suited to study stress-driven compositional dynamics, metabolism, and functions of lipid metabolites. When Arabidopsis plants were subjected to wounding, infection by *Pseudomonas syringae* pv *tomato* DC3000 expressing *AvrRpt2* (*Pst*Avr), infection by *Pseudomonas syringae* pv. *maculicola* (*Psm*), and low temperature, and 86 oxidized and acylated lipids were analyzed using mass spectrometry, different sets of lipids were found to change in level in response to the various stresses. Analysis of plant species (wheat versus Arabidopsis), ecotypes (Arabidopsis Columbia 0 versus Arabidopsis C24), and stresses (wounding, bacterial infection, and freezing) showed that acylated monogalactosyldiacylglycerol was a major and diverse lipid class that differed in acyl composition among plant species when plants were subjected to different stresses. Mass spectrometry analysis provided evidence that oxophytodienoic acid, an oxidized fatty acid, is significantly more concentrated on the galactosyl ring of monogalactosyldiacylglycerol than on the glycerol backbone. A mass spectrometry method, measuring 272 lipid analytes with high precision in a relatively short time, was developed. Application of the method to plants subjected to wounding and freezing stress in large-scale experiments showed the method produces data suitable for lipid co-occurrence analysis, which identifies groups of lipid analytes produced by identical or inter-twined enzymatic pathways. The mass spectrometry method and lipid co-occurrence analysis were utilized to study the nature of lipid modifications and the roles of lipoxygenases and patatin-like acyl hydrolases in Arabidopsis during cold acclimation, freezing, and thawing.

MEMBRANE LIPID CHANGES IN *ARABIDOPSIS THALIANA* IN RESPONSE TO ENVIRONMENTAL STRESSES

by

HIEU SY VU

B.A., Vietnam National University-Ho Chi Minh City, 2005

A DISSERTATION

submitted in partial fulfillment of the requirements for the degree

DOCTOR OF PHILOSOPHY

Division of Biology
College of Arts and Sciences

KANSAS STATE UNIVERSITY
Manhattan, Kansas

2014

Approved by:

Major Professor
Ruth Welti

Copyright

Abstract

The molecular mechanisms by which plants respond to environmental stresses to sustain growth and yield have great importance to agriculture. Lipid metabolites are a major element of plant stress responses. The model plant *Arabidopsis thaliana* is well-suited to study stress-driven compositional dynamics, metabolism, and functions of lipid metabolites. When Arabidopsis plants were subjected to wounding, infection by *Pseudomonas syringae* pv *tomato* DC3000 expressing *AvrRpt2* (*Pst*Avr), infection by *Pseudomonas syringae* pv. *maculicola* (*Psm*), and low temperature, and 86 oxidized and acylated lipids were analyzed using mass spectrometry, different sets of lipids were found to change in level in response to the various stresses. Analysis of plant species (wheat versus Arabidopsis), ecotypes (Arabidopsis Columbia 0 versus Arabidopsis C24), and stresses (wounding, bacterial infection, and freezing) showed that acylated monogalactosyldiacylglycerol was a major and diverse lipid class that differed in acyl composition among plant species when plants were subjected to different stresses. Mass spectrometry analysis provided evidence that oxophytodienoic acid, an oxidized fatty acid, is significantly more concentrated on the galactosyl ring of monogalactosyldiacylglycerol than on the glycerol backbone. A mass spectrometry method, measuring 272 lipid analytes with high precision in a relatively short time, was developed. Application of the method to plants subjected to wounding and freezing stress in large-scale experiments showed the method produces data suitable for lipid co-occurrence analysis, which identifies groups of lipid analytes produced by identical or inter-twined enzymatic pathways. The mass spectrometry method and lipid co-occurrence analysis were utilized to study the nature of lipid modifications and the roles of lipoxygenases and patatin-like acyl hydrolases in Arabidopsis during cold acclimation, freezing, and thawing.

Table of Contents

List of Abbreviations xi
List of Figures xiii
List of Tables xv
Acknowledgements xvi
Chapter 1 - Introduction 1
Rationale of studying stress responses in plants 1
Arabidopsis thaliana: a well-established model 1
Stress-induced damages and plant physiological responses 2
Overview of plant molecular responses to stresses 4
Plant lipid metabolism and stress-induced lipid modifications 5
Plant lipid metabolism under normal conditions 5
Stress-induced membrane lipid modifications 6
Hydrolysis 6
Oxidation 7
Acylation 8
Transgalactosylation 8
Hypotheses 8
Lipidomics: an excellent tool 9
Internal standards 10
Lipid extraction 11
Ionization of lipid in mass spectrometer 11
Mass analyzer and ion fragmentation 11
Data processing 12
References 13
Figures 21
Chapter 2 - Direct infusion mass spectrometry of oxylipin-containing Arabidopsis membrane lipids reveals varied patterns in different stress responses. 24
Abstract 24

Introduction 25
Results 26
Triple Quadrupole MS Precursor Scanning for Lipids with 18-Carbon Oxidized Acyl Chains 26
Identification of the Detected Oxidized Complex Lipids using QTOF and FTICR MS 28
Experimental Design and Measurements of Oxidized Complex Leaf Membrane Lipids during Stress Responses 31
Total Oxidized Lipid Accumulation as a Function of Stress 32
Patterns of Oxidized Lipid Accumulation as a Function of Stress 33
Patterns of Oxidized Lipid Accumulation in Wounding 34
Patterns of Oxidized Lipid Accumulation in Bacterial Infection 35
Patterns of Oxidized Lipid Accumulation in Freezing 37
Other Stress-Associated Lipids 37
Discussion 37
Conclusion 40
Materials and Methods 41
Growth Conditions and Sampling for Stress Treatments 41
Stress Treatments 41
Bacterial Counts 42
Lipid Extraction 43
Tissue Mass Determination 43
Extracts used for QTOF and FTICR MS Analysis and Fractionation for QTOF Analysis 44
Triple Quadrupole MS Analysis of Ox-lipids 44
Triple Quadrupole MS Analysis of Normal-Chain Lipids 46
QTOF MS Analysis 46
FTICR MS Analysis 47
Statistical analysis 48
Acknowledgements 48
References 49
Figure and Tables 54
Supplemental Data 68

Chapter 3 - Head-group acylation of monogalactosyldiacylglycerol is a common stress response, and the acyl-galactose acyl composition varies among plant species and with applied stress 75
Abstract 75
Introduction 76
Materials and Methods 77
Plant materials 77
Treatments 78
Ion leakage measurement 78
Lipid extraction 79
Modified Bligh–Dyer method (Bligh and Dyer, 1959) for polar lipid analysis 79
Alternate extraction method (for polar lipid analysis) 79
For gas chromatography-MS (free oxylipin analysis) 79
Mass spectrometry 79
Mass spectral data processing and analysis 81
Results 82
Wound-induced acylation of the galactose of MGDG occurs in multiple plant species 82
acMGDGs accumulate following stress, including sub-lethal freezing 83
The composition of induced acMGDGs varies among stresses 84
The proportions of 16:3, 16:0 and 18:3 in the Gal-esterified acyl chains in acMGDGs resemble proportions in DGDG 85
The oxidized fatty acyl chain OPDA is enriched on the Gal of acMGDG 86
Oxidized acMGDG induction is enhanced by re-wounding 87
Discussion 87
Acknowledgements 89
References 90
Figures and Tables 92
Supplemental Data 103
Chapter 4 - Lipid changes after leaf wounding in *Arabidopsis thaliana*: Expanded lipidomic data form the basis for lipid co-occurrence analysis 107
Abstract 107

Introduction 108
Results 109
Plant wounding 109
Extraction of leaves 109
MS analysis of lipids 110
Variations in lipid analytes among individual plants and in response to wounding treatment 112
Discussion 115
Experimental procedures 118
Plant material, growth, and wounding treatment 118
Lipid extraction 119
Lipid profiling by ESI triple quadrupole MS 119
Data processing and calculation of normalized lipid intensities 121
Statistical analysis and figure and table production 122
Acknowledgements 123
References 123
Figures and Tables 126
Supplemental Data 155
Chapter 5 - Roles of lipoxygenases and lipases in Arabidopsis in response to freezing 168
Abstract 168
Introduction 168
Materials and Methods 170
Overall experimental design 170
Arabidopsis lines 171
Plant growth conditions 172
Cold acclimation and freezing treatment 172
Sampling and lipid extraction 173
Plant phenotyping 174
Mass spectrometry analysis 175
Data processing and statistical analysis 176
Results 177

Ablation of pPLAIIγ enhances cold acclimation effect on freezing tolerance 177
Freezing-induced lipid changes occur in clusters 178
Lipid changes correlate with freezing-induced leaf damage 181
Formation of OPDA-containing acMGDG is enhanced in pPLAIIγ knockout 181
Discussion 182
References 184
Figures and Tables 186
Chapter 6 - Conclusions and future directions 202
Conclusions 202
Future directions 202
References 203
Appendix A – Permission to release copyrighted material 205

List of Abbreviations

ac (prefix)	acylated
ACP	Acyl carrier protein
AH	Acyl hydrolase
ASG	Acylated sterol glucoside
CID	Collision induced dissociation
DAG	Diacylglycerol
DGDG	Digalactosyldiacylglycerol
dnOPDA	Dinor-oxophytodienoic acid
ER	Endoplasmic reticulum
ESI	Electrospray ionization
FAD	Fatty acid desaturase
FT-ICR	Fourier-transformed Ion Cyclotron Resonance
Gal	Galactose
GC	Gas chromatography
GIPC	Glycosylinositolphosphoceramide
GlcCer	Glycosylceramide
LC	Liquid chromatography
LOX	Lipoxygenase
LPC	Lysophosphatidylcholine
LPE	Lysophosphatidylethanolamine
MGDG	Monogalactosyldiacylglycerol
MRM	Multiple reaction monitoring
MS	Mass spectrometry
MS/MS	Tandem mass spectrometry
NL	Neutral loss
OPDA	Oxophytodienoic acid
ox (prefix)	oxidized
PA	Phosphatidic acid

PC	Phosphatidylcholine
PE	Phosphatidylethanolamine
PG	Phosphatidylglycerol
PI	Phosphatidylinositol
PLA	Phospholipase A
PLC	Phospholipase C
PLD	Phospholipase D
pPLA	Patatin-related phospholipase A
Pre	Precursor
PS	Phosphatidylserine
Q	Quadrupole
Q-TOF	Quadrupole time-of-flight
ROS	Reactive oxygen species
SG	Sterol glucoside
SQDG	Sulfoquinovosyldiacylglycerol
TAG	Triacylglycerol
TeGDG	Tetragalactosyldiacylglycerol
TrGDG	Trigalactosyldiacylglycerol

List of Figures

Figure 1.1 Examples of normal-chain plant lipids. 21
Figure 1.2 Arabidopsis lipid metabolism in normal and stress conditions. 22
Figure 1.3 Examples of oxidized and acylated membrane lipids in Arabidopsis. 23
Figure 2.1 ESI triple quadrupole MS precursor ion spectra, acquired on extracts of leaves of Arabidopsis plants infected with *Pst*Avr for 24 h. 54
Figure 2.2 Treatments of 5 week-old wild-type Arabidopsis plants. 55
Figure 2.3 Oxidized membrane lipid levels following treatments shown in Figure 2.2. 56
Figure 2.4 Oxidized membrane lipids under stress conditions as quantified by triple quadrupole MS precursor scanning. 57
Figure 2.5 Summary of changes in ox-lipids and PA in response to stress treatments. 58
Figure 3.1 acMGDG structure and occurrence upon wounding. 92
Figure 3.2 Levels of acMGDG (grouped by fatty acyl moiety on the Gal) in leaves of Arabidopsis Col-0 (A) and C24 (B), tomato (C), and wheat (D) 45 min after wounding. ... 93
Figure 3.3 acMGDG forms in leaves of Arabidopsis Col-0 after application of different stresses, and its occurrence during freezing is not directly associated with cell membrane ion leakage. 94
Figure 3.4 Levels of acMGDG (grouped by fatty acyl moiety on the Gal) in leaves of Arabidopsis Col-0 after application of different stresses. 96
Figure 3.5 Comparison of fatty acyl composition. 98
Figure 3.6 Levels of oxidized MGDG, DGDG, and acMGDG, measured by Pre 277.2 (18:3) and Pre 291.2 (18:4-O) using direct infusion ESI triple quadrupole MS in negative mode..... 100
Figure 4.1 Heatmap of autoscaled lipid levels determined by MS analysis. 126
Figure 4.2 Autoscaled levels of representative lipid analytes in individual plants. 127
Figure 4.3 Lipid dendrogram. 129
Figure 4.4 Autoscaled levels of representative lipid analytes in sub-clusters A1, A4, and A5.. 130
Figure 4.5 Autoscaled levels of representative lipid analytes in sub-clusters C2 and C9. 132
Figure 4.6 Autoscaled levels of representative lipid analytes in sub-clusters C5, C7, and C8... 134
Figure 4.7 Autoscaled levels of a representative lipid from each sub-cluster. 136

Figure 5.1 Seed position in trays..... 186
Figure 5.2 Example of tray and plant labeling..... 187
Figure 5.3 Cold acclimation and freezing experiment design. 189
Figure 5.4 Low-temperature-induced leaf damage assessed by relative ion leakage. 190
Figure 5.5 Plant appearance followed freezing treatments. 190
Figure 5.6 Dendrogram describing lipid co-occurrence of Col-0 plants in response to low temperature treatments. 192
Figure 5.7 Comparisons of autoscaled lipid levels of sub-clusters between Col-0 and pPLAIIγ (line E) plants that underwent low temperature treatments. 194

List of Tables

Table 2.1 Oxidized fatty acyl chains detected in extracts from leaves of *Arabidopsis thaliana* infected with *Pst*Avr for 24 h. 59
Table 2.2 Lipids detected by ESI MS/MS negative ion precursor ion scans, Pre 291.2, Pre 293.2, and Pre 295.2. 60
Table 3.1 NL fragments used to detect acMGDGs by ESI triple quadrupole MS in positive mode 101
Table 3.2 Ratio of signals from OPDA/18:3 in galactolipids of *Arabidopsis thaliana.* 102
Table 4.1 Characteristics of three lipid extraction methods. 138
Table 4.2 Lipid name abbreviations 140
Table 4.3 ANOVA and post-hoc test results. 143
Table 5.1 List of Arabidopsis lines used in the experiment. 197
Table 5.2 Internal standards used in lipid profiling. 198
Table 5.3 Positions of sample vials on a mass spectrometry sample tray. 199
Table 5.4 Correlation of lipids in sub-clusters with leaf damage as quantified by ion leakage. 201

Acknowledgements

First and foremost, I would like to thank my advisor, Ruth Welti, for teaching me mass spectrometry, lipidomics, and plant biology, for helping me in designing experiments, for writing, editing, and correcting my publications and dissertation, for finding me funding and professional opportunities, for guiding me in science, and for everything. I truly appreciate her dedication. I want to thank other past and current members of the Welti lab, including Gail Ragan, Giorgis Isaac, Richard Jeannotte, Thilani Samarakoon, Libin Yao, Sam Honey, Joe Bloomfield, Kelly Zachariasen, Morgan Ambruster, David Hwang, Mohammed Sbeih, Kaleb Lowe, Neema Prakash, Dedan McEllhiney, Charles "Drew" Roach, Allison McKiearnan, Samantha Elledge, Laura Welti, Hollie Wickham, Tingting Song, Nancy Huls, and Ariel Burns for helping me with my research. I specifically thank Ruth for making data processing templates for Chapter 2, 3, 4, and 5, and for measuring ion conductivity in Chapter 5. I would like to thank Mary Roth, Pam Tamura, and Sunitha Shiva for maintaining instruments, maintaining a fantastic laboratory, and for their help with my samples, experiments, talks, publications, and dissertation. Specifically, I thank Pam for Q-TOF MS lipid identification and figure preparation in Chapters 2 and 3, and for lipid extraction in Chapter 4. I thank Mary for lipid profiling of wheat and tomato samples in Chapter 3. I thank Sunitha for her contribution in development of the lipid profiling method in Chapters 4 and 5. I thank Thilani for GC-MS quantification in Chapter 3. I thank Sam, Drew, Sunitha, Thilani, Neema, Kaleb, Mary, Pam, Morgan, Libin, and Ruth for planting, taking care of plants, treating plants, sampling, measuring ion conductivity, and preparing samples in Chapters 4 and 5. I thank Sunitha and Dedan for Q-TOF MS lipid identification in Chapter 4.

I would like to thank Jyoti Shah for helping me with experimental design and procedures, for giving me research materials, for guiding and supporting me in science. I would like to thank members of the Shah lab, including Ratnesh Chaturvedi, Katie Lorenc-Kukula, Vamsi Nalam, Vijay Singh, Joe Louis, Kartikeya Krothapalli, and Sujon Sarowar for their help with my samples, research materials, experiments, publications and dissertation. I thank Sujon for RT-PCR analysis shown in Chapter 4.

I would like to thank Xuemin Wang and Maoyin Li for research materials and for their help in experimental design and preparation of my publications and dissertation.

I would like to thank Todd Williams, Nadya Galeva, and Lawrence Seib for acquisition and processing of mass spectral data.

I would like to thank Gary Gadbury, Dilan Paranagama, Lixia Fan, and Lianqing Zheng for their help in experimental design, data processing, and publication preparation.

I would like to thank Kathrin Schrick, and her lab members, including Hanh Nguyen, Page Cox, and Daniel Stucky; Susan Brown, and her lab members, including Michelle Coleman, Sherry Miller, Jinping Fu, and Barbara Van Slyke; Mark Ungerer, and his lab members, including Bradley Bakken, Taki Kawakami, Hannah Tetreault, and Ying Zhen; Timothy Durrett, and Tam Thu Tran Nguyen; Ari Jumponen; Eric Schmelz; Cong Son Tuan Van; and Haibao Tang for their expertise and/or lending me research tools and instruments.

I would like to thank Paul Hinkes, Jeff Ramey, Yuriy Pyatkivskyy, and Dennis Karote for fixing instruments and Iggy Kass for writing a data extraction script.

I would like to thank Ernst Heinz and Mats Ellerström for research ideas and encouragement.

I would like to thank the current members, Ruth Welti, Mark Ungerer, Kathrin Schrick, and Timothy Durrett, and the past members of my committee, Rachel Zufferey and James C. Nelson, for guiding me through my graduate education. I want to thank Michal Zolkiewski for serving as the outside chair on my committee.

I want to specially thank my father, Vu Sy Van, my mother, Vu Thi Chuot, my sister, Vu Thi Thanh Hien, my aunt, Tho Knapp, my uncle, Orson Knapp, and Mrs. Hoa Cocozzoli for their support. I truly appreciate my wife, Tam Thu Tran Nguyen, who has always been very supportive and understanding.

Chapter 1 - Introduction

Rationale of studying stress responses in plants

The large and increasing human population requires continuous growth in global food production; such growth requires increasing yields on currently arable lands or increasing arable land area. And, as crude oil reserves diminish, humans may turn to crops for chemicals, materials, and biofuels, increasing pressure on food production even further. Environmental stresses limit crop yields and the arability of land. Indeed, many regions of the world are currently abandoned due to stresses such as high salinity, flooding, water deficit, and harsh winter weather. This not only reduces food production capacity but, in many parts of the world, leads to deforestation as people convert land to agriculture. Deforestation, in turn, creates even more problems for agriculture such as erosion, drought, and flooding. The problem of providing for an enormous and growing human population in a world with limited resources requires multiple solutions, including increasing the efficiency of food production. More efficient food production can be achieved with better agricultural practices that minimize yield loss due to weather, pathogens, and pests and better crop varieties with increased stress tolerance and higher yields. Improved stress tolerance also translates to expansion of cultivated lands. For example, an improved salinity-tolerant rice variety can be grown in coastal areas otherwise abandoned due to salt stress. Similarly, development of more freezing-resistant winter wheat can help expand cultivation with winter wheat northward to increase grain production. All of these promising crop technologies are, however, not feasible without a deep basic understanding of how environmental stresses affect plants and how plants respond to those stresses.

Arabidopsis thaliana: a well-established model

While essential in food production, crop plants are not best-suited for fast-paced basic research due to characteristics that include large sizes, long life cycles, and complicated genomes. *Arabidopsis thaliana* (Arabidopsis), on the other hand, is small in size, making it feasible to grow large numbers in well-controlled laboratory environments. Its short life cycle (40-45 days) is a great advantage in genetic studies. Its small and diploid genome facilitates genetic manipulation and its strict self-pollination allows easy maintenance of mutated lines. Arabidopsis

tissues are relatively soft, making handling, especially metabolite extraction, very easy. Arabidopsis is widely distributed across very different climate zones and its populations thus express great diversity in genetics, phenotype, and biochemistry which are valuable resources for basic research. Over the last two decades, a tremendous amount of Arabidopsis knowledge and research materials have been accumulated and made available to the scientific community. High similarities with crop species, including canola, turnip, cabbage, and broccoli, facilitate the transfer of Arabidopsis-based discoveries to crop plants.

Stress-induced damages and plant physiological responses

In the living environment of most plants, there are many stress agents. Biotic stressors include living organisms such as bacteria, fungi, nematodes, insects, rodents, and grazers. Abiotic stressors are non-living agents such as temperature, wind, water, salt, heavy metals, and toxic chemicals. In this dissertation, I mainly focused on mechanical wounding, bacterial infection, cold, and freezing as plant stressors. These stresses have great agricultural significance, and yet are relatively simple so that they can be applied reproducibly to a large number of Arabidopsis plants, providing a system that is amenable to experimentation.

Mechanical wounding (by hemostat or needle) is carried out in the laboratory to imitate wounds that plants sustain in nature, where wounding is caused by insect bites, large herbivore grazing, wind and hail damage. Wounded plants may suffer from both the primary damage, including ruptured cells, tissue and fluid loss, and secondary damage, caused by attack of opportunistic pathogens via wound openings.

Bacterial pathogens infect plants via wound openings, stomata, root tips, or cracks created by lateral roots. There are intracellular, extracellular and vascular plant bacteria. Symptoms caused by bacterial pathogens include wilts, mosaics, blights, spots, rots or abnormal growths (Mansfield et al., 2012). Plant defense against biotic agents, including bacteria, may be constitutive or inducible. Constitutive defense includes specialized structures (e.g., thorns, trichomes); natural barriers (e.g., cell walls, epidermal wax cuticles, thick bark); preformed chemicals, such as phenolics (e.g., anthocyanin, tannins, lignin), nitrogenous compounds (e.g., caffeine, nicotine, capsaisin), and proteins (e.g., defensins, chitinases, glucanases) (Wittstock and

Gershenzon, 2002; Kaplan et al., 2008; Kempel et al., 2011). Inducible defense is triggered by the presence of pathogens or pests. There are different types of inducible defenses. Inducible defense of a plant species against a whole group of pathogens by recognition of microbe-associated molecular patterns (MAMPs) is called basal resistance or innate immunity. Plant innate immunity against viral pathogens also includes small-RNA-based degradation of viral RNA or DNA (for review, see Peláez and Sanchez, 2013). Innate immunity is non-specific and is very difficult for pathogens to overcome. If a pathogen can overcome plant immunity and cause disease, the plant is called the host species. Within a host species, there are still individuals that will not develop disease when exposed to the pathogen; such interactions are deemed incompatible. Inducible defense that is specifically induced by a pathogen effector is called effector-triggered immunity (ETI). ETI results in what is termed the hypersensitive response (HR), a deliberate suicide of infected tissues to prevent the pathogen from extracting nutrients and spreading. Although effective, ETI is easily evaded by pathogens with a high mutation rate. When HR occurs in one tissue, other uninfected tissues of the plant can become resistant to a wide range of pathogens. This phenomenon is referred to as systemic-acquired resistance (SAR).

In addition to wounding, freezing is another major abiotic plant stress. Freezing injuries to plant cells occur mainly at cell membranes. Ice crystals usually form first in the intercellular space due to its high freezing point because of low solute concentration; the ice crystals can directly rupture cell membranes. However, the major freezing damage is caused by intensive dehydration. As ice crystals form, the water potential drops drastically in the intercellular space, creating a massive rush of water from the cytoplasm. This dehydration causes membrane lysis induced by expansion, membrane lipids undergo a transition to hexagonal II phase, and fracture jump lesions occur (Uemura et al., 1995). Other dehydration-related factors that can cause injury include protein instability and accumulation of harmful reactive oxygen species (ROS). Freezing tolerance of Arabidopsis and many other plants growing in the temperate zone can be significantly increased by cold acclimation. Cold acclimation occurs when plants are exposed to low non-freezing temperatures. The plants change their gene expression, protein composition, and metabolite composition in ways that help them survive the coming freezing temperature.

Overview of plant molecular responses to stresses

Within the first few seconds or minutes after exposure to stress, a number of common molecular changes occur in plants. Oligosaccharides are released from cell walls (bacterial infection, Nothnagel et al., 1983). Plasma membrane microdomains may be rigidified, followed by rearrangement of actin in the cytoskeleton (cold acclimation, Örvar et al., 2000). These changes trigger activation of ROS-forming enzymes and changes in Ca^{2+} fluxes (Prasad et al., 1994; Orozco-Cardenas and Ryan, 1999; León et al., 2001). The massive accumulation of superoxide anion and peroxide is referred to as oxidative burst. ROS and Ca^{2+} activate mitogen-activated protein kinase (MAPK), which in turn activates downstream gene expression. Massive changes in gene expression induced by stress lead to changes in protein and metabolite composition of the cells and ultimately to adaptive responses. For example, genes induced by cold acclimation include those encoding hydrophilic late embryogenesis abundant (LEA) polypeptides, such as COR15a in Arabidopsis (Wang and Hua, 2009). There is evidence suggesting that they might be involved in membrane stabilization (Koag et al., 2003; Koag et al., 2009).

With the development of microarray and mass spectrometry technology and the availability of complete plant genome sequences, global changes in gene expression and protein profiles of plant cells in response to different environmental stresses have been intensively studied, especially in *Arabidopsis thaliana* (Fowler and Thomashow, 2002; Rabbani et al., 2003; Thilmony et al., 2006; Matsui et al., 2008; Li et al., 2012; Niehl et al., 2013; Rocco et al., 2013). As results of gene expression and protein changes, the totality of the cell metabolites changes, including sugars, amino acids, lipids, and secondary metabolites. Therefore, the study of the total composition of metabolites or metabolomics, is a critical tool (together with genomics, transcriptomics, and proteomics) in understanding plant adaptations to stresses. Lipidomics is the branch of metabolomics that deals with analysis of non-water-soluble metabolites. In this dissertation, I focus on the dynamics of plant lipid composition (the plant lipidome) under stresses.

Plant lipid metabolism and stress-induced lipid modifications

Plant lipid metabolism under normal conditions

In plants, fatty acid synthesis occurs in the plastid, where two type of fatty acids, palmitic acid, 16:0 (number of carbon: number of double bond equivalent), and oleic acid, 18:1, are produced. In the plastid, 16:0 and 18:1 linked to acyl carrier protein (ACP) are used in the acylation of glycerol-3-phosphate (G3P) to form phosphatidic acid (PA) (Kunst et al., 1988; Bin et al., 2004; Kim and Huang, 2004; Xu et al., 2006), which can be hydrolyzed to form diacylglycerol (DAG) by the action of phosphatase (Ohlrogge and Browse, 1995). PA can then be converted to phosphatidylglycerol (PG) (Andrews and Mudd, 1985; Müller and Frentzen, 2001). DAG can be converted to monogalactosyldiacylglycerol (MGDG) and further to digalactosyldiacylglycerol (DGDG) by accepting galactose from UDP-Gal (Kelly and Dörmann, 2004). Esterified 16:0 and 18:1 can be desaturated by various fatty acid desaturases (FADs). While the 18:1 at the *sn-1* position on the glycerol backbone can be desaturated from 18:1 to 18:3 in PG, MGDG, and DGDG, 16:0 at the *sn-2* position can only be desaturated to 16:3 in MGDG; in PG, 16:0 is converted to 3,4-*trans*-16:1 (Gao et al., 2009) and in DGDG, 16:0 is not affected by FAD. MGDG and DGDG can also be synthesized using a DAG backbone imported to the plastid from the endoplasmic reticulum (ER) in the eukaryotic pathway. In the ER, 16:0 and 18:1 are linked to coenzyme A (CoA) and used to acylate G3P to form PA, which can be converted to PG, phosphatidylinositol (PI), and DAG. DAG may be the substrate for phosphatidylethanolamine (PE) and phosphatidylcholine (PC) synthesis. Phosphatidylserine (PS) can be synthesized from PE in a serine exchange reaction (Yamaoka et al., 2011). Fatty acids esterified to PC may undergo desaturation (Browse et al., 1993; Sperling and Heinz, 1993) and removal which feeds 16:0-CoA, 18:2-CoA, and 18:3-CoA back to the fatty acyl pool. In addition to incorporation of fatty acids from fatty acyl-CoAs into PA, an alternative route for phospholipid synthesis involves incorporation of acyl chains from fatty acyl-CoA directly into PC by "acyl editing", which may involve acylation of a lysophosphatidylcholine (LPC) (Bates et al., 2007; Bates et al., 2009). A fatty acyl group from PE can also be transferred to sterols to form sterol esters (Banaś et al., 2005). In plants, the most abundant sterols are sitosterol, campesterol, and stigmasterol. Other major derivatives of sterols include steryl glycoside (SG) and acylated steryl glycoside (ASG). SG is synthesized from sterol and UDP-glucose by UDP-glucose: sterol glucosyltransferase

(DeBolt et al., 2009). Figure 1.1 shows some examples of the polar lipids mentioned above. Figure 1.2 summarizes the biosynthesis of polar lipids in plant cells (solid arrows).

Stress-induced membrane lipid modifications

When a plant is stressed, several lipid modifications occur, including hydrolysis, fatty acid oxidation, polar head-group acylation, and trans-galactosylation (oligo-galactosyldiacylglycerol synthesis from MGDG). The dashed-arrows in Figure 1.2 indicate reactions that are induced by stresses.

Hydrolysis

There are many types of enzymes carrying out membrane lipid hydrolysis by different reactions. Phospholipase A cleaves a fatty acyl group from the glycerol backbone, producing lyso-phospholipids and free fatty acids. The patatin-related phospholipase A (pPLA) is an important enzyme family. In Arabidopsis, pPLA family consists of 10 genes divided into three subfamilies, pPLAI, pPLAII (α, β, γ, δ, ε), and pPLAIII (α, β, γ, δ) (Scherer et al., 2010). Patatin is a group of storage glycoproteins first found in potato tubers (Galliard, 1971). Patatin-related enzymes usually contain an esterase-specific sequence, GXSXG (Scherer et al., 2010). In the pPLAIII subfamily, this sequence is GXGXG and in the pPLAI and pPLAII subfamilies, this sequence is GXSXG (Scherer et al., 2010). Although pPLAs are known as "phospholipases", some members of the family can act on galactolipids as well as phospholipids, and in most cases, *in-vivo* substrates of these enzymes are not well characterized. pPLAs are involved in various processes, including plant responses to fungal and bacterial infection, phosphate deficiency, and cellulose content (La Camera et al., 2005; Yang et al., 2007; Rietz et al., 2010; Li et al., 2011). However, the detailed pPLA catalytic mechanism, as well as substrate and product identities of most pPLAs are still unclear. They might be involved in releasing bioactive oxidized fatty acids (oxylipins) from complex membrane lipids. AtPLAI (At1g61850) preferentially hydrolyzes oxidized galactolipids as compared to the non-oxidized substrates (Yang et al., 2007). pPLAIIIδ was shown to promote the synthesis of TAG with 20- and 22-carbon fatty acids (Li et al., 2013).

Phospholipase C hydrolyzes the glycerol-phosphate linkage in a glycerophospholipid, producing DAG, while phospholipase D hydrolyzes the head-group phosphoester linkage forming free

choline (from PC) or ethanolamine (from PE) and PA. Phospholipases C and D are activated in many stresses including wounding, bacterial infection and freezing. In Arabidopsis, recognition of avirulent factors, AvrRpm1 or AvrRpt2, causes two distinct activations of phospholipases. PLC is activated first, producing PA with the action of DAGK. This PA is shown to cause an influx of extracellular Ca^{2+}, followed by the second, much greater accumulation of PA due to phospholipase D (PLD) activation (Andersson et al., 2006b). Finally, PA is found to regulate both ROS production via NADPH oxidase activity and stomata closing induced by ABA, H_2O_2, and NO (Zhang et al., 2009). When Arabidopsis is exposed to sub-lethal freezing, phospholipase Dα (PLDα) catalyzes the degradation of phosphatidylcholine (PC), the major component of membrane bilayer, and produces PA, perhaps resulting in decreased cryostability of membranes (Welti et al., 2002). Interestingly, the membrane-bound PLDδ, which produces about 20% of the total PA, has the opposite effect of PLDα. Its knockout decreases Arabidopsis freezing tolerance although it does not affect induction of cold-regulated genes COR47 and COR78, nor the accumulation of proline and soluble sugars (Li et al., 2004). Damage to plants not only occurrs during the freezing period but also during the thawing afterward (Steponkus and Lynch, 1989). Whereas during the freezing period, mainly extraplastidic membrane phospholipids (PC and PE) are hydrolyzed by PLDα (Welti et al., 2002), plastidic MGDG and PG are hydrolyzed intensively during the thawing period; hydrolysis is increased by knocking out PLDδ (Li et al., 2008). PLDδ's ability to decrease the post-freezing hydrolysis of plastidic membrane lipids might contribute to its beneficial effect on Arabidopsis freezing tolerance.

Oxidation

Fatty acyl oxidation can occur enzymatically or non-enzymatically. Enzymatically, fatty acyl oxidation is often initiated by lipoxygenases (LOXs) or dioxygenases (DOXs). In Arabidopsis, there are two major groups of LOXs, 9-LOXs and 13-LOXs with designation dependent on the position of the introduced oxygen (Porta and Rocha-Sosa, 2002). In the Arabidopsis genome, there are two genes annotated as 9-LOX, *AtLOX1* (At1G55020) and *AtLOX5* (At3G22400) and 4 genes annotated as 13-LOX, *AtLOX2* (At3G45140), *AtLOX3* (At1G17420), *AtLOX4* (At1G72520), and *AtLOX6* (At1G67560). Two of the major products of enzymatic fatty acyl oxidation by 13-LOXs in Arabidopsis are oxophytodienoic acid (OPDA) and dinor-oxophytodienoic acid (dnOPDA), which are precursors of jasmonic acid (JA). ODPA and

dnOPDA production is induced drastically in response to wounding and avirulent bacterial infection. Although it is still unclear whether the acyl substrates of LOXs can be esterified or not, the majority of induced OPDA and dnOPDA are found in galactolipids (Andersson et al., 2006a; Buseman et al., 2006; Kourtchenko et al., 2007). Some examples of oxidized glycerolipids are shown in Figure 1.3. Non-enzymatic fatty acyl peroxidation occurrs in wounding and fungal infection due to ROS, producing oxidized fatty acids such as malondialdehyde and phytoprostanes (Imbusch and Mueller, 2000; Thoma et al., 2003; Mène-Saffrané et al., 2009).

Acylation

In Arabidopsis, a massive accumulation of OPDA- and dnOPDA-containing MGDG with the *sn-6* position of the galactose ring acylated to yet another OPDA occurred in response to wounding and avirulent bacterial infection (Andersson et al., 2006a; Kourtchenko et al., 2007). Very little is known about this acylation as well as the enzymes that catalyze the process. Much earlier in vitro experiments suggested that MGDG can be acylated with acyl groups from DGDG (Heinz, 1972). An example of acylated MGDG (acMGDG), acMGDG(16:0/18:4-O/16:4-O), is shown in Figure 1.3.

Transgalactosylation

Transgalactosylation has only been reported in Arabidopsis responding to freezing. The galactosyl group from an MGDG can be transferred to another MGDG to form DAG, DGDG and higher oligogalactolipids, which are believed to prevent the fusion of membrane bilayers following freezing. DAG, which is not desirable due to its nonlamellar phase forming nature, is converted to TAG (Moellering et al., 2010).

Hypotheses

There are many remaining questions about stress-induced lipids and lipid metabolizing enzymes, including their identities, their substrates, biosynthesis, catabolism, and especially their functions in stress responses. The motivation for the research presented in this dissertation was to address these questions. The hypotheses tested are:

(1) Different stresses or stress responses result in distinct lipidomes (holistic lipid compositions).
(2) In response to a stress, groups of lipid analytes that are metabolized by the same enzyme or pathway change together.
(3) Ablation of LOXs and pPLAs lead to altered stress-induced lipidomes and altered stress response outcomes.

Lipidomics: an excellent tool

To test the above hypotheses, lipidomes of wild-type Arabidopsis plants exposed to wounding, bacterial infection, and low temperature stresses were obtained and compared. Lipidomes of stressed knockout mutants are obtained and analyzed to reveal the roles of LOXs and pPLAs in stress responses.

Throughout the research, the capacity to quantitatively monitor large numbers of lipids efficiently was critical. Mass spectrometry-based lipidomics was the method of choice due to its many advantages including low detection limit, high sensitivity, vast dynamic range, good resolution and precision, reliable compound identification, good compound coverage, and short sample analysis time. A low detection limit (low background noise) is critical to detect low abundant compounds, especially early signaling molecules. Sensitivity is the efficiency of detection. A high-sensitivity method requires a small number of ions to give a signal that is higher than the detection limit and vice versa. Linear dynamic range is the range of concentrations in which the quantification is linear; a wide dynamic range is required when a structural lipid is measured simultaneously with a signaling lipid. Resolution (resolving power) refers the mass difference between two compounds required for the mass spectrometer to accurately distinguish them. Reproducibility (precision) is evaluated by the variation between replicates of the same measurement. Compound identification quality is the type and amount of information utilized to identify compounds. For example, an identification based only on the mass of an intact ion is not as strong as one based on masses of an intact ion plus a fragment ion. Compound coverage or comprehensiveness is the number of lipid classes and compounds that

can be measured simultaneously. Time and labor consumption are critical aspects to consider, especially in large scale experiments.

Lipidomics is a multi-step procedure starting from lipid extraction. The extracted total lipids can be separated into fractions by liquid chromatography (LC) or directly introduced into a mass spectrometer (direct infusion). For quantification purposes, internal standard(s) with known amounts are co-analyzed with target lipids. Inside a mass spectrometer, the lipid analytes are ionized, filtered, fragmented (in tandem MS analyses), and detected. This provides information on the identities (defined by the lipid ion masses and, in tandem MS analyses, their fragment masses) and the abundance of lipid analytes. For the purpose of this dissertation research, direct-infusion electrospray ionization (ESI) tandem mass spectrometry (MS/MS), operated in neutral loss scan mode (NL scan), precursor scan mode (Pre scan), and multiple reaction monitoring (MRM), was employed to profile plant lipidomes. Rationales of key components of the employed analytical approaches are discussed below.

Internal standards

An internal standard is a quantitative standard present in the same sample as the analytes. Without internal standards, mass spectral signals can be used to calculate the percentage of the target compounds of the total signals to compare samples of the same experiment. However, lack of quantification by normalization of MS intensity to internal standards will significantly limit comparison between different experiments among experiments in the literature. The two most important criteria for internal standards are: (1) they are not present in the biological samples being analyzed and (2) their chemistry and ionization are the same or highly similar to those of the target compounds. Therefore, it is ideal to use stable-isotope labeled lipids as internal standards since they satisfy both criteria. Since the cell lipidome is so diverse, stable isotope-labeled internal standards are not available in every class of lipids in every organism. Non-native lipids, such as odd-chain lipids and saturated lipids, are currently the most commonly used internal standards (Koivusalo et al., 2001; Welti et al., 2002; Ejsing et al., 2006). Although these internal standards would not allow absolute quantification of many lipid classes, they provide good sample-to-sample quantification, which was the main goal of this dissertation research.

Lipid extraction

Total lipids are most commonly extracted by chloroform-based procedures developed by Bligh and Dyer (1959) and Folch et al. (1957). The total extracts produced by these procedures contain almost all lipid classes present in the samples. However, these extraction methods are time-consuming, labor-consuming, and prone to human error. These disadvantages hinder their application in large-scale experiments. Therefore, a simpler extraction method is presented in Chapter 4. In this method, leaf tissues are directly submerged in a large volume (compared to tissue volume) of mass spectral solvent for a long period. The extracts can be injected directly to a mass spectrometer without any further treatment.

Ionization of lipid in mass spectrometer

The ionization method of choice was ESI (Han and Gross, 1994; Kerwin et al., 1994; Kim et al., 1994). ESI has two main advantages: (1) its great sensitivity (several orders of magnitude higher than fast atom bombardment, FAB) and the "softness" of the ionization (producing a single intact ion for each target analyte, rather than fragmenting the intact ion).

Mass analyzer and ion fragmentation

One or more mass analyzers, i.e., the electrical and physical components that guide, select and separate ions based on their mass-to-charge ratios, are the core of every mass spectrometer. A triple-quadrupole mass spectrometer contains three linearly arranged sets of four parallel metal rods (each called a quadrupole). From the front end of the mass spectrometer, the quadrupoles can be named Q1, Q2, and Q3, respectively. In Q1 and Q3, the opposing pairs of metal rods create an oscillating electric field by applying specific values of direct current (DC) and radio frequency (RF) potentials to move ions of particular mass to charge ratios (*m/z*). By varying the DC and RF values to transmit varied *m/z*, the mass spectrometer creates a mass spectrum. Q2 is in the collision cell between the Q1 and Q3 mass analyzers. In Q2, only RF potential is applied so that all ions (above a threshold) can pass through. Q2 is usually partly enclosed and inert gas (nitrogen or argon) can be introduced; collision of ions with the inert gas causes fragmentation

(collision induced dissociation, CID). Ion fragmentation in tandem mass spectrometry gives structural information (beside intact ion molecular mass information) on the targets being analyzed (de Hoffmann, 1996).

In a triple quadrupole mass spectrometer, there are four scanning modes that involve CID: product ion scan, Pre scan, NL scan, and MRM. The latter 3 scanning modes are commonly utilized in both LC-MS and direct infusion lipidomics. In all three scanning modes, Q2 is always activated. In Pre scan, Q1 sequentially transmits precursor ions of a specified mass range, whereas Q3 only allow ions with a specified fragment mass to pass through to the ion detector. In NL scan, both Q1 and Q3 sequentially transmit precursor ions and fragments with a specified offset (the mass of the neutral fragment). In MRM, for a short specified period of time (the dwell time), Q1 and Q3 only transmit a pair of specified precursor ion and fragment. Although MRM does not produce a conventional spectrum, it is highly sensitive, precise and especially time efficient. MRM is usually coupled with LC in LC-MRM lipidomics (Bielawski et al., 2006; Deems et al., 2007; Ikeda et al., 2008; Ikeda et al., 2009; Mesaros et al., 2009; Scherer et al., 2009). Inherent disadvantages of LC-MS include the unstable ion stream, which reduces precision, and the limited detection window per lipid analyte, which limits the comprehensiveness of LC-based lipidomics. In Chapter 4, MRM was combined with direct infusion MS to improve compound coverage and precision.

Data processing

Lipidomics, like other –omics research, produces large amounts of data. Due the intrinsic structural diversity of lipids, lipidomics data is also highly complicated. Multiple calculation steps have to be carried out to turn mass spectrometry output into meaningful data amenable to statistical study. These steps may include peak annotation, isotopic deconvolution, and quantification (normalization to internal standard). Especially in large scale experiments, it is impractical to manually process raw mass spectral data for statistical analysis. Several softwares have been developed to automate data processing in lipidomics. Lipid Profiler is commercially provided by MDS Sciex for handling LC-MS lipidomics data. LIMSA, TriglyAPCI, and MSPECTRA are open source software also designed for LC-MS lipidomics (Cvačka et al., 2006;

Haimi et al., 2006). To improve data processing in this dissertation research, LipidomeDB Data Calculation Environment (LipidomeDB DCE) was utilized. This is an online calculating environment that can take spectrum lists (including mass and intensity information) in Excel files (exported from mass spectral raw data) and perform peak identification, isotopic deconvolution, and quantification based on researcher-provided target compound lists (Zhou et al., 2011). Also because of the bulkiness of lipidomic data, statistical analysis can be time consuming and error-prone without suitable tools. The MetaboAnalyst website provides user-friendly, online statistical tools that are well designed to handle large datasets (Xia et al., 2009; Xia et al., 2012).

In this dissertation research, Arabidopsis responses to environmental stresses were studied at the molecular level using reverse genetics and lipidomics. Firstly, lipidomics was used to globally monitor membrane lipid changes in stressed Arabidopsis (Chapter 2 and 3). From these data, hypotheses about roles of membrane lipid modifications in plant stress responses were made. An improved lipidomics strategy coupled with co-occurrence analysis was employed in Chapter 4 to study the metabolic modularity of lipid changes in response to wounding. The analytical approach and co-occurrence analysis were applied in a large scale experiment in which lipidomes of 22 Arabidopsis knockouts (21 lines ablated in membrane lipid metabolizing enzymes and an OPDA reductase knockout line) under cold acclimation and freezing stress were documented and analyzed (Chapter 5).

References

Andersson MX, Hamberg M, Kourtchenko O, Brunnström A, McPhail KL, Gerwick WH, Göbel C, Feussner I, and Ellerström M (2006a) Oxylipin profiling of the hypersensitive response in *Arabidopsis thaliana*. Formation of a novel oxo-phytodienoic acid-containing galactolipid, arabidopside E. J. Biol. Chem. **281**, 31528-31537.

Andersson MX, Kourtchenko O, Dangl JL, Mackey D, and Ellerström M (2006b) Phospholipase-dependent signalling during the AvrRpm1- and AvrRpt2-induced disease resistance responses in *Arabidopsis thaliana*. Plant J. **47**, 947-959.

Andrews J, and Mudd JB (1985) Phosphatidylglycerol synthesis in pea chloroplasts: pathway and localization. Plant Physiol. **79**, 259-265.

Banaś A, Carlsson AS, Huang B, Lenman M, Banaś W, Lee M, Noiriel A, Benveniste P, Schaller H, Bouvier-Navé P, and Stymne S (2005) Cellular sterol ester synthesis in plants is performed by an enzyme (phospholipid:sterol acyltransferase) different from the yeast and mammalian acyl-CoA:sterol acyltransferases. J. Biol. Chem. **280**, 34626-34634.

Bates PD, Durrett TP, Ohlrogge JB, and Pollard M (2009) Analysis of acyl fluxes through multiple pathways of triacylglycerol synthesis in developing soybean embryos. Plant Physiol. **150**, 55-72.

Bates PD, Ohlrogge JB, and Pollard M (2007) Incorporation of newly synthesized fatty acids into cytosolic glycerolipids in pea leaves occurs via acyl editing. J. Biol. Chem. **282**, 31206-31216.

Bielawski J, Szulc ZM, Hannun YA, and Bielawska A (2006) Simultaneous quantitative analysis of bioactive sphingolipids by high-performance liquid chromatography-tandem mass spectrometry. Methods **39**, 82-91.

Bin Y, Wakao S, Fan J, and Benning C (2004) Loss of plastidic lysophosphatidic acid acyltransferase causes embryo-lethality in Arabidopsis. Plant Cell Physiol. **45**, 503-510.

Bligh EG, and Dyer WJ (1959) A rapid method of total lipid extraction and purification. Can. J. Biochem. Physiol. **37**, 911-917.

Browse J, McConn M, James D,Jr, and Miquel M (1993) Mutants of Arabidopsis deficient in the synthesis of alpha-linolenate. Biochemical and genetic characterization of the endoplasmic reticulum linoleoyl desaturase. J. Biol. Chem. **268**, 16345-16351.

Buseman CM, Tamura P, Sparks AA, Baughman EJ, Maatta S, Zhao J, Roth MR, Esch SW, Shah J, Williams TD, and Welti R (2006) Wounding stimulates the accumulation of glycerolipids containing oxophytodienoic acid and dinor-oxophytodienoic acid in Arabidopsis leaves. Plant Physiol. **142**, 28-39.

Cvačka J, Krafková E, Jiroš P, and Valterová I (2006) Computer-assisted interpretation of atmospheric pressure chemical ionization mass spectra of triacylglycerols. Rapid Commun. Mass Spectrom. **20**, 3586-3594.

de Hoffmann E (1996) Tandem mass spectrometry: a primer. J. Mass Spectrom. **31**, 129-137.

DeBolt S, Scheible WR, Schrick K, Auer M, Beisson F, Bischoff V, Bouvier-Nave P, Carroll A, Hematy K, Li Y, Milne J, Nair M, Schaller H, Zemla M, and Somerville C (2009)

Mutations in UDP-glucose:sterol glucosyltransferase in Arabidopsis cause transparent testa phenotype and suberization defect in seeds. Plant Physiol. **151**, 78-87.

Deems R, Buczynski MW, Bowers-Gentry R, Harkewicz R, and Dennis EA (2007) Detection and quantitation of eicosanoids via high performance liquid chromatography-electrospray ionization-mass spectrometry. Methods Enzymol. **432**, 59-82.

Ejsing CS, Duchoslav E, Sampaio J, Simons K, Bonner R, Thiele C, Ekroos K, and Shevchenko A (2006) Automated identification and quantification of glycerophospholipid molecular species by multiple precursor ion scanning. Anal. Chem. **78**, 6202-6214.

Folch J, Lees M, and Sloane Stanley GH (1957) A simple method for the isolation and purification of total lipides from animal tissues. J. Biol. Chem. **226**, 497-509.

Fowler S, and Thomashow MF (2002) Arabidopsis transcriptome profiling indicates that multiple regulatory pathways are activated during cold acclimation in addition to the CBF cold response pathway. Plant Cell **14**, 1675-1690.

Galliard T (1971) The enzymic deacylation of phospholipids and galactolipids in plants. Purification and properties of a lipolytic acyl-hydrolase from potato tubers. Biochem. J. **121**, 379-390.

Gao J, Ajjawi I, Manoli A, Sawin A, Xu C, Froehlich JE, Last RL, and Benning C (2009) *FATTY ACID DESATURASE4* of Arabidopsis encodes a protein distinct from characterized fatty acid desaturases. Plant J. **60**, 832-839.

Haimi P, Uphoff A, Hermansson M, and Somerharju P (2006) Software tools for analysis of mass spectrometric lipidome data. Anal. Chem. **78**, 8324-8331.

Han X, and Gross RW (1994) Electrospray ionization mass spectroscopic analysis of human erythrocyte plasma membrane phospholipids. Proc. Natl. Acad. Sci. U. S. A. **91**, 10635-10639.

Heinz E (1972) Some properties of the acyl galactosyl diglyceride-forming enzyme from leaves. Zeitschrift fur Pflanzenphysiologie **69**, 359-360.

Ikeda K, Oike Y, Shimizu T, and Taguchi R (2009) Global analysis of triacylglycerols including oxidized molecular species by reverse-phase high resolution LC/ESI-QTOF MS/MS. J. Chromatogr. B. Analyt Technol. Biomed. Life. Sci. **877**, 2639-2647.

Ikeda K, Shimizu T, and Taguchi R (2008) Targeted analysis of ganglioside and sulfatide molecular species by LC/ESI-MS/MS with theoretically expanded multiple reaction monitoring. J. Lipid Res. **49**, 2678-2689.

Imbusch R, and Mueller MJ (2000) Analysis of oxidative stress and wound-inducible dinor isoprostanes F(1) (phytoprostanes F(1)) in plants. Plant Physiol. **124**, 1293-1304.

Kaplan I, Halitschke R, Kessler A, Sardanelli S, and Denno RF (2008) Constitutive and induced defenses to herbivory in above- and belowground plant tissues. Ecology **89**, 392-406.

Kelly AA, and Dörmann P (2004) Green light for galactolipid trafficking. Curr. Opin. Plant Biol. **7**, 262-269.

Kempel A, Schadler M, Chrobock T, Fischer M, and van Kleunen M (2011) Tradeoffs associated with constitutive and induced plant resistance against herbivory. Proc. Natl. Acad. Sci. U. S. A. **108**, 5685-5689.

Kerwin JL, Tuininga AR, and Ericsson LH (1994) Identification of molecular species of glycerophospholipids and sphingomyelin using electrospray mass spectrometry. J. Lipid Res. **35**, 1102-1114.

Kim HU, and Huang AH (2004) Plastid lysophosphatidyl acyltransferase is essential for embryo development in Arabidopsis. Plant Physiol. **134**, 1206-1216.

Kim HY, Wang TC, and Ma YC (1994) Liquid chromatography/mass spectrometry of phospholipids using electrospray ionization. Anal. Chem. **66**, 3977-3982.

Koag MC, Fenton RD, Wilkens S, and Close TJ (2003) The binding of maize DHN1 to lipid vesicles. Gain of structure and lipid specificity. Plant Physiol. **131**, 309-316.

Koag MC, Wilkens S, Fenton RD, Resnik J, Vo E, and Close TJ (2009) The K-segment of maize DHN1 mediates binding to anionic phospholipid vesicles and concomitant structural changes. Plant Physiol. **150**, 1503-1514.

Koivusalo M, Haimi P, Heikinheimo L, Kostiainen R, and Somerharju P (2001) Quantitative determination of phospholipid compositions by ESI-MS: effects of acyl chain length, unsaturation, and lipid concentration on instrument response. J. Lipid Res. **42**, 663-672.

Kourtchenko O, Andersson MX, Hamberg M, Brunnström A, Göbel C, McPhail KL, Gerwick WH, Feussner I, and Ellerström M (2007) Oxo-phytodienoic acid-containing

galactolipids in Arabidopsis: jasmonate signaling dependence. Plant Physiol. **145**, 1658-1669.

Kunst L, Browse J, and Somerville C (1988) Altered regulation of lipid biosynthesis in a mutant of Arabidopsis deficient in chloroplast glycerol-3-phosphate acyltransferase activity. Proc. Natl. Acad. Sci. U. S. A. **85**, 4143-4147.

León J, Rojo E, and Sánchez-Serrano JJ (2001) Wound signalling in plants. J. Exp. Bot. **52**, 1-9.

Li B, Takahashi D, Kawamura Y, and Uemura M (2012) Comparison of plasma membrane proteomic changes of Arabidopsis suspension-cultured cells (T87 Line) after cold and ABA treatment in association with freezing tolerance development. Plant Cell Physiol. **53**, 543-554.

Li M, Bahn SC, Fan C, Li J, Phan T, Ortiz M, Roth MR, Welti R, Jaworski J, and Wang X (2013) Patatin-Related Phospholipase pPLAIIIδ Increases Seed Oil Content with Long-Chain Fatty Acids in Arabidopsis. Plant Physiol. **162**, 39-51.

Li W, Li M, Zhang W, Welti R, and Wang X (2004) The plasma membrane-bound phospholipase Dδ enhances freezing tolerance in *Arabidopsis thaliana*. Nat. Biotechnol. **22**, 427-433.

Li W, Wang R, Li M, Li L, Wang C, Welti R, and Wang X (2008) Differential degradation of extraplastidic and plastidic lipids during freezing and post-freezing recovery in *Arabidopsis thaliana*. J. Biol. Chem. **283**, 461-468.

Maatta S, Scheu B, Roth MR, Tamura P, Li M, Williams TD, Wang X, and Welti R (2012) Levels of *Arabidopsis thaliana* leaf phosphatidic acids, phosphatidylserines, and most trienoate-containing polar lipid molecular species increase during the dark period of the diurnal cycle. Front. Plant. Sci. **3**, 49.

Mansfield J, Genin S, Magori S, Citovsky V, Sriariyanum M, Ronald P, Dow M, Verdier V, Beer SV, Machado MA, Toth I, Salmond G, and Foster GD (2012) Top 10 plant pathogenic bacteria in molecular plant pathology. Mol. Plant. Pathol. **13**, 614-629.

Matsui A, Ishida J, Morosawa T, Mochizuki Y, Kaminuma E, Endo TA, Okamoto M, Nambara E, Nakajima M, Kawashima M, Satou M, Kim JM, Kobayashi N, Toyoda T, Shinozaki K, and Seki M (2008) Arabidopsis transcriptome analysis under drought, cold,

high-salinity and ABA treatment conditions using a tiling array. Plant Cell Physiol. **49**, 1135-1149.

Mène-Saffrané L, Dubugnon L, Chételat A, Stolz S, Gouhier-Darimont C, and Farmer EE (2009) Nonenzymatic oxidation of trienoic fatty acids contributes to reactive oxygen species management in Arabidopsis. J. Biol. Chem. **284**, 1702-1708.

Mesaros C, Lee SH, and Blair IA (2009) Targeted quantitative analysis of eicosanoid lipids in biological samples using liquid chromatography-tandem mass spectrometry. J. Chromatogr. B. Analyt Technol. Biomed. Life. Sci. **877**, 2736-2745.

Moellering ER, Muthan B, and Benning C (2010) Freezing tolerance in plants requires lipid remodeling at the outer chloroplast membrane. Science **330**, 226-228.

Müller F, and Frentzen M (2001) Phosphatidylglycerophosphate synthases from *Arabidopsis thaliana*. FEBS Lett. **509**, 298-302.

Narashimhan R, Wang G, Li M, Roth M, Welti R, and Wang X (2013) Differential changes in galactolipid and phospholipid species in soybean leaves and roots under nitrogen deficiency and after nodulation. Phytochemitry **96**, 81-91.

Niehl A, Zhang ZJ, Kuiper M, Peck SC, and Heinlein M (2013) Label-free quantitative proteomic analysis of systemic responses to local wounding and virus infection in *Arabidopsis thaliana*. J. Proteome Res. **12**, 2491-2503.

Nothnagel EA, McNeil M, Albersheim P, and Dell A (1983) Host-pathogen interactions : XXII. A galacturonic acid oligosaccharide from plant cell walls elicits phytoalexins. Plant Physiol. **71**, 916-926.

Ohlrogge J, and Browse J (1995) Lipid biosynthesis. Plant Cell **7**, 957-970.

Orozco-Cardenas M, and Ryan CA (1999) Hydrogen peroxide is generated systemically in plant leaves by wounding and systemin via the octadecanoid pathway. Proc. Natl. Acad. Sci. U. S. A. **96**, 6553-6557.

Örvar BL, Sangwan V, Omann F, and Dhindsa RS (2000) Early steps in cold sensing by plant cells: the role of actin cytoskeleton and membrane fluidity. Plant J. **23**, 785-794.

Peláez P, and Sanchez F (2013) Small RNAs in plant defense responses during viral and bacterial interactions: similarities and differences. Front. Plant. Sci. **4**, 343.

Porta H, and Rocha-Sosa M (2002) Plant lipoxygenases. Physiological and molecular features. Plant Physiol. **130**, 15-21.

Prasad TK, Anderson MD, Martin BA, and Stewart CR (1994) Evidence for chilling-induced oxidative stress in maize seedlings and a regulatory role for hydrogen peroxide. Plant Cell **6**, 65-74.

Rabbani MA, Maruyama K, Abe H, Khan MA, Katsura K, Ito Y, Yoshiwara K, Seki M, Shinozaki K, and Yamaguchi-Shinozaki K (2003) Monitoring expression profiles of rice genes under cold, drought, and high-salinity stresses and abscisic acid application using cDNA microarray and RNA gel-blot analyses. Plant Physiol. **133**, 1755-1767.

Rocco M, Arena S, Renzone G, Scippa GS, Lomaglio T, Verrillo F, Scaloni A, and Marra M (2013) Proteomic analysis of temperature stress-responsive proteins in Arabidopsis thaliana rosette leaves. Mol. Biosyst **9**, 1257-1267.

Scherer GF, Ryu SB, Wang X, Matos AR, and Heitz T (2010) Patatin-related phospholipase A: nomenclature, subfamilies and functions in plants. Trends Plant Sci. **15**, 693-700.

Scherer M, Schmitz G, and Liebisch G (2009) High-throughput analysis of sphingosine 1-phosphate, sphinganine 1-phosphate, and lysophosphatidic acid in plasma samples by liquid chromatography-tandem mass spectrometry. Clin. Chem. **55**, 1218-1222.

Sperling P, and Heinz E (1993) Isomeric sn-1-octadecenyl and sn-2-octadecenyl analogues of lysophosphatidylcholine as substrates for acylation and desaturation by plant microsomal membranes. Eur. J. Biochem. **213**, 965-971.

Steponkus PL, and Lynch DV (1989) Freeze/thaw-induced destabilization of the plasma membrane and the effects of cold acclimation. J. Bioenerg. Biomembr. **21**, 21-41.

Thilmony R, Underwood W, and He SY (2006) Genome-wide transcriptional analysis of the Arabidopsis thaliana interaction with the plant pathogen Pseudomonas syringae pv. tomato DC3000 and the human pathogen Escherichia coli O157:H7. Plant J. **46**, 34-53.

Thoma I, Loeffler C, Sinha AK, Gupta M, Krischke M, Steffan B, Roitsch T, and Mueller MJ (2003) Cyclopentenone isoprostanes induced by reactive oxygen species trigger defense gene activation and phytoalexin accumulation in plants. Plant J. **34**, 363-375.

Uemura M, Joseph RA, and Steponkus PL (1995) Cold acclimation of *Arabidopsis thaliana* (Effect on plasma membrane lipid composition and freeze-induced lesions). Plant Physiol. **109**, 15-30.

Wang Y, and Hua J (2009) A moderate decrease in temperature induces COR15a expression through the CBF signaling cascade and enhances freezing tolerance. Plant J. **60**, 340-349.

Welti R, Li W, Li M, Sang Y, Biesiada H, Zhou HE, Rajashekar CB, Williams TD, and Wang X (2002) Profiling membrane lipids in plant stress responses. Role of phospholipase Dα in freezing-induced lipid changes in Arabidopsis. J. Biol. Chem. **277**, 31994-32002.

Wittstock U, and Gershenzon J (2002) Constitutive plant toxins and their role in defense against herbivores and pathogens. Curr. Opin. Plant Biol. **5**, 300-307.

Xia J, Mandal R, Sinelnikov IV, Broadhurst D, and Wishart DS (2012) MetaboAnalyst 2.0--a comprehensive server for metabolomic data analysis. Nucleic Acids Res. **40**, W127-33.

Xia J, Psychogios N, Young N, and Wishart DS (2009) MetaboAnalyst: a web server for metabolomic data analysis and interpretation. Nucleic Acids Res. **37**, W652-60.

Xu C, Yu B, Cornish AJ, Froehlich JE, and Benning C (2006) Phosphatidylglycerol biosynthesis in chloroplasts of Arabidopsis mutants deficient in acyl-ACP glycerol-3-phosphate acyltransferase. Plant J. **47**, 296-309.

Yamaoka Y, Yu Y, Mizoi J, Fujiki Y, Saito K, Nishijima M, Lee Y, and Nishida I (2011) *PHOSPHATIDYLSERINE SYNTHASE1* is required for microspore development in *Arabidopsis thaliana*. Plant J. **67**, 648-661.

Yang W, Devaiah SP, Pan X, Isaac G, Welti R, and Wang X (2007) AtPLAI is an acyl hydrolase involved in basal jasmonic acid production and *Arabidopsis* resistance to *Botrytis cinerea*. J. Biol. Chem. **282**, 18116-18128.

Zhang Y, Zhu H, Zhang Q, Li M, Yan M, Wang R, Wang L, Welti R, Zhang W, and Wang X (2009) Phospholipase Dα1 and phosphatidic acid regulate NADPH oxidase activity and production of reactive oxygen species in ABA-mediated stomatal closure in *Arabidopsis*. Plant Cell **21**, 2357-2377.

Zhou Z, Marepally SR, Nune DS, Pallakollu P, Ragan G, Roth MR, Wang L, Lushington GH, Visvanathan M, and Welti R (2011) LipidomeDB data calculation environment: online processing of direct-infusion mass spectral data for lipid profiles. Lipids **46**, 879-884.

Figures

Figure 1.1 Examples of normal-chain plant lipids.

This figure is adapted, with modifications, from Narashimhan et al. (Supplemental Figure 1, 2013).

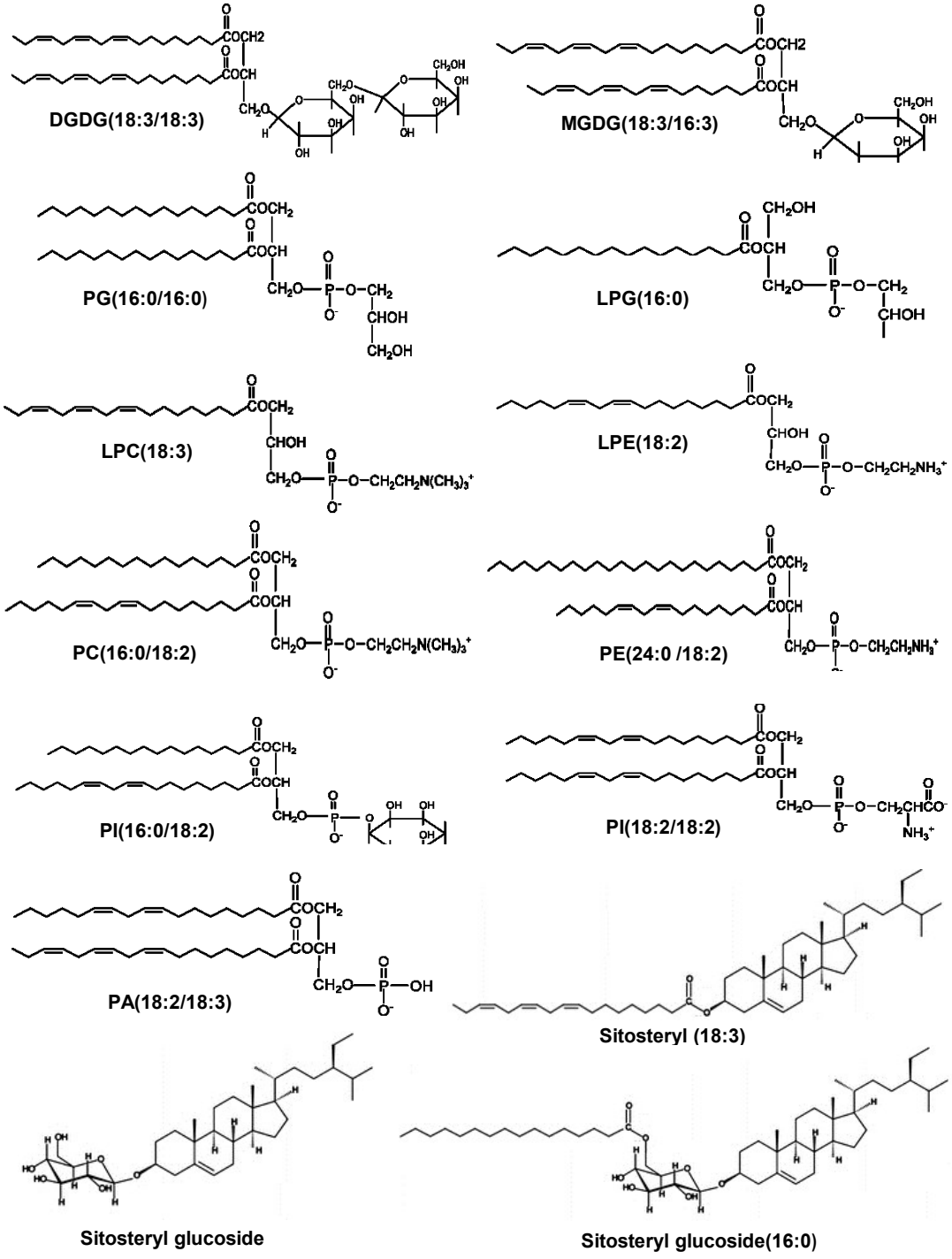

Figure 1.2 Arabidopsis lipid metabolism in normal and stress conditions.

Solid arrows indicate reactions that occur in normal conditions. Dashed arrows indicate reaction that occurs in stress conditions. Abbreviations not explained elsewhere: CoA (Coenzyme A); ac-PG, -MGDG, -DGDG (acylated PG, MGDG, DGDG); ox-PC, -PE, PG,-MGDG,-DGDG (oxidized PC, PE, PG, MGDG, DGDG); and ACP (acyl carrier protein). This figure is adapted, with modifications, from Maatta et al. (Figure 5, 2012).

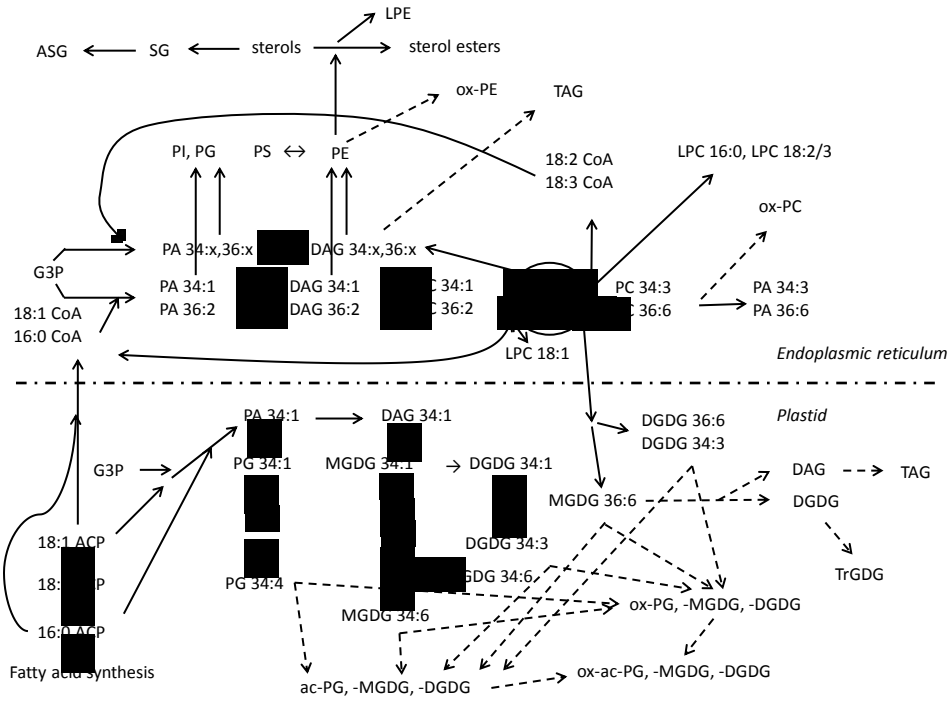

Figure 1.3 Examples of oxidized and acylated membrane lipids in Arabidopsis.

This figure is adapted from Vu et al. (2012) with modifications.

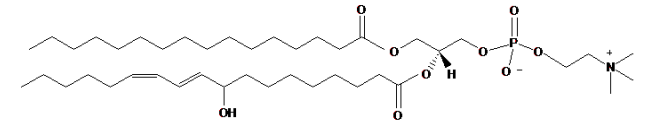

PC(18:2-O/16:0)

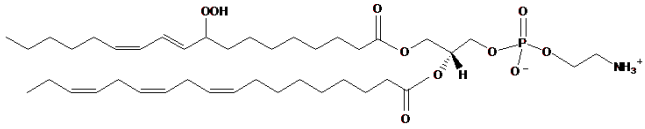

PE(18:2-2O/18:3)

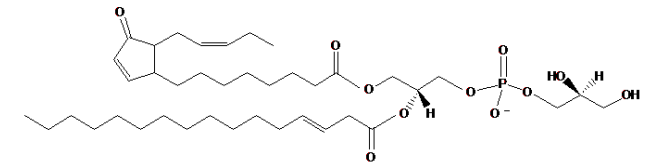

PG(18:4-O/16:1)

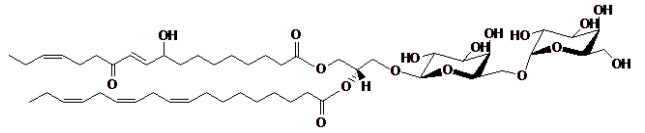

DGDG(18:3-2O/18:3)

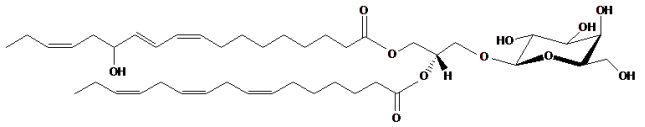

MGDG(18:3-O/16:3)

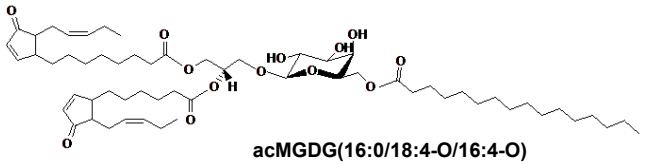

acMGDG(16:0/18:4-O/16:4-O)

Chapter 2 - Direct infusion mass spectrometry of oxylipin-containing Arabidopsis membrane lipids reveals varied patterns in different stress responses.

Abstract

Direct infusion electrospray ionization triple quadrupole precursor scanning for three oxidized fatty acyl anions revealed 86 mass spectral peaks representing polar membrane lipids in extracts from *Arabidopsis thaliana* infected with *Pseudomonas syringae* pv *tomato* DC3000 expressing *AvrRpt2* (*Pst*Avr). Quadrupole time-of-flight and Fourier transform ion cyclotron resonance mass spectrometry provided evidence for the presence of membrane lipids containing one or more oxidized acyl chains. The membrane lipids included molecular species of phosphatidylcholine, phosphatidylethanolamine, phosphatidylglycerol, digalactosyldiacylglycerol, monogalactosyldiacylglycerol, and acylated monogalactosyldiacylglycerol. The oxidized chains were identified at the level of chemical formula and included $C_{18}H_{27}O_3$ (abbreviated 18:4-O, to indicate four double bond equivalents and one oxygen beyond the carbonyl group), $C_{18}H_{29}O_3$ (18:3-O), $C_{18}H_{31}O_3$ (18:2-O), $C_{18}H_{29}O_4$ (18:3-2O), $C_{18}H_{31}O_4$ (18:2-2O), and $C_{16}H_{23}O_3$ (16:4-O). Mass spectral signals from the polar oxidized lipid (ox-lipid) species were quantified in extracts of Arabidopsis leaves subjected to wounding, infection by *Pst*Avr, infection by a virulent strain of *P. syringae*, and low temperature. Ox-lipids produced low amounts of mass spectral signal, 0.1 to 3.2% as much as obtained in typical direct infusion profiling of normal-chain membrane lipids of the same classes. Analysis of the oxidized membrane lipid species and normal-chain phosphatidic acids indicated that stress-induced ox-lipid composition differs from the basal ox-lipid composition. Additionally, different stresses result in production of varied amounts, different timing, and different compositional patterns of stress-induced membrane lipids. The data form the basis for a working hypothesis that the stress-specific signatures of ox-lipids, like those of oxylipins, are indicative of their functions.

Introduction

Biotic and abiotic stresses result in lipid oxidation, and there is strong evidence for the importance of oxidized free fatty acids, also known as oxylipins, in plant stress responses (Imbusch and Mueller, 2000; Vollenweider et al., 2000; Stintzi et al., 2001; Howe and Schilmiller, 2002; Stenzel et al., 2003; Thoma et al., 2003; Taki et al., 2005; Sattler et al., 2006; Thines et al., 2007; Chehab et al., 2008; Katsir et al., 2008; Mueller et al., 2008). Recent studies indicate that oxidized fatty acyl chains also occur in complex polar lipids and that plants produce complex oxidized lipids under stress conditions, including wounding (Buseman et al., 2006), bacterial infection (Andersson et al., 2006; Grun et al., 2007; Kourtchenko et al., 2007), fungal infection (Thoma et al., 2003), extended dark (Seltmann et al., 2010), aging (Xiao et al., 2010), and osmotic stress (Seltmann et al., 2010).

A number of plastid-derived, complex lipid molecular species that contain oxophytodienoic acid (OPDA) and dinor-oxophytodienoic acid (dnOPDA) have been characterized (Stelmach et al., 2001; Hisamatsu et al., 2003; 2005; Andersson et al., 2006; Buseman et al., 2006; Kourtchenko et al., 2007; Glauser et al., 2008; Maeda et al., 2008). Some of the characterized oxidized lipid species have been shown to occur in thylakoid membranes (Böttcher and Weiler, 2007). In Arabidopsis (*Arabidopsis thaliana*), some of the OPDA- and dnOPDA-containing monogalactosyldiacylglycerols (MGDGs) contain two esterified oxidized fatty acid chains or, when the 6-position of the MGDG galactose ring is acylated, three oxidized chains. These lipid species with multiple isopentenone (OPDA or dnOPDA)-containing chains are sometimes called arabidopsides (Hisamatsu et al., 2003; 2005; Andersson et al., 2006). Characterized galactose-acylated MGDG (acMGDG) molecular species include OPDA/dnOPDA MGDG with OPDA on the galactose ring (arabidopside E) and a tri-OPDA MGDG species (arabidopside G; Andersson et al., 2006; Kourtchenko et al., 2007). OPDA also has been identified in phosphatidylglycerol (PG) (Buseman et al., 2006). MGDG and digalactosyldiacylglycerol (DGDG) contain, in addition to OPDA and dnOPDA, 16- and 18-carbon ketols, both in combination with normal chains and with OPDA (Buseman et al., 2006). Membrane lipids also contain other oxidized acyl species, including phytoprostanes and hydroxy fatty acids (Thoma et al., 2003; Imbusch and Mueller, 2000; Grun et al., 2007).

In some studies of oxidized membrane lipids, the oxidized fatty acyl chains have been analyzed after releasing the chains from the membrane lipids (Thoma et al., 2003; Grun et al., 2007), while in other studies, the intact membrane lipid species have been measured directly (Stelmach et al., 2001; Andersson et al., 2006; Buseman et al., 2006; Böttcher and Weiler, 2007; Kourtchenko et al., 2007; Thiocone et al., 2008; Seltmann et al., 2010). Several mass spectrometry strategies have been utilized for intact lipid oxylipin-containing plant lipid profiling. Buseman et al. (2006) used precursor ion scanning by direct infusion electrospray ionization (ESI) triple quadrupole mass spectrometry (MS) to quantify multiple oxylipin-containing complex lipids. Liquid chromatography or liquid chromatography-mass spectrometry approaches have also been used (Stelmach et al., 2001; Andersson et al., 2006; Böttcher and Weiler, 2007; Kourtchenko et al., 2007; Glauser et al., 2008; Thiocone et al., 2008; Seltmann et al., 2010). However, most analyses have been limited to fewer than 20 oxidized membrane lipid species.

In the current work, we utilized a direct-infusion ESI triple quadrupole MS strategy to quantify a larger group of oxidized membrane lipids. By precursor scanning in negative mode, 86 peaks representing combinations of intact ion *m/z* and oxidized acyl fragment *m/z* were identified. The chemical formulas of the fatty acyl substituents of each peak were determined by accurate mass analysis. In so doing, oxidized Arabidopsis phosphatidylcholine (PC) and phosphatidylethanolamine (PE) molecular species, as well as PG, DGDG, MGDG, and acMGDG species, were characterized. We tested the hypothesis that different environmental cues trigger different changes in oxidized lipid profiles of Arabidopsis by challenging wild-type Arabidopsis with mechanical wounding, infection with avirulent and virulent bacteria, and low temperature, and monitoring the oxidized membrane lipid changes.

Results

Triple Quadrupole MS Precursor Scanning for Lipids with 18-Carbon Oxidized Acyl Chains

With the goal of investigating the formation of oxidized lipids in Arabidopsis leaves on a broad scale and in an expeditious manner, ionizable membrane lipids with at least one oxidized fatty acid of known chemical formula were identified using a semi-targeted, direct infusion mass spectrometry approach. In the polar lipid fraction of Arabidopsis, five 18-carbon oxidized fatty acids (first 5 entries in Table 2.1) can be detected with three ESI triple quadrupole MS scans in negative mode. The five 18-carbon oxidized fatty acids include $C_{18}H_{27}O_3$ (designated as 18:4-O; nomenclature indicates "acyl carbons: double bond equivalents beyond the acid carbonyl-number of oxygens in addition to the carbonyl group"), $C_{18}H_{29}O_3$ (18:3-O), $C_{18}H_{31}O_3$ (18:2-O), $C_{18}H_{29}O_4$ (18:3-2O), and $C_{18}H_{31}O_4$ (18:2-2O). 18:3-2O and 18:2-2O each undergo a water loss during collision induced dissociation to produce 18:4-O and 18:3-O, respectively. The dehydration allows 18:3-2O and 18:2-2O to be detected by scans for 18:4-O and 18:3-O, respectively (Buseman et al., 2006; Maeda et al., 2008). Thus, scanning for precursors of 291.2 (Pre 291.2) detects precursors of 18:4-O and 18:3-2O, scanning for Pre 293.2 detects precursors of 18:3-O and 18:2-2O, and scanning for Pre 295.2 detects precursors of 18:2-O. Using a single scan to detect membrane lipids with two different acyl species reduces scan time. Also, importantly, using Pre 291.2 and Pre 293.2 to detect lipids containing oxidized acyl chains with *m/z* 309.2 (e.g. 18:3-2O) and 311.2 (e.g. 18:2-2O) provides increased specificity compared to scanning for Pre 309.2 and Pre 311.2, because anions of 18:3-2O and 18:2-2O share the same nominal *m/z* as normal-chain fatty acyl chains 20:1 and 20:0, respectively. 20:1 and 20:0 are not detected by scans for Pre 291.2 and Pre 293.2, because 20:1 and 20:0 do not undergo water losses.

Scanning for negatively charged precursors of *m/z* 291.2, 293.2, and 295.2, while infusing an extract of Arabidopsis leaves infected with *Pseudomonas syringae* pv. *tomato* DC3000 expressing the *AvrRpt2* avirulence gene (*Pst*Avr), reveals the spectral peaks shown in Figure 2.1. Scans were repeated on a series of similar samples, and peaks detected in any *Pst*Avr-infected sample were numbered **1** through **86**. With the samples dissolved in solvent containing ammonium acetate, for various lipids, peaks represent $[M - H]^-$ (indicated by peak numbers in parentheses in Figure 2.1), $[M + C_2H_3O_2]^-$, where $C_2H_3O_2$ is acetate (indicated by peak numbers without parentheses), or both adducts.

Identification of the Detected Oxidized Complex Lipids using QTOF and FTICR MS

Identifying information for the observed peaks is presented in Table 2.2 and Tables S2.1 and S2.2. Quadrupole time-of-flight (QTOF) MS aided in definition of the compounds. The extracts were batch-fractionated by normal-phase chromatography. A fraction or the whole extract (as indicated in Table S2.1) was directly infused into the ESI source, operating in negative mode, of a QTOF mass spectrometer. Each oxidized lipid precursor ion, previously detected by precursor scanning by triple quadrupole MS (Figure 2.1), was selected with the first quadrupole and subjected to collision induced dissociation. The fragments were scanned with the time-of-flight analyzer to obtain accurate *m/z* ratios of the acyl anions; the *m/z*s were used to determine the chemical formulas of the acyl chains. Together, the precursor and fragment *m/z*s allowed identification of lipid species indicated by nearly all of the peaks detected by precursor spectral scanning (Figure 2.1, Table 2.2, and Table S2.1). The identities of 24 of the 86 observed peaks were additionally confirmed at the level of intact ion chemical formula by determination of accurate *m/z* of precursor ions in positive mode by Fourier transform ion cyclotron resonance (FTICR) MS. The compounds confirmed in this way are indicated in Table 2.2, which summarizes the evidence for each identification, and the FTICR MS data are shown in Table S2.2. To help the reader in visualizing the observed compounds, Figure S2.1 shows examples of structures consistent with the data for some compounds. As described in the legend, the depicted structures are possibilities only.

Twelve oxidized PC (ox-PC; **1-12**) and twelve oxidized PE (ox-PE) species (**13-24**) were identified by precursor scanning and confirmed by QTOF MS analysis (Table 2.2). Each detected ox-PC and ox-PE molecular species has a normal chain fatty acid, 16:0, 18:3, or 18:2, in combination with an oxidized chain, 18:3-O, 18:3-2O, 18:2-O, or 18:2-2O. The detected combinations are analogous to the most common Arabidopsis PC and PE species, which are 16:0/18:3, 16:0/18:2, 18:3/18:3, 18:3/18:2, and 18:2/18:2 (Devaiah et al., 2006), if 18:3 were substituted with 18:4-O (OPDA), 18:3-O, and 18:3-2O, and 18:2 were substituted with 18:2-O and 18:2-2O. Eight oxidized PG (ox-PG) species (**25-32**) were identified by triple quadrupole and QTOF MS (Table 2.2). These species included a normal chain, 16:0 or 16:1, in combination with 18:4-O, 18:3-O, 18:2-O, or 18:2-2O. The 18:4-O ox-PG species were identified previously

(Buseman et al., 2006). The acyl combinations found in ox-PG are again analogous to the most common PG species, 18:3/16:1, 18:2/16:1, 18:3/16:0, and 18:2/16:0 (Devaiah et al., 2006). No ox-PC, ox-PE, or ox-PG species with multiple oxidized fatty acid chains were detected.

Fifteen oxidized DGDG (ox-DGDG) species (Table 2.2, **33**-**47**) were identified by triple quadrupole MS precursor scanning. These include normal chains 16:3, 16:0, or 18:3, or oxidized chains 16:4-O or 18:4-O, in combination with oxidized chains 18:4-O, 18:3-O, or 18:3-2O. Five of the detected species were previously identified (Hisamatsu et al., 2005; Buseman et al., 2006). Again, the acyl combinations found in the oxidized molecular species were structurally related to the major molecular species of Arabidopsis DGDGs, 18:3/16:3, 18:3/16:0, and 18:3/18:3 (Devaiah et al., 2006). Twelve oxidized MGDG (ox-MGDG) species (**48**-**59**) were characterized (Table 2.2). 16:3, 16:4-O, 18:3, or 18:4-O were found in combination with 18:4-O, 18:3-O, or 18:3-2O. The combinations observed also are analogous to the major molecular species of MGDG, 18:3/16:3 and 18:3/18:3 (Devaiah et al., 2006). Identities of detected diacyl compounds (i.e., compounds **1**-**59**) are summarized in brief form in Table S2.3.

Twenty-seven oxidized acMGDG (ox-acMGDG) peaks (**60**-**86**) were identified by precursor scanning (Table 2.2). Previous work has indicated that MGDG can be acylated at the 6-position on the galactose ring when plant leaves are wounded by grinding or stressed by bacterial infection (Heinz, 1967a; Heinz and Tulloch, 1969; Andersson et al., 2006). The current analysis did not determine the positions of the three chains, i.e., on the glycerol backbone or on the galactose. Besides the two previously identified acMGDGs, with combinations of 16:4-O and 18:4-O only, additional acMGDGs included various combinations of non-oxidized chains, 16:3, 16:1, 16:0, 18:3, 18:2, 18:1, 18:0, and oxidized chains, 16:4-O, 18:4-O, 16:3-2O, and 18:3-2O. Identities of detected acMGDGs are summarized in brief form in Table S2.4.

In addition to the species detected by precursor scanning, QTOF MS analysis detected two additional PCs (Table S2.1, **87**-**88**), two PEs (**89**, **90**), one PG (**91**), five DGDGs (**92**-**96**), two MGDGs (**97**, **98**), and 17 acMGDGs (**99**-**115**). These entries represent oxidized and non-oxidized species with the same nominal *m/z*s as peaks detected by triple quadrupole MS precursor scanning. However, **87**-**115** were not targeted by the precursor scans because most

don't contain the scanned precursor fragment. Thus, although they were noted as being present in pathogen infection, lipids **87-115** were not determined, nor quantified, in the remaining analyses.

Most of the 86 peaks listed in Table 2.2 represented a single combination of a head group and acyl species, and their identifications were straightforward (Table 2.2, Table S2.1), but a few identifications require some explanation. The identifications of several peaks (**45**, **78**, **79**, **80a**, **82**), indicated by a prime symbol (') in Table 2.2, were ambiguous. The precursor *m/z*, in combination with the acyl chains observed, indicated that one fragment was dehydrated. Because the QTOF mass spectra did not detect the hydrated fragment, its identity is not clear. Thus, both possible acyl chain combinations are indicated for peaks with the prime (') symbol; the peaks detected by triple quadrupole MS scanning may represent one or both of the indicated species. Additionally, peak **31**, representing an ox-PG species, occurred at the same nominal *m/z* as the $[M - H]^-$ ion of an ox-MGDG species. The same ox-MGDG species was detected separately in peak **53** as its $[M + C_2H_3O_2]^-$ ion. Lastly, thirteen spectral peaks (**63**, **67**, **68**, **69**, **70**, **71**, **72**, **76**, **77**, **80**, **81**, **83**, **84**) observed by triple quadrupole MS scanning represented a combination of at least two members of the acMGDG class. These species are designated with the same number, but with a different letter, in Table 2.2 and Tables S2.1 and S2.2. The multiple identifications arose from two situations: (1) ox-acMGDG species with the same chemical formula, but multiple acyl combinations (e.g., **68a** and **b**; 18:4-O/16:4-O/18:3 acMGDG and 18:4-O/18:4-O/16:3 acMGDG), and (2) ox-acMGDG species with different chemical formulas with the same nominal *m/z*, also with heterogeneity derived from multiple acyl combinations (e.g., **84a** and **b**; 18:3-2O/18:4-O/16:4-O acMGDG and 18:3-2O/18:3/18:3 acMGDG).

In the current work, acyl components of the membrane lipids were identified at the level of chemical formula. Potential identities of the identified oxidized acyl anions are indicated in Table 2.1 and possible structures for some detected compounds shown in Figure S2.1. Previous data indicated that in *Arabidopisis thaliana*, 18:4-O and 16:4-O in the complex lipids represent primarily OPDA and dnOPDA (Stelmach et al., 2001; Hisamatsu et al., 2003; 2005; Buseman et al., 2006). 18:3-O may be a keto fatty acid (Vollenweider et al., 2000) and/or a hydroxy fatty acid, as may 16:3-O. 18:2-O also may be a hydroxy fatty acid. 18:3-2O and 16:3-2O may be

ketols (Hamberg, 1988; Weber et al., 1997), fatty acid hydroperoxides, and/or dihydroxy fatty acids (e.g., Hamberg et al., 2003). 18:2-2O may also represent a dihydroxy fatty acid or a fatty acid hydroperoxide. In future work, as links are established between specific oxidized membrane lipid species and physiological function via quantitative analyses of intact membrane lipid molecular species, the fatty acyl structures associated with the identified chemical formulas of the physiologically relevant membrane molecular species will be determined. The experiment described next is a start toward establishing functional links.

Experimental Design and Measurements of Oxidized Complex Leaf Membrane Lipids during Stress Responses

A and B, Pre 291.2. C, Pre 293.2. D, Pre 295.2. Pre 291.2 scan detects ox-lipids containing 18:4-O and 18:3-2O, Pre 293.2 scan detects ox-lipids containing 18:3-O and 18:2-2O, and Pre 295.2 scan detects ox-lipids containing 18:2-O. Peaks with labels in parentheses are $[M - H]^-$ adducts. Peak labels with no parentheses indicate $[M + C_2H_3O_2]^-$ adducts. Please note that intensity and *m/z* scales of the spectra differ. Panels A and B have breaks in the intensity axes. Details of peaks numbered 1-86 are shown in Table 2.2.

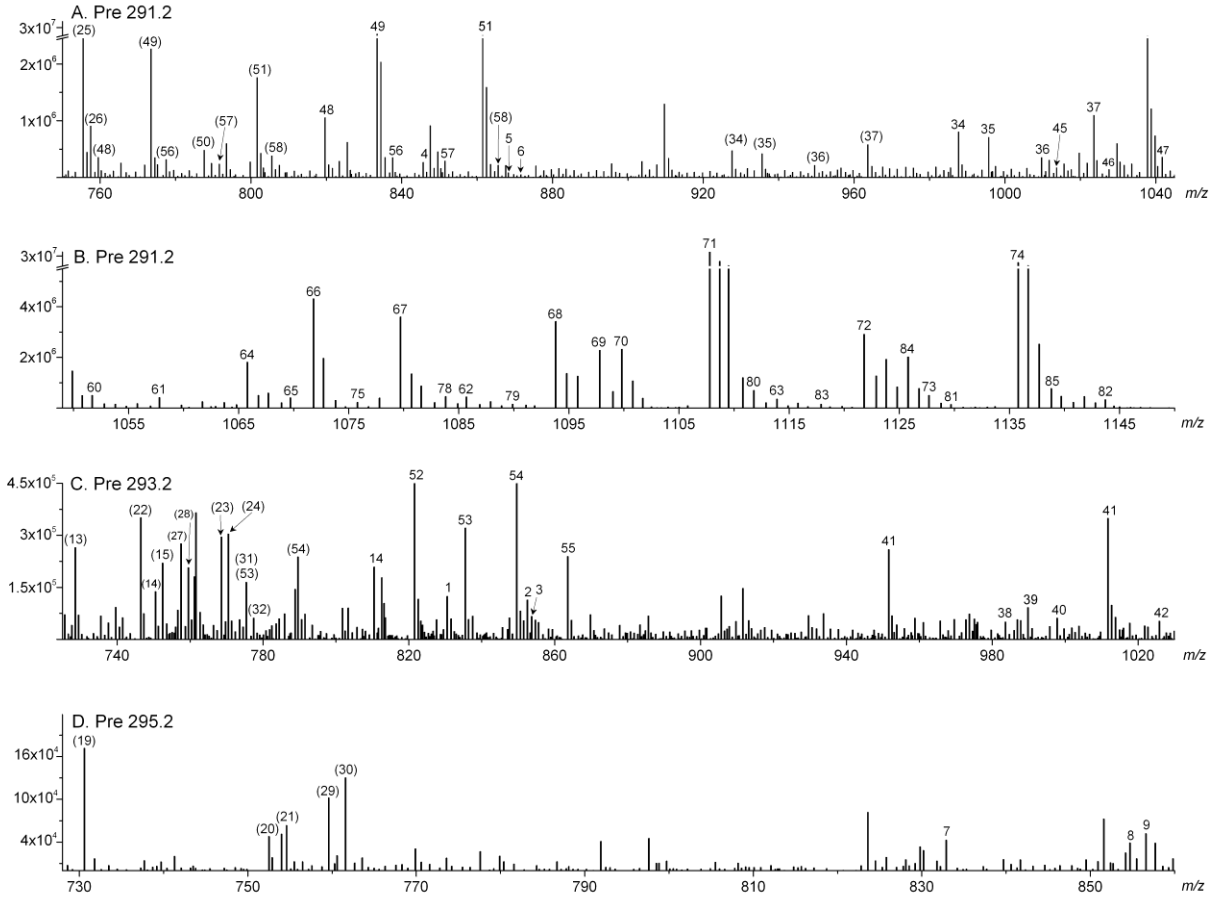

Figure 2.3 Oxidized membrane lipid levels following treatments shown in Figure 2.2.

A, Total oxidized lipids with colors indicating classes. B, ox-PC. C, ox-PE. D, ox-PG. E, ox-DGDG. F, ox-MGDG. G, ox-acMGDG. In B-G, colors indicate individual peaks detected by triple quadrupole MS precursor scanning in negative mode (Table 2.2). The size of each color-coded block represents the quantity of the ox-lipid classes (A) or of individual peaks 1–86 (B-G). Vertical axes have different scales.

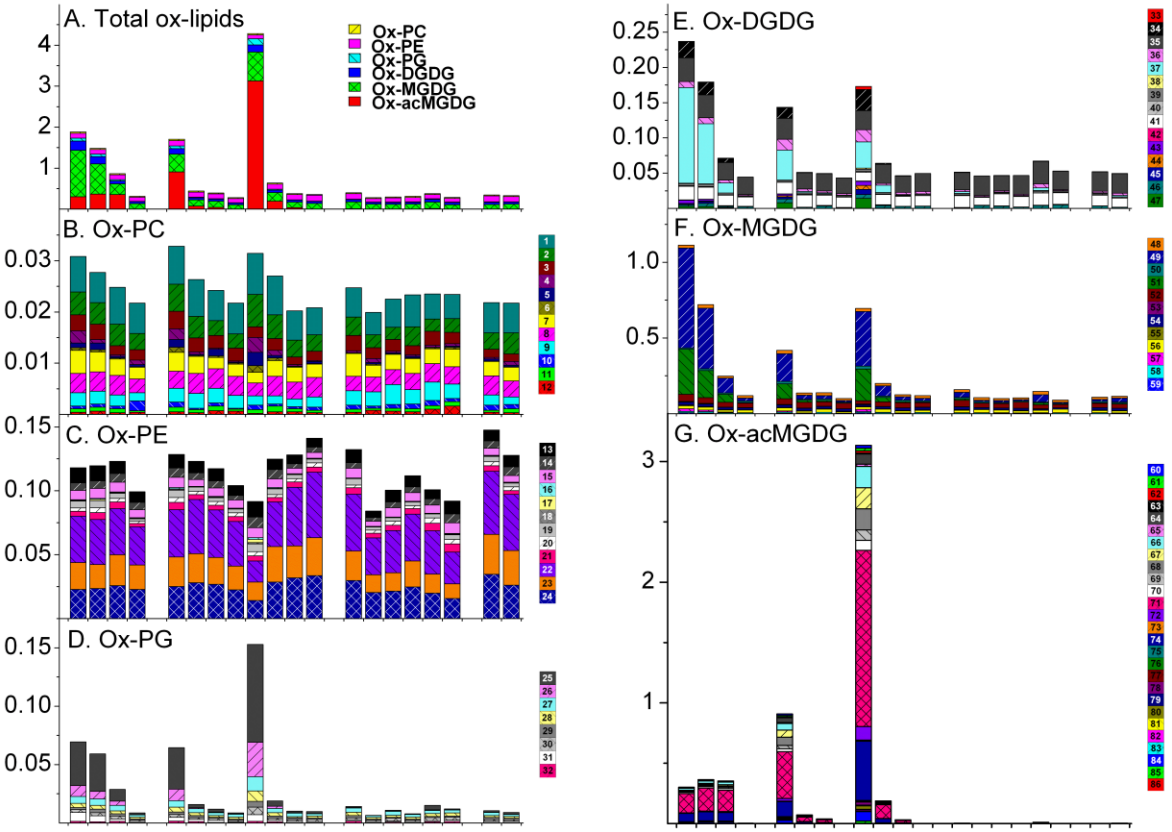

Figure 2.4 Oxidized membrane lipids under stress conditions as quantified by triple quadrupole MS precursor scanning.

A, Wounded, 15 min. B, Wounded, 45 min. C, Wounded, 6 h. D, *Pst*Avr, 12 h. E, *Pst*Avr, 24 h. F, *Psm*, 24 h. G, Freezing (-8° C, 2 h). Numbers along top *x*-axis refer to peaks/compounds in Table 2.2. In each panel, the white bars denote the basal amount as determined under the corresponding control condition: Unwounded, for A, B, and C; $MgCl_2$, 12 h, for D; $MgCl_2$, 24 h, for E and F; and 4° C, 84 h, for G. The black bars denote the amount of each ox-lipid measured in each stress treatment. Both white and black bars start at the *x*-axis. The smaller of the white and black bars is "in front" of the other bar. Increments on the vertical scales of panels A and B (below break) and C are the same; so are those on panel D and E (below break). $p < 0.05$, $n = 5$.

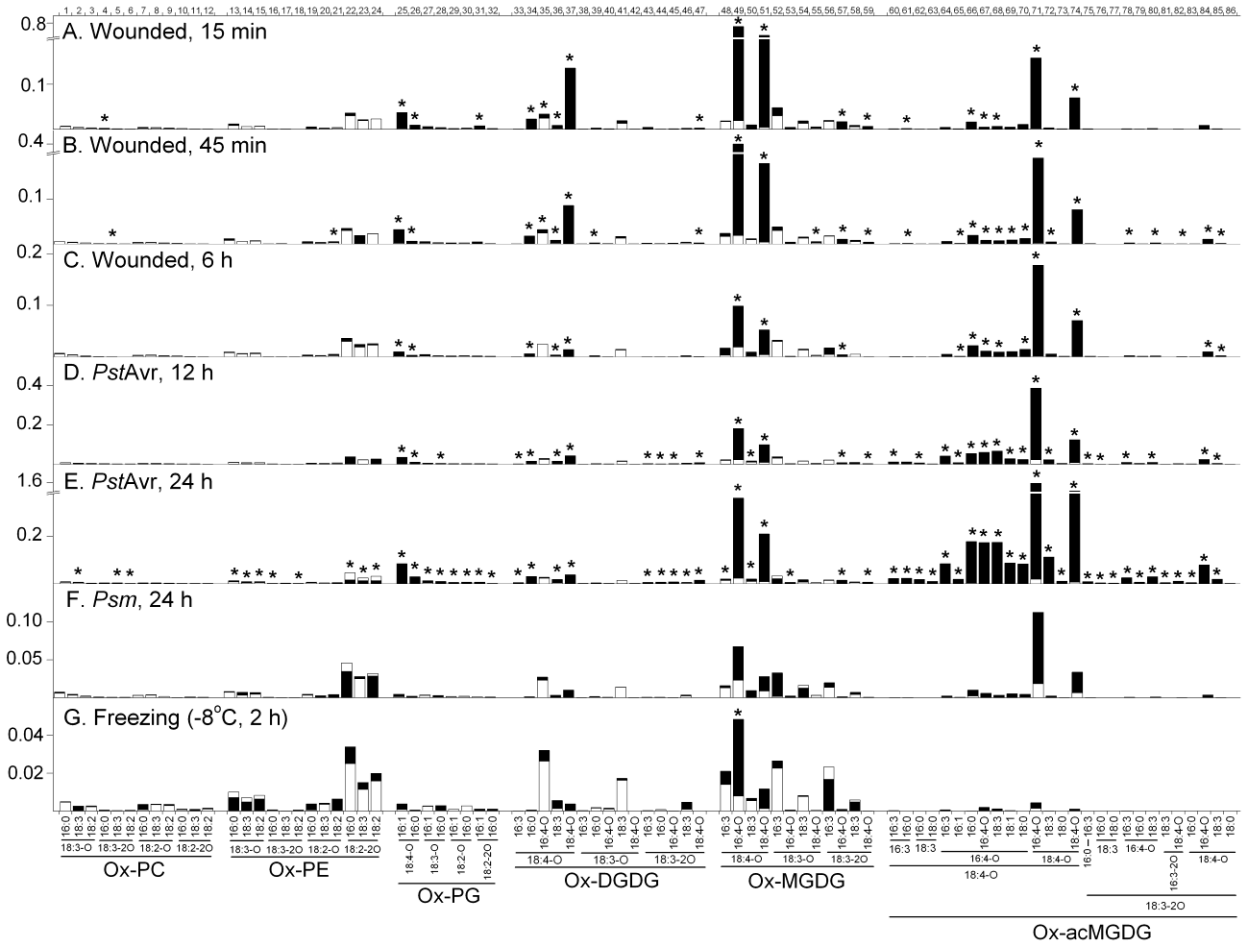

Table 2.1 Oxidized fatty acyl chains detected in extracts from leaves of *Arabidopsis thaliana* infected with *Pst*Avr for 24 h.

Figure S2.1 shows examples of possible structures and fragmentation of oxidized lipids from each class.

Triple quadrupole MS precursor scan	**Chemical formula of oxidized fatty acyl anion**	***m/z* of anion**	**Abbreviation**	**Examples of compounds consistent with detected formula**
Acyl formulas directly scanned				
Pre 291.20	$C_{18}H_{27}O_3$	291.1966	18:4-O	OPDA, keto 18:3
Pre 293.21	$C_{18}H_{29}O_3$	293.2122	18:3-O	hydroxy 18:3, keto fatty acid
Pre 295.23	$C_{18}H_{31}O_3$	295.2279	18:2-O	hydroxy 18:2
Pre 291.20	$C_{18}H_{29}O_4$	309.2071	18:3-2O	ketol fatty acid, hydroperoxy 18:3, dihydroxy 18:3
Pre 293.21	$C_{18}H_{31}O_4$	311.2228	18:2-2O	hydroperoxy 18:2, dihydroxy 18:2
Acyl formulas identified by scanning of above anions or as a result of QTOF MS analysis				
-	$C_{16}H_{23}O_3$	263.1653	16:4-O	dnOPDA
-	$C_{16}H_{25}O_3$	265.1809	16:3-O	hydroxy 16:3
-	$C_{16}H_{25}O_4$	281.1758	16:3-2O	ketol fatty acid, hydroperoxy 16:3, dihydroxy 16:3
-	$C_{18}H_{25}O_4$	305.1758	18:5-2O	-

Table 2.2 Lipids detected by ESI MS/MS negative ion precursor ion scans, Pre 291.2, Pre 293.2, and Pre 295.2.

Tables S2.3 and S2.4 indicate the compounds detected in a simplified form.

Number[a]	M mass	M formula	Identification[b]	Detection Method[c]	Identification Evidence[d]
1	771	C42H78O9PN	18:3-O/16:0 PC	Pre 293.2, [M + $C_2H_3O_2$]$^-$	Tentative, Table S2.1
2	793	C44H76O9PN	18:3-O/18:3 PC	Pre 293.2, [M + $C_2H_3O_2$]$^-$	Table S2.1
3	795	C44H78O9PN	18:3-O/18:2 PC	Pre 293.2, [M + $C_2H_3O_2$]$^-$	Table S2.1
4	787	C42H78O10PN	18:3-2O/16:0 PC	Pre 291.2, [M + $C_2H_3O_2$]$^-$	Table S2.1
5	809	C44H76O10PN	18:3-2O/18:3 PC	Pre 291.2, [M + $C_2H_3O_2$]$^-$	Table S2.1
6	811	C44H78O10PN	18:3-2O/18:2 PC	Pre 291.2, [M + $C_2H_3O_2$]$^-$	Table S2.1
7	773	C42H80O9PN	18:2-O/16:0 PC	Pre 295.2, [M + $C_2H_3O_2$]$^-$	Table S2.1
8	795	C44H78O9PN	18:2-O/18:3 PC	Pre 295.2, [M + $_2H_3O_2$]$^-$	Table S2.1
9	797	C44H80O9PN	18:2-O/18:2 PC	Pre 295.2, [M + $C_2H_3O_2$]$^-$	Tentative, Table S2.1
10	789	C42H80O10PN	18:2-2O/16:0 PC	Pre 293.2, [M + $C_2H_3O_2$]$^-$	Table S2.1
11	811	C44H78O10PN	18:2-2O/18:3 PC	Pre 293.2, [M + $C_2H_3O_2$]$^-$	Table S2.1
12	813	C44H80O10PN	18:2-2O/18:2 PC	Pre 293.2, [M + $C_2H_3O_2$]$^-$	Tentative, Table S2.1

13	729	C39H72O9PN	18:3-O/16:0 PE	Pre 293.2, $[M - H]^-$	Table S2.1
14	751	C41H70O9PN	18:3-O/18:3 PE	Pre 293.2, $[M - H]^-$	Table S2.1
15	753	C41H72O9PN	18:3-O/18:2 PE	Pre 293.2, $[M - H]^-$	Table S2.1
16	745	C39H72O10PN	18:3-2O/16:0 PE	Pre 291.2, $[M - H]^-$	Table S2.1
17	767	C41H70O10PN	18:3-2O/18:3 PE	Pre 291.2, $[M - H]^-$	Table S2.1
18	769	C41H72O10PN	18:3-2O/18:2 PE	Pre 291.2, $[M - H]^-$	Table S2.1
19	731	C39H74O9PN	18:2-O/16:0 PE	Pre 295.2, $[M - H]^-$	Table S2.1, S2.2
20	753	C41H72O9PN	18:2-O/18:3 PE	Pre 295.2, $[M - H]^-$	Table S2.1
21	755	C41H74O9PN	18:2-O/18:2 PE	Pre 295.2, $[M - H]^-$	Table S2.1
22	747	C39H74O10PN	18:2-2O/16:0 PE	Pre 293.2, $[M - H]^-$	Table S2.1, S2.2
23	769	C41H72O10PN	18:2-2O/18:3 PE	Pre 293.2, $[M - H]^-$	Tentative, Table S2.1
24	771	C41H74O10PN	18:2-2O/18:2 PE	Pre 293.2, $[M - H]^-$	Tentative, Table S2.1
25	756	C40H69O11P	18:4-O/16:1 PG	Pre 291.2, $[M - H]^-$	Buseman et al., 2006
26	758	C40H71O11P	18:4-O/16:0 PG	Pre 291.2, $[M - H]^-$	Buseman et al., 2006
27	758	C40H71O11P	18:3-O/16:1 PG	Pre 293.2, $[M - H]^-$	Table S2.1
28	760	C40H73O11P	18:3-O/16:0 PG	Pre 293.2, $[M - H]^-$	Table S2.1
29	760	C40H73O11P	18:2-O/16:1 PG	Pre 295.2, $[M - H]^-$	Table S2.1
30	762	C40H75O11P	18:2-O/16:0 PG	Pre 295.2, $[M - H]^-$	Table S2.1
31*	776	C40H73O12P	18:2-2O/16:1 PG	Pre 293.2, $[M - H]^-$	Table S2.1
31*	776	C43H68O12	18:3-O/16:4-O MGDG	Pre 293.2, $[M - H]^-$	Table S2.1
32	778	C40H75O12P	18:2-2O/16:0 PG	Pre 293.2, $[M - H]^-$	Table S2.1
33	922	C49H78O16	18:4-O/16:3 DGDG	Pre 291.2, $[M - H]^-$	Table S2.1
34	928	C49H84O16	18:4-O/16:0 DGDG	Pre 291.2, [M +	Table S2.1

				$C_2H_3O_2]^-$	
35	936	C49H76O17	18:4-O/16:4-O DGDG	Pre 291.2, [M + $C_2H_3O_2]^-$	Hisamatsu et al., 2005
36	950	C51H82O16	18:4-O/18:3 DGDG	Pre 291.2, [M + $C_2H_3O_2]^-$	Buseman et al., 2006
37	964	C51H80O17	18:4-O/18:4-O DGDG	Pre 291.2, [M + $C_2H_3O_2]^-$	Buseman et al., 2006; Hisamatsu et al., 2005
38	924	C49H80O16	18:3-O/16:3 DGDG	Pre 293.2, [M + $C_2H_3O_2]^-$	Table S2.1
39	930	C49H86O16	18:3-O/16:0 DGDG	Pre 293.2, [M +$C_2H_3O_2]^-$	Table S2.1
40	938	C49H78O17	18:3-O/16:4-O DGDG	Pre 293.2, [M + $C_2H_3O_2]^-$	Table S2.1
41	952	C51H84O16	18:3-O/18:3 DGDG	Pre 293.2, [M + $C_2H_3O_2]^-$	Table S2.1
42	966	C51H82O17	18:3-O/18:4-O DGDG	Pre 293.2, [M + $C_2H_3O_2]^-$	Table S2.1
43	940	C49H80O17	18:3-2O/16:3 DGDG	Pre 291.2, [M + $C_2H_3O_2]^-$	Table S2.1
44	946	C49H86O17	18:3-2O/16:0 DGDG	Pre 291.2, [M - H]$^-$	Table S2.1
45'	954	C49H78O18	18:3-2O/16:4-O DGDG	Pre 291.2, [M + $C_2H_3O_2]^-$	Table S2.1
45'	954	C49H78O18	18:4-O/16:3-2O DGDG	Pre 291.2, [M + $C_2H_3O_2]^-$	Table S2.1
46	968	C51H84O17	18:3-2O/18:3 DGDG	Pre 291.2, [M + $C_2H_3O_2]^-$	Buseman et al., 2006
47	982	C51H82O18	18:3-2O/18:4-O DGDG	Pre 291.2, [M + $C_2H_3O_2]^-$	Buseman et al., 2006

48	760	C43H68O11	18:4-O/16:3 MGDG	Pre 291.2, $[M - H]^-$	Table S2.2, Buseman et al., 2006; Stelmach et al., 2001,
49	774	C43H66O12	18:4-O/16:4-O MGDG	Pre 291.2, $[M + C_2H_3O_2]^-$	Table S2.2, Buseman et al., 2006; Hisamatsu et al., 2003
50	788	C45H72O11	18:4-O/18:3 MGDG	Pre 291.2, $[M - H]^-$	Buseman et al., 2006
51	802	C45H70O12	18:4-O/18:4-O MGDG	Pre 291.2, $[M + C_2H_3O_2]^-$	Table S2.2, Buseman et al., 2006; Hisamatsu et al., 2003
52	762	C43H70O11	18:3-O/16:3 MGDG	Pre 293.2, $[M + C_2H_3O_2]^-$	Table S2.1
53	776	C43H68O12	18:3-O/16:4-O MGDG	Pre 293.2, $[M + C_2H_3O_2]^-$	Tentative, Table S2.1
54	790	C45H74O11	18:3-O/18:3 MGDG	Pre 293.2, $[M - H]^-$	Table S2.1
55	804	C45H72O12	18:3-O/18:4-O MGDG	Pre 293.2, $[M + C_2H_3O_2]^-$	Table S2.1
56	778	C43H70O12	18:3-2O/16:3 MGDG	Pre 291.2, $[M + C_2H_3O_2]^-$	Buseman et al., 2006
57	792	C43H68O13	18:3-2O/16:4-O MGDG	Pre 291.2, $[M + C_2H_3O_2]^-$	Buseman et al., 2006
58	806	C45H74O12	18:3-2O/18:3 MGDG	Pre 291.2, $[M + C_2H_3O_2]^-$	Buseman et al., 2006
59	820	C45H72O13	18:3-2O/18:4-O	Pre 291.2, [M +	Buseman et

			MGDG	$C_2H_3O_2]^-$	al., 2006
60	992	C59H92O12	18:4-O/16:3/16:3 acMGDG	Pre 291.2, [M + $C_2H_3O_2]^-$	Table S2.1, S2.2
61	998	C59H98O12	18:4-O/16:3/16:0 acMGDG	Pre 291.2, [M + $C_2H_3O_2]^-$	Table S2.1, S2.2
62	1026	C61H102O12	18:4-O/18:3/16:0 acMGDG	Pre 291.2, [M + $C_2H_3O_2]^-$	Table S2.1
63a	1054	C63H106O12	18:4-O/18:3/18:0 acMGDG	Pre 291.2, [M + $C_2H_3O_2]^-$	Table S2.1
63b	1054	C63H106O12	18:4-O/18:2/18:1 acMGDG	Pre 291.2, [M + $C_2H_3O_2]^-$	Table S2.1
64	1006	C59H90O13	18:4-O/16:4-O/16:3 acMGDG	Pre 291.2, [M + $C_2H_3O_2]^-$	Table S2.1, S2.2
65	1010	C59H94O13	18:4-O/16:4-O/16:1 acMGDG	Pre 291.2, [M + $C_2H_3O_2]^-$	Table S2.1, S2.2
66	1012	C59H96O13	18:4-O/16:4-O/16:0 acMGDG	Pre 291.2, [M + $C_2H_3O_2]^-$	Table S2.1, S2.2
67a	1020	C59H88O14	18:4-O/16:4-O/16:4-O acMGDG	Pre 291.2, [M + $C_2H_3O_2]^-$	Table S2.1, S2.2
67b	1020	C61H96O12	18:4-O/18:3/16:3 acMGDG	Pre 291.2, [M + $C_2H_3O_2]^-$	Table S2.1
68a	1034	C61H94O13	18:4-O/16:4-O/18:3 acMGDG	Pre 291.2, [M + $C_2H_3O_2]^-$	Table S2.1, S2.2
68b	1034	C61H94O13	18:4-O/18:4-O/16:3 acMGDG	Pre 291.2, [M + $C_2H_3O_2]^-$	Table S2.1, S2.2
69a	1038	C61H98O13	18:4-O/16:4-O/18:1 acMGDG	Pre 291.2, [M +$C_2H_3O_2]^-$	Table S2.1, S2.2
69b	1038	C61H98O13	18:4-O/18:4-O/16:1 acMGDG	Pre 291.2, [M +$C_2H_3O_2]^-$	Table S2.1, S2.2
70a	1040	C61H100O13	18:4-O/16:4-O/18:0	Pre 291.2, [M +	Table S2.1,

			acMGDG	$C_2H_3O_2]^-$	S2.2
70b	1040	C61H100O13	18:4-O/18:4-O/16:0 acMGDG	Pre 291.2, [M + $C_2H_3O_2]^-$	Table S2.1, S2.2
71a	1048	C61H92O14	18:4-O/18:4-O/16:4-O acMGDG	Pre 291.2, [M + $C_2H_3O_2]^-$	Table S2.1, S2.2, Andersson et al., 2006
71b	1048	C63H100O12	18:4-O/18:3/18:3 acMGDG	Pre 291.2, [M + $C_2H_3O_2]^-$	Table S2.1, S2.2
72a	1062	C63H98O13	18:4-O/18:4-O/18:3 acMGDG	Pre 291.2, [M + $C_2H_3O_2]^-$	Table S2.1, S2.2
72b	1062	C61H90O15	18:4-O/18:5-2O/16:4-O acMGDG	Pre 291.2, [M + $C_2H_3O_2]^-$	Table S2.1, S2.2
73	1068	C63H104O13	18:4-O/18:4-O/18:0 acMGDG	Pre 291.2, [M + $C_2H_3O_2]^-$	Table S2.1
74	1076	C63H96O14	18:4-O/18:4-O/18:4-O acMGDG	Pre 291.2, [M + $C_2H_3O_2]^-$	Table S2.1, S2.2, Kourtchenko et al., 2007
75	1016	C59H100O13	18:3-2O/16:0/16:3 acMGDG	Pre 291.2, [M + $C_2H_3O_2]^-$	Table S2.1
76a	1044	C61H104O13	18:3-2O/18:3/16:0 acMGDG	Pre 291.2, [M + $C_2H_3O_2]^-$	Table S2.1
76b	1044	C61H104O13	18:3-2O/18:0/16:3 acMGDG	Pre 291.2, [M + $C_2H_3O_2]^-$	Tentative, Table S2.1
77a	1072	C63H108O13	18:3-2O/18:3/18:0 acMGDG	Pre 291.2, [M + $C_2H_3O_2]^-$	Table S2.1
77b	1072	C61H100O15	18:3-2O/18:2/16:3-2O acMGDG	Pre 291.2, [M + $C_2H_3O_2]^-$	Table S2.1
77c	1072	C63H108O13	18:3-2O/18:2/18:1	Pre 291.2, [M +	Table S2.1

			acMGDG	$C_2H_3O_2]^-$	
78'	1024	C59H92O14	18:3-2O/16:4-O/16:3 acMGDG	Pre 291.2, [M + $C_2H_3O_2]^-$	Table S2.1
78'	1024	C59H92O14	18:4-O/16:3-2O/16:3 acMGDG	Pre 291.2, [M + $C_2H_3O_2]^-$	Table S2.1
79'	1030	C59H98O14	18:3-2O/16:4-O/16:0 acMGDG	Pre 291.2, [M + $C_2H_3O_2]^-$	Table S2.1, S2.2
79'	1030	C59H98O14	18:4-O/16:3-2O/16:0 acMGDG	Pre 291.2, [M + $C_2H_3O_2]^-$	Table S2.1, S2.2
80a'	1052	C61H96O14	18:3-2O/16:4-O/18:3 acMGDG	Pre 291.2, [M + $C_2H_3O_2]^-$	Table S2.1
80a'	1052	C61H96O14	18:4-O/16:3-2O/18:3 acMGDG	Pre 291.2, [M + $C_2H_3O_2]^-$	Table S2.1
80b	1052	C61H96O14	18:3-2O/18:4-O/16:3 acMGDG	Pre 291.2, [M + $C_2H_3O_2]^-$	Table S2.1
81a	1070	C61H98O15	18:3-2O/16:3-2O/18:3 acMGDG	Pre 291.2, [M + $C_2H_3O_2]^-$	Table S2.1
81b	1070	C61H98O15	18:3-2O/18:3-2O/16:3 acMGDG	Pre 291.2, [M + $C_2H_3O_2]^-$	Tentative, Table S2.1
81c	1070	C63H106O13	18:3-2O/18:2/18:2 acMGDG	Pre 291.2, [M + $C_2H_3O_2]^-$	Table S2.1
82'	1084	C61H96O16	18:3-2O/16:3-2O/18:4-O acMGDG	Pre 291.2, [M + $C_2H_3O_2]^-$	Table S2.1, S2.2
82'	1084	C61H96O16	18:3-2O/18:3-2O/16:4-O acMGDG	Pre 291.2, [M + $C_2H_3O_2]^-$	Table S2.1, S2.2
83a	1058	C61H102O14	18:3-2O/18:4-O/16:0 acMGDG	Pre 291.2, [M + $C_2H_3O_2]^-$	Table S2.1
83b	1058	C61H102O14	18:3-2O/16:4-O/18:0 acMGDG	Pre 291.2, [M + $C_2H_3O_2]^-$	Tentative, Table S2.1
84a	1066	C61H94O15	18:3-2O/18:4-	Pre 291.2, [M +	Table S2.1,

			O/16:4-O acMGDG	$C_2H_3O_2]^-$	S2.2
84b	1066	C63H102O13	18:3-2O/18:3/18:3 acMGDG	Pre 291.2, [M + $C_2H_3O_2]^-$	Table S2.1, S2.2
85	1080	C63H100O14	18:3-2O/18:4-O/18:3 acMGDG	Pre 291.2, [M + $C_2H_3O_2]^-$	Table S2.1
86	1086	C63H106O14	18:3-2O/18:4-O/18:0 acMGDG	Pre 291.2, [M + $C_2H_3O_2]^-$	Table S2.1

[a]Each number (1-86) represents a peak observed in triple quadrupole MS spectra (Figure 2.1). An asterisk (*) indicates peaks resulting from two compounds of different lipid classes with the same ion mass. A prime symbol (') indicates peaks with at least two possible identifications, where it is unclear whether the peak represents one or both compounds. Numbers followed by a, b, or c signify that accurate *m/z* analysis indicates that the peak represents multiple lipid species detected by the stated precursor scan (Tables S2.1 and S2.2).

[b]Abbreviations: acMGDG, acylated monogalactosyldiacylglycerol; DGDG, digalactosyldiacylglycerol; MGDG, monogalactosyldiacylglycerol; PC, phosphatidylcholine; PE, phosphatidylethanolamine; PG, phosphatidylglycerol.

[c]Peaks were identified in triple quadrupole MS spectra with three negative precursor scans, Pre 291.2, Pre 293.2, and Pre 295.2; each species was observed as the $[M - H]^-$ and/or $[M + C_2H_3O_2]^-$ ion.

[d]QTOF MS peak data are provided in Table S2.1. FTICR MS peak data are provided in Table S2.2. Peak identification is indicated as "Tentative" if QTOF MS *m/z* values for one acyl group (or more) were greater than 10 parts per million (ppm) from the theoretical *m/z*, and the compound was not previously identified or identified by accurate *m/z* of the intact compound in FTICR MS spectra. Previously identified peaks/compounds are marked with corresponding references.

Supplemental Data

Supplemental Data in this chapter include:

- Figure S2.1 Examples of possible structures and fragmentation of oxidized lipids from each class.
- Figure S2.2 Bacterial counts (colony forming unit (CFU) per mg of leaf dry mass) at 12 h and 24 h post-infection.
- Figure S2.3 Oxidized membrane lipid levels during various control conditions and conditions with low ox-lipid levels as quantified by triple quadrupole MS precursor scanning.
- Figure S2.4 Levels of ox-MGDG, ox-acMGDG and PA in Arabidopsis leaves during stress and control treatments.
- Figure S2.5 Levels of LPC, LPE, and PA, in Arabidopsis leaves during stress and control treatments.

Tables S2.1-S2.8 are supplied as a separate Excel file.

- Table S2.1 QTOF MS m/z data supporting compound identifications in Table 2.2. Analysis was performed on extracts from leaves of Arabidopsis thaliana infected with PstAvr for 24 h.
- Table S2.2 FTICR MS m/z data supporting compound identifications in Table 2.2. Analysis was performed on extracts from leaves of Arabidopsis thaliana infected with PstAvr for 24 h.
- Table S2.3 Simplified designation of diacyl oxidized compounds (1-59).
- Table S2.4 Simplified table of acMGDGs (60-86) identified by precursor scanning.
- Table S2.5 Levels (individual sample data) of ox-lipids during plant stress responses.
- Table S2.6 Levels (averages and standard deviations) of ox-lipids during plant stress responses.
- Table S2.7 Levels (individual sample data) of normal lipids during plant stress responses.
- Table S2.8 Levels (averages and standard deviations) of normal lipids during plant stress responses.

Figure S2.1 Examples of possible structures for anions of oxidized lipids from each class. These structures are consistent with current data, but, in fact, the acyl chain structures shown in Table 2.1 and identified with specific compounds in Table 2.2 have been identified only at the level of chemical formula. The specific structural features (e.g. presence of C=O vs. C=C double bonds vs. rings, presence of specific functional groups, positions of double bonds and functional groups, and positions of acyl chains on glycerol) have not been determined. Table 2.1 indicates some additional possibilities for acyl chain structures.

Compounds shown:

7. 18:2-O/16:0 PC, shown as the $[M + C_2H_3O_2]^-$ ion of 1-hexadecanoyl-2-(9-hydroxy-10E,12Z-octadecadienoyl)-*sn*-glycero-3-phosphocholine;

23. 18:2-2O/18:3 PE, shown as the $[M - H]^-$ ion of 1-(9-hydroperoxy-10E,12Z-octadecadienoyl)-2-(9Z,12Z,15Z-octadecatrienoyl)-*sn*-glycero-3-phosphoethanolamine;

25. 18:4-O/16:1 PG, shown as the $[M - H]^-$ ion of 1-(8-[2-(cis-pent-2'-enyl)-3-oxo-cis-cyclo-pent-4-enyl]octanoyl)-2-(3E-hexadecenoyl)-*sn*-glycero-3-phospho-(1'-*sn*-glycerol), where 8-[2-(cis-pent-2'-enyl)-3-oxo-cis-cyclo-pent-4-enyl]octanoyl is also known as 12-oxo-10,15-phytodienoyl and OPDA;

46. 18:3-2O/18:3 DGDG, shown as the $[M + C_2H_3O_2]^-$ ion of 1-(9-hydroxy-12-oxo-10E,15Z-octadecadienoyl)-2-(9Z,12Z, 15Z-octadecatrienoyl)-3-O-[α-D-galactosyl-(1→6)-O-β-D-galactosyl]-*sn*-glycerol, where 9-hydroxy-12-oxo-10E,15Z-octadecadienoyl is also known as γ-ketol;

52. 18:3-O/16:3 MGDG, shown as the $[M + C_2H_3O_2]^-$ ion of 1-(13-hydroxy-9Z,11E,15Z-octadecatrienoyl)-2-(7Z,10Z,13Z-hexadecatrienoyl)-3-O-β-D-galactosyl-*sn*-glycerol;

66. 18:4-O/16:4-O/16:0 acMGDG, shown as the $[M + C_2H_3O_2]^-$ ion of 1-(8-[2-(cis-pent-2'-enyl)-3-oxo-cis-cyclo-pent-4-enyl]octanoyl)-2-(6-[2-(cis-pent-2'-enyl)-3-oxo-cis-cyclo-pent-4-enyl]hexanoyl)-3-O-(6-O-hexadecanoyl-β-D-galactosyl)-*sn*-glycerol, where 8-[2-(cis-pent-2'-enyl)-3-oxo-cis-cyclo-pent-4-enyl]octanoyl is also known as 12-oxo-10,15-phytodienoyl and OPDA, and 6-[2-(cis-pent-2'-enyl)-3-oxo-cis-cyclo-pent-4-enyl]hexanoyl is known as dinor-oxo-phytodienoyl and dnOPDA.

OPDA = 8-[2-(cis-pent-2'-enyl)-3-oxo-cis-cyclo-pent-4-enyl]octanoic acid

dnOPDA = 6-[2-(cis-pent-2'-enyl)-3-oxo-cis-cyclo-pent-4-enyl]hexanoic acid

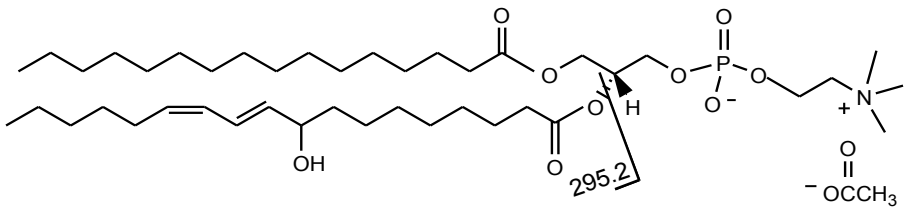

7

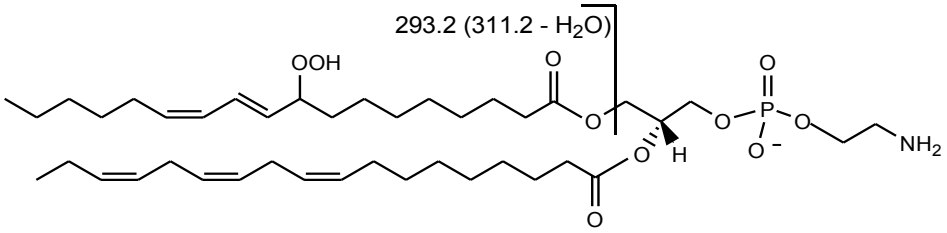

23

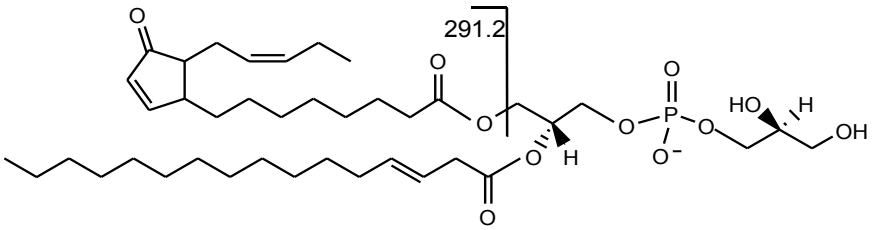

25

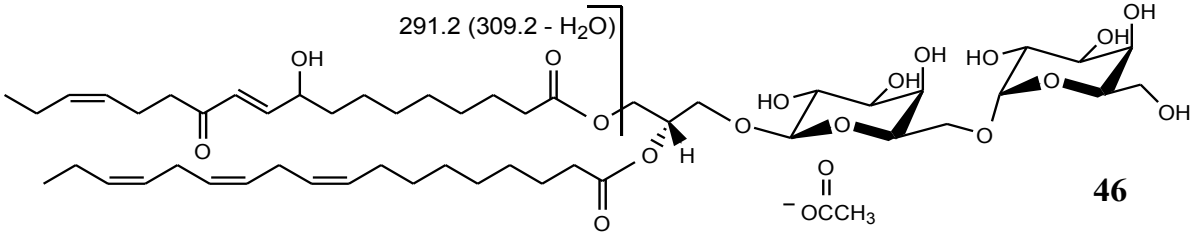

46

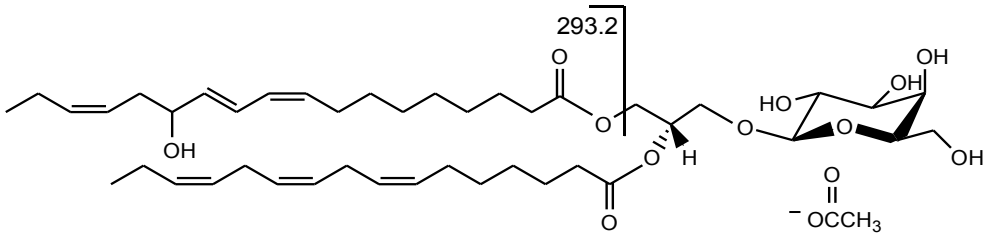

52

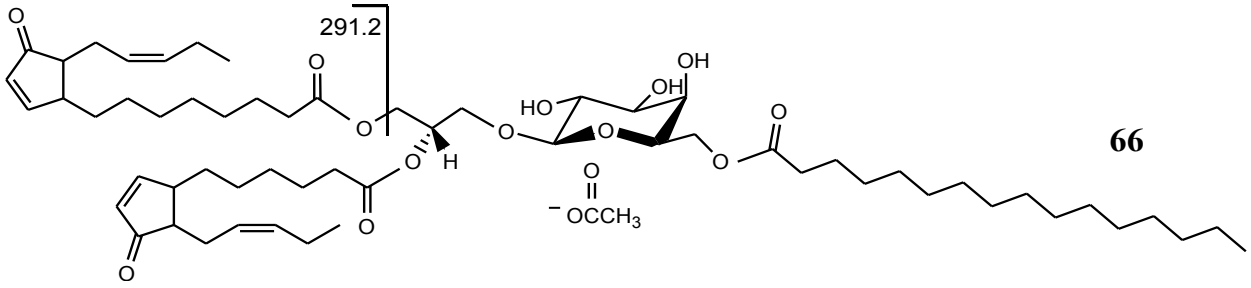

66

Figure S2.2 Bacterial counts (colony forming unit (CFU) per mg of leaf dry mass) at 12 h and 24 h post-infection.

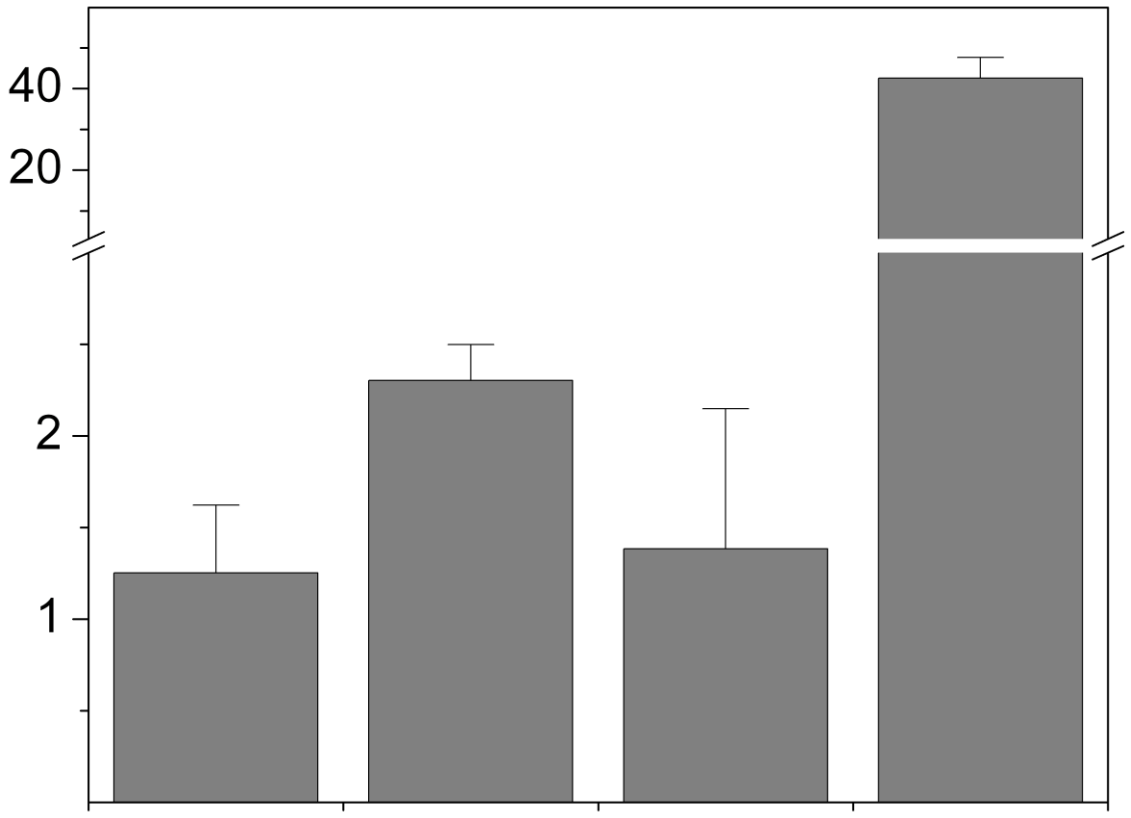

Figure S2.3 Oxidized membrane lipid levels during various control conditions and conditions with low ox-lipid levels (indicated on the panels) as quantified by triple quadrupole MS precursor scanning. Numbers along top x-axis refer to peaks/compounds in Table 2.2. Error bars indicate standard deviation.

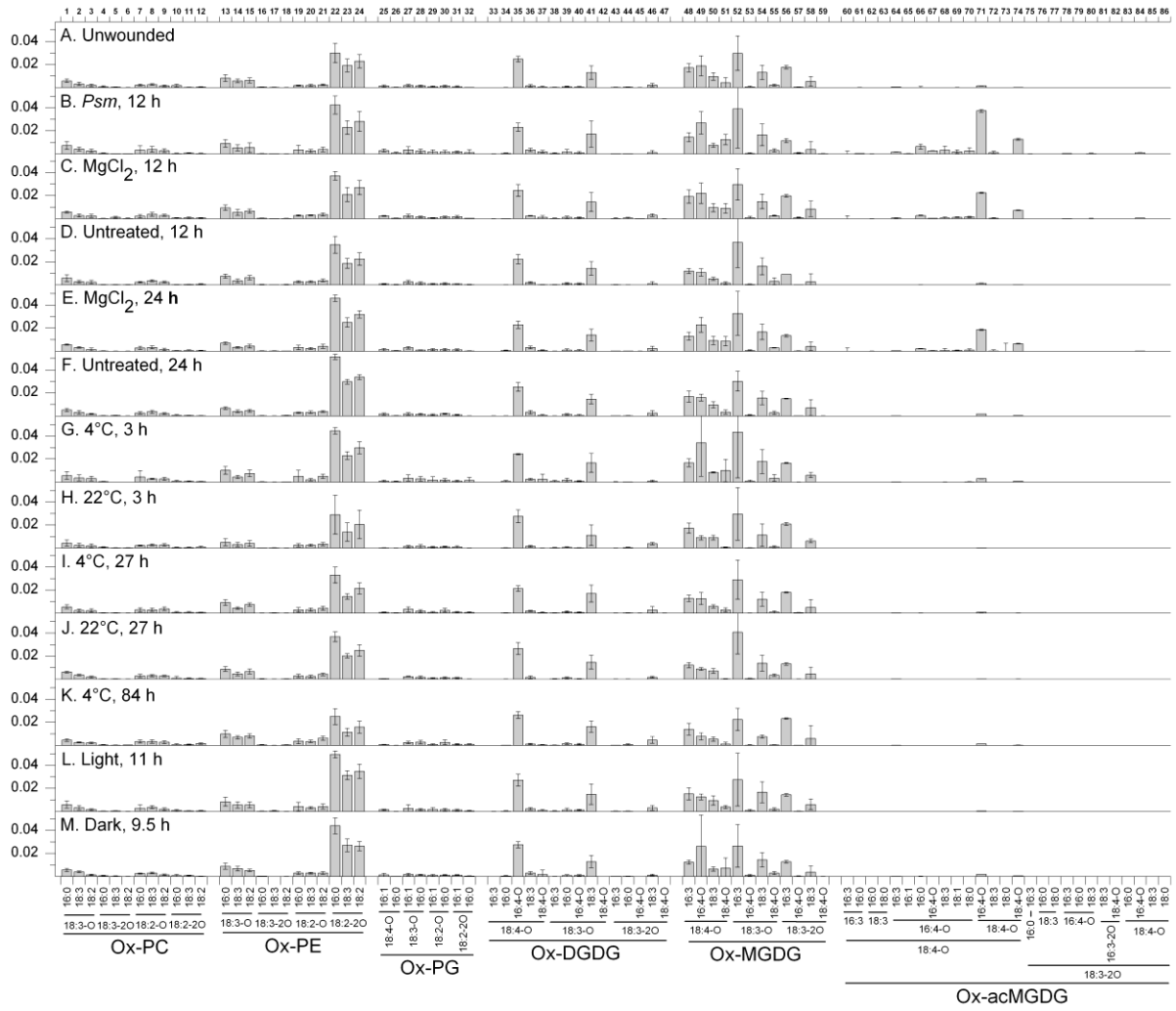

Figure S2.4 Levels of ox-MGDG, ox-acMGDG and PA in Arabidopsis leaves during stress and control treatments. Panels A, B, and C are ox-MGDG and ox-acMGDG as indicated. Panels D, E and F are PA. Error bars indicate standard deviation.

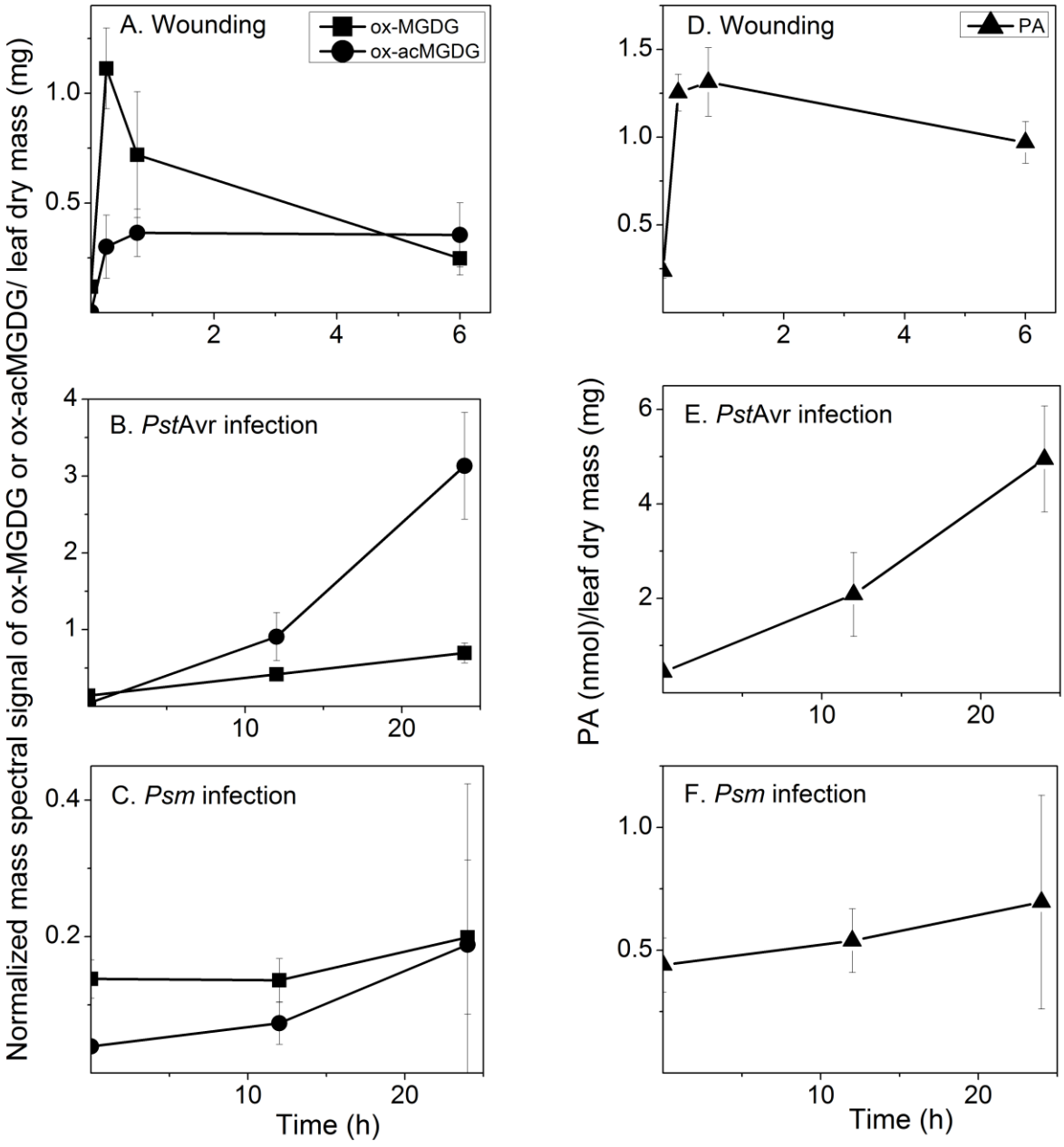

Figure S2.5 Levels of LPC, LPE, and PA, in Arabidopsis leaves during stress and control treatments. Average data used in this figure are presented in Table 2.8. Error bars indicate standard deviation. T-test was performed on 12 treatment-control pairs: **Wounded, 15 min** vs. Unwounded; **Wounded, 45 min** vs. Unwounded; **Wounded, 6 h** vs. Unwounded; ***Pst*Avr, 12 h** vs. $MgCl_2$, 12 h; ***Psm*, 12 h** vs. $MgCl_2$, 12 h; **$MgCl_2$, 12 h** vs. Untreated, 12 h; ***Pst*Avr, 24 h** vs. $MgCl_2$, 12 h; ***Psm*, 24 h** vs. $MgCl_2$, 24 h; **$MgCl_2$, 24 h** vs. Untreated, 24 h; **4°C, 3 h** vs. 22°C, 3 h; **4°C, 27 h** vs. 22°C, 27 h; **Freezing (-8°C, 2 h)** vs. 4°C, 84 h; *p < 0.05, n = 5 (except for 4°C, 3 h, n = 4).

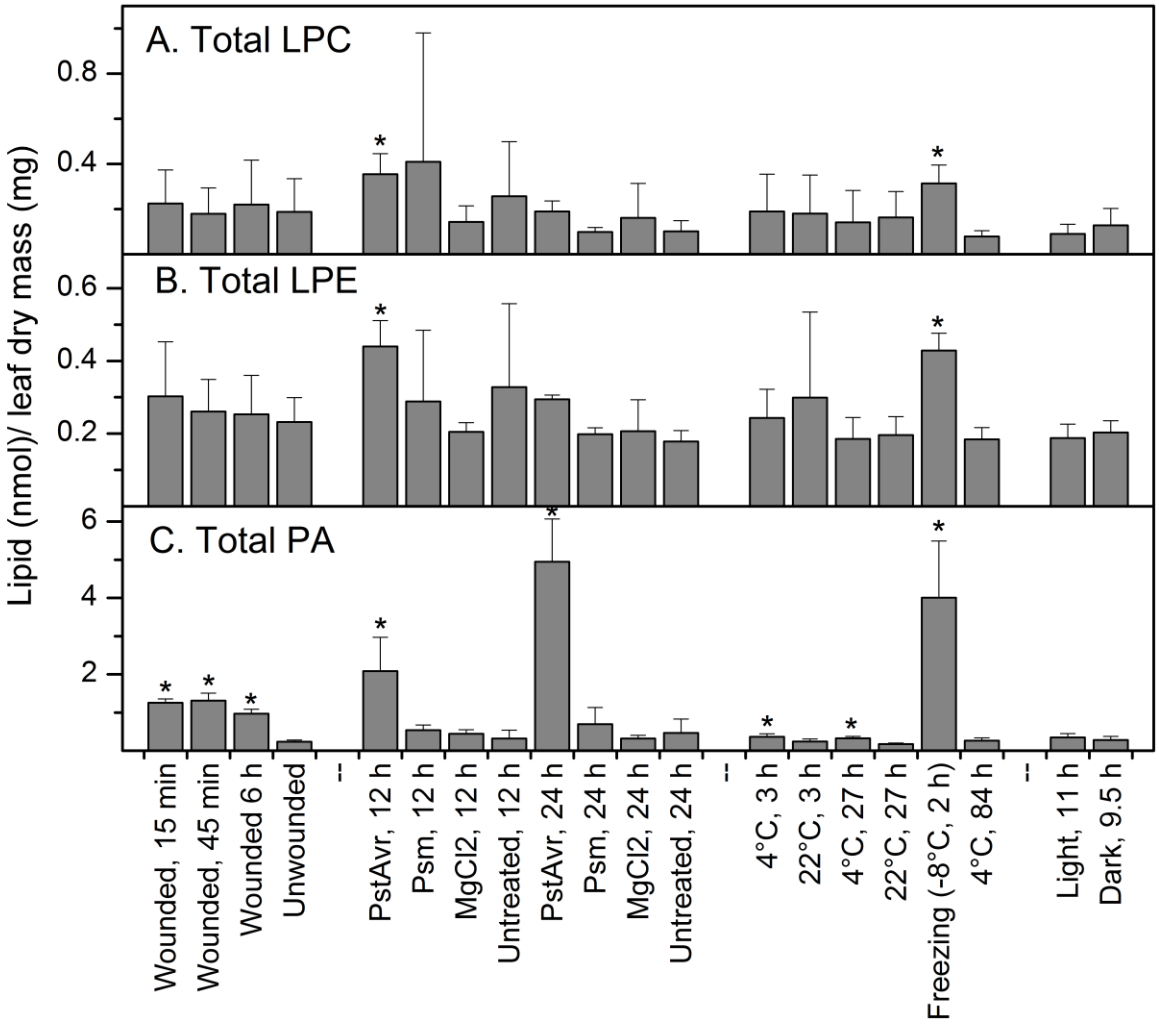

Chapter 3 - Head-group acylation of monogalactosyldiacylglycerol is a common stress response, and the acyl-galactose acyl composition varies among plant species and with applied stress

Abstract

Formation of galactose-acylated monogalactosyldiacylglycerols has been shown to be induced by leaf homogenization, mechanical wounding, avirulent bacterial infection and thawing after snap-freezing. Here, lipidomic analysis using mass spectrometry showed that galactose-acylated monogalactosyldiacylglycerols, formed in wheat (*Triticum aestivum*) and tomato (*Solanum lycopersicum*) leaves upon wounding, have acyl-galactose profiles that differ from those of wounded *Arabidopsis thaliana*, indicating that different plant species accumulate different acyl-galactose components in response to the same stress. Additionally, the composition of the acyl-galactose component of Arabidopsis acMGDG (galactose-acylated monogalactosyldiacylglycerol) depends on the stress treatment. After sub-lethal freezing treatment, acMGDG contained mainly non-oxidized fatty acids esterified to galactose, whereas mostly oxidized fatty acids accumulated on galactose after wounding or bacterial infection. Compositional data are consistent with acMGDG being formed in vivo by transacylation with fatty acids from digalactosyldiacylglycerols. Oxophytodienoic acid, an oxidized fatty acid, was more concentrated on the galactosyl ring of acylated monogalactosyldiacylglycerols than in galactolipids in general. Also, oxidized fatty acid-containing acylated monogalactosyldiacylglycerols increased cumulatively when wounded Arabidopsis leaves were wounded again. These findings suggest that, in Arabidopsis, the pool of galactose-acylated monogalactosyldiacylglycerols may serve to sequester oxidized fatty acids during stress responses.

Introduction

Membranes of plant chloroplasts contain glyco-glycerolipids with three major head groups: galactose (Gal, in monogalactosyldiacylglycerol, MGDG), digalactose (in digalactosyldiacylglycerol, DGDG) and sulfonated glucose (in sulfoquinovosyldiacylglycerol, SQDG). The Gal component of MGDG can be enzymatically modified by fatty acylation (esterification) at the 6′-hydroxyl group. Over 40 years ago, this head group acylation was characterized in spinach homogenates (Heinz, 1967a; Heinz and Tulloch, 1969). Fatty acid compositional analysis of in vitro incubation products from an ammonium sulfate-precipitated protein fraction with purified lipid substrates indicated that, when only MGDG was present, galactose-acylated MGDG (acMGDG) was formed via a dismutation reaction, i.e. 2 MGDG → acMGDG + monogalactosylmonoacylglycerol (MGMG). However, when both MGDG and DGDG were present, acMGDG was formed exclusively by transacylation from DGDG, i.e. DGDG + MGDG → acMGDG + digalactosylmonoacylglycerol (DGMG; Heinz 1967b, Heinz 1972). This early work focused on acMGDG formation in homogenized leaf tissues; however, the potential physiological role for the acylation reaction was not considered.

More recently, acMGDGs with the structure 1-(12-oxophytodienoic acid) (OPDA), 2-dinor-oxophytodienoic acid (dnOPDA), 3-(OPDA-Gal) glycerol (Arabidopside E) and acMGDG with 3 OPDA chains (Arabidopside G) were identified in Arabidopsis leaves under stress. These acMGDGs can accumulate to as much as 8% of the Arabidopsis total leaf lipid when the leaves are infected with the bacteria *Pseudomonas syringae* carrying the avirulence factor AvrRpt2 (Pst) or AvrRpm1 (Andersson et al., 2006; Kourtchenko et al., 2007). Indeed, in vitro testing indicated that Arabidopsides E and G have antimicrobial activities against the virulent bacterium *Pseudomonas syringae* DC3000 (Andersson et al., 2006) and the necrotrophic fungus *Botrytis cinerea* (Kourtchenko et al., 2007). Forty additional acMGDG molecular species (13 non-oxidized and 27 oxidized) were measured after wounding of Arabidopsis leaves (Ibrahim et al., 2011) and 27 additional acMGDGs, each with at least one oxidized fatty acid chain, were characterized as being induced significantly after wounding or avirulent bacterial infection of Arabidopsis leaves (Vu et al., 2012).

Galactolipids with cyclic oxidized acyl chains, or oxylipins, such as OPDA, esterified to glycerol are rare in plant species outside the genus *Arabidopsis* (Bottcher and Weiler, 2007). The current study adds to the evidence that, although cyclic fatty acids in membrane lipids may be restricted in occurrence, Gal acylation of MGDG is a relatively conserved process that occurs in tomato and wheat, in addition to Arabidopsis, spinach, and broad bean (Heinz, 1967b; Heinz, 1967a; Heinz and Tulloch, 1969; Heinz, 1972; Andersson et al., 2006; Kourtchenko et al., 2007; Ibrahim et al., 2011; Vu et al., 2012). MGDG Gal acylation is demonstrated to be a common response to stresses including wounding, freezing and infection with avirulent bacteria. The data show major variation in composition of the Gal-esterified acyl group, both among plant species and in response to different stresses. Furthermore, comparison of the profiles of the fatty acyl chain on the Gal of acMGDG and the fatty acyl chains of DGDG supports the notion that DGDG is the usual acyl donor for MGDG Gal acylation *in vivo*.

Materials and Methods

Plant materials

Mature wheat leaves (*Triticum aestivum* 'Thatcher') were collected from the North Agronomy Farm, Kansas State University, Manhattan, KS. Tomato plants (*Solanum lycopersicum* 'Better Boy') were purchased from Westside Market, Manhattan, KS. *Arabidopsis thaliana* accessions Columbia-0 (Col-0) and C24 were grown one plant per well in Pro-Mix 'PGX' soil (Hummert International, Earth City, MO) in 72-well plug trays (Hummert International, Earth City, MO). Trays were kept in a Conviron growth chamber under a 14/10 h light/dark cycle with 60% humidity at 21°C. Light intensity in growth chambers was maintained at 80 μmol m−2 s−1 with cool white fluorescent lights (Sylvania, Danvers, MA). Plants were fertilized twice, once when sowing and once at 20 days old, by irrigation with a 1% solution of 20-20-20 Miracle-Gro plant food (Scotts Miracle-Gro, Marysville, OH). Col-0 was harvested after 30 days and C24 after 42 days of growth.

Treatments

Arabidopsis plants were infected with bacteria (*Pseudomonas syringae*) as previously described (Vu et al., 2012). Cold acclimation was performed in a 4°C room equipped with light carts. Freezing treatment was performed in a programmable freezing chamber (Espec Corporation, Hudsonville, MI). Each tray of plants in soil was partly submerged in an ice slurry (made by adding tap water to approximately 1.5 kg of ice chips to a total volume of 4 l) to avoid supercooling during freezing treatment at −8°C for 2 h. The soil was completely in contact with the ice slurry through the irrigation holes at the bottom of the growing tray. The temperature was dropped to −8°C without gradual decreasing; at the end of the freezing treatment, plants were transferred to their growth condition (21°C, 60% humidity) and sampled after 3 and 24 h. Leaf numbers 5 and 6 were collected for ion leakage measurement (see next section), and the remaining portion of the rosette was dropped into 4 ml of 75°C isopropanol with 0.01% butylated hydroxytoluene (BHT) for lipid analysis. Leaf number is the order of leaf appearance, determined as described previously (Telfer et al., 1997). Wounding was performed by applying pressure with a hemostat across the leaf mid-vein, leaving wound marks about 6 mm apart. For the re-wounding experiment, plants were randomly assigned to one of three groups. Plants of the 'control' singly wounded group were harvested at 0 min, 5 min, 15 min, 45 min, 4 h, 24 h and 48 h after wounding. For the other two groups, a second wound was applied at the same location as the first wound either 24 or 48 h after the first wound was applied. The leaves were harvested at 0 min, 5 min, 15 min, 45 min, 4 h, 24 h and 48 h after the second wound. In the re-wounding experiment, four leaves (leaf numbers 5, 6, 7 and 8) were harvested at each time point; leaf number 5 was dropped into 2 ml of 75°C isopropanol with 0.01% BHT for lipid analysis, and leaf numbers 6, 7 and 8 were put together into a 1.5-ml tube and frozen in liquid nitrogen for phytohormone analysis by gas chromatography – mass spectrometry (MS).

Ion leakage measurement

Two leaves from each rosette were rinsed with deionized water before being dropped into a a 50-ml PYREX glass tube (Corning Inc., Corning, NY) containing 25 ml of distilled water (Dillons Supermarket, Manhattan, KS). The tubes were shaken for 2 h at 100 rpm before the first ion conductivity reading with Oakton CON 510 electrical conductivity meter (Oakton Instruments,

Vernon Hills, IL). After the first reading, the tubes were incubated at 95–100°C in a water bath for 2 h, and a second conductivity reading was taken. Relative ion leakage, as a percentage, was reported as (the first over the second conductivity reading) × 100 (%).

Lipid extraction

Modified Bligh–Dyer method (Bligh and Dyer, 1959) for polar lipid analysis

For the *Pst* and wounding experiments, three leaves were dropped into 3 ml of 75°C isopropanol containing 0.01% BHT; heating at 75°C was continued for 15 min. Chloroform (1.5 ml) and water (0.6 ml) were added, and the tube was shaken for 1 h before the solvent was transferred to another tube. For the second round of extraction, 4 ml of chloroform: methanol (2:1) was added to the leaves, followed by shaking for 30 min and combination of the solvent with the previous extract. After repeating the extraction three more times and combining the extracts, the combined extract was evaporated under a nitrogen stream and re-dissolved in 1 ml of chloroform. The extracted leaf residue was dried overnight at 105°C and the dry mass obtained by weighing.

Alternate extraction method (for polar lipid analysis)

For the freezing and re-wounding experiments, leaves were dropped into a 20-ml vial with a Teflon-lined cap containing 4 ml (2 ml in the re-wounding experiment) of 75°C isopropanol with 0.01% BHT. After 15 min at 75°C, 12 ml (6 ml in the re-wounding experiment) of extraction solvent (chloroform: methanol: 300 mM ammonium acetate in water, 30:41.5:3.5, v/v/v) were added, and the tube was shaken at room temperature for 24 h.

For gas chromatography-MS (free oxylipin analysis)

Extraction and derivatization were carried out as described previously (Schmelz et al., 2004).

Mass spectrometry

For samples extracted by the modified Bligh–Dyer method (stored in 1 ml chloroform), a volume (x µl) containing 0.2 mg leaf dry mass was diluted by adding (360 − x) µl of chloroform and 840

µl of methanol: 300 mM ammonium acetate in water (95:5, v/v). For samples extracted by the alternate method, a volume (y µl) containing 0.2 mg leaf dry mass was diluted with (1200 − y) µl of chloroform: methanol: isopropanol: 300 mM ammonium acetate in water (30:41.5:25:3.5, v/v/v/v).

Phospholipids and galactolipids with normal chains were analyzed by triple quadrupole MS using head group-specific scans and standards as described previously (Xiao et al., 2010). Precursor scans of m/z 277.2 (Pre 277.2, 18:3), m/z 291.2 (Pre 291.2, 18:4-O), m/z 293.2 (Pre 293.2, 18:3-O), m/z 295.2 (Pre 295.2, 18:2-O or 17:3-2O) and m/z 283.2 (Pre 283.2, 18:0, to detect internal standard 16:0/18:0 MGDG) were performed in negative mode as described previously (Vu et al., 2012), except that 1.505 nmol of 18:0/16:0 MGDG was used in each vial as an internal standard.

Scans for neutral loss (NL) fragments composed of Gal and a fatty acid (Table 3.1) were carried out in positive mode using an ABI 4000 triple quadrupole mass spectrometer (Applied Biosystems, Foster City, CA) with an electrospray ionization (ESI) source. To perform the NL scans listed in Table 3.1, three identical sample vials were used to provide enough volume for the analysis of each sample. To each sample vial, 0.95 nmol of di18:0 DGDG was added as an internal standard; this was detected by NL scan of m/z 341.2 (NL 341.2), with a target of m/z 966.7. The infusion flow rate was 30 µl min−1. The scan rate was 36 u s−1 for 75 cycles. Other parameters were: collision gas, 2 (arbitrary units); curtain gas, 20 (arbitrary units); ion source gases 1 and 2, 45 (arbitrary units); source temperature, 100°C; interface heater, ‘on’; ion spray voltage, 5500 V; declustering potential, 90 V; entrance potential, 10 V; collision energy, 24 V and collision cell exit potential, 23 V.

Accurate acyl mass analysis by quadrupole time-of-flight (Q-TOF) MS was performed on unfractionated lipid extracts with a Q-TOF-2 tandem mass spectrometer (Micromass Ltd., Manchester, UK), using the solvent, parameters and processing method described by Buseman et al. (2006), with a few changes. Charged precursor ions were subjected to product ion scanning in negative or positive ion mode. Precursor ions were selected by the quadrupole, tuned to transmit at 0.8 u full width at half height (i.e. monoisotopic selection). Extracts were infused into the ESI source at 20 µl min^{-1}; collision energy was 30 V.

Chemical ionization gas chromatography – MS was used to profile phytohormones of samples harvested from the re-wounding experiment following the procedure described by Schmelz et al. (2004).

Mass spectral data processing and analysis

Peak smoothing, background subtraction and peak centroiding for triple quadrupole MS data were carried out using a custom script with Applied Biosystems analyst software. After targeted peaks were identified, isotopic overlaps were calculated and subtracted from peaks within each spectrum. For NL scans, spectra were also corrected for isotopic overlaps of head group fragments. Signals of targeted peaks were normalized to the signal of the corresponding internal standard (18:0/16:0 MGDG for negative precursor scans and di18:0 DGDG for positive NL scans) and reported as normalized mass spectral signal per mg of leaf dry mass, where amount of signal produced by 1 nmol internal standard is 1 unit of signal.

To calculate the OPDA to 18:3 signal ratio in MGDGs and DGDGs in Arabidopsis, the ESI triple quadrupole MS signals were detected by scanning in negative mode for Pre 291.2 (OPDA) and Pre 277.2 (18:3). The sum of signals from MGDGs and DGDGs containing combinations of OPDA (18:4-O) with each of the five major fatty acids [16:3, 16:0, dnOPDA (16:4-O), 18:3 and OPDA] was divided by the sum of MGDGs and DGDGs containing combinations of 18:3 with each of the same five major fatty acids. To calculate the Gal-OPDA to Gal-18:3 signal ratio in acMGDGs, the sum of signals of Gal-OPDA acMGDGs [with each of the 35 diacylglycerol (DAG) combinations listed in Table S3.1], detected by scanning in positive mode for NL 453.3 (Gal-OPDA), was divided by the sum of signals of Gal-18:3 acMGDGs (with the 35 DAGs listed in Table S3.1), detected by scanning in positive mode for NL 439.3 (Gal-18:3).

Q-TOF mass spectra obtained in negative mode were mass-corrected by using, as a lock mass, the theoretical exact mass of the acyl anion of 18:3 fatty acid or OPDA, m/z 277.2173 or 291.1966, respectively. Q-TOF spectra obtained in positive mode were mass-corrected by locking on the mass of a fragment containing the glycerol backbone attached to either 18:3 fatty acid or OPDA (m/z 335.2581 or 349.2373, respectively). With the locked mass correction, the exact masses of product ions were determined to ten thousandths of a mass unit.

Results

Wound-induced acylation of the galactose of MGDG occurs in multiple plant species

acMGDGs are formed by acylation of MGDG on the carbon at the 6-position of galactose (Heinz and Tulloch, 1969). Utilizing direct infusion ESI triple quadrupole MS, acMGDG levels can be measured by NL scanning in the positive mode. Figure 3.1A depicts an acMGDG molecule, showing formation of the NL fragment, $C_{22}H_{43}O_6N$ (417.3 u), by collision-induced dissociation. The fragment is composed of a palmitoyl chain, 16:0 (where 16 is the number of carbons and 0 is the number of double bond equivalents, excluding the carbonyl double bond), esterified to Gal. Other NL fragments used for detection of acMGDGs are listed in Table 3.1. Each NL scan targets an acMGDG group with a common acyl-Gal component and varied DAG components. The DAG components targeted in each NL scan (Table 3.1) are listed in Table S3.1. In contrast to the previous method used by our group to detect acMGDGs by targeting fatty acyl anions (Vu et al., 2012), which did not identify the position of the detected fatty acid among the three positions in acMGDG, the current method detects the fatty acid linked to the galactose. To compare amounts of acMGDGs, signals were normalized to the signal of an internal standard, with an amount of signal equal to that of 1 nmol of the standard equal to 1. This approach allows sample-to-sample comparison of signals. More detail on the acMGDGs (as defined by DAG species in combination with each acyl-galactose species) may be viewed in Table S3.2.

Figure 3.1B shows that various plant species, from the monocot wheat to eudicots tomato and Arabidopsis, produce acMGDG in response to wounding. acMGDG is formed within 45 min after wounding with a hemostat. Fold increases of acMGDG in leaves 45 min after wounding were 3 for tomato, 18 for wheat, 20 for Arabidopsis C24 and 130 for Arabidopsis Col-0.

In acMGDG produced in response to wounding, the fatty acyl species linked to Gal varied among plant species (Figure 3.2). Figure 3.2A shows that in Arabidopsis Col-0, the most abundant Gal-linked fatty acids were 18:4-O, which has been identified as OPDA in galactolipids (Stelmach et al., 2001; Buseman et al., 2006), 16:0, 18:3-2O/20:1, 18:3 and 18:3-O (49, 19, 11, 7 and 4%, respectively, of the total acMGDG measured). Gal-linked fatty acids 18:3-2O and 20:1 have the same nominal mass and thus are not differentiated by this method. In agreement with previous analyses of *Arabidopsis thaliana* Col-0, three acMGDGs with the most abundant signals were 1-OPDA,2-dnOPDA,3-(OPDA-galactosyl) glycerol (Arabidopside E,

38% of total acMGDG signal), 1-OPDA,2-dnOPDA,3-(16:0-galactosyl) glycerol (14%) and 1,2-diOPDA,3-(OPDA-galactosyl) glycerol (7%, Arabidopside G) (Table S3.2; Andersson et al., 2006, Ibrahim et al., 2011, Kourtchenko et al., 2007, Vu et al., 2012). In Arabidopsis C24, Gal linkage of unoxidized fatty acids was more prevalent: 18:3 (32% of total acMGDG signal), 16:0 (19%), OPDA (18%), 18:2 (6%), 18:3-O (6%) and 18:3-2O/20:1 (6%) compared to Col-0 after the same wounding treatment (Figure 3.2B). While the amount of acMGDG with OPDA esterified to Gal is approximately 10-fold less in Arabidopsis C24 than in Arabidopsis Col-0, the amount of acMGDG with 18:3 esterified to Gal was slightly higher in C24 than in Col-0. Similarly, MS signals from acMGDGs in wounded tomato and wheat leaves were derived primarily from unoxidized Gal-linked fatty acids: 16:0 (40%), 18:3 (27%) and 18:2 (15%) in tomato; 18:3 (73%), 16:0 (9%) and 18:2 (6%) in wheat (Figure 3.2C–D). Scanning for NL 439.3 (18:3-containing Gal) in samples from wheat 45 min after wounding produced a massive peak at m/z 1052.8, whose signal accounted for 72% of the total acMGDG signal (Table S3.2). Accurate-mass product ion analysis of this species (acetate adduct, $[M + C_2H_3O_2]^-$, m/z 1093.8) by Q-TOF MS in the negative mode (Buseman et al., 2006, Vu et al., 2012) showed that this largest acMGDG component of wheat contained only 18:3 acyl chains, consistent with a structure of 1,2-di18:3,3-(18:3-galactosyl) glycerol (Figure S3.1). Table S3.3 shows the acyl composition (three chains) of the major acMGDG molecular species detected in Arabidopsis Col-0, tomato and wheat and the supporting accurate-mass product ion analysis.

acMGDGs accumulate following stress, including sub-lethal freezing

The total amounts of acMGDG formed under different stress treatments were determined using the NL scans indicated in Table 3.1 (Figure 3.3). As shown previously by precursor scanning for acyl anions, infection of *Arabidopsis thaliana* Col-0 with the avirulent bacteria *Pst* induced large amounts of acMGDG (Figure 3.3A; Vu et al., 2012). Wounding also induced acMGDG (Figure 3.3B). Similarly, sub-lethal freezing induced synthesis of acMGDG (Figure 3.3C). Levels of acMGDG with unoxidized fatty acyl chains had not been previously determined (Vu et al., 2012; next section). In the experiment shown in Figure 3.3C–E, Arabidopsis Col-0 plants were cold-acclimated at 4°C for 3 days or not acclimated (remained at the growth temperature of 21°C) until the freezing treatment (2 h at −8°C). Plants were returned to 21°C after freezing and sampled 3 h or 24 h later. As indicated by measurement of ion leakage at 24 h (Figure 3.3D),

non-acclimated plants sustained more damage than acclimated plants ($P < 0.001$). Figure 3.3C indicates that levels of acMGDG increased during the post-freezing period in both acclimated and non-acclimated plants, but that the levels were always higher in non-acclimated than in acclimated plants. Ion leakage measurements (Figure 3.3D) indicate that the membranes of acclimated plants were quite permeable at 3 h into the recovery period, but less so at 24 h ($P < 0.01$). In contrast, the non-acclimated plants showed greater leaf membrane damage after 24 h post freezing than at 3 h ($P < 0.05$) and much more damage at 24 h than observed in acclimated plants. Indeed, acclimated plants sustained visible damage to leaves, but the leaves were able to recover, while the damaged leaves of non-acclimated plants died, although the plant did not (see Figure S3.2). Levels of the phospholipid hydrolytic product phosphatidic acid (PA) are shown in Figure 3.3E. (Levels of other membrane lipids are shown in Table S3.4). Whereas total PA levels (Figure 3.3E) were closely correlated with leaf ion leakage (Figure 3.3D), the total acMGDG signal (Figure 3.3C) did not correlate strictly with leaf injury. Acclimated plants tended to accumulate acMGDG between 3 h and 24 h ($P < 0.1$) after freezing treatment as ion leakage dropped. Taken together, comparison of acMGDG signals in acclimated and non-acclimated plants demonstrates a link between treatment and total acMGDG accumulation, but acMGDG accumulated even during recovery.

The composition of induced acMGDGs varies among stresses

The most abundant acMGDGs in Col-0 leaves after infection of the plants by *Pst* (24 h) were those with Gal-linked fatty acids OPDA (56%), 16:0 (17%), 18:3 (10%), 18:3-2O/20:1 (6%) and 16:4-O (4%) (Figure 3.4A). The acMGDG composition, with a prevalence of OPDA and 16:0 on Gal, was similar to that formed after wounding (Figure 3.4B). The acMGDG Gal-linked acyl composition was drastically different in plants 24 h after freezing. In acclimated plants (Figure 3.4C), 18:3 (48%), 16:0 (14%), OPDA (14%), 16:3 (10%) and 18:2 (6%) were most prevalent, and in non-acclimated plants (Figure 3.4D), 18:3 (58%), 16:3 (13%), 16:0 (11%), 18:2 (7%) and OPDA (4%) were highest. Although acclimated plants accumulated approximately five-fold less acMGDG than non-acclimated plants, they accumulated approximately the same amount of OPDA-Gal acMGDG (0.48 ± 0.23 normalized MS units mg^{-1} dry mass in acclimated plants compared with 0.59 ± 0.17 units in non-acclimated plants).

Overall, the data demonstrate that during recovery from freezing, as well as during Pst infection and after wounding, significant acylation of the Gal of MGDG was induced. However, in contrast to the composition during other stresses, after freezing, the Gal-linked acyl chains were mostly unoxidized.

The proportions of 16:3, 16:0 and 18:3 in the Gal-esterified acyl chains in acMGDGs resemble proportions in DGDG

The formation of acMGDG, by a dismutation reaction when MGDG was the only substrate or by transacylation from DGDG when both MGDG and DGDG were present, has been demonstrated in in vitro experiments (Heinz, 1967b; Heinz, 1972). To define the in vivo substrate(s) for acMGDG formation, we considered the acyl compositions of Arabidopsis MGDG and DGDG. Leaf MGDG contains two major molecular species; 18:3/16:3 MGDG is present at higher levels than di18:3 MGDG. Leaf DGDG has three major molecular species: di18:3 DGDG > (16:0/18:3 DGDG + 18:3/16:0 DGDG) > 18:3/16:3 DGDG. The acyl composition of MGDG has previously been analyzed: 59% 18:3, 33% 16:3 and only 1% 16:0, whereas the acyl composition of DGDG contains 77% 18:3, 3% 16:3 and 12% 16:0 (Miquel et al., 1998). Comparing the percentages of 16:0 and 16:3 (and other acyls) esterified to the Gal of acMGDG of stressed (induced) samples to the percentages in MGDG and DGDG of untreated samples should shed light on the origin(s) of the acyl groups (Figure 3.5). The fatty acid compositions of MGDG and DGDG used in the current analysis were estimated from the percentage of each MGDG and DGDG molecular species determined by head-group scanning of untreated samples, with assignment of molecular species based on previous product ion analysis (Devaiah et al., 2006). Detailed estimation is shown in Table S3.5. The percentages of each fatty acid in MGDG and DGDG determined in this way on the untreated samples were in close agreement with the previously published data (Miquel et al., 1998). When acMGDG formation is induced by stresses in Col-0, fatty acid oxidation also occurs at various levels. Hence, for comparison of normal and head group-acylated galactolipid compositions, the contents of unoxidized fatty acids and their oxidized derivatives were summed: i.e. 16:3 and its major oxidized derivative, 16:4-O, were combined; similarly, 18:3, 18:4-O, 18:3-O and 18:3-2O were combined, as were 18:2 and 18:2-2O. The composition of the fatty acids linked to Gal in acMGDG during stress responses, reveals that the percentage of 16:0, ranging from 11 to 19%, is similar to the percentage in DGDG (11%) and

much higher than in MGDG (0.1%, Figure 3.5). While it is possible that under certain circumstances, some fatty acyl chains used to esterify Gal might come from MGDG, as suggested by the somewhat higher percentage of 16:3 and 16:4-O incorporated on the Gal of acMGDG following freezing stress (Figure 3.5E–F), the data are consistent with DGDG as the major source of the Gal-esterified fatty acids in acMGDG formed in vivo.

The oxidized fatty acyl chain OPDA is enriched on the Gal of acMGDG

To determine relative amounts of OPDA and 18:3 in MGDG, DGDG and acMGDG, ratios of MS signals for OPDA and 18:3 in MGDG and DGDG were measured using ESI triple quadrupole MS precursor scanning in negative mode, while ratios of MS signals for OPDA and 18:3 on the Gal of acMGDG were measured using NL scanning in positive mode. Levels of MGDG and DGDG detected by negative precursor scans for 18:4-O (includes OPDA), 18:3-O and 18:2-O are shown in Table S3.6. The ratios of OPDA to 18:3 signals under different treatments are shown in Table 3.2. *Pst* infection and wounding of Col-0 significantly increased the OPDA level in MGDG and DGDG ($P < 0.001$) and the OPDA/18:3 signal ratio in MGDG and DGDG ($P < 0.05$). However, the OPDA/18:3 signal ratio was several orders of magnitude higher on the Gal of acMGDG than in MGDG and DGDG under both induced and non-induced conditions. Although neither acclimated nor non-acclimated plants accumulated much OPDA in galactolipids after freezing treatment, the OPDA/18:3 signal ratio from the acyl chains on the Gal of acMGDG was significantly greater than the OPDA/18:3 signal ratio from the acyl chains esterified to the glycerols of MGDG and DGDG. Interestingly, OPDA enrichment on the Gal of induced acMGDG in cold-acclimated Col-0 plants is greater than in non-acclimated Col-0 recovering from sub-lethal freezing (Table 3.2). Taken together, the data in Table 3.2 indicate that the enrichment of OPDA on the Gal of acMGDG is roughly correlated with the availability of OPDA in MGDG and DGDG, and OPDA is concentrated in the pool of fatty acids linked to the Gal of acMGDG.

Oxidized acMGDG induction is enhanced by re-wounding

Although the existence of acMGDG has long been known, its physiological roles are still largely unclear. The fully oxidized acMGDGs Arabidopside E and Arabidopside G have been demonstrated to have anti-fungal and anti-bacterial activities in vitro (Andersson et al., 2006; Kourtchenko et al., 2007). One hypothesis about acMGDG function is that oxidized fatty acid-containing complex lipids may serve as reservoirs for precursors of oxylipin-derived phytohormones such as jasmonic acid (JA). In order to test this hypothesis, we wounded Col-0 leaves twice at the same place, with the second wound occurring either 24 or 48 h after the first. Leaves were harvested for lipid extraction at 0 min, 5 min, 15 min, 45 min, 4 h, 24 h and 48 h following each wounding event. Harvested leaves were extracted and analyzed for both complex lipids and the free phytohormones JA and OPDA. There was no enhancement by re-wounding in levels of induced total free JA and total free OPDA (Figure S3.3), indicating that the accumulation of pools of esterified oxylipins did not trigger a significantly faster or stronger response in levels of free JA or OPDA upon re-wounding.

Figure 3.6 shows levels of plastidic complex lipids MGDG, DGDG and acMGDG. Whereas free oxylipin content was not significantly higher upon re-wounding, signals from oxidized MGDG and DGDG (Figure 3.6A–C) were clearly increased by a second wounding to levels higher than by a single wounding. The second wounding did not induce major and sustained increases in signals from unoxidized acMGDG (Figure 3.6D–F). In contrast, the levels of oxidized acMGDGs (Figure 3.6G–H) were much higher during re-wounding and remained higher than the levels induced by the first wounding for up to 48 h after re-wounding.

Discussion

The present work demonstrates that acMGDGs are formed in planta across species (Figure 3.1B). Prior work established that wounding and bacterial infection induce acMGDG production in Arabidopsis (Andersson et al., 2006; Kourtchenko et al., 2007; Vu et al., 2012). Homogenization was also reported to induce MGDG acylation in spinach and broad bean leaves (Heinz 1967a, Heinz 1972). Here, we demonstrated that acMGDG is also formed in tomato and wheat in response to wounding, suggesting that Gal acylation of MGDG is a conserved response

to stress in plants. We also demonstrate that sub-lethal freezing induces acMGDG synthesis in the post-freezing period (Figure 3.3C). This was not observed in our previous study, which focused only on oxidized acMGDG and analyzed lipid levels only to the end of the freezing period (Vu et al., 2012).

The acyl composition of the acyl-Gal in acMGDG differs in different circumstances. Factors that affect the composition include the plant species, the applied stress, and, likely, other factors that affect the composition of the galactolipid pool. In general the data support the notion that in vivo formation of acMGDG occurs via transacylation from DGDG, as demonstrated previously for in vitro formation (Heinz, 1967b; Heinz, 1972). Species and accessions with more oxidized lipids in the galactolipid pool (Col-0 > C24 > other species) have more oxidized lipids in acMGDG. Stresses that induce more lipid oxidation (bacterial infection and wounding) vs those that induce less (freezing) also result in production of acMGDG with more oxidized molecular species. Wound-induced acMGDGs containing Gal-linked OPDA (Arabidopsides E and G) were not detected in *Brassica napus*, *Nicotiana tabacum*, *Pisum sativum*, *Spinacia oleracea*, *Avena sativa* and barley (Kourtchenko et al., 2007). However, we cannot rule out the possibility that acMGDG is produced in these species with unoxidized fatty acids linked to Gal, similar to the observed reaction products in wheat.

At the same time, the composition of the acyl-Gal in Arabidopsis acMGDG was determined to be more oxidized than the galactolipid acyl pool as a whole. Ibrahim et al. (2011) reported that the ratio of unoxidized acMGDG to oxidized acMGDG in Col-0 leaves harvested 30 min after wounding (regardless of the positions of oxidized fatty acids on acMGDGs) is 0.6; the detection of such a high level of oxidation agrees with our data showing that oxidized fatty acids are enriched in acMGDG. Two possible explanations for the enrichment of OPDA on the Gal of acMGDG are: (1) that an acyltransferase preferentially acylates Gal with an oxidized fatty acid compared to an unoxidized one or (2) that an oxidizing enzyme, such as a lipoxygenase, can act efficiently and directly on an unoxidized fatty acid bound to Gal. The data suggest that, as previously demonstrated in vitro, DGDG in particular is likely to be the source of acyl chains for MGDG acylation to acMGDG in vivo. To date, no protein or gene directly responsible for acylation of acMGDG has been identified. The oxidized MGDGs and DGDGs, such as

Arabidopsides A, B and D (OPDA/dnOPDA MGDG, diOPDA MGDG and diOPDA DGDG, respectively, Figure 3.6A–C) are among the most rapidly formed compounds during stress responses, and the production of acMGDG always lags behind the production of these potential substrate species. This might support the idea of preferential acylation with oxidized fatty acids. On the other hand, Nilsson et al. (2012) presented data suggesting that oxidizing enzymes can directly catalyze oxidation of membrane bound fatty acids. Interaction between a soluble lipoxygenase and a Gal-linked acyl chain might be even more likely. If an oxidizing enzyme could preferentially interact with head group-linked fatty acyl chains, this would support the second possibility.

One potential function for acMGDGs might be as a reservoir for signaling compounds. Another possibility is that acMGDGs are just signs of damage. The current work did not provide support for either of those possibilities. JA and OPDA production was not directly correlated with acMGDG levels, nor was leaf damage linked with acMGDG levels in the recovery period after freezing. An alternative notion is that the acMGDG pool serves to sequester potentially harmful fatty acids from the main membrane lipid pool. Two examples of accumulation of acMGDG during stress responses support this idea. In the period after freezing, cold-acclimated plants accumulated acMGDG as the leaves recovered and ion leakage decreased (Figure 3.3). This acMGDG in acclimated leaves was enriched in oxidized fatty acid more than the acMGDG accumulated in non-acclimated leaves which do not recover from freezing damage. The second example is accumulation of acMGDG during re-wounding (Figure 3.6). In this case, upon rewounding, levels of acMGDG with oxidized fatty acids linked to Gal appeared to increase more and to stay increased longer than other galactolipid derivatives. These examples imply that acMGDG species are relatively long-lived and may persist and increase as recovery from stress occurs.

Acknowledgements

The authors would like to thank Dr Ernst Heinz for his encouragement and helpful comments. We are grateful to Drs Xuemin Wang and Jyoti Shah for their participation in related studies. We thank Dr Mark Ungerer for use of a freezing chamber and Dr Ari Jumponen for use of a light

cart. We appreciate Dr Sunish Sehgal allowing us to harvest wheat leaves from his plantings. This work was supported by the National Science Foundation (MCB 0920663 to R. W.). Instrument acquisition at the Kansas Lipidomics Research Center was supported by National Science Foundation (EPS 0236913, DBI 0521587, DBI 1228622), Kansas Technology Enterprise Corporation, K-IDeA Networks of Biomedical Research Excellence (INBRE) of National Institutes of Health (P20RR16475) and Kansas State University. Contribution no. 13-362-J from the Kansas Agricultural Experiment Station.

References

Andersson MX, **Hamberg M**, **Kourtchenko O**, **Brunnström A**, **McPhail KL**, **Gerwick WH**, **Gobel C**, **Feussner I**, **Ellerström M** (2006) Oxylipin profiling of the hypersensitive response in Arabidopsis thaliana. Formation of a novel oxo-phytodienoic acid-containing galactolipid, arabidopside E. J Biol Chem **281**: 31528–31537

Bligh EG, **Dyer WJ** (1959) A rapid method for total lipid extraction and purification. Can J Biochem Physiol **37**: 911–917

Bottcher C, **Weiler EW** (2007) cyclo-Oxylipin-galactolipids in plants: occurrence and dynamics. Planta **226**: 629–637

Buseman CM, **Tamura P**, **Sparks AA**, **Baughman EJ**, **Maatta S**, **Zhao J**, **Roth MR**, **Esch SW**, **Shah J**, **Williams TD**, **Welti R** (2006) Wounding stimulates the accumulation of glycerolipids containing oxophytodienoic acid and dinor-oxophytodienoic acid in Arabidopsis leaves. Plant Physiol **142**: 28–39

Devaiah SP, **Roth MR**, **Baughman E**, **Li M**, **Tamura P**, **Jeannotte R**, **Welti R**, **Wang X** (2006) Quantitative profiling of polar glycerolipid species from organs of wild-type Arabidopsis and a PHOSPHOLIPASE Dα1 knockout mutant. Phytochemistry **67**: 1907–1924

Heinz E (1967a) Acylgalactosyldiglyceride from leaf homogenates. Biochim Biophys Acta **144**: 321–332

Heinz E (1967b) On the enzymatic formation of acylgalactosyldiglyceride. Biochim Biophys Acta **144**: 333–343

Heinz E (1972) Some properties of the acyl galactosyl diglyceride-forming enzyme from leaves. Z Pflanzenphysiol **69**: 359–376

Heinz E, **Tulloch AP** (1969) Reinvestigation of the structure of acyl galactosyl diglyceride from spinach leaves. Hoppe-Seyler's Z Physiol Chem **350**: 493–498

Ibrahim A, **Schutz AL**, **Galano JM**, **Herrfurth C**, **Feussner K**, **Durand T**, **Brodhun F**, **Feussner I** (2011) The Alphabet of Galactolipids in Arabidopsis thaliana. Front Plant Sci **2**: 95

Kourtchenko O, **Andersson MX**, **Hamberg M**, **Brunnström A**, **Gobel C**, **McPhail KL**, **Gerwick WH**, **Feussner I**, **Ellerström M** (2007) Oxo-phytodienoic acid-containing galactolipids in Arabidopsis: jasmonate signaling dependence. Plant Physiol **145**: 1658–1669

Miquel M, **Cassagne C**, **Browse J** (1998) A new class of Arabidopsis mutants with reduced hexadecatrienoic acid fatty acid levels. Plant Physiol **117**: 923–930

Nilsson AK, **Fahlberg P**, **Ellerström M**, **Andersson MX** (2012) Oxo-phytodienoic acid (OPDA) is formed on fatty acids esterified to galactolipids after tissue disruption in Arabidopsis thaliana. FEBS Lett **586**: 2483–2487

Schmelz EA, **Engelberth J**, **Tumlinson JH**, **Block A**, **Alborn HT** (2004) The use of vapor phase extraction in metabolic profiling of phytohormones and other metabolites. Plant J **39**: 790–808

Stelmach BA, **Muller A**, **Hennig P**, **Gebhardt S**, **Schubert-Zsilavecz M**, **Weiler EW** (2001) A novel class of oxylipins, sn1-O-(12-oxophytodienoyl)-sn2-O-(hexadecatrienoyl)-monogalactosyl Diglyceride, from Arabidopsis thaliana. J Biol Chem **276**: 12832–12838

Telfer A, **Bollman KM**, **Poethig RS** (1997) Phase change and the regulation of trichome distribution in Arabidopsis thaliana. Development **124**: 645–654

Vu HS, **Tamura P**, **Galeva NA**, **Chaturvedi R**, **Roth MR**, **Williams TD**, **Wang X**, **Shah J**, **Welti R** (2012) Direct infusion mass spectrometry of oxylipin-containing Arabidopsis membrane lipids reveals varied patterns in different stress responses. Plant Physiol **158**: 324–339

Xiao S, **Gao W**, **Chen QF**, **Chan SW**, **Zheng SX**, **Ma J**, **Wang M**, **Welti R**, **Chye ML** (2010) Overexpression of Arabidopsis acyl-CoA binding protein ACBP3 promotes starvation-induced and age-dependent leaf senescence. Plant Cell **22**: 1463–1482

Figures and Tables

Figure 3.1 acMGDG structure and occurrence upon wounding.

A) Structure of a representative acMGDG molecule, 1-18:4-O,2-16:4-O,3-(16:0-galactosyl)glycerol and the fragmentation that gives rise to the NL fragment by collision induced dissociation. A proton moves from right to left during fragmentation. B) Total acMGDG induced by wounding, measured by the 11 NL scans indicated in Table 3.1, in Arabidopsis Col-0 and C24, tomato, and wheat leaves. Units are in relation to amount of signal detected for 1 nmol of internal standard (di18:0 DGDG), which is denoted as 1. Error bars are standard deviation, n = 5. The numbers above the bars of wounded samples show the fold induction compared to corresponding unwounded samples.

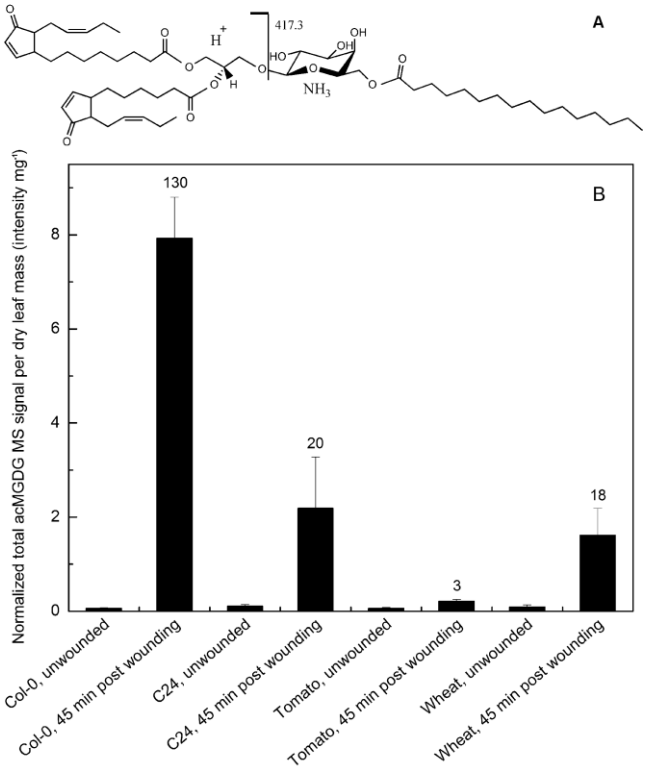

Figure 3.2 Levels of acMGDG (grouped by fatty acyl moiety on the Gal) in leaves of Arabidopsis Col-0 (A) and C24 (B), tomato (C), and wheat (D) 45 min after wounding.
The y axes have different scales. Error bars are standard deviation, n = 5. The numbers above the bars show the percentage of the corresponding acMGDG group over the sum of the 11 measured acMGDG groups.

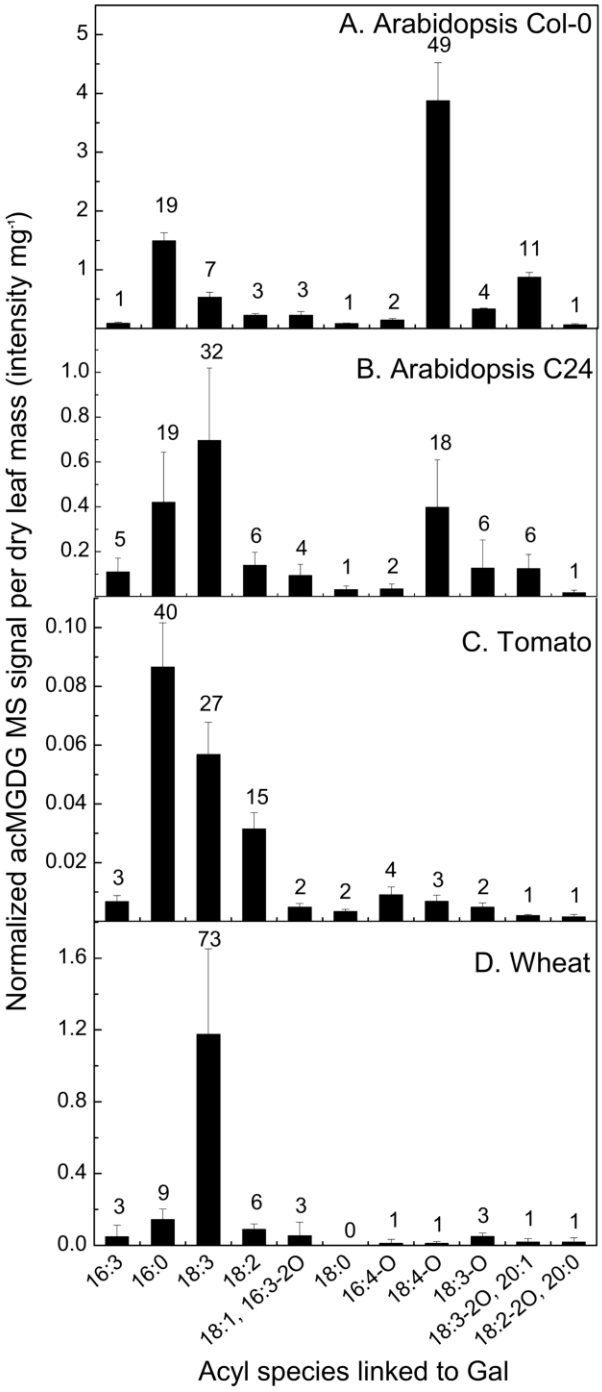

Figure 3.3 acMGDG forms in leaves of Arabidopsis Col-0 after application of different stresses, and its occurrence during freezing is not directly associated with cell membrane ion leakage.

Panels A, B, and C: acMGDG induced by Pst infection, wounding, and freezing. The y axes have different scales. Panel C shares an x-axis with Panels D and E. Panel D: Relative ion leakage (%) of acclimated and non-acclimated Arabidopsis Col-0 leaves at 3 h and 24 h after freezing treatment. Panel E: Level of total phosphatidic acid as measured by MS in acclimated and non-acclimated Arabidopsis Col-0 leaves at 3 h and 24 h after freezing treatment. Error bars are standard deviation; panels A and B: n = 5; panels C, D, and E: n = 6.

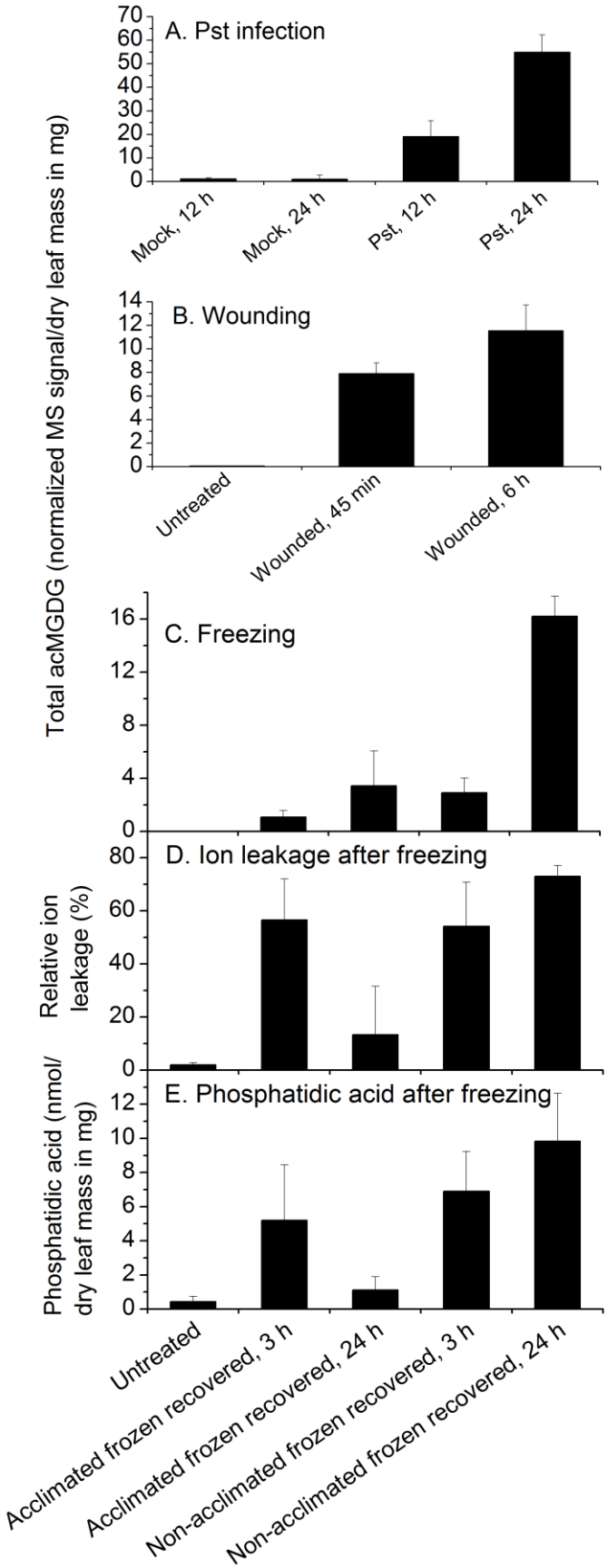
A. Pst infection
B. Wounding
C. Freezing
D. Ion leakage after freezing
E. Phosphatidic acid after freezing
Total acMGDG (normalized MS signal/dry leaf mass in mg)
Relative ion leakage (%)
Phosphatidic acid (nmol/ dry leaf mass in mg)
Mock, 12 h
Mock, 24 h
Pst, 12 h
Pst, 24 h
Untreated
Wounded, 45 min
Wounded, 6 h
Untreated
Acclimated frozen recovered, 3 h
Acclimated frozen recovered, 24 h
Non-acclimated frozen recovered, 3 h
Non-acclimated frozen recovered, 24 h

Figure 3.4 Levels of acMGDG (grouped by fatty acyl moiety on the Gal) in leaves of Arabidopsis Col-0 after application of different stresses.

Panel A: acMGDG at 24 h post Pst infection, n = 5; panel B: acMGDG at 45 min post wounding, n = 5; panel C: acMGDG of cold acclimated Col-0 plants at 24 h post freezing, n= 6; panel D: acMGDG of non-acclimated Col-0 plants at 24 h post freezing, n = 6. Y axes have different scales. Error bars are standard deviation. The numbers above the bars show the percentage of the corresponding acMGDG group over the sum of the 11 measured acMGDG groups.

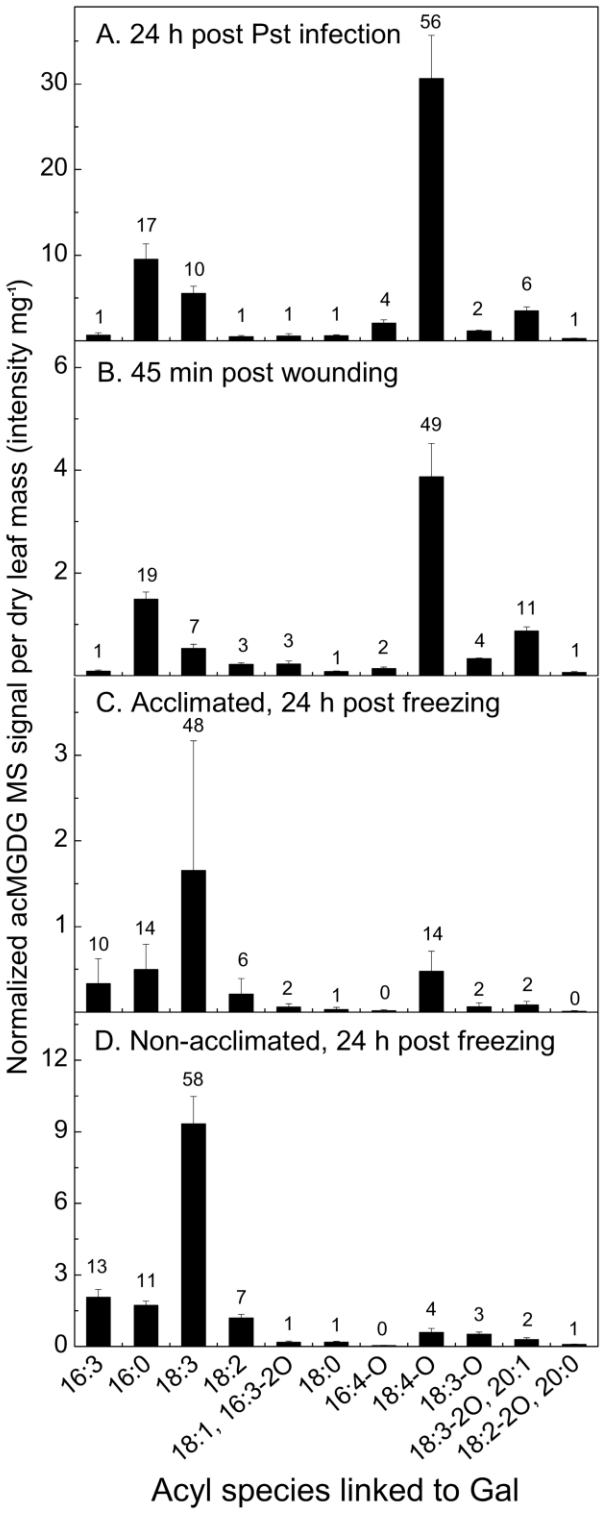
A. 24 h post Pst infection
B. 45 min post wounding
C. Acclimated, 24 h post freezing
D. Non-acclimated, 24 h post freezing
Normalized acMGDG MS signal per dry leaf mass (intensity mg-1)
Acyl species linked to Gal
16:3
16:0
18:3
18:2
18:1, 16:3-2O
18:0
16:4-O
18:4-O
18:3-O
18:3-2O, 20:1
18:2-2O, 20:0

Figure 3.5 Comparison of fatty acyl composition.

Fatty acyl composition (%) of MGDG (A) and DGDG (B) in untreated leaves and fatty acid composition of acyl-Gal in acMGDG of Col-0 plants at 24 h post Pst infection (C), n = 5; and at 45 min post wounding (D), n = 5; of cold acclimated (E) and of non-acclimated (F) Col-0 plants at 24 h post freezing, n = 6.

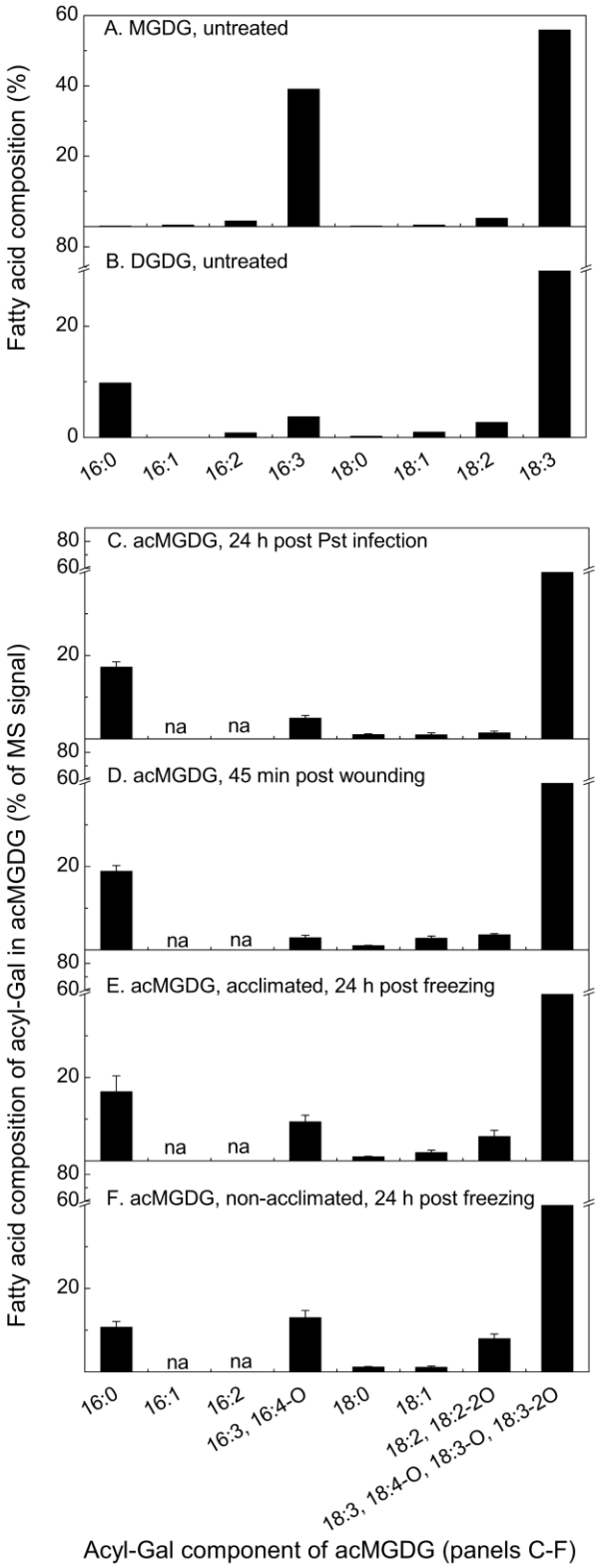
A. MGDG, untreated
B. DGDG, untreated
Fatty acid composition (%)
C. acMGDG, 24 h post Pst infection
D. acMGDG, 45 min post wounding
E. acMGDG, acclimated, 24 h post freezing
F. acMGDG, non-acclimated, 24 h post freezing
Fatty acid composition of acyl-Gal in acMGDG (% of MS signal)
na
16:0
16:1
16:2
16:3, 16:4-O
18:0
18:1
18:2, 18:2-2O
18:3, 18:4-O, 18:3-O, 18:3-2O
Acyl-Gal component of acMGDG (panels C-F)

Figure 3.6 Levels of oxidized MGDG, DGDG, and acMGDG, measured by Pre 277.2 (18:3) and Pre 291.2 (18:4-O) using direct infusion ESI triple quadrupole MS in negative mode. Levels of lipids were measured at various time points after wounding was performed at 0 h (squares). Data denoted by circles show levels of lipids after a second wounding at the 24 h time point of the first wounding, and data denoted by triangles show levels of lipids after a second wounding at the 48 h time point of the first wounding. The x-axis indicates time (h) starting from the only wounding event (squares) or final wounding event (circles and triangles). Y axes are mass spectral signal for the indicated compound, where 1 is the amount of signal detected for 1 nmol of internal standard (18:0/16:0 MGDG), The y axes have different scales. Error bars are standard deviation, n = 5.

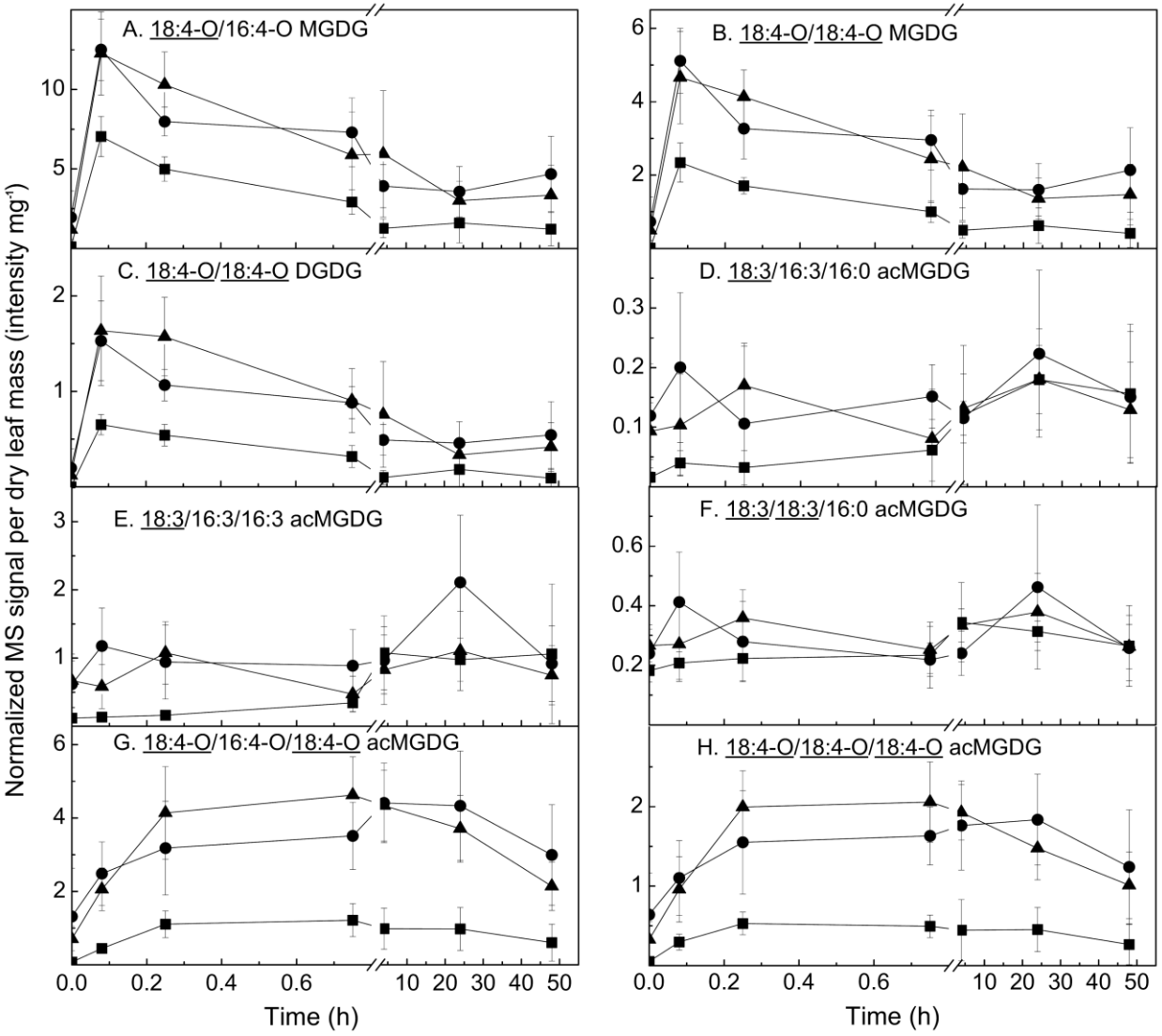

Table 3.1 NL fragments used to detect acMGDGs by ESI triple quadrupole MS in positive mode

m/z of NL fragment	Fatty acyl chain	Chemical formula of NL fragment
411.3	16:3	$C_{22}H_{37}O_6N$
417.3	16:0	$C_{22}H_{43}O_6N$
425.3	16:4-O	$C_{22}H_{35}O_7N$
439.3	18:3	$C_{24}H_{41}O_6N$
441.3	18:2	$C_{24}H_{43}O_6N$
443.3	18:1, 16:3-2O	$C_{24}H_{45}O_6N$, $C_{22}H_{37}O_7N$
445.3	18:0	$C_{24}H_{47}O_6N$
453.3	18:4-O	$C_{24}H_{39}O_7N$
455.3	18:3-O	$C_{24}H_{41}O_7N$
471.3	18:3-2O, 20:1	$C_{24}H_{41}O_8N$, $C_{26}H_{49}O_6N$
473.3	18:2-2O, 20:0	$C_{24}H_{43}O_8N$, $C_{26}H_{51}O_6N$

Table 3.2 Ratio of signals from OPDA/18:3 in galactolipids of *Arabidopsis thaliana.*

Total OPDA-containing MGDG and DGDG (normalized mass spectral signal unit per dry leaf mass), measured by scanning Pre 291.2 in negative mode (complete data in Table S3.6), are shown in the second column. Col-0 was subjected to Pst infection ("Pst, 24 h", n = 5), freezing and post-freezing at 21 °C with or without prior cold acclimation ("acclimated, 24 h" or "non-acclimated, 24 h", n = 6), and wounding ("wounded, 45 min", n = 5). C24 was also wounded and sampled after 45 min ("wounded, 45 min", n = 5). The third through fifth columns indicate the ratio of signals derived from OPDA to signals derived from 18:3 in acyl chains of MGDG, acyl chains of DGDG, or from the acyl chain on the Gal of acMGDG. Errors are standard deviation.

Treatment	**OPDA-containing MGDG and DGDG (intensity mg^{-1})**	**Ratio of OPDA/18:3 signals**		
		in MGDG	**in DGDG**	**on Gal of acMGDG**
Col-0, untreated	0.02 ± 0.01	0.0005 ± 0.0002	0.0049 ± 0.0005	5.39 ± 3.50
Col-0, Pst, 24 h	0.81 ± 0.15	0.022 ± 0.006	0.041 ± 0.010	5.82 ± 1.95
Col-0, acclimated, 24 h	0.013 ± 0.013	0.0006 ± 0.0010	0.0008 ± 0.0006	0.51 ± 0.36
Col-0, non-acclimated, 24 h	0.017 ± 0.009	0.0092 ± 0.0080	0.0080 ± 0.0070	0.063 ± 0.017
Col-0, wounded, 45 min	1.26 ± 0.23	0.0085 ± 0.0053	0.022 ± 0.011	24.1 ± 6.5
C24, untreated	0.17 ± 0.07	0.0004 ± 0.0003	0.0027 ± 0.0026	0.39 ± 0.21
C24, wounded, 45 min	0.26 ± 0.13	0.0013 ± 0.0007	0.0058 ± 0.0018	0.56 ± 0.07

Supplemental Data

Supplemental data for this chapter include:

Figure S3.1 Tentative structure of 18:3/18:3/18:3 acMGDG detected in wounded wheat leaves

Figure S3.2 Acclimated and non-acclimated *Arabidopsis thaliana* Col-0 after freezing at -8 °C for 2 h

Figure S3.3 Total free OPDA and JA after wounding and re-wounding of Col-0 plants

Tables S3.1-S3.6 are in a separate Excel file

Table S3.1 DAG fragments of acMGDG determined during NL scanning by ESI triple quadrupole mass spectrometry in positive mode using scan modes listed in Table 3.1

Table S3.2 Levels of acMGDG detected by NL scans of individual replicates (in normalized mass spectral signal unit mg-1 leaf dry mass)

Table S3.3 Accurate masses of acyl groups of acMGDG from wounded Col-0, tomato and wheat provided by Q-TOF mass spectrometry in negative mode

Table S3.4 Levels of normal chain phospholipids and galactolipids detected by triple quadrupole mass spectrometry (in nmol mg-1 leaf dry mass), performed as described in Xiao et al. (2010, supplemental data)

Table S3.5 Estimation of fatty acid composition in MGDG and DGDG

Table S3.6 Levels of 18:4-O- and 18:3-O-containing MGDG, DGDG, and phosphatidylglycerol (PG) detected by Pre scans of 291.2, 293.2 and 295.2 in negative mode, as described by Vu et al. (2012)

Figure S3.1 Tentative structure of 18:3/18:3/18:3 acMGDG detected in wounded wheat leaves.

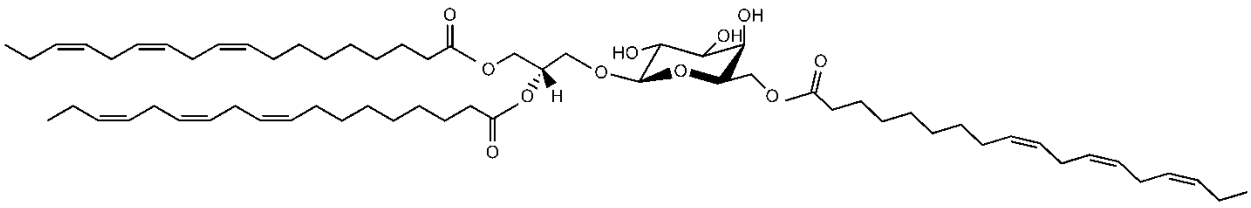

Figure S3.2 Acclimated and non-acclimated *Arabidopsis thaliana* Col-0 after freezing at -8 °C for 2 h. Numbers on the left indicate time (h) at 21 °C after freezing treatment.

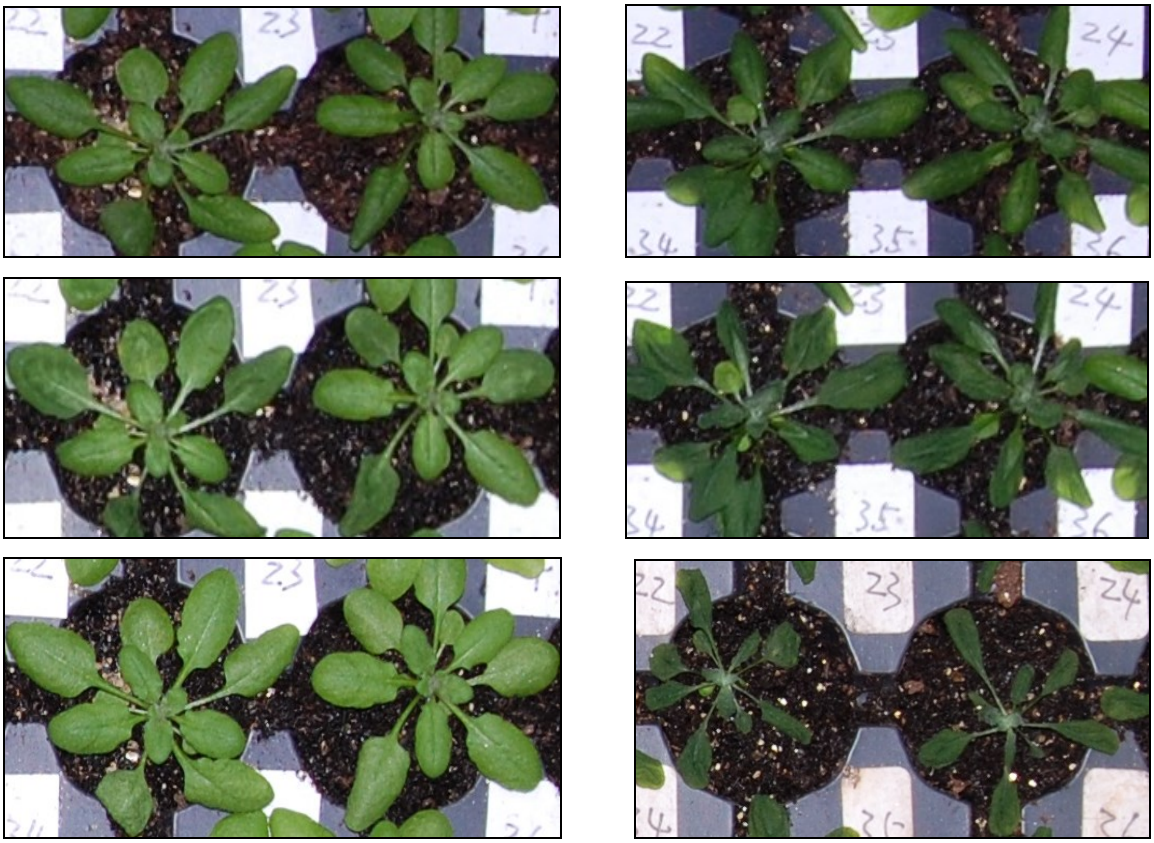

Figure S3.3 Total free OPDA and JA after wounding and re-wounding of Col-0 plants. A: total free OPDA, B: total free JA in ng/mg of leaf fresh weight. Total OPDA is sum of *cis*- and *trans*-OPDA. Total JA is sum of *cis*- and *trans*-JA.

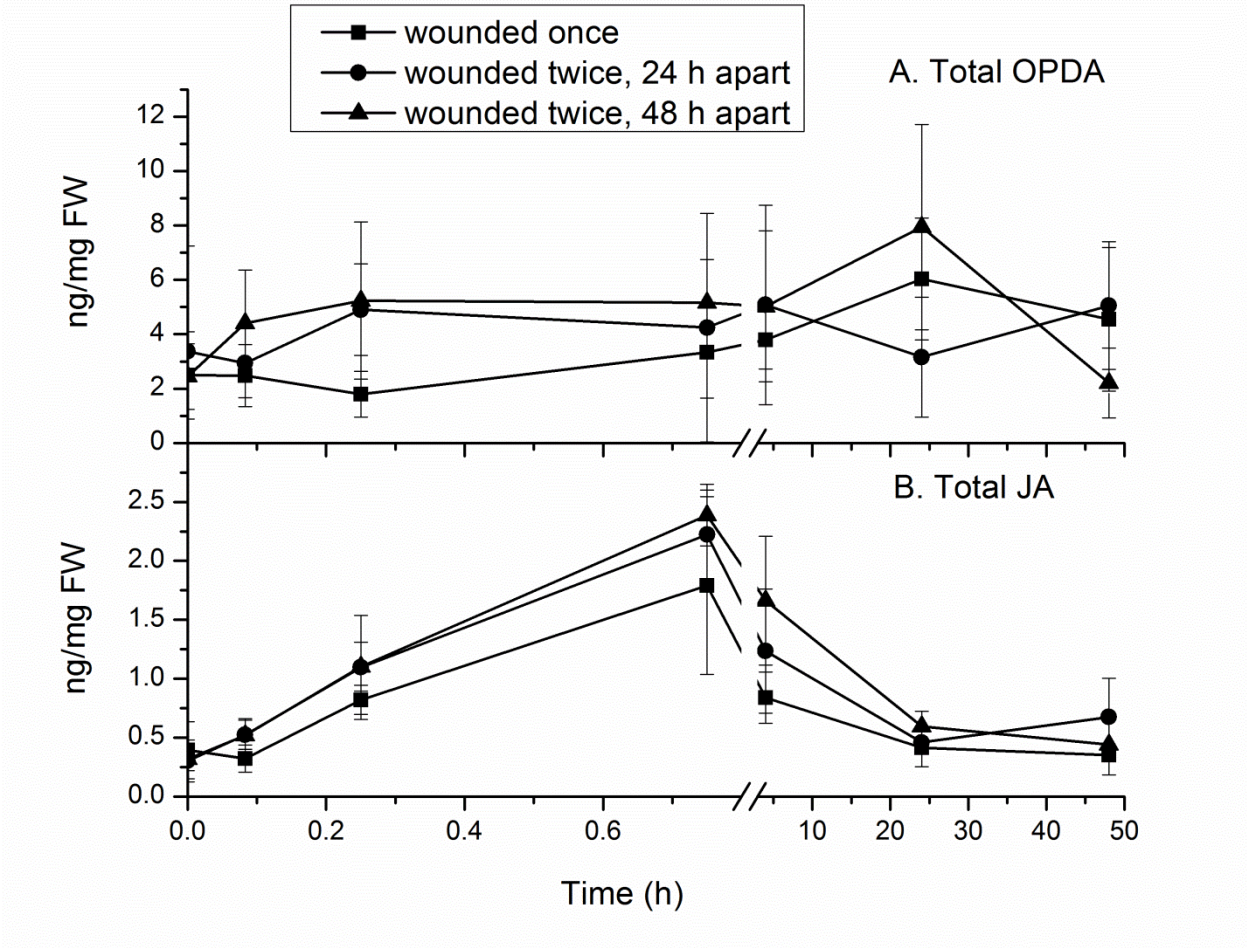

Chapter 4 - Lipid changes after leaf wounding in *Arabidopsis thaliana*: Expanded lipidomic data form the basis for lipid co-occurrence analysis

Abstract

A direct-infusion electrospray ionization triple quadrupole mass spectrometry method with multiple reaction monitoring (MRM) was employed to measure 272 lipid analytes extracted from leaves of *Arabidopsis thaliana* subjected to mechanical wounding. The lipid classes analyzed comprised galactolipids and phospholipids (including monoacyl molecular species, molecular species with oxidized acyl chains, phosphatidic acids (PAs), tri-and tetra-galactosyldiacylglycerols (TrGDGs and TeGDGs), head-group-acylated galactolipids, and head-group-acylated phosphatidylglycerol (acPG), sulfoquinovosyldiacylglycerols (SQDGs), sphingolipids, di- and tri-acylglycerols (DAGs and TAGs), and sterol derivatives. Of the 272 lipid analytes, 256 changed significantly in response to wounding. In general, levels of structural lipids decreased, whereas monoacyl molecular species, galactolipids and phosphatidylglycerols (PGs) with oxidized fatty acyl chains, PAs, TrGDGs, TeGDGs, TAGs, head-group-acylated galactolipids, acPG, and some sterol derivatives increased, many transiently. The observed changes are consistent with activation of lipid oxidizing, hydrolyzing, glycosylating, and acylating activities in the wounding response. Correlation analysis of the levels of lipid analytes across individual control and treated plants was used to construct a lipid dendrogram and to define clusters and sub-clusters of lipid analytes, each composed of a group of lipids which occurred in a coordinated manner. Current knowledge of metabolism supports the notion that observed sub-clusters comprise lipids generated by parallel metabolism or formed from sub-cluster members by a non-rate-limiting process. This work demonstrates that co-occurrence analysis, based on correlation of lipid levels among plants, is a powerful approach to defining lipids generated *in vivo* by identical or inter-twined enzymatic pathways.

Introduction

As lipid biochemists have long known, and computational biologists have recently confirmed, lipid metabolism contains more than its share of reactions catalyzed by enzymes with broad substrate selectivity, i.e., those that act on more than one substrate and produce multiple products (Carbonell et al., 2011). Indeed, knock-out or suppression of single genes has indicated that, during stress responses in plants, individual lipid-metabolizing enzymes act on multiple substrates and produce multiple products (e.g., Welti et al., 2002; Peters et al., 2010). On the other hand, application of stress to a plant activates multiple metabolic pathways. In lipid metabolism, wounding stress causes phospholipase D activation, phospholipase A activation, oxidation of fatty acids on galactolipids, and head-group acylation of monogalactosyldiacylglycerols (Narváez-Vásquez et al., 1999; Zien et al., 2001; Ryu et al., 2004; Buseman et al., 2006; Vu et al., 2014). Steuer et al. (2003) observed that individual plants under the same treatment show small biological variations in the rate and extent of activation of various metabolic pathways. Taken together, current knowledge suggests that (1) when a stress is applied, plant lipid composition will change due to activation of an array of enzymes, (2) under each treatment condition, individual plants will vary slightly in lipid composition, due to varied responses of individual pathways, and, (3) in most cases, activation of a pathway will result in simultaneous change in members of a group of lipids that represent substrates or products of the activated pathway.

Lipidomic analysis can be employed to reveal the levels of plant lipid molecular species. In the current work we have developed a direct-infusion electrospray ionization (ESI) triple-quadrupole mass spectrometry (MS) method to analyze a wide array of lipid species, with a focus on ability to analyze compositional patterns of lipids among individual plants and during stress. This approach provides good sensitivity and precision.

We predicted that lipid intermediates or products produced by the same enzyme(s) or pathway would co-occur when their metabolic pathway is activated and/or repressed in individual plants. Using tools developed for metabolomics and drawing on recent thinking about the use of metabolite level correlations to further understanding of metabolism (Camacho et al., 2005; Xia et al., 2009 and 2012; Toubiana et al., 2013), lipidomic data were analyzed to reveal lipid groups

defined by co-occurrence through stresses and among individual plants. The relationships between the revealed co-occurring groups and known plant lipid metabolism were examined.

Results

Plant wounding

To test the hypothesis described in the Introduction, we conducted a leaf-wounding experiment. Wild-type Arabidopsis (accession Columbia-0) plants were wounded with a hemostat by crimping twice across the mid-vein of three leaves. Wounded leaves were harvested 45 min and 6 h after wounding as were the leaves in the same position on unwounded control plants (n = 31 for each treatment group). Wounding at this level produces ion leakage (Figure S4.1) and an increase in expression of genes encoding enzymes involved in production of oxidized fatty acids (*ALLENE OXIDE SYNTHASE* (*AOS*) and *LIPOXYGENASE2* (*LOX2*); Figure S4.2a and b), but the leaves undergo recovery, as indicated by reduced ion leakage at 24 h (Figure S4.1). Some crimped leaf areas appear to heal, while marks remain visible in other areas at 24 h (Figure S4.3). All leaves remain green, and improvement in appearance is apparent within 24 h after wounding (Figure S4.3).

Extraction of leaves

Because our goal is to apply lipidomics in a high-throughput manner and because extraction can be a time-consuming part of lipid analysis, a streamlined extraction method was developed. After quenching of potential phospholipase D activity by immersion of leaves harvested 45 min after wounding in hot isopropanol for 15 min, a polar solvent mixture was added. After shaking for 24 h and removing the leaves, the extract was subjected to mass spectral analysis. Comparison with a modified Bligh-Dyer method (Bligh and Dyer, 1959; Welti et al., 2002) and a Bligh-Dyer type extraction, followed by additional extraction targeted at sphingolipids (Toledo et al., 1995; Markham et al., 2006), showed that the three methods each extracted similar amounts of lipid and there was only minor variation in the composition of lipids extracted by the three methods (Table 4.1 and full data set in Table S4.1).

MS analysis of lipids

To analyze stress-induced Arabidopsis leaf lipids, a direct-infusion ESI triple quadrupole MS method with MRM was developed. Each lipid analyte is defined by its mode of analysis (positive or negative), its intact ion mass/change (*m/z*), and a fragment *m/z*; an arbitrary "lipid number" corresponds to the set of parameters used in the analysis. Each analyte has been annotated, based on available information; information supporting annotations (accurate mass and LC-MS data indicating the presence of the annotated lipids in Arabidopsis thaliana tissues) is compiled in Table S4.2. Supporting quadrupole time-of-flight (QTOF) MS data not previously published are provided in Table S4.3. Abbreviations used in lipid annotations are summarized in Table 4.2, and examples of possible structures for oxidized fatty acid chains are provided in Table S4.4. MS settings for each analyte are also listed in Table S4.2. Some analytes have multiple annotations because a triple quadrupole MS, in direct infusion mode, is unable to differentiate compounds and fragments with the same nominal *m/zs*. Available data provide confidence that the vast majority of the annotations are correct, i.e., the annotation(s) indicates the major lipid(s) detected by the stated MS settings.

Infusion profiles of representative lipid analytes showed that the detected intensity varied somewhat as a function of infusion time (Figure S4.4). Some analytes, particularly negatively charged lipids including PA and phosphatidylserine (PS), were relatively retained in the loop and/or tubing, but elution of all analytes was essentially complete within 15 min of the start of infusion. To avoid variation in analyte levels due to uneven infusion, the MRM transition intensity for each analyte was acquired repeatedly throughout the entire infusion period and the intensities were averaged. Separate infusions were made for acquisition in the negative and positive modes, because initial experiments indicated that it took several seconds after mode switching for the intensity to stabilize. Infusion of a single plant extract took 35 min: a 15 min infusion in positive mode with 2.5 min of washing, followed by a 15 min infusion in negative mode with 2.5 min of washing.

Intensities were normalized to internal standards analyzed by the same method as the lipid analytes. Instrumental parameters for the internal standards are indicated in Table S4.5, and Table S4.2 indicates the internal standard(s) used for normalization of each analyte. Background

values for each lipid analyte were calculated in samples of the internal standards alone and subtracted from values in samples containing plant lipids.

The goal of the quantification was to compare levels of each lipid analyte in various plant samples, rather than to compare various lipid levels with each other. Absolute analyte levels are unreliable due to the limited number of internal standards and the variations in instrumental parameters among analytes and internal standards. In many cases, analyte intensities were normalized to intensities of standards of substantially different structure. To assure consistent data for each analyte throughout long periods of mass spectral data collection, an adaptation of the "quality control" approach suggested by Dunn et al. (2011) was employed. Representative samples from all treatments were pooled. The pooled sample, called the quality control (QC) sample, was analyzed recurrently among the experimental samples (Table S4.6). The QC analyte intensities were used to normalize the intensities in the experimental samples, as described in Experimental Procedures. Data for the lipid analytes are presented as (1) normalized intensity per mg of leaf dry mass, where a value of 1 corresponds to the same amount of intensity as derived from 1 pmol of internal standard(s) and (2) autoscaled values, produced by dividing the difference between an intensity and the mean intensity of the 93 samples by the standard deviation of the intensity of the 93 samples (Xia et al., 2009; 2012). The autoscaled values allow easy comparison of lipid levels across various samples, because all analytes can be plotted on similar scales, but do not provide information about the absolute lipid levels.

In total, the intensities of 377 MRM transitions were quantified and measurements of 272 of these lipid analytes are described here. Of these, 268 represent unique analytes, whereas four represent the same lipid measured with different instrument parameters. Each lipid analyte described in this work met the following criteria: (1) the background MRM intensity (in the internal standard-only samples) was less than 40% of the average intensity of the QC samples; and (2) the coefficient of variation, i.e., the standard deviation divided by the mean of the level of the analyte in the (identical) QC samples, was less than 20%. Coefficients of variation for individual analytes are shown in Table S4.2.

Variations in lipid analytes among individual plants and in response to wounding treatment

The full set of data for lipid analyte levels in normalized intensity per mg of leaf dry mass and as autoscaled values is provided in Tables S4.6 and S4.7. Original and autoscaled data of each lipid analyte are plotted as a function of wounding treatment (Figure S4.5). Of the 268 unique lipid analytes, 256 were significantly different in at least one of the three pairwise comparisons by ANOVA ($p < 0.01$) (Table 4.3 and Table S4.9). Tukey's post-hoc test indicates that 143 lipids were significantly different in all three pairwise comparisons and 74 lipids in comparisons between both "Wounded; 45 min" versus "Unwounded" and "Wounded; 6 h" versus "Unwounded" (Table 4.3).

The autoscaled lipid levels of individual samples are displayed as a heat map in Figure 1, and the levels of 10 lipid analytes as a function of autoscaled levels are shown in Figure 4.2. The data in Figures 4.1 and 4.2 both show that variation in lipid levels was observed in samples subjected to the same treatment, in most cases, as well as among treatments. To test the hypothesis that variation in lipid levels is due to increased or decreased activities of specific lipid pathways in individual plants and that analysis of the lipidomic data can reveal groups of lipids defined by lipid co-occurrence, correlations in the levels of the lipid analytes were determined. Spearman's correlation coefficient, ρ, was calculated for each lipid analyte with each other lipid analyte across all 93 lipid samples, including 31 samples subjected to each treatment (unwounded, wounded and harvested after 45 min, and wounded and harvested after 6 h) (Table S4.10). Spearman's correlation coefficient can range from -1 (perfect negative correlation) to 1 (perfect positive correlation) with 0 indicating no correlation.

Levels of every lipid analyte were positively correlated with the levels of at least one other lipid analyte. Of the 268 unique analytes, 264 were correlated with another lipid with a $\rho > 0.60$. By matching each lipid analyte with the one to which it was most highly correlated, a dendrogram was constructed (Figure 4.3). The dendrogram includes seven clusters of lipids, labeled A-G, corresponding to groups in which every lipid is correlated with another lipid with $\rho > 0.80$. Two of the clusters, A and C, are large, and contain 60 and 146 lipid analytes, respectively. Comparison of various correlation "cutoffs" in light of understanding of metabolism (described

in the Discussion) indicated that, within these clusters, lipids that were likely to be metabolically related were those with the highest correlation values, i.e., $\rho > 0.96$. There are 6 sub-clusters (A1-A6) in A with lipids with $\rho > 0.96$. Within C, there are 12 such sub-clusters (C1-C12).

Cluster A contains structural (i.e., membrane) lipids that are decreased as a function of wounding treatment (Figures 4.2 and S4.5, Table 4.3). These include normal chain species of DGDG, MGDG, GlcCer, GIPC, PC, PE, PG, and SQDG. Cluster B contains 3 PE species containing a normal acyl chain and 18:3-O. These analytes exhibited no change in response to wounding at 45 min but decreased at 6 h post-wounding. Cluster C contains many lipids induced by wounding. These include monoacyl lipids, including DGMGs, MGMGs, LPCs, and LPEs. Cluster C also contains head group-acylated galactolipids, acMGDG and acDGDG, as well as the only acPG species that was measured. DAG, TAG, and PA species are located in Cluster C, as are poly-galactosylated lipids, TrGDG and TeGDG. A large portion of the galactolipid analytes (acDGDG, acMGDG, DGDG, DGMG, MGDG, and MGMG) in Cluster C contains oxidized fatty acyl chains, whereas only 5 phospholipids with oxidized fatty acyl chains, i.e., PC(16:0/18:3-2O), PE(18:3/18:3-2O), PG(18:3-O/16:0), PG(18:4-O/16:0), and PG(18:4-O/16:1), fell within Cluster C. Cluster C contains several normal diacyl lipids that are likely to contain 16:3. These lipids include DAG(34:6), PA(34:6), PC(34:6), PC(32:3), and PE(32:3). Finally, Cluster C contains sterol glucosides and acyl sterol glucosides. Cluster D consists of sterol esters that change little in response to wounding. Cluster E contains two PCs with long acyl chains, PC(40:2) and PC(40:3), while Cluster F consists of 3 PEs, each with a normal-chain fatty acid and 18:3-3O. Cluster G is composed of PC(34:4) and PE(34:4).

The most highly correlated lipid analyte groups are the 18 sub-clusters, A1-A6 and C1-C12, each of which contains lipids linked by $\rho > 0.96$. Examples showing the correlation of lipid analyte levels in these clusters are provided in Figures 4.4, 4.5 and 4.6, and Figure 4.7 presents boxplots of lipid levels in response to wounding for an example lipid from each of the 18 sub-clusters. Figure 4.4 shows autoscaled values for the lipids in sub-cluster A1 (4.4a), A4 (4.4b), and A5 (4.4c) as a function of individual plant and treatment. Sub-cluster A1 includes PC(32:1) and PE(32:1), which has been identified previously as PE(16:0/16:1) (Samarakoon et al., 2012, Table S4.2). Sub-cluster A4 includes PE species (PE(34:3), PE(36:5) and PE(36:6)), which previous

analysis has shown to contain 18:3 (Welti et al., 2002; Table S4.2). Sub-cluster A5 consists of PC and PE species (PC(34:2), PE(34:2), and PE(36:4)) containing 18:2 (Welti et al., 2002; Table S4.2). Lipid analytes within the same sub-cluster vary similarly across the samples and treatments (Figure 4.4a-c). There is slightly lower co-occurrence when an analyte from each of sub-clusters A1, A4, and A5 is compared (Figure 4.4d). In addition to A1, A4, and A5, A3 is an additional PC-PE sub-cluster, which contains PC species with limited desaturation and which may contain 18:1 and/or 18:2 (Welti et al., 2002; Table S4.2). On the other hand, sub-cluster A2 consists of the incompletely desaturated MGDG species, MGDG(34:4) and MGDG(34:5), whereas A6 is comprised of completely desaturated galactolipid species, DGDG(34:6), DGDG(36:6), and MGDG(34:6). Each sub-cluster within Cluster A thus represents either a PC + PE or MGDG + DGDG group of molecular species related by acyl composition.

Figure 4.5a and 4.5b show sub-cluster C2 (PA(34:6), TeGDG(34:6), and TrGDG(34:6)) and sub-cluster C9, which includes PA(34:2), PA(34:3), PA(36:2), PA(36:3), PA(36:4), PA(36:5), and PA(36:6). The analytes within each of these sub-clusters are closely correlated, but these sub-clusters are not well correlated to each other, as illustrated by comparison of levels of PA(34:6) from sub-cluster C2 and PA(36:6) from sub-cluster C9 (Figure 4.5c). Figure 4.6a, 4.6b, and 4.6c depict the changes in sterol glucosides and acyl sterol glucosides of sub-clusters C5, C7, and C8. Again, these show a higher level of in-sub-cluster lipid co-occurence compared with inter-sub-cluster co-occurence (Figure 4.6d).

Overall, sub-clusters in Cluster C are diverse. In addition to previously mentioned sub-clusters, there is a sub-cluster (C4) composed of all four TAG species determined, a sub-cluster of Arabidopsides A and B (MGDG(18:4-O/16:4-O) and MGDG(18:4-O/18:4-O); C6), and 5 sub-clusters containing acDGDG/acMGDG. The five acDGDG/acMGDG sub-clusters (C1, C3, C10, C11, and C12) fall into two groups. Sub-clusters C1 and C3 are moderately related with the highest inter-sub-cluster ρ, ρ(C1,C3), equal to 0.91 and sub-clusters C10, C11, and C12 are closely related with the highest ρs among all 3 sub-clusters falling just short of 0.96. On the other hand, the highest ρ between any lipid in sub-clusters C1 or C3 with one in C10, C11, or C12 is 0.77. There is some potential ambiguity in annotation of the acylated galactolipid sub-clusters, which makes it difficult to fully interpret the sub-clustering. (Note that only one

annotation per lipid is shown in the dendrogram, but complete annotations including alternative interpretations are shown in Tables 4.3 and S4.2) Still, sub-cluster C3 contains some clearly normal-chain acyl species, whereas sub-clusters C10, C11, and C12 contain highly oxidized acylated galactolipids. Figure 4.7g, i, p, q, and r show examples of the patterns of lipid changes during the wounding response for a lipid from each of the 5 acylated galactolipid sub-clusters. The levels of lipids in sub-clusters C1 and C3 continued to rise between 45 min and 6 h post-wounding, while the levels of acylated galactolipids in sub-clusters C10, C11, and C12 were reduced at 6 h compared to 45 min post-wounding.

Discussion

Lipids are modular, with many different molecular species containing the same component acyl chain or head group. This modularity goes hand-in-hand with the promiscuity of lipid-metabolizing enzymes, many of which act on multiple, related substrates. Here, we show that data support the hypothesis that correlation analysis can reveal groups of lipids acted on by the same enzyme(s), using lipidomic data from control plants and plants subjected to wounding. By metabolic control analysis and computer simulation, Camacho et al. (2005) found that many cases of high correlations in the levels of different metabolites among profiles of biological replicate samples are due to control of the metabolite levels by a single enzyme. Based on current knowledge of lipid metabolism, we infer that the highly correlated sub-clusters detected here by correlation analysis ($\rho > 0.96$) may (1) consist of substrates or products of the same enzyme(s), (2) may include a lipid formed from a common starting material by a metabolic branch, and/or (3) may include a lipid formed from another member of the group by a non-rate-limiting process.

Among the sub-clusters, several are likely to be produced by parallel metabolism by the same enzyme. These include the steryl glucosides in sub-cluster C5, which are likely to have been produced by the glycosylation of sterols by UDP-Glc:sterol glycosyltransferase(s) described by DeBolt et al. (2009). It's probable that each of the acyl sterol glucoside sub-clusters (C7 and C8) was formed by parallel acylation of two sterol glucosides with the same acyl chain, although the acylating enzymes acting on sterol glucosides have not been identified. Sub-cluster C9, which

consists of PAs with fatty acids similar to extraplastidic phospholipids, may have been derived largely from the activity of phospholipases D (e.g., Zien et al., 2001; Welti et al., 2002), though it has been suggested that diacylglycerol kinase also can contribute to PA formation in stress conditions (e.g., Arisz et al., 2013). Recent data support the notion that sub-cluster C6 (Arabidopsides A and B) may have been formed by a common enzymatic pathway acting on similar, but distinct, substrates. Nilsson et al. (2012) showed that 18:4-O (oxophytodienoic acid) and 16:4-O (dinor-oxophytodienoic acid) are formed without release of the acyl chains from the galactolipid pool. It follows that the two molecular species in sub-cluster C6 would be formed from the two most abundant MGDG species, MGDG(18:3/16:3) and MGDG(18:3/18:3), by analogous pathways involving oxidation and cyclization of the esterified fatty acyl chains.

The formation of sub-cluster C2, which consists of TrGDG(34:6), TeGDG(34:6), and PA(34:6) likely involves the action of SENSITIVE TO FREEZING 2 (SFR2) (Moellering et al., 2010), a processive galactosylating enzyme that transfers a galactose from MGDGs to successively yield β-linked DGDG, TrGDG, and TeGDG from MGDG. The resulting DAG does not accumulate (Moellering et al., 2010), and while Moellering et al. (2010) provide evidence that TAG may be formed from it, the inclusion of PA(34:6) in the sub-cluster suggests that a DAG kinase may phosphorylate the DAG in a branch step. Several molecular species of TAGs are formed in response to wounding (sub-cluster C4); formation of these TAGs may involve phospholipid:diacylglycerol acyltransferase (PDAT1) (Fan et al., 2013). TAG may serve as a transient buffer for leaf acyl chains present in excess (Troncoso-Ponce et al., 2013). Unfortunately, we did not determine the level of a TAG species containing 34:6 (i.e., 18:3/16:3), which could be derived from MGDG by SFR2.

While all the sub-clusters within Cluster A are quite closely correlated, the components of the four sub-clusters containing PC and PE (A1, A3, A4, A5) and two sub-clusters of MGDG and DGDG (A2, A6) vary in their fatty acyl composition. In the plastid, DGDG is formed from MGDG by a UDP-galactose-dependent DGDG synthase (DGDGS; Kelly and Dörmann, 2002; reviewed in Li-Beisson et al., 2013). Fatty acyl chains can undergo desaturation on either MGDG or DGDG (except that FAD5 acts only on MGDG; Kunst et al., 1989). Sub-cluster A2 includes MGDG species that are not fully desaturated; their co-accumulation may indicate that

the rate of the final desaturation of MGDG acyl chains by FAD7 and/or FAD8 varied among plants and limited the rate of formation of fully desaturated species. Indeed, the level of plastidic trienoic fatty acids is regulated in stress responses and affects the ability of plants to withstand stresses, including cold and bacterial infection (Kodama et al., 1994; Routaboul et al., 2000; Yaeno et al., 2004; Chaturvedi et al., 2008). On the other hand, the occurrence of DGDG(34:6) with MGDG(34:6) in sub-cluster A6 is due to a near-constant ratio of these lipids among plants, suggesting that the conversion of MGDG to DGDG is not rate-limiting. The high correlation coefficients between PCs and PEs with the same acyl chains in sub-clusters A1 and A5 could mean either that the rate of production of acyl-identical PCs and PEs is similar and/or that enzymes involved in PC-PE (inter)conversion, perhaps through a DAG intermediate, function near equilibrium, maintaining a near-constant ratio of acyl-identical PE and PC molecular species (found together in sub-clusters). In pea leaves, PC is labeled from acetate much more rapidly than PE during a 10-min time course, suggesting that PC and PE molecular species with the same acyl chains are unlikely to be formed initially by parallel pathways (Bates et al., 2007), and that it is more likely that PC species are converted to PEs during the wounding experiment.

The modular nature and the typical action of lipid-metabolizing enzymes on multiple substrates may make complex lipids especially amenable to co-occurrence analysis as a mechanism for extending our understanding of compound relationships and metabolism. In the current analysis, acDGDGs, acPG, and many acMGDGs are a large group of lipids that has not been extensively studied. Evidence has been presented that acMGDG is formed by the reaction MGDG + DGDG → acMGDG + DGMG (Heinz, 1967; Heinz, 1972; Vu et al., 2014). The current results show that two groups of acMGDGs are formed with different kinetics. acMGDGs in sub-clusters C10, C11, and C12, most of which are rich in oxidized fatty acids, are formed rapidly (i.e., their levels are high at 45 min) and their levels drop by 6 h post-wounding (Figure 4.7p, 4.7q, 4.7r). Other acMGDGs (sub-clusters C1 and C3; Figure 4.7g, 4.7i), including all quantified molecular species unambiguously annotated as having entirely normal-chain fatty acids (acMGDG(16:0/34:6), acMGDG(16:3/34:6), acMGDG(18:2/34:6), acMGDG(18:3/34:6)), were formed more slowly, with levels considerably higher at 6 h than at 45 min. A similar phenomenon was observed previously when galactolipids containing two oxidized acyl chains accumulated much faster in response to wounding than galactolipids with a single oxidized acyl

chain (Buseman et al., 2006). Thus, the acMGDG pool reflects the diacyl species that serve as substrates for acMGDG formation; however, oxidized chains are concentrated in the acMGDG pool (Vu et al., 2014). Still, the mechanism for the rapid rise and decline in species containing two oxidized chains and the identity of the acylating enzyme(s) forming the head-group-acylated molecular species remains unknown. Additionally, the placement of a number of analytes that are not obviously structurally similar in sub-clusters C1 and C3 provides a catalyst for future reassessment of the tentative annotations.

In the current work, we have developed an MS-based analytical approach targeting a wide range of lipid molecular species. The current approach has demonstrated that levels of lipids differed among individual Arabidopsis plants, and levels of nearly all of the lipids in wild-type plants changed in response to wounding, with normal-chain "traditional" structural lipids decreasing and many other lipids increasing. The analytical precision was sufficient for a number of lipid species to be clustered based on co-occurrence among individual plants and across the stress conditions. The levels of seventy-nine percent of the lipid analytes were correlated with $\rho > 0.80$ with at least one other analyte, placing them in a lipid cluster, and 24% of the lipids were correlated with $\rho > 0.96$, placing them in a sub-cluster. While lack of high correlation can be due to either excessive analytical variation or true lack of co-occurrence, interpretation of the lipid analytical results in light of knowledge of lipid metabolism demonstrates that high positive correlation reflects metabolic relationships. At the current stage of plant lipidomic development, careful and highly replicated MS analysis can provide large amounts of information about lipid dynamics in plants under stress. The current work highlights the value of co-occurrence analysis in defining groups of metabolically-related lipids. Undoubtedly, application of co-occurrence analysis to additional lipids and to plants subjected to other perturbations will provide further metabolic insight.

Experimental procedures

Plant material, growth, and wounding treatment

Plant material and growth are described in Method S4.1. For the wounding treatment, a hemostat was used to wound leaves number 5, 6, 7 and 8 of 30-day-old plants across the mid-vein, twice

and about 6 mm apart. Leaf numbers were determined as described by Telfer et al. (1997). Leaves 6, 7, and 8 were harvested 45 min or 6 h after being wounded. For the control, leaves 6, 7, and 8 were harvested from unwounded plants. For the extraction test, fifteen plants were harvested 45 min after wounding. For the main experiment, thirty-two samples (one each from 32 plants) were collected for each of the two wounding treatments and for control plants. Each sample for lipid analysis corresponded to the three harvested leaves from one plant. In the main experiment, one sample in each treatment group (i.e., sample 23) was removed from the analysis due to technical problems; thus, n for each group is 31. The extraction test and the main experiment were performed on separate sets of plants.

Lipid extraction

In the main experiment, harvested leaves number 6, 7, and 8 were immediately dropped into 4 ml of isopropanol with 0.01% butylated hydroxytoluene (BHT) at 75°C in a 20-ml EPA vial with Teflon-lined screw-cap (Thermo Fisher Scientific, Inc., thermofisher.com). Vials were kept at 75°C for 15 min to deactivate lipid-hydrolyzing enzymes. Vials were cooled to room temperature and stored overnight at -80°C before adding 12 ml of chloroform: methanol: 300 mM ammonium acetate in water (30:41.5:3.5, v/v/v) and shaking at 100 rpm on an orbital shaker for 24 h at room temperature. Extracted leaves were transferred to a new vial and dried overnight at 105°C. The extract was stored at -80°C. Dried extracted leaves were cooled and weighed on a balance with 2 µg detection limit (Mettler Toledo, mt.com). The precision and accuracy of the balance were previously described (Vu et al., 2012). For the extraction test, 5 leaves harvested 45 min after wounding were extracted as just described (Method 1), 5 leaves were extracted as described by Welti et al. (2002; Method 2), and 5 leaves were extracted as described by Welti et al. (2002), skipping the backwash steps, followed by 4 extractions with "Solvent H" (lower phase of isopropanol/hexane/water, 55:20:25, v/v/v; Toledo et al., 1995, Markham et al., 2006; Method 3).

Lipid profiling by ESI triple quadrupole MS

To prepare analytical samples for mass spectrometry, from each sample, the volume corresponding to 0.04 mg extracted leaf dry mass was determined and that volume of sample was

transferred to a 2-ml amber vial, containing 20 µl of internal standard mix. Components of the internal standard mix are listed in Table S4.5. Isopropanol: chloroform: methanol: 300 mM ammonium acetate in water (25: 30: 41.5: 3.5, v/v/v/v) was added to make the total volume 1.4 ml. The vial was sealed with a snap-cap with a crisscross, pre-slit septum.

Quality control (QC) samples were prepared for data normalization by first pooling 300 µl of extract from samples 1-9 from each treatment (unwounded, wounded 45 min, and wounded 6 h) to make a QC stock solution. Based on the dry leaf mass of the samples used to make the combined extract, the concentration was calculated to be 0.40 mg (of leaf dry mass) ml-1 (8.1 ml total volume). To prepare working QC samples, the internal standard mixture was added and the stock was diluted, so that each working QC sample contained lipid extract corresponding to 0.04 mg combined leaf dry mass, 20 µl of the internal standard mix (as used in the other samples), and mass spectrometry solvent (isopropanol: chloroform: methanol: 300 mM ammonium acetate in water, 25: 30: 41.5: 3.5, v/v/v/v) in 1.4 ml. The QC mass spectrometry samples were labeled "QC1" to "QC39", stored at -80°C, and brought to room temperature 1 h before analysis. Analytical samples and QC samples from the main experiment were arranged in a VT 54 rack as shown in Table S4.6. For the lipid extraction test, the same analytical set-up was used.

Data were acquired with a Xevo TQ-S mass spectrometer (Waters Corporation, waters.com) equipped with an ESI source operating in direct infusion mode. Each sample was infused twice, once to acquire positive and once for negative multiple reaction monitoring (MRM) transitions. Samples were injected into a 300-µl PEEK sample loop with a 2777 autosampler (Waters Corporation). To make sure the loop was completely filled, the injection volume was set at 400 µl. The sample in the loop was infused to the mass spectrometer with an Acquity pump (Waters Corporation) controlled by an "inlet method" in MassLynx (software from Waters Corporation). Each inlet method was 17.5 min with solvents and flow rates as follows: from 0 to 11 min, methanol at 0.03 ml min-1; from 11 to 15 min, methanol at 0.09 ml min-1; from 15 to 17 min, methanol: acetic acid (9: 1, v/v) at 0.5 ml min-1; from 17 to 17.1 min, 17.1 to 17.2 min, 17.2 to 17.3 min, 17.3 to 17.4 min, and 17.4 to 17.5 min, methanol at 0.4, 0.3, 0.2, 0.1, and 0.03 ml min-1, respectively. The mass spectrometer acquired data from 0 to 15 min. The positive mode and negative mode data acquisition methods had 13 and 7 functions, respectively. Every function

acquired data on lipid analytes and internal standard components in MRM mode throughout the 15 min. Each function contained from 12 to 28 transitions which were allocated the same dwell time. In the positive mode, 130-131 scans (cycles) and, in the negative mode, 38 scans of each function were performed (Table S4.2). Parameters for each MRM transition are listed in Table S4.2 for the plant lipid analytes and in Table S4.5 for the internal standards. Other mass spectrometry parameters are indicated Method S4.4.

Samples were analyzed at the rate of 1 tray (Table S4.6) per day with a total daily analysis time of 22.75 h. Each day, a cleaned source cone was installed and an Xpertek 0.5-µm PEEK filter (P.J. Cobert Associates, Inc., cobertassociates.com) in the line between the autosampler and source was changed.

Data processing and calculation of normalized lipid intensities

"Spectrum Combine" software (a process file called SpectrumCombine_4p0p0) and a parameter file, custom-developed by Iggy Kass (Waters Corporation), was employed to process and export MassLynx data to Excel. MRM scans were combined by averaging the scans for each MRM channel within each function before export. Exported data were processed in an in-house Excel template in which the data from all samples (i.e., QC, "internal standard only", and analytical samples) were isotopically deconvoluted. The intensity per nmol of each internal standard in each sample was calculated; these values for internal standards for the same class were averaged. The deconvoluted data for each lipid were normalized to the internal standard(s) of the same lipid class (if possible) or another lipid class analyzed under similar experimental conditions (in cases where an appropriate internal standard was not available). The internal standard used for normalization of each MRM signal is indicated in Table S4.2.

Once normalized intensities were calculated, the average level of the background, as indicated by the average of the "internal standard only" samples from that tray, was subtracted from every other sample in the tray. An adaptation of the method of Dunn et al. (2011) was used to assure that the data could be compared throughout extended acquisition periods. The values for the first 5 QC samples in each set of analytes (Table S4.6) were eliminated, due to potential instrument

instability when the instrument is first started after installation of a cleaned cone. To correct for any drift during acquisition of each tray's data, a trend line was constructed of the intensity data for each lipid in the remaining 8 identical QC samples as a function of vial position number in the tray. Each lipid intensity in each analytical sample was multiplied by the average of that lipid's level in the QC samples on that tray divided by the level of the lipid on the QC trend line at the sample's vial position. To correct for any variability across different trays (days), the trend-corrected value of each lipid in each sample was multiplied by the average of the QC values for that lipid from the entire acquisition process divided by the average of that lipid's level in the QC samples on the sample's own tray. After calculation of the lipid levels in each sample, the values were divided by the dry mass of the sample analyzed (0.04 mg).

The lipid values are normalized intensity per mg leaf dry mass, where a value of 1 is the intensity of 1 pmol of internal standard. Because the internal standards were not uniformly well-matched to the lipids analyzed (some differ in class; many differ substantially in m/z), the absolute values of the analytes provide only a rough guide to absolute amount of each lipid.

Statistical analysis and figure and table production

Auto-scaling and analysis of variance (ANOVA) with Tukey's post hoc tests were performed (Table S4.9), and the heat map (Figure 4.1), correlation table (Table S4.10), and Figure S4.5 were produced using utilities at the Metaboanalyst website (metabolanalyst.ca; Xia et al., 2009 and 2012). Autoscaling allows easy comparison of patterns of the levels of different lipids across samples. The autoscaled value of a lipid in a sample is equal to: [(the original value of the lipid in the sample) – (the average value for that lipid among all samples)] divided by (the standard deviation for that lipid among all samples). Figures 4.2, 4.4, 4.5, 4.6, and 4.7 were produced using Origin 8.5 (OriginLab Corporation, originlab.com). Clustering was performed using Cluster 3.0 (Eisen et al., 1997). The output was imported to Dendroscope (Huson et al., 2007; Huson and Scornavacca, 2012) to produce the dendrogram, which was modified in color.

Acknowledgements

The authors thank Iggy Kass of Waters Corporation for writing the program to export data from MassLynx, and Samantha Elledge, Laura Welti, Cong Tuan Son Van, and Haibao Tang for help in production of the figures. This material is based upon work supported by the National Science Foundation under Collaborative Research Grant Nos. MCB-0920663 (to RW and GG), MCB-0920600 (to XW), and MCB-0920681 (to JS). The mass spectrometers used in the analyses were acquired with NSF funding under Grant Nos. DBI-1228622, DBI 0521587, and EPS 0236913. Contribution no. 14-244-J from the Kansas Agricultural Experiment Station.

References

Arisz SA, van Wijk R, Roels W, Zhu JK, Haring MA and Munnik T (2013) Rapid phosphatidic acid accumulation in response to low temperature stress in Arabidopsis is generated through diacylglycerol kinase. Front Plant Sci. 4, 1. doi: 10.3389/fpls.2013.00001

Bates PD, Ohlrogge JB and Pollard M (2007) Incorporation of newly synthesized fatty acids into cytosolic glycerolipids in pea leaves occurs via acyl editing. J. Biol. Chem. **282**, 31206-31216.

Bligh EG and Dyer WJ (1959) A rapid method of total lipid extraction and purification. Can. J. Biochem. Physiol. **37**, 911-917.

Buseman CM, Tamura P, Sparks AA, Baughman EJ, Maatta S, Zhao J, Roth MR, Esch SW, Shah J, Williams TD and Welti R (2006) Wounding stimulates the accumulation of glycerolipids containing oxophytodienoic acid and dinor-oxophytodienoic acid in Arabidopsis leaves. Plant Physiol. **142**, 28-39.

Camacho D, Fuente A and Mendes P (2005) The origin of correlations in metabolomics data. Metabolomics **1**, 53-63.

Carbonell P, Lecointre G and Faulon J-L (2011) Origins of specificity and promiscuity in metabolic networks. J. Biol. Chem. **286**, 43994-44004.

Chaturvedi R, Krothapalli K, Makandar R, Nandi A, Sparks AA, Roth MR, Welti R and Shah J (2008) Plastid omega3-fatty acid desaturase-dependent accumulation of a systemic acquired resistance inducing activity in petiole exudates of Arabidopsis thaliana is independent of jasmonic acid. Plant J. **54**, 106-117.

DeBolt S, Scheible WR, Schrick K, Auer M, Beisson F, Bischoff V, Bouvier-Navé P, Carroll A, Hematy K, Li Y, Milne J, Nair M, Schaller H, Zemla M and Somerville C (2009) Mutations in UDP-Glucose:sterol glucosyltransferase in Arabidopsis cause transparent testa phenotype and suberization defect in seeds. Plant Physiol. **151**, 78-87.

Dunn WB, Broadhurst D, Begley P, Zelena E, Francis-McIntyre S, Anderson N, Brown M, Knowles JD, Halsall A, Haselden JN, Nicholls AW, Wilson ID, Kell DB, Goodacre R and Human Serum Metabolome (HUSERMET) Consortium. (2011) Procedures for large-scale metabolic profiling of serum and plasma using gas chromatography and liquid chromatography coupled to mass spectrometry. Nat. Protoc. **6**, 1060-1083.

Eisen MB, Spellman PT, Brown PO and Botstein D (1997) Cluster analysis and display of genome-wide expression patterns. Proc. Natl. Acad. Sci. USA **95**, 14863-14868.

Fan J, Yan C and Xu C (2013) Phospholipid:diacylglycerol acyltransferase-mediated triacylglycerol biosynthesis is crucial for protection against fatty acid-induced cell death in growing tissues of Arabidopsis. Plant J. **76**, 930-942.

Heinz E. (1967) On the enzymatic formation of acyl galactosyldiglyceride. Biochim. Biophys. Acta **144**, 333–343.

Heinz E. (1972) Some properties of the acyl galactosyl diglyceride-forming enzyme from leaves. Z. Pflanzenphysiol. **69**, 359–376.

Huson DH and Scornavacca C (2012) Dendroscope 3: An interactive tool for rooted phylogenetic trees and networks. Syst. Biol. **61**, 1061-1067.

Huson DH, Richter DC, Rausch C, Dezulian T, Franz M and Rupp R (2007) Dendroscope: An interactive viewer for large phylogenetic trees. BMC Bioinformatics. **8**, 460.

Kelly AA, and Dörmann P (2002) DGD2, an Arabidopsis gene encoding a UDP-galactose-dependent digalactosyldiacylglycerol synthase is expressed during growth under phosphate-limiting conditions. J. Biol. Chem. **277**, 1166–1173.

Kodama H, Hamada T, Horiguchi G, Nishimura M and Iba K (1994) Genetic enhancement of cold tolerance by expression of a gene for chloroplast [omega]-3 fatty acid desaturase in transgenic tobacco. Plant Physiol. **105**, 601-605.

Kunst L, Browse J and Somerville C (1989) A mutant of Arabidopsis deficient in desaturation of palmitic acid in leaf lipids. Plant Physiol. **90**, 943-947.

Markham JE, Li J, Cahoon EB and Jaworski JG (2006) Separation and identification of major plant sphingolipid classes from leaves. J. Biol. Chem. **281**, 22684-22694.

Moellering ER, Muthan B and Benning C (2010) Freezing tolerance in plants requires lipid remodeling at the outer chloroplast membrane. Science **330**, 226-228.

Narváez-Vásquez J, Florin-Christensen J and Ryan CA (1999) Positional specificity of a phospholipase A activity induced by wounding, systemin, and oligosaccharide elicitors in tomato leaves. Plant Cell **11**, 2249-2260.

Nilsson AK, Fahlberg P, Ellerström M and Andersson MX (2012) Oxo-phytodienoic acid (OPDA) is formed on fatty acids esterified to galactolipids after tissue disruption in Arabidopsis thaliana. FEBS Lett. **586**, 2483-2487.

Peters C, Li M, Narasimhan R, Roth M, Welti R and Wang X (2010) Non-specific phospholipase C NPC4 promotes response to abscisic acid and tolerance to hyperosmotic stress in Arabidopsis. Plant Cell **22**, 2642-2659.

Routaboul JM, Fischer SF and Browse J (2000) Trienoic fatty acids are required to maintain chloroplast function at low temperatures. Plant Physiol. **124**, 1697-1705.

Ryu SB (2004) Phospholipid-derived signaling mediated by phospholipase A in plants. Trends Plant Sci. **9**, 229-235.

Steuer R, Kurths J, Fiehn O and Weckwerth W (2003) Observing and interpreting correlations in metabolomics networks. Bioinformatics **19**, 1019-1026.

Telfer A, Bollman KM and Poething RS (1997) Phase change and the regulation of trichome distribution in Arabidopsis thaliana. Development **124**, 645-654.

Toledo MS, Suzuki E, Straus AH and Takahashi, HK (1995) Glycolipids from Paracoccidioides brasiliensis. Isolation of a galactofuranose-containing glycolipid reactive with sera of patients with paracoccidioidomycosis. J. Med. Vet. Mycol. **33**, 247-251.

Toubiana D, Fernie AR, Nikoloski Z and Fait A (2013) Network analysis: tackling complex data to study plant metabolism. Trends Biotechnol. **31**, 29-36.

Troncoso-Ponce MA, Cao X, Yang Z and Ohlrogge JB (2013) Lipid turnover during senescence. Plant Sci. 205-206, 13-19.

Vu HS, Tamura P, Galeva NA, Chaturvedi R, Williams TD, Wang X, Shah J and Welti R (2012) Direct infusion mass spectrometry of oxylipin-containing Arabidopsis thaliana

membrane lipids reveals varied patterns in different stress responses. Plant Physiol. **158**, 324-339.

Vu HS, Roth MR, Tamura P, Samarakoon T, Shiva S., Honey S, Lowe K, Schmelz EA, Williams TD and Welti R (2014) Head-group acylation of monogalactosyldiacylglycerol is a common stress response, and the acyl-galactose acyl composition varies with the plant species and applied stress. Physiol Plant. In press.

Welti R, Li W, Li M, Sang Y, Biesiada H, Zhou H-E, Rajashekar CB, Williams TD and Wang X (2002) Profiling membrane lipids in plant stress responses. Role of phospholipase Dα in freezing-induced lipid changes in Arabidopsis. J. Biol. Chem. **277**, 31994-32002.

Xia J, Psychogios N, Young N and Wishart DS (2009) MetaboAnalyst: a web server for metabolomic data analysis and interpretation. Nucl. Acids Res. **37**, W652-660.

Xia J, Mandal R, Sinelnikov I, Broadhurst D and Wishart DS (2012) MetaboAnalyst 2.0 - a comprehensive server for metabolomic data analysis. Nucl. Acids Res. **40**, W127-133.

Yaeno T, Matsuda O and Iba K (2004) Role of chloroplast trienoic fatty acids in plant disease defense responses. Plant J. **40**, 931-941.

Zien CA, Wang C, Wang X and Welti R (2001). In-vivo substrates and the contribution of the common phospholipase D, PLDa, to wound-induced metabolism of lipids in Arabidopsis. Biochim. Biophys. Acta **1530**, 236-248.

Figures and Tables

Figure 4.1 Heatmap of autoscaled lipid levels determined by MS analysis.

272 analytes are shown in 93 samples. Each sample represents one plant under control (unwounded) or wounding treatment (n = 31 for each treatment).

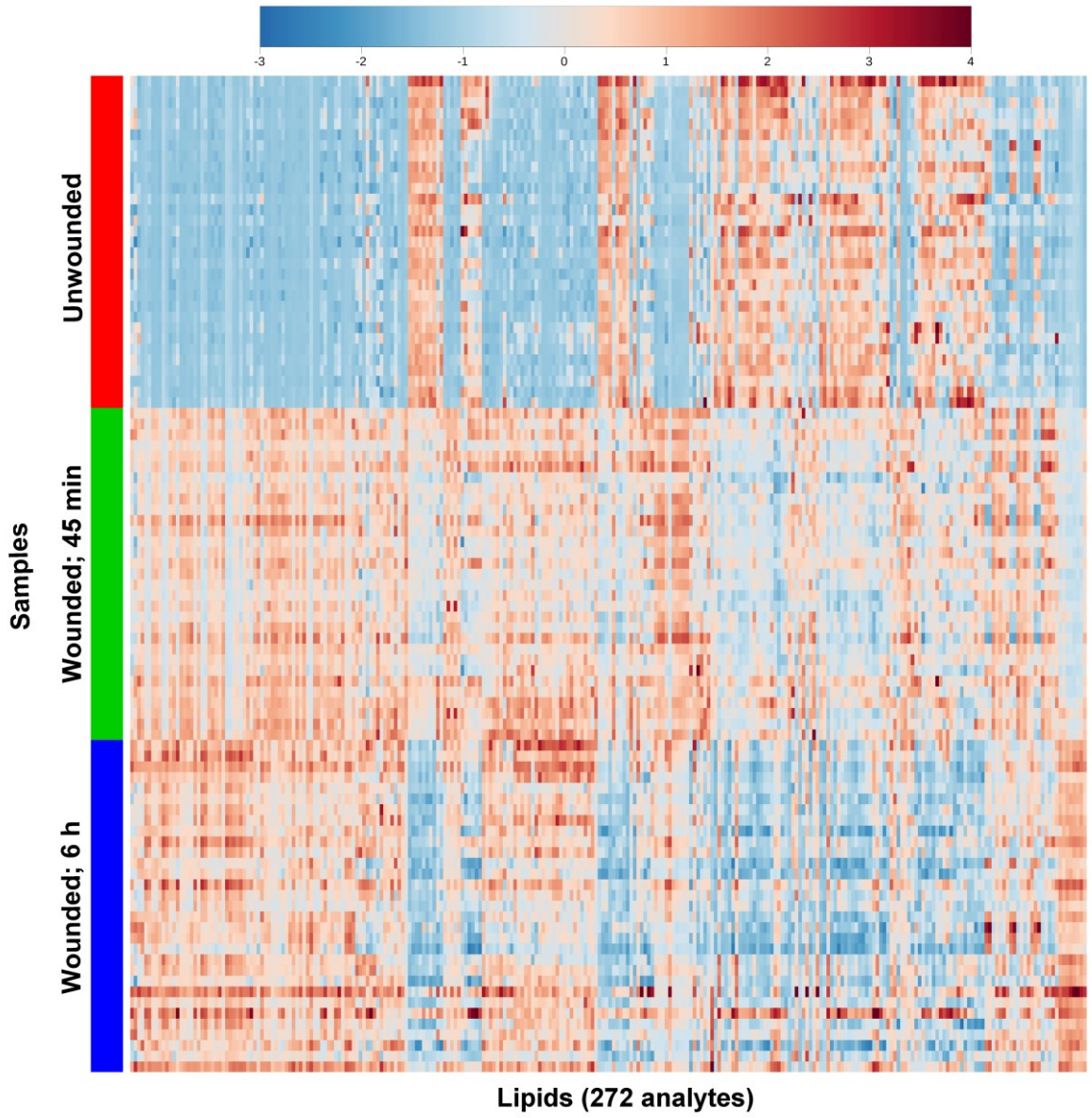

Figure 4.2 Autoscaled levels of representative lipid analytes in individual plants.
Each sample represents one plant under control (unwounded) or wounding treatment (n = 31 for each treatment). Connections between points were included to make it easier to visualize the variations in lipid levels across samples.

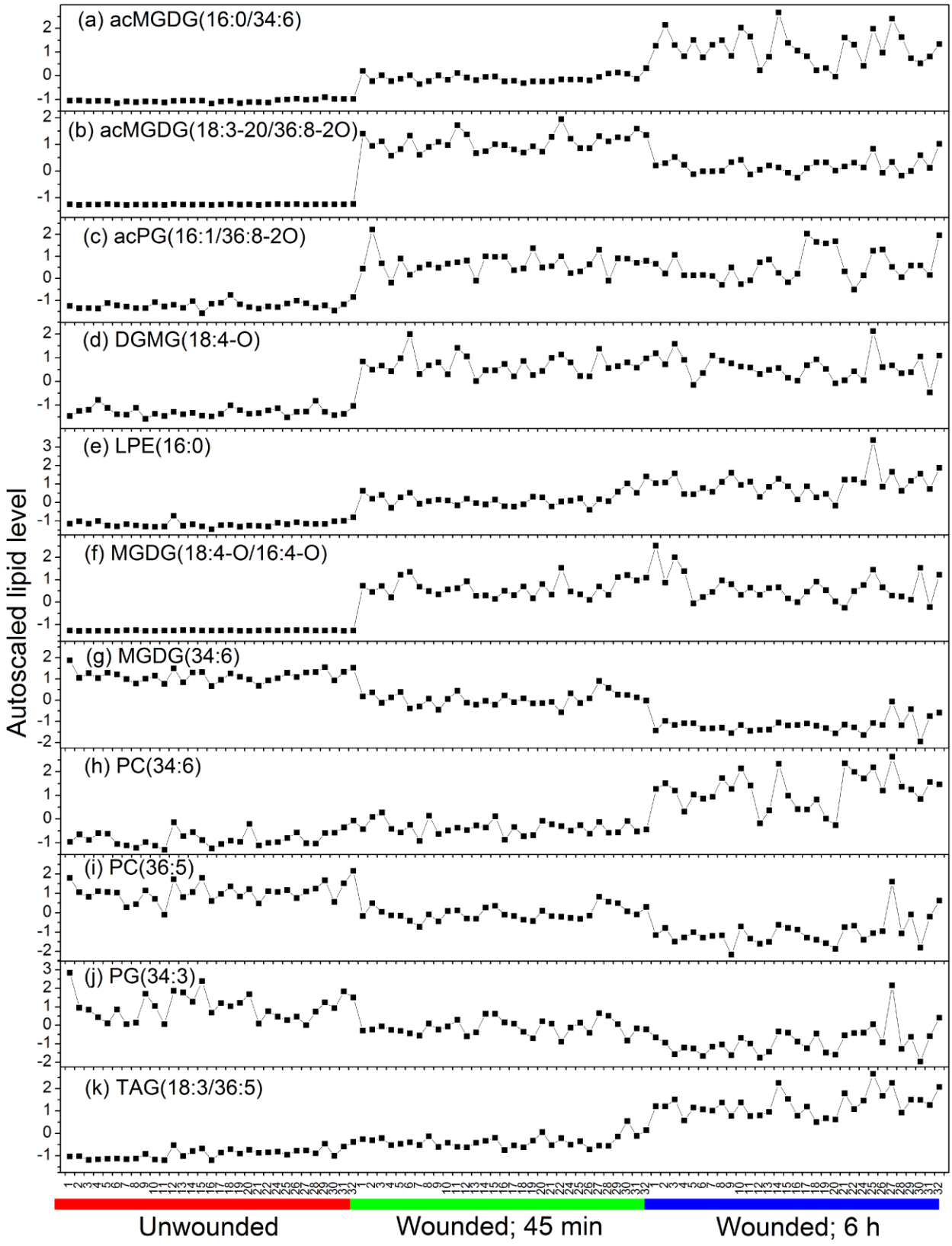
(a) acMGDG(16:0/34:6)
(b) acMGDG(18:3-20/36:8-2O)
(c) acPG(16:1/36:8-2O)
(d) DGMG(18:4-O)
(e) LPE(16:0)
(f) MGDG(18:4-O/16:4-O)
(g) MGDG(34:6)
(h) PC(34:6)
(i) PC(36:5)
(j) PG(34:3)
(k) TAG(18:3/36:5)
Autoscaled lipid level
Unwounded
Wounded; 45 min
Wounded; 6 h

Figure 4.3 Lipid dendrogram.

272 lipid analytes were clustered using a single-linkage hierarchical algorithm based on Spearman's correlation coefficient, ρ (Table S4.10). The center of the dendrogram is at ρ = 0.305. There is a scale break from ρ = 0.340 to ρ = 0.590. Eight analytes were excluded from the dendrogram due to their low level of correlation with other analytes (maximal ρ < 0.6) or because they were repeat measurements of included lipids. A single annotation is provided for each analyte; additional potential annotations are indicated in Table 4.3. Seven clusters with ρ > 0.8 are indicated by letters and colors: A (blue), B (orange), C (green), D (lavender), E (aqua), F (pink), and G (rust). Six sub-clusters of ρ > 0.96 within cluster A and twelve sub-clusters of ρ > 0.96 within cluster C are indicated as A1-A6 and C1-C12. The sub-cluster lines are red, and the lipid annotations within sub-clusters are bold.

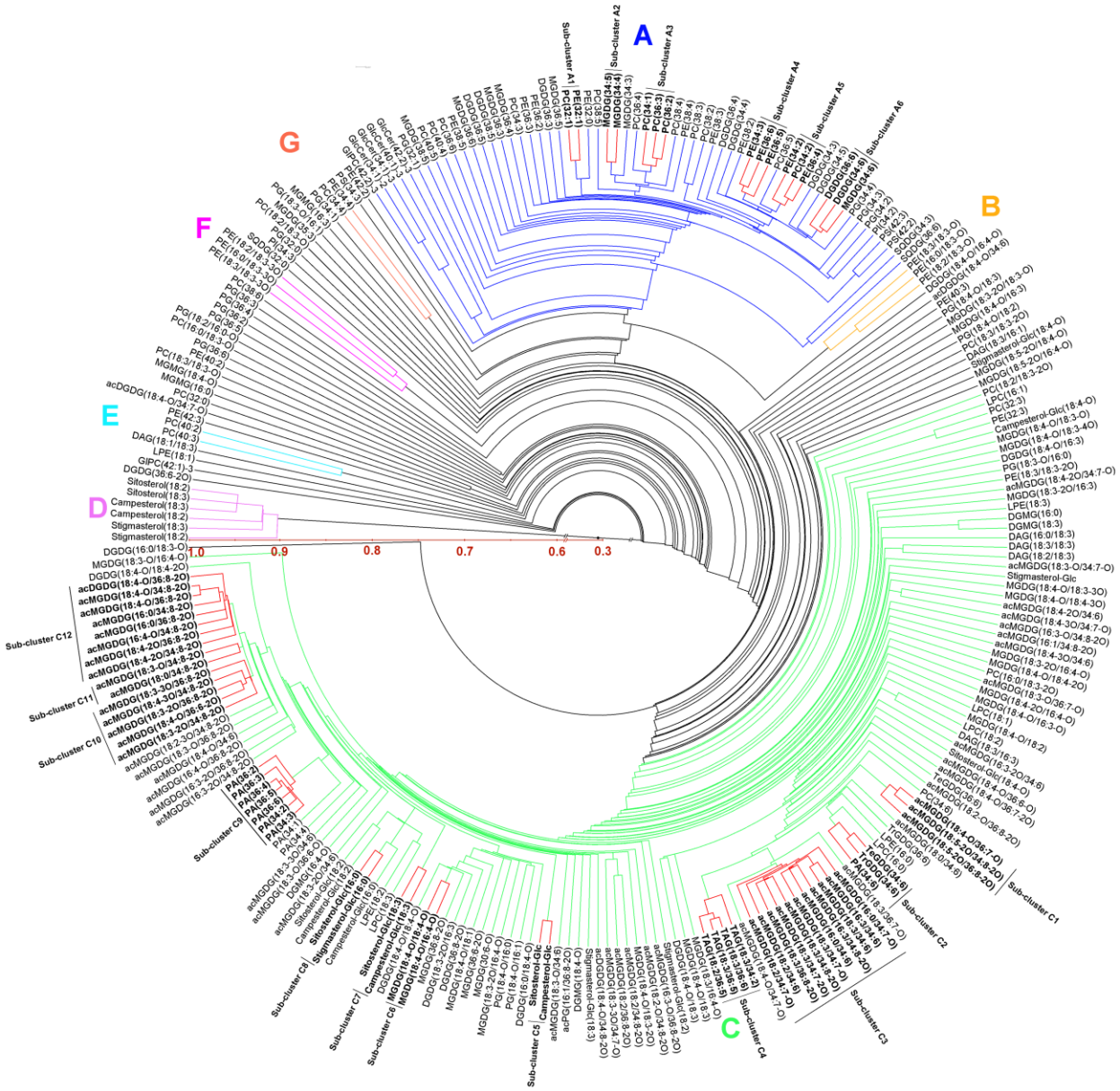

Figure 4.4 Autoscaled levels of representative lipid analytes in sub-clusters A1, A4, and A5. Points represent individual plants subjected to control or wounding treatment as indicated. Panels a, b, and c represent the three clusters, and panel d shows lipid levels for one lipid from each cluster. Text or insets show Spearman's correlation coefficient for pairs of lipids within the clusters (a, b, and c) and for representative pairs of lipids in different clusters (d).

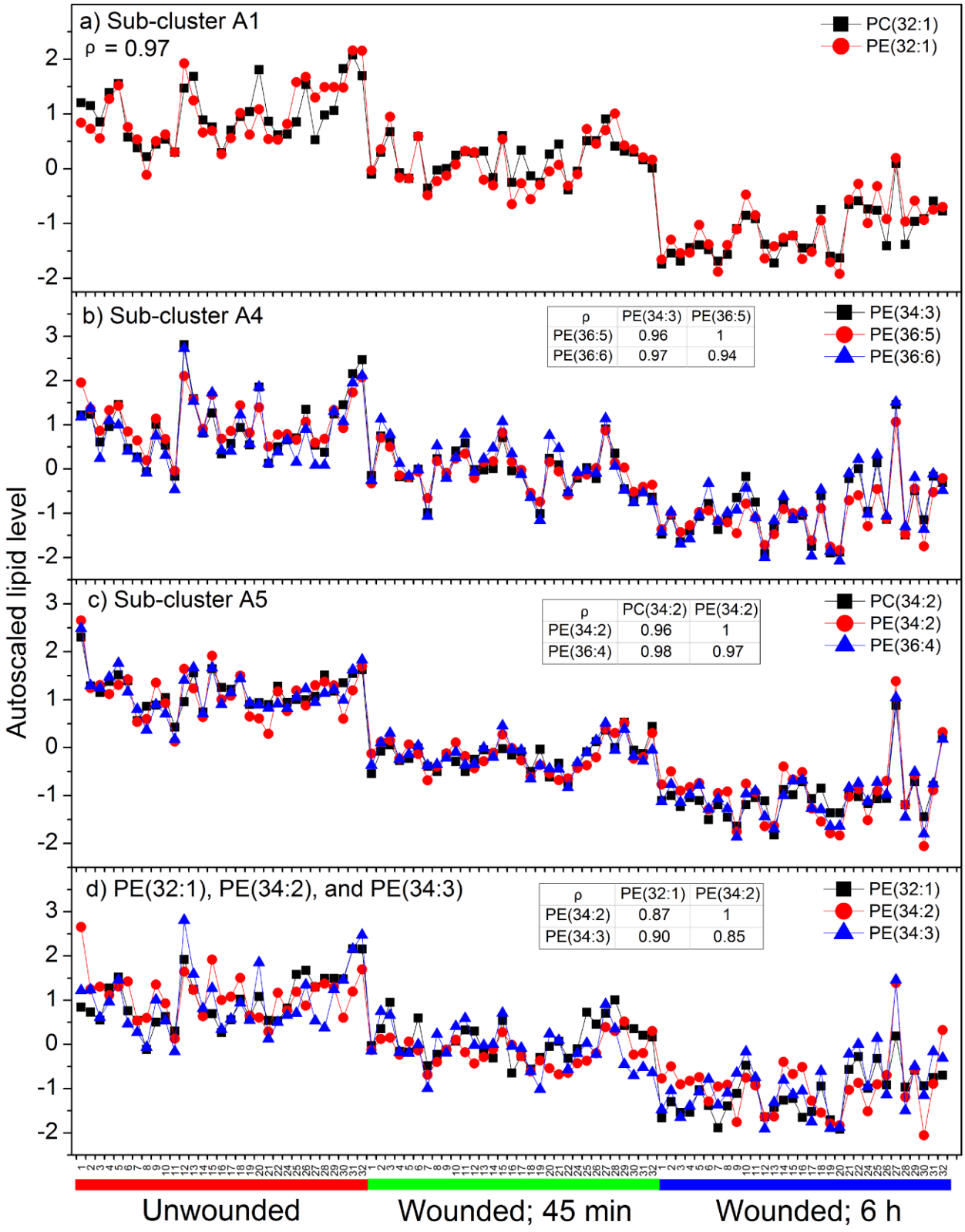
a) Sub-cluster A1
ρ = 0.97
PC(32:1)
PE(32:1)
b) Sub-cluster A4
ρ | PE(34:3) | PE(36:5)
PE(36:5) | 0.96 | 1
PE(36:6) | 0.97 | 0.94
PE(34:3)
PE(36:5)
PE(36:6)
c) Sub-cluster A5
ρ | PC(34:2) | PE(34:2)
PE(34:2) | 0.96 | 1
PE(36:4) | 0.98 | 0.97
PC(34:2)
PE(34:2)
PE(36:4)
d) PE(32:1), PE(34:2), and PE(34:3)
ρ | PE(32:1) | PE(34:2)
PE(34:2) | 0.87 | 1
PE(34:3) | 0.90 | 0.85
PE(32:1)
PE(34:2)
PE(34:3)
Autoscaled lipid level
Unwounded
Wounded; 45 min
Wounded; 6 h

Figure 4.5 Autoscaled levels of representative lipid analytes in sub-clusters C2 and C9. Points represent individual plants subjected to control or wounding treatment as indicated. Panels a and b represent the two clusters, and panel c shows lipid levels for one lipid from each cluster. Text or insets show Spearman's correlation coefficient for pairs of lipids within the clusters (a and b) and for representative pairs of lipids in different clusters (c).

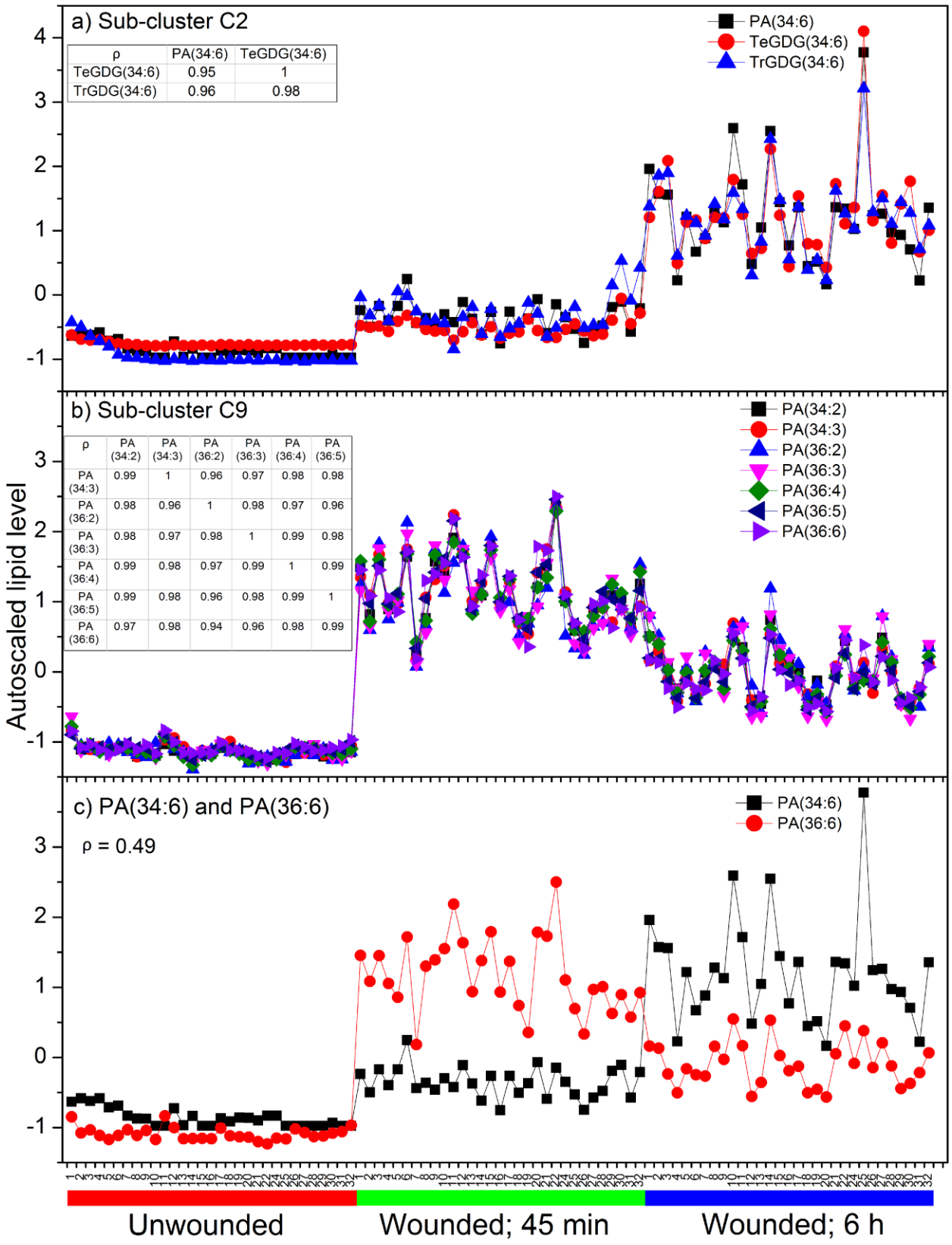
a) Sub-cluster C2
PA(34:6)
TeGDG(34:6)
TrGDG(34:6)
ρ | PA(34:6) | TeGDG(34:6)
TeGDG(34:6) | 0.95 | 1
TrGDG(34:6) | 0.96 | 0.98
b) Sub-cluster C9
PA(34:2)
PA(34:3)
PA(36:2)
PA(36:3)
PA(36:4)
PA(36:5)
PA(36:6)
ρ | PA (34:2) | PA (34:3) | PA (36:2) | PA (36:3) | PA (36:4) | PA (36:5)
PA (34:3) | 0.99 | 1 | 0.96 | 0.97 | 0.98 | 0.98
PA (36:2) | 0.98 | 0.96 | 1 | 0.98 | 0.97 | 0.96
PA (36:3) | 0.98 | 0.97 | 0.98 | 1 | 0.99 | 0.98
PA (36:4) | 0.99 | 0.98 | 0.97 | 0.99 | 1 | 0.99
PA (36:5) | 0.99 | 0.98 | 0.96 | 0.98 | 0.99 | 1
PA (36:6) | 0.97 | 0.98 | 0.94 | 0.96 | 0.98 | 0.99
Autoscaled lipid level
c) PA(34:6) and PA(36:6)
ρ = 0.49
PA(34:6)
PA(36:6)
Unwounded
Wounded; 45 min
Wounded; 6 h

Figure 4.6 Autoscaled levels of representative lipid analytes in sub-clusters C5, C7, and C8. Points represent individual plants subjected to control or wounding treatment as indicated. Panels a, b, and c represent the three clusters, and panel d shows lipid levels for one lipid from each cluster. Text or insets show Spearman's correlation coefficient for pairs of lipids within the clusters (a, b, and c) and for representative pairs of lipids in different clusters (d).

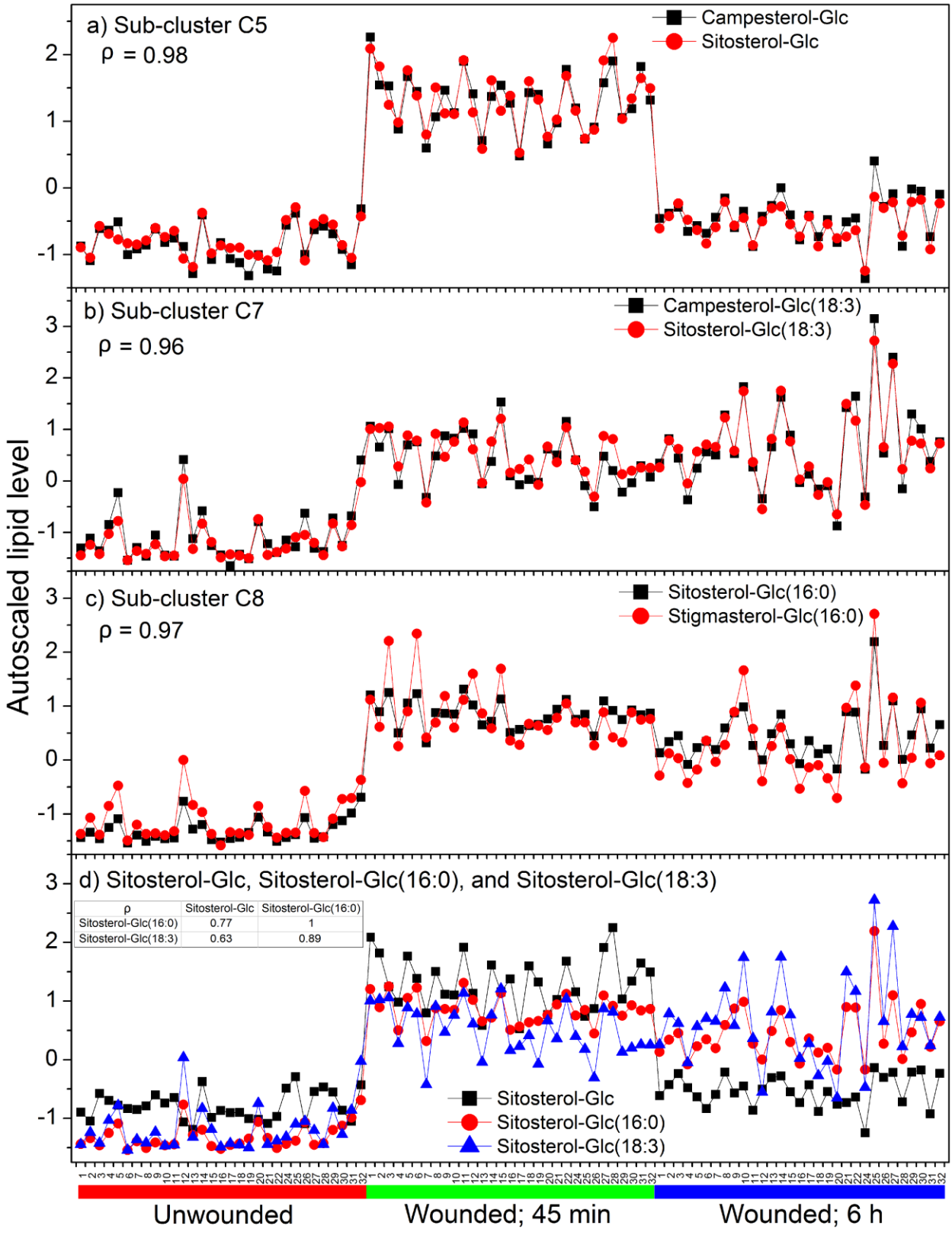
a) Sub-cluster C5
ρ = 0.98
Campesterol-Glc
Sitosterol-Glc
b) Sub-cluster C7
ρ = 0.96
Campesterol-Glc(18:3)
Sitosterol-Glc(18:3)
c) Sub-cluster C8
ρ = 0.97
Sitosterol-Glc(16:0)
Stigmasterol-Glc(16:0)
d) Sitosterol-Glc, Sitosterol-Glc(16:0), and Sitosterol-Glc(18:3)
ρ | Sitosterol-Glc | Sitosterol-Glc(16:0)
Sitosterol-Glc(16:0) | 0.77 | 1
Sitosterol-Glc(18:3) | 0.63 | 0.89
Sitosterol-Glc
Sitosterol-Glc(16:0)
Sitosterol-Glc(18:3)
Autoscaled lipid level
Unwounded
Wounded; 45 min
Wounded; 6 h

Figure 4.7 Autoscaled levels of a representative lipid from each sub-cluster.

The box depicts the middle 50% of the autoscaled values. The line within the box represents the median and the error bars represent standard deviation. n = 31 for each treatment.

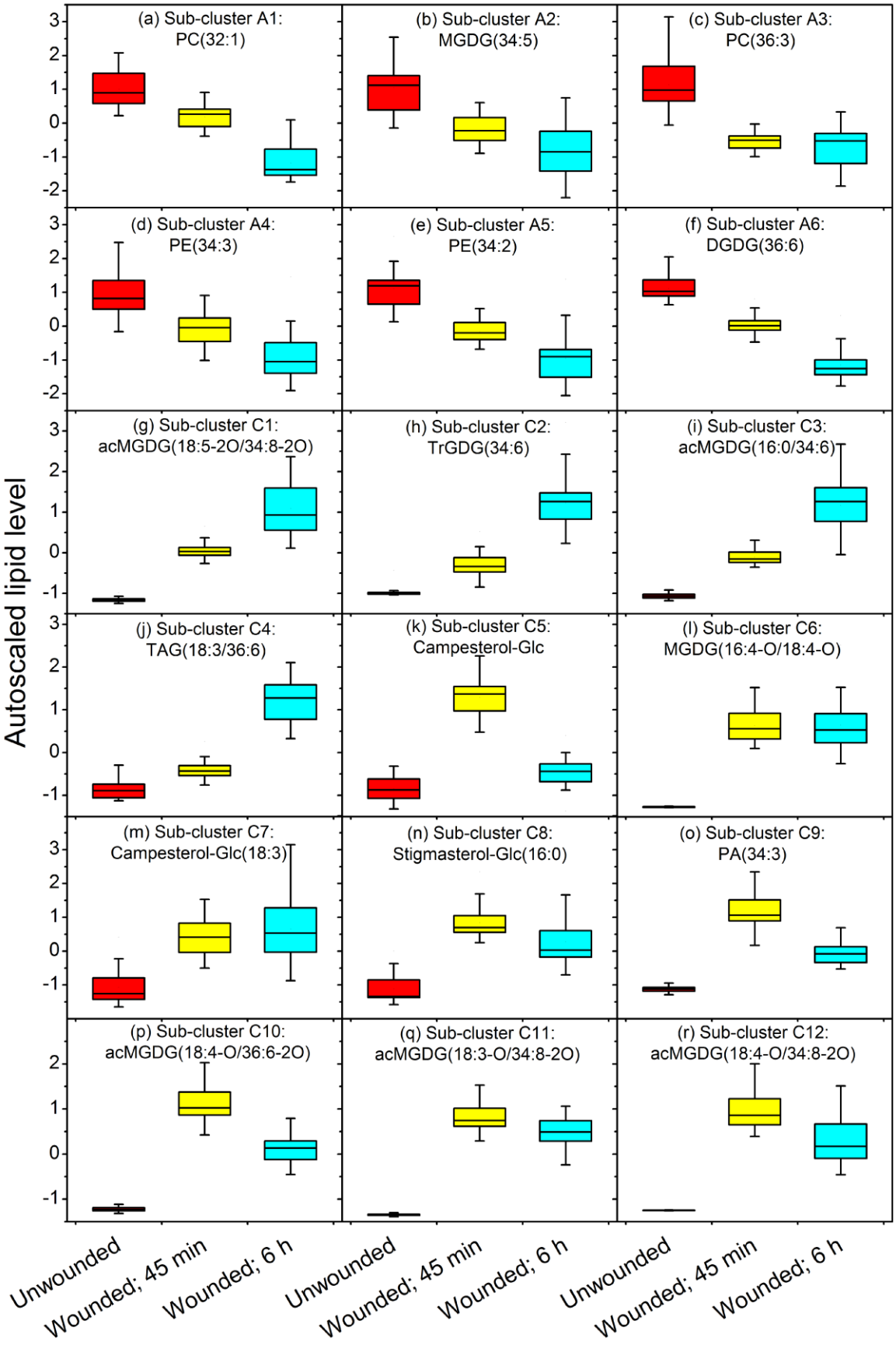
Autoscaled lipid level
(a) Sub-cluster A1: PC(32:1)
(b) Sub-cluster A2: MGDG(34:5)
(c) Sub-cluster A3: PC(36:3)
(d) Sub-cluster A4: PE(34:3)
(e) Sub-cluster A5: PE(34:2)
(f) Sub-cluster A6: DGDG(36:6)
(g) Sub-cluster C1: acMGDG(18:5-2O/34:8-2O)
(h) Sub-cluster C2: TrGDG(34:6)
(i) Sub-cluster C3: acMGDG(16:0/34:6)
(j) Sub-cluster C4: TAG(18:3/36:6)
(k) Sub-cluster C5: Campesterol-Glc
(l) Sub-cluster C6: MGDG(16:4-O/18:4-O)
(m) Sub-cluster C7: Campesterol-Glc(18:3)
(n) Sub-cluster C8: Stigmasterol-Glc(16:0)
(o) Sub-cluster C9: PA(34:3)
(p) Sub-cluster C10: acMGDG(18:4-O/36:6-2O)
(q) Sub-cluster C11: acMGDG(18:3-O/34:8-2O)
(r) Sub-cluster C12: acMGDG(18:4-O/34:8-2O)
Unwounded
Wounded; 45 min
Wounded; 6 h
Unwounded
Wounded; 45 min
Wounded; 6 h
Unwounded
Wounded; 45 min
Wounded; 6 h

Table 4.1 Characteristics of three lipid extraction methods.

Method 1 is the single-step extraction method used for the main experiment in the current work. Method 2 is a modification of the Bligh and Dyer (1959) method (Welti et al., 2002). Method 3 includes Method 2, omitting backwashes, followed by additional extraction with solvent containing isopropanol, hexane, and water (Toledo et al., 1995; Markham et al., 2006). "Intensity normalized to internal standards per dry mass" indicates the total amount of mass spectral signal detected by each method in all lipid classes in comparison to internal standards added at the time of mass spectral analysis (post-extraction). "Percent of total intensity" indicates the intensity detected in each class by each method. Abbreviations are indicated in Table 4.2.

	Composition of extracts from Arabidopsis 45 min after wounding (Intensity normalized to internal standards per dry mass (units · mg^{-1}))		
	Extraction method 1 (Single-step)	Extraction method 2	Extraction method 3
Total intensity	634334 ± 12830	609413 ± 31828	604970 ± 57144
	Percent of total intensity		
Lipid class	Extraction method 1 (Single-step)	Extraction method 2	Extraction method 3
acDGDG	0.0070 ± 0.0029	0.0060 ± 0.0008	0.0069 ± 0.0010
acMGDG	2.33 ± 0.22	2.42 ± 0.23	2.82 ± 0.41
acPG	0.0023 ± 0.0005	0.0017 ± 0.0004	0.0024 ± 0.0007
DAG	0.0064 ± 0.0006	0.0079 ± 0.0010	0.0090 ± 0.0009
DGDG	11.80 ± 0.45	11.35 ± 0.33	9.75 ± 0.70
DGMG	0.0403 ± 0.0036	0.0372 ± 0.0238	0.0184 ± 0.0023
GIPC	0.0086 ± 0.0016	0.0072 ± 0.0027	0.0278 ± 0.0015
GlcCer	2.70 ± 0.13	2.16 ± 0.09	1.96 ± 0.12
LPC	0.0560 ± 0.0208	0.3235 ± 0.4332	0.0482 ± 0.0111
LPE	0.0372 ± 0.0086	0.0513 ± 0.0374	0.0251 ± 0.0040
MGDG	66.22 ± 1.08	68.15 ± 1.20	70.32 ± 1.24

MGMG	0.0745 ± 0.0031	0.0201 ± 0.0056	0.0206 ± 0.0026
PA	0.297 ± 0.039	0.484 ± 0.045	0.505 ± 0.033
PC	4.21 ± 0.33	4.46 ± 0.366	3.84 ± 0.31
PE	2.19 ± 0.03	2.23 ± 0.10	2.20 ± 0.16
PG	4.92 ± 0.18	5.10 ± 0.17	5.19 ± 0.26
PI	1.12 ± 0.03	1.18 ± 0.02	1.17 ± 0.05
PS	0.0482 ± 0.0015	0.0508 ± 0.0017	0.0476 ± 0.0020
SQDG	0.297 ± 0.020	0.313 ± 0.007	0.302 ± 0.020
Sterol derivatives	3.60 ± 0.46	1.61 ± 0.06	1.72 ± 0.06
TAG	0.0114 ± 0.0005	0.0131 ± 0.0037	0.0122 ± 0.0006
TeGDG	0.0010 ± 0.0003	0.0010 ± 0.0001	0.0012 ± 0.0001
TrGDG	0.0169 ± 0.0016	0.0175 ± 0.0017	0.0167 ± 0.0032

Table 4.2 Lipid name abbreviations

Lipid group	Example abbreviation	Abbreviation explanation
Monoacyl glycerophospholipids		
digalactosylmonoacylglycerol	DGMG(18:3)	(Acyl carbons: acyl carbon-carbon double bonds[a])
lysophosphatidylcholine	LPC(16:0)	
lysophosphatidylethanolamine	LPE(16:0)	
monogalactosylmonoacylglycerol	MGMG(18:3)	
Polar diacyl glycerolipids		
phosphatidic acid	PA(34:3)	(Total acyl carbons: total carbon-carbon double bonds)
phosphatidylcholine	PC(32:0)	
phosphatidylethanolamine	PE(36:2)	
phosphatidylglycerol	PG(34:1)	
phosphatidylinositol	PI(38:4)	
phosphatidylserine	PS(36:5)	
digalactosyldiacylglycerol	DGDG(36:6)	
monogalactosyldiacylglycerol	MGDG(34:6)	
sulfoquinovosyldiacylglycerol	SQDG(34:3)	
tetragalactosyldiacylglycerol	TeGDG(34:6)	
trigalactosyldiacylglycerol	TrGDG(34:6)	
Head-group-acylated polar glycerolipids		
acylated digalactosyldiacylglycerol	acDGDG(18:4-O/36:8-2O)	(Head-group acyl carbons: head-group acyl carbon-carbon double bonds/total *sn-1,2* acyl carbons: total *sn-1,2* carbon-carbon double bonds)

acylated monogalactosyldiacylglycerol	acMGDG(16:0/34:6)	
acylated phosphatidylglycerol	acPG(16:1/36:8-2O)	(Acyl carbons: carbon-carbon double bonds for one acyl chain/total acyl carbons: total carbon-carbon double bonds for the other two acyl chains combined)
Neutral glycerolipids		
triacylglycerol	TAG(18:3/36:6)	(Acyl carbons: carbon-carbon double bonds for one acyl chain/total acyl carbons: total carbon-carbon double bonds for the other two acyl chains combined)
diacylglycerol	DAG(16:0/18:3)	(Acyl carbons: carbon-carbon double bonds for one acyl chain/acyl carbons: carbon-carbon double bonds for the other acyl chain)
Polar diacyl lipids measured in negative mode		
DGDG, MGDG, PC, PE, PG	PC(16:0/18:3-O)	(Acyl carbons: carbon-carbon double bonds for one acyl chain/acyl carbons: carbon-carbon double bonds for the other acyl chain)[b]
Sphingolipids		
glycosylinositolphosphoceramide	GIPC(42:2)-3	(Carbons: carbon-carbon double bonds of sphingoid base + fatty amide)-number of hydroxyl groups in base plus acyl chain

glycosylceramide	GlcCer(42:2)-3	
Sterol derivatives		
acylated sterol glucoside	Sitosterol-Glc(18:3)	(Acyl carbons: acyl carbon-carbon double bonds)
sterol ester	Campesterol(18:3)	
sterol glucoside	Sitosterol-Glc	---

[a]"Double bonds" can also indicate double bond equivalents, such as rings. "Extra" oxygen atoms in acyl chains are indicated by a "-O"; for example, oxophytodienoic acid is 18:4-O to indicate 4 double bond equivalents and 1 "extra" oxygen atom.

[b]Note: *sn*-1 and *sn*-2 positions of acyl chains on the glycerol were not determined.

Table 4.3 ANOVA and post-hoc test results.

One-way ANOVA was performed to compare the levels of the lipids among the three treatments. If a significant difference ($p < 0.01$) was detected for a lipid, a Tukey post-hoc test was performed to identify the differing treatments. Significantly different lipids were marked "up" if the lipid was higher at 45 min after wounding than in unwounded plants, at 6 h than in unwounded plants, or at 6 h than at 45 min. "Down" indicates significant changes in the opposite direction. Comparisons that are not significantly different are marked "-". The "Cluster/Sub-cluster" column shows the cluster/sub-cluster name for each lipid in a labeled unit in the dendrogram (Figure 4.3).

Lipid Name	**Wounded; 45 min vs Unwounded**	**Wounded; 6 h vs Unwounded**	**Wounded, 6 h vs Wounded; 45 min**	**Cluster/Sub-cluster**
acDGDG(18:4-O/34:6)	up	up	-	not in a cluster[f]
acDGDG(18:4-O/34:7-O)	-	up	-	not in a cluster[f]
acDGDG(18:4-O/34:8-2O) or acDGDG(18:4-O/36:6)	up	up	-	C
acDGDG(18:4-O/36:8-2O)	up	up	-	C12
acMGDG(16:0/34:6)	up	up	up	C3
acMGDG(16:0/34:7-O)	up	up	up	C3
acMGDG(16:0/34:8-2O) or acMGDG(16:0/36:6)	up	up	-	C12
acMGDG(16:0/36:8-2O)	up	up	-	C12
acMGDG(16:1/34:8-2O) or acMGDG(16:1/36:6)	up	up	up	C
acMGDG(16:3/34:6)	up	up	up	C3
acMGDG(16:3/34:8-2O) or acMGDG(16:3/36:6)	up	up	up	C3
acMGDG(16:3-O/34:8-2O) or acMGDG(16:3-O/36:6)	up	up	-	C
acMGDG(16:3-O/36:8-2O)	up	up	-	C

acMGDG(16:3-2O/34:6) or acMGDG(18:1/34:6)	up	up	up	C
acMGDG(16:3-2O/34:8-2O) or acMGDG(16:3-2O/36:6) or acMGDG(18:1/34:8-2O) or acMGDG(18:1/36:6)	up	up	down	C
acMGDG(16:3-2O/36:8-2O) or acMGDG(18:1/36:8-2O)	up	up	down	C
acMGDG(16:4-O/34:8-2O) or acMGDG(16:4-O/36:6)	up	up	down	C12
acMGDG(16:4-O/36:8-2O)	up	up	down	C
acMGDG(18:0/34:6)	up	up	up	C
acMGDG(18:0/34:8-2O) or acMGDG(18:0/36:6)	up	up	down	C11
acMGDG(18:2/34:6)	up	up	up	C3
acMGDG(18:2/34:7-O)	up	up	up	C3
acMGDG(18:2/34:8-2O) or acMGDG(18:2/36:6)	up	up	-	C
acMGDG(18:2/36:8-2O)	up	up	down	C
acMGDG(18:2-O/34:8-2O) or acMGDG(18:2-O/36:6)	up	up	-	C
acMGDG(18:2-O/36:8-2O)	up	up	up	C
acMGDG(18:2-3O/34:8-2O) or acMGDG(18:2-3O/36:6)	up	up	down	C
acMGDG(18:3/34:6)	up	up	up	C3
acMGDG(18:3/34:7-O)	up	up	up	C3
acMGDG(18:3/34:7-2O) or acMGDG(18:3/36:5)	up	up	up	C3
acMGDG(18:3/34:8-2O) or acMGDG(18:3/36:6)	up	up	up	C3
acMGDG(18:3/36:7-O)	up	up	up	C

acMGDG(18:3/36:8-2O)	up	up	up	C3
acMGDG(18:3-O/34:6)	up	up	-	C
acMGDG(18:3-O/34:7-O)	up	up	up	C
acMGDG(18:3-O/34:8-2O) or acMGDG(18:3-O/36:6)	up	up	down	C11
acMGDG(18:3-O/36:6-O)	up	up	down	C
acMGDG(18:3-O/36:7-O)	up	up	up	C
acMGDG(18:3-O/36:8-2O)	up	up	-	C
acMGDG(18:3-2O/34:6)	up	up	-	C
acMGDG(18:3-2O/34:8-2O) or acMGDG(18:3-2O/36:6)	up	up	down	C10
acMGDG(18:3-2O/36:8-2O)	up	up	down	C10
acMGDG(18:3-3O/34:6)	up	up	down	C
acMGDG(18:3-3O/34:7-O)	up	up	down	C
acMGDG(18:3-3O/36:8-2O)	up	up	down	C10
acMGDG(18:4-O/34:6)	up	up	down	C
acMGDG(18:4-O/34:7-O)	up	up	up	C
Arabidopside E: acMGDG(18:4-O/34:8-2O) or acMGDG(18:4-O/36:6)	up	up	down	C12
acMGDG(18:4-O/36:6-O)	up	up	up	C
acMGDG(18:4-O/36:6-2O)	up	up	down	C10
acMGDG(18:4-O/36:7-2O) (alternative fragmentation)	up	up	up	C
acMGDG(18:4-O/36:7-O)	up	up	up	C1
[a]Arabidopside G: acMGDG(18:4-O/36:8-2O)	up	up	down	C12
[a]Arabidopside G: acMGDG(18:4-O/36:8-2O) (alternative fragmentation)	up	up	down	not in dendrogram[a]
acMGDG(18:4-2O/34:6)	up	up	-	C

acMGDG(18:4-2O/34:7-O)	up	up	up	C
acMGDG(18:4-2O/34:8-2O) or acMGDG(18:4-2O/36:6)	up	up	down	C12
acMGDG(18:4-2O/36:8-2O)	up	up	-	C12
acMGDG(18:4-3O/34:6)	up	up	-	C
acMGDG(18:4-3O/34:7-O)	up	up	-	C
acMGDG(18:4-3O/34:8-2O) or acMGDG(18:4-3O/36:6)	up	up	down	C10
acMGDG(18:5-2O/34:8-2O) or acMGDG(18:5-2O/36:6)	up	up	up	C1
acMGDG(18:5-2O/36:8-2O)	up	up	up	C1
acPG(16:1/36:8-2O)	up	up	-	C
DAG(34:3)	up	up	-	C
DAG(34:4)	up	up	-	not in a cluster[f]
DAG(34:6)	up	up	up	C
DAG(36:4)	-	-	up	not in a cluster[f]
DAG(36:5)	up	up	-	C
DAG(36:6)	up	up	-	C
DGDG(16:0/18:3-2O)	up	-	down	not in dendrogram[e]
DGDG(16:0/18:3-O)	up	up	-	not in a cluster[f]
DGDG(16:0/18:4-O)	up	up	-	C
DGDG(18:3-2O/16:3)	up	up	down	C
DGDG(18:4-O/16:3)	up	up	-	C
Arabidopside C: DGDG(18:4-O/16:4-O)	up	up	-	not in a cluster[f]
DGDG(18:4-O/18:3)	up	up	up	C
Arabidopside D: DGDG(18:4-O/18:4-O)	up	up	-	C
DGDG(18:4-O/18:4-2O) or DGDG(18:4-O/20:2)	up	up	down	C
DGDG(34:3)	down	down	down	A

DGDG(34:4)	down	down	down	A
DGDG(34:5)	down	down	down	A
DGDG(34:6)	down	down	down	A6
DGDG(36:3)	down	down	down	A
DGDG(36:4)	down	down	down	A
DGDG(36:5)	down	down	-	A
DGDG(36:6)	down	down	down	A6
DGDG(36:6-2O) or DGDG(38:4)	-	-	-	not in a cluster[f]
DGDG(36:8-2O) or DGDG(38:6)	up	up	down	C
DGDG(38:5) or DGDG(36:7-2O)	down	down	-	A
DGMG(16:0)	up	up	down	C
DGMG(16:4-O)	up	up	-	C
DGMG(18:3)	up	up	down	C
DGMG(18:4-O)	up	up	-	C
GIPC(42:1)-3	down	down	-	not in a cluster[f]
GIPC(42:2)-3	down	down	-	A
GlcCer(34:1)-2	-	down	down	A
GlcCer(34:1)-3	-	-	-	A
GlcCer(40:1)-3	-	-	-	A
GlcCer(42:2)-3	-	down	down	A
LPC(16:0)	up	up	up	C
LPC(16:1)	up	up	-	C
LPC(18:1)	up	up	up	C
LPC(18:2)	up	up	-	C
LPC(18:3)	up	up	down	C
LPE(16:0)	up	up	up	C
LPE(18:1)	up	-	-	not in a cluster[f]
LPE(18:2)	up	up	down	C
LPE(18:3)	up	up	down	C

MGDG(18:3/16:4-O)	up	up	up	C
MGDG(18:3-O/16:4-O)	up	up	-	C
MGDG(18:3-2O/16:3)	up	up	-	C
MGDG(18:3-2O/16:4-O) or MGDG(20:1/16:4-O) (16:4-O as fragment)	up	up	-	C
MGDG(18:3-2O/16:4-O) (18:4-O as fragment)	up	up	-	C
MGDG(18:3-2O/18:3-O)	up	up	down	not in a cluster[f]
MGDG(18:4-O/16:3)	up	up	-	not in a cluster[f]
MGDG(18:4-O/16:3-O)	up	up	up	C
[b]Arabidopside A: MGDG(18:4-O/16:4-O) (16:4-O as fragment)	up	up	-	C6
[b]Arabidopside A: MGDG(18:4-O/16:4-O) (18:4-O as fragment)	up	up	-	not in dendrogram[b]
MGDG(18:4-O/18:1) or MGDG(18:4-O/16:3-2O)	up	up	-	C
MGDG(18:4-O/18:2)	up	up	up	C
MGDG(18:4-O/18:3)	up	up	up	C
MGDG(18:4-O/18:3-O)	up	up	-	C
MGDG(18:4-O/18:3-2O) or MGDG(18:4-O/20:3)	up	up	-	C
MGDG(18:4-O/18:3-3O)	up	up	-	C
MGDG(18:4-O/18:3-4O)	up	up	-	C
Arabidopside B: MGDG(18:4-O/18:4-O)	up	up	-	C6
MGDG(18:4-O/18:4-2O)	up	up	-	C
MGDG(18:4-O/18:4-3O)	up	up	down	C
MGDG(18:4-2O/16:4-O) or MGDG(20:2/16:4-O)	up	up	up	C

MGDG(18:5-2O/16:4-O) or MGDG(20:3/16:4-O)	up	up	up	not in a cluster[f]
MGDG(18:5-2O/18:4-O) or MGDG(20:3/18:4-O)	up	up	-	not in a cluster[f]
MGDG(30:6-O)	up	up	down	C
MGDG(34:3)	down	down	down	A
MGDG(34:4)	down	down	down	A2
MGDG(34:5)	down	down	down	A2
MGDG(34:6)	down	down	down	A6
MGDG(35:3)	up	-	down	not in a cluster[f]
MGDG(36:3)	down	down	-	A
MGDG(36:4) or MGDG(34:6-2O)	down	down	-	A
MGDG(36:5) or MGDG(34:7-2O)	down	down	down	A
MGDG(36:6) or MGDG(34:8-2O)	down	down	down	A
MGDG(36:6-2O) or MGDG(38:4)	up	up	down	C
MGDG(36:8-2O) or MGDG(38:6)	up	up	-	C
MGDG(38:5) or MGDG(36:7-2O)	down	down	down	A
MGMG(16:0)	up	-	-	not in a cluster[f]
MGMG(16:3)	-	-	-	not in a cluster[f]
MGMG(18:3)	-	-	down	not in dendrogram[e]
MGMG(18:4-O)	up	-	-	not in a cluster[f]
PA(34:1)	up	up	down	C
PA(34:2)	up	up	down	C9
PA(34:3)	up	up	down	C9
PA(34:4)	up	up	-	C
PA(34:6)	up	up	up	C2
PA(36:2)	up	up	down	C9
PA(36:3)	up	up	down	C9

PA(36:4)	up	up	down	C9
PA(36:5)	up	up	down	C9
PA(36:6)	up	up	down	C9
PC(16:0/18:3-O)	-	down	down	not in a cluster[f]
PC(16:0/18:3-2O)	up	up	-	C
PC(18:2/18:3-O)	-	down	down	not in a cluster[f]
PC(18:2/18:3-2O)	up	up	down	C
PC(18:3/18:3-O)	-	down	down	not in a cluster[f]
PC(18:3/18:3-2O)	up	up	down	not in a cluster[f]
PC(32:0)	-	-	-	not in a cluster[f]
PC(32:1)	down	down	down	A1
PC(32:3)	-	up	up	C
PC(34:1)	down	down	-	A3
PC(34:2)	down	down	down	A5
PC(34:3)	down	down	down	A
PC(34:4)	down	down	-	G
PC(34:6)	up	up	up	C
PC(36:2)	down	down	-	A3
PC(36:3)	down	down	-	A3
PC(36:4)	down	down	-	A
PC(36:5)	down	down	down	A
PC(36:6)	-	down	down	A
PC(38:2)	down	down	down	A
PC(38:3)	down	down	down	A
PC(38:4)	down	down	down	A
PC(38:5)	down	down	down	A
PC(38:6)	-	-	-	not in a cluster[f]
PC(40:2)	down	-	up	E
PC(40:3)	down	-	up	E
PC(40:4)	down	down	-	A
PC(40:5)	down	down	-	A

PE(16:0/18:3-O)	-	down	down	B
PE(16:0/18:3-2O)	-	-	down	not in dendrogram[e]
PE(16:0/18:3-3O)	up	up	up	F
PE(18:2/18:3-O)	-	down	down	B
PE(18:2/18:3-2O)	up	down	down	not in dendrogram[e]
PE(18:2/18:3-3O)	-	up	up	F
PE(18:3/18:3-O)	-	down	down	B
PE(18:3/18:3-2O)	up	up	down	C
PE(18:3/18:3-3O)	-	up	up	F
PE(32:0)	down	down	down	A
PE(32:1)	down	down	down	A1
PE(32:3)	-	up	up	C
PE(34:2)	down	down	down	A5
PE(34:3)	down	down	down	A4
PE(34:4)	down	-	-	G
PE(36:2)	down	down	-	A
PE(36:3)	down	down	-	A
PE(36:4)	down	down	down	A5
PE(36:5)	down	down	down	A4
PE(36:6)	down	down	down	A4
PE(38:2)	down	down	down	A
PE(38:3)	down	down	down	A
PE(38:4)	down	down	down	A
PE(38:5)	down	down	-	A
PE(40:2)	down	-	up	not in a cluster[f]
PE(40:3)	-	up	up	not in a cluster[f]
PE(42:2)	down	down	-	not in a cluster[f]
[c]PE(42:3) (measured in positive mode)	down	down	down	not in a cluster[f]
[c]PE(42:3) (measured in negative mode)	-	-	-	not in dendrogram[c]

PG(18:3-O/16:0)	up	up	up	C
PG(18:3-O/16:1)	up	up	-	not in a cluster[f]
PG(18:2/16:0-O)	down	down	down	not in a cluster[f]
PG(18:4-O/16:0)	up	up	down	C
PG(18:4-O/16:1)	up	up	down	C
PG(18:4-O/18:2)	up	up	down	not in a cluster[f]
PG(18:4-O/18:3)	up	up	down	not in a cluster[f]
PG(32:0)	-	-	-	not in a cluster[f]
PG(32:1)	-	down	down	A
PG(34:1)	down	down	-	not in a cluster[f]
PG(34:2)	down	down	down	A
PG(34:3)	down	down	down	A
PG(34:4)	down	down	down	A
PG(36:2)	-	-	down	not in a cluster[f]
PG(36:3)	-	down	-	not in a cluster[f]
PG(36:4)	-	down	-	not in a cluster[f]
PG(36:5)	-	-	-	not in a cluster[f]
PG(36:6)	-	-	-	not in a cluster[f]
PI(34:2)	down	down	down	A
[d]PI(34:3) (measured in positive mode)	-	down	-	not in a cluster[f]
[d]PI(34:3) (measured in negative mode)	-	-	-	not in dendrogram[d]
PS(34:3)	down	down	-	not in a cluster[f]
PS(42:2)	down	down	down	A
PS(42:3)	down	down	down	A
SQDG(32:0)	up	down	down	not in a cluster[f]
SQDG(34:3)	down	down	down	A
SQDG(36:6)	-	down	down	A
Campesterol(18:2)	-	-	-	D
Campesterol(18:3)	-	-	up	D

Campesterol-Glc	up	up	down	C5
Campesterol-Glc(16:0)	up	up	-	C
Campesterol-Glc(18:2)	up	up	down	C
Campesterol-Glc(18:3)	up	up	-	C7
Campesterol-Glc(18:4-O)	up	up	-	C
Sitosterol(18:2)	-	-	-	D
Sitosterol(18:3)	-	-	up	D
Sitosterol-Glc	up	up	down	C5
Sitosterol-Glc(16:0)	up	up	down	C8
Sitosterol-Glc(18:2)	up	up	down	C
Sitosterol-Glc(18:3)	up	up	-	C7
Sitosterol-Glc(18:4-O)	up	up	up	C
Stigmasterol(18:2)	-	-	up	D
Stigmasterol(18:3)	down	-	up	D
Stigmasterol-Glc	up	-	down	C
Stigmasterol-Glc(16:0)	up	up	down	C8
Stigmasterol-Glc(18:2)	up	-	down	C
Stigmasterol-Glc(18:3)	up	up	-	C
Stigmasterol-Glc(18:4-O)	up	up	-	not in a cluster[f]
TAG(18:2/36:5)	up	up	up	C4
TAG(18:3/34:2)	up	up	up	C4
TAG(18:3/36:5)	up	up	up	C4
TAG(18:3/36:6)	up	up	up	C4
TeGDG(34:6)	-	up	up	C2
TeGDG(36:6)	-	up	up	C
TrGDG(34:6)	up	up	up	C2
TrGDG(36:6)	up	up	up	C

[a] and [b] Indicates lipid measured twice in the same mode by different fragmentation events. For each, the second measurement was not included in the dendrogram.

[c] and [d] Indicate lipid measured once by a fragmentation event in the positive and once by a fragmentation event in negative mode. For each, the second measurement (in negative mode) had poor sensitivity

compared to the positive measurement and was not included in the dendrogram.

[e] Not in dendrogram due to $\rho < 0.6$.

[f] Not in a cluster due to $\rho < 0.8$, but still in dendrogram, because $\rho > 0.6$.

Supplemental Data

Supplemental data for this chapter include:

Figure S4.1 Ion leakage of Arabidopsis Col-0 control (unwounded) and wounded plants.

Figure S4.2 Expression of *ALLENE OXIDE SYNTHASE* (*AOS*) and *LIPOXYGENASE2* (*LOX2*) as quantified by qRT-PCR.

Figure S4.3 Leaf appearance before and after wounding.

Figure S4.4 Infusion profiles of representative lipids, as a function of time.

Figure S4.5 Levels of lipids as a function of wounding treatment. (This figure is supplied in a separate PDF file)

Tables S4.1-S4.10 are in a separate Excel file

Table S4.1 Comparison of three extraction methods**.**

Table S4.2 Lipids analyzed with their experimental parameters and evidence for their identification.

Table S4.3 Accurate masses of acyl groups of acMGDG from wounded *Arabidopsis thaliana* (Col-0) by Q-TOF mass spectrometry.

Table S4.4 Oxidized fatty acyl species relevant to this work.

Table S4.5 Internal standards employed in lipid profiling.

Table S4.6 Arrangement of samples in mass spectral lipid profiling in 4 mass spectrometry sample trays.

Table S4.7 Lipid amounts (normalized intensity per mg of leaf dry mass)

Table S4.8 Autoscaled lipid profiling data.

Table S4.9 One-way ANOVA and Tukey's post-hoc test results.

Table S4.10 Correlation among amounts of lipids across plant samples.

Methods S4.1 Plant material and growth

Method S4.2 Ion leakage measurement

Method S4.3 Quantification of gene expression by Real-Time-PCR

Method S4.4 Instrument parameters for analyses on the XevoTS-Q mass spectrometer

Method S4.5 Dendrogram file format conversion

Appendix S4.1 References cited in Supporting Information

Figure S4.1 Ion leakage of Arabidopsis Col-0 control (unwounded) and wounded plants.
*Student's t-test indicated a significant difference from unwounded leaves; $p < 0.001$, $n = 10$.

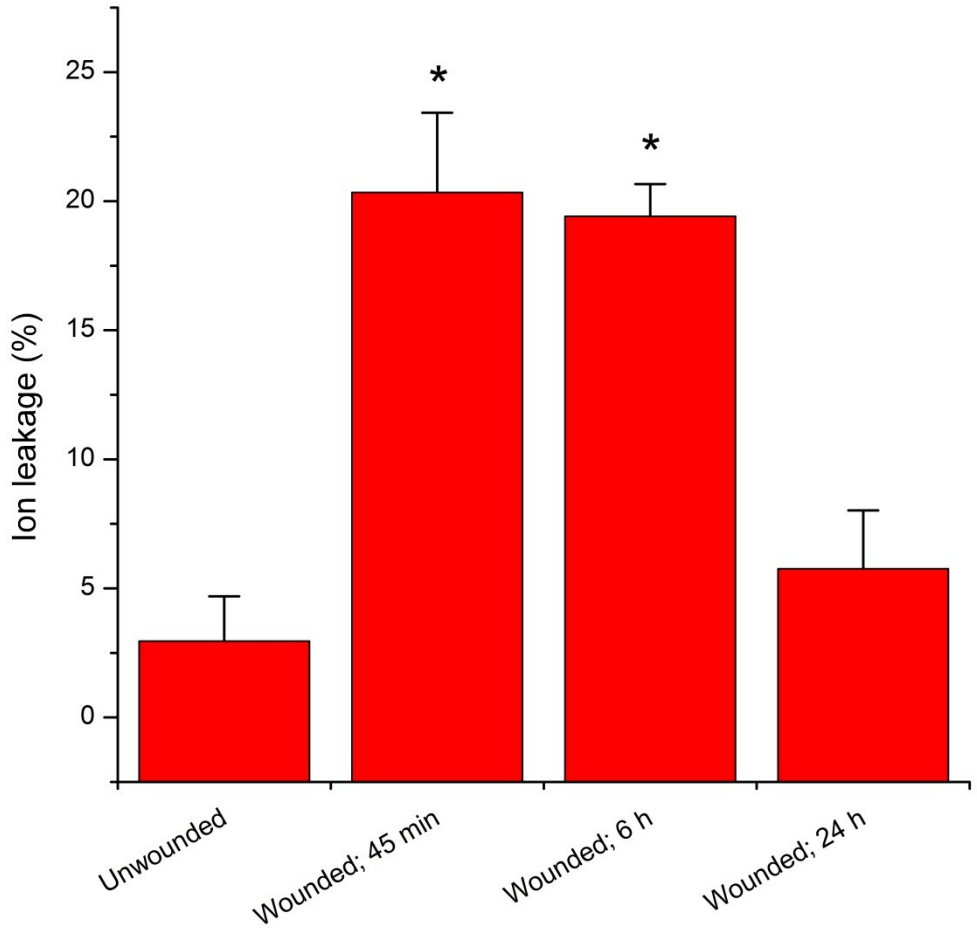

Figure S4.2 Expression of *ALLENE OXIDE SYNTHASE* (*AOS*) and *LIPOXYGENASE2* (*LOX2*) as quantified by qRT-PCR. The levels of *AOS* and *LOX2* expression were normalized to that of a constitutive control gene, *EF1α*. Six unwounded plants and 6 wounded plants were sampled. The Q test for discordant data (Shoemaker et al., 1974) was applied, resulting in removal of one datum in the unwounded *AOS* data set and one datum in the *LOX2* wounded data set. The data indicate that *AOS* expression was 3.9-fold greater and *LOX2* expression was 7.3-fold greater in leaf 6 of wounded plants, compared to leaf 6 of unwounded plants.
*The p-value for the comparison of unwounded and wounded plant gene expression was < 0.001 for both genes by Student's t-test.

Figure S4.3 Leaf appearance before and after wounding. Plants were 4-week old.

Figure S4.4 Infusion profiles of representative lipids, as a function of time. The vertical axis is relative intensity (%). The horizontal axis is time (min) from 0 to 15 min. Following lipid names are the polarity of the mass spectrometer (positive/negative), the intact ion *m/z*>fragment *m/z*, and the maximum intensity (i.e., the intensity of 100%). The samples were directly infused from a 300 µl loop. The initial period of no intensity represents the time it took for the sample to reach the mass spectrometer. The sample solvent was isopropanol: chloroform: methanol: 300 mM ammonium acetate in water (25: 30: 41.5: 3.5, v/v/v/v). From 0 to 11 min, the sample was pushed through the loop with methanol at 30 µl min^{-1} and, from 11 to 15 min, with methanol at 90 µl min^{-1}. In positive mode each lipid was scanned 130 or 131 times, and in negative mode each lipid was scanned 38 times, during the 15 min of data acquisition.

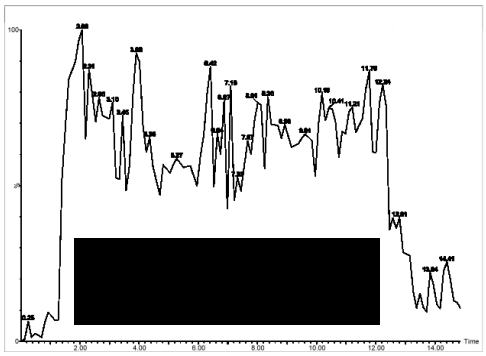

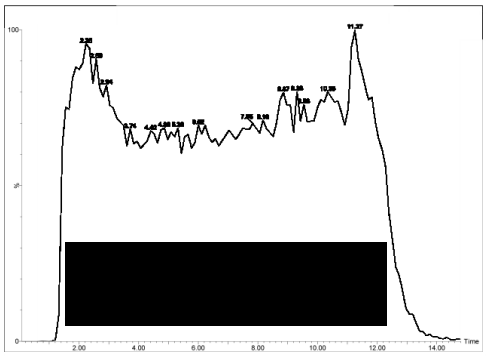

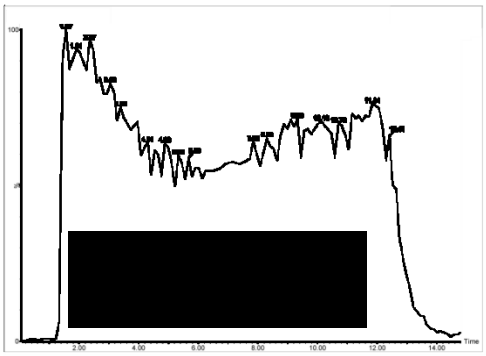

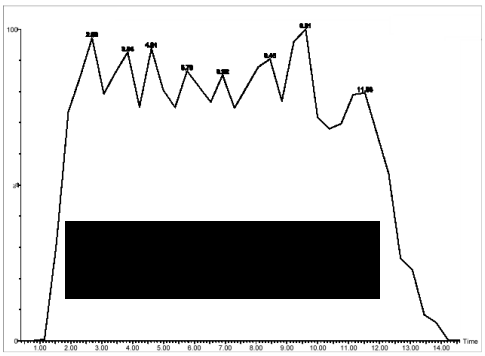

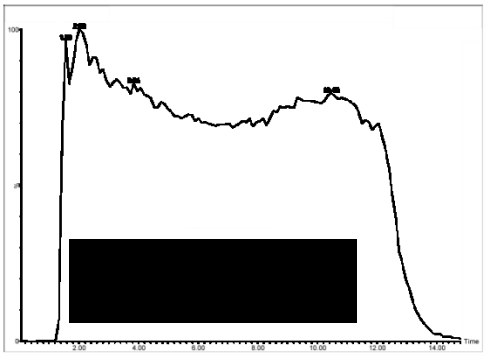

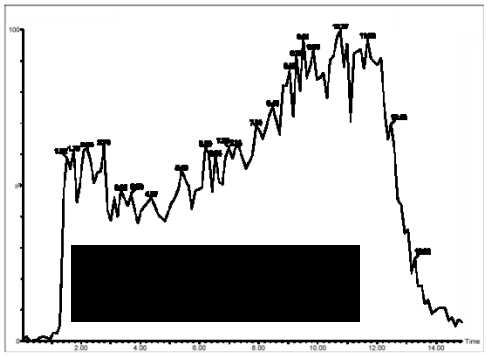

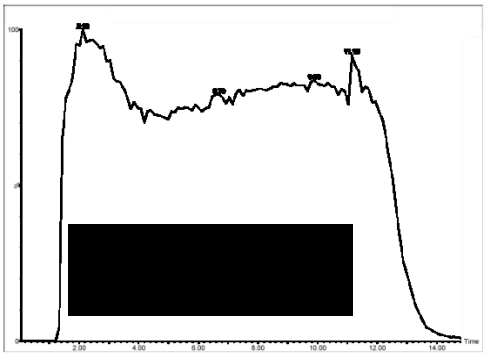

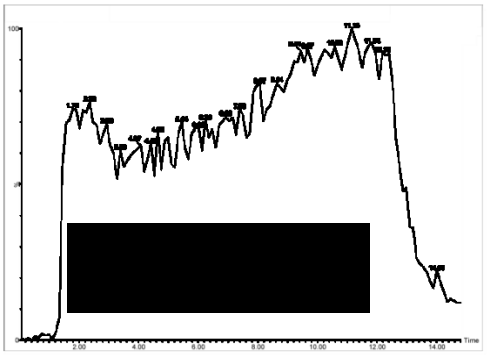

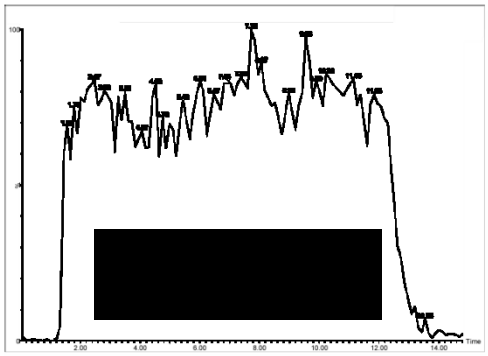

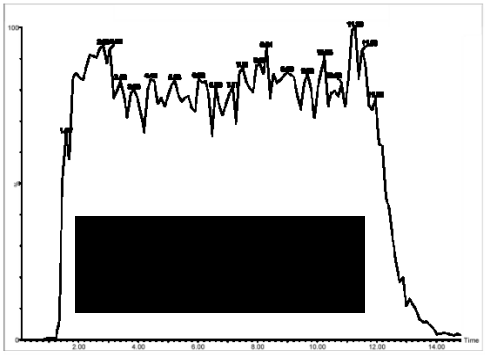

Methods S4.1 Plant material and growth

Arabidopsis thaliana accession Columbia-0 (Col-0) seeds were soaked in tap water at 4°C for 2 days before being sown at 4 seeds per well in 72-well plug trays (International Green House Company, Danville, IL, USA) filled with loosely packed, water-saturated, autoclaved, and cooled Pro-Mix "PGX" soil (Hummert International, Springfield, MO, USA). Trays were placed in a growth chamber under a 14/10 h light/dark cycle at 21°C with 60% humidity. Light intensity was maintained at 80 μmol m^{-2} sec^{-1} with cool white fluorescent lights. Trays were covered with propagation domes for the first 7 days to maintain high humidity. Trays were watered once per week. On day 12 after sowing, plants were reduced to one plant per well. On day 19, trays were fertilized with 0.01% Miracle-Gro 20-20-20 (Scotts Miracle-Gro Co., Marysville, OH, USA).

Method S4.2 Ion leakage measurement

Ion leakage was measured as described previously (Vu et al., 2014). Briefly, leaves were harvested at 45 min, 6 h, and 24 h after wounding, rinsed with distilled water, and shaken in a test tube containing 25 ml of distilled water at 100 rpm for 2 h before the conductivity of the solution was measured. The solution was then heated to and maintained at 95-100°C for 2 h to fully release the leaves' ions. After cooling to room temperature, a second conductivity measurement was taken. The ion leakage (%) was calculated as the first measurement over the second measurement x 100.

Method S4.3 Quantification of gene expression by real-time-PCR

Total RNA was extracted from wounded and unwounded leaf samples by the acid guanidinium thiocyanate-phenol-chloroform extraction method according to Chomczynski and Sachhi (1987). DNA contamination in isolated RNA samples was removed by treatment with RNase-free DNase

(Ambion, lifetechnologies.com), and RNA was spectrophotometrically quantified at 260 nm. DNA-free total RNA (2 μg) from each sample was used for cDNA synthesis. The first-strand cDNA synthesis was performed with Oligo (dT) primer using M-MLV Reverse Transcriptase (Promega, promega.com) according to the manufacturer's instructions. Individual real-time PCR reactions contained 5 μL of the SYBR Green PCR master mix (Applied Biosystems, *appliedbiosystems.com*), 2 μL of cDNA, 0.3 μL of 10 μM forward and reverse primers, and 2.4 μL of distilled water on an Eco qPCR system (Illumina, illumina.com) using the following amplification protocol: 10 min polymerase activation and denaturation at 95°C, and 40 cycles of 95°C for 10 sec, 60°C for 30 sec, and 72°C for 30 sec. This was followed by denaturation to confirm a single PCR product. Melt curves were obtained by slow heating at 0.5°C sec^{-1}, from 55°C to 95°C while continuously monitoring the fluorescence signal. A negative control without a cDNA template and a positive control with a known cDNA template were run to evaluate the overall specificity. The levels of *AOS* (At5g42650) and *LOX2* (At3g45140) expression was normalized to that of a constitutive control gene *EF1α* (At5g60390) by subtracting the cycle threshold value of control *EF1α* from the cycle threshold value of *AOS* and *LOX2*. The *EF1α*-F (5′- accaagattgacaggcgttc-3′) and *EF1α*-R (5′- tgcaacagtctgcctcatgt -3′), *AOS*-F (5'-ccctttttccgatttctctcc-3') and *AOS*-R (5'-acggtagcctccggttagtt-3'), and *LOX2*-F (5′-ggtctcgatgacattgctga-3′) and *LOX2*-R (5′-aggcatctcaaactcgcact-3′) gene-specific primers were used for PCR amplification of *EF1α*, *AOS*, and *LOX2*, respectively. Expression was measured in leaf 6 of 4-week-old wild-type (Col-0) Arabidopsis, either unwounded or subjected to wounding on leaves 5, 6, and 7.

Method S4.4 Instrument parameters for analyses on the XevoTS-Q mass spectrometer

The global settings for all analyses on the Xevo TS-Q mass spectrometer were: capillary voltage, ±2.8 kV; source offset voltage, ±30.0 V; cone voltage, ±40.0 V; source temperature, 150°C; desolvation temperature, 250°C; cone gas flow, 150 L h^{-1}; desolvation gas flow, 650 L h^{-1}; collision gas flow, 0.1 mL min^{-1}; nebulizer gas pressure, 7 bar; low mass 1 and 2 resolution, 2.5; high mass 1 and 2 resolution, 14.5; ion energy 1 and 2, 1.0. Interchannel delay (ICD) was 0.006-0.012 sec in positive mode and 0.100 sec in negative mode. Interscan delay (ISD) was 0.020 sec in positive mode and 0.100 sec in negative mode.

Method S4.5 Dendrogram file format conversion

Clustering results produced by Cluster 3.0 (Eisen et al., 1997) (.gtr and .cdt files) were converted to NEWICK format (.nwk) using a Python script written by Haibao Tang (J. Craig Venter Institute, Rockville, MD, USA). The script can be obtained from the following link: https://github.com/tanghaibao/treecut/blob/master/scripts/eisen_to_newick.py.

Appendix S4.1 References cited in Suppplemental data

Andersson MX, Hamberg M, Kourtchenko O, Brunnström A, McPhail KL, Gerwick WH, Goebel C, Feussner I and Ellerström M (2006) Oxylipin profiling of the hypersensitive response in *Arabidopsis thaliana*. Formation of a novel oxo-phytodienoic acid-containing galactolipid Arabidopside E. J. Biol. Chem. 281, 31528-31537.

Burgos A, Szymanski J, Seiwert B, Degenkolbe T, Hannah MA, Giavalisco P and Willmitzer L (2011) Analysis of short-term changes in the *Arabidopsis thaliana* glycerolipidome in response to temperature and light. The Plant Journal 66, 656–666.

Buseman CM, Tamura P, Sparks AA, Baughman EJ, Maatta S, Zhao J, Roth MR, Esch SW, Shah J, Williams TD and Welti R (2006) Wounding stimulates the accumulation of

glycerolipids containing oxophytodienoic acid and dinor-oxophytodienoic acid in Arabidopsis leaves. Plant Physiol. 142, 28-39.

Chomczynski P and Sachhi N (1987) Single-step method of RNA isolation by acid guanidinium thiocyanate-phenol-chloroform extraction. Anal. Biochem. 162, 156-159.

Devaiah SP, Roth MR, Baugham E, Li M, Tamura P, Jeannotte R, Welti R and Wang XM (2006) Quantitative profiling of polar glycerolipid species and the role of phospholipase Dα1 in defining the lipid species in Arabidopsis tissues. Phytochemistry 67, 1907-1924.

Eisen MB, Spellman PT, Brown PO and Botstein D (1997) Cluster analysis and display of genome-wide expression patterns. Proc. Natl. Acad. Sci. USA 95, 14863-14868.

Esch, S.W., Tamura, P., Sparks, A.A., Roth, M.R., Devaiah, S.P., Heinz, E., Wang, X., Williams TD and Welti R (2007) Rapid characterization of fatty acyl composition of complex lipids by collision-induced dissociation time-of-flight mass spectrometry. J. Lipid. Res. 48, 235-241.

Glauser G, Grata E, Rudaz S and Wolfender JL (2008) High-resolution profiling of oxylipin containing galactolipids in Arabidopsis extracts by ultraperformance liquid chromatography/time-of-flight mass spectrometry. Rapid Commun. Mass Spectrom. 22, 3154-3160.

Grun G, Berger S, Matthes D and Mueller MJ (2007) Early accumulation of non-enzymatically synthesized oxylipins in *Arabidopsis thaliana* after infection with *Pseudomonas syringae*. Funct. Plant Biol. 34**,** 65-71.

Hisamatsu Y, Goto N, Hasegawa K and Shigemori H (2003) Arabidopsides A and B, two new oxylipins from *Arabidopsis thaliana*. Tetrahedron Lett. 44, 5553-5556.

Hisamatsu Y, Goto N, Sekiguchi M, Hasegawa K and Shigemori H (2005) Oxylipins arabidopsides C and D from *Arabidopsis thaliana*. J. Nat. Prod. 68, 600-603.

Hsu F-F, Turk J, Williams TD and Welti R (2007) Electrospray ionization multiple stage quadrupole ion-trap and tandem quadrupole mass spectrometric studies on phosphatidylglycerol from Arabidopsis leaves. J. Am. So.c Mass Spectrom. 18, 783-90.

Ibrahim A, Schütz AL, Galano JM, Herrfurth C, Feussner K, Durand T, Brodhun F and Feussner I (2011) The alphabet of galactolipids in *Arabidopsis thaliana*. Front Plant Sci. DOI: 10.3389/fpls.2011.00095.

Kourtchenko O, Andersson MX, Hamberg M, Brunnström A, Goebel C, McPhail KL, Gerwick WH, Feussner I and Ellerström M (2007) Oxo-phytodienoic acid containing galactolipids in Arabidopsis: Jasmonate signaling dependence. Plant Physiol. 145, 1658-1669.

Li M, Baughman E, Roth MR, Han X, Welti R, and Wang X (2014) Quantitative profiling and pattern analysis of triacylglycerol species in Arabidopsis seeds by electrospray ionization mass spectrometry. Plant J. 77, 160-172.

Maeda H, Sage TL, Isaac G, Welti R and DellaPenna D (2008) Tocopherols modulate extra-plastidic polyunsaturated fatty acid metabolism in *Arabidopsis* at low temperature. Plant Cell 20, 452-470.

Markham JE and Jaworski JG (2007) Rapid measurement of sphingolipids from Arabidopsis thaliana by reversed-phase high-performance liquid chromatography coupled to electrospray ionization tandem mass spectrometry. Rapid Commun. Mass Spectrom. 21, 1304-1314.

Okazaki Y, Shimojima M, Sawada Y, Toyooka K, Narisawa T, Mochida K, Tanaka H, Matsuda F, Hirai A, Hirai MY, Ohta H and Saito K (2009) A chloroplastic UDP-glucose pyrophosphorylase from Arabidopsis is the committed enzyme for the first step of sulfolipid biosynthesis. Plant Cell 21, 892-909.

Peters C, Li M, Narasimhan R, Roth MR, Welti R and Wang X (2010) Nonspecific phospholipase C NPC4 promotes responses to abscisic acid and tolerance to hyperosmotic stress in Arapidopsis. Plant Cell 22, 2642-2659.

Samarakoon T, Shiva S, Lowe K, Tamura P, Roth MR and Welti R (2012) Arabidopsis thaliana membrane lipid molecular species and their mass spectral analysis. In *High throughput phenotyping in plants, Methods in Molecular Biology*. Ed., J. Normanly. Humana Press, New York, NY. 918, 179-268.

Schrick K, Shiva S, Arpin J, Delimont N, Isaac G, Tamura P and Welti R (2012) Steryl glucoside and acyl steryl glucoside analysis of Arabidopsis seeds by electrospray ionization tandem mass spectrometry. Lipids 47, 185-193.

Shigemori H, Nakajyo H, Hisamatsu Y, Sekiguchi M, Goto N and Hasegawa K (2006) Arabidopside F, a new oxylipin from *Arabidopsis thaliana*. Heterocycles 69, 295-301.

Shoemaker JP, Garland CW and Steinfeld JI (1974) "Experiments in Physical Chemistry", McGraw-Hill, Inc., pp. 34-39.

Stelmach BA, Mueller A, Hennig P, Gebhardt S, Schubert-Zsilavecz M and Weiler EW (2001) A novel class of oxylipins, sn1-O-(12-oxophytodienoyl)-sn2-O-(hexadecatrienoyl)-monogalactosyl diglyceride, from *Arabidopsis thaliana*. J. Biol. Chem 276, 12832-12838.

Vu HS, Tamura P, Galeva NA, Chaturvedi R, Williams TD, Wang X, Shah J and Welti R (2012) Direct infusion mass spectrometry of oxylipin-containing Arabidopsis thaliana membrane lipids reveals varied patterns in different stress responses. Plant Physiol. 158, 324-339.

Vu HS, Roth MR, Tamura P, Samarakoon T, Shiva S, Honey S, Lowe K, Schmelz EA, Williams TD and Welti R (2014) Head-group acylation of monogalactosyldiacylglycerol is a common stress response, and the acyl-galactose acyl composition varies with the plant species and applied stress. Physiol Plant. In press.

Welti R, Li W, Li M, Sang Y, Biesiada H, Zhou H, Rajashekar CB, Williams TD and Wang X (2002) Profiling membrane lipids in plant stress responses. Role of phospholipase Dα in freezing-induced lipid changes in Arabidopsis. J. Biol. Chem. 277, 31994-32002.

Welti R, Wang X and Williams TD (2003) Electrospray ionization tandem mass spectrometry scan modes for plant chloroplast lipids. Anal. Biochem. 314, 149-152.

Wewer V, Dombrink I, Vom Dorp K and Dörmann P (2011) Quantification of sterol lipids in plants by quadrupole time-of-flight mass spectrometry. J. Lipid Res. 52, 1039–1054.

Xiao S, Gao W, Chen Q, Chan S, Zheng S, Ma J, Wang M, Welti, R and Chye M-L. (2010) Overexpression of Arabidopsis acyl-CoA binding protein ACBP3 promotes starvation-induced and age-dependent leaf senescence. Plant Cell 22, 1463-1482

Yang W, Zheng Y, Bahn SC, Pan X, Li M, Vu HS, Roth MR, Scheu B, Welti R, Hong Y and Wang X (2011) The patatin-containing phospholipase A pPLAIIα modulates oxylipin formation and water loss in Arabidopsis thaliana. Mol. Plant 5, 452-460.

Zoeller M, Stingl N, Krischke M, Fekete A, Waller F, Berger S and Mueller MJ (2012) Lipid profiling of the Arabidopsis hypersensitive response reveals specific lipid peroxidation and fragmentation processes: biogenesis of pimelic and azelaic acid. Plant Physiol. 160, 365-378.

Chapter 5 - Roles of lipoxygenases and lipases in Arabidopsis in response to freezing

Abstract

The analytical approach developed in Chapter 4 was used to measure 331 lipids extracted from Arabidopsis exposed to cold acclimation, freezing and thawing. The data from wild-type plants were used to construct a dendrogram depicting clusters and sub-clusters of lipids that have similar patterns in response to treatments. The levels of these lipids were compared between the wild-type and 22 lines with knockout mutations in oxophytodienoic reductase, lipoxygenase and acyl hydrolase genes. Preliminary analysis of the data suggests that an increased formation of oxophytodienoic-acid-containing acylated monogalactosyldiacylglycerols (Arabidopsides E and G) during tissue thawing of cold-acclimated, frozen *pPLAIIγ* knockout coincided with a better recovery compared to wild-type.

Introduction

Lipoxygenases (LOXs) initiate lipid oxidation under various stresses. The enzymatic lipid oxidation catalyzed either by 9-LOXs or 13-LOXs produces either 9- or 13-hydroperoxy fatty acids, which are the precursors of many oxylipins. In Arabidopsis, the 9-LOX pathway, which includes LOX1 and LOX5, has been shown to have an antagonistic interaction with the ethylene pathway in the control of oxidative stress and modulation of bacterial defense (López et al., 2011). LOX1 was demonstrated to be essential in stomatal closing in response to bacterial infection (Montillet et al., 2013) and to be involved in Arabidopsis early response to cadmium exposure (Keunen et al., 2013). All four Arabidopsis 13-LOXs, LOX2, LOX3, LOX4, and LOX6 were shown to contribute to jasmonate synthesis in wounded leaves (Chauvin et al., 2013). Chauvin et al. (2013) also showed that LOX6 was the only 13-LOX necessary for the initiation of early jasmonate synthesis in systemic leaves. In an earlier study, LOX2 was shown to be required for wound-induced accumulation of jasmonic acid (Bell et al., 1995). These results suggest that the involvements of individual LOX genes in plant responses to different stresses are

different. Although LOX-derived products are induced by many abiotic and biotic stresses (Feussner and Wasternack, 2002; Weber, 2002; Hamberg et al., 2005; Shah, 2005; and Shah and Chaturvedi, 2008), the potential roles of each LOX gene in biosynthesis of oxidized lipids under plant stress conditions are understudied. Therefore, analyses of LOX mutants are critical to define specific roles of each LOX gene in the formation of stress-induced oxidized membrane lipids.

Acyl hydrolases (AHs) affect plant stress responses and might be involved in metabolism of oxidized membrane lipids. The Arabidopsis genome has many gene families tentatively encoding acyl hydrolase such as DEFECTIVE IN ANTHER DEHISENCE 1 (DAD-1)-like proteins (Ishiguro et al., 2001), secreted phospholipase A2 (Lee et al., 2005), GDSL lipases (Oh et al., 2005), and patatin-like proteins (PLP) (La Camera et al., 2005). PLP2 is involved in cell death execution, oxylipin synthesis, and pathogen resistance (La Camera et al., 2009). In a research on gene expression response to stresses, out of six PLPs: At4g37070, At2g26560, At4g37050, At2g39220, At3g54950 and At3g63200 (PLP1, PLP2, PLP3, PLP6, PLP7, and PLP9, respectively) only PLP2, PLP3, and PLP7 were induced by drought and PLP2 was further demonstrated to be induced in wounding and have AH activity *in vitro* (Matos et al., 2008). PLP1, PLP3, and PLP5 were demonstrated to have different roles in root response to phosphate deprivation (Rietz et al., 2010). It is clear that the PLPs play important roles in plant stress responses and are possibly involved in membrane lipid metabolism. However, very little is know about their substrates, products, and especially functions of each PLP under stress conditions. Although many phospholipases have been demonstrated to activate and play important roles in plant responses to cold and freezing (Welti et al., 2002; Li et al., 2004; Li et al., 2008), the roles of PLP in low temperature stress are still poorly studied (Li et al., 2013). Therefore, it is important to study PLP mutants to define their roles in stress-induced metabolism of oxidized membrane lipids.

Improving plant freezing tolerance has great agricultural significance. Naturally, some plants, including Arabidopsis, can increase their freezing tolerance after a period of exposure to low, non-freezing temperature; this is termed cold acclimation. Changes in lipid composition during cold acclimation are very important among the molecular strategies that help plants increase their

freezing tolerance. ACYL-LIPID DESATURASE 2 (ADS2) was shown to desaturate esterified 16:0 at low temperature, and this was shown to be important for freezing tolerance (Chen and Thelen, 2013). The accumulation of triacylglycerols during the acclimation period was reported to be a distinguishing factor between Arabidopsis ecotypes with different freezing tolerance (Degenkolbe et al., 2012). A distinct, acclimation-independent freezing tolerating mechanism is the converting of monogalactosyldiacylglycerol to oligogalactosyldiaclyglycerol by SENSITIVE TO FREEZING 2 (SFR2), a constitutively expressed protein (Moellering et al., 2010). Thus, cold acclimation and ultimately freezing tolerance involve diverse lipid compositional changes. To better understand the changes and their bases, a systematic approach is needed to study mechanisms underlying plant freezing tolerance.

In this research, we applied the high throughput lipidomics strategy developed in Chapter 4 to study Arabidopsis oxophytodienoic reductase, LOX and AH knockout mutants responding to cold acclimation and freezing. Six wild-type control plants and three plants of each knockout line were grown in a tray. Each tray was exposed to a unique temperature treatment. Afterward, the plants were harvested for both leaf damage assesment by ion leakage and lipid analysis. The whole treatment was repeated three times. Analysis of the first round is complete and analysis of rounds 2 and 3 is in progress. The direct infusion of total lipids, combined with the sensitivity of the mass spectrometer operated in MRM mode, offer relatively comprehensive snapshots of lipidomes. We employed a quality control strategy to enhance precision. This chapter presents data obtained from the first round of the experiment. The data provide novel preliminary findings about the production and metabolism of oxidized membrane lipids and the involvement of LOXs and AHs in cold and freezing responses in Arabidopsis.

Materials and Methods

Overall experimental design

In this research, we utilized 23 Arabidopsis lines; each of which was given a letter label from A to X for convenient handling (Table 5.1), except for the wild-type Columbia-0 (Col-0) accession which was duplicated (A and M, treated as 2 different lines during the experiment) due to its critical role as a control. The 24 lines were grown in triplicate in 72-well plug trays (Figure 5.1

and Figure 5.2). Each tray was treated with one of the conditions described in Figure 5.3. All 17 treatments (17 trays) were repeated three times (referred to as replication rounds 1, 2, and 3). Each well of the plug tray was labeled with a number from 1 – 72. Therefore, each line was associated with three different numbers indicating its positions on the plug tray. The positions of each line were different in the three replication rounds. For example, in replication round 1, line H was grown in wells numbered 1, 15, and 38 of each of the 17 trays; in replication round 2, line H was grown in wells numbered 13, 46, and 62 (Figure 5.1). The positions of each line in a tray were randomized in a controlled manner so that there was always at least 1 plant of all 24 lines on the outside wells. Seed sowing of the 17 trays of each replication round was done on 5 consecutive days (day 1: tray 1, 2, 4, 7, 10, and 12; day 2: 3, 5, 8, and 11; day 3: 6, 9, 14, and 16; day 4: tray 13 and 17; day 5: tray 15). All handlings and treatments of each tray (watering, thinning, fertilizing, photographing, treating, and harvesting) were done according to a staggered schedule so that time-consuming steps such as thinning or harvesting could be performed by no more than 4 laboratory workers at a time, and so that no more than two trays (the maximal capacity of the freezing chamber) would require freezing treatment on the same day.

Each tray was photographed to record visible phenotypes. In parallel with lipid analysis, ion leakage measurements were performed to detect membrane damage caused by the treatments.

Arabidopsis lines

We studied 22 mutant lines (including single, double, and triple knockouts) and wild-type, i.e. accession Columbia-0 (Col-0). Each line was given a letter label from A to X for easy handling throughout the experiment, as listed in Table 5.1. Col-0 was duplicated (A and M).

All the *pPLA* knockout lines were provided by Xuemin Wang and Maoyin Li (Danforth Plant Science Center, St Louis, MO, USA). All the *lox* lines except for *lox4* were provided by Jyoti Shah (University of North Texas, Denton, TX, USA). The l*ox4* knockout line was ordered directly from Arabidopsis Biological Resource Center (ABRC). The *lox4* seeds were sown and grown for 30 days before leaves were harvested for DNA extraction. Genotype with respect to *lox4* was confirmed by PCR using forward primer GACGCGTTCGTGTCTGACT and reverse

primer GGACTCTTTCCGCCTTTGA. Seeds collected from plants confirmed to be *lox4* homozygous recessive were used as line N. The *opr3* knockout line (X) was kindly shared by Jianmin Zhou. The *opr3* knockout line (in Col-0 background with RAP-luciferase transgene inserted) was induced by EMS mutagenesis giving the G2471A base substitution which results in replacement of Trp138 by a stop codon.

Plant growth conditions

Pro-Mix "PGX" soil (Hummert International, Earth City, MO, USA) was mixed with tap water to saturation and autoclaved for 1 h and was cooled to room temperature before potting. The pots for planting were a 72-well TLC Square Plug tray (International Greenhouse Company, Danville, IL, USA), placed inside a tray with holes, then both were placed inside another tray without holes (Hummert International). To prepare for sowing, a tray was filled with 2.5 L of fertilizer solution (0.01 % Peters 20: 20: 20 (Hummert International) in tap water).

Randomized seed positions used in the three rounds of the experiment are shown in Figure 5.1. Each plant has a combined label including the tray label (e.g., F1-1, Figure 5.2) and the well number (Figure 5.1A). When sowing, a bamboo toothpick was used to place four seeds, evenly spaced, at the center of a well. After sowing, a tray was drained, covered with a propagation dome (Hummert International) and kept at 4 °C for 2 days before transfer to growth conditions (21 °C, 60 % humidity, 80 – 100 $\mu E\ m^{-2}\ s^{-1}$). On day 9 counting from the time the tray was transferred, the propagation dome was removed. On day 11, plants were thinned so that only one healthiest plant remained. Trays were watered by sub-irrigation once a week. On day 20, trays were irrigated with the 0.01 % fertilizer solution. Plants were subjected to low temperature treatments on day 28.

Cold acclimation and freezing treatment

Plants were cold acclimated and frozen using the protocol described in Chapter 3. Figure 5.3 describes the temperature regimes applied.

Sampling and lipid extraction

Two types of samples were collected from each plant (72 plants per tray): (1) leaves 5 and 6 in a 50-ml tube containing 25 ml of distilled water (Dillons Supermarket, Manhattan, KS, USA) and (2) the rest of the rosette in a 20-ml vial containing 4 ml of isopropanol with 0.01% butylated hydroxytoluene (BHT) at 75 °C. The two samples from each plant were each labeled to indicate the plant from which they were derived (for example, the two samples from plant 3 of tray F1-1 in Figure 5.2 were both labeled "F1-1-3"). The sample labels were printed on Tough Tag labels (Diversified Biotech, Dedham, MA, USA), which were used to label the 50-ml tubes and the 20-ml vials.

Harvesting was carried out on a cart carrying two heat blocks with the blocks removed to house the 20-ml vials (the vials sat in the area where the blocks normally sit). The thermal blocks were maintained at 75 °C. Other material included four 40-slot racks to hold 72 tubes containing distilled water (two racks to hold tubes before harvesting, 2 racks to hold tubes after leaves 5 and 6 had been dropped in). For trays 1, 2, 4, 6, 9, 10, 11, 12, 13, 14, 15, 16, and 17 (treatments which ended with a period at 21 °C), the rolling cart was positioned right next to the growth chamber (at room temperature). For trays 3 and 5, the cart was situated inside the cold room where the trays were treated (the heating block heaters were set at 90 °C to compensate for the cold air and still maintain the vials at 75 °C). For trays 7 and 8, the cart was positioned next to the freezing chamber in which the trays were frozen (harvesting occurred at room temperature). At the end of each of the indicated treatment periods (Figure 5.3), the leaf material from each corresponding tray was harvested simultaneously by four laboratory personnel so that the average harvesting time was less than 20 min per tray. The four personnel worked in two pairs, each pair had one "cutter" and one "dipper" who stood facing each other across the cart. The "cutter" procedure for each plant was: (1) cut the whole rosette off the roots, (2) cut leaves 5 and 6 and drop them into the gloved palm of the corresponding "dipper", and (3) drop the rest of the rosette into the corresponding pre-labeled, pre-heated 20-ml vial, cap the vial, shake the vial slightly to fully submerge the rosette, and return the vial to the heating block heaters. The "dipper" procedure for each plant included: (1) receive leaves 5 and 6 from the corresponding "cutter", (2) rinse the leaves in a beaker of distilled water, and (2) drop the leaves into the pre-labeled 50-ml tube, cap the tube, and shake the tube to completely submerge the leaves in water.

For all trays except for trays 7 and 8, the tray was set on the cart during harvesting and the two pairs of personnel sequentially harvested the plants in order from 1 to 72. For trays 7 and 8, the trays were pre-cut (before seed sowing) into blocks of 4 plants with consecutive labels (e.g., 1-4, 5-8, 9-12…). At the end of the freezing treatment, the freezing chamber continued to maintain temperature at -8 °C. The blocks of 4 plants were taken out of the freezing chamber one at a time and were quickly harvested (two plants per harvesting pair) before thawing occurred. The freezing chamber was opened and closed quickly; the temperature increased from -8 °C to -7 °C or -6 °C; the awaiting plants remained well frozen. In all cases, after the last plant of a tray was harvested, the vials were incubated at 75 °C for an additional 15 min and were allowed to cool to room temperature before being stored at -80 °C.

To begin lipid extraction, each cardboard box of 72 samples from one tray stored at -80 °C was allowed to warm to room temperature. To each vial, 12 ml of the extraction solvent (chloroform: methanol: 300 mM ammonium acetate in water, 30: 41.5: 3.5, v/v/v) were added. The vials were shaken on an orbital shaker at 100 rpm for 24 h. After being shaken, the extracted rosette from each vial was removed and put into an empty vial with the same label. The original vials with solvent were stored at -20 °C. The extracted rosettes in non-capped vials were dried first in a fume hood for 1-2 h and then in an oven at 105 °C overnight. The dried rosettes were allowed to cool to room temperature and weighed using a Mettler-Toledo AX balance (Mettler-Toledo, Greifensee, Switzerland). To eliminate electrostatic forces resulting from drying of the rosettes, the rosettes were passed through an anti-static U ionizer (Haug, Germany).

Plant phenotyping

Photos of each tray were taken at multiple times including: (1) immediately before fertilizing at 20 days old, (2) immediately before the last watering which occurred on the day before the tray was harvested (trays 1, 2, 4, 6, 9, 12, and 15) or treated (trays 3, 5, 7, 8, 10, 11, 13, 14, 16, and 17), and (3) immediately before the tray was harvested (trays 7 and 8 were not photographed immediately prior to harvesting to avoid thawing). At each time point, a tray was photographed three times with three F-stop values (f/11, f/13, and f/14), using a Nikon D40 camera with an 18-55 mm lens. Other camera parameters were: ISO 200, focal length 35-45 mm, exposure time 250

s^{-1}, built-in flash "ON". One high quality photo of each tray at each time point was chosen (total of three photos per tray) for determining the number of leaves of each plant. The cotyledons were not counted in the total number of leaves. For an emerging leaf, it was only counted if the width of the petiole was estimated to be less than half of the maximal width of the leaf.

For ion leakage measurements, when each plant was harvested, leaves number 5 and 6 (as determined by Telfer et al., 1997) were dropped into a 50-ml glass tube containing 25 ml of distilled water (purchased from Dillons Supermarket, Manhattan, KS). The tubes were tightly capped and shaken at 150 rpm for 2 h. Conductivity was measured using an electrical conductivity meter CON 510 (Oakton Instruments, Vernon Hills, IL). After the first measurement, the tubes were re-capped and incubated in a water bath at 80 - 90 °C for 2 h and were allowed to cool to room temperature so the total ion leakage could be measured. Ion leakage was the percentage of the first conductivity value in relation to the total conductivity value (second value) for each plant.

Mass spectrometry analysis

A mixture of internal standards in chloroform was included in all mass spectrometry samples for analysis (including the sample vials, the internal standard-only vials, and the quality control (QC) vials). The composition of the internal standard mixture (20 µl) added per 0.04 mg dry mass of leaf tissue is listed in Table 5.2.

A quality control (QC) stock was prepared by pooling 1 ml from samples 1-10 of all the trays of replication round 1 and 2 (a total of 34 trays). The total volume of the QC stock was 340 ml and the concentration was 0.688 mg leaf dry mass ml^{-1}. The stock was divided into 34 aliquots of 10 ml each and the aliquots were stored at -20 °C. To make mass spectrometry QC vials, a QC stock aliquot was mixed with 3.4 ml of the internal standard mix (measured with a 1-ml glass syringe) and 224.6 ml (measured with a 250-ml glass cylinder) of mass spectrometry solvent (isopropanol: chloroform: methanol: 300 mM ammonium acetate in water, 25: 30: 41.5: 3.5, v/v/v/v). After being shaken, 1.4 ml of the mixture was dispensed into each of 156 amber 2-ml vials labeled "QC1" to "QC39" (four sets). The prepared QC mass spectrometry vials were stored at -80 °C and were brought to room temperature 1 h before analysis.

To prepare the sample mass spectrometry vials, the 20-ml vials containing the extracted total lipids were brought to room temperature from -20 °C ~2 h prior to handling, one tray (72 vials) at a time. To each of the 72 2-ml amber vials (labeled "1" to "72", the tray name, for example "F1-1", was written on the rack), 20 µl of the internal standard mixture (measured with a 100-µl syringe) was added first. In sequential order from 1 to 72, a volume that contained 0.04 mg leaf dry mass from a 20-ml vial was added to the similarly labeled 2-ml amber vial; a volume of mass spectrometry solvent (isopropanol: chloroform: methanol: 300 mM ammonium acetate in water, 25: 30: 41.5: 3.5, v/v/v/v) was added to the total volume of 1.4 ml; and the amber vial was capped before the next sample was added to the next amber vial. The mass spectrometry solvent volume was measured and dispensed with a 2.5-ml dispenser (Eppendorf, Hamburg, Germany) mounted on top of the solvent bottle. Since the smallest increment of dispenser was 50 µl, the calculated mass spectrometry solvent volume was adjusted to the closest marked level of the dispenser. For example, all volumes from 1226-1275 µl were adjusted to 1250 µl and all volumes from 1276-1325 µl were adjusted to 1300 µl. In each tray, 6 internal standard-only vials were included (labeled "IS1" to "IS6"); each contained 20 µl of the internal standard mix and 1.38 ml (total of 1.4 ml) of the mass spectrometry solvent. For mass spectrometry analysis, the 72 sample vials from each tray, together with 6 "IS" vials, and 39 "QC" vials were arranged in 3 VT-54 racks.

Table 5.3 lists the positions of mass spectrometry vials in the first VT-54 rack with QC vial 1-13, IS vial 1-2, and sample vial 1-24. The second and third VT-54 rack have the same arrangement with the QC 14-26, IS 3-4, sample 25-48 for the second VT-54 rack and QC 27-39, IS 5-6, sample 49-72 for the third VT-54 rack.

Data processing and statistical analysis

Data from experimental samples were normalized to QC samples, dendrogram, and graphs were produced using the same methods in Chapter 4. T-tests were done using Excel. The Spearman's correlation coefficient ρ between lipid analytes and ion leakage were calculated using the Metaboanalyst website.

Results

Our analysis of lipid compositions and phenotypes of wild-type, AH, and LOX knockouts were designed to capture behaviors of Arabidopsis plants at critical points during a cold acclimation/freezing/thawing time course. They included early cold acclimation (1 h at 4 °C, tray 3), late cold acclimation (three days at 4 °C, tray 5), right after freezing treatment at -8 °C for 2 h with or without cold acclimation (trays 8 and 7, respectively), 1 h, 3 h, and 24 h of thawing at 21 °C after freezing treatment with cold acclimation (tray 11, 14, and 17, respectively) or without cold acclimation (tray 10, 13, and 16, respectively).

Ablation of pPLAIIγ enhances cold acclimation effect on freezing tolerance

Electrolyte leakage measurements provided a quantitative assessment of leaf damage throughout the course of low temperature exposure. As shown in Figure 5.4, ion leakage in non-acclimated Col-0 plants was at its highest level immediately after the plants were removed from the freezing chamber (74-h point). The cold acclimation effect, i.e. the increased freezing tolerance, was demonstrated by the lower ion leakage percentage of acclimated Col-0 plants at this time. In the thawing phase (75-h, 77-h, and 98-h time points), the acclimated Col-0 plants showed clear signs of recovery as the ion leakage dropped close to the level of the untreated control plants, especially at 24 h after freezing. On the other hand, the ion leakage of the non-acclimated Col-0 plants stayed high even 24 h after freezing. Differences between acclimated and non-acclimated Col-0 plants during the thawing phase were also visible as shown in Figure 5.5. At 24 h after freezing, the acclimated plants appeared normal, except for some leaf areas with visible damage. Similarly treated plants were observed to continue growing, bolting, and eventually produce seeds. On the other hand, the non-acclimated plants were shrunken and dry. Leaves of similarly treated plants were observed to turn yellow and die, but the shoots were able to make new leaves after 7 – 10 days.

To identify mutants that affect freezing response of Arabidopsis, the ion leakage percentages of the 22 lines during exposure to freezing and thawing were compared to those of Col-0. Line E (*pPLAIIγ* knockout) had lower ion leakage in cold acclimated plants during recovery compared to wild-type, especially at the 77 h time point (3 h of thawing after freezing, $p < 0.1$), as depicted

in Figure 5.4. Acclimated pPLAIIγ knockout plants were visibly less damaged than acclimated Col-0 at 3 h after freezing (77 h time point, Figure 5.5).

Freezing-induced lipid changes occur in clusters

In 35 min per sample, our MRM-based analysis was able to measure 377 lipid species. Before further data analysis, several rules were applied to ensure quality of the data. First, we eliminated lipid species with background (average intensity measured in internal-standard-only samples) higher than 40% of the averaged signals detected in all QC samples. Second, we eliminated lipids with background higher than 20% of the QC average if the majority of the chemically similar lipid analytes were eliminated by the first rule. Applying the first two rules eliminated 34 compounds. Third, we eliminated 12 more lipids that measured less than 0.1 pmol in more than 1000 experimental samples (out of 17*72 = 1224 experimental samples). Our dataset contains 331 lipid analytes, each with 1224 measurements.

Since the dataset was acquired over a long period (~ two months), variation due to instrumental performance was very likely to occur. To correct for this variation, signals of each lipid in all experimental samples were normalized to the QC samples using the same method as described in Chapter 4.

It is hypothesized that cold-acclimation, freezing and thawing affect different biochemical pathways. Each pathway, in turn, controls the biosynthesis and metabolism of multiple lipid analytes. With the assumption that metabolites affected by the same pathway will behave in the same manner as a function of cold, freezing, and thawing treatments, pathways that are affected by low temperature treatments can be identified by clustering lipids that vary together across treatments and individual plants. To identify the clusters formed in low temperature stress, we calculated a 331 x 331 distance matrix using data from 102 (17 conditions x 6 replicates) wild-type Col-0 plants of the first round of the experiment. The level of each lipid analyte in all samples was ranked (1 to 1224), and Spearman's correlation coefficient ρ was calculated for each pair of compounds. A single linkage hierarchical clustering algorithm, using the maximal ρ for each lipid analyte, was applied to generate clusters. Figure 5.6 is a dendrogram of lipids that

correlate with $\rho > 0.6$ (301 lipids). Lipids that correlate with maximal $\rho > 0.8$ form clusters labeled from A to J. Within clusters A, B, and J, 94 lipids correlate with maximal $\rho > 0.95$ forming 16 sub-clusters. For each sub-cluster, levels of 1 or 2 representative lipids of Col-0 and pPLAIIγ mutant (line E) are shown in Figure 5.7 as a function of temperature treatment.

Many known cold- and freezing-induced pathways are visible in treated Col-0 via the sub-clusters shown in Figure 5.6 and their patterns shown in Figure 5.7. The degradation of PC (sub-cluster B1, B2, and B5), PE (sub-cluster B3 and B4), MGDG (sub-cluster B6), and DGDG (sub-cluster B7, and B8), together with the formation of PA (sub-cluster A2) can be explained, at least partially, by the activation of phospholipase D (Welti et al., 2002). Also, it cannot be ruled out that PAs are synthesized from DAGs produced by phospholipase C (Testerink and Munnik, 2005). The cold acclimation effect is evident as the degradation that occurred in acclimated Col-0 plants was not as severe and the plants almost recovered to control levels by 24 h after freezing while the lipids in non-acclimated plants were largely hydrolyzed and showed no sign of recovery. Interestingly, in acclimated plants, PE with long chain fatty acids (sub-cluster B4) accumulated after the cold acclimation and maintained higher levels thoughout the freezing and thawing treatments compared to the control, instead of being degraded as in the non-acclimated plants.

Although both LPC (sub-cluster A1) and PA (sub-cluster A2) are products of membrane lipid hydrolysis, their patterns of changes in response to low temperature treatments are substantially different. While PA was induced significantly more in non-acclimated plants than in acclimated thoughout the post-freezing period, LPC was induced more in acclimated plants, especially immediately and 1 h after freezing.

The formation of TrGDG (sub-cluster A5), coupled closely with TeGDG synthesis (Figure 5.6), was more dramatic in acclimated plants than in non-acclimated plants during the thawing process. The formation of TAG (sub-cluster A3) followed a similar pattern (much more in acclimated plants than in non-acclimated plants) and TAG seemed to keep accumulating in acclimated plants even at 3 h and 24 h after freezing.

The Gal-acylation of MGDG to form acMGDG (sub-cluster 6 and sub-cluster 7) was complex to interpret as the acyl groups involved were also affected by induced oxidation. acMGDG with three non-oxidized acyl groups (most of sub-cluster A7a) was induced in both non-acclimated and acclimated plants immediately at the end of the freezing period and was induced to significantly higher levels in non-acclimated plants than in acclimated plants. Even at 24 h, when the levels in acclimated plants tended to decrease to control level, the levels in non-acclimated plants showed little reduction, making the difference even greater. Sub-cluster A7b includes mostly acMGDGs with 2 oxidized acyl groups out of the total 3 acyl groups. The overall pattern of sub-cluster A7b somewhat resembles that of sub-cluster A7a and non-acclimated plants accumulated more at 24 h into thawing. A very striking difference occurred after 1 h of thawing, when the more oxidized acMGDGs (cluster A7b) were much higher in the acclimated plants compared to the non-acclimated ones. Fully oxidized acMGDGs (sub-cluster A6) were distinctive from less oxidized acMGDG in that they were not only more induced in acclimated plants but also maintained higher levels after 1 h, 3 h, and 24 h of thawing. This pattern also helped to distinguish between possible annotations of some acMGDG. For example, acMGDG(18:4-O/36:6) and acMGDG(18:4-O/34:8-2O) have the same mass and same head-group fragment but the pattern and clustering with acMGDG(18:4-O/36:8-2O) (sub-cluster A6) suggests that the fully oxidized annotation, acMGDG(18:4-O/34:8-2O), may be the correct one for the majority of lipid detected with the relevant analytical parameters in the current experiment.

The induction pattern of ASG (sub-cluster A4) was relatively similar to that of non-oxidized acMGDG (sub-cluster A7a). ASG was induced significantly in both acclimated and non-acclimated plants as early as 1 h after freezing. Especially at 24 h post-freezing, non-acclimated plants maintained a higher level of ASG compared to acclimated ones. The changes in sterol ester synthesis in response to low temperature, on the other hand, occurred in a unique pattern: sterol esters (cluster J1) were induced during the acclimation period. Freezing temperature also induced synthesis of sterol esters; however, after 24 h of thawing, markedly higher levels of sterol esters were detected in acclimated plants, which were exposed to both cold and freezing, compared to non-acclimated plants, which were exposed only to freezing.

Lipid changes correlate with freezing-induced leaf damage

It is hypothesized that freezing- and thawing-induced changes in lipid sub-clusters play different roles in determining the ultimate fate of the plants in response to the stress. Degradation of structural lipids and synthesis of antagonistic lipids might coincide with more severe tissue damage; whereas, induction and stably high levels of healing lipids could result in recovery from stress damage. To further investigate possible roles of lipids in each sub-cluster (Figure 5.6) in plant response to freezing, the Spearman's correlation coefficient ρ between lipids and leaf damage as measure by ion leakage was calculated using data from Col-0 plants. Table 5.4 shows the average and standard deviation of all ρ values within each lipid sub-cluster. It is obvious that non-structural, freezing induced lipids (cluster A) positively correlate with leaf damage, while structural lipids (cluster B) negatively correlate with leaf ion leakage. Highest among sub-clusters that have positive ρ are A2 (PA), A7a (acMGDG with mostly non-oxidized acyl groups), and A4 (ASG). The structural lipids with lowest negative ρ values are PCs (sub-cluster B1, B5, and B2) and MGDGs (sub-cluster B6). Interestingly, among the A-cluster lipids, TAG (sub-cluster A3) express distinctively less correlation with leaf damage, suggesting different involvement in plant responses compared to its stress-induced counterparts. Similarly, the long-chain PE (sub-cluster B4) has significantly higher correlation with leaf ion leakage, compared to other presumably structural lipid classes.

Formation of OPDA-containing acMGDG is enhanced in pPLAIIγ knockout

A hypothesis which might explain why cold-acclimated line E plants (*pPLAII γ* knockout) showed better appearance (Figure 5.5) and lower ion leakage (Figure 5.4) than Col-0 plants after 3 h and 24 h of thawing is that ablation of pPLAIIγ causes alteration(s) in how lipids in sub-clusters (Figure 5.6) respond to cold-acclimation, freezing, and thawing. To test this hypothesis, autoscaled lipid levels of representative lipids of all sub-clusters of *pPLAIIγ* knockouts were compared to those of Col-0 plants throughout the temperature regime. Figure 5.7 shows comparisons of autoscaled lipid levels between Col-0 and *pPLAIIγ* knockout of all 17 sub-clusters. The majority of sub-clusters are not different between knockout and wild-type except for PC with 38 acyl carbons (sub-cluster B1, Figure 5.7i) and oxidized acMGDG (sub-cluster A6, Figure 5.7f). Since the levels of PC with 38 acyl carbons were inconsistent across untreated

plants, the differences observed are not very likely to be related to the applied temperature treatments. Sub-cluster A6, (oxidized acMGDG), on the other hand, shows consistently low levels in untreated controls. As shown in Figure 5.7f, cold-acclimated *pPLAIIγ* knockouts expressed higher levels of lipids in sub-cluster A6 (acMGDG(18:4-O/34:8-2O) and acMGDG(18:4-O/36:8-2O)) at 0 h (74^{th} h time point, $p = 0.002$), 1 h (75^{th} h time point, $p = 0.07$) and 24 h (98^{th} h time point, $p = 0.02$) of thawing after freezing compared to Col-0 plants.

Discussion

In this chapter, the analytical approach and the co-occurrence analysis developed in Chapter 4 were applied to identify lipid analytes that were similarly metabolized when Arabidopsis responded to low temperature stress. Similar to wounding response, low temperature response induced changes in levels of the majority of lipid analytes, either increasing (cluster A) or decreasing (cluster B, Figure 5.6 and Figure 5.7). Similar sub-clusters were observed in low temperature response, including acMGDG (sub-cluster A6, A7a, and A7b), ASG (sub-cluster A4), PA (sub-cluster A2), TAG (sub-cluster A3), DGDG (sub-cluster B7 and B8), MGDG (sub-cluster B6), PC (sub-cluster B5), and PE (sub-cluster B3). Some sub-clusters only formed in low temperature reponse, not in wounding response, including long-chain PC (sub-cluster B2) and long-chain PE (sub-cluster B4). This suggests that unique lipid metabolizing enzyme(s) may have been activated only in response to low temperature and not in wounding response. On the other hand, MGDG(18:4-O/16:4-O) and MGDG(18:4-O/18:4-O) did not formed a sub-cluster in low temperature response. This suggests that acyl oxidation was activated to a lesser extent in low temperature response compared to wounding response (Vu et al., 2014). This might also explain the smaller sub-cluster of fully oxidized acMGDGs with only two members, acMGDG(18:4-O/34:8-2O) and acMGDG(18:4-O/36:8-2O) induced by low temperature (sub-cluster A6).

The TrGDG formation (sub-cluster A5) was presumably catalyzed by the galactolipid: galactolipid galactosyl transferase encoded by SFR2 (Moellering et al., 2010). In this reaction, a galactose from an MGDG is transferred onto MGDG, DGDG, and TrGDG forming β-linked

DGDG, TrGDG, and TeGDG, respectively. In wounding response, the inclusion of PA(34:6) in the same sub-cluster as TrGDG(34:6) and TeGDG(34:6) suggests that DAG(34:6) released by SFR2 was converted to PA(34:6). In low temperature response, PA(34:6) was not in the TrGDG sub-cluster; instead, PA(34:6) more closely correlated with the PA sub-cluster (A2). This suggests that PA(34:6) may have been formed mostly from MGDG(34:6) hydrolysis in low temperature stress.

Co-occurrence analysis of lipid analytes in low temperature response provides biochemical insights into cold acclimation. Many sub-clusters were specifically induced more in cold-acclimated plants including LPC and LPE (sub-cluster A1), TAG (sub-cluster A3), TrGDG (sub-cluster A5, oxidized acMGDG (sub-cluster A6), long-chain PE (sub-cluster B4), and sterol esters (sub-cluster J1, Figure 5.7). Some sub-clusters were hydrolyzed to a lesser extent in cold-acclimated plants compared to non-acclimated plants: PC with 38 acyl carbons (sub-cluster B1), long-chain PC (sub-cluster B2), PE with 36 acyl carbons (sub-cluster B3), PC and PS (sub-cluster B5), MGDG (sub-cluster B6), and DGDG (sub-cluster B7 and B8, Figure 5.7). On the other hand, some sub-clusters were specifically induced more in non-acclimated plants compared to acclimated plants including PA (sub-cluster A2), ASG (sub-cluster A4), and normal-chain acMGDG (sub-cluster A7a, Figure 5.7). It is noted that while the majority of the metabolic differences between non-acclimated and acclimated plants occurred during the thawing period, fewer changes were detected during the cold acclimation period. Lipid analytes that were induced during cold acclimation include PE (sub-cluster B3 and B4) and sterol esters (sub-cluster J1, Figure 5.7).

In this chapter, co-occurrence analysis was employed to identify metabolically active lipid analytes in response to low temperature. The knowledge was utilized to focus our comparisons between knockouts and wild-types on these metabolically important lipid analytes. Cold-acclimated *pPLAIIγ* knockout plants were found to induce higher levels of OPDA-containing acMGDGs (sub-cluster A6) compared to cold-acclimated Col-0 plants during thawing (Figure 5.7f). The coincidence between higher levels of acMGDG(18:4-O/34:8-2O) and acMGDG(18:4-O/36:8-2O) and faster recovery of cold-acclimated *pPLAIIγ* knockout plants suggests a "healing" role of the concentration of OPDA in acMGDG (reported by Vu et al., 2014). pPLAIIγ may

encode an acyl hydrolase that tends to hydrolyze OPDA-containing acMGDGs specifically. pPLAIIγ was previously shown to have higher galactolipase activity than phospholipase activity in vitro (Rietz et al., 2010).

References

Bell E, Creelman RA, and Mullet JE (1995) A chloroplast lipoxygenase is required for wound-induced jasmonic acid accumulation in Arabidopsis. Proc. Natl. Acad. Sci. U. S. A. **92**, 8675-8679.

Chauvin A, Caldelari D, Wolfender JL, and Farmer EE (2013) Four 13-lipoxygenases contribute to rapid jasmonate synthesis in wounded *Arabidopsis thaliana* leaves: a role for lipoxygenase 6 in responses to long-distance wound signals. New Phytol. **197**, 566-575.

Chen M, and Thelen JJ (2013) ACYL-LIPID DESATURASE2 Is Required for Chilling and Freezing Tolerance in Arabidopsis. Plant Cell **25**, 1430-1444.

Comfurius P, and Zwaal RF (1977) The enzymatic synthesis of phosphatidylserine and purification by CM-cellulose column chromatography. Biochim. Biophys. Acta **488**, 36-42.

Degenkolbe T, Giavalisco P, Zuther E, Seiwert B, Hincha DK, and Willmitzer L (2012) Differential remodeling of the lipidome during cold acclimation in natural accessions of *Arabidopsis thaliana*. Plant J. **72**, 972-982.

Feussner, I., and Wasternack, C. (2002) The lipoxygenase pathway. Annu. Rev. Plant Biol. **53**, 275- 297.

Hamberg, M., de Leon, I.P., Rodriguez, M.J., and Castresana, C. (2005) α-Dioxygenases. Biochem. Biophys. Res. Comm. **338**, 169-174.

Ishiguro S, Kawai-Oda A, Ueda J, Nishida I, and Okada K (2001) The *DEFECTIVE IN ANTHER DEHISCIENCE* gene encodes a novel phospholipase A1 catalyzing the initial step of jasmonic acid biosynthesis, which synchronizes pollen maturation, anther dehiscence, and flower opening in Arabidopsis. Plant Cell **13**, 2191-2209.

Keunen E, Remans T, Opdenakker K, Jozefczak M, Gielen H, Guisez Y, Vangronsveld J, and Cuypers A (2013) A mutant of the *Arabidopsis thaliana* LIPOXYGENASE1 gene

shows altered signalling and oxidative stress related responses after cadmium exposure. Plant Physiol. Biochem. **63**, 272-280.

La Camera S, Balagué C, Göbel C, Geoffroy P, Legrand M, Feussner I, Roby D, and Heitz T (2009) The Arabidopsis patatin-like protein 2 (PLP2) plays an essential role in cell death execution and differentially affects biosynthesis of oxylipins and resistance to pathogens. Mol. Plant Microbe Interact. **22**, 469-481.

La Camera S, Geoffroy P, Samaha H, Ndiaye A, Rahim G, Legrand M, and Heitz T (2005) A pathogen-inducible patatin-like lipid acyl hydrolase facilitates fungal and bacterial host colonization in Arabidopsis. Plant J. **44**, 810-825.

Lee HY, Bahn SC, Shin JS, Hwang I, Back K, Doelling JH, and Ryu SB (2005) Multiple forms of secretory phospholipase A2 in plants. Prog. Lipid Res. **44**, 52-67.

Li M, Bahn SC, Fan C, Li J, Phan T, Ortiz M, Roth MR, Welti R, Jaworski J, and Wang X (2013) Patatin-Related Phospholipase pPLAIIIδ Increases Seed Oil Content with Long-Chain Fatty Acids in Arabidopsis. Plant Physiol. **162**, 39-51.

Li W, Li M, Zhang W, Welti R, and Wang X (2004) The plasma membrane-bound phospholipase Dδ enhances freezing tolerance in *Arabidopsis thaliana*. Nat. Biotechnol. **22**, 427-433.

Li W, Wang R, Li M, Li L, Wang C, Welti R, and Wang X (2008) Differential degradation of extraplastidic and plastidic lipids during freezing and post-freezing recovery in *Arabidopsis thaliana*. J. Biol. Chem. **283**, 461-468.

López MA, Vicente J, Kulasekaran S, Vellosillo T, Martínez M, Irigoyen ML, Cascón T, Bannenberg G, Hamberg M, and Castresana C (2011) Antagonistic role of 9-lipoxygenase-derived oxylipins and ethylene in the control of oxidative stress, lipid peroxidation and plant defence. Plant J. **67**, 447-458.

Matos AR, Gigon A, Laffray D, Pêtres S, Zuily-Fodil Y, and Pham-Thi AT (2008) Effects of progressive drought stress on the expression of patatin-like lipid acyl hydrolase genes in Arabidopsis leaves. Physiol. Plant. **134**, 110-120.

Moellering ER, Muthan B, and Benning C (2010) Freezing tolerance in plants requires lipid remodeling at the outer chloroplast membrane. Science **330**, 226-228.

Montillet JL, Leonhardt N, Mondy S, Tranchimand S, Rumeau D, Boudsocq M, Garcia AV, Douki T, Bigeard J, Laurière C, Chevalier A, Castresana C, and Hirt H (2013) An

abscisic acid-independent oxylipin pathway controls stomatal closure and immune defense in Arabidopsis. PLoS Biol. **11**, e1001513.

Oh IS, Park AR, Bae MS, Kwon SJ, Kim YS, Lee JE, Kang NY, Lee S, Cheong H, and Park OK (2005) Secretome analysis reveals an Arabidopsis lipase involved in defense against *Alternaria brassicicola*. Plant Cell **17**, 2832-2847.

Rietz S, Dermendjiev G, Oppermann E, Tafesse FG, Effendi Y, Holk A, Parker JE, Teige M, and Sherer GFE (2009) Roles of *Arabidopsis* Patatin-Related Phospholipases A in Root Development Are Related to Auxin Responses and Phosphate Deficiency. Mol. Plant **3**, 524-538.

Shah, J. (2005) Lipids, lipases and lipid modifying enzymes in plant disease resistance. Annu Rev. Phytopathol. **43**, 229-260.

Shah, J., and Chaturvedi, R. (2008) Lipid signals in plant-pathogen interaction**.** Annu. Plant Rev. 34, 292-333.

Telfer A, Bollman KM, and Poethig RS (1997) Phase change and the regulation of trichome distribution in *Arabidopsis thaliana*. Development **124**, 645-654.

Testerink C, and Munnik T (2005) Phosphatidic acid: a multifunctional stress signaling lipid in plants. Trends Plant Sci. **10**, 368-375.

Vu HS, Roth MR, Tamura P, Samarakoon T, Shiva S, Honey S, Lowe K, Schmelz EA, Williams TD, and Welti R (2014) Head-group acylation of monogalactosyldiacylglycerol is a common stress response, and the acyl-galactose acyl composition varies with the plant species and applied stress. Physiol. Plant., In press.

Weber, H. (2002) Fatty acid-derived signals in plants. Trends Plant Sci. **7**, 217-224.

Welti R, Li W, Li M, Sang Y, Biesiada H, Zhou HE, Rajashekar CB, Williams TD, and Wang X (2002) Profiling membrane lipids in plant stress responses. Role of phospholipase Dα in freezing-induced lipid changes in Arabidopsis. J. Biol. Chem. **277**, 31994-32002.

Figures and Tables

Figure 5.1 Seed position in trays

(A) Schematic numbering of wells within a 72-well plug tray. (B), (C), and (D) Positions of letter-coded seeds for all trays of round 1, 2, and 3, respectively.

A

1	2	3	4	5	6	7	8	9	10	11	12
13	14	15	16	17	18	19	20	21	22	23	24
25	26	27	28	29	30	31	32	33	34	35	36
37	38	39	40	41	42	43	44	45	46	47	48
49	50	51	52	53	54	55	56	57	58	59	60
61	62	63	64	65	66	67	68	69	70	71	72

B

H	V	K	G	I	T	Q	C	A	W	X	P
W	P	H	O	J	P	U	L	O	M	A	D
V	J	F	M	C	S	V	C	I	I	S	T
N	H	G	B	B	K	N	E	E	R	T	X
U	Q	R	X	W	A	K	L	G	D	F	Q
J	D	U	S	O	R	L	E	N	F	M	B

C

P	L	E	U	X	Q	G	A	B	O	N	V
H	M	B	N	D	G	L	F	I	J	B	A
K	U	Q	F	T	W	T	I	P	V	X	L
Q	C	G	D	K	V	W	X	N	H	R	E
R	O	A	U	M	S	O	E	C	P	S	J
I	H	J	D	S	R	K	F	C	T	M	W

D

M	Q	I	X	A	G	J	E	D	U	T	B
H	O	B	I	U	V	J	T	C	E	J	V
L	K	B	A	A	I	Q	E	D	M	O	P
F	X	L	R	X	W	N	N	M	F	S	C
W	U	G	G	R	P	H	T	S	K	Q	D
N	F	S	W	C	R	K	V	P	L	H	O

Figure 5.2 Example of tray and plant labeling.

Each plant is referred to by a combined label including the tray label, e.g. “F1-1”, and the well position from 1 to 72. For example, the plants shown in this figure are labeled F1-1-1 to F1-1-72.

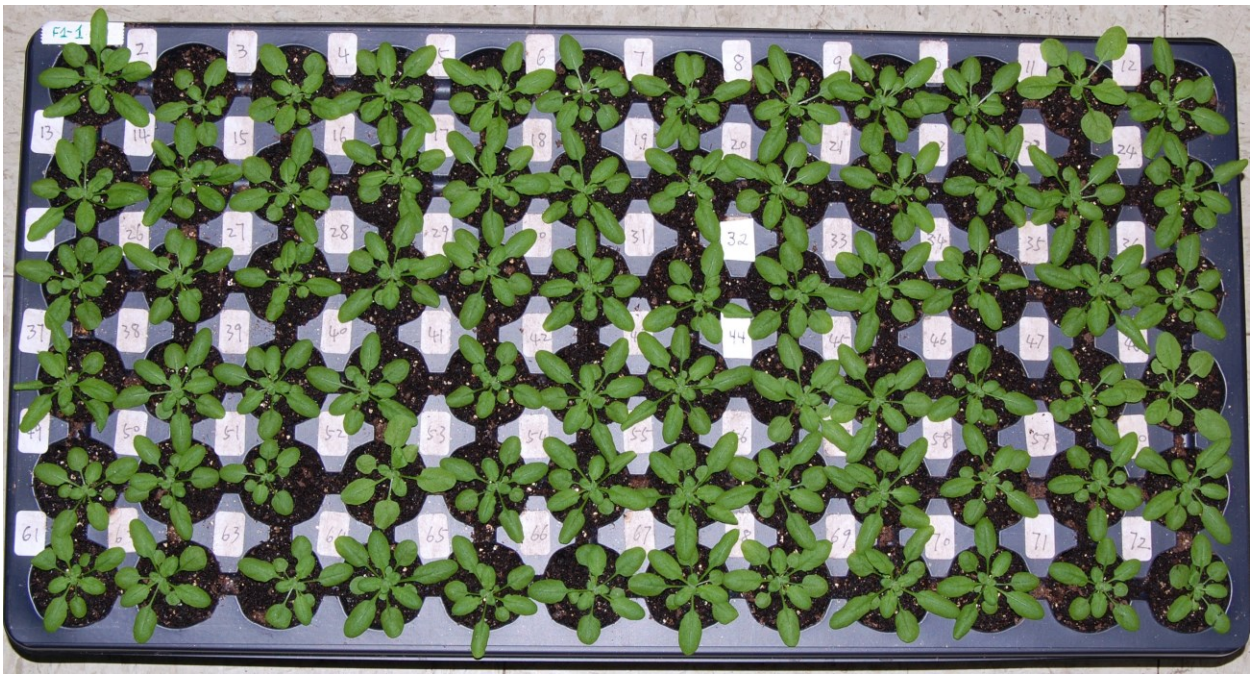
F2-1

Figure 5.3 Cold acclimation and freezing experiment design.

Plants entered the experiment at 30-day old. The X-axis is time (h) starting from the beginning of cold acclimation treatment at 4 °C. The Y-axis is temperature (°C). Each circle marks the time and temperature when and in which the correspondingly numbered tray was harvested. The line leading to each circle represents the temperature regime applied to the tray. Red line is untreated control (C); yellow line is non-acclimated (N); and blue is acclimated (A). In words, treatments applied to each tray are: tray **1** (no treatment), tray **2** (1 h at 21 °C), tray **3** (1 h at 4 °C), tray **4** (72 h at 21 °C), tray **5** (72 h at 4 °C), tray **6** (74 h at 21 °C), tray **7** (72 h at 21 °C and 2 h at -8 °C), tray **8** (72 h at 4 °C and 2 h at -8 °C), tray **9** (75 h at 21 °C), tray **10** (72 h at 21°C, 2 h at -8 °C, and 1 h at 21 °C), tray **11** (72 h at 4 °C, 2 h at -8 °C, and 1 h at 21 °C), tray **12** (77 h at 21 °C), tray **13** (72 h at 21 °C, 2 h at -8 °C, and 3 h at 21 °C), tray **14** (72 h at 4 °C, 2 h at -8 °C, and 3 h at 21 °C), tray **15** (98 h at 21 °C), tray **16** (72 h at 21 °C, 2 h at -8 °C, and 24 h at 21 °C), tray **17** (72 h at 4 °C, 2 h at -8 °C, and 24 h at 21 °C).

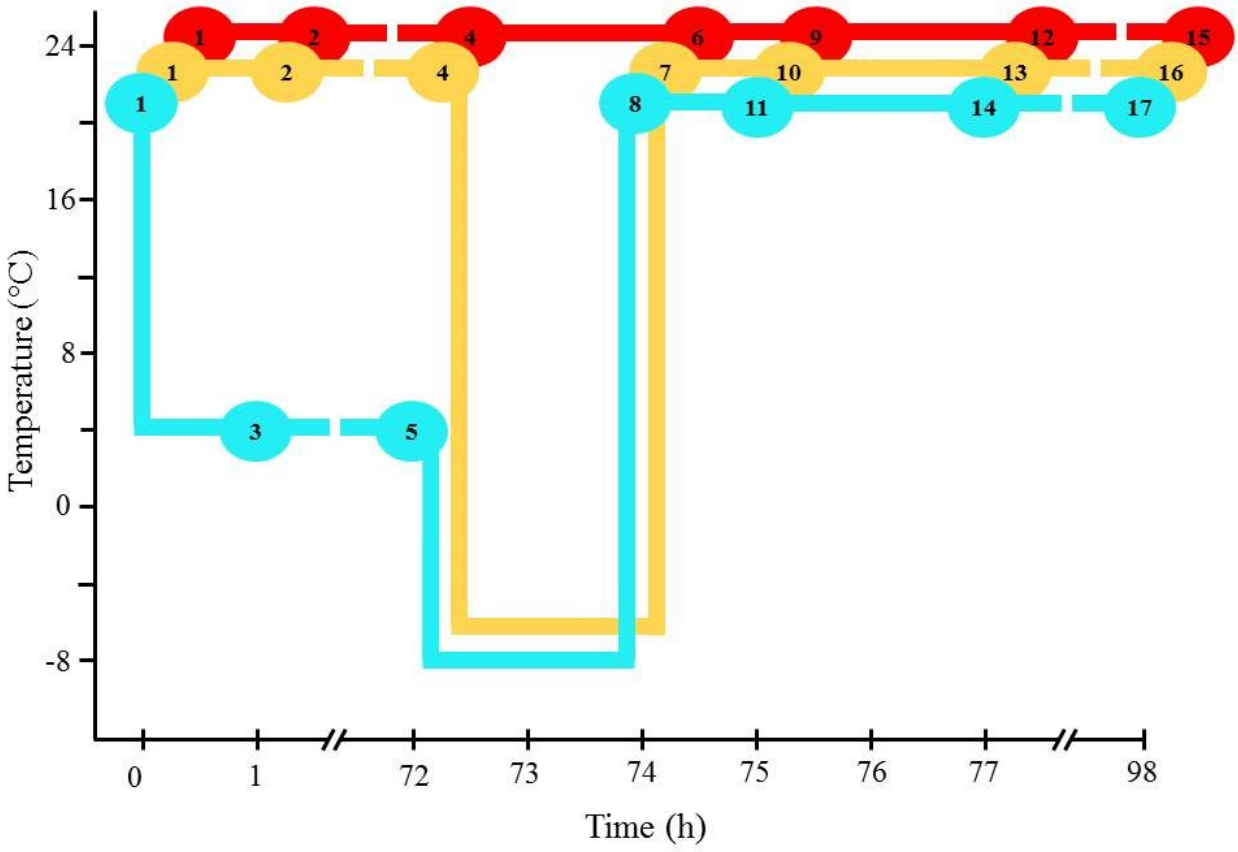

Figure 5.4 Low-temperature-induced leaf damage assessed by relative ion leakage.

The Y-axis is autoscaled level of ion leakage. The X-axis is the time course (h) of the temperature treatment (details of which are shown in Figure 5.3). At each time point, a set of six variables are shown, including untreated control (C), non-acclimated (N), and acclimated (A) of Col-0 and *pPLAIIγ* knockout (E). The box corresponding to each variable is also color-coded. The boxes summarize 6 replicates for Col-0 plants and 3 replicates for line E plants. The top and bottom of the boxes represent the 75 and 25 percentile; the bar inside the box marks the median, while the whisker is standard deviation.

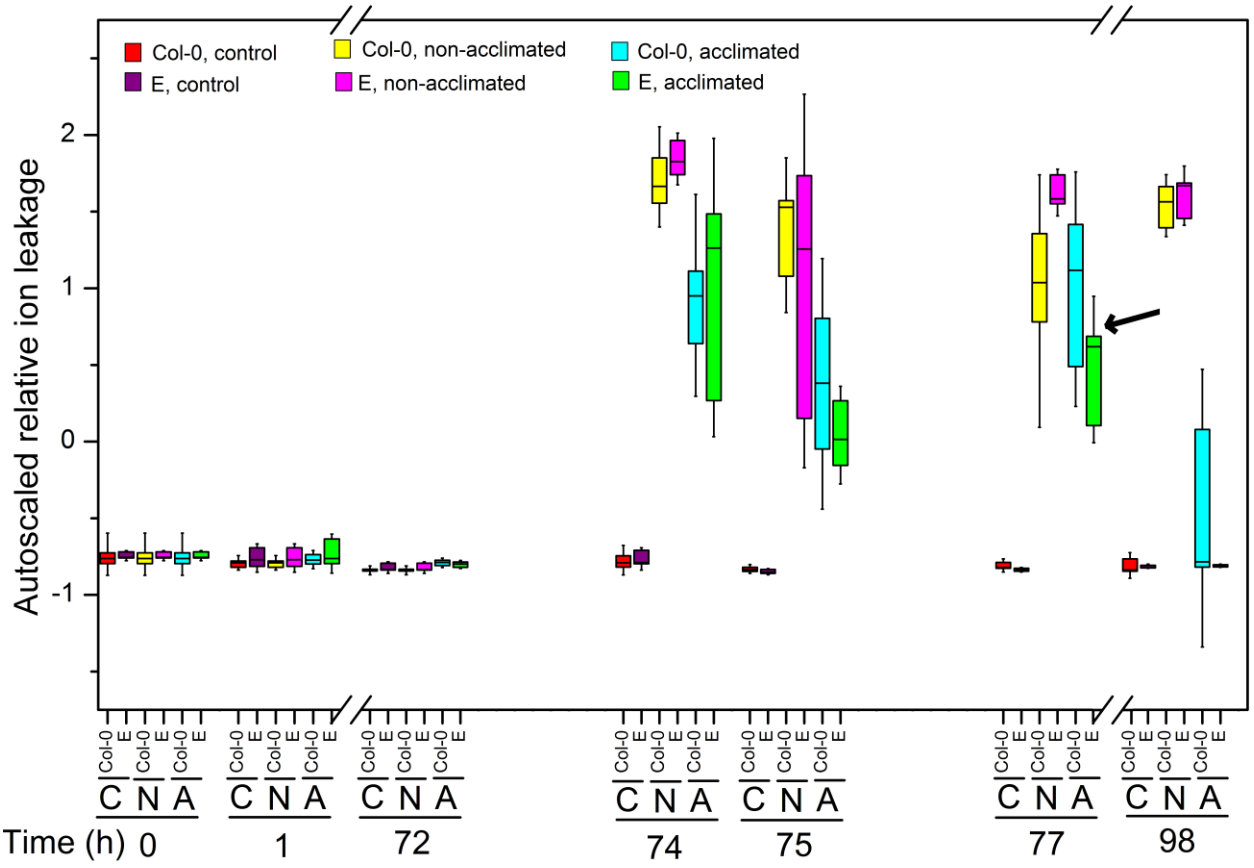

Figure 5.5 Plant appearance followed freezing treatments.

Photographs depict three wild-type plants (line A) and three line E plants (*pPLAIIγ* knockout) of untreated (control, C), non-acclimated frozen (N), and acclimated frozen (A) trays after 1 h (75th hour), 3 h (77th hour), and 24 h (98th hour) of thawing.

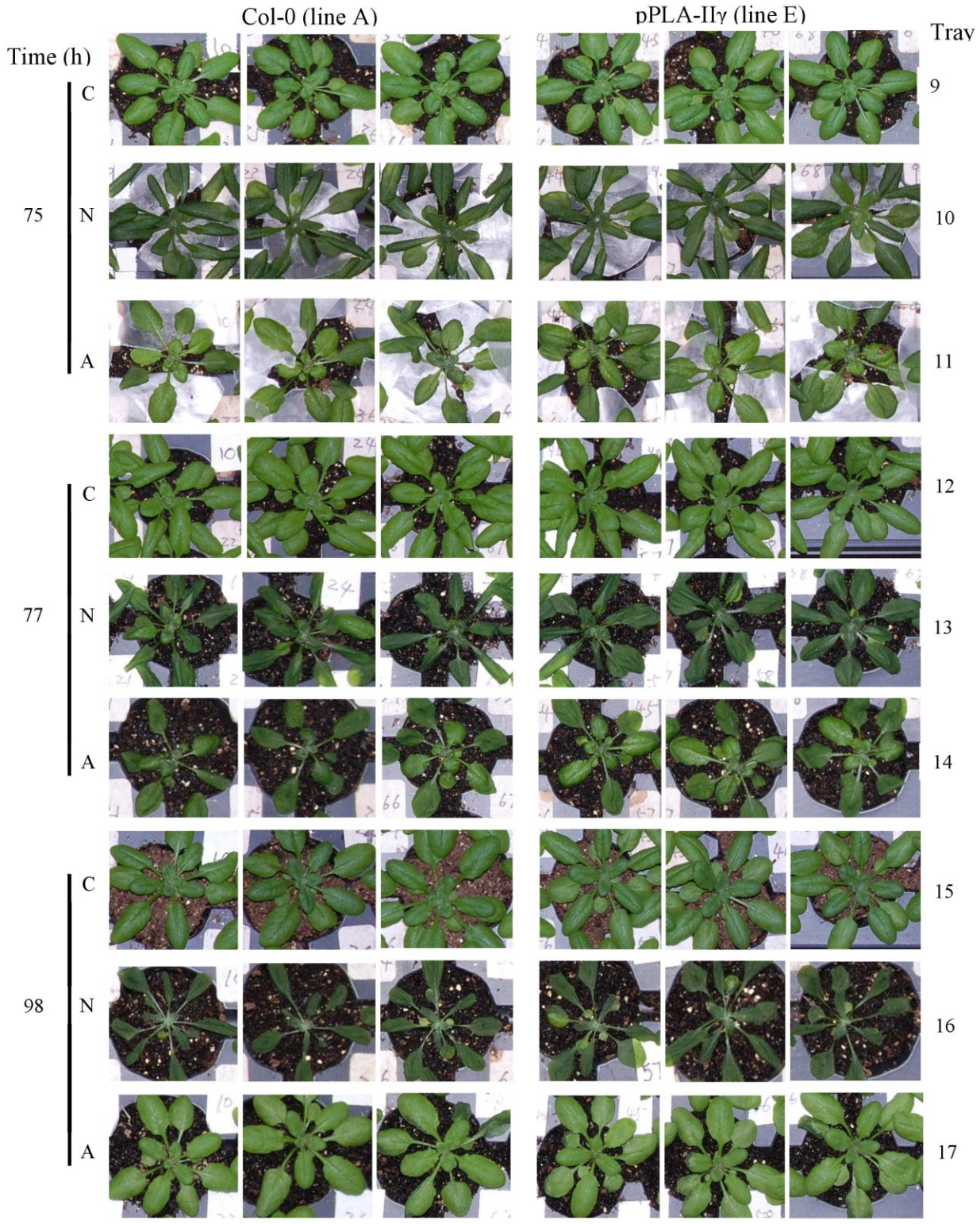
Col-0 (line A)
pPLA-IIγ (line E)
Time (h)
Tray
C
N
A
75
77
98
9
10
11
12
13
14
15
16
17

Figure 5.6 Dendrogram describing lipid co-occurrence of Col-0 plants in response to low temperature treatments.

The distance from the center to the circumference of the dendrogram represents Spearman's correlation coefficient ρ, measured by the horizontal scale in red. Only lipids with at least one $\rho > 0.6$ are shown in this dendrogram. Branches of lipids that correlate with all $\rho > 0.8$ are color-coded, labeled by a letter with the same color, from A to J, and are referred to as "clusters". Within cluster A, B, and J, branches of lipids correlate with each other with all $\rho > 0.95$ are called sub-clusters which are marked with red edges and bolded lipid names. Sub-cluster A7 is further divided into sub-cluster A7a and A7b due the difference in acyl composition. Sub-cluster A7a contains mostly acMGDG with all non-oxidized acyl groups, while sub-cluster A7b contains mostly acMGDG with two oxidized acyl groups.

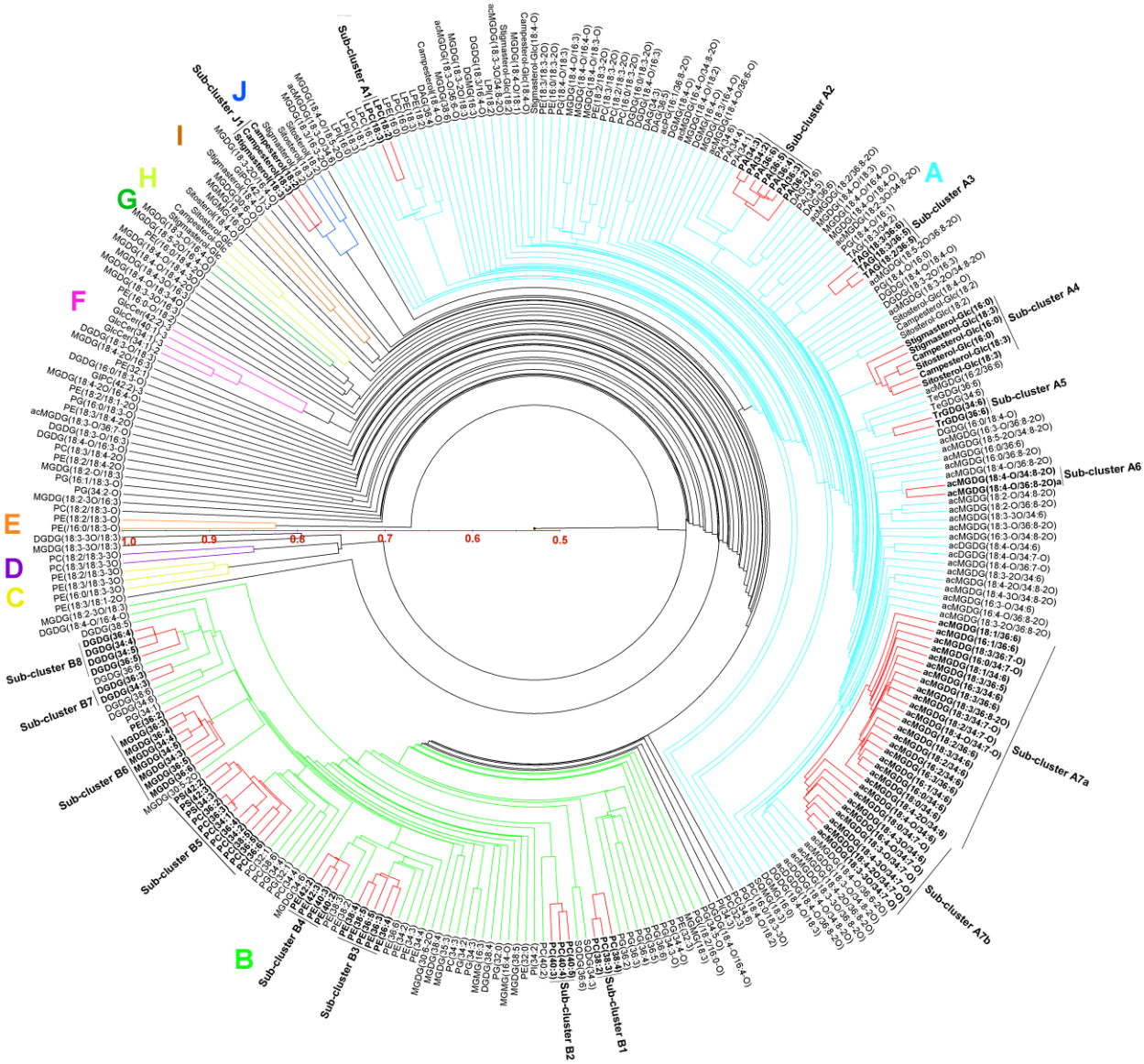
A
B
C
D
E
F
G
H
I
J
1.0
0.9
0.8
0.7
0.6
0.5
Sub-cluster A1
Sub-cluster A2
Sub-cluster A3
Sub-cluster A4
Sub-cluster A5
Sub-cluster A6
Sub-cluster A7a
Sub-cluster A7b
Sub-cluster B1
Sub-cluster B2
Sub-cluster B3
Sub-cluster B4
Sub-cluster B5
Sub-cluster B6
Sub-cluster B7
Sub-cluster B8
Sub-cluster J1

Figure 5.7 Comparisons of autoscaled lipid levels of sub-clusters between Col-0 and pPLAIIγ (line E) plants that underwent low temperature treatments. shows the design of stress treatments for quantitative analysis of oxidized polar lipid molecular species in *Arabidopsis thaliana* accession Columbia Col-0. In order to compare the patterns of oxidized lipids produced in various stresses, plants were grown simultaneously in a growth chamber at 22°C under 14 h light/10 h dark cycles. The experimental sample collection occurred in one 24 h period on 5-week-old plants. The experimental design included three experiments: wounding with a hemostat (first four conditions), infection with *Pseudomonas syringae* pv. *tomato* DC3000 expressing *AvrRpt2* (*Pst*Avr) and infection with *Pseudomonas syringae* pv. *maculicola* (*Psm*) (next eight conditions), and cold acclimation and freezing six conditions). Each sub-experiment included appropriate control conditions, including sampling at 4°C at various time points and mock-inoculated sampling at 12 and 24 h time (

A and B, Pre 291.2. C, Pre 293.2. D, Pre 295.2. Pre 291.2 scan detects ox-lipids containing 18:4-O and 18:3-2O, Pre 293.2 scan detects ox-lipids containing 18:3-O and 18:2-2O, and Pre 295.2 scan detects ox-lipids containing 18:2-O. Peaks with labels in parentheses are $[M - H]^-$ adducts. Peak labels with no parentheses indicate $[M + C_2H_3O_2]^-$ adducts. Please note that intensity and *m/z* scales of the spectra differ. Panels A and B have breaks in the intensity axes. Details of peaks numbered 1-86 are shown in Table 2.2.

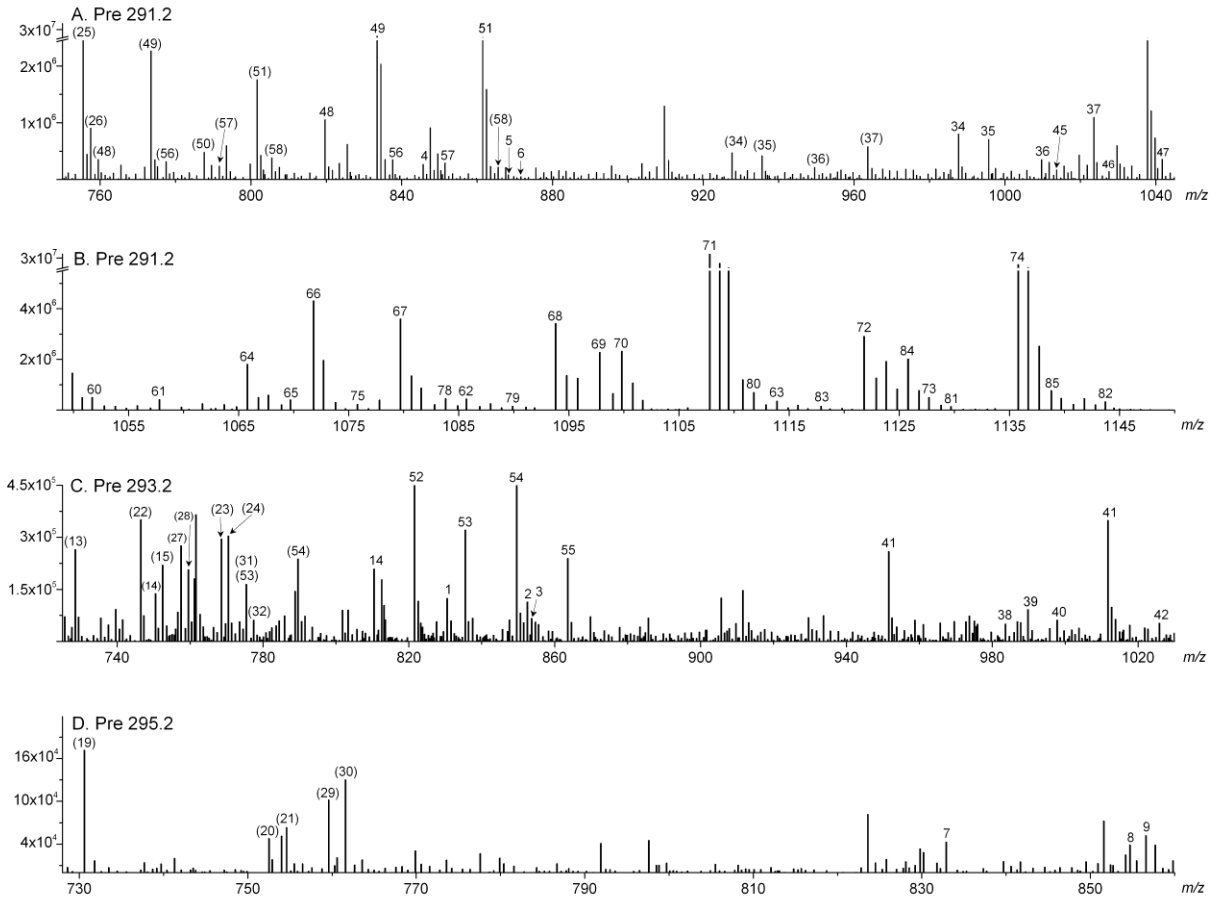
A. Pre 291.2
B. Pre 291.2
C. Pre 293.2
D. Pre 295.2
m/z

Figure 2.3 Oxidized membrane lipid levels following treatments shown in Figure 2.2.

A, Total oxidized lipids with colors indicating classes. B, ox-PC. C, ox-PE. D, ox-PG. E, ox-DGDG. F, ox-MGDG. G, ox-acMGDG. In B-G, colors indicate individual peaks detected by triple quadrupole MS precursor scanning in negative mode (Table 2.2). The size of each color-coded block represents the quantity of the ox-lipid classes (A) or of individual peaks 1–86 (B-G). Vertical axes have different scales.

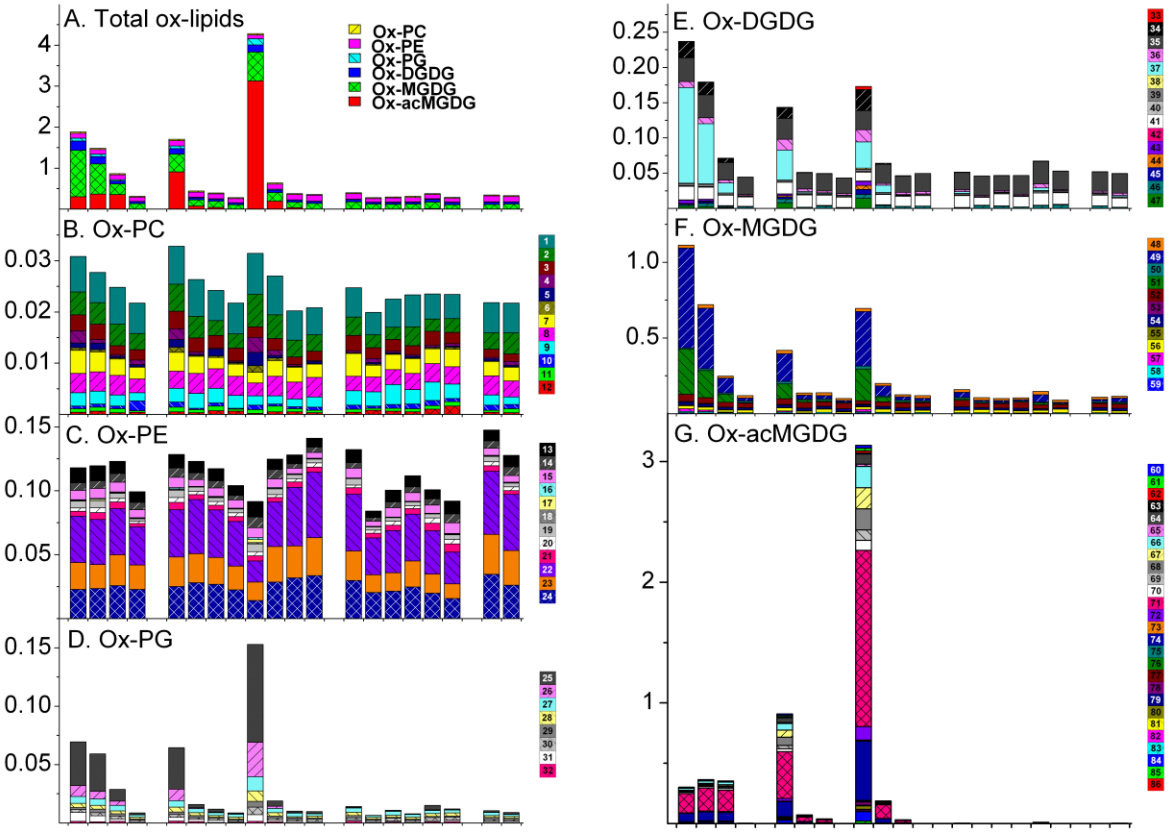

Figure 2.4 Oxidized membrane lipids under stress conditions as quantified by triple quadrupole MS precursor scanning.

A, Wounded, 15 min. B, Wounded, 45 min. C, Wounded, 6 h. D, *Pst*Avr, 12 h. E, *Pst*Avr, 24 h. F, *Psm*, 24 h. G, Freezing (-8° C, 2 h). Numbers along top *x*-axis refer to peaks/compounds in Table 2.2. In each panel, the white bars denote the basal amount as determined under the corresponding control condition: Unwounded, for A, B, and C; $MgCl_2$, 12 h, for D; $MgCl_2$, 24 h, for E and F; and 4° C, 84 h, for G. The black bars denote the amount of each ox-lipid measured in each stress treatment. Both white and black bars start at the *x*-axis. The smaller of the white and black bars is "in front" of the other bar. Increments on the vertical scales of panels A and B (below break) and C are the same; so are those on panel D and E (below break). $p < 0.05$, $n = 5$.

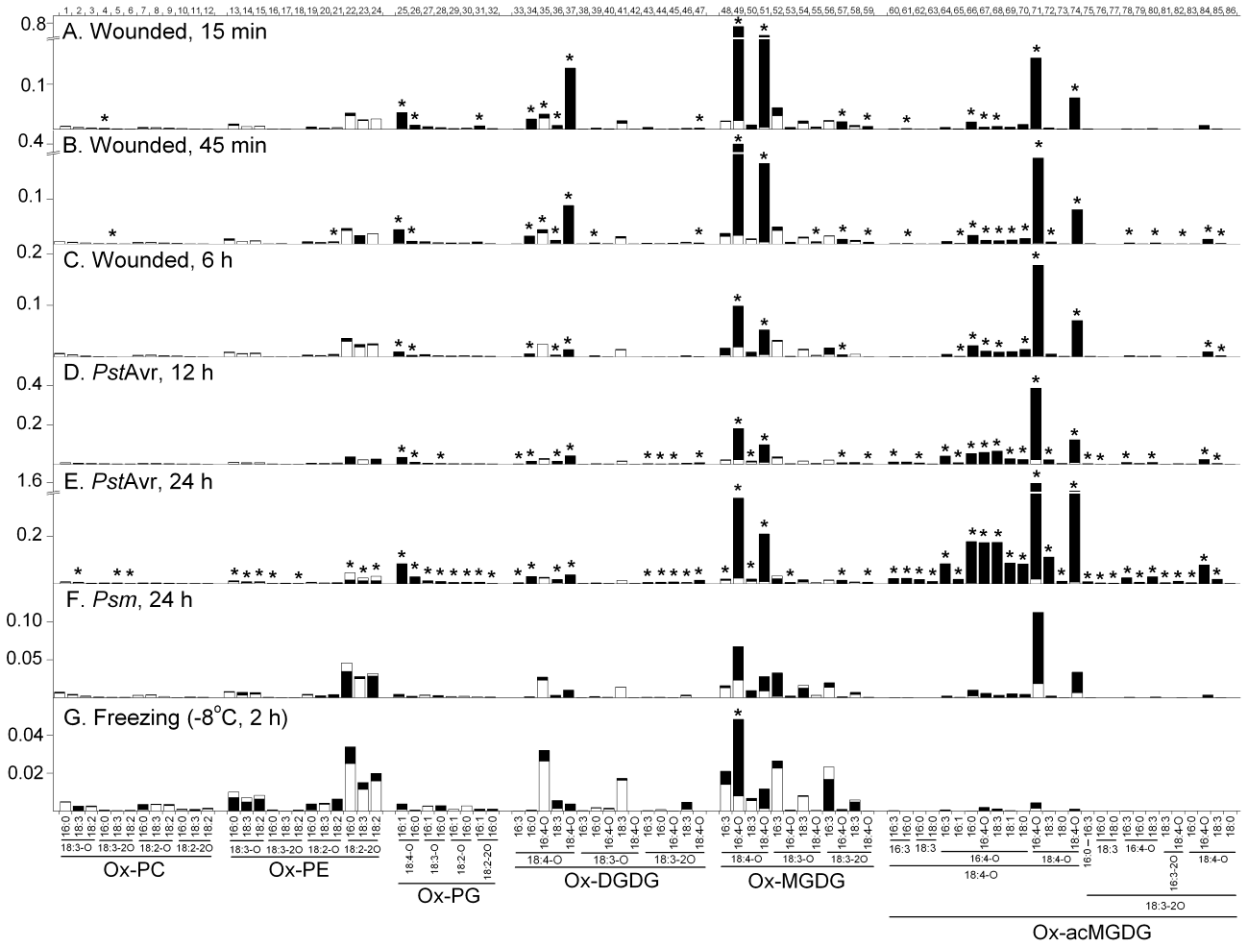

Table 2.1 Oxidized fatty acyl chains detected in extracts from leaves of *Arabidopsis thaliana* infected with *Pst*Avr for 24 h.

Figure S2.1 shows examples of possible structures and fragmentation of oxidized lipids from each class.

Triple quadrupole MS precursor scan	**Chemical formula of oxidized fatty acyl anion**	***m/z* of anion**	**Abbreviation**	**Examples of compounds consistent with detected formula**
Acyl formulas directly scanned				
Pre 291.20	$C_{18}H_{27}O_3$	291.1966	18:4-O	OPDA, keto 18:3
Pre 293.21	$C_{18}H_{29}O_3$	293.2122	18:3-O	hydroxy 18:3, keto fatty acid
Pre 295.23	$C_{18}H_{31}O_3$	295.2279	18:2-O	hydroxy 18:2
Pre 291.20	$C_{18}H_{29}O_4$	309.2071	18:3-2O	ketol fatty acid, hydroperoxy 18:3, dihydroxy 18:3
Pre 293.21	$C_{18}H_{31}O_4$	311.2228	18:2-2O	hydroperoxy 18:2, dihydroxy 18:2
Acyl formulas identified by scanning of above anions or as a result of QTOF MS analysis				
-	$C_{16}H_{23}O_3$	263.1653	16:4-O	dnOPDA
-	$C_{16}H_{25}O_3$	265.1809	16:3-O	hydroxy 16:3
-	$C_{16}H_{25}O_4$	281.1758	16:3-2O	ketol fatty acid, hydroperoxy 16:3, dihydroxy 16:3
-	$C_{18}H_{25}O_4$	305.1758	18:5-2O	-

Table 2.2 Lipids detected by ESI MS/MS negative ion precursor ion scans, Pre 291.2, Pre 293.2, and Pre 295.2.

Tables S2.3 and S2.4 indicate the compounds detected in a simplified form.

Number[a]	M mass	M formula	Identification[b]	Detection Method[c]	Identification Evidence[d]
1	771	C42H78O9PN	18:3-O/16:0 PC	Pre 293.2, [M + $C_2H_3O_2$]$^-$	Tentative, Table S2.1
2	793	C44H76O9PN	18:3-O/18:3 PC	Pre 293.2, [M + $C_2H_3O_2$]$^-$	Table S2.1
3	795	C44H78O9PN	18:3-O/18:2 PC	Pre 293.2, [M + $C_2H_3O_2$]$^-$	Table S2.1
4	787	C42H78O10PN	18:3-2O/16:0 PC	Pre 291.2, [M + $C_2H_3O_2$]$^-$	Table S2.1
5	809	C44H76O10PN	18:3-2O/18:3 PC	Pre 291.2, [M + $C_2H_3O_2$]$^-$	Table S2.1
6	811	C44H78O10PN	18:3-2O/18:2 PC	Pre 291.2, [M + $C_2H_3O_2$]$^-$	Table S2.1
7	773	C42H80O9PN	18:2-O/16:0 PC	Pre 295.2, [M + $C_2H_3O_2$]$^-$	Table S2.1
8	795	C44H78O9PN	18:2-O/18:3 PC	Pre 295.2, [M + $_2H_3O_2$]$^-$	Table S2.1
9	797	C44H80O9PN	18:2-O/18:2 PC	Pre 295.2, [M + $C_2H_3O_2$]$^-$	Tentative, Table S2.1
10	789	C42H80O10PN	18:2-2O/16:0 PC	Pre 293.2, [M + $C_2H_3O_2$]$^-$	Table S2.1
11	811	C44H78O10PN	18:2-2O/18:3 PC	Pre 293.2, [M + $C_2H_3O_2$]$^-$	Table S2.1
12	813	C44H80O10PN	18:2-2O/18:2 PC	Pre 293.2, [M + $C_2H_3O_2$]$^-$	Tentative, Table S2.1

13	729	C39H72O9PN	18:3-O/16:0 PE	Pre 293.2, $[M - H]^-$	Table S2.1
14	751	C41H70O9PN	18:3-O/18:3 PE	Pre 293.2, $[M - H]^-$	Table S2.1
15	753	C41H72O9PN	18:3-O/18:2 PE	Pre 293.2, $[M - H]^-$	Table S2.1
16	745	C39H72O10PN	18:3-2O/16:0 PE	Pre 291.2, $[M - H]^-$	Table S2.1
17	767	C41H70O10PN	18:3-2O/18:3 PE	Pre 291.2, $[M - H]^-$	Table S2.1
18	769	C41H72O10PN	18:3-2O/18:2 PE	Pre 291.2, $[M - H]^-$	Table S2.1
19	731	C39H74O9PN	18:2-O/16:0 PE	Pre 295.2, $[M - H]^-$	Table S2.1, S2.2
20	753	C41H72O9PN	18:2-O/18:3 PE	Pre 295.2, $[M - H]^-$	Table S2.1
21	755	C41H74O9PN	18:2-O/18:2 PE	Pre 295.2, $[M - H]^-$	Table S2.1
22	747	C39H74O10PN	18:2-2O/16:0 PE	Pre 293.2, $[M - H]^-$	Table S2.1, S2.2
23	769	C41H72O10PN	18:2-2O/18:3 PE	Pre 293.2, $[M - H]^-$	Tentative, Table S2.1
24	771	C41H74O10PN	18:2-2O/18:2 PE	Pre 293.2, $[M - H]^-$	Tentative, Table S2.1
25	756	C40H69O11P	18:4-O/16:1 PG	Pre 291.2, $[M - H]^-$	Buseman et al., 2006
26	758	C40H71O11P	18:4-O/16:0 PG	Pre 291.2, $[M - H]^-$	Buseman et al., 2006
27	758	C40H71O11P	18:3-O/16:1 PG	Pre 293.2, $[M - H]^-$	Table S2.1
28	760	C40H73O11P	18:3-O/16:0 PG	Pre 293.2, $[M - H]^-$	Table S2.1
29	760	C40H73O11P	18:2-O/16:1 PG	Pre 295.2, $[M - H]^-$	Table S2.1
30	762	C40H75O11P	18:2-O/16:0 PG	Pre 295.2, $[M - H]^-$	Table S2.1
31*	776	C40H73O12P	18:2-2O/16:1 PG	Pre 293.2, $[M - H]^-$	Table S2.1
31*	776	C43H68O12	18:3-O/16:4-O MGDG	Pre 293.2, $[M - H]^-$	Table S2.1
32	778	C40H75O12P	18:2-2O/16:0 PG	Pre 293.2, $[M - H]^-$	Table S2.1
33	922	C49H78O16	18:4-O/16:3 DGDG	Pre 291.2, $[M - H]^-$	Table S2.1
34	928	C49H84O16	18:4-O/16:0 DGDG	Pre 291.2, [M +	Table S2.1

				$C_2H_3O_2]^-$	
35	936	C49H76O17	18:4-O/16:4-O DGDG	Pre 291.2, [M + $C_2H_3O_2]^-$	Hisamatsu et al., 2005
36	950	C51H82O16	18:4-O/18:3 DGDG	Pre 291.2, [M + $C_2H_3O_2]^-$	Buseman et al., 2006
37	964	C51H80O17	18:4-O/18:4-O DGDG	Pre 291.2, [M + $C_2H_3O_2]^-$	Buseman et al., 2006; Hisamatsu et al., 2005
38	924	C49H80O16	18:3-O/16:3 DGDG	Pre 293.2, [M + $C_2H_3O_2]^-$	Table S2.1
39	930	C49H86O16	18:3-O/16:0 DGDG	Pre 293.2, [M +$C_2H_3O_2]^-$	Table S2.1
40	938	C49H78O17	18:3-O/16:4-O DGDG	Pre 293.2, [M + $C_2H_3O_2]^-$	Table S2.1
41	952	C51H84O16	18:3-O/18:3 DGDG	Pre 293.2, [M + $C_2H_3O_2]^-$	Table S2.1
42	966	C51H82O17	18:3-O/18:4-O DGDG	Pre 293.2, [M + $C_2H_3O_2]^-$	Table S2.1
43	940	C49H80O17	18:3-2O/16:3 DGDG	Pre 291.2, [M + $C_2H_3O_2]^-$	Table S2.1
44	946	C49H86O17	18:3-2O/16:0 DGDG	Pre 291.2, [M - H]$^-$	Table S2.1
45'	954	C49H78O18	18:3-2O/16:4-O DGDG	Pre 291.2, [M + $C_2H_3O_2]^-$	Table S2.1
45'	954	C49H78O18	18:4-O/16:3-2O DGDG	Pre 291.2, [M + $C_2H_3O_2]^-$	Table S2.1
46	968	C51H84O17	18:3-2O/18:3 DGDG	Pre 291.2, [M + $C_2H_3O_2]^-$	Buseman et al., 2006
47	982	C51H82O18	18:3-2O/18:4-O DGDG	Pre 291.2, [M + $C_2H_3O_2]^-$	Buseman et al., 2006

48	760	C43H68O11	18:4-O/16:3 MGDG	Pre 291.2, $[M - H]^-$	Table S2.2, Buseman et al., 2006; Stelmach et al., 2001,
49	774	C43H66O12	18:4-O/16:4-O MGDG	Pre 291.2, $[M + C_2H_3O_2]^-$	Table S2.2, Buseman et al., 2006; Hisamatsu et al., 2003
50	788	C45H72O11	18:4-O/18:3 MGDG	Pre 291.2, $[M - H]^-$	Buseman et al., 2006
51	802	C45H70O12	18:4-O/18:4-O MGDG	Pre 291.2, $[M + C_2H_3O_2]^-$	Table S2.2, Buseman et al., 2006; Hisamatsu et al., 2003
52	762	C43H70O11	18:3-O/16:3 MGDG	Pre 293.2, $[M + C_2H_3O_2]^-$	Table S2.1
53	776	C43H68O12	18:3-O/16:4-O MGDG	Pre 293.2, $[M + C_2H_3O_2]^-$	Tentative, Table S2.1
54	790	C45H74O11	18:3-O/18:3 MGDG	Pre 293.2, $[M - H]^-$	Table S2.1
55	804	C45H72O12	18:3-O/18:4-O MGDG	Pre 293.2, $[M + C_2H_3O_2]^-$	Table S2.1
56	778	C43H70O12	18:3-2O/16:3 MGDG	Pre 291.2, $[M + C_2H_3O_2]^-$	Buseman et al., 2006
57	792	C43H68O13	18:3-2O/16:4-O MGDG	Pre 291.2, $[M + C_2H_3O_2]^-$	Buseman et al., 2006
58	806	C45H74O12	18:3-2O/18:3 MGDG	Pre 291.2, $[M + C_2H_3O_2]^-$	Buseman et al., 2006
59	820	C45H72O13	18:3-2O/18:4-O	Pre 291.2, [M +	Buseman et

			MGDG	$C_2H_3O_2]^-$	al., 2006
60	992	C59H92O12	18:4-O/16:3/16:3 acMGDG	Pre 291.2, [M + $C_2H_3O_2]^-$	Table S2.1, S2.2
61	998	C59H98O12	18:4-O/16:3/16:0 acMGDG	Pre 291.2, [M + $C_2H_3O_2]^-$	Table S2.1, S2.2
62	1026	C61H102O12	18:4-O/18:3/16:0 acMGDG	Pre 291.2, [M + $C_2H_3O_2]^-$	Table S2.1
63a	1054	C63H106O12	18:4-O/18:3/18:0 acMGDG	Pre 291.2, [M + $C_2H_3O_2]^-$	Table S2.1
63b	1054	C63H106O12	18:4-O/18:2/18:1 acMGDG	Pre 291.2, [M + $C_2H_3O_2]^-$	Table S2.1
64	1006	C59H90O13	18:4-O/16:4-O/16:3 acMGDG	Pre 291.2, [M + $C_2H_3O_2]^-$	Table S2.1, S2.2
65	1010	C59H94O13	18:4-O/16:4-O/16:1 acMGDG	Pre 291.2, [M + $C_2H_3O_2]^-$	Table S2.1, S2.2
66	1012	C59H96O13	18:4-O/16:4-O/16:0 acMGDG	Pre 291.2, [M + $C_2H_3O_2]^-$	Table S2.1, S2.2
67a	1020	C59H88O14	18:4-O/16:4-O/16:4-O acMGDG	Pre 291.2, [M + $C_2H_3O_2]^-$	Table S2.1, S2.2
67b	1020	C61H96O12	18:4-O/18:3/16:3 acMGDG	Pre 291.2, [M + $C_2H_3O_2]^-$	Table S2.1
68a	1034	C61H94O13	18:4-O/16:4-O/18:3 acMGDG	Pre 291.2, [M + $C_2H_3O_2]^-$	Table S2.1, S2.2
68b	1034	C61H94O13	18:4-O/18:4-O/16:3 acMGDG	Pre 291.2, [M + $C_2H_3O_2]^-$	Table S2.1, S2.2
69a	1038	C61H98O13	18:4-O/16:4-O/18:1 acMGDG	Pre 291.2, [M +$C_2H_3O_2]^-$	Table S2.1, S2.2
69b	1038	C61H98O13	18:4-O/18:4-O/16:1 acMGDG	Pre 291.2, [M +$C_2H_3O_2]^-$	Table S2.1, S2.2
70a	1040	C61H100O13	18:4-O/16:4-O/18:0	Pre 291.2, [M +	Table S2.1,

			acMGDG	$C_2H_3O_2]^-$	S2.2
70b	1040	C61H100O13	18:4-O/18:4-O/16:0 acMGDG	Pre 291.2, [M + $C_2H_3O_2]^-$	Table S2.1, S2.2
71a	1048	C61H92O14	18:4-O/18:4-O/16:4-O acMGDG	Pre 291.2, [M + $C_2H_3O_2]^-$	Table S2.1, S2.2, Andersson et al., 2006
71b	1048	C63H100O12	18:4-O/18:3/18:3 acMGDG	Pre 291.2, [M + $C_2H_3O_2]^-$	Table S2.1, S2.2
72a	1062	C63H98O13	18:4-O/18:4-O/18:3 acMGDG	Pre 291.2, [M + $C_2H_3O_2]^-$	Table S2.1, S2.2
72b	1062	C61H90O15	18:4-O/18:5-2O/16:4-O acMGDG	Pre 291.2, [M + $C_2H_3O_2]^-$	Table S2.1, S2.2
73	1068	C63H104O13	18:4-O/18:4-O/18:0 acMGDG	Pre 291.2, [M + $C_2H_3O_2]^-$	Table S2.1
74	1076	C63H96O14	18:4-O/18:4-O/18:4-O acMGDG	Pre 291.2, [M + $C_2H_3O_2]^-$	Table S2.1, S2.2, Kourtchenko et al., 2007
75	1016	C59H100O13	18:3-2O/16:0/16:3 acMGDG	Pre 291.2, [M + $C_2H_3O_2]^-$	Table S2.1
76a	1044	C61H104O13	18:3-2O/18:3/16:0 acMGDG	Pre 291.2, [M + $C_2H_3O_2]^-$	Table S2.1
76b	1044	C61H104O13	18:3-2O/18:0/16:3 acMGDG	Pre 291.2, [M + $C_2H_3O_2]^-$	Tentative, Table S2.1
77a	1072	C63H108O13	18:3-2O/18:3/18:0 acMGDG	Pre 291.2, [M + $C_2H_3O_2]^-$	Table S2.1
77b	1072	C61H100O15	18:3-2O/18:2/16:3-2O acMGDG	Pre 291.2, [M + $C_2H_3O_2]^-$	Table S2.1
77c	1072	C63H108O13	18:3-2O/18:2/18:1	Pre 291.2, [M +	Table S2.1

			acMGDG	$C_2H_3O_2]^-$	
78'	1024	C59H92O14	18:3-2O/16:4-O/16:3 acMGDG	Pre 291.2, [M + $C_2H_3O_2]^-$	Table S2.1
78'	1024	C59H92O14	18:4-O/16:3-2O/16:3 acMGDG	Pre 291.2, [M + $C_2H_3O_2]^-$	Table S2.1
79'	1030	C59H98O14	18:3-2O/16:4-O/16:0 acMGDG	Pre 291.2, [M + $C_2H_3O_2]^-$	Table S2.1, S2.2
79'	1030	C59H98O14	18:4-O/16:3-2O/16:0 acMGDG	Pre 291.2, [M + $C_2H_3O_2]^-$	Table S2.1, S2.2
80a'	1052	C61H96O14	18:3-2O/16:4-O/18:3 acMGDG	Pre 291.2, [M + $C_2H_3O_2]^-$	Table S2.1
80a'	1052	C61H96O14	18:4-O/16:3-2O/18:3 acMGDG	Pre 291.2, [M + $C_2H_3O_2]^-$	Table S2.1
80b	1052	C61H96O14	18:3-2O/18:4-O/16:3 acMGDG	Pre 291.2, [M + $C_2H_3O_2]^-$	Table S2.1
81a	1070	C61H98O15	18:3-2O/16:3-2O/18:3 acMGDG	Pre 291.2, [M + $C_2H_3O_2]^-$	Table S2.1
81b	1070	C61H98O15	18:3-2O/18:3-2O/16:3 acMGDG	Pre 291.2, [M + $C_2H_3O_2]^-$	Tentative, Table S2.1
81c	1070	C63H106O13	18:3-2O/18:2/18:2 acMGDG	Pre 291.2, [M + $C_2H_3O_2]^-$	Table S2.1
82'	1084	C61H96O16	18:3-2O/16:3-2O/18:4-O acMGDG	Pre 291.2, [M + $C_2H_3O_2]^-$	Table S2.1, S2.2
82'	1084	C61H96O16	18:3-2O/18:3-2O/16:4-O acMGDG	Pre 291.2, [M + $C_2H_3O_2]^-$	Table S2.1, S2.2
83a	1058	C61H102O14	18:3-2O/18:4-O/16:0 acMGDG	Pre 291.2, [M + $C_2H_3O_2]^-$	Table S2.1
83b	1058	C61H102O14	18:3-2O/16:4-O/18:0 acMGDG	Pre 291.2, [M + $C_2H_3O_2]^-$	Tentative, Table S2.1
84a	1066	C61H94O15	18:3-2O/18:4-	Pre 291.2, [M +	Table S2.1,

			O/16:4-O acMGDG	$C_2H_3O_2]^-$	S2.2
84b	1066	C63H102O13	18:3-2O/18:3/18:3 acMGDG	Pre 291.2, [M + $C_2H_3O_2]^-$	Table S2.1, S2.2
85	1080	C63H100O14	18:3-2O/18:4-O/18:3 acMGDG	Pre 291.2, [M + $C_2H_3O_2]^-$	Table S2.1
86	1086	C63H106O14	18:3-2O/18:4-O/18:0 acMGDG	Pre 291.2, [M + $C_2H_3O_2]^-$	Table S2.1

[a]Each number (1-86) represents a peak observed in triple quadrupole MS spectra (Figure 2.1). An asterisk (*) indicates peaks resulting from two compounds of different lipid classes with the same ion mass. A prime symbol (') indicates peaks with at least two possible identifications, where it is unclear whether the peak represents one or both compounds. Numbers followed by a, b, or c signify that accurate *m/z* analysis indicates that the peak represents multiple lipid species detected by the stated precursor scan (Tables S2.1 and S2.2).

[b]Abbreviations: acMGDG, acylated monogalactosyldiacylglycerol; DGDG, digalactosyldiacylglycerol; MGDG, monogalactosyldiacylglycerol; PC, phosphatidylcholine; PE, phosphatidylethanolamine; PG, phosphatidylglycerol.

[c]Peaks were identified in triple quadrupole MS spectra with three negative precursor scans, Pre 291.2, Pre 293.2, and Pre 295.2; each species was observed as the $[M - H]^-$ and/or $[M + C_2H_3O_2]^-$ ion.

[d]QTOF MS peak data are provided in Table S2.1. FTICR MS peak data are provided in Table S2.2. Peak identification is indicated as "Tentative" if QTOF MS *m/z* values for one acyl group (or more) were greater than 10 parts per million (ppm) from the theoretical *m/z*, and the compound was not previously identified or identified by accurate *m/z* of the intact compound in FTICR MS spectra. Previously identified peaks/compounds are marked with corresponding references.

Supplemental Data

Supplemental Data in this chapter include:

- Figure S2.1 Examples of possible structures and fragmentation of oxidized lipids from each class.
- Figure S2.2 Bacterial counts (colony forming unit (CFU) per mg of leaf dry mass) at 12 h and 24 h post-infection.
- Figure S2.3 Oxidized membrane lipid levels during various control conditions and conditions with low ox-lipid levels as quantified by triple quadrupole MS precursor scanning.
- Figure S2.4 Levels of ox-MGDG, ox-acMGDG and PA in Arabidopsis leaves during stress and control treatments.
- Figure S2.5 Levels of LPC, LPE, and PA, in Arabidopsis leaves during stress and control treatments.

Tables S2.1-S2.8 are supplied as a separate Excel file.

- Table S2.1 QTOF MS m/z data supporting compound identifications in Table 2.2. Analysis was performed on extracts from leaves of Arabidopsis thaliana infected with PstAvr for 24 h.
- Table S2.2 FTICR MS m/z data supporting compound identifications in Table 2.2. Analysis was performed on extracts from leaves of Arabidopsis thaliana infected with PstAvr for 24 h.
- Table S2.3 Simplified designation of diacyl oxidized compounds (1-59).
- Table S2.4 Simplified table of acMGDGs (60-86) identified by precursor scanning.
- Table S2.5 Levels (individual sample data) of ox-lipids during plant stress responses.
- Table S2.6 Levels (averages and standard deviations) of ox-lipids during plant stress responses.
- Table S2.7 Levels (individual sample data) of normal lipids during plant stress responses.
- Table S2.8 Levels (averages and standard deviations) of normal lipids during plant stress responses.

Figure S2.1 Examples of possible structures for anions of oxidized lipids from each class. These structures are consistent with current data, but, in fact, the acyl chain structures shown in Table 2.1 and identified with specific compounds in Table 2.2 have been identified only at the level of chemical formula. The specific structural features (e.g. presence of C=O vs. C=C double bonds vs. rings, presence of specific functional groups, positions of double bonds and functional groups, and positions of acyl chains on glycerol) have not been determined. Table 2.1 indicates some additional possibilities for acyl chain structures.

Compounds shown:

7. 18:2-O/16:0 PC, shown as the $[M + C_2H_3O_2]^-$ ion of 1-hexadecanoyl-2-(9-hydroxy-10E,12Z-octadecadienoyl)-*sn*-glycero-3-phosphocholine;

23. 18:2-2O/18:3 PE, shown as the $[M - H]^-$ ion of 1-(9-hydroperoxy-10E,12Z-octadecadienoyl)-2-(9Z,12Z,15Z-octadecatrienoyl)-*sn*-glycero-3-phosphoethanolamine;

25. 18:4-O/16:1 PG, shown as the $[M - H]^-$ ion of 1-(8-[2-(cis-pent-2'-enyl)-3-oxo-cis-cyclo-pent-4-enyl]octanoyl)-2-(3E-hexadecenoyl)-*sn*-glycero-3-phospho-(1'-*sn*-glycerol), where 8-[2-(cis-pent-2'-enyl)-3-oxo-cis-cyclo-pent-4-enyl]octanoyl is also known as 12-oxo-10,15-phytodienoyl and OPDA;

46. 18:3-2O/18:3 DGDG, shown as the $[M + C_2H_3O_2]^-$ ion of 1-(9-hydroxy-12-oxo-10E,15Z-octadecadienoyl)-2-(9Z,12Z, 15Z-octadecatrienoyl)-3-O-[α-D-galactosyl-(1→6)-O-β-D-galactosyl]-*sn*-glycerol, where 9-hydroxy-12-oxo-10E,15Z-octadecadienoyl is also known as γ-ketol;

52. 18:3-O/16:3 MGDG, shown as the $[M + C_2H_3O_2]^-$ ion of 1-(13-hydroxy-9Z,11E,15Z-octadecatrienoyl)-2-(7Z,10Z,13Z-hexadecatrienoyl)-3-O-β-D-galactosyl-*sn*-glycerol;

66. 18:4-O/16:4-O/16:0 acMGDG, shown as the $[M + C_2H_3O_2]^-$ ion of 1-(8-[2-(cis-pent-2'-enyl)-3-oxo-cis-cyclo-pent-4-enyl]octanoyl)-2-(6-[2-(cis-pent-2'-enyl)-3-oxo-cis-cyclo-pent-4-enyl]hexanoyl)-3-O-(6-O-hexadecanoyl-β-D-galactosyl)-*sn*-glycerol, where 8-[2-(cis-pent-2'-enyl)-3-oxo-cis-cyclo-pent-4-enyl]octanoyl is also known as 12-oxo-10,15-phytodienoyl and OPDA, and 6-[2-(cis-pent-2'-enyl)-3-oxo-cis-cyclo-pent-4-enyl]hexanoyl is known as dinor-oxo-phytodienoyl and dnOPDA.

OPDA = 8-[2-(cis-pent-2'-enyl)-3-oxo-cis-cyclo-pent-4-enyl]octanoic acid

dnOPDA = 6-[2-(cis-pent-2'-enyl)-3-oxo-cis-cyclo-pent-4-enyl]hexanoic acid

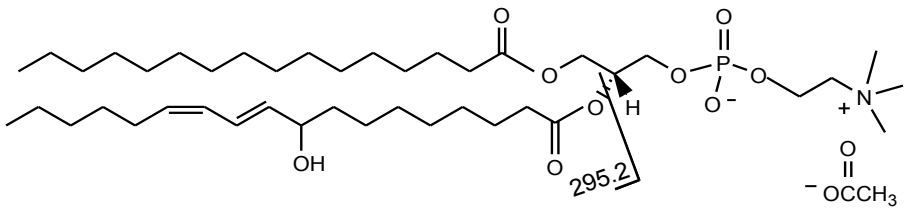

7

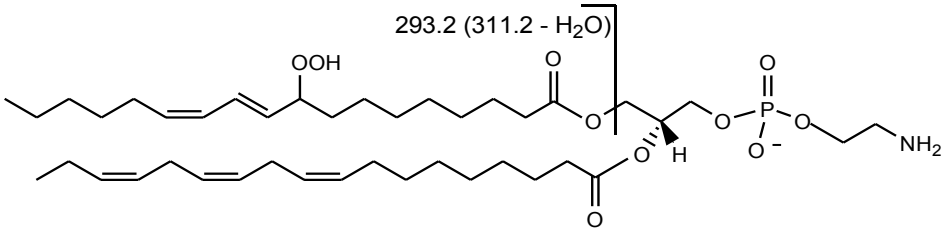

23

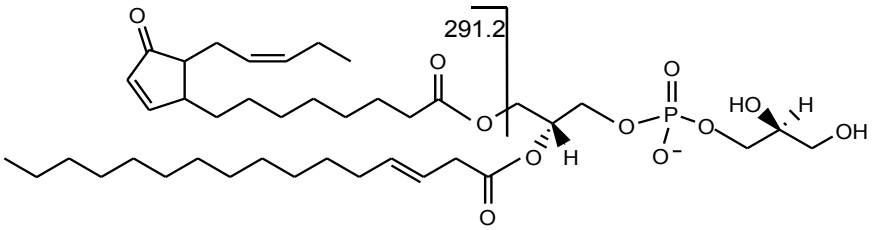

25

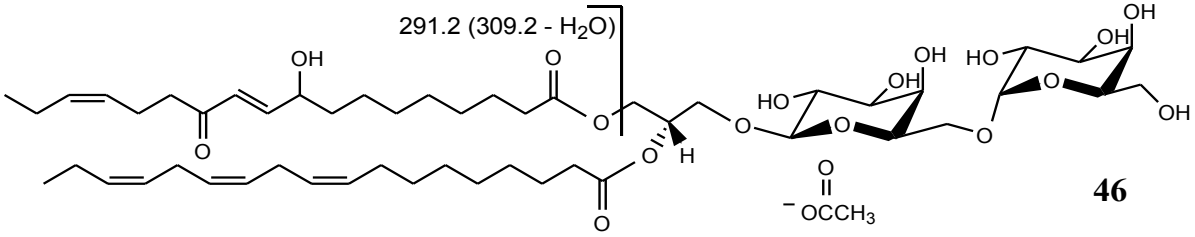

46

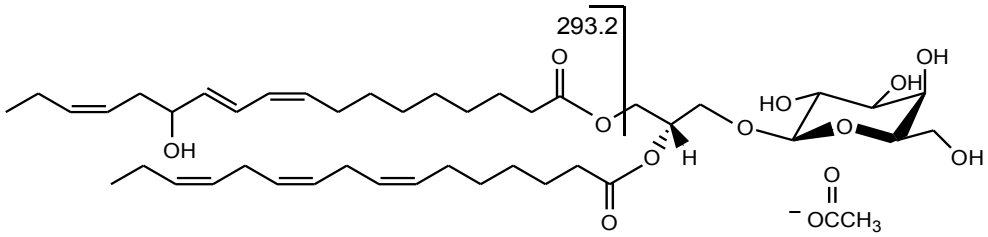

52

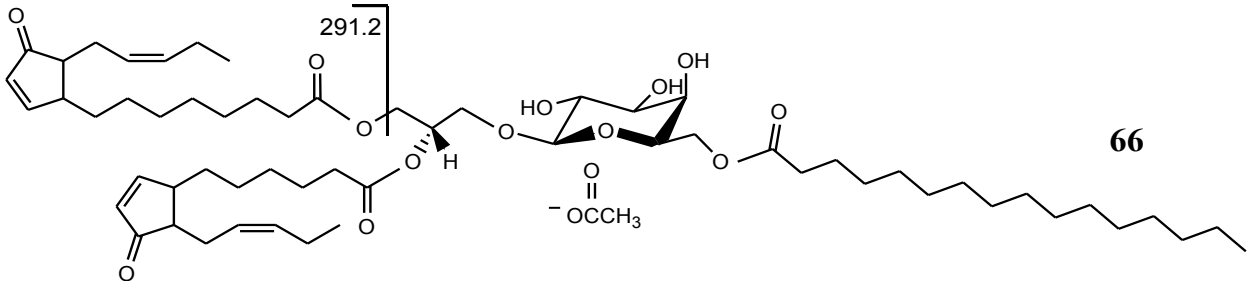

66

Figure S2.2 Bacterial counts (colony forming unit (CFU) per mg of leaf dry mass) at 12 h and 24 h post-infection.

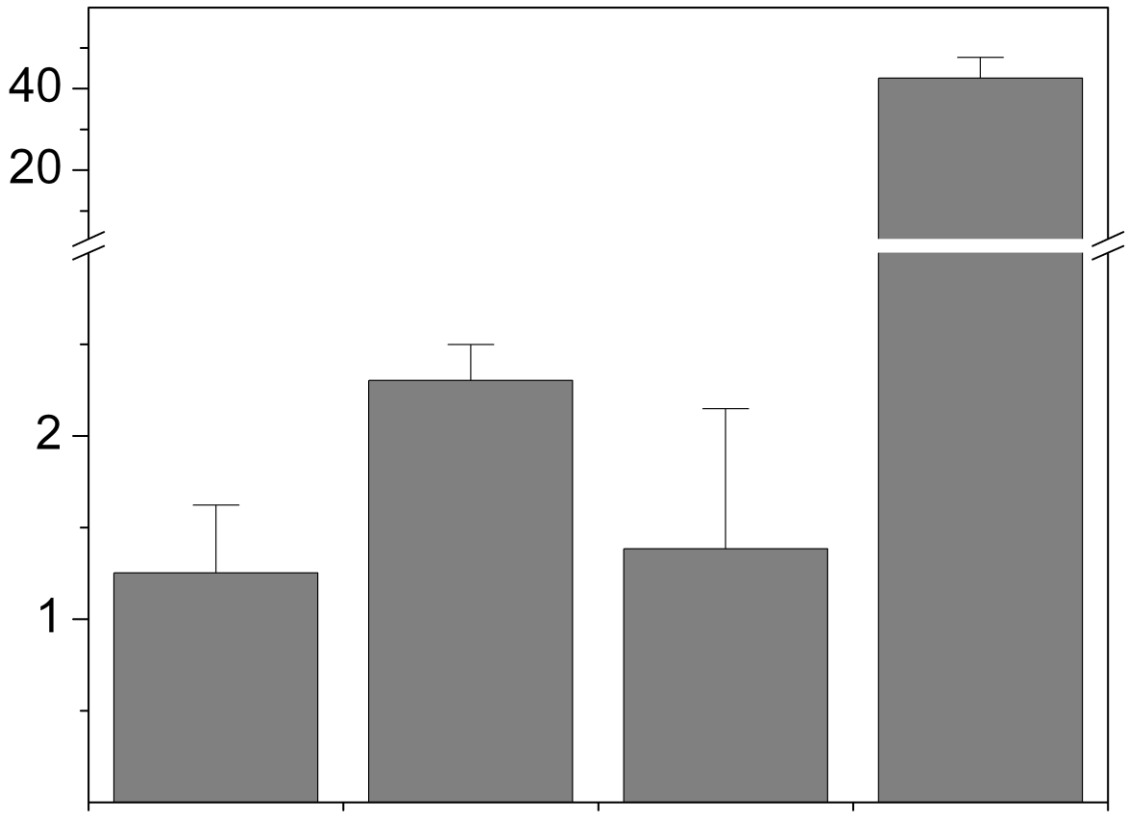

Figure S2.3 Oxidized membrane lipid levels during various control conditions and conditions with low ox-lipid levels (indicated on the panels) as quantified by triple quadrupole MS precursor scanning. Numbers along top x-axis refer to peaks/compounds in Table 2.2. Error bars indicate standard deviation.

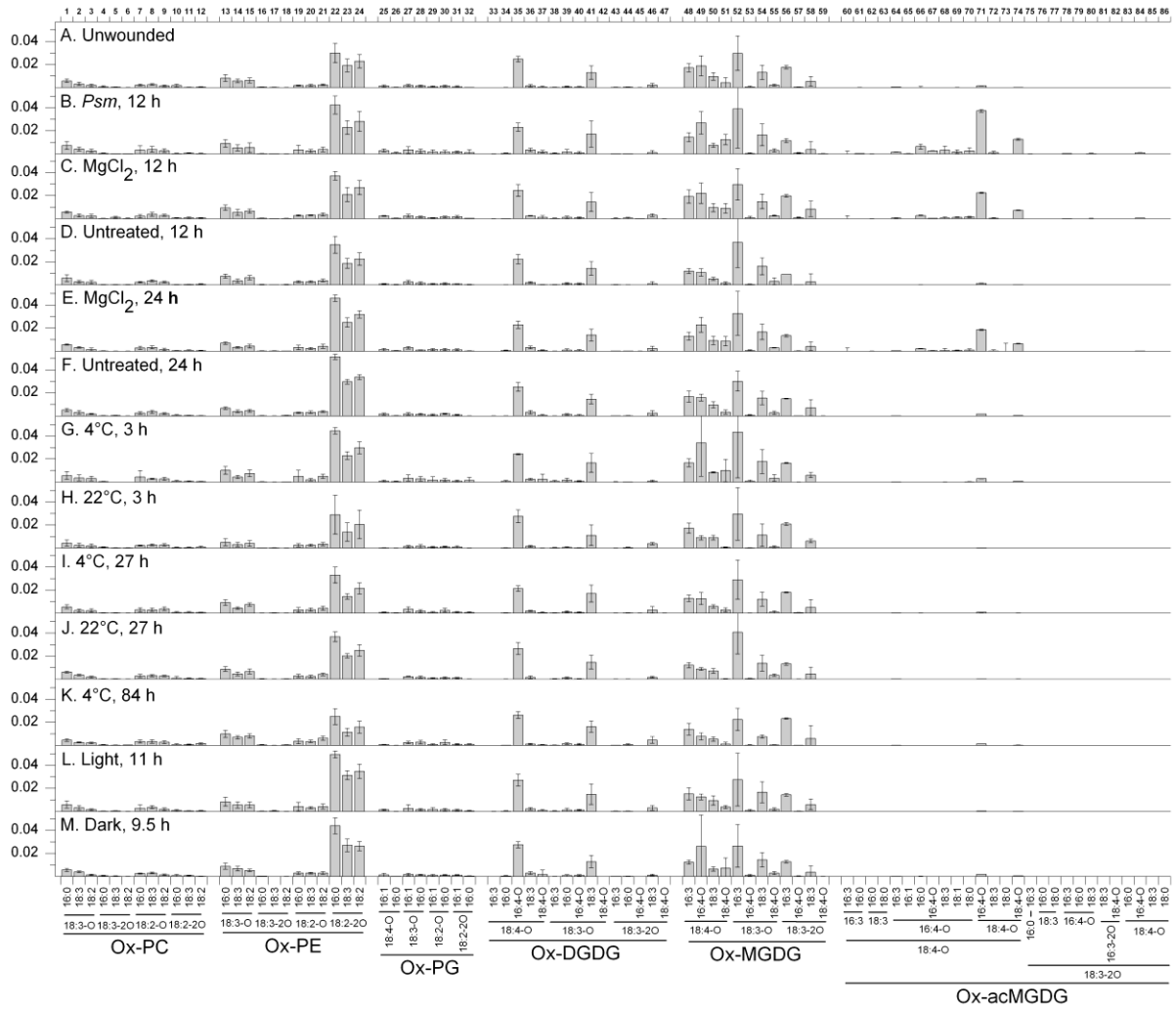

Figure S2.4 Levels of ox-MGDG, ox-acMGDG and PA in Arabidopsis leaves during stress and control treatments. Panels A, B, and C are ox-MGDG and ox-acMGDG as indicated. Panels D, E and F are PA. Error bars indicate standard deviation.

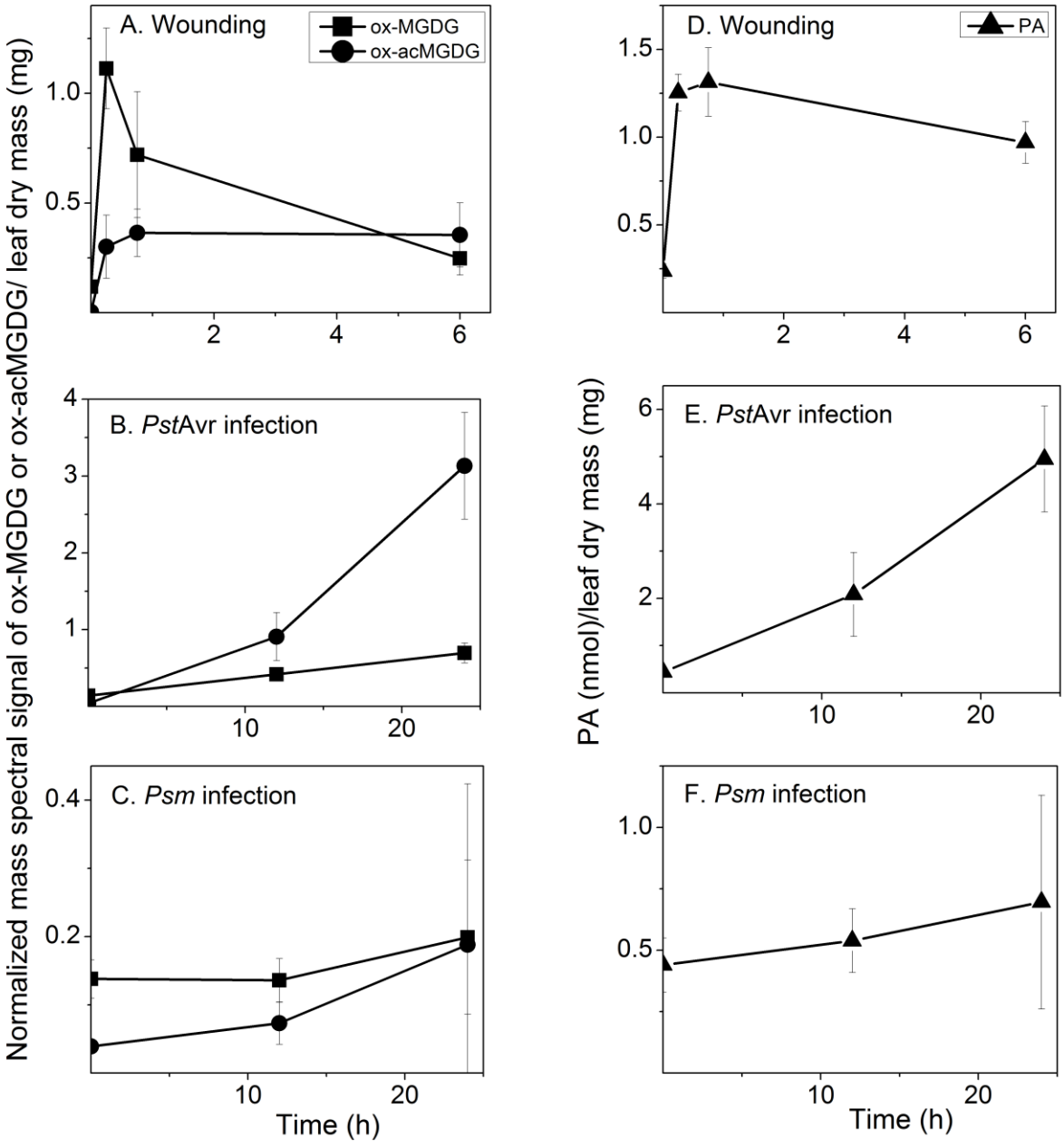

Figure S2.5 Levels of LPC, LPE, and PA, in Arabidopsis leaves during stress and control treatments. Average data used in this figure are presented in Table 2.8. Error bars indicate standard deviation. T-test was performed on 12 treatment-control pairs: **Wounded, 15 min** vs. Unwounded; **Wounded, 45 min** vs. Unwounded; **Wounded, 6 h** vs. Unwounded; ***Pst*Avr, 12 h** vs. $MgCl_2$, 12 h; ***Psm*, 12 h** vs. $MgCl_2$, 12 h; **$MgCl_2$, 12 h** vs. Untreated, 12 h; ***Pst*Avr, 24 h** vs. $MgCl_2$, 12 h; ***Psm*, 24 h** vs. $MgCl_2$, 24 h; **$MgCl_2$, 24 h** vs. Untreated, 24 h; **4°C, 3 h** vs. 22°C, 3 h; **4°C, 27 h** vs. 22°C, 27 h; **Freezing (-8°C, 2 h)** vs. 4°C, 84 h; *p < 0.05, n = 5 (except for 4°C, 3 h, n = 4).

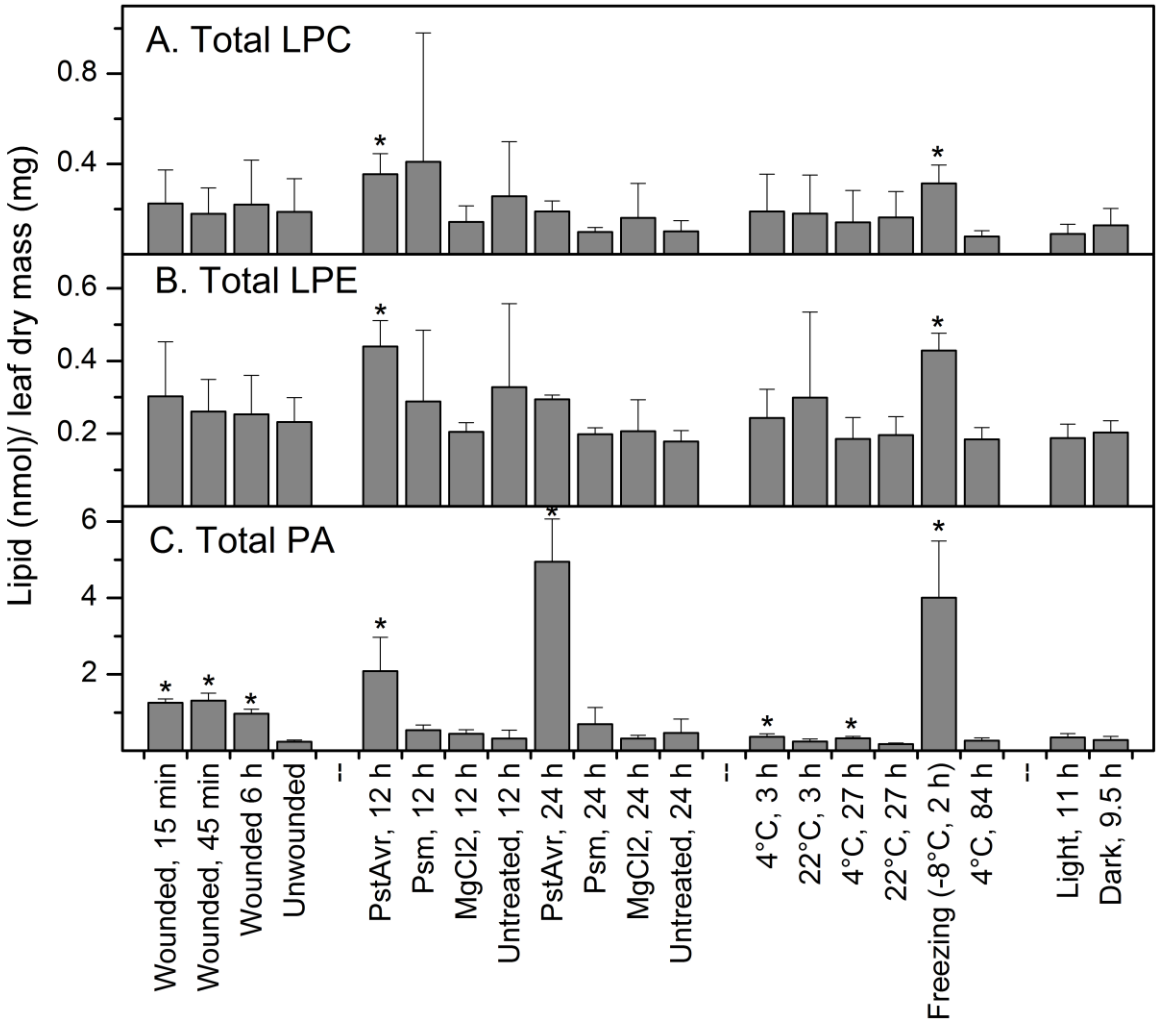

Chapter 6 - Head-group acylation of monogalactosyldiacylglycerol is a common stress response, and the acyl-galactose acyl composition varies among plant species and with applied stress

Abstract

Formation of galactose-acylated monogalactosyldiacylglycerols has been shown to be induced by leaf homogenization, mechanical wounding, avirulent bacterial infection and thawing after snap-freezing. Here, lipidomic analysis using mass spectrometry showed that galactose-acylated monogalactosyldiacylglycerols, formed in wheat (*Triticum aestivum*) and tomato (*Solanum lycopersicum*) leaves upon wounding, have acyl-galactose profiles that differ from those of wounded *Arabidopsis thaliana*, indicating that different plant species accumulate different acyl-galactose components in response to the same stress. Additionally, the composition of the acyl-galactose component of Arabidopsis acMGDG (galactose-acylated monogalactosyldiacylglycerol) depends on the stress treatment. After sub-lethal freezing treatment, acMGDG contained mainly non-oxidized fatty acids esterified to galactose, whereas mostly oxidized fatty acids accumulated on galactose after wounding or bacterial infection. Compositional data are consistent with acMGDG being formed in vivo by transacylation with fatty acids from digalactosyldiacylglycerols. Oxophytodienoic acid, an oxidized fatty acid, was more concentrated on the galactosyl ring of acylated monogalactosyldiacylglycerols than in galactolipids in general. Also, oxidized fatty acid-containing acylated monogalactosyldiacylglycerols increased cumulatively when wounded Arabidopsis leaves were wounded again. These findings suggest that, in Arabidopsis, the pool of galactose-acylated monogalactosyldiacylglycerols may serve to sequester oxidized fatty acids during stress responses.

Introduction

Membranes of plant chloroplasts contain glyco-glycerolipids with three major head groups: galactose (Gal, in monogalactosyldiacylglycerol, MGDG), digalactose (in digalactosyldiacylglycerol, DGDG) and sulfonated glucose (in sulfoquinovosyldiacylglycerol, SQDG). The Gal component of MGDG can be enzymatically modified by fatty acylation (esterification) at the 6′-hydroxyl group. Over 40 years ago, this head group acylation was characterized in spinach homogenates (Heinz, 1967a; Heinz and Tulloch, 1969). Fatty acid compositional analysis of in vitro incubation products from an ammonium sulfate-precipitated protein fraction with purified lipid substrates indicated that, when only MGDG was present, galactose-acylated MGDG (acMGDG) was formed via a dismutation reaction, i.e. 2 MGDG → acMGDG + monogalactosylmonoacylglycerol (MGMG). However, when both MGDG and DGDG were present, acMGDG was formed exclusively by transacylation from DGDG, i.e. DGDG + MGDG → acMGDG + digalactosylmonoacylglycerol (DGMG; Heinz 1967b, Heinz 1972). This early work focused on acMGDG formation in homogenized leaf tissues; however, the potential physiological role for the acylation reaction was not considered.

More recently, acMGDGs with the structure 1-(12-oxophytodienoic acid) (OPDA), 2-dinor-oxophytodienoic acid (dnOPDA), 3-(OPDA-Gal) glycerol (Arabidopside E) and acMGDG with 3 OPDA chains (Arabidopside G) were identified in Arabidopsis leaves under stress. These acMGDGs can accumulate to as much as 8% of the Arabidopsis total leaf lipid when the leaves are infected with the bacteria *Pseudomonas syringae* carrying the avirulence factor AvrRpt2 (Pst) or AvrRpm1 (Andersson et al., 2006; Kourtchenko et al., 2007). Indeed, in vitro testing indicated that Arabidopsides E and G have antimicrobial activities against the virulent bacterium *Pseudomonas syringae* DC3000 (Andersson et al., 2006) and the necrotrophic fungus *Botrytis cinerea* (Kourtchenko et al., 2007). Forty additional acMGDG molecular species (13 non-oxidized and 27 oxidized) were measured after wounding of Arabidopsis leaves (Ibrahim et al., 2011) and 27 additional acMGDGs, each with at least one oxidized fatty acid chain, were characterized as being induced significantly after wounding or avirulent bacterial infection of Arabidopsis leaves (Vu et al., 2012).

Galactolipids with cyclic oxidized acyl chains, or oxylipins, such as OPDA, esterified to glycerol are rare in plant species outside the genus *Arabidopsis* (Bottcher and Weiler, 2007). The current study adds to the evidence that, although cyclic fatty acids in membrane lipids may be restricted in occurrence, Gal acylation of MGDG is a relatively conserved process that occurs in tomato and wheat, in addition to Arabidopsis, spinach, and broad bean (Heinz, 1967b; Heinz, 1967a; Heinz and Tulloch, 1969; Heinz, 1972; Andersson et al., 2006; Kourtchenko et al., 2007; Ibrahim et al., 2011; Vu et al., 2012). MGDG Gal acylation is demonstrated to be a common response to stresses including wounding, freezing and infection with avirulent bacteria. The data show major variation in composition of the Gal-esterified acyl group, both among plant species and in response to different stresses. Furthermore, comparison of the profiles of the fatty acyl chain on the Gal of acMGDG and the fatty acyl chains of DGDG supports the notion that DGDG is the usual acyl donor for MGDG Gal acylation *in vivo*.

Materials and Methods

Plant materials

Mature wheat leaves (*Triticum aestivum* 'Thatcher') were collected from the North Agronomy Farm, Kansas State University, Manhattan, KS. Tomato plants (*Solanum lycopersicum* 'Better Boy') were purchased from Westside Market, Manhattan, KS. *Arabidopsis thaliana* accessions Columbia-0 (Col-0) and C24 were grown one plant per well in Pro-Mix 'PGX' soil (Hummert International, Earth City, MO) in 72-well plug trays (Hummert International, Earth City, MO). Trays were kept in a Conviron growth chamber under a 14/10 h light/dark cycle with 60% humidity at 21°C. Light intensity in growth chambers was maintained at 80 μmol m−2 s−1 with cool white fluorescent lights (Sylvania, Danvers, MA). Plants were fertilized twice, once when sowing and once at 20 days old, by irrigation with a 1% solution of 20-20-20 Miracle-Gro plant food (Scotts Miracle-Gro, Marysville, OH). Col-0 was harvested after 30 days and C24 after 42 days of growth.

Treatments

Arabidopsis plants were infected with bacteria (*Pseudomonas syringae*) as previously described (Vu et al., 2012). Cold acclimation was performed in a 4°C room equipped with light carts. Freezing treatment was performed in a programmable freezing chamber (Espec Corporation, Hudsonville, MI). Each tray of plants in soil was partly submerged in an ice slurry (made by adding tap water to approximately 1.5 kg of ice chips to a total volume of 4 l) to avoid supercooling during freezing treatment at −8°C for 2 h. The soil was completely in contact with the ice slurry through the irrigation holes at the bottom of the growing tray. The temperature was dropped to −8°C without gradual decreasing; at the end of the freezing treatment, plants were transferred to their growth condition (21°C, 60% humidity) and sampled after 3 and 24 h. Leaf numbers 5 and 6 were collected for ion leakage measurement (see next section), and the remaining portion of the rosette was dropped into 4 ml of 75°C isopropanol with 0.01% butylated hydroxytoluene (BHT) for lipid analysis. Leaf number is the order of leaf appearance, determined as described previously (Telfer et al., 1997). Wounding was performed by applying pressure with a hemostat across the leaf mid-vein, leaving wound marks about 6 mm apart. For the re-wounding experiment, plants were randomly assigned to one of three groups. Plants of the 'control' singly wounded group were harvested at 0 min, 5 min, 15 min, 45 min, 4 h, 24 h and 48 h after wounding. For the other two groups, a second wound was applied at the same location as the first wound either 24 or 48 h after the first wound was applied. The leaves were harvested at 0 min, 5 min, 15 min, 45 min, 4 h, 24 h and 48 h after the second wound. In the re-wounding experiment, four leaves (leaf numbers 5, 6, 7 and 8) were harvested at each time point; leaf number 5 was dropped into 2 ml of 75°C isopropanol with 0.01% BHT for lipid analysis, and leaf numbers 6, 7 and 8 were put together into a 1.5-ml tube and frozen in liquid nitrogen for phytohormone analysis by gas chromatography – mass spectrometry (MS).

Ion leakage measurement

Two leaves from each rosette were rinsed with deionized water before being dropped into a a 50-ml PYREX glass tube (Corning Inc., Corning, NY) containing 25 ml of distilled water (Dillons Supermarket, Manhattan, KS). The tubes were shaken for 2 h at 100 rpm before the first ion conductivity reading with Oakton CON 510 electrical conductivity meter (Oakton Instruments,

Vernon Hills, IL). After the first reading, the tubes were incubated at 95–100°C in a water bath for 2 h, and a second conductivity reading was taken. Relative ion leakage, as a percentage, was reported as (the first over the second conductivity reading) × 100 (%).

Lipid extraction

Modified Bligh–Dyer method (Bligh and Dyer, 1959) for polar lipid analysis

For the *Pst* and wounding experiments, three leaves were dropped into 3 ml of 75°C isopropanol containing 0.01% BHT; heating at 75°C was continued for 15 min. Chloroform (1.5 ml) and water (0.6 ml) were added, and the tube was shaken for 1 h before the solvent was transferred to another tube. For the second round of extraction, 4 ml of chloroform: methanol (2:1) was added to the leaves, followed by shaking for 30 min and combination of the solvent with the previous extract. After repeating the extraction three more times and combining the extracts, the combined extract was evaporated under a nitrogen stream and re-dissolved in 1 ml of chloroform. The extracted leaf residue was dried overnight at 105°C and the dry mass obtained by weighing.

Alternate extraction method (for polar lipid analysis)

For the freezing and re-wounding experiments, leaves were dropped into a 20-ml vial with a Teflon-lined cap containing 4 ml (2 ml in the re-wounding experiment) of 75°C isopropanol with 0.01% BHT. After 15 min at 75°C, 12 ml (6 ml in the re-wounding experiment) of extraction solvent (chloroform: methanol: 300 mM ammonium acetate in water, 30:41.5:3.5, v/v/v) were added, and the tube was shaken at room temperature for 24 h.

For gas chromatography-MS (free oxylipin analysis)

Extraction and derivatization were carried out as described previously (Schmelz et al., 2004).

Mass spectrometry

For samples extracted by the modified Bligh–Dyer method (stored in 1 ml chloroform), a volume (x µl) containing 0.2 mg leaf dry mass was diluted by adding (360 − x) µl of chloroform and 840

µl of methanol: 300 mM ammonium acetate in water (95:5, v/v). For samples extracted by the alternate method, a volume (y µl) containing 0.2 mg leaf dry mass was diluted with (1200 − y) µl of chloroform: methanol: isopropanol: 300 mM ammonium acetate in water (30:41.5:25:3.5, v/v/v/v).

Phospholipids and galactolipids with normal chains were analyzed by triple quadrupole MS using head group-specific scans and standards as described previously (Xiao et al., 2010). Precursor scans of m/z 277.2 (Pre 277.2, 18:3), m/z 291.2 (Pre 291.2, 18:4-O), m/z 293.2 (Pre 293.2, 18:3-O), m/z 295.2 (Pre 295.2, 18:2-O or 17:3-2O) and m/z 283.2 (Pre 283.2, 18:0, to detect internal standard 16:0/18:0 MGDG) were performed in negative mode as described previously (Vu et al., 2012), except that 1.505 nmol of 18:0/16:0 MGDG was used in each vial as an internal standard.

Scans for neutral loss (NL) fragments composed of Gal and a fatty acid (Table 3.1) were carried out in positive mode using an ABI 4000 triple quadrupole mass spectrometer (Applied Biosystems, Foster City, CA) with an electrospray ionization (ESI) source. To perform the NL scans listed in Table 3.1, three identical sample vials were used to provide enough volume for the analysis of each sample. To each sample vial, 0.95 nmol of di18:0 DGDG was added as an internal standard; this was detected by NL scan of m/z 341.2 (NL 341.2), with a target of m/z 966.7. The infusion flow rate was 30 µl min−1. The scan rate was 36 u s−1 for 75 cycles. Other parameters were: collision gas, 2 (arbitrary units); curtain gas, 20 (arbitrary units); ion source gases 1 and 2, 45 (arbitrary units); source temperature, 100°C; interface heater, ‘on’; ion spray voltage, 5500 V; declustering potential, 90 V; entrance potential, 10 V; collision energy, 24 V and collision cell exit potential, 23 V.

Accurate acyl mass analysis by quadrupole time-of-flight (Q-TOF) MS was performed on unfractionated lipid extracts with a Q-TOF-2 tandem mass spectrometer (Micromass Ltd., Manchester, UK), using the solvent, parameters and processing method described by Buseman et al. (2006), with a few changes. Charged precursor ions were subjected to product ion scanning in negative or positive ion mode. Precursor ions were selected by the quadrupole, tuned to transmit at 0.8 u full width at half height (i.e. monoisotopic selection). Extracts were infused into the ESI source at 20 µl min^{-1}; collision energy was 30 V.

Chemical ionization gas chromatography – MS was used to profile phytohormones of samples harvested from the re-wounding experiment following the procedure described by Schmelz et al. (2004).

Mass spectral data processing and analysis

Peak smoothing, background subtraction and peak centroiding for triple quadrupole MS data were carried out using a custom script with Applied Biosystems analyst software. After targeted peaks were identified, isotopic overlaps were calculated and subtracted from peaks within each spectrum. For NL scans, spectra were also corrected for isotopic overlaps of head group fragments. Signals of targeted peaks were normalized to the signal of the corresponding internal standard (18:0/16:0 MGDG for negative precursor scans and di18:0 DGDG for positive NL scans) and reported as normalized mass spectral signal per mg of leaf dry mass, where amount of signal produced by 1 nmol internal standard is 1 unit of signal.

To calculate the OPDA to 18:3 signal ratio in MGDGs and DGDGs in Arabidopsis, the ESI triple quadrupole MS signals were detected by scanning in negative mode for Pre 291.2 (OPDA) and Pre 277.2 (18:3). The sum of signals from MGDGs and DGDGs containing combinations of OPDA (18:4-O) with each of the five major fatty acids [16:3, 16:0, dnOPDA (16:4-O), 18:3 and OPDA] was divided by the sum of MGDGs and DGDGs containing combinations of 18:3 with each of the same five major fatty acids. To calculate the Gal-OPDA to Gal-18:3 signal ratio in acMGDGs, the sum of signals of Gal-OPDA acMGDGs [with each of the 35 diacylglycerol (DAG) combinations listed in Table S3.1], detected by scanning in positive mode for NL 453.3 (Gal-OPDA), was divided by the sum of signals of Gal-18:3 acMGDGs (with the 35 DAGs listed in Table S3.1), detected by scanning in positive mode for NL 439.3 (Gal-18:3).

Q-TOF mass spectra obtained in negative mode were mass-corrected by using, as a lock mass, the theoretical exact mass of the acyl anion of 18:3 fatty acid or OPDA, m/z 277.2173 or 291.1966, respectively. Q-TOF spectra obtained in positive mode were mass-corrected by locking on the mass of a fragment containing the glycerol backbone attached to either 18:3 fatty acid or OPDA (m/z 335.2581 or 349.2373, respectively). With the locked mass correction, the exact masses of product ions were determined to ten thousandths of a mass unit.

Results

Wound-induced acylation of the galactose of MGDG occurs in multiple plant species

acMGDGs are formed by acylation of MGDG on the carbon at the 6-position of galactose (Heinz and Tulloch, 1969). Utilizing direct infusion ESI triple quadrupole MS, acMGDG levels can be measured by NL scanning in the positive mode. Figure 3.1A depicts an acMGDG molecule, showing formation of the NL fragment, C22H43O6N (417.3 u), by collision-induced dissociation. The fragment is composed of a palmitoyl chain, 16:0 (where 16 is the number of carbons and 0 is the number of double bond equivalents, excluding the carbonyl double bond), esterified to Gal. Other NL fragments used for detection of acMGDGs are listed in Table 3.1. Each NL scan targets an acMGDG group with a common acyl-Gal component and varied DAG components. The DAG components targeted in each NL scan (Table 3.1) are listed in Table S3.1. In contrast to the previous method used by our group to detect acMGDGs by targeting fatty acyl anions (Vu et al., 2012), which did not identify the position of the detected fatty acid among the three positions in acMGDG, the current method detects the fatty acid linked to the galactose. To compare amounts of acMGDGs, signals were normalized to the signal of an internal standard, with an amount of signal equal to that of 1 nmol of the standard equal to 1. This approach allows sample-to-sample comparison of signals. More detail on the acMGDGs (as defined by DAG species in combination with each acyl-galactose species) may be viewed in Table S3.2.

Figure 3.1B shows that various plant species, from the monocot wheat to eudicots tomato and Arabidopsis, produce acMGDG in response to wounding. acMGDG is formed within 45 min after wounding with a hemostat. Fold increases of acMGDG in leaves 45 min after wounding were 3 for tomato, 18 for wheat, 20 for Arabidopsis C24 and 130 for Arabidopsis Col-0.

In acMGDG produced in response to wounding, the fatty acyl species linked to Gal varied among plant species (Figure 3.2). Figure 3.2A shows that in Arabidopsis Col-0, the most abundant Gal-linked fatty acids were 18:4-O, which has been identified as OPDA in galactolipids (Stelmach et al., 2001; Buseman et al., 2006), 16:0, 18:3-2O/20:1, 18:3 and 18:3-O (49, 19, 11, 7 and 4%, respectively, of the total acMGDG measured). Gal-linked fatty acids 18:3-2O and 20:1 have the same nominal mass and thus are not differentiated by this method. In agreement with previous analyses of *Arabidopsis thaliana* Col-0, three acMGDGs with the most abundant signals were 1-OPDA,2-dnOPDA,3-(OPDA-galactosyl) glycerol (Arabidopside E,

38% of total acMGDG signal), 1-OPDA,2-dnOPDA,3-(16:0-galactosyl) glycerol (14%) and 1,2-diOPDA,3-(OPDA-galactosyl) glycerol (7%, Arabidopside G) (Table S3.2; Andersson et al., 2006, Ibrahim et al., 2011, Kourtchenko et al., 2007, Vu et al., 2012). In Arabidopsis C24, Gal linkage of unoxidized fatty acids was more prevalent: 18:3 (32% of total acMGDG signal), 16:0 (19%), OPDA (18%), 18:2 (6%), 18:3-O (6%) and 18:3-2O/20:1 (6%) compared to Col-0 after the same wounding treatment (Figure 3.2B). While the amount of acMGDG with OPDA esterified to Gal is approximately 10-fold less in Arabidopsis C24 than in Arabidopsis Col-0, the amount of acMGDG with 18:3 esterified to Gal was slightly higher in C24 than in Col-0. Similarly, MS signals from acMGDGs in wounded tomato and wheat leaves were derived primarily from unoxidized Gal-linked fatty acids: 16:0 (40%), 18:3 (27%) and 18:2 (15%) in tomato; 18:3 (73%), 16:0 (9%) and 18:2 (6%) in wheat (Figure 3.2C–D). Scanning for NL 439.3 (18:3-containing Gal) in samples from wheat 45 min after wounding produced a massive peak at m/z 1052.8, whose signal accounted for 72% of the total acMGDG signal (Table S3.2). Accurate-mass product ion analysis of this species (acetate adduct, $[M + C_2H_3O_2]^-$, m/z 1093.8) by Q-TOF MS in the negative mode (Buseman et al., 2006, Vu et al., 2012) showed that this largest acMGDG component of wheat contained only 18:3 acyl chains, consistent with a structure of 1,2-di18:3,3-(18:3-galactosyl) glycerol (Figure S3.1). Table S3.3 shows the acyl composition (three chains) of the major acMGDG molecular species detected in Arabidopsis Col-0, tomato and wheat and the supporting accurate-mass product ion analysis.

acMGDGs accumulate following stress, including sub-lethal freezing

The total amounts of acMGDG formed under different stress treatments were determined using the NL scans indicated in Table 3.1 (Figure 3.3). As shown previously by precursor scanning for acyl anions, infection of *Arabidopsis thaliana* Col-0 with the avirulent bacteria *Pst* induced large amounts of acMGDG (Figure 3.3A; Vu et al., 2012). Wounding also induced acMGDG (Figure 3.3B). Similarly, sub-lethal freezing induced synthesis of acMGDG (Figure 3.3C). Levels of acMGDG with unoxidized fatty acyl chains had not been previously determined (Vu et al., 2012; next section). In the experiment shown in Figure 3.3C–E, Arabidopsis Col-0 plants were cold-acclimated at 4°C for 3 days or not acclimated (remained at the growth temperature of 21°C) until the freezing treatment (2 h at −8°C). Plants were returned to 21°C after freezing and sampled 3 h or 24 h later. As indicated by measurement of ion leakage at 24 h (Figure 3.3D),

non-acclimated plants sustained more damage than acclimated plants ($P < 0.001$). Figure 3.3C indicates that levels of acMGDG increased during the post-freezing period in both acclimated and non-acclimated plants, but that the levels were always higher in non-acclimated than in acclimated plants. Ion leakage measurements (Figure 3.3D) indicate that the membranes of acclimated plants were quite permeable at 3 h into the recovery period, but less so at 24 h ($P < 0.01$). In contrast, the non-acclimated plants showed greater leaf membrane damage after 24 h post freezing than at 3 h ($P < 0.05$) and much more damage at 24 h than observed in acclimated plants. Indeed, acclimated plants sustained visible damage to leaves, but the leaves were able to recover, while the damaged leaves of non-acclimated plants died, although the plant did not (see Figure S3.2). Levels of the phospholipid hydrolytic product phosphatidic acid (PA) are shown in Figure 3.3E. (Levels of other membrane lipids are shown in Table S3.4). Whereas total PA levels (Figure 3.3E) were closely correlated with leaf ion leakage (Figure 3.3D), the total acMGDG signal (Figure 3.3C) did not correlate strictly with leaf injury. Acclimated plants tended to accumulate acMGDG between 3 h and 24 h ($P < 0.1$) after freezing treatment as ion leakage dropped. Taken together, comparison of acMGDG signals in acclimated and non-acclimated plants demonstrates a link between treatment and total acMGDG accumulation, but acMGDG accumulated even during recovery.

The composition of induced acMGDGs varies among stresses

The most abundant acMGDGs in Col-0 leaves after infection of the plants by *Pst* (24 h) were those with Gal-linked fatty acids OPDA (56%), 16:0 (17%), 18:3 (10%), 18:3-2O/20:1 (6%) and 16:4-O (4%) (Figure 3.4A). The acMGDG composition, with a prevalence of OPDA and 16:0 on Gal, was similar to that formed after wounding (Figure 3.4B). The acMGDG Gal-linked acyl composition was drastically different in plants 24 h after freezing. In acclimated plants (Figure 3.4C), 18:3 (48%), 16:0 (14%), OPDA (14%), 16:3 (10%) and 18:2 (6%) were most prevalent, and in non-acclimated plants (Figure 3.4D), 18:3 (58%), 16:3 (13%), 16:0 (11%), 18:2 (7%) and OPDA (4%) were highest. Although acclimated plants accumulated approximately five-fold less acMGDG than non-acclimated plants, they accumulated approximately the same amount of OPDA-Gal acMGDG (0.48 ± 0.23 normalized MS units mg^{-1} dry mass in acclimated plants compared with 0.59 ± 0.17 units in non-acclimated plants).

Overall, the data demonstrate that during recovery from freezing, as well as during Pst infection and after wounding, significant acylation of the Gal of MGDG was induced. However, in contrast to the composition during other stresses, after freezing, the Gal-linked acyl chains were mostly unoxidized.

The proportions of 16:3, 16:0 and 18:3 in the Gal-esterified acyl chains in acMGDGs resemble proportions in DGDG

The formation of acMGDG, by a dismutation reaction when MGDG was the only substrate or by transacylation from DGDG when both MGDG and DGDG were present, has been demonstrated in in vitro experiments (Heinz, 1967b; Heinz, 1972). To define the in vivo substrate(s) for acMGDG formation, we considered the acyl compositions of Arabidopsis MGDG and DGDG. Leaf MGDG contains two major molecular species; 18:3/16:3 MGDG is present at higher levels than di18:3 MGDG. Leaf DGDG has three major molecular species: di18:3 DGDG > (16:0/18:3 DGDG + 18:3/16:0 DGDG) > 18:3/16:3 DGDG. The acyl composition of MGDG has previously been analyzed: 59% 18:3, 33% 16:3 and only 1% 16:0, whereas the acyl composition of DGDG contains 77% 18:3, 3% 16:3 and 12% 16:0 (Miquel et al., 1998). Comparing the percentages of 16:0 and 16:3 (and other acyls) esterified to the Gal of acMGDG of stressed (induced) samples to the percentages in MGDG and DGDG of untreated samples should shed light on the origin(s) of the acyl groups (Figure 3.5). The fatty acid compositions of MGDG and DGDG used in the current analysis were estimated from the percentage of each MGDG and DGDG molecular species determined by head-group scanning of untreated samples, with assignment of molecular species based on previous product ion analysis (Devaiah et al., 2006). Detailed estimation is shown in Table S3.5. The percentages of each fatty acid in MGDG and DGDG determined in this way on the untreated samples were in close agreement with the previously published data (Miquel et al., 1998). When acMGDG formation is induced by stresses in Col-0, fatty acid oxidation also occurs at various levels. Hence, for comparison of normal and head group-acylated galactolipid compositions, the contents of unoxidized fatty acids and their oxidized derivatives were summed: i.e. 16:3 and its major oxidized derivative, 16:4-O, were combined; similarly, 18:3, 18:4-O, 18:3-O and 18:3-2O were combined, as were 18:2 and 18:2-2O. The composition of the fatty acids linked to Gal in acMGDG during stress responses, reveals that the percentage of 16:0, ranging from 11 to 19%, is similar to the percentage in DGDG (11%) and

much higher than in MGDG (0.1%, Figure 3.5). While it is possible that under certain circumstances, some fatty acyl chains used to esterify Gal might come from MGDG, as suggested by the somewhat higher percentage of 16:3 and 16:4-O incorporated on the Gal of acMGDG following freezing stress (Figure 3.5E–F), the data are consistent with DGDG as the major source of the Gal-esterified fatty acids in acMGDG formed in vivo.

The oxidized fatty acyl chain OPDA is enriched on the Gal of acMGDG

To determine relative amounts of OPDA and 18:3 in MGDG, DGDG and acMGDG, ratios of MS signals for OPDA and 18:3 in MGDG and DGDG were measured using ESI triple quadrupole MS precursor scanning in negative mode, while ratios of MS signals for OPDA and 18:3 on the Gal of acMGDG were measured using NL scanning in positive mode. Levels of MGDG and DGDG detected by negative precursor scans for 18:4-O (includes OPDA), 18:3-O and 18:2-O are shown in Table S3.6. The ratios of OPDA to 18:3 signals under different treatments are shown in Table 3.2. *Pst* infection and wounding of Col-0 significantly increased the OPDA level in MGDG and DGDG ($P < 0.001$) and the OPDA/18:3 signal ratio in MGDG and DGDG ($P < 0.05$). However, the OPDA/18:3 signal ratio was several orders of magnitude higher on the Gal of acMGDG than in MGDG and DGDG under both induced and non-induced conditions. Although neither acclimated nor non-acclimated plants accumulated much OPDA in galactolipids after freezing treatment, the OPDA/18:3 signal ratio from the acyl chains on the Gal of acMGDG was significantly greater than the OPDA/18:3 signal ratio from the acyl chains esterified to the glycerols of MGDG and DGDG. Interestingly, OPDA enrichment on the Gal of induced acMGDG in cold-acclimated Col-0 plants is greater than in non-acclimated Col-0 recovering from sub-lethal freezing (Table 3.2). Taken together, the data in Table 3.2 indicate that the enrichment of OPDA on the Gal of acMGDG is roughly correlated with the availability of OPDA in MGDG and DGDG, and OPDA is concentrated in the pool of fatty acids linked to the Gal of acMGDG.

Oxidized acMGDG induction is enhanced by re-wounding

Although the existence of acMGDG has long been known, its physiological roles are still largely unclear. The fully oxidized acMGDGs Arabidopside E and Arabidopside G have been demonstrated to have anti-fungal and anti-bacterial activities in vitro (Andersson et al., 2006; Kourtchenko et al., 2007). One hypothesis about acMGDG function is that oxidized fatty acid-containing complex lipids may serve as reservoirs for precursors of oxylipin-derived phytohormones such as jasmonic acid (JA). In order to test this hypothesis, we wounded Col-0 leaves twice at the same place, with the second wound occurring either 24 or 48 h after the first. Leaves were harvested for lipid extraction at 0 min, 5 min, 15 min, 45 min, 4 h, 24 h and 48 h following each wounding event. Harvested leaves were extracted and analyzed for both complex lipids and the free phytohormones JA and OPDA. There was no enhancement by re-wounding in levels of induced total free JA and total free OPDA (Figure S3.3), indicating that the accumulation of pools of esterified oxylipins did not trigger a significantly faster or stronger response in levels of free JA or OPDA upon re-wounding.

Figure 3.6 shows levels of plastidic complex lipids MGDG, DGDG and acMGDG. Whereas free oxylipin content was not significantly higher upon re-wounding, signals from oxidized MGDG and DGDG (Figure 3.6A–C) were clearly increased by a second wounding to levels higher than by a single wounding. The second wounding did not induce major and sustained increases in signals from unoxidized acMGDG (Figure 3.6D–F). In contrast, the levels of oxidized acMGDGs (Figure 3.6G–H) were much higher during re-wounding and remained higher than the levels induced by the first wounding for up to 48 h after re-wounding.

Discussion

The present work demonstrates that acMGDGs are formed in planta across species (Figure 3.1B). Prior work established that wounding and bacterial infection induce acMGDG production in Arabidopsis (Andersson et al., 2006; Kourtchenko et al., 2007; Vu et al., 2012). Homogenization was also reported to induce MGDG acylation in spinach and broad bean leaves (Heinz 1967a, Heinz 1972). Here, we demonstrated that acMGDG is also formed in tomato and wheat in response to wounding, suggesting that Gal acylation of MGDG is a conserved response

to stress in plants. We also demonstrate that sub-lethal freezing induces acMGDG synthesis in the post-freezing period (Figure 3.3C). This was not observed in our previous study, which focused only on oxidized acMGDG and analyzed lipid levels only to the end of the freezing period (Vu et al., 2012).

The acyl composition of the acyl-Gal in acMGDG differs in different circumstances. Factors that affect the composition include the plant species, the applied stress, and, likely, other factors that affect the composition of the galactolipid pool. In general the data support the notion that in vivo formation of acMGDG occurs via transacylation from DGDG, as demonstrated previously for in vitro formation (Heinz, 1967b; Heinz, 1972). Species and accessions with more oxidized lipids in the galactolipid pool (Col-0 > C24 > other species) have more oxidized lipids in acMGDG. Stresses that induce more lipid oxidation (bacterial infection and wounding) vs those that induce less (freezing) also result in production of acMGDG with more oxidized molecular species. Wound-induced acMGDGs containing Gal-linked OPDA (Arabidopsides E and G) were not detected in *Brassica napus*, *Nicotiana tabacum*, *Pisum sativum*, *Spinacia oleracea*, *Avena sativa* and barley (Kourtchenko et al., 2007). However, we cannot rule out the possibility that acMGDG is produced in these species with unoxidized fatty acids linked to Gal, similar to the observed reaction products in wheat.

At the same time, the composition of the acyl-Gal in Arabidopsis acMGDG was determined to be more oxidized than the galactolipid acyl pool as a whole. Ibrahim et al. (2011) reported that the ratio of unoxidized acMGDG to oxidized acMGDG in Col-0 leaves harvested 30 min after wounding (regardless of the positions of oxidized fatty acids on acMGDGs) is 0.6; the detection of such a high level of oxidation agrees with our data showing that oxidized fatty acids are enriched in acMGDG. Two possible explanations for the enrichment of OPDA on the Gal of acMGDG are: (1) that an acyltransferase preferentially acylates Gal with an oxidized fatty acid compared to an unoxidized one or (2) that an oxidizing enzyme, such as a lipoxygenase, can act efficiently and directly on an unoxidized fatty acid bound to Gal. The data suggest that, as previously demonstrated in vitro, DGDG in particular is likely to be the source of acyl chains for MGDG acylation to acMGDG in vivo. To date, no protein or gene directly responsible for acylation of acMGDG has been identified. The oxidized MGDGs and DGDGs, such as

Arabidopsides A, B and D (OPDA/dnOPDA MGDG, diOPDA MGDG and diOPDA DGDG, respectively, Figure 3.6A–C) are among the most rapidly formed compounds during stress responses, and the production of acMGDG always lags behind the production of these potential substrate species. This might support the idea of preferential acylation with oxidized fatty acids. On the other hand, Nilsson et al. (2012) presented data suggesting that oxidizing enzymes can directly catalyze oxidation of membrane bound fatty acids. Interaction between a soluble lipoxygenase and a Gal-linked acyl chain might be even more likely. If an oxidizing enzyme could preferentially interact with head group-linked fatty acyl chains, this would support the second possibility.

One potential function for acMGDGs might be as a reservoir for signaling compounds. Another possibility is that acMGDGs are just signs of damage. The current work did not provide support for either of those possibilities. JA and OPDA production was not directly correlated with acMGDG levels, nor was leaf damage linked with acMGDG levels in the recovery period after freezing. An alternative notion is that the acMGDG pool serves to sequester potentially harmful fatty acids from the main membrane lipid pool. Two examples of accumulation of acMGDG during stress responses support this idea. In the period after freezing, cold-acclimated plants accumulated acMGDG as the leaves recovered and ion leakage decreased (Figure 3.3). This acMGDG in acclimated leaves was enriched in oxidized fatty acid more than the acMGDG accumulated in non-acclimated leaves which do not recover from freezing damage. The second example is accumulation of acMGDG during re-wounding (Figure 3.6). In this case, upon rewounding, levels of acMGDG with oxidized fatty acids linked to Gal appeared to increase more and to stay increased longer than other galactolipid derivatives. These examples imply that acMGDG species are relatively long-lived and may persist and increase as recovery from stress occurs.

Acknowledgements

The authors would like to thank Dr Ernst Heinz for his encouragement and helpful comments. We are grateful to Drs Xuemin Wang and Jyoti Shah for their participation in related studies. We thank Dr Mark Ungerer for use of a freezing chamber and Dr Ari Jumponen for use of a light

cart. We appreciate Dr Sunish Sehgal allowing us to harvest wheat leaves from his plantings. This work was supported by the National Science Foundation (MCB 0920663 to R. W.). Instrument acquisition at the Kansas Lipidomics Research Center was supported by National Science Foundation (EPS 0236913, DBI 0521587, DBI 1228622), Kansas Technology Enterprise Corporation, K-IDeA Networks of Biomedical Research Excellence (INBRE) of National Institutes of Health (P20RR16475) and Kansas State University. Contribution no. 13-362-J from the Kansas Agricultural Experiment Station.

References

Andersson MX, **Hamberg M**, **Kourtchenko O**, **Brunnström A**, **McPhail KL**, **Gerwick WH**, **Gobel C**, **Feussner I**, **Ellerström M** (2006) Oxylipin profiling of the hypersensitive response in Arabidopsis thaliana. Formation of a novel oxo-phytodienoic acid-containing galactolipid, arabidopside E. J Biol Chem **281**: 31528–31537

Bligh EG, **Dyer WJ** (1959) A rapid method for total lipid extraction and purification. Can J Biochem Physiol **37**: 911–917

Bottcher C, **Weiler EW** (2007) cyclo-Oxylipin-galactolipids in plants: occurrence and dynamics. Planta **226**: 629–637

Buseman CM, **Tamura P**, **Sparks AA**, **Baughman EJ**, **Maatta S**, **Zhao J**, **Roth MR**, **Esch SW**, **Shah J**, **Williams TD**, **Welti R** (2006) Wounding stimulates the accumulation of glycerolipids containing oxophytodienoic acid and dinor-oxophytodienoic acid in Arabidopsis leaves. Plant Physiol **142**: 28–39

Devaiah SP, **Roth MR**, **Baughman E**, **Li M**, **Tamura P**, **Jeannotte R**, **Welti R**, **Wang X** (2006) Quantitative profiling of polar glycerolipid species from organs of wild-type Arabidopsis and a PHOSPHOLIPASE Dα1 knockout mutant. Phytochemistry **67**: 1907–1924

Heinz E (1967a) Acylgalactosyldiglyceride from leaf homogenates. Biochim Biophys Acta **144**: 321–332

Heinz E (1967b) On the enzymatic formation of acylgalactosyldiglyceride. Biochim Biophys Acta **144**: 333–343

Heinz E (1972) Some properties of the acyl galactosyl diglyceride-forming enzyme from leaves. Z Pflanzenphysiol **69**: 359–376

Heinz E, **Tulloch AP** (1969) Reinvestigation of the structure of acyl galactosyl diglyceride from spinach leaves. Hoppe-Seyler's Z Physiol Chem **350**: 493–498

Ibrahim A, **Schutz AL**, **Galano JM**, **Herrfurth C**, **Feussner K**, **Durand T**, **Brodhun F**, **Feussner I** (2011) The Alphabet of Galactolipids in Arabidopsis thaliana. Front Plant Sci **2**: 95

Kourtchenko O, **Andersson MX**, **Hamberg M**, **Brunnström A**, **Gobel C**, **McPhail KL**, **Gerwick WH**, **Feussner I**, **Ellerström M** (2007) Oxo-phytodienoic acid-containing galactolipids in Arabidopsis: jasmonate signaling dependence. Plant Physiol **145**: 1658–1669

Miquel M, **Cassagne C**, **Browse J** (1998) A new class of Arabidopsis mutants with reduced hexadecatrienoic acid fatty acid levels. Plant Physiol **117**: 923–930

Nilsson AK, **Fahlberg P**, **Ellerström M**, **Andersson MX** (2012) Oxo-phytodienoic acid (OPDA) is formed on fatty acids esterified to galactolipids after tissue disruption in Arabidopsis thaliana. FEBS Lett **586**: 2483–2487

Schmelz EA, **Engelberth J**, **Tumlinson JH**, **Block A**, **Alborn HT** (2004) The use of vapor phase extraction in metabolic profiling of phytohormones and other metabolites. Plant J **39**: 790–808

Stelmach BA, **Muller A**, **Hennig P**, **Gebhardt S**, **Schubert-Zsilavecz M**, **Weiler EW** (2001) A novel class of oxylipins, sn1-O-(12-oxophytodienoyl)-sn2-O-(hexadecatrienoyl)-monogalactosyl Diglyceride, from Arabidopsis thaliana. J Biol Chem **276**: 12832–12838

Telfer A, **Bollman KM**, **Poethig RS** (1997) Phase change and the regulation of trichome distribution in Arabidopsis thaliana. Development **124**: 645–654

Vu HS, **Tamura P**, **Galeva NA**, **Chaturvedi R**, **Roth MR**, **Williams TD**, **Wang X**, **Shah J**, **Welti R** (2012) Direct infusion mass spectrometry of oxylipin-containing Arabidopsis membrane lipids reveals varied patterns in different stress responses. Plant Physiol **158**: 324–339

Xiao S, **Gao W**, **Chen QF**, **Chan SW**, **Zheng SX**, **Ma J**, **Wang M**, **Welti R**, **Chye ML** (2010) Overexpression of Arabidopsis acyl-CoA binding protein ACBP3 promotes starvation-induced and age-dependent leaf senescence. Plant Cell **22**: 1463–1482

Figures and Tables

Figure 3.1 acMGDG structure and occurrence upon wounding.

A) Structure of a representative acMGDG molecule, 1-18:4-O,2-16:4-O,3-(16:0-galactosyl)glycerol and the fragmentation that gives rise to the NL fragment by collision induced dissociation. A proton moves from right to left during fragmentation. B) Total acMGDG induced by wounding, measured by the 11 NL scans indicated in Table 3.1, in Arabidopsis Col-0 and C24, tomato, and wheat leaves. Units are in relation to amount of signal detected for 1 nmol of internal standard (di18:0 DGDG), which is denoted as 1. Error bars are standard deviation, n = 5. The numbers above the bars of wounded samples show the fold induction compared to corresponding unwounded samples.

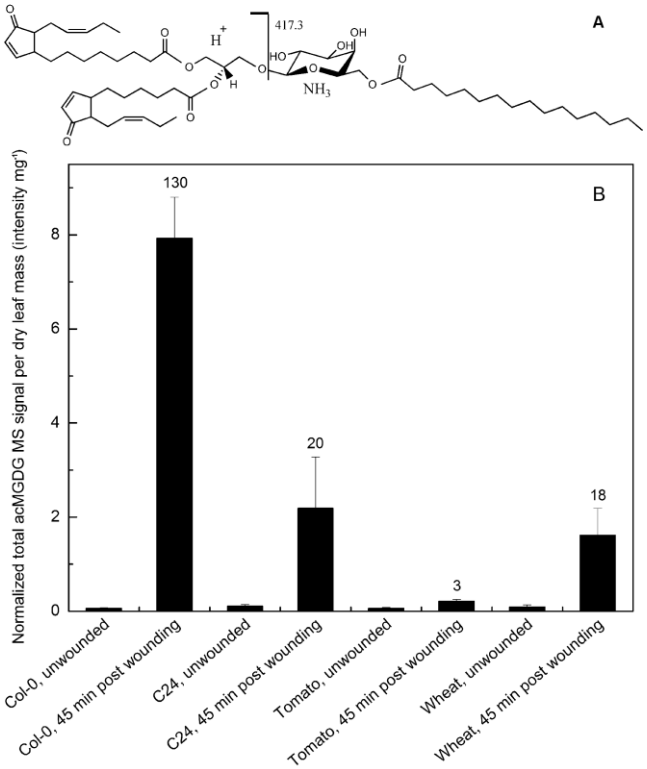

Figure 3.2 Levels of acMGDG (grouped by fatty acyl moiety on the Gal) in leaves of Arabidopsis Col-0 (A) and C24 (B), tomato (C), and wheat (D) 45 min after wounding. The y axes have different scales. Error bars are standard deviation, n = 5. The numbers above the bars show the percentage of the corresponding acMGDG group over the sum of the 11 measured acMGDG groups.

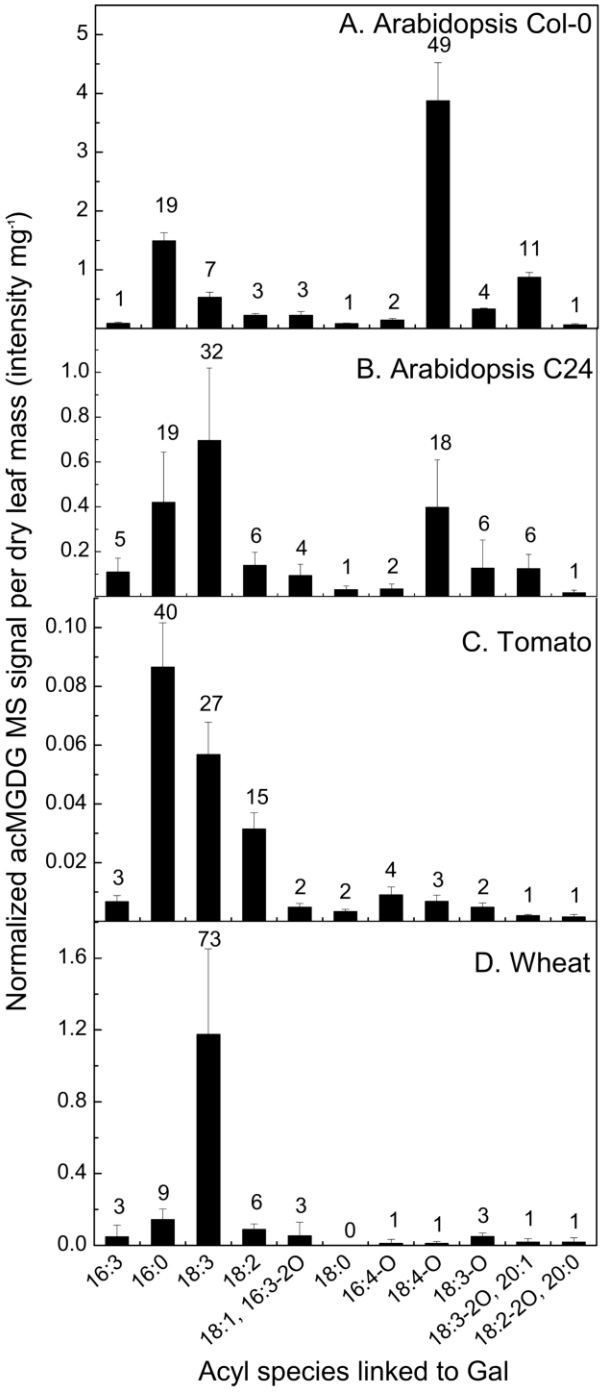

Figure 3.3 acMGDG forms in leaves of Arabidopsis Col-0 after application of different stresses, and its occurrence during freezing is not directly associated with cell membrane ion leakage.

Panels A, B, and C: acMGDG induced by Pst infection, wounding, and freezing. The y axes have different scales. Panel C shares an x-axis with Panels D and E. Panel D: Relative ion leakage (%) of acclimated and non-acclimated Arabidopsis Col-0 leaves at 3 h and 24 h after freezing treatment. Panel E: Level of total phosphatidic acid as measured by MS in acclimated and non-acclimated Arabidopsis Col-0 leaves at 3 h and 24 h after freezing treatment. Error bars are standard deviation; panels A and B: n = 5; panels C, D, and E: n = 6.

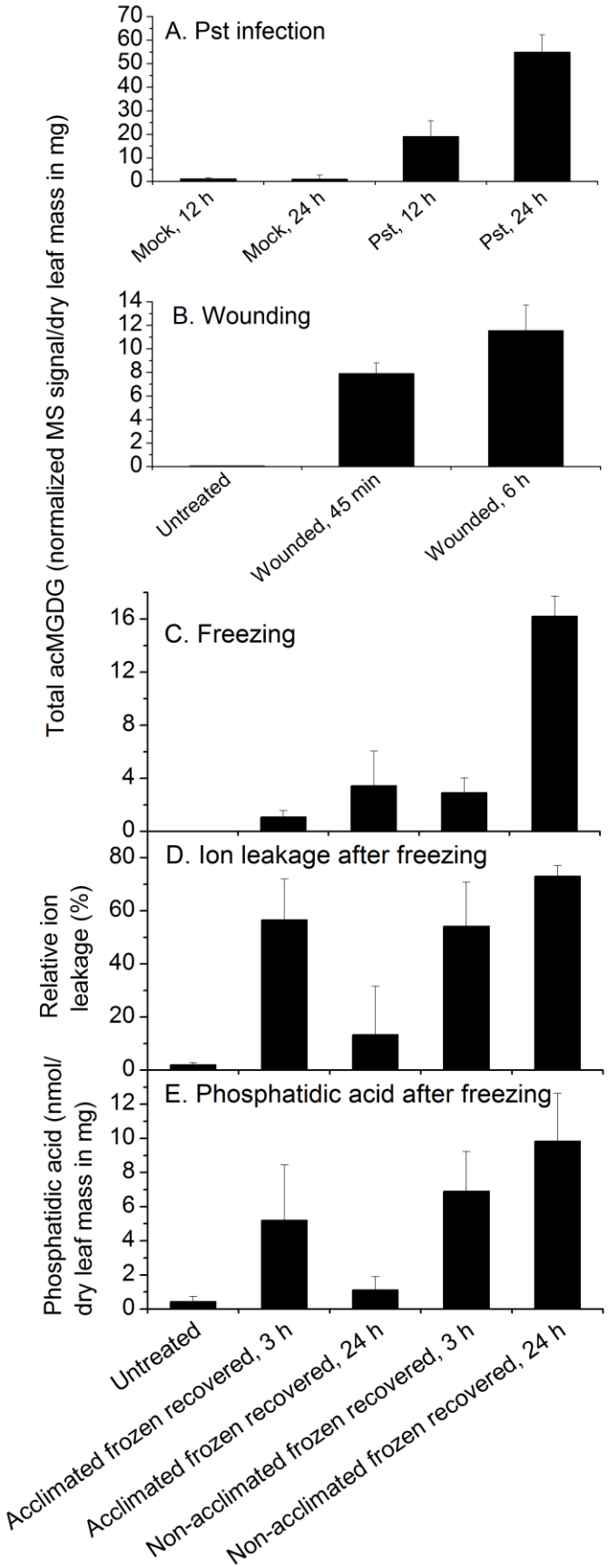
A. Pst infection
B. Wounding
C. Freezing
D. Ion leakage after freezing
E. Phosphatidic acid after freezing
Total acMGDG (normalized MS signal/dry leaf mass in mg)
Relative ion leakage (%)
Phosphatidic acid (nmol/ dry leaf mass in mg)
Mock, 12 h
Mock, 24 h
Pst, 12 h
Pst, 24 h
Untreated
Wounded, 45 min
Wounded, 6 h
Untreated
Acclimated frozen recovered, 3 h
Acclimated frozen recovered, 24 h
Non-acclimated frozen recovered, 3 h
Non-acclimated frozen recovered, 24 h

Figure 3.4 Levels of acMGDG (grouped by fatty acyl moiety on the Gal) in leaves of Arabidopsis Col-0 after application of different stresses.

Panel A: acMGDG at 24 h post Pst infection, n = 5; panel B: acMGDG at 45 min post wounding, n = 5; panel C: acMGDG of cold acclimated Col-0 plants at 24 h post freezing, n= 6; panel D: acMGDG of non-acclimated Col-0 plants at 24 h post freezing, n = 6. Y axes have different scales. Error bars are standard deviation. The numbers above the bars show the percentage of the corresponding acMGDG group over the sum of the 11 measured acMGDG groups.

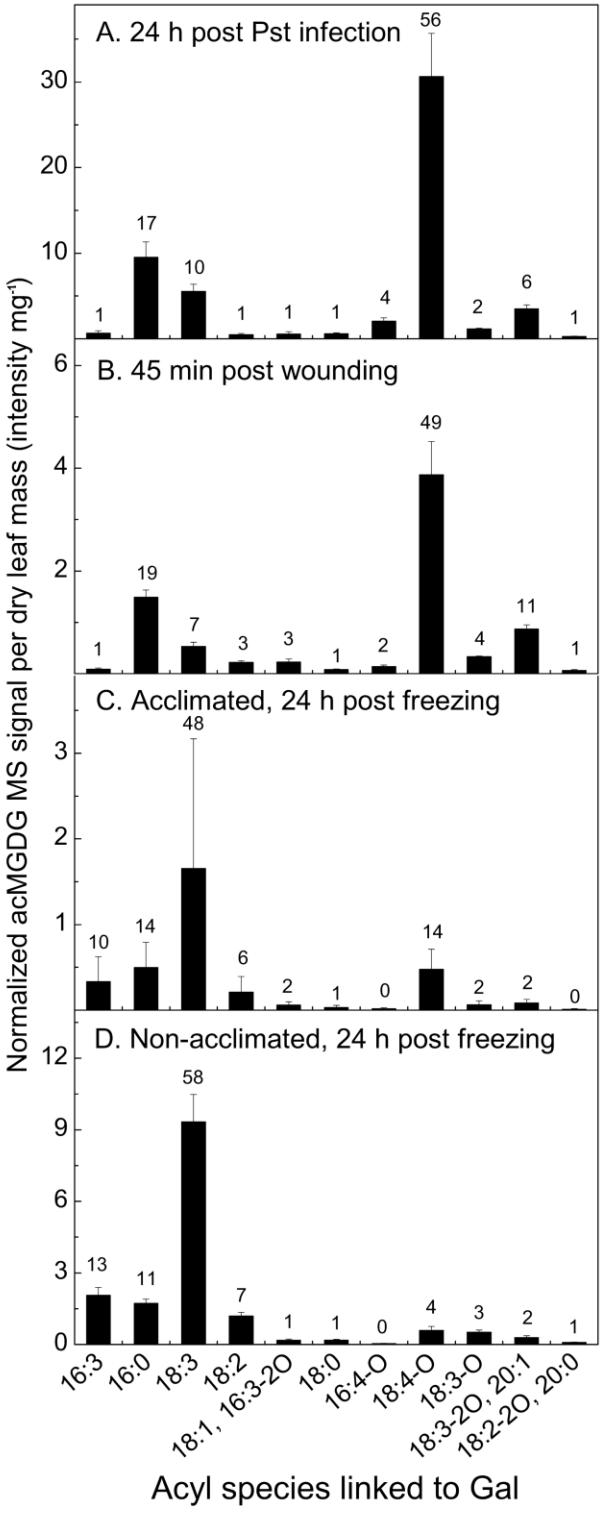
A. 24 h post Pst infection
B. 45 min post wounding
C. Acclimated, 24 h post freezing
D. Non-acclimated, 24 h post freezing
Normalized acMGDG MS signal per dry leaf mass (intensity mg-1)
Acyl species linked to Gal
16:3
16:0
18:3
18:2
18:1, 16:3-2O
18:0
16:4-O
18:4-O
18:3-O
18:3-2O, 20:1
18:2-2O, 20:0

Figure 3.5 Comparison of fatty acyl composition.

Fatty acyl composition (%) of MGDG (A) and DGDG (B) in untreated leaves and fatty acid composition of acyl-Gal in acMGDG of Col-0 plants at 24 h post Pst infection (C), n = 5; and at 45 min post wounding (D), n = 5; of cold acclimated (E) and of non-acclimated (F) Col-0 plants at 24 h post freezing, n = 6.

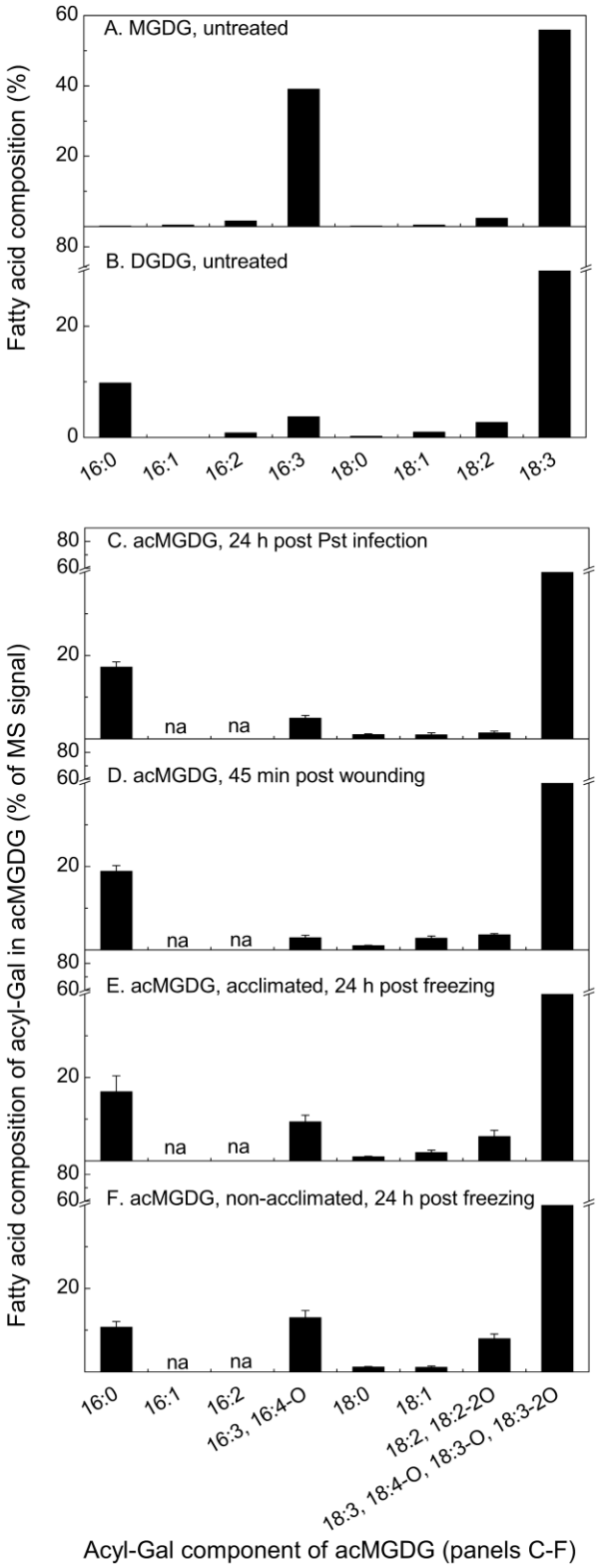
A. MGDG, untreated
B. DGDG, untreated
Fatty acid composition (%)
C. acMGDG, 24 h post Pst infection
D. acMGDG, 45 min post wounding
E. acMGDG, acclimated, 24 h post freezing
F. acMGDG, non-acclimated, 24 h post freezing
Fatty acid composition of acyl-Gal in acMGDG (% of MS signal)
na
16:0
16:1
16:2
16:3, 16:4-O
18:0
18:1
18:2, 18:2-2O
18:3, 18:4-O, 18:3-O, 18:3-2O
Acyl-Gal component of acMGDG (panels C-F)

Figure 3.6 Levels of oxidized MGDG, DGDG, and acMGDG, measured by Pre 277.2 (18:3) and Pre 291.2 (18:4-O) using direct infusion ESI triple quadrupole MS in negative mode. Levels of lipids were measured at various time points after wounding was performed at 0 h (squares). Data denoted by circles show levels of lipids after a second wounding at the 24 h time point of the first wounding, and data denoted by triangles show levels of lipids after a second wounding at the 48 h time point of the first wounding. The x-axis indicates time (h) starting from the only wounding event (squares) or final wounding event (circles and triangles). Y axes are mass spectral signal for the indicated compound, where 1 is the amount of signal detected for 1 nmol of internal standard (18:0/16:0 MGDG), The y axes have different scales. Error bars are standard deviation, n = 5.

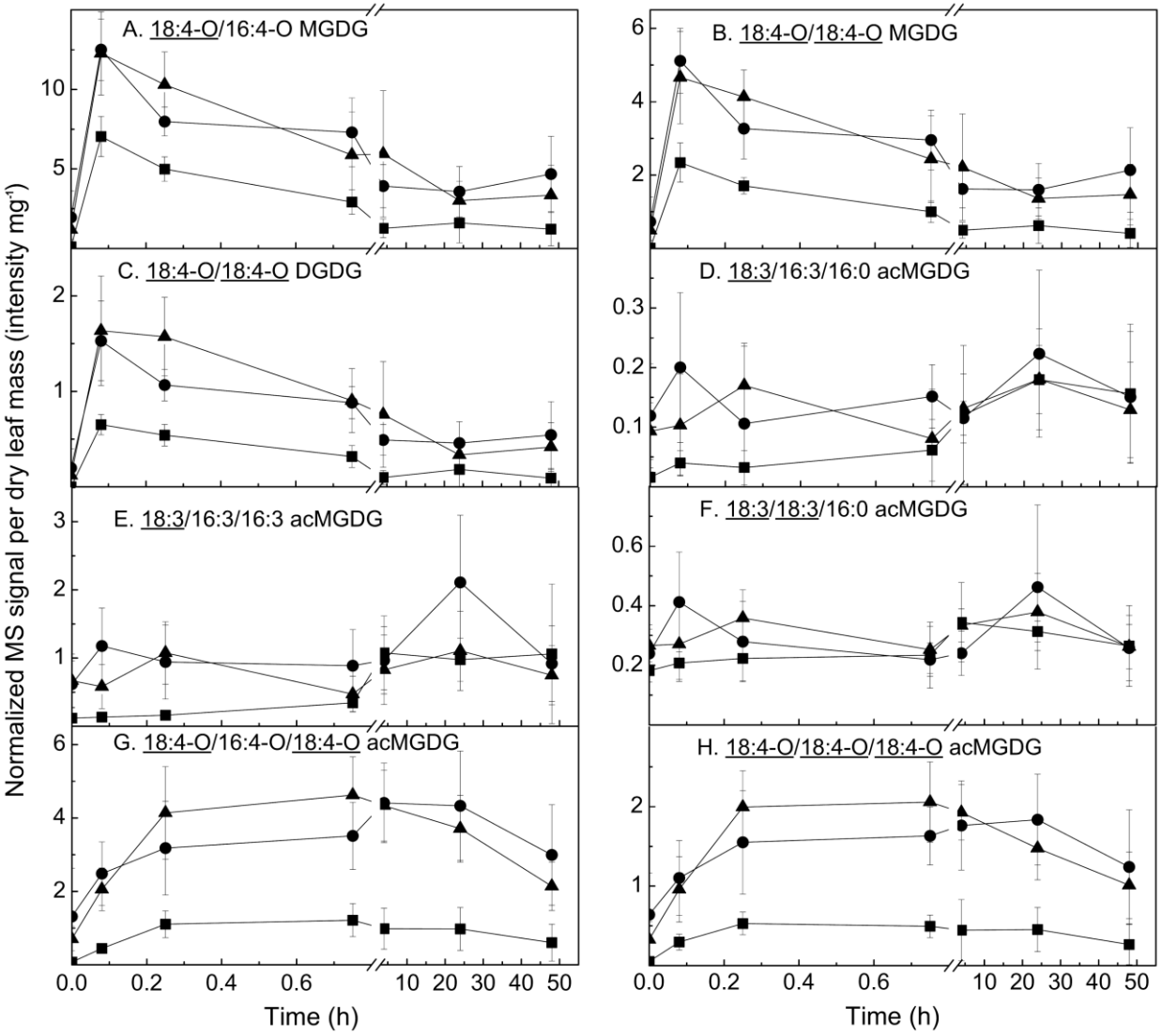

Table 3.1 NL fragments used to detect acMGDGs by ESI triple quadrupole MS in positive mode

m/z of NL fragment	Fatty acyl chain	Chemical formula of NL fragment
411.3	16:3	$C_{22}H_{37}O_6N$
417.3	16:0	$C_{22}H_{43}O_6N$
425.3	16:4-O	$C_{22}H_{35}O_7N$
439.3	18:3	$C_{24}H_{41}O_6N$
441.3	18:2	$C_{24}H_{43}O_6N$
443.3	18:1, 16:3-2O	$C_{24}H_{45}O_6N$, $C_{22}H_{37}O_7N$
445.3	18:0	$C_{24}H_{47}O_6N$
453.3	18:4-O	$C_{24}H_{39}O_7N$
455.3	18:3-O	$C_{24}H_{41}O_7N$
471.3	18:3-2O, 20:1	$C_{24}H_{41}O_8N$, $C_{26}H_{49}O_6N$
473.3	18:2-2O, 20:0	$C_{24}H_{43}O_8N$, $C_{26}H_{51}O_6N$

Table 3.2 Ratio of signals from OPDA/18:3 in galactolipids of *Arabidopsis thaliana.*

Total OPDA-containing MGDG and DGDG (normalized mass spectral signal unit per dry leaf mass), measured by scanning Pre 291.2 in negative mode (complete data in Table S3.6), are shown in the second column. Col-0 was subjected to Pst infection ("Pst, 24 h", n = 5), freezing and post-freezing at 21 °C with or without prior cold acclimation ("acclimated, 24 h" or "non-acclimated, 24 h", n = 6), and wounding ("wounded, 45 min", n = 5). C24 was also wounded and sampled after 45 min ("wounded, 45 min", n = 5). The third through fifth columns indicate the ratio of signals derived from OPDA to signals derived from 18:3 in acyl chains of MGDG, acyl chains of DGDG, or from the acyl chain on the Gal of acMGDG. Errors are standard deviation.

Treatment	**OPDA-containing MGDG and DGDG (intensity mg^{-1})**	**Ratio of OPDA/18:3 signals**		
		in MGDG	**in DGDG**	**on Gal of acMGDG**
Col-0, untreated	0.02 ± 0.01	0.0005 ± 0.0002	0.0049 ± 0.0005	5.39 ± 3.50
Col-0, Pst, 24 h	0.81 ± 0.15	0.022 ± 0.006	0.041 ± 0.010	5.82 ± 1.95
Col-0, acclimated, 24 h	0.013 ± 0.013	0.0006 ± 0.0010	0.0008 ± 0.0006	0.51 ± 0.36
Col-0, non-acclimated, 24 h	0.017 ± 0.009	0.0092 ± 0.0080	0.0080 ± 0.0070	0.063 ± 0.017
Col-0, wounded, 45 min	1.26 ± 0.23	0.0085 ± 0.0053	0.022 ± 0.011	24.1 ± 6.5
C24, untreated	0.17 ± 0.07	0.0004 ± 0.0003	0.0027 ± 0.0026	0.39 ± 0.21
C24, wounded, 45 min	0.26 ± 0.13	0.0013 ± 0.0007	0.0058 ± 0.0018	0.56 ± 0.07

Supplemental Data

Supplemental data for this chapter include:

Figure S3.1 Tentative structure of 18:3/18:3/18:3 acMGDG detected in wounded wheat leaves

Figure S3.2 Acclimated and non-acclimated *Arabidopsis thaliana* Col-0 after freezing at -8 °C for 2 h

Figure S3.3 Total free OPDA and JA after wounding and re-wounding of Col-0 plants

Tables S3.1-S3.6 are in a separate Excel file

Table S3.1 DAG fragments of acMGDG determined during NL scanning by ESI triple quadrupole mass spectrometry in positive mode using scan modes listed in Table 3.1

Table S3.2 Levels of acMGDG detected by NL scans of individual replicates (in normalized mass spectral signal unit mg-1 leaf dry mass)

Table S3.3 Accurate masses of acyl groups of acMGDG from wounded Col-0, tomato and wheat provided by Q-TOF mass spectrometry in negative mode

Table S3.4 Levels of normal chain phospholipids and galactolipids detected by triple quadrupole mass spectrometry (in nmol mg-1 leaf dry mass), performed as described in Xiao et al. (2010, supplemental data)

Table S3.5 Estimation of fatty acid composition in MGDG and DGDG

Table S3.6 Levels of 18:4-O- and 18:3-O-containing MGDG, DGDG, and phosphatidylglycerol (PG) detected by Pre scans of 291.2, 293.2 and 295.2 in negative mode, as described by Vu et al. (2012)

Figure S3.1 Tentative structure of 18:3/18:3/18:3 acMGDG detected in wounded wheat leaves.

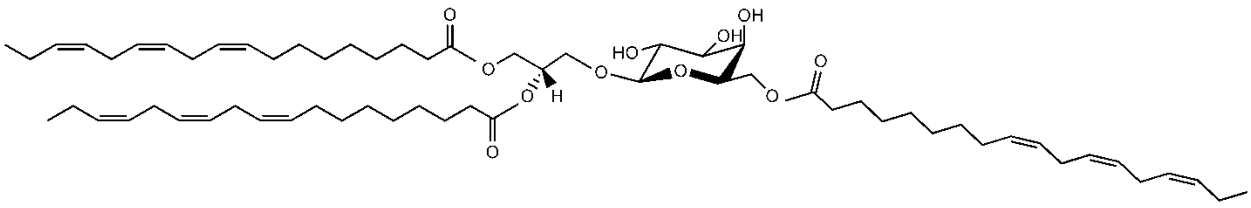

Figure S3.2 Acclimated and non-acclimated *Arabidopsis thaliana* Col-0 after freezing at -8 °C for 2 h. Numbers on the left indicate time (h) at 21 °C after freezing treatment.

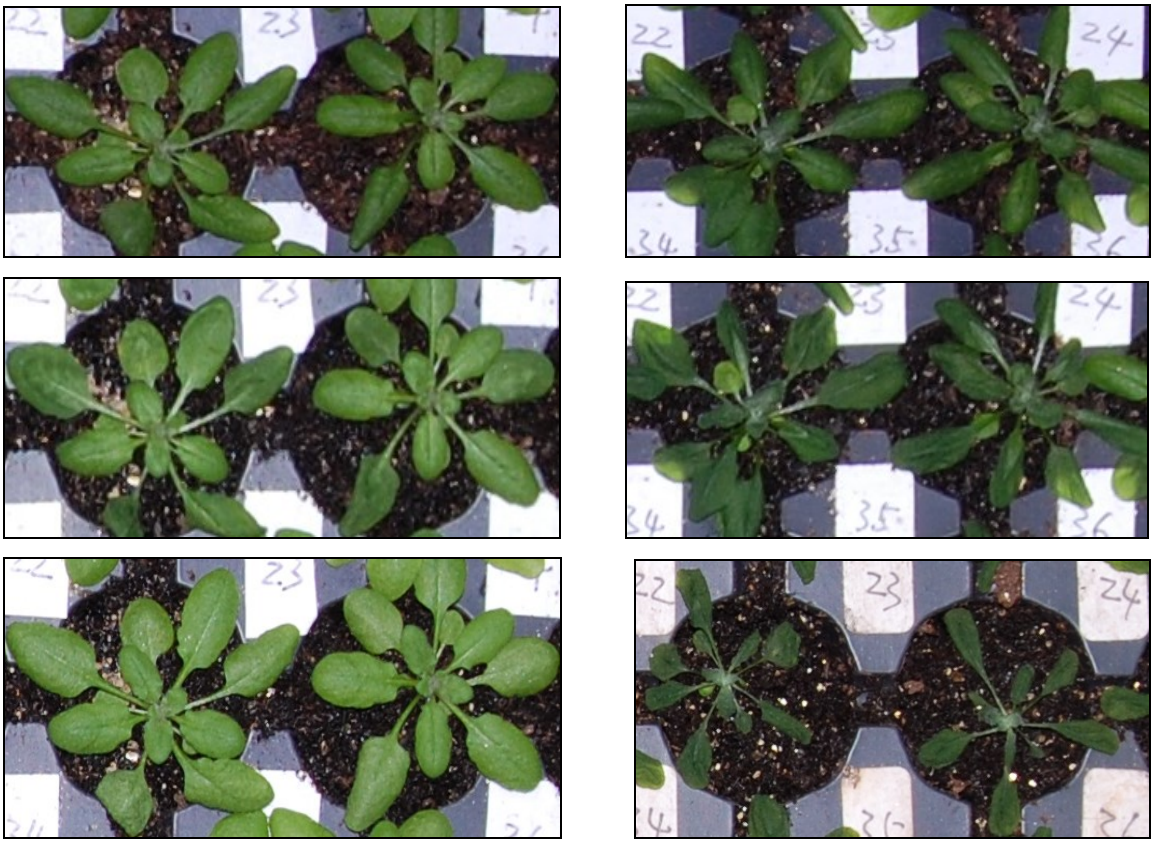

Figure S3.3 Total free OPDA and JA after wounding and re-wounding of Col-0 plants. A: total free OPDA, B: total free JA in ng/mg of leaf fresh weight. Total OPDA is sum of *cis*- and *trans*-OPDA. Total JA is sum of *cis*- and *trans*-JA.

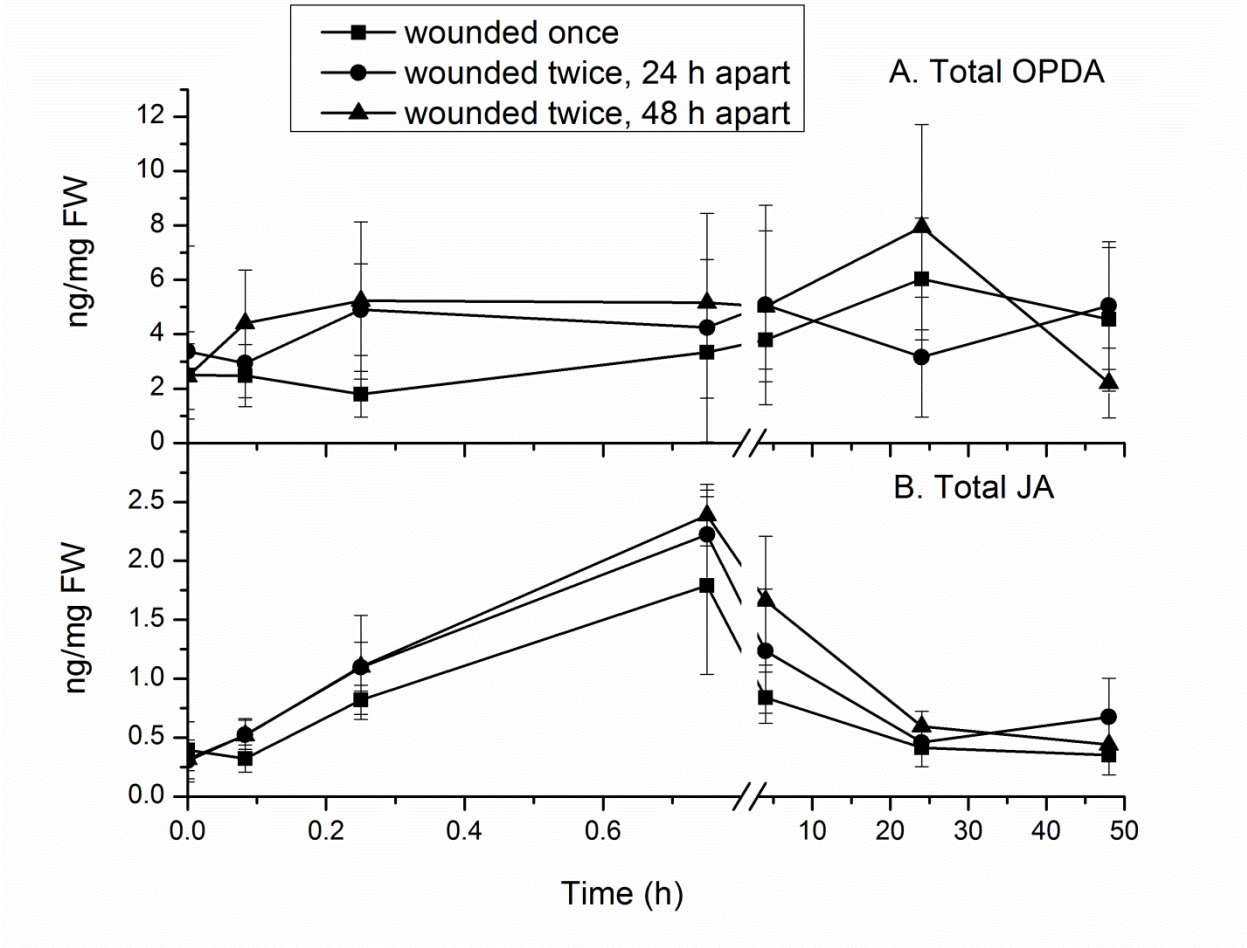

Chapter 7 - Lipid changes after leaf wounding in *Arabidopsis thaliana*: Expanded lipidomic data form the basis for lipid co-occurrence analysis

Abstract

A direct-infusion electrospray ionization triple quadrupole mass spectrometry method with multiple reaction monitoring (MRM) was employed to measure 272 lipid analytes extracted from leaves of *Arabidopsis thaliana* subjected to mechanical wounding. The lipid classes analyzed comprised galactolipids and phospholipids (including monoacyl molecular species, molecular species with oxidized acyl chains, phosphatidic acids (PAs), tri-and tetra-galactosyldiacylglycerols (TrGDGs and TeGDGs), head-group-acylated galactolipids, and head-group-acylated phosphatidylglycerol (acPG), sulfoquinovosyldiacylglycerols (SQDGs), sphingolipids, di- and tri-acylglycerols (DAGs and TAGs), and sterol derivatives. Of the 272 lipid analytes, 256 changed significantly in response to wounding. In general, levels of structural lipids decreased, whereas monoacyl molecular species, galactolipids and phosphatidylglycerols (PGs) with oxidized fatty acyl chains, PAs, TrGDGs, TeGDGs, TAGs, head-group-acylated galactolipids, acPG, and some sterol derivatives increased, many transiently. The observed changes are consistent with activation of lipid oxidizing, hydrolyzing, glycosylating, and acylating activities in the wounding response. Correlation analysis of the levels of lipid analytes across individual control and treated plants was used to construct a lipid dendrogram and to define clusters and sub-clusters of lipid analytes, each composed of a group of lipids which occurred in a coordinated manner. Current knowledge of metabolism supports the notion that observed sub-clusters comprise lipids generated by parallel metabolism or formed from sub-cluster members by a non-rate-limiting process. This work demonstrates that co-occurrence analysis, based on correlation of lipid levels among plants, is a powerful approach to defining lipids generated *in vivo* by identical or inter-twined enzymatic pathways.

Introduction

As lipid biochemists have long known, and computational biologists have recently confirmed, lipid metabolism contains more than its share of reactions catalyzed by enzymes with broad substrate selectivity, i.e., those that act on more than one substrate and produce multiple products (Carbonell et al., 2011). Indeed, knock-out or suppression of single genes has indicated that, during stress responses in plants, individual lipid-metabolizing enzymes act on multiple substrates and produce multiple products (e.g., Welti et al., 2002; Peters et al., 2010). On the other hand, application of stress to a plant activates multiple metabolic pathways. In lipid metabolism, wounding stress causes phospholipase D activation, phospholipase A activation, oxidation of fatty acids on galactolipids, and head-group acylation of monogalactosyldiacylglycerols (Narváez-Vásquez et al., 1999; Zien et al., 2001; Ryu et al., 2004; Buseman et al., 2006; Vu et al., 2014). Steuer et al. (2003) observed that individual plants under the same treatment show small biological variations in the rate and extent of activation of various metabolic pathways. Taken together, current knowledge suggests that (1) when a stress is applied, plant lipid composition will change due to activation of an array of enzymes, (2) under each treatment condition, individual plants will vary slightly in lipid composition, due to varied responses of individual pathways, and, (3) in most cases, activation of a pathway will result in simultaneous change in members of a group of lipids that represent substrates or products of the activated pathway.

Lipidomic analysis can be employed to reveal the levels of plant lipid molecular species. In the current work we have developed a direct-infusion electrospray ionization (ESI) triple-quadrupole mass spectrometry (MS) method to analyze a wide array of lipid species, with a focus on ability to analyze compositional patterns of lipids among individual plants and during stress. This approach provides good sensitivity and precision.

We predicted that lipid intermediates or products produced by the same enzyme(s) or pathway would co-occur when their metabolic pathway is activated and/or repressed in individual plants. Using tools developed for metabolomics and drawing on recent thinking about the use of metabolite level correlations to further understanding of metabolism (Camacho et al., 2005; Xia et al., 2009 and 2012; Toubiana et al., 2013), lipidomic data were analyzed to reveal lipid groups

defined by co-occurrence through stresses and among individual plants. The relationships between the revealed co-occurring groups and known plant lipid metabolism were examined.

Results

Plant wounding

To test the hypothesis described in the Introduction, we conducted a leaf-wounding experiment. Wild-type Arabidopsis (accession Columbia-0) plants were wounded with a hemostat by crimping twice across the mid-vein of three leaves. Wounded leaves were harvested 45 min and 6 h after wounding as were the leaves in the same position on unwounded control plants (n = 31 for each treatment group). Wounding at this level produces ion leakage (Figure S4.1) and an increase in expression of genes encoding enzymes involved in production of oxidized fatty acids (*ALLENE OXIDE SYNTHASE* (*AOS*) and *LIPOXYGENASE2* (*LOX2*); Figure S4.2a and b), but the leaves undergo recovery, as indicated by reduced ion leakage at 24 h (Figure S4.1). Some crimped leaf areas appear to heal, while marks remain visible in other areas at 24 h (Figure S4.3). All leaves remain green, and improvement in appearance is apparent within 24 h after wounding (Figure S4.3).

Extraction of leaves

Because our goal is to apply lipidomics in a high-throughput manner and because extraction can be a time-consuming part of lipid analysis, a streamlined extraction method was developed. After quenching of potential phospholipase D activity by immersion of leaves harvested 45 min after wounding in hot isopropanol for 15 min, a polar solvent mixture was added. After shaking for 24 h and removing the leaves, the extract was subjected to mass spectral analysis. Comparison with a modified Bligh-Dyer method (Bligh and Dyer, 1959; Welti et al., 2002) and a Bligh-Dyer type extraction, followed by additional extraction targeted at sphingolipids (Toledo et al., 1995; Markham et al., 2006), showed that the three methods each extracted similar amounts of lipid and there was only minor variation in the composition of lipids extracted by the three methods (Table 4.1 and full data set in Table S4.1).

MS analysis of lipids

To analyze stress-induced Arabidopsis leaf lipids, a direct-infusion ESI triple quadrupole MS method with MRM was developed. Each lipid analyte is defined by its mode of analysis (positive or negative), its intact ion mass/change (*m/z*), and a fragment *m/z*; an arbitrary "lipid number" corresponds to the set of parameters used in the analysis. Each analyte has been annotated, based on available information; information supporting annotations (accurate mass and LC-MS data indicating the presence of the annotated lipids in Arabidopsis thaliana tissues) is compiled in Table S4.2. Supporting quadrupole time-of-flight (QTOF) MS data not previously published are provided in Table S4.3. Abbreviations used in lipid annotations are summarized in Table 4.2, and examples of possible structures for oxidized fatty acid chains are provided in Table S4.4. MS settings for each analyte are also listed in Table S4.2. Some analytes have multiple annotations because a triple quadrupole MS, in direct infusion mode, is unable to differentiate compounds and fragments with the same nominal *m/zs*. Available data provide confidence that the vast majority of the annotations are correct, i.e., the annotation(s) indicates the major lipid(s) detected by the stated MS settings.

Infusion profiles of representative lipid analytes showed that the detected intensity varied somewhat as a function of infusion time (Figure S4.4). Some analytes, particularly negatively charged lipids including PA and phosphatidylserine (PS), were relatively retained in the loop and/or tubing, but elution of all analytes was essentially complete within 15 min of the start of infusion. To avoid variation in analyte levels due to uneven infusion, the MRM transition intensity for each analyte was acquired repeatedly throughout the entire infusion period and the intensities were averaged. Separate infusions were made for acquisition in the negative and positive modes, because initial experiments indicated that it took several seconds after mode switching for the intensity to stabilize. Infusion of a single plant extract took 35 min: a 15 min infusion in positive mode with 2.5 min of washing, followed by a 15 min infusion in negative mode with 2.5 min of washing.

Intensities were normalized to internal standards analyzed by the same method as the lipid analytes. Instrumental parameters for the internal standards are indicated in Table S4.5, and Table S4.2 indicates the internal standard(s) used for normalization of each analyte. Background

values for each lipid analyte were calculated in samples of the internal standards alone and subtracted from values in samples containing plant lipids.

The goal of the quantification was to compare levels of each lipid analyte in various plant samples, rather than to compare various lipid levels with each other. Absolute analyte levels are unreliable due to the limited number of internal standards and the variations in instrumental parameters among analytes and internal standards. In many cases, analyte intensities were normalized to intensities of standards of substantially different structure. To assure consistent data for each analyte throughout long periods of mass spectral data collection, an adaptation of the "quality control" approach suggested by Dunn et al. (2011) was employed. Representative samples from all treatments were pooled. The pooled sample, called the quality control (QC) sample, was analyzed recurrently among the experimental samples (Table S4.6). The QC analyte intensities were used to normalize the intensities in the experimental samples, as described in Experimental Procedures. Data for the lipid analytes are presented as (1) normalized intensity per mg of leaf dry mass, where a value of 1 corresponds to the same amount of intensity as derived from 1 pmol of internal standard(s) and (2) autoscaled values, produced by dividing the difference between an intensity and the mean intensity of the 93 samples by the standard deviation of the intensity of the 93 samples (Xia et al., 2009; 2012). The autoscaled values allow easy comparison of lipid levels across various samples, because all analytes can be plotted on similar scales, but do not provide information about the absolute lipid levels.

In total, the intensities of 377 MRM transitions were quantified and measurements of 272 of these lipid analytes are described here. Of these, 268 represent unique analytes, whereas four represent the same lipid measured with different instrument parameters. Each lipid analyte described in this work met the following criteria: (1) the background MRM intensity (in the internal standard-only samples) was less than 40% of the average intensity of the QC samples; and (2) the coefficient of variation, i.e., the standard deviation divided by the mean of the level of the analyte in the (identical) QC samples, was less than 20%. Coefficients of variation for individual analytes are shown in Table S4.2.

Variations in lipid analytes among individual plants and in response to wounding treatment

The full set of data for lipid analyte levels in normalized intensity per mg of leaf dry mass and as autoscaled values is provided in Tables S4.6 and S4.7. Original and autoscaled data of each lipid analyte are plotted as a function of wounding treatment (Figure S4.5). Of the 268 unique lipid analytes, 256 were significantly different in at least one of the three pairwise comparisons by ANOVA ($p < 0.01$) (Table 4.3 and Table S4.9). Tukey's post-hoc test indicates that 143 lipids were significantly different in all three pairwise comparisons and 74 lipids in comparisons between both "Wounded; 45 min" versus "Unwounded" and "Wounded; 6 h" versus "Unwounded" (Table 4.3).

The autoscaled lipid levels of individual samples are displayed as a heat map in Figure 1, and the levels of 10 lipid analytes as a function of autoscaled levels are shown in Figure 4.2. The data in Figures 4.1 and 4.2 both show that variation in lipid levels was observed in samples subjected to the same treatment, in most cases, as well as among treatments. To test the hypothesis that variation in lipid levels is due to increased or decreased activities of specific lipid pathways in individual plants and that analysis of the lipidomic data can reveal groups of lipids defined by lipid co-occurrence, correlations in the levels of the lipid analytes were determined. Spearman's correlation coefficient, ρ, was calculated for each lipid analyte with each other lipid analyte across all 93 lipid samples, including 31 samples subjected to each treatment (unwounded, wounded and harvested after 45 min, and wounded and harvested after 6 h) (Table S4.10). Spearman's correlation coefficient can range from -1 (perfect negative correlation) to 1 (perfect positive correlation) with 0 indicating no correlation.

Levels of every lipid analyte were positively correlated with the levels of at least one other lipid analyte. Of the 268 unique analytes, 264 were correlated with another lipid with a $\rho > 0.60$. By matching each lipid analyte with the one to which it was most highly correlated, a dendrogram was constructed (Figure 4.3). The dendrogram includes seven clusters of lipids, labeled A-G, corresponding to groups in which every lipid is correlated with another lipid with $\rho > 0.80$. Two of the clusters, A and C, are large, and contain 60 and 146 lipid analytes, respectively. Comparison of various correlation "cutoffs" in light of understanding of metabolism (described

in the Discussion) indicated that, within these clusters, lipids that were likely to be metabolically related were those with the highest correlation values, i.e., $\rho > 0.96$. There are 6 sub-clusters (A1-A6) in A with lipids with $\rho > 0.96$. Within C, there are 12 such sub-clusters (C1-C12).

Cluster A contains structural (i.e., membrane) lipids that are decreased as a function of wounding treatment (Figures 4.2 and S4.5, Table 4.3). These include normal chain species of DGDG, MGDG, GlcCer, GIPC, PC, PE, PG, and SQDG. Cluster B contains 3 PE species containing a normal acyl chain and 18:3-O. These analytes exhibited no change in response to wounding at 45 min but decreased at 6 h post-wounding. Cluster C contains many lipids induced by wounding. These include monoacyl lipids, including DGMGs, MGMGs, LPCs, and LPEs. Cluster C also contains head group-acylated galactolipids, acMGDG and acDGDG, as well as the only acPG species that was measured. DAG, TAG, and PA species are located in Cluster C, as are poly-galactosylated lipids, TrGDG and TeGDG. A large portion of the galactolipid analytes (acDGDG, acMGDG, DGDG, DGMG, MGDG, and MGMG) in Cluster C contains oxidized fatty acyl chains, whereas only 5 phospholipids with oxidized fatty acyl chains, i.e., PC(16:0/18:3-2O), PE(18:3/18:3-2O), PG(18:3-O/16:0), PG(18:4-O/16:0), and PG(18:4-O/16:1), fell within Cluster C. Cluster C contains several normal diacyl lipids that are likely to contain 16:3. These lipids include DAG(34:6), PA(34:6), PC(34:6), PC(32:3), and PE(32:3). Finally, Cluster C contains sterol glucosides and acyl sterol glucosides. Cluster D consists of sterol esters that change little in response to wounding. Cluster E contains two PCs with long acyl chains, PC(40:2) and PC(40:3), while Cluster F consists of 3 PEs, each with a normal-chain fatty acid and 18:3-3O. Cluster G is composed of PC(34:4) and PE(34:4).

The most highly correlated lipid analyte groups are the 18 sub-clusters, A1-A6 and C1-C12, each of which contains lipids linked by $\rho > 0.96$. Examples showing the correlation of lipid analyte levels in these clusters are provided in Figures 4.4, 4.5 and 4.6, and Figure 4.7 presents boxplots of lipid levels in response to wounding for an example lipid from each of the 18 sub-clusters. Figure 4.4 shows autoscaled values for the lipids in sub-cluster A1 (4.4a), A4 (4.4b), and A5 (4.4c) as a function of individual plant and treatment. Sub-cluster A1 includes PC(32:1) and PE(32:1), which has been identified previously as PE(16:0/16:1) (Samarakoon et al., 2012, Table S4.2). Sub-cluster A4 includes PE species (PE(34:3), PE(36:5) and PE(36:6)), which previous

analysis has shown to contain 18:3 (Welti et al., 2002; Table S4.2). Sub-cluster A5 consists of PC and PE species (PC(34:2), PE(34:2), and PE(36:4)) containing 18:2 (Welti et al., 2002; Table S4.2). Lipid analytes within the same sub-cluster vary similarly across the samples and treatments (Figure 4.4a-c). There is slightly lower co-occurrence when an analyte from each of sub-clusters A1, A4, and A5 is compared (Figure 4.4d). In addition to A1, A4, and A5, A3 is an additional PC-PE sub-cluster, which contains PC species with limited desaturation and which may contain 18:1 and/or 18:2 (Welti et al., 2002; Table S4.2). On the other hand, sub-cluster A2 consists of the incompletely desaturated MGDG species, MGDG(34:4) and MGDG(34:5), whereas A6 is comprised of completely desaturated galactolipid species, DGDG(34:6), DGDG(36:6), and MGDG(34:6). Each sub-cluster within Cluster A thus represents either a PC + PE or MGDG + DGDG group of molecular species related by acyl composition.

Figure 4.5a and 4.5b show sub-cluster C2 (PA(34:6), TeGDG(34:6), and TrGDG(34:6)) and sub-cluster C9, which includes PA(34:2), PA(34:3), PA(36:2), PA(36:3), PA(36:4), PA(36:5), and PA(36:6). The analytes within each of these sub-clusters are closely correlated, but these sub-clusters are not well correlated to each other, as illustrated by comparison of levels of PA(34:6) from sub-cluster C2 and PA(36:6) from sub-cluster C9 (Figure 4.5c). Figure 4.6a, 4.6b, and 4.6c depict the changes in sterol glucosides and acyl sterol glucosides of sub-clusters C5, C7, and C8. Again, these show a higher level of in-sub-cluster lipid co-occurence compared with inter-sub-cluster co-occurence (Figure 4.6d).

Overall, sub-clusters in Cluster C are diverse. In addition to previously mentioned sub-clusters, there is a sub-cluster (C4) composed of all four TAG species determined, a sub-cluster of Arabidopsides A and B (MGDG(18:4-O/16:4-O) and MGDG(18:4-O/18:4-O); C6), and 5 sub-clusters containing acDGDG/acMGDG. The five acDGDG/acMGDG sub-clusters (C1, C3, C10, C11, and C12) fall into two groups. Sub-clusters C1 and C3 are moderately related with the highest inter-sub-cluster ρ, ρ(C1,C3), equal to 0.91 and sub-clusters C10, C11, and C12 are closely related with the highest ρs among all 3 sub-clusters falling just short of 0.96. On the other hand, the highest ρ between any lipid in sub-clusters C1 or C3 with one in C10, C11, or C12 is 0.77. There is some potential ambiguity in annotation of the acylated galactolipid sub-clusters, which makes it difficult to fully interpret the sub-clustering. (Note that only one

annotation per lipid is shown in the dendrogram, but complete annotations including alternative interpretations are shown in Tables 4.3 and S4.2) Still, sub-cluster C3 contains some clearly normal-chain acyl species, whereas sub-clusters C10, C11, and C12 contain highly oxidized acylated galactolipids. Figure 4.7g, i, p, q, and r show examples of the patterns of lipid changes during the wounding response for a lipid from each of the 5 acylated galactolipid sub-clusters. The levels of lipids in sub-clusters C1 and C3 continued to rise between 45 min and 6 h post-wounding, while the levels of acylated galactolipids in sub-clusters C10, C11, and C12 were reduced at 6 h compared to 45 min post-wounding.

Discussion

Lipids are modular, with many different molecular species containing the same component acyl chain or head group. This modularity goes hand-in-hand with the promiscuity of lipid-metabolizing enzymes, many of which act on multiple, related substrates. Here, we show that data support the hypothesis that correlation analysis can reveal groups of lipids acted on by the same enzyme(s), using lipidomic data from control plants and plants subjected to wounding. By metabolic control analysis and computer simulation, Camacho et al. (2005) found that many cases of high correlations in the levels of different metabolites among profiles of biological replicate samples are due to control of the metabolite levels by a single enzyme. Based on current knowledge of lipid metabolism, we infer that the highly correlated sub-clusters detected here by correlation analysis ($\rho > 0.96$) may (1) consist of substrates or products of the same enzyme(s), (2) may include a lipid formed from a common starting material by a metabolic branch, and/or (3) may include a lipid formed from another member of the group by a non-rate-limiting process.

Among the sub-clusters, several are likely to be produced by parallel metabolism by the same enzyme. These include the steryl glucosides in sub-cluster C5, which are likely to have been produced by the glycosylation of sterols by UDP-Glc:sterol glycosyltransferase(s) described by DeBolt et al. (2009). It's probable that each of the acyl sterol glucoside sub-clusters (C7 and C8) was formed by parallel acylation of two sterol glucosides with the same acyl chain, although the acylating enzymes acting on sterol glucosides have not been identified. Sub-cluster C9, which

consists of PAs with fatty acids similar to extraplastidic phospholipids, may have been derived largely from the activity of phospholipases D (e.g., Zien et al., 2001; Welti et al., 2002), though it has been suggested that diacylglycerol kinase also can contribute to PA formation in stress conditions (e.g., Arisz et al., 2013). Recent data support the notion that sub-cluster C6 (Arabidopsides A and B) may have been formed by a common enzymatic pathway acting on similar, but distinct, substrates. Nilsson et al. (2012) showed that 18:4-O (oxophytodienoic acid) and 16:4-O (dinor-oxophytodienoic acid) are formed without release of the acyl chains from the galactolipid pool. It follows that the two molecular species in sub-cluster C6 would be formed from the two most abundant MGDG species, MGDG(18:3/16:3) and MGDG(18:3/18:3), by analogous pathways involving oxidation and cyclization of the esterified fatty acyl chains.

The formation of sub-cluster C2, which consists of TrGDG(34:6), TeGDG(34:6), and PA(34:6) likely involves the action of SENSITIVE TO FREEZING 2 (SFR2) (Moellering et al., 2010), a processive galactosylating enzyme that transfers a galactose from MGDGs to successively yield β-linked DGDG, TrGDG, and TeGDG from MGDG. The resulting DAG does not accumulate (Moellering et al., 2010), and while Moellering et al. (2010) provide evidence that TAG may be formed from it, the inclusion of PA(34:6) in the sub-cluster suggests that a DAG kinase may phosphorylate the DAG in a branch step. Several molecular species of TAGs are formed in response to wounding (sub-cluster C4); formation of these TAGs may involve phospholipid:diacylglycerol acyltransferase (PDAT1) (Fan et al., 2013). TAG may serve as a transient buffer for leaf acyl chains present in excess (Troncoso-Ponce et al., 2013). Unfortunately, we did not determine the level of a TAG species containing 34:6 (i.e., 18:3/16:3), which could be derived from MGDG by SFR2.

While all the sub-clusters within Cluster A are quite closely correlated, the components of the four sub-clusters containing PC and PE (A1, A3, A4, A5) and two sub-clusters of MGDG and DGDG (A2, A6) vary in their fatty acyl composition. In the plastid, DGDG is formed from MGDG by a UDP-galactose-dependent DGDG synthase (DGDGS; Kelly and Dörmann, 2002; reviewed in Li-Beisson et al., 2013). Fatty acyl chains can undergo desaturation on either MGDG or DGDG (except that FAD5 acts only on MGDG; Kunst et al., 1989). Sub-cluster A2 includes MGDG species that are not fully desaturated; their co-accumulation may indicate that

the rate of the final desaturation of MGDG acyl chains by FAD7 and/or FAD8 varied among plants and limited the rate of formation of fully desaturated species. Indeed, the level of plastidic trienoic fatty acids is regulated in stress responses and affects the ability of plants to withstand stresses, including cold and bacterial infection (Kodama et al., 1994; Routaboul et al., 2000; Yaeno et al., 2004; Chaturvedi et al., 2008). On the other hand, the occurrence of DGDG(34:6) with MGDG(34:6) in sub-cluster A6 is due to a near-constant ratio of these lipids among plants, suggesting that the conversion of MGDG to DGDG is not rate-limiting. The high correlation coefficients between PCs and PEs with the same acyl chains in sub-clusters A1 and A5 could mean either that the rate of production of acyl-identical PCs and PEs is similar and/or that enzymes involved in PC-PE (inter)conversion, perhaps through a DAG intermediate, function near equilibrium, maintaining a near-constant ratio of acyl-identical PE and PC molecular species (found together in sub-clusters). In pea leaves, PC is labeled from acetate much more rapidly than PE during a 10-min time course, suggesting that PC and PE molecular species with the same acyl chains are unlikely to be formed initially by parallel pathways (Bates et al., 2007), and that it is more likely that PC species are converted to PEs during the wounding experiment.

The modular nature and the typical action of lipid-metabolizing enzymes on multiple substrates may make complex lipids especially amenable to co-occurrence analysis as a mechanism for extending our understanding of compound relationships and metabolism. In the current analysis, acDGDGs, acPG, and many acMGDGs are a large group of lipids that has not been extensively studied. Evidence has been presented that acMGDG is formed by the reaction MGDG + DGDG → acMGDG + DGMG (Heinz, 1967; Heinz, 1972; Vu et al., 2014). The current results show that two groups of acMGDGs are formed with different kinetics. acMGDGs in sub-clusters C10, C11, and C12, most of which are rich in oxidized fatty acids, are formed rapidly (i.e., their levels are high at 45 min) and their levels drop by 6 h post-wounding (Figure 4.7p, 4.7q, 4.7r). Other acMGDGs (sub-clusters C1 and C3; Figure 4.7g, 4.7i), including all quantified molecular species unambiguously annotated as having entirely normal-chain fatty acids (acMGDG(16:0/34:6), acMGDG(16:3/34:6), acMGDG(18:2/34:6), acMGDG(18:3/34:6)), were formed more slowly, with levels considerably higher at 6 h than at 45 min. A similar phenomenon was observed previously when galactolipids containing two oxidized acyl chains accumulated much faster in response to wounding than galactolipids with a single oxidized acyl

chain (Buseman et al., 2006). Thus, the acMGDG pool reflects the diacyl species that serve as substrates for acMGDG formation; however, oxidized chains are concentrated in the acMGDG pool (Vu et al., 2014). Still, the mechanism for the rapid rise and decline in species containing two oxidized chains and the identity of the acylating enzyme(s) forming the head-group-acylated molecular species remains unknown. Additionally, the placement of a number of analytes that are not obviously structurally similar in sub-clusters C1 and C3 provides a catalyst for future reassessment of the tentative annotations.

In the current work, we have developed an MS-based analytical approach targeting a wide range of lipid molecular species. The current approach has demonstrated that levels of lipids differed among individual Arabidopsis plants, and levels of nearly all of the lipids in wild-type plants changed in response to wounding, with normal-chain "traditional" structural lipids decreasing and many other lipids increasing. The analytical precision was sufficient for a number of lipid species to be clustered based on co-occurrence among individual plants and across the stress conditions. The levels of seventy-nine percent of the lipid analytes were correlated with $\rho > 0.80$ with at least one other analyte, placing them in a lipid cluster, and 24% of the lipids were correlated with $\rho > 0.96$, placing them in a sub-cluster. While lack of high correlation can be due to either excessive analytical variation or true lack of co-occurrence, interpretation of the lipid analytical results in light of knowledge of lipid metabolism demonstrates that high positive correlation reflects metabolic relationships. At the current stage of plant lipidomic development, careful and highly replicated MS analysis can provide large amounts of information about lipid dynamics in plants under stress. The current work highlights the value of co-occurrence analysis in defining groups of metabolically-related lipids. Undoubtedly, application of co-occurrence analysis to additional lipids and to plants subjected to other perturbations will provide further metabolic insight.

Experimental procedures

Plant material, growth, and wounding treatment

Plant material and growth are described in Method S4.1. For the wounding treatment, a hemostat was used to wound leaves number 5, 6, 7 and 8 of 30-day-old plants across the mid-vein, twice

and about 6 mm apart. Leaf numbers were determined as described by Telfer et al. (1997). Leaves 6, 7, and 8 were harvested 45 min or 6 h after being wounded. For the control, leaves 6, 7, and 8 were harvested from unwounded plants. For the extraction test, fifteen plants were harvested 45 min after wounding. For the main experiment, thirty-two samples (one each from 32 plants) were collected for each of the two wounding treatments and for control plants. Each sample for lipid analysis corresponded to the three harvested leaves from one plant. In the main experiment, one sample in each treatment group (i.e., sample 23) was removed from the analysis due to technical problems; thus, n for each group is 31. The extraction test and the main experiment were performed on separate sets of plants.

Lipid extraction

In the main experiment, harvested leaves number 6, 7, and 8 were immediately dropped into 4 ml of isopropanol with 0.01% butylated hydroxytoluene (BHT) at 75°C in a 20-ml EPA vial with Teflon-lined screw-cap (Thermo Fisher Scientific, Inc., thermofisher.com). Vials were kept at 75°C for 15 min to deactivate lipid-hydrolyzing enzymes. Vials were cooled to room temperature and stored overnight at -80°C before adding 12 ml of chloroform: methanol: 300 mM ammonium acetate in water (30:41.5:3.5, v/v/v) and shaking at 100 rpm on an orbital shaker for 24 h at room temperature. Extracted leaves were transferred to a new vial and dried overnight at 105°C. The extract was stored at -80°C. Dried extracted leaves were cooled and weighed on a balance with 2 µg detection limit (Mettler Toledo, mt.com). The precision and accuracy of the balance were previously described (Vu et al., 2012). For the extraction test, 5 leaves harvested 45 min after wounding were extracted as just described (Method 1), 5 leaves were extracted as described by Welti et al. (2002; Method 2), and 5 leaves were extracted as described by Welti et al. (2002), skipping the backwash steps, followed by 4 extractions with "Solvent H" (lower phase of isopropanol/hexane/water, 55:20:25, v/v/v; Toledo et al., 1995, Markham et al., 2006; Method 3).

Lipid profiling by ESI triple quadrupole MS

To prepare analytical samples for mass spectrometry, from each sample, the volume corresponding to 0.04 mg extracted leaf dry mass was determined and that volume of sample was

transferred to a 2-ml amber vial, containing 20 µl of internal standard mix. Components of the internal standard mix are listed in Table S4.5. Isopropanol: chloroform: methanol: 300 mM ammonium acetate in water (25: 30: 41.5: 3.5, v/v/v/v) was added to make the total volume 1.4 ml. The vial was sealed with a snap-cap with a crisscross, pre-slit septum.

Quality control (QC) samples were prepared for data normalization by first pooling 300 µl of extract from samples 1-9 from each treatment (unwounded, wounded 45 min, and wounded 6 h) to make a QC stock solution. Based on the dry leaf mass of the samples used to make the combined extract, the concentration was calculated to be 0.40 mg (of leaf dry mass) ml-1 (8.1 ml total volume). To prepare working QC samples, the internal standard mixture was added and the stock was diluted, so that each working QC sample contained lipid extract corresponding to 0.04 mg combined leaf dry mass, 20 µl of the internal standard mix (as used in the other samples), and mass spectrometry solvent (isopropanol: chloroform: methanol: 300 mM ammonium acetate in water, 25: 30: 41.5: 3.5, v/v/v/v) in 1.4 ml. The QC mass spectrometry samples were labeled "QC1" to "QC39", stored at -80°C, and brought to room temperature 1 h before analysis. Analytical samples and QC samples from the main experiment were arranged in a VT 54 rack as shown in Table S4.6. For the lipid extraction test, the same analytical set-up was used.

Data were acquired with a Xevo TQ-S mass spectrometer (Waters Corporation, waters.com) equipped with an ESI source operating in direct infusion mode. Each sample was infused twice, once to acquire positive and once for negative multiple reaction monitoring (MRM) transitions. Samples were injected into a 300-µl PEEK sample loop with a 2777 autosampler (Waters Corporation). To make sure the loop was completely filled, the injection volume was set at 400 µl. The sample in the loop was infused to the mass spectrometer with an Acquity pump (Waters Corporation) controlled by an "inlet method" in MassLynx (software from Waters Corporation). Each inlet method was 17.5 min with solvents and flow rates as follows: from 0 to 11 min, methanol at 0.03 ml min-1; from 11 to 15 min, methanol at 0.09 ml min-1; from 15 to 17 min, methanol: acetic acid (9: 1, v/v) at 0.5 ml min-1; from 17 to 17.1 min, 17.1 to 17.2 min, 17.2 to 17.3 min, 17.3 to 17.4 min, and 17.4 to 17.5 min, methanol at 0.4, 0.3, 0.2, 0.1, and 0.03 ml min-1, respectively. The mass spectrometer acquired data from 0 to 15 min. The positive mode and negative mode data acquisition methods had 13 and 7 functions, respectively. Every function

acquired data on lipid analytes and internal standard components in MRM mode throughout the 15 min. Each function contained from 12 to 28 transitions which were allocated the same dwell time. In the positive mode, 130-131 scans (cycles) and, in the negative mode, 38 scans of each function were performed (Table S4.2). Parameters for each MRM transition are listed in Table S4.2 for the plant lipid analytes and in Table S4.5 for the internal standards. Other mass spectrometry parameters are indicated Method S4.4.

Samples were analyzed at the rate of 1 tray (Table S4.6) per day with a total daily analysis time of 22.75 h. Each day, a cleaned source cone was installed and an Xpertek 0.5-µm PEEK filter (P.J. Cobert Associates, Inc., cobertassociates.com) in the line between the autosampler and source was changed.

Data processing and calculation of normalized lipid intensities

"Spectrum Combine" software (a process file called SpectrumCombine_4p0p0) and a parameter file, custom-developed by Iggy Kass (Waters Corporation), was employed to process and export MassLynx data to Excel. MRM scans were combined by averaging the scans for each MRM channel within each function before export. Exported data were processed in an in-house Excel template in which the data from all samples (i.e., QC, "internal standard only", and analytical samples) were isotopically deconvoluted. The intensity per nmol of each internal standard in each sample was calculated; these values for internal standards for the same class were averaged. The deconvoluted data for each lipid were normalized to the internal standard(s) of the same lipid class (if possible) or another lipid class analyzed under similar experimental conditions (in cases where an appropriate internal standard was not available). The internal standard used for normalization of each MRM signal is indicated in Table S4.2.

Once normalized intensities were calculated, the average level of the background, as indicated by the average of the "internal standard only" samples from that tray, was subtracted from every other sample in the tray. An adaptation of the method of Dunn et al. (2011) was used to assure that the data could be compared throughout extended acquisition periods. The values for the first 5 QC samples in each set of analytes (Table S4.6) were eliminated, due to potential instrument

instability when the instrument is first started after installation of a cleaned cone. To correct for any drift during acquisition of each tray's data, a trend line was constructed of the intensity data for each lipid in the remaining 8 identical QC samples as a function of vial position number in the tray. Each lipid intensity in each analytical sample was multiplied by the average of that lipid's level in the QC samples on that tray divided by the level of the lipid on the QC trend line at the sample's vial position. To correct for any variability across different trays (days), the trend-corrected value of each lipid in each sample was multiplied by the average of the QC values for that lipid from the entire acquisition process divided by the average of that lipid's level in the QC samples on the sample's own tray. After calculation of the lipid levels in each sample, the values were divided by the dry mass of the sample analyzed (0.04 mg).

The lipid values are normalized intensity per mg leaf dry mass, where a value of 1 is the intensity of 1 pmol of internal standard. Because the internal standards were not uniformly well-matched to the lipids analyzed (some differ in class; many differ substantially in m/z), the absolute values of the analytes provide only a rough guide to absolute amount of each lipid.

Statistical analysis and figure and table production

Auto-scaling and analysis of variance (ANOVA) with Tukey's post hoc tests were performed (Table S4.9), and the heat map (Figure 4.1), correlation table (Table S4.10), and Figure S4.5 were produced using utilities at the Metaboanalyst website (metabolanalyst.ca; Xia et al., 2009 and 2012). Autoscaling allows easy comparison of patterns of the levels of different lipids across samples. The autoscaled value of a lipid in a sample is equal to: [(the original value of the lipid in the sample) – (the average value for that lipid among all samples)] divided by (the standard deviation for that lipid among all samples). Figures 4.2, 4.4, 4.5, 4.6, and 4.7 were produced using Origin 8.5 (OriginLab Corporation, originlab.com). Clustering was performed using Cluster 3.0 (Eisen et al., 1997). The output was imported to Dendroscope (Huson et al., 2007; Huson and Scornavacca, 2012) to produce the dendrogram, which was modified in color.

Acknowledgements

The authors thank Iggy Kass of Waters Corporation for writing the program to export data from MassLynx, and Samantha Elledge, Laura Welti, Cong Tuan Son Van, and Haibao Tang for help in production of the figures. This material is based upon work supported by the National Science Foundation under Collaborative Research Grant Nos. MCB-0920663 (to RW and GG), MCB-0920600 (to XW), and MCB-0920681 (to JS). The mass spectrometers used in the analyses were acquired with NSF funding under Grant Nos. DBI-1228622, DBI 0521587, and EPS 0236913. Contribution no. 14-244-J from the Kansas Agricultural Experiment Station.

References

Arisz SA, van Wijk R, Roels W, Zhu JK, Haring MA and Munnik T (2013) Rapid phosphatidic acid accumulation in response to low temperature stress in Arabidopsis is generated through diacylglycerol kinase. Front Plant Sci. 4, 1. doi: 10.3389/fpls.2013.00001

Bates PD, Ohlrogge JB and Pollard M (2007) Incorporation of newly synthesized fatty acids into cytosolic glycerolipids in pea leaves occurs via acyl editing. J. Biol. Chem. **282**, 31206-31216.

Bligh EG and Dyer WJ (1959) A rapid method of total lipid extraction and purification. Can. J. Biochem. Physiol. **37**, 911-917.

Buseman CM, Tamura P, Sparks AA, Baughman EJ, Maatta S, Zhao J, Roth MR, Esch SW, Shah J, Williams TD and Welti R (2006) Wounding stimulates the accumulation of glycerolipids containing oxophytodienoic acid and dinor-oxophytodienoic acid in Arabidopsis leaves. Plant Physiol. **142**, 28-39.

Camacho D, Fuente A and Mendes P (2005) The origin of correlations in metabolomics data. Metabolomics **1**, 53-63.

Carbonell P, Lecointre G and Faulon J-L (2011) Origins of specificity and promiscuity in metabolic networks. J. Biol. Chem. **286**, 43994-44004.

Chaturvedi R, Krothapalli K, Makandar R, Nandi A, Sparks AA, Roth MR, Welti R and Shah J (2008) Plastid omega3-fatty acid desaturase-dependent accumulation of a systemic acquired resistance inducing activity in petiole exudates of Arabidopsis thaliana is independent of jasmonic acid. Plant J. **54**, 106-117.

DeBolt S, Scheible WR, Schrick K, Auer M, Beisson F, Bischoff V, Bouvier-Navé P, Carroll A, Hematy K, Li Y, Milne J, Nair M, Schaller H, Zemla M and Somerville C (2009) Mutations in UDP-Glucose:sterol glucosyltransferase in Arabidopsis cause transparent testa phenotype and suberization defect in seeds. Plant Physiol. **151**, 78-87.

Dunn WB, Broadhurst D, Begley P, Zelena E, Francis-McIntyre S, Anderson N, Brown M, Knowles JD, Halsall A, Haselden JN, Nicholls AW, Wilson ID, Kell DB, Goodacre R and Human Serum Metabolome (HUSERMET) Consortium. (2011) Procedures for large-scale metabolic profiling of serum and plasma using gas chromatography and liquid chromatography coupled to mass spectrometry. Nat. Protoc. **6**, 1060-1083.

Eisen MB, Spellman PT, Brown PO and Botstein D (1997) Cluster analysis and display of genome-wide expression patterns. Proc. Natl. Acad. Sci. USA **95**, 14863-14868.

Fan J, Yan C and Xu C (2013) Phospholipid:diacylglycerol acyltransferase-mediated triacylglycerol biosynthesis is crucial for protection against fatty acid-induced cell death in growing tissues of Arabidopsis. Plant J. **76**, 930-942.

Heinz E. (1967) On the enzymatic formation of acyl galactosyldiglyceride. Biochim. Biophys. Acta **144**, 333–343.

Heinz E. (1972) Some properties of the acyl galactosyl diglyceride-forming enzyme from leaves. Z. Pflanzenphysiol. **69**, 359–376.

Huson DH and Scornavacca C (2012) Dendroscope 3: An interactive tool for rooted phylogenetic trees and networks. Syst. Biol. **61**, 1061-1067.

Huson DH, Richter DC, Rausch C, Dezulian T, Franz M and Rupp R (2007) Dendroscope: An interactive viewer for large phylogenetic trees. BMC Bioinformatics. **8**, 460.

Kelly AA, and Dörmann P (2002) DGD2, an Arabidopsis gene encoding a UDP-galactose-dependent digalactosyldiacylglycerol synthase is expressed during growth under phosphate-limiting conditions. J. Biol. Chem. **277**, 1166–1173.

Kodama H, Hamada T, Horiguchi G, Nishimura M and Iba K (1994) Genetic enhancement of cold tolerance by expression of a gene for chloroplast [omega]-3 fatty acid desaturase in transgenic tobacco. Plant Physiol. **105**, 601-605.

Kunst L, Browse J and Somerville C (1989) A mutant of Arabidopsis deficient in desaturation of palmitic acid in leaf lipids. Plant Physiol. **90**, 943-947.

Markham JE, Li J, Cahoon EB and Jaworski JG (2006) Separation and identification of major plant sphingolipid classes from leaves. J. Biol. Chem. **281**, 22684-22694.

Moellering ER, Muthan B and Benning C (2010) Freezing tolerance in plants requires lipid remodeling at the outer chloroplast membrane. Science **330**, 226-228.

Narváez-Vásquez J, Florin-Christensen J and Ryan CA (1999) Positional specificity of a phospholipase A activity induced by wounding, systemin, and oligosaccharide elicitors in tomato leaves. Plant Cell **11**, 2249-2260.

Nilsson AK, Fahlberg P, Ellerström M and Andersson MX (2012) Oxo-phytodienoic acid (OPDA) is formed on fatty acids esterified to galactolipids after tissue disruption in Arabidopsis thaliana. FEBS Lett. **586**, 2483-2487.

Peters C, Li M, Narasimhan R, Roth M, Welti R and Wang X (2010) Non-specific phospholipase C NPC4 promotes response to abscisic acid and tolerance to hyperosmotic stress in Arabidopsis. Plant Cell **22**, 2642-2659.

Routaboul JM, Fischer SF and Browse J (2000) Trienoic fatty acids are required to maintain chloroplast function at low temperatures. Plant Physiol. **124**, 1697-1705.

Ryu SB (2004) Phospholipid-derived signaling mediated by phospholipase A in plants. Trends Plant Sci. **9**, 229-235.

Steuer R, Kurths J, Fiehn O and Weckwerth W (2003) Observing and interpreting correlations in metabolomics networks. Bioinformatics **19**, 1019-1026.

Telfer A, Bollman KM and Poething RS (1997) Phase change and the regulation of trichome distribution in Arabidopsis thaliana. Development **124**, 645-654.

Toledo MS, Suzuki E, Straus AH and Takahashi, HK (1995) Glycolipids from Paracoccidioides brasiliensis. Isolation of a galactofuranose-containing glycolipid reactive with sera of patients with paracoccidioidomycosis. J. Med. Vet. Mycol. **33**, 247-251.

Toubiana D, Fernie AR, Nikoloski Z and Fait A (2013) Network analysis: tackling complex data to study plant metabolism. Trends Biotechnol. **31**, 29-36.

Troncoso-Ponce MA, Cao X, Yang Z and Ohlrogge JB (2013) Lipid turnover during senescence. Plant Sci. 205-206, 13-19.

Vu HS, Tamura P, Galeva NA, Chaturvedi R, Williams TD, Wang X, Shah J and Welti R (2012) Direct infusion mass spectrometry of oxylipin-containing Arabidopsis thaliana

membrane lipids reveals varied patterns in different stress responses. Plant Physiol. **158**, 324-339.

Vu HS, Roth MR, Tamura P, Samarakoon T, Shiva S., Honey S, Lowe K, Schmelz EA, Williams TD and Welti R (2014) Head-group acylation of monogalactosyldiacylglycerol is a common stress response, and the acyl-galactose acyl composition varies with the plant species and applied stress. Physiol Plant. In press.

Welti R, Li W, Li M, Sang Y, Biesiada H, Zhou H-E, Rajashekar CB, Williams TD and Wang X (2002) Profiling membrane lipids in plant stress responses. Role of phospholipase Dα in freezing-induced lipid changes in Arabidopsis. J. Biol. Chem. **277**, 31994-32002.

Xia J, Psychogios N, Young N and Wishart DS (2009) MetaboAnalyst: a web server for metabolomic data analysis and interpretation. Nucl. Acids Res. **37**, W652-660.

Xia J, Mandal R, Sinelnikov I, Broadhurst D and Wishart DS (2012) MetaboAnalyst 2.0 - a comprehensive server for metabolomic data analysis. Nucl. Acids Res. **40**, W127-133.

Yaeno T, Matsuda O and Iba K (2004) Role of chloroplast trienoic fatty acids in plant disease defense responses. Plant J. **40**, 931-941.

Zien CA, Wang C, Wang X and Welti R (2001). In-vivo substrates and the contribution of the common phospholipase D, PLDa, to wound-induced metabolism of lipids in Arabidopsis. Biochim. Biophys. Acta **1530**, 236-248.

Figures and Tables

Figure 4.1 Heatmap of autoscaled lipid levels determined by MS analysis.

272 analytes are shown in 93 samples. Each sample represents one plant under control (unwounded) or wounding treatment (n = 31 for each treatment).

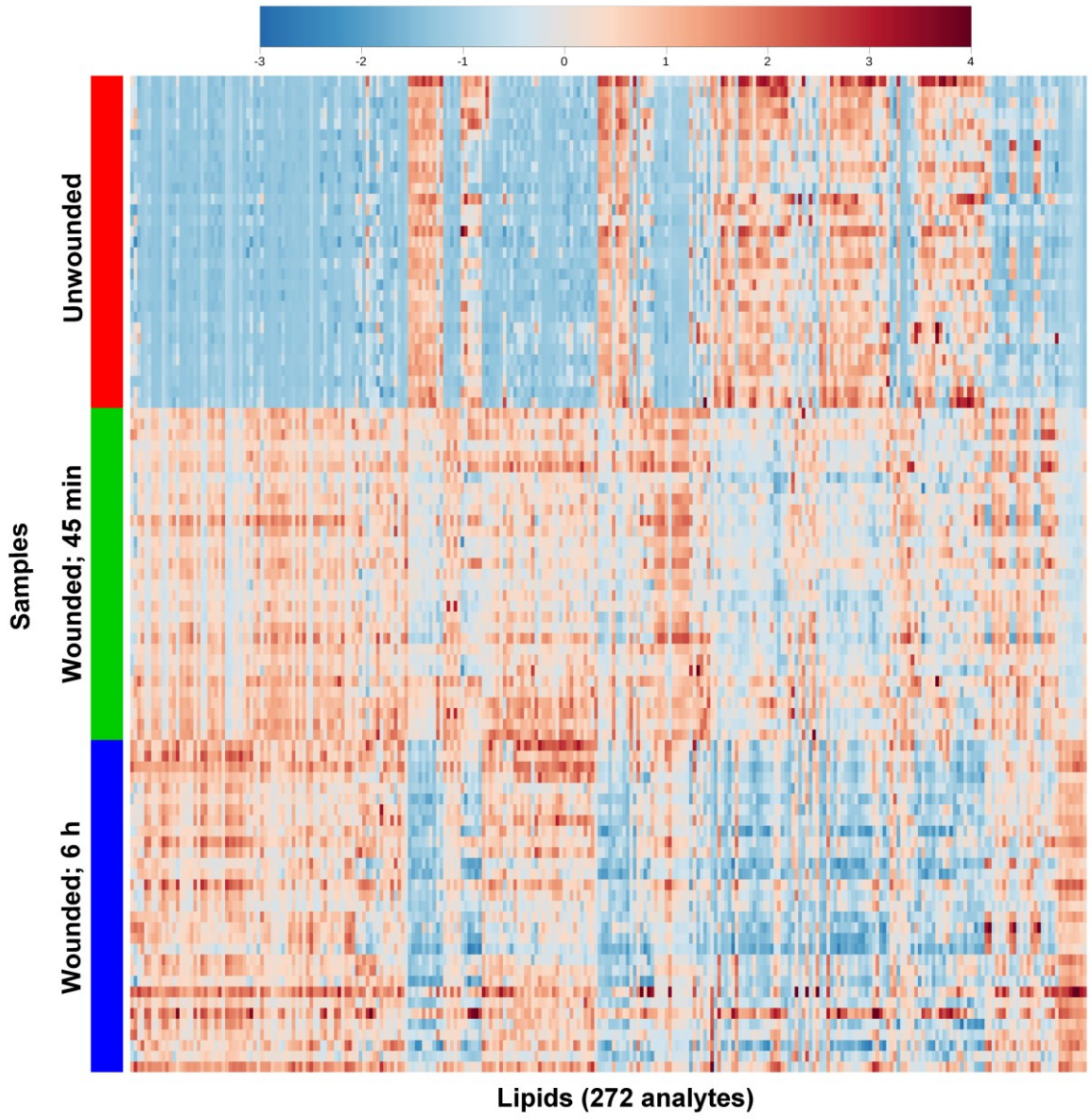

Figure 4.2 Autoscaled levels of representative lipid analytes in individual plants.
Each sample represents one plant under control (unwounded) or wounding treatment (n = 31 for each treatment). Connections between points were included to make it easier to visualize the variations in lipid levels across samples.

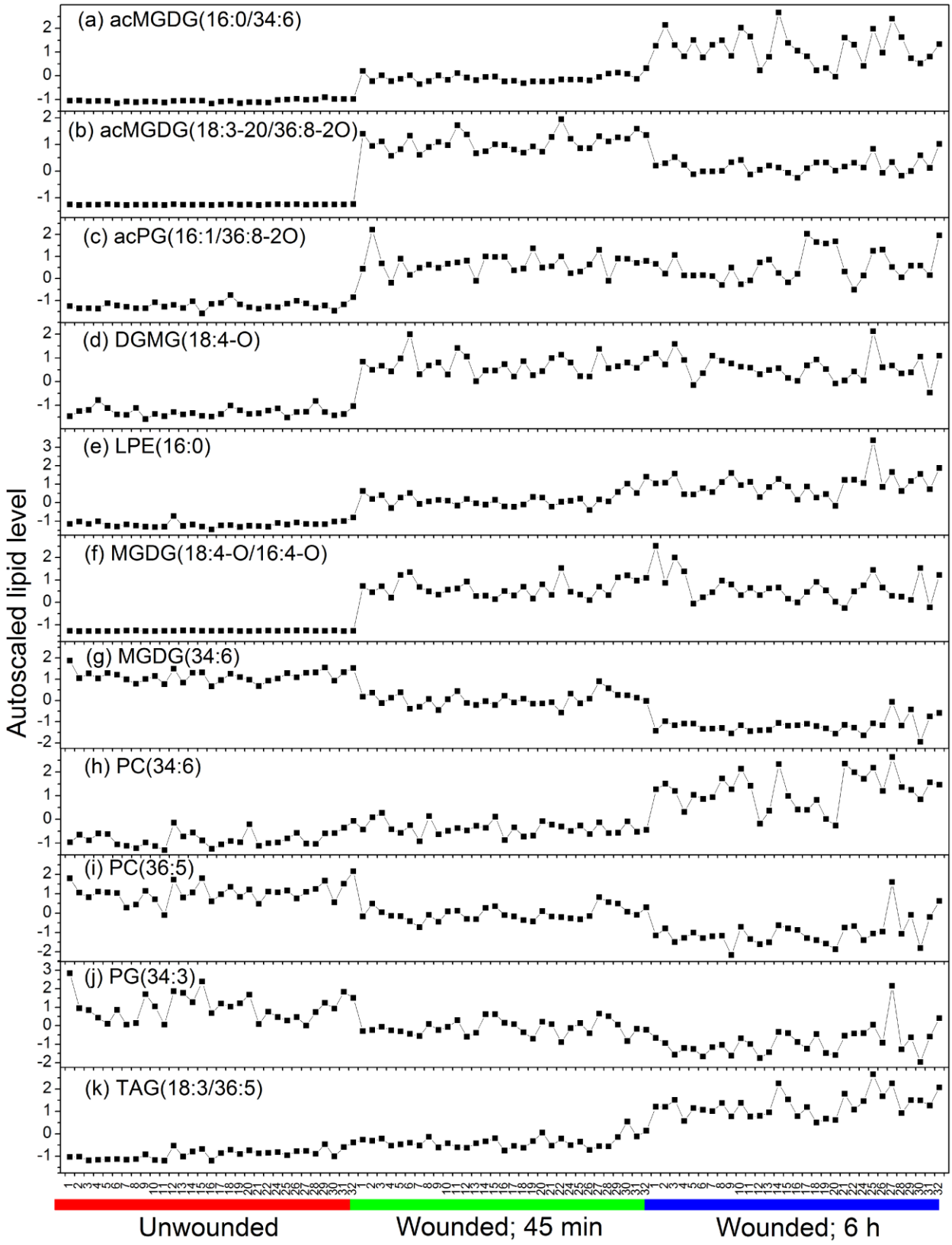
(a) acMGDG(16:0/34:6)
(b) acMGDG(18:3-20/36:8-2O)
(c) acPG(16:1/36:8-2O)
(d) DGMG(18:4-O)
(e) LPE(16:0)
(f) MGDG(18:4-O/16:4-O)
(g) MGDG(34:6)
(h) PC(34:6)
(i) PC(36:5)
(j) PG(34:3)
(k) TAG(18:3/36:5)
Autoscaled lipid level
Unwounded
Wounded; 45 min
Wounded; 6 h

Figure 4.3 Lipid dendrogram.

272 lipid analytes were clustered using a single-linkage hierarchical algorithm based on Spearman's correlation coefficient, ρ (Table S4.10). The center of the dendrogram is at ρ = 0.305. There is a scale break from ρ = 0.340 to ρ = 0.590. Eight analytes were excluded from the dendrogram due to their low level of correlation with other analytes (maximal ρ < 0.6) or because they were repeat measurements of included lipids. A single annotation is provided for each analyte; additional potential annotations are indicated in Table 4.3. Seven clusters with ρ > 0.8 are indicated by letters and colors: A (blue), B (orange), C (green), D (lavender), E (aqua), F (pink), and G (rust). Six sub-clusters of ρ > 0.96 within cluster A and twelve sub-clusters of ρ > 0.96 within cluster C are indicated as A1-A6 and C1-C12. The sub-cluster lines are red, and the lipid annotations within sub-clusters are bold.

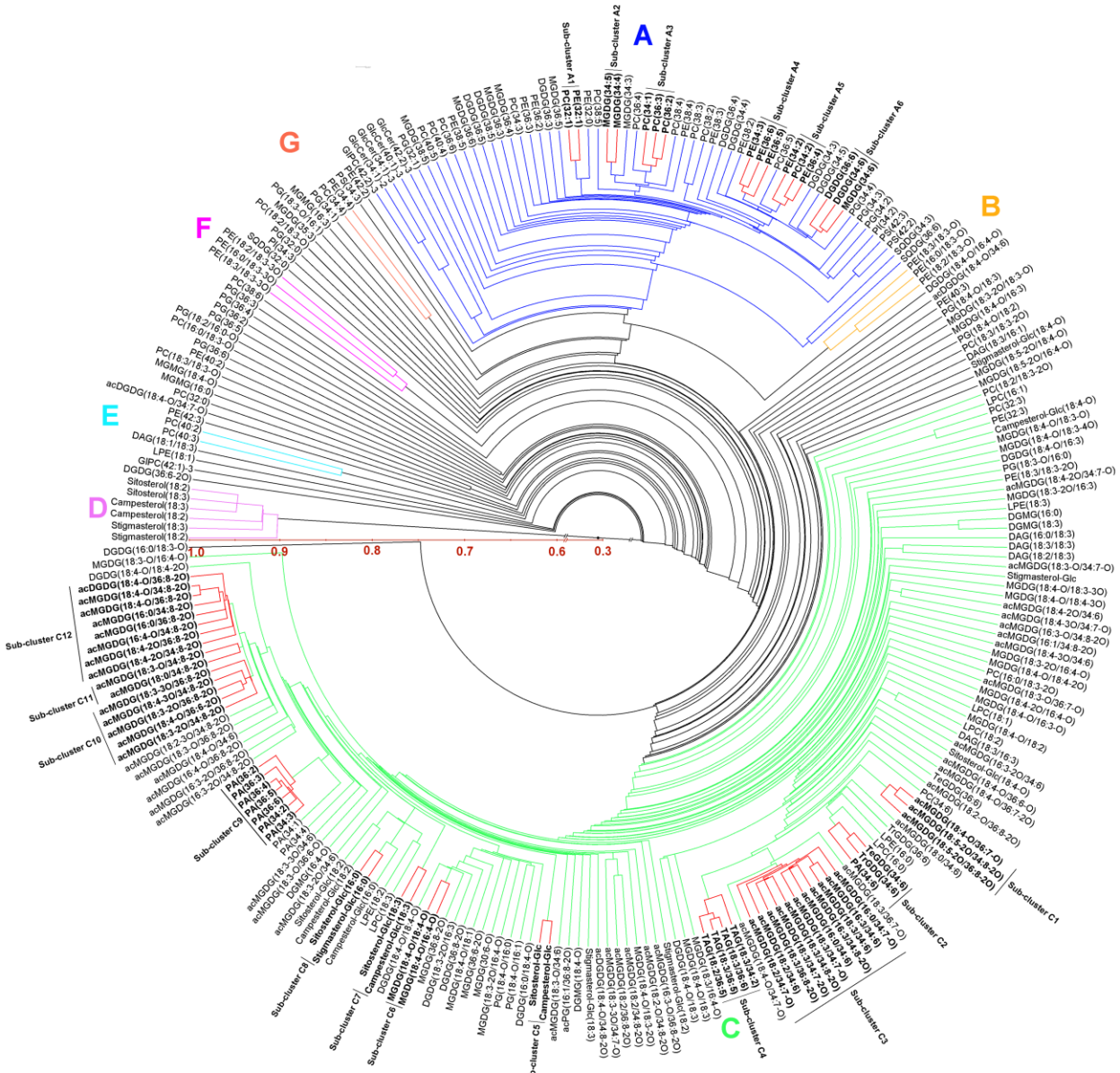

Figure 4.4 Autoscaled levels of representative lipid analytes in sub-clusters A1, A4, and A5. Points represent individual plants subjected to control or wounding treatment as indicated. Panels a, b, and c represent the three clusters, and panel d shows lipid levels for one lipid from each cluster. Text or insets show Spearman's correlation coefficient for pairs of lipids within the clusters (a, b, and c) and for representative pairs of lipids in different clusters (d).

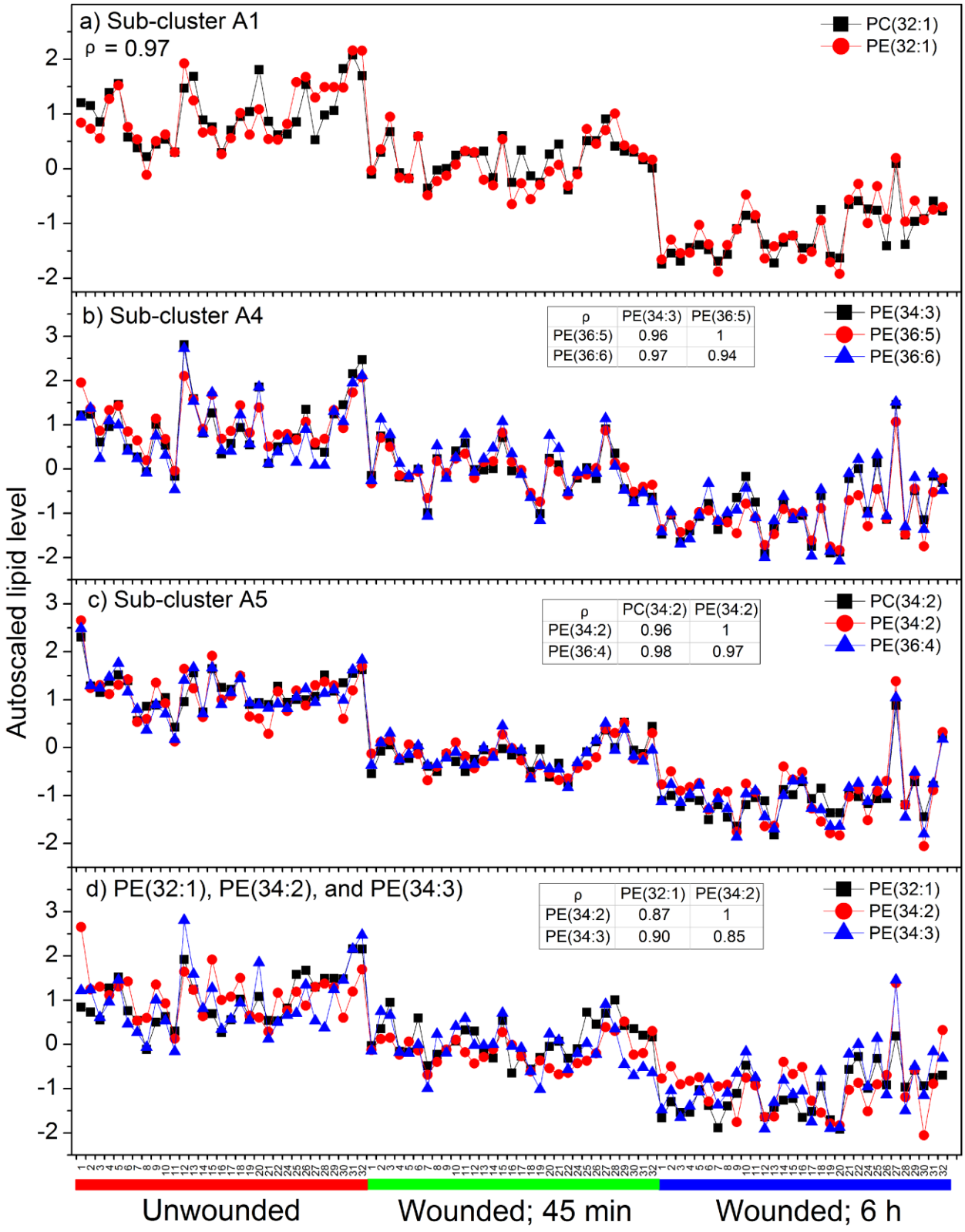
a) Sub-cluster A1
ρ = 0.97
PC(32:1)
PE(32:1)
b) Sub-cluster A4
ρ | PE(34:3) | PE(36:5)
PE(36:5) | 0.96 | 1
PE(36:6) | 0.97 | 0.94
PE(34:3)
PE(36:5)
PE(36:6)
c) Sub-cluster A5
ρ | PC(34:2) | PE(34:2)
PE(34:2) | 0.96 | 1
PE(36:4) | 0.98 | 0.97
PC(34:2)
PE(34:2)
PE(36:4)
d) PE(32:1), PE(34:2), and PE(34:3)
ρ | PE(32:1) | PE(34:2)
PE(34:2) | 0.87 | 1
PE(34:3) | 0.90 | 0.85
PE(32:1)
PE(34:2)
PE(34:3)
Autoscaled lipid level
Unwounded
Wounded; 45 min
Wounded; 6 h

Figure 4.5 Autoscaled levels of representative lipid analytes in sub-clusters C2 and C9. Points represent individual plants subjected to control or wounding treatment as indicated. Panels a and b represent the two clusters, and panel c shows lipid levels for one lipid from each cluster. Text or insets show Spearman's correlation coefficient for pairs of lipids within the clusters (a and b) and for representative pairs of lipids in different clusters (c).

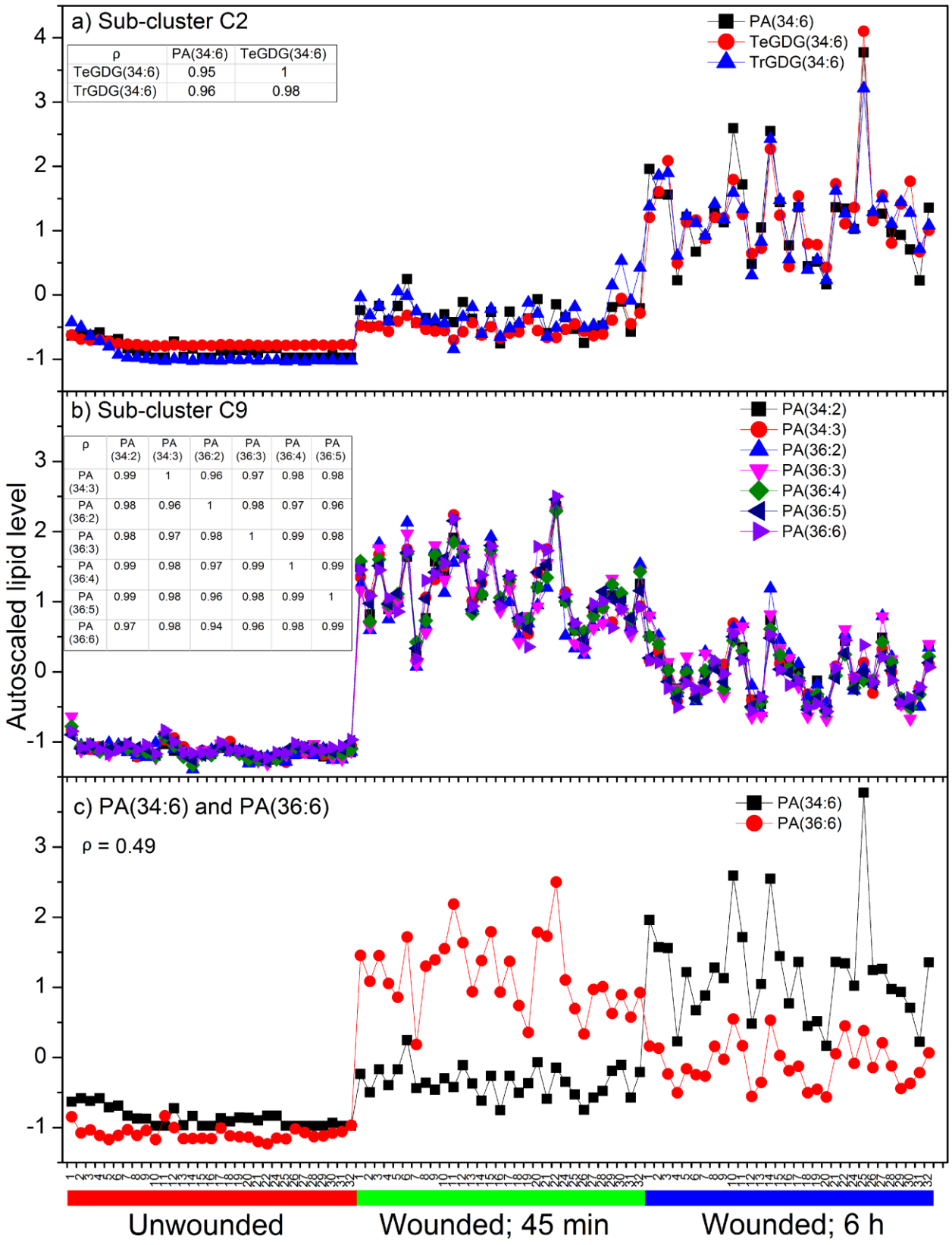
a) Sub-cluster C2
PA(34:6)
TeGDG(34:6)
TrGDG(34:6)
ρ | PA(34:6) | TeGDG(34:6)
TeGDG(34:6) | 0.95 | 1
TrGDG(34:6) | 0.96 | 0.98
b) Sub-cluster C9
PA(34:2)
PA(34:3)
PA(36:2)
PA(36:3)
PA(36:4)
PA(36:5)
PA(36:6)
ρ | PA (34:2) | PA (34:3) | PA (36:2) | PA (36:3) | PA (36:4) | PA (36:5)
PA (34:3) | 0.99 | 1 | 0.96 | 0.97 | 0.98 | 0.98
PA (36:2) | 0.98 | 0.96 | 1 | 0.98 | 0.97 | 0.96
PA (36:3) | 0.98 | 0.97 | 0.98 | 1 | 0.99 | 0.98
PA (36:4) | 0.99 | 0.98 | 0.97 | 0.99 | 1 | 0.99
PA (36:5) | 0.99 | 0.98 | 0.96 | 0.98 | 0.99 | 1
PA (36:6) | 0.97 | 0.98 | 0.94 | 0.96 | 0.98 | 0.99
Autoscaled lipid level
c) PA(34:6) and PA(36:6)
ρ = 0.49
PA(34:6)
PA(36:6)
Unwounded
Wounded; 45 min
Wounded; 6 h

Figure 4.6 Autoscaled levels of representative lipid analytes in sub-clusters C5, C7, and C8. Points represent individual plants subjected to control or wounding treatment as indicated. Panels a, b, and c represent the three clusters, and panel d shows lipid levels for one lipid from each cluster. Text or insets show Spearman's correlation coefficient for pairs of lipids within the clusters (a, b, and c) and for representative pairs of lipids in different clusters (d).

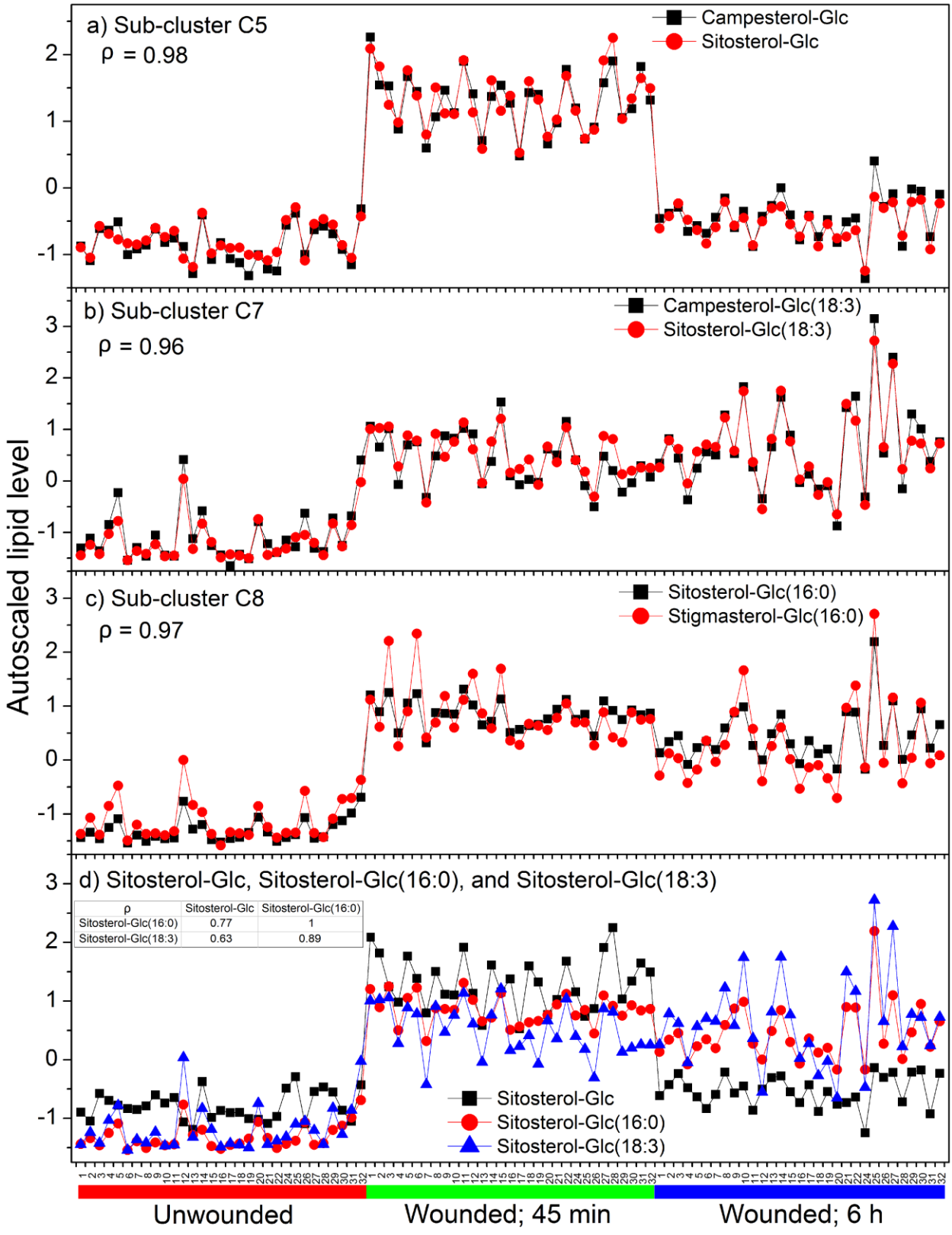
a) Sub-cluster C5
ρ = 0.98
Campesterol-Glc
Sitosterol-Glc
b) Sub-cluster C7
ρ = 0.96
Campesterol-Glc(18:3)
Sitosterol-Glc(18:3)
c) Sub-cluster C8
ρ = 0.97
Sitosterol-Glc(16:0)
Stigmasterol-Glc(16:0)
d) Sitosterol-Glc, Sitosterol-Glc(16:0), and Sitosterol-Glc(18:3)
ρ | Sitosterol-Glc | Sitosterol-Glc(16:0)
Sitosterol-Glc(16:0) | 0.77 | 1
Sitosterol-Glc(18:3) | 0.63 | 0.89
Sitosterol-Glc
Sitosterol-Glc(16:0)
Sitosterol-Glc(18:3)
Autoscaled lipid level
Unwounded
Wounded; 45 min
Wounded; 6 h

Figure 4.7 Autoscaled levels of a representative lipid from each sub-cluster.

The box depicts the middle 50% of the autoscaled values. The line within the box represents the median and the error bars represent standard deviation. n = 31 for each treatment.

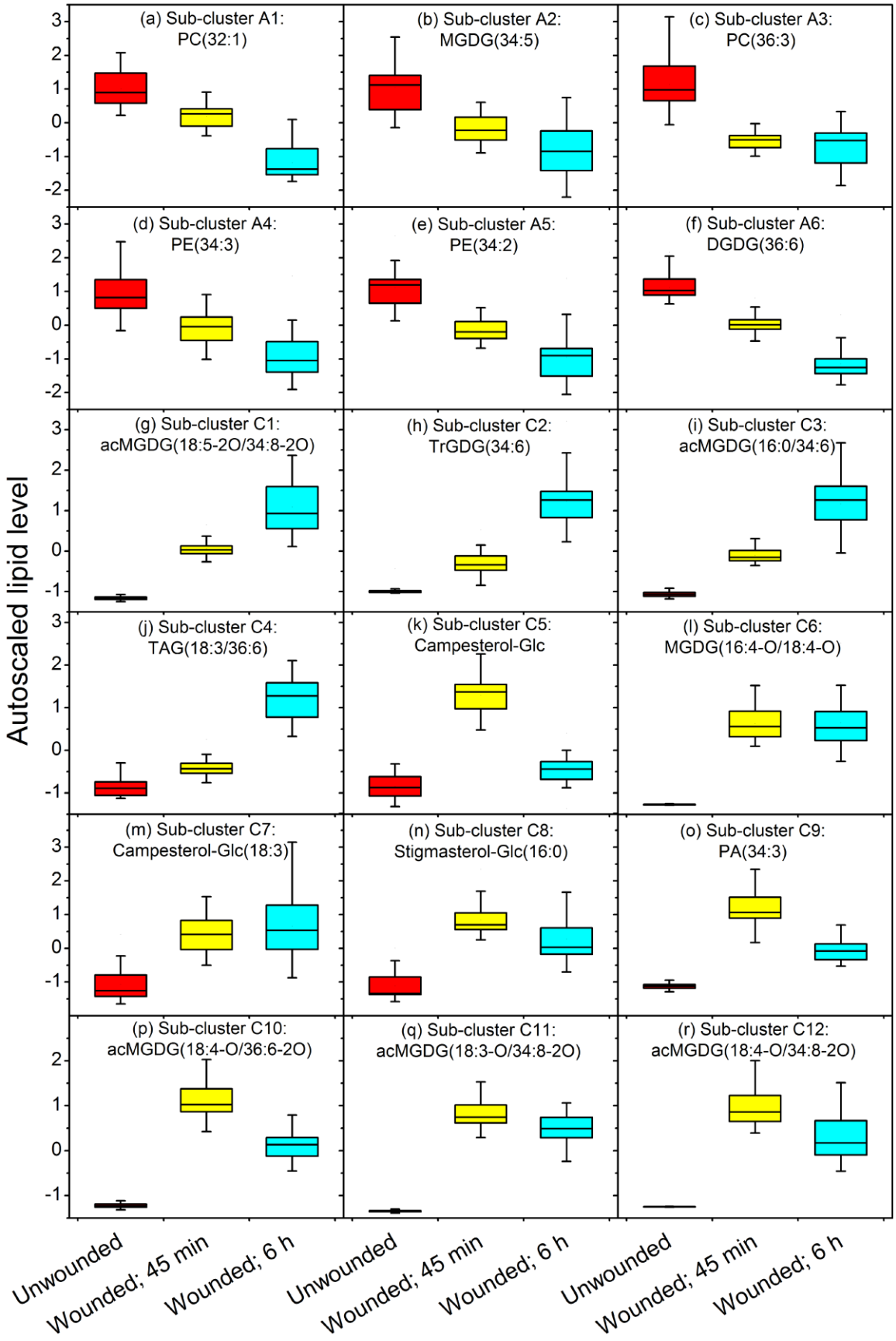
Autoscaled lipid level
(a) Sub-cluster A1: PC(32:1)
(b) Sub-cluster A2: MGDG(34:5)
(c) Sub-cluster A3: PC(36:3)
(d) Sub-cluster A4: PE(34:3)
(e) Sub-cluster A5: PE(34:2)
(f) Sub-cluster A6: DGDG(36:6)
(g) Sub-cluster C1: acMGDG(18:5-2O/34:8-2O)
(h) Sub-cluster C2: TrGDG(34:6)
(i) Sub-cluster C3: acMGDG(16:0/34:6)
(j) Sub-cluster C4: TAG(18:3/36:6)
(k) Sub-cluster C5: Campesterol-Glc
(l) Sub-cluster C6: MGDG(16:4-O/18:4-O)
(m) Sub-cluster C7: Campesterol-Glc(18:3)
(n) Sub-cluster C8: Stigmasterol-Glc(16:0)
(o) Sub-cluster C9: PA(34:3)
(p) Sub-cluster C10: acMGDG(18:4-O/36:6-2O)
(q) Sub-cluster C11: acMGDG(18:3-O/34:8-2O)
(r) Sub-cluster C12: acMGDG(18:4-O/34:8-2O)
Unwounded
Wounded; 45 min
Wounded; 6 h

Table 4.1 Characteristics of three lipid extraction methods.

Method 1 is the single-step extraction method used for the main experiment in the current work. Method 2 is a modification of the Bligh and Dyer (1959) method (Welti et al., 2002). Method 3 includes Method 2, omitting backwashes, followed by additional extraction with solvent containing isopropanol, hexane, and water (Toledo et al., 1995; Markham et al., 2006). "Intensity normalized to internal standards per dry mass" indicates the total amount of mass spectral signal detected by each method in all lipid classes in comparison to internal standards added at the time of mass spectral analysis (post-extraction). "Percent of total intensity" indicates the intensity detected in each class by each method. Abbreviations are indicated in Table 4.2.

	Composition of extracts from Arabidopsis 45 min after wounding (Intensity normalized to internal standards per dry mass (units · mg^{-1}))		
	Extraction method 1 (Single-step)	Extraction method 2	Extraction method 3
Total intensity	634334 ± 12830	609413 ± 31828	604970 ± 57144
	Percent of total intensity		
Lipid class	Extraction method 1 (Single-step)	Extraction method 2	Extraction method 3
acDGDG	0.0070 ± 0.0029	0.0060 ± 0.0008	0.0069 ± 0.0010
acMGDG	2.33 ± 0.22	2.42 ± 0.23	2.82 ± 0.41
acPG	0.0023 ± 0.0005	0.0017 ± 0.0004	0.0024 ± 0.0007
DAG	0.0064 ± 0.0006	0.0079 ± 0.0010	0.0090 ± 0.0009
DGDG	11.80 ± 0.45	11.35 ± 0.33	9.75 ± 0.70
DGMG	0.0403 ± 0.0036	0.0372 ± 0.0238	0.0184 ± 0.0023
GIPC	0.0086 ± 0.0016	0.0072 ± 0.0027	0.0278 ± 0.0015
GlcCer	2.70 ± 0.13	2.16 ± 0.09	1.96 ± 0.12
LPC	0.0560 ± 0.0208	0.3235 ± 0.4332	0.0482 ± 0.0111
LPE	0.0372 ± 0.0086	0.0513 ± 0.0374	0.0251 ± 0.0040
MGDG	66.22 ± 1.08	68.15 ± 1.20	70.32 ± 1.24

MGMG	0.0745 ± 0.0031	0.0201 ± 0.0056	0.0206 ± 0.0026
PA	0.297 ± 0.039	0.484 ± 0.045	0.505 ± 0.033
PC	4.21 ± 0.33	4.46 ± 0.366	3.84 ± 0.31
PE	2.19 ± 0.03	2.23 ± 0.10	2.20 ± 0.16
PG	4.92 ± 0.18	5.10 ± 0.17	5.19 ± 0.26
PI	1.12 ± 0.03	1.18 ± 0.02	1.17 ± 0.05
PS	0.0482 ± 0.0015	0.0508 ± 0.0017	0.0476 ± 0.0020
SQDG	0.297 ± 0.020	0.313 ± 0.007	0.302 ± 0.020
Sterol derivatives	3.60 ± 0.46	1.61 ± 0.06	1.72 ± 0.06
TAG	0.0114 ± 0.0005	0.0131 ± 0.0037	0.0122 ± 0.0006
TeGDG	0.0010 ± 0.0003	0.0010 ± 0.0001	0.0012 ± 0.0001
TrGDG	0.0169 ± 0.0016	0.0175 ± 0.0017	0.0167 ± 0.0032

Table 4.2 Lipid name abbreviations

Lipid group	Example abbreviation	Abbreviation explanation
Monoacyl glycerophospholipids		
digalactosylmonoacylglycerol	DGMG(18:3)	(Acyl carbons: acyl carbon-carbon double bonds[a])
lysophosphatidylcholine	LPC(16:0)	
lysophosphatidylethanolamine	LPE(16:0)	
monogalactosylmonoacylglycerol	MGMG(18:3)	
Polar diacyl glycerolipids		
phosphatidic acid	PA(34:3)	(Total acyl carbons: total carbon-carbon double bonds)
phosphatidylcholine	PC(32:0)	
phosphatidylethanolamine	PE(36:2)	
phosphatidylglycerol	PG(34:1)	
phosphatidylinositol	PI(38:4)	
phosphatidylserine	PS(36:5)	
digalactosyldiacylglycerol	DGDG(36:6)	
monogalactosyldiacylglycerol	MGDG(34:6)	
sulfoquinovosyldiacylglycerol	SQDG(34:3)	
tetragalactosyldiacylglycerol	TeGDG(34:6)	
trigalactosyldiacylglycerol	TrGDG(34:6)	
Head-group-acylated polar glycerolipids		
acylated digalactosyldiacylglycerol	acDGDG(18:4-O/36:8-2O)	(Head-group acyl carbons: head-group acyl carbon-carbon double bonds/total *sn-1,2* acyl carbons: total *sn-1,2* carbon-carbon double bonds)

acylated monogalactosyldiacylglycerol	acMGDG(16:0/34:6)	
acylated phosphatidylglycerol	acPG(16:1/36:8-2O)	(Acyl carbons: carbon-carbon double bonds for one acyl chain/total acyl carbons: total carbon-carbon double bonds for the other two acyl chains combined)
Neutral glycerolipids		
triacylglycerol	TAG(18:3/36:6)	(Acyl carbons: carbon-carbon double bonds for one acyl chain/total acyl carbons: total carbon-carbon double bonds for the other two acyl chains combined)
diacylglycerol	DAG(16:0/18:3)	(Acyl carbons: carbon-carbon double bonds for one acyl chain/acyl carbons: carbon-carbon double bonds for the other acyl chain)
Polar diacyl lipids measured in negative mode		
DGDG, MGDG, PC, PE, PG	PC(16:0/18:3-O)	(Acyl carbons: carbon-carbon double bonds for one acyl chain/acyl carbons: carbon-carbon double bonds for the other acyl chain)[b]
Sphingolipids		
glycosylinositolphosphoceramide	GIPC(42:2)-3	(Carbons: carbon-carbon double bonds of sphingoid base + fatty amide)-number of hydroxyl groups in base plus acyl chain

glycosylceramide	GlcCer(42:2)-3	
Sterol derivatives		
acylated sterol glucoside	Sitosterol-Glc(18:3)	(Acyl carbons: acyl carbon-carbon double bonds)
sterol ester	Campesterol(18:3)	
sterol glucoside	Sitosterol-Glc	---

[a]"Double bonds" can also indicate double bond equivalents, such as rings. "Extra" oxygen atoms in acyl chains are indicated by a "-O"; for example, oxophytodienoic acid is 18:4-O to indicate 4 double bond equivalents and 1 "extra" oxygen atom.

[b]Note: *sn*-1 and *sn*-2 positions of acyl chains on the glycerol were not determined.

Table 4.3 ANOVA and post-hoc test results.

One-way ANOVA was performed to compare the levels of the lipids among the three treatments. If a significant difference ($p < 0.01$) was detected for a lipid, a Tukey post-hoc test was performed to identify the differing treatments. Significantly different lipids were marked "up" if the lipid was higher at 45 min after wounding than in unwounded plants, at 6 h than in unwounded plants, or at 6 h than at 45 min. "Down" indicates significant changes in the opposite direction. Comparisons that are not significantly different are marked "-". The "Cluster/Sub-cluster" column shows the cluster/sub-cluster name for each lipid in a labeled unit in the dendrogram (Figure 4.3).

Lipid Name	**Wounded; 45 min vs Unwounded**	**Wounded; 6 h vs Unwounded**	**Wounded, 6 h vs Wounded; 45 min**	**Cluster/Sub-cluster**
acDGDG(18:4-O/34:6)	up	up	-	not in a cluster[f]
acDGDG(18:4-O/34:7-O)	-	up	-	not in a cluster[f]
acDGDG(18:4-O/34:8-2O) or acDGDG(18:4-O/36:6)	up	up	-	C
acDGDG(18:4-O/36:8-2O)	up	up	-	C12
acMGDG(16:0/34:6)	up	up	up	C3
acMGDG(16:0/34:7-O)	up	up	up	C3
acMGDG(16:0/34:8-2O) or acMGDG(16:0/36:6)	up	up	-	C12
acMGDG(16:0/36:8-2O)	up	up	-	C12
acMGDG(16:1/34:8-2O) or acMGDG(16:1/36:6)	up	up	up	C
acMGDG(16:3/34:6)	up	up	up	C3
acMGDG(16:3/34:8-2O) or acMGDG(16:3/36:6)	up	up	up	C3
acMGDG(16:3-O/34:8-2O) or acMGDG(16:3-O/36:6)	up	up	-	C
acMGDG(16:3-O/36:8-2O)	up	up	-	C

acMGDG(16:3-2O/34:6) or acMGDG(18:1/34:6)	up	up	up	C
acMGDG(16:3-2O/34:8-2O) or acMGDG(16:3-2O/36:6) or acMGDG(18:1/34:8-2O) or acMGDG(18:1/36:6)	up	up	down	C
acMGDG(16:3-2O/36:8-2O) or acMGDG(18:1/36:8-2O)	up	up	down	C
acMGDG(16:4-O/34:8-2O) or acMGDG(16:4-O/36:6)	up	up	down	C12
acMGDG(16:4-O/36:8-2O)	up	up	down	C
acMGDG(18:0/34:6)	up	up	up	C
acMGDG(18:0/34:8-2O) or acMGDG(18:0/36:6)	up	up	down	C11
acMGDG(18:2/34:6)	up	up	up	C3
acMGDG(18:2/34:7-O)	up	up	up	C3
acMGDG(18:2/34:8-2O) or acMGDG(18:2/36:6)	up	up	-	C
acMGDG(18:2/36:8-2O)	up	up	down	C
acMGDG(18:2-O/34:8-2O) or acMGDG(18:2-O/36:6)	up	up	-	C
acMGDG(18:2-O/36:8-2O)	up	up	up	C
acMGDG(18:2-3O/34:8-2O) or acMGDG(18:2-3O/36:6)	up	up	down	C
acMGDG(18:3/34:6)	up	up	up	C3
acMGDG(18:3/34:7-O)	up	up	up	C3
acMGDG(18:3/34:7-2O) or acMGDG(18:3/36:5)	up	up	up	C3
acMGDG(18:3/34:8-2O) or acMGDG(18:3/36:6)	up	up	up	C3
acMGDG(18:3/36:7-O)	up	up	up	C

acMGDG(18:3/36:8-2O)	up	up	up	C3
acMGDG(18:3-O/34:6)	up	up	-	C
acMGDG(18:3-O/34:7-O)	up	up	up	C
acMGDG(18:3-O/34:8-2O) or acMGDG(18:3-O/36:6)	up	up	down	C11
acMGDG(18:3-O/36:6-O)	up	up	down	C
acMGDG(18:3-O/36:7-O)	up	up	up	C
acMGDG(18:3-O/36:8-2O)	up	up	-	C
acMGDG(18:3-2O/34:6)	up	up	-	C
acMGDG(18:3-2O/34:8-2O) or acMGDG(18:3-2O/36:6)	up	up	down	C10
acMGDG(18:3-2O/36:8-2O)	up	up	down	C10
acMGDG(18:3-3O/34:6)	up	up	down	C
acMGDG(18:3-3O/34:7-O)	up	up	down	C
acMGDG(18:3-3O/36:8-2O)	up	up	down	C10
acMGDG(18:4-O/34:6)	up	up	down	C
acMGDG(18:4-O/34:7-O)	up	up	up	C
Arabidopside E: acMGDG(18:4-O/34:8-2O) or acMGDG(18:4-O/36:6)	up	up	down	C12
acMGDG(18:4-O/36:6-O)	up	up	up	C
acMGDG(18:4-O/36:6-2O)	up	up	down	C10
acMGDG(18:4-O/36:7-2O) (alternative fragmentation)	up	up	up	C
acMGDG(18:4-O/36:7-O)	up	up	up	C1
[a]Arabidopside G: acMGDG(18:4-O/36:8-2O)	up	up	down	C12
[a]Arabidopside G: acMGDG(18:4-O/36:8-2O) (alternative fragmentation)	up	up	down	not in dendrogram[a]
acMGDG(18:4-2O/34:6)	up	up	-	C

acMGDG(18:4-2O/34:7-O)	up	up	up	C
acMGDG(18:4-2O/34:8-2O) or acMGDG(18:4-2O/36:6)	up	up	down	C12
acMGDG(18:4-2O/36:8-2O)	up	up	-	C12
acMGDG(18:4-3O/34:6)	up	up	-	C
acMGDG(18:4-3O/34:7-O)	up	up	-	C
acMGDG(18:4-3O/34:8-2O) or acMGDG(18:4-3O/36:6)	up	up	down	C10
acMGDG(18:5-2O/34:8-2O) or acMGDG(18:5-2O/36:6)	up	up	up	C1
acMGDG(18:5-2O/36:8-2O)	up	up	up	C1
acPG(16:1/36:8-2O)	up	up	-	C
DAG(34:3)	up	up	-	C
DAG(34:4)	up	up	-	not in a cluster[f]
DAG(34:6)	up	up	up	C
DAG(36:4)	-	-	up	not in a cluster[f]
DAG(36:5)	up	up	-	C
DAG(36:6)	up	up	-	C
DGDG(16:0/18:3-2O)	up	-	down	not in dendrogram[e]
DGDG(16:0/18:3-O)	up	up	-	not in a cluster[f]
DGDG(16:0/18:4-O)	up	up	-	C
DGDG(18:3-2O/16:3)	up	up	down	C
DGDG(18:4-O/16:3)	up	up	-	C
Arabidopside C: DGDG(18:4-O/16:4-O)	up	up	-	not in a cluster[f]
DGDG(18:4-O/18:3)	up	up	up	C
Arabidopside D: DGDG(18:4-O/18:4-O)	up	up	-	C
DGDG(18:4-O/18:4-2O) or DGDG(18:4-O/20:2)	up	up	down	C
DGDG(34:3)	down	down	down	A

DGDG(34:4)	down	down	down	A
DGDG(34:5)	down	down	down	A
DGDG(34:6)	down	down	down	A6
DGDG(36:3)	down	down	down	A
DGDG(36:4)	down	down	down	A
DGDG(36:5)	down	down	-	A
DGDG(36:6)	down	down	down	A6
DGDG(36:6-2O) or DGDG(38:4)	-	-	-	not in a cluster[f]
DGDG(36:8-2O) or DGDG(38:6)	up	up	down	C
DGDG(38:5) or DGDG(36:7-2O)	down	down	-	A
DGMG(16:0)	up	up	down	C
DGMG(16:4-O)	up	up	-	C
DGMG(18:3)	up	up	down	C
DGMG(18:4-O)	up	up	-	C
GIPC(42:1)-3	down	down	-	not in a cluster[f]
GIPC(42:2)-3	down	down	-	A
GlcCer(34:1)-2	-	down	down	A
GlcCer(34:1)-3	-	-	-	A
GlcCer(40:1)-3	-	-	-	A
GlcCer(42:2)-3	-	down	down	A
LPC(16:0)	up	up	up	C
LPC(16:1)	up	up	-	C
LPC(18:1)	up	up	up	C
LPC(18:2)	up	up	-	C
LPC(18:3)	up	up	down	C
LPE(16:0)	up	up	up	C
LPE(18:1)	up	-	-	not in a cluster[f]
LPE(18:2)	up	up	down	C
LPE(18:3)	up	up	down	C

MGDG(18:3/16:4-O)	up	up	up	C
MGDG(18:3-O/16:4-O)	up	up	-	C
MGDG(18:3-2O/16:3)	up	up	-	C
MGDG(18:3-2O/16:4-O) or MGDG(20:1/16:4-O) (16:4-O as fragment)	up	up	-	C
MGDG(18:3-2O/16:4-O) (18:4-O as fragment)	up	up	-	C
MGDG(18:3-2O/18:3-O)	up	up	down	not in a cluster[f]
MGDG(18:4-O/16:3)	up	up	-	not in a cluster[f]
MGDG(18:4-O/16:3-O)	up	up	up	C
[b]Arabidopside A: MGDG(18:4-O/16:4-O) (16:4-O as fragment)	up	up	-	C6
[b]Arabidopside A: MGDG(18:4-O/16:4-O) (18:4-O as fragment)	up	up	-	not in dendrogram[b]
MGDG(18:4-O/18:1) or MGDG(18:4-O/16:3-2O)	up	up	-	C
MGDG(18:4-O/18:2)	up	up	up	C
MGDG(18:4-O/18:3)	up	up	up	C
MGDG(18:4-O/18:3-O)	up	up	-	C
MGDG(18:4-O/18:3-2O) or MGDG(18:4-O/20:3)	up	up	-	C
MGDG(18:4-O/18:3-3O)	up	up	-	C
MGDG(18:4-O/18:3-4O)	up	up	-	C
Arabidopside B: MGDG(18:4-O/18:4-O)	up	up	-	C6
MGDG(18:4-O/18:4-2O)	up	up	-	C
MGDG(18:4-O/18:4-3O)	up	up	down	C
MGDG(18:4-2O/16:4-O) or MGDG(20:2/16:4-O)	up	up	up	C

MGDG(18:5-2O/16:4-O) or MGDG(20:3/16:4-O)	up	up	up	not in a cluster[f]
MGDG(18:5-2O/18:4-O) or MGDG(20:3/18:4-O)	up	up	-	not in a cluster[f]
MGDG(30:6-O)	up	up	down	C
MGDG(34:3)	down	down	down	A
MGDG(34:4)	down	down	down	A2
MGDG(34:5)	down	down	down	A2
MGDG(34:6)	down	down	down	A6
MGDG(35:3)	up	-	down	not in a cluster[f]
MGDG(36:3)	down	down	-	A
MGDG(36:4) or MGDG(34:6-2O)	down	down	-	A
MGDG(36:5) or MGDG(34:7-2O)	down	down	down	A
MGDG(36:6) or MGDG(34:8-2O)	down	down	down	A
MGDG(36:6-2O) or MGDG(38:4)	up	up	down	C
MGDG(36:8-2O) or MGDG(38:6)	up	up	-	C
MGDG(38:5) or MGDG(36:7-2O)	down	down	down	A
MGMG(16:0)	up	-	-	not in a cluster[f]
MGMG(16:3)	-	-	-	not in a cluster[f]
MGMG(18:3)	-	-	down	not in dendrogram[e]
MGMG(18:4-O)	up	-	-	not in a cluster[f]
PA(34:1)	up	up	down	C
PA(34:2)	up	up	down	C9
PA(34:3)	up	up	down	C9
PA(34:4)	up	up	-	C
PA(34:6)	up	up	up	C2
PA(36:2)	up	up	down	C9
PA(36:3)	up	up	down	C9

PA(36:4)	up	up	down	C9
PA(36:5)	up	up	down	C9
PA(36:6)	up	up	down	C9
PC(16:0/18:3-O)	-	down	down	not in a cluster[f]
PC(16:0/18:3-2O)	up	up	-	C
PC(18:2/18:3-O)	-	down	down	not in a cluster[f]
PC(18:2/18:3-2O)	up	up	down	C
PC(18:3/18:3-O)	-	down	down	not in a cluster[f]
PC(18:3/18:3-2O)	up	up	down	not in a cluster[f]
PC(32:0)	-	-	-	not in a cluster[f]
PC(32:1)	down	down	down	A1
PC(32:3)	-	up	up	C
PC(34:1)	down	down	-	A3
PC(34:2)	down	down	down	A5
PC(34:3)	down	down	down	A
PC(34:4)	down	down	-	G
PC(34:6)	up	up	up	C
PC(36:2)	down	down	-	A3
PC(36:3)	down	down	-	A3
PC(36:4)	down	down	-	A
PC(36:5)	down	down	down	A
PC(36:6)	-	down	down	A
PC(38:2)	down	down	down	A
PC(38:3)	down	down	down	A
PC(38:4)	down	down	down	A
PC(38:5)	down	down	down	A
PC(38:6)	-	-	-	not in a cluster[f]
PC(40:2)	down	-	up	E
PC(40:3)	down	-	up	E
PC(40:4)	down	down	-	A
PC(40:5)	down	down	-	A

PE(16:0/18:3-O)	-	down	down	B
PE(16:0/18:3-2O)	-	-	down	not in dendrogram[e]
PE(16:0/18:3-3O)	up	up	up	F
PE(18:2/18:3-O)	-	down	down	B
PE(18:2/18:3-2O)	up	down	down	not in dendrogram[e]
PE(18:2/18:3-3O)	-	up	up	F
PE(18:3/18:3-O)	-	down	down	B
PE(18:3/18:3-2O)	up	up	down	C
PE(18:3/18:3-3O)	-	up	up	F
PE(32:0)	down	down	down	A
PE(32:1)	down	down	down	A1
PE(32:3)	-	up	up	C
PE(34:2)	down	down	down	A5
PE(34:3)	down	down	down	A4
PE(34:4)	down	-	-	G
PE(36:2)	down	down	-	A
PE(36:3)	down	down	-	A
PE(36:4)	down	down	down	A5
PE(36:5)	down	down	down	A4
PE(36:6)	down	down	down	A4
PE(38:2)	down	down	down	A
PE(38:3)	down	down	down	A
PE(38:4)	down	down	down	A
PE(38:5)	down	down	-	A
PE(40:2)	down	-	up	not in a cluster[f]
PE(40:3)	-	up	up	not in a cluster[f]
PE(42:2)	down	down	-	not in a cluster[f]
[c]PE(42:3) (measured in positive mode)	down	down	down	not in a cluster[f]
[c]PE(42:3) (measured in negative mode)	-	-	-	not in dendrogram[c]

PG(18:3-O/16:0)	up	up	up	C
PG(18:3-O/16:1)	up	up	-	not in a cluster[f]
PG(18:2/16:0-O)	down	down	down	not in a cluster[f]
PG(18:4-O/16:0)	up	up	down	C
PG(18:4-O/16:1)	up	up	down	C
PG(18:4-O/18:2)	up	up	down	not in a cluster[f]
PG(18:4-O/18:3)	up	up	down	not in a cluster[f]
PG(32:0)	-	-	-	not in a cluster[f]
PG(32:1)	-	down	down	A
PG(34:1)	down	down	-	not in a cluster[f]
PG(34:2)	down	down	down	A
PG(34:3)	down	down	down	A
PG(34:4)	down	down	down	A
PG(36:2)	-	-	down	not in a cluster[f]
PG(36:3)	-	down	-	not in a cluster[f]
PG(36:4)	-	down	-	not in a cluster[f]
PG(36:5)	-	-	-	not in a cluster[f]
PG(36:6)	-	-	-	not in a cluster[f]
PI(34:2)	down	down	down	A
[d]PI(34:3) (measured in positive mode)	-	down	-	not in a cluster[f]
[d]PI(34:3) (measured in negative mode)	-	-	-	not in dendrogram[d]
PS(34:3)	down	down	-	not in a cluster[f]
PS(42:2)	down	down	down	A
PS(42:3)	down	down	down	A
SQDG(32:0)	up	down	down	not in a cluster[f]
SQDG(34:3)	down	down	down	A
SQDG(36:6)	-	down	down	A
Campesterol(18:2)	-	-	-	D
Campesterol(18:3)	-	-	up	D

Campesterol-Glc	up	up	down	C5
Campesterol-Glc(16:0)	up	up	-	C
Campesterol-Glc(18:2)	up	up	down	C
Campesterol-Glc(18:3)	up	up	-	C7
Campesterol-Glc(18:4-O)	up	up	-	C
Sitosterol(18:2)	-	-	-	D
Sitosterol(18:3)	-	-	up	D
Sitosterol-Glc	up	up	down	C5
Sitosterol-Glc(16:0)	up	up	down	C8
Sitosterol-Glc(18:2)	up	up	down	C
Sitosterol-Glc(18:3)	up	up	-	C7
Sitosterol-Glc(18:4-O)	up	up	up	C
Stigmasterol(18:2)	-	-	up	D
Stigmasterol(18:3)	down	-	up	D
Stigmasterol-Glc	up	-	down	C
Stigmasterol-Glc(16:0)	up	up	down	C8
Stigmasterol-Glc(18:2)	up	-	down	C
Stigmasterol-Glc(18:3)	up	up	-	C
Stigmasterol-Glc(18:4-O)	up	up	-	not in a cluster[f]
TAG(18:2/36:5)	up	up	up	C4
TAG(18:3/34:2)	up	up	up	C4
TAG(18:3/36:5)	up	up	up	C4
TAG(18:3/36:6)	up	up	up	C4
TeGDG(34:6)	-	up	up	C2
TeGDG(36:6)	-	up	up	C
TrGDG(34:6)	up	up	up	C2
TrGDG(36:6)	up	up	up	C

[a] and [b] Indicates lipid measured twice in the same mode by different fragmentation events. For each, the second measurement was not included in the dendrogram.

[c] and [d] Indicate lipid measured once by a fragmentation event in the positive and once by a fragmentation event in negative mode. For each, the second measurement (in negative mode) had poor sensitivity

compared to the positive measurement and was not included in the dendrogram.

[e] Not in dendrogram due to $\rho < 0.6$.

[f] Not in a cluster due to $\rho < 0.8$, but still in dendrogram, because $\rho > 0.6$.

Supplemental Data

Supplemental data for this chapter include:

Figure S4.1 Ion leakage of Arabidopsis Col-0 control (unwounded) and wounded plants.

Figure S4.2 Expression of *ALLENE OXIDE SYNTHASE* (*AOS*) and *LIPOXYGENASE2* (*LOX2*) as quantified by qRT-PCR.

Figure S4.3 Leaf appearance before and after wounding.

Figure S4.4 Infusion profiles of representative lipids, as a function of time.

Figure S4.5 Levels of lipids as a function of wounding treatment. (This figure is supplied in a separate PDF file)

Tables S4.1-S4.10 are in a separate Excel file

Table S4.1 Comparison of three extraction methods**.**

Table S4.2 Lipids analyzed with their experimental parameters and evidence for their identification.

Table S4.3 Accurate masses of acyl groups of acMGDG from wounded *Arabidopsis thaliana* (Col-0) by Q-TOF mass spectrometry.

Table S4.4 Oxidized fatty acyl species relevant to this work.

Table S4.5 Internal standards employed in lipid profiling.

Table S4.6 Arrangement of samples in mass spectral lipid profiling in 4 mass spectrometry sample trays.

Table S4.7 Lipid amounts (normalized intensity per mg of leaf dry mass)

Table S4.8 Autoscaled lipid profiling data.

Table S4.9 One-way ANOVA and Tukey's post-hoc test results.

Table S4.10 Correlation among amounts of lipids across plant samples.

Methods S4.1 Plant material and growth

Method S4.2 Ion leakage measurement

Method S4.3 Quantification of gene expression by Real-Time-PCR

Method S4.4 Instrument parameters for analyses on the XevoTS-Q mass spectrometer

Method S4.5 Dendrogram file format conversion

Appendix S4.1 References cited in Supporting Information

Figure S4.1 Ion leakage of Arabidopsis Col-0 control (unwounded) and wounded plants.
*Student's t-test indicated a significant difference from unwounded leaves; $p < 0.001$, $n = 10$.

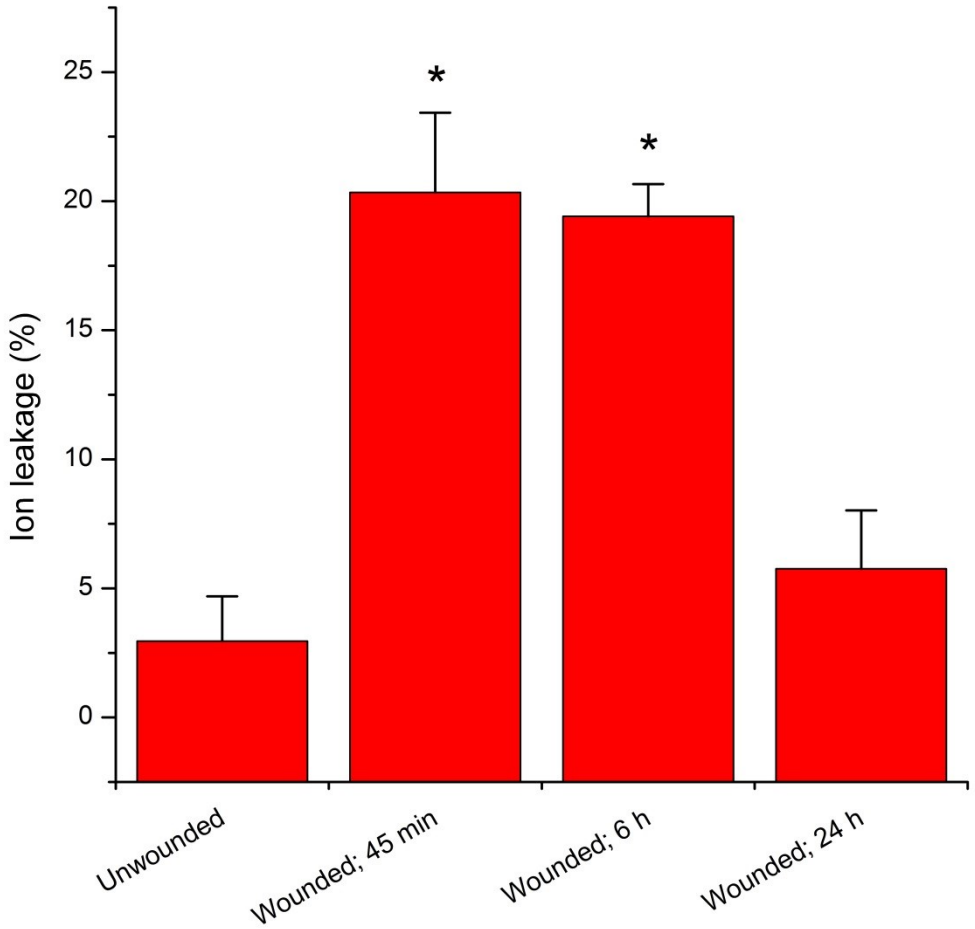

Figure S4.2 Expression of *ALLENE OXIDE SYNTHASE* (*AOS*) and *LIPOXYGENASE2* (*LOX2*) as quantified by qRT-PCR. The levels of *AOS* and *LOX2* expression were normalized to that of a constitutive control gene, *EF1α*. Six unwounded plants and 6 wounded plants were sampled. The Q test for discordant data (Shoemaker et al., 1974) was applied, resulting in removal of one datum in the unwounded *AOS* data set and one datum in the *LOX2* wounded data set. The data indicate that *AOS* expression was 3.9-fold greater and *LOX2* expression was 7.3-fold greater in leaf 6 of wounded plants, compared to leaf 6 of unwounded plants.
*The p-value for the comparison of unwounded and wounded plant gene expression was < 0.001 for both genes by Student's t-test.

Figure S4.3 Leaf appearance before and after wounding. Plants were 4-week old.

Figure S4.4 Infusion profiles of representative lipids, as a function of time. The vertical axis is relative intensity (%). The horizontal axis is time (min) from 0 to 15 min. Following lipid names are the polarity of the mass spectrometer (positive/negative), the intact ion *m/z*>fragment *m/z*, and the maximum intensity (i.e., the intensity of 100%). The samples were directly infused from a 300 µl loop. The initial period of no intensity represents the time it took for the sample to reach the mass spectrometer. The sample solvent was isopropanol: chloroform: methanol: 300 mM ammonium acetate in water (25: 30: 41.5: 3.5, v/v/v/v). From 0 to 11 min, the sample was pushed through the loop with methanol at 30 µl min^{-1} and, from 11 to 15 min, with methanol at 90 µl min^{-1}. In positive mode each lipid was scanned 130 or 131 times, and in negative mode each lipid was scanned 38 times, during the 15 min of data acquisition.

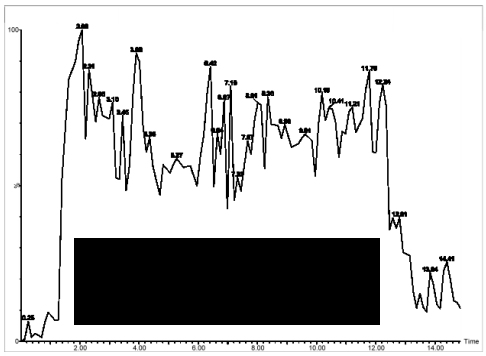
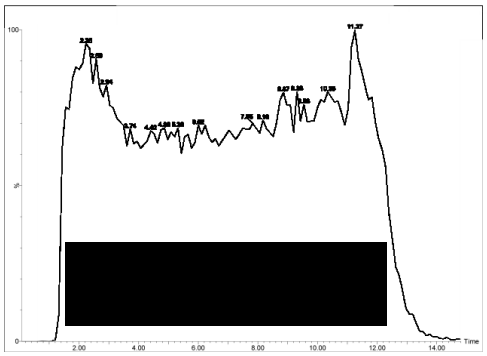
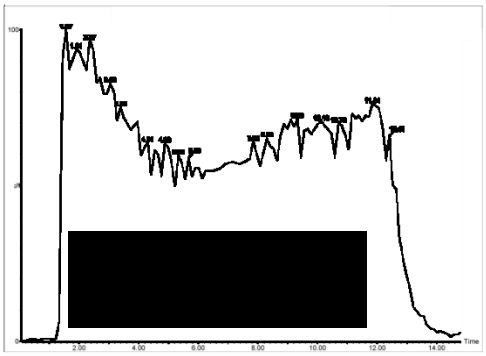
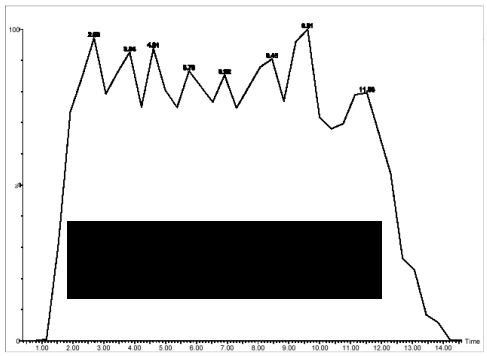
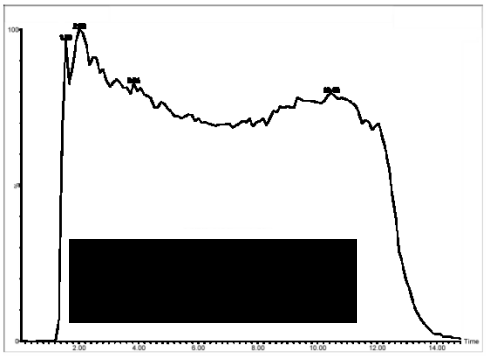
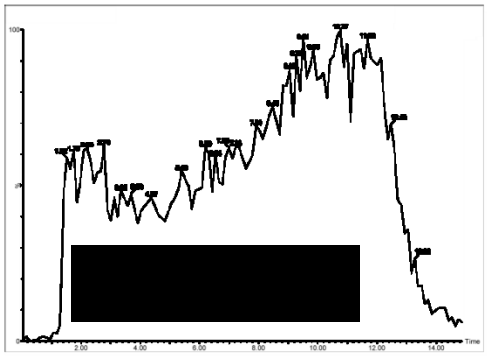
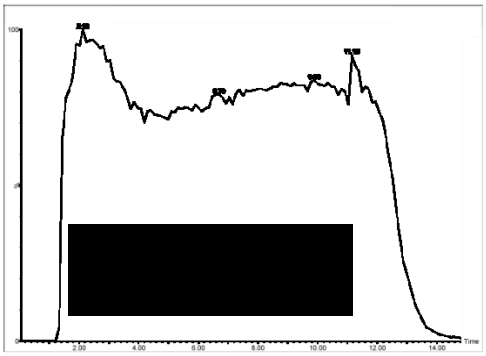
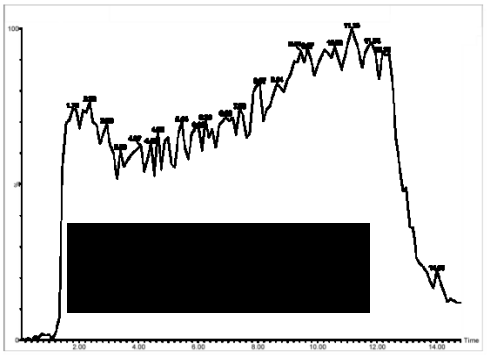

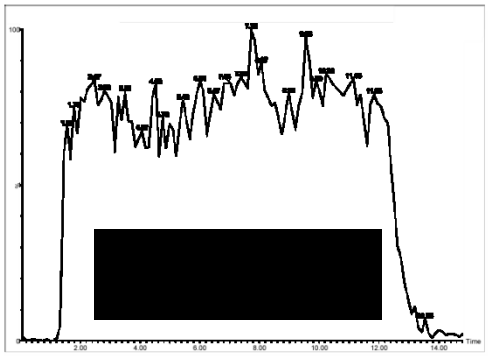

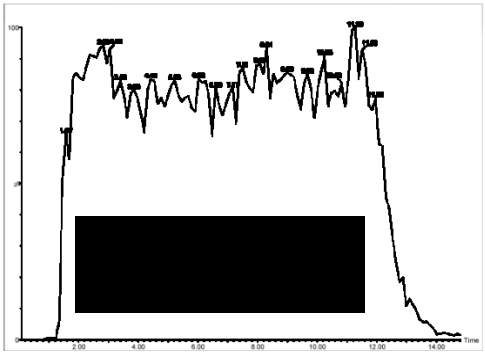

Methods S4.1 Plant material and growth

Arabidopsis thaliana accession Columbia-0 (Col-0) seeds were soaked in tap water at 4°C for 2 days before being sown at 4 seeds per well in 72-well plug trays (International Green House Company, Danville, IL, USA) filled with loosely packed, water-saturated, autoclaved, and cooled Pro-Mix "PGX" soil (Hummert International, Springfield, MO, USA). Trays were placed in a growth chamber under a 14/10 h light/dark cycle at 21°C with 60% humidity. Light intensity was maintained at 80 μmol m^{-2} sec^{-1} with cool white fluorescent lights. Trays were covered with propagation domes for the first 7 days to maintain high humidity. Trays were watered once per week. On day 12 after sowing, plants were reduced to one plant per well. On day 19, trays were fertilized with 0.01% Miracle-Gro 20-20-20 (Scotts Miracle-Gro Co., Marysville, OH, USA).

Method S4.2 Ion leakage measurement

Ion leakage was measured as described previously (Vu et al., 2014). Briefly, leaves were harvested at 45 min, 6 h, and 24 h after wounding, rinsed with distilled water, and shaken in a test tube containing 25 ml of distilled water at 100 rpm for 2 h before the conductivity of the solution was measured. The solution was then heated to and maintained at 95-100°C for 2 h to fully release the leaves' ions. After cooling to room temperature, a second conductivity measurement was taken. The ion leakage (%) was calculated as the first measurement over the second measurement x 100.

Method S4.3 Quantification of gene expression by real-time-PCR

Total RNA was extracted from wounded and unwounded leaf samples by the acid guanidinium thiocyanate-phenol-chloroform extraction method according to Chomczynski and Sachhi (1987). DNA contamination in isolated RNA samples was removed by treatment with RNase-free DNase

(Ambion, lifetechnologies.com), and RNA was spectrophotometrically quantified at 260 nm. DNA-free total RNA (2 μg) from each sample was used for cDNA synthesis. The first-strand cDNA synthesis was performed with Oligo (dT) primer using M-MLV Reverse Transcriptase (Promega, promega.com) according to the manufacturer's instructions. Individual real-time PCR reactions contained 5 μL of the SYBR Green PCR master mix (Applied Biosystems, *appliedbiosystems.com*), 2 μL of cDNA, 0.3 μL of 10 μM forward and reverse primers, and 2.4 μL of distilled water on an Eco qPCR system (Illumina, illumina.com) using the following amplification protocol: 10 min polymerase activation and denaturation at 95°C, and 40 cycles of 95°C for 10 sec, 60°C for 30 sec, and 72°C for 30 sec. This was followed by denaturation to confirm a single PCR product. Melt curves were obtained by slow heating at 0.5°C sec^{-1}, from 55°C to 95°C while continuously monitoring the fluorescence signal. A negative control without a cDNA template and a positive control with a known cDNA template were run to evaluate the overall specificity. The levels of *AOS* (At5g42650) and *LOX2* (At3g45140) expression was normalized to that of a constitutive control gene *EF1α* (At5g60390) by subtracting the cycle threshold value of control *EF1α* from the cycle threshold value of *AOS* and *LOX2*. The *EF1α*-F (5′- accaagattgacaggcgttc-3′) and *EF1α*-R (5′- tgcaacagtctgcctcatgt -3′), *AOS*-F (5'-ccctttttccgatttctctcc-3') and *AOS*-R (5'-acggtagcctccggttagtt-3'), and *LOX2*-F (5′-ggtctcgatgacattgctga-3′) and *LOX2*-R (5′-aggcatctcaaactcgcact-3′) gene-specific primers were used for PCR amplification of *EF1α*, *AOS*, and *LOX2*, respectively. Expression was measured in leaf 6 of 4-week-old wild-type (Col-0) Arabidopsis, either unwounded or subjected to wounding on leaves 5, 6, and 7.

Method S4.4 Instrument parameters for analyses on the XevoTS-Q mass spectrometer

The global settings for all analyses on the Xevo TS-Q mass spectrometer were: capillary voltage, ±2.8 kV; source offset voltage, ±30.0 V; cone voltage, ±40.0 V; source temperature, 150°C; desolvation temperature, 250°C; cone gas flow, 150 L h^{-1}; desolvation gas flow, 650 L h^{-1}; collision gas flow, 0.1 mL min^{-1}; nebulizer gas pressure, 7 bar; low mass 1 and 2 resolution, 2.5; high mass 1 and 2 resolution, 14.5; ion energy 1 and 2, 1.0. Interchannel delay (ICD) was 0.006-0.012 sec in positive mode and 0.100 sec in negative mode. Interscan delay (ISD) was 0.020 sec in positive mode and 0.100 sec in negative mode.

Method S4.5 Dendrogram file format conversion

Clustering results produced by Cluster 3.0 (Eisen et al., 1997) (.gtr and .cdt files) were converted to NEWICK format (.nwk) using a Python script written by Haibao Tang (J. Craig Venter Institute, Rockville, MD, USA). The script can be obtained from the following link: https://github.com/tanghaibao/treecut/blob/master/scripts/eisen_to_newick.py.

Appendix S4.1 References cited in Suppplemental data

Andersson MX, Hamberg M, Kourtchenko O, Brunnström A, McPhail KL, Gerwick WH, Goebel C, Feussner I and Ellerström M (2006) Oxylipin profiling of the hypersensitive response in *Arabidopsis thaliana*. Formation of a novel oxo-phytodienoic acid-containing galactolipid Arabidopside E. J. Biol. Chem. 281, 31528-31537.

Burgos A, Szymanski J, Seiwert B, Degenkolbe T, Hannah MA, Giavalisco P and Willmitzer L (2011) Analysis of short-term changes in the *Arabidopsis thaliana* glycerolipidome in response to temperature and light. The Plant Journal 66, 656–666.

Buseman CM, Tamura P, Sparks AA, Baughman EJ, Maatta S, Zhao J, Roth MR, Esch SW, Shah J, Williams TD and Welti R (2006) Wounding stimulates the accumulation of

glycerolipids containing oxophytodienoic acid and dinor-oxophytodienoic acid in Arabidopsis leaves. Plant Physiol. 142, 28-39.

Chomczynski P and Sachhi N (1987) Single-step method of RNA isolation by acid guanidinium thiocyanate-phenol-chloroform extraction. Anal. Biochem. 162, 156-159.

Devaiah SP, Roth MR, Baugham E, Li M, Tamura P, Jeannotte R, Welti R and Wang XM (2006) Quantitative profiling of polar glycerolipid species and the role of phospholipase Dα1 in defining the lipid species in Arabidopsis tissues. Phytochemistry 67, 1907-1924.

Eisen MB, Spellman PT, Brown PO and Botstein D (1997) Cluster analysis and display of genome-wide expression patterns. Proc. Natl. Acad. Sci. USA 95, 14863-14868.

Esch, S.W., Tamura, P., Sparks, A.A., Roth, M.R., Devaiah, S.P., Heinz, E., Wang, X., Williams TD and Welti R (2007) Rapid characterization of fatty acyl composition of complex lipids by collision-induced dissociation time-of-flight mass spectrometry. J. Lipid. Res. 48, 235-241.

Glauser G, Grata E, Rudaz S and Wolfender JL (2008) High-resolution profiling of oxylipin containing galactolipids in Arabidopsis extracts by ultraperformance liquid chromatography/time-of-flight mass spectrometry. Rapid Commun. Mass Spectrom. 22, 3154-3160.

Grun G, Berger S, Matthes D and Mueller MJ (2007) Early accumulation of non-enzymatically synthesized oxylipins in *Arabidopsis thaliana* after infection with *Pseudomonas syringae*. Funct. Plant Biol. 34**,** 65-71.

Hisamatsu Y, Goto N, Hasegawa K and Shigemori H (2003) Arabidopsides A and B, two new oxylipins from *Arabidopsis thaliana*. Tetrahedron Lett. 44, 5553-5556.

Hisamatsu Y, Goto N, Sekiguchi M, Hasegawa K and Shigemori H (2005) Oxylipins arabidopsides C and D from *Arabidopsis thaliana*. J. Nat. Prod. 68, 600-603.

Hsu F-F, Turk J, Williams TD and Welti R (2007) Electrospray ionization multiple stage quadrupole ion-trap and tandem quadrupole mass spectrometric studies on phosphatidylglycerol from Arabidopsis leaves. J. Am. So.c Mass Spectrom. 18, 783-90.

Ibrahim A, Schütz AL, Galano JM, Herrfurth C, Feussner K, Durand T, Brodhun F and Feussner I (2011) The alphabet of galactolipids in *Arabidopsis thaliana*. Front Plant Sci. DOI: 10.3389/fpls.2011.00095.

Kourtchenko O, Andersson MX, Hamberg M, Brunnström A, Goebel C, McPhail KL, Gerwick WH, Feussner I and Ellerström M (2007) Oxo-phytodienoic acid containing galactolipids in Arabidopsis: Jasmonate signaling dependence. Plant Physiol. 145, 1658-1669.

Li M, Baughman E, Roth MR, Han X, Welti R, and Wang X (2014) Quantitative profiling and pattern analysis of triacylglycerol species in Arabidopsis seeds by electrospray ionization mass spectrometry. Plant J. 77, 160-172.

Maeda H, Sage TL, Isaac G, Welti R and DellaPenna D (2008) Tocopherols modulate extra-plastidic polyunsaturated fatty acid metabolism in *Arabidopsis* at low temperature. Plant Cell 20, 452-470.

Markham JE and Jaworski JG (2007) Rapid measurement of sphingolipids from Arabidopsis thaliana by reversed-phase high-performance liquid chromatography coupled to electrospray ionization tandem mass spectrometry. Rapid Commun. Mass Spectrom. 21, 1304-1314.

Okazaki Y, Shimojima M, Sawada Y, Toyooka K, Narisawa T, Mochida K, Tanaka H, Matsuda F, Hirai A, Hirai MY, Ohta H and Saito K (2009) A chloroplastic UDP-glucose pyrophosphorylase from Arabidopsis is the committed enzyme for the first step of sulfolipid biosynthesis. Plant Cell 21, 892-909.

Peters C, Li M, Narasimhan R, Roth MR, Welti R and Wang X (2010) Nonspecific phospholipase C NPC4 promotes responses to abscisic acid and tolerance to hyperosmotic stress in Arapidopsis. Plant Cell 22, 2642-2659.

Samarakoon T, Shiva S, Lowe K, Tamura P, Roth MR and Welti R (2012) Arabidopsis thaliana membrane lipid molecular species and their mass spectral analysis. In *High throughput phenotyping in plants, Methods in Molecular Biology*. Ed., J. Normanly. Humana Press, New York, NY. 918, 179-268.

Schrick K, Shiva S, Arpin J, Delimont N, Isaac G, Tamura P and Welti R (2012) Steryl glucoside and acyl steryl glucoside analysis of Arabidopsis seeds by electrospray ionization tandem mass spectrometry. Lipids 47, 185-193.

Shigemori H, Nakajyo H, Hisamatsu Y, Sekiguchi M, Goto N and Hasegawa K (2006) Arabidopside F, a new oxylipin from *Arabidopsis thaliana*. Heterocycles 69, 295-301.

Shoemaker JP, Garland CW and Steinfeld JI (1974) "Experiments in Physical Chemistry", McGraw-Hill, Inc., pp. 34-39.

Stelmach BA, Mueller A, Hennig P, Gebhardt S, Schubert-Zsilavecz M and Weiler EW (2001) A novel class of oxylipins, sn1-O-(12-oxophytodienoyl)-sn2-O-(hexadecatrienoyl)-monogalactosyl diglyceride, from *Arabidopsis thaliana*. J. Biol. Chem 276, 12832-12838.

Vu HS, Tamura P, Galeva NA, Chaturvedi R, Williams TD, Wang X, Shah J and Welti R (2012) Direct infusion mass spectrometry of oxylipin-containing Arabidopsis thaliana membrane lipids reveals varied patterns in different stress responses. Plant Physiol. 158, 324-339.

Vu HS, Roth MR, Tamura P, Samarakoon T, Shiva S, Honey S, Lowe K, Schmelz EA, Williams TD and Welti R (2014) Head-group acylation of monogalactosyldiacylglycerol is a common stress response, and the acyl-galactose acyl composition varies with the plant species and applied stress. Physiol Plant. In press.

Welti R, Li W, Li M, Sang Y, Biesiada H, Zhou H, Rajashekar CB, Williams TD and Wang X (2002) Profiling membrane lipids in plant stress responses. Role of phospholipase Dα in freezing-induced lipid changes in Arabidopsis. J. Biol. Chem. 277, 31994-32002.

Welti R, Wang X and Williams TD (2003) Electrospray ionization tandem mass spectrometry scan modes for plant chloroplast lipids. Anal. Biochem. 314, 149-152.

Wewer V, Dombrink I, Vom Dorp K and Dörmann P (2011) Quantification of sterol lipids in plants by quadrupole time-of-flight mass spectrometry. J. Lipid Res. 52, 1039–1054.

Xiao S, Gao W, Chen Q, Chan S, Zheng S, Ma J, Wang M, Welti, R and Chye M-L. (2010) Overexpression of Arabidopsis acyl-CoA binding protein ACBP3 promotes starvation-induced and age-dependent leaf senescence. Plant Cell 22, 1463-1482

Yang W, Zheng Y, Bahn SC, Pan X, Li M, Vu HS, Roth MR, Scheu B, Welti R, Hong Y and Wang X (2011) The patatin-containing phospholipase A pPLAIIα modulates oxylipin formation and water loss in Arabidopsis thaliana. Mol. Plant 5, 452-460.

Zoeller M, Stingl N, Krischke M, Fekete A, Waller F, Berger S and Mueller MJ (2012) Lipid profiling of the Arabidopsis hypersensitive response reveals specific lipid peroxidation and fragmentation processes: biogenesis of pimelic and azelaic acid. Plant Physiol. 160, 365-378.

Chapter 8 - Roles of lipoxygenases and lipases in Arabidopsis in response to freezing

Abstract

The analytical approach developed in Chapter 4 was used to measure 331 lipids extracted from Arabidopsis exposed to cold acclimation, freezing and thawing. The data from wild-type plants were used to construct a dendrogram depicting clusters and sub-clusters of lipids that have similar patterns in response to treatments. The levels of these lipids were compared between the wild-type and 22 lines with knockout mutations in oxophytodienoic reductase, lipoxygenase and acyl hydrolase genes. Preliminary analysis of the data suggests that an increased formation of oxophytodienoic-acid-containing acylated monogalactosyldiacylglycerols (Arabidopsides E and G) during tissue thawing of cold-acclimated, frozen *pPLAIIγ* knockout coincided with a better recovery compared to wild-type.

Introduction

Lipoxygenases (LOXs) initiate lipid oxidation under various stresses. The enzymatic lipid oxidation catalyzed either by 9-LOXs or 13-LOXs produces either 9- or 13-hydroperoxy fatty acids, which are the precursors of many oxylipins. In Arabidopsis, the 9-LOX pathway, which includes LOX1 and LOX5, has been shown to have an antagonistic interaction with the ethylene pathway in the control of oxidative stress and modulation of bacterial defense (López et al., 2011). LOX1 was demonstrated to be essential in stomatal closing in response to bacterial infection (Montillet et al., 2013) and to be involved in Arabidopsis early response to cadmium exposure (Keunen et al., 2013). All four Arabidopsis 13-LOXs, LOX2, LOX3, LOX4, and LOX6 were shown to contribute to jasmonate synthesis in wounded leaves (Chauvin et al., 2013). Chauvin et al. (2013) also showed that LOX6 was the only 13-LOX necessary for the initiation of early jasmonate synthesis in systemic leaves. In an earlier study, LOX2 was shown to be required for wound-induced accumulation of jasmonic acid (Bell et al., 1995). These results suggest that the involvements of individual LOX genes in plant responses to different stresses are

different. Although LOX-derived products are induced by many abiotic and biotic stresses (Feussner and Wasternack, 2002; Weber, 2002; Hamberg et al., 2005; Shah, 2005; and Shah and Chaturvedi, 2008), the potential roles of each LOX gene in biosynthesis of oxidized lipids under plant stress conditions are understudied. Therefore, analyses of LOX mutants are critical to define specific roles of each LOX gene in the formation of stress-induced oxidized membrane lipids.

Acyl hydrolases (AHs) affect plant stress responses and might be involved in metabolism of oxidized membrane lipids. The Arabidopsis genome has many gene families tentatively encoding acyl hydrolase such as DEFECTIVE IN ANTHER DEHISENCE 1 (DAD-1)-like proteins (Ishiguro et al., 2001), secreted phospholipase A2 (Lee et al., 2005), GDSL lipases (Oh et al., 2005), and patatin-like proteins (PLP) (La Camera et al., 2005). PLP2 is involved in cell death execution, oxylipin synthesis, and pathogen resistance (La Camera et al., 2009). In a research on gene expression response to stresses, out of six PLPs: At4g37070, At2g26560, At4g37050, At2g39220, At3g54950 and At3g63200 (PLP1, PLP2, PLP3, PLP6, PLP7, and PLP9, respectively) only PLP2, PLP3, and PLP7 were induced by drought and PLP2 was further demonstrated to be induced in wounding and have AH activity *in vitro* (Matos et al., 2008). PLP1, PLP3, and PLP5 were demonstrated to have different roles in root response to phosphate deprivation (Rietz et al., 2010). It is clear that the PLPs play important roles in plant stress responses and are possibly involved in membrane lipid metabolism. However, very little is know about their substrates, products, and especially functions of each PLP under stress conditions. Although many phospholipases have been demonstrated to activate and play important roles in plant responses to cold and freezing (Welti et al., 2002; Li et al., 2004; Li et al., 2008), the roles of PLP in low temperature stress are still poorly studied (Li et al., 2013). Therefore, it is important to study PLP mutants to define their roles in stress-induced metabolism of oxidized membrane lipids.

Improving plant freezing tolerance has great agricultural significance. Naturally, some plants, including Arabidopsis, can increase their freezing tolerance after a period of exposure to low, non-freezing temperature; this is termed cold acclimation. Changes in lipid composition during cold acclimation are very important among the molecular strategies that help plants increase their

freezing tolerance. ACYL-LIPID DESATURASE 2 (ADS2) was shown to desaturate esterified 16:0 at low temperature, and this was shown to be important for freezing tolerance (Chen and Thelen, 2013). The accumulation of triacylglycerols during the acclimation period was reported to be a distinguishing factor between Arabidopsis ecotypes with different freezing tolerance (Degenkolbe et al., 2012). A distinct, acclimation-independent freezing tolerating mechanism is the converting of monogalactosyldiacylglycerol to oligogalactosyldiaclyglycerol by SENSITIVE TO FREEZING 2 (SFR2), a constitutively expressed protein (Moellering et al., 2010). Thus, cold acclimation and ultimately freezing tolerance involve diverse lipid compositional changes. To better understand the changes and their bases, a systematic approach is needed to study mechanisms underlying plant freezing tolerance.

In this research, we applied the high throughput lipidomics strategy developed in Chapter 4 to study Arabidopsis oxophytodienoic reductase, LOX and AH knockout mutants responding to cold acclimation and freezing. Six wild-type control plants and three plants of each knockout line were grown in a tray. Each tray was exposed to a unique temperature treatment. Afterward, the plants were harvested for both leaf damage assesment by ion leakage and lipid analysis. The whole treatment was repeated three times. Analysis of the first round is complete and analysis of rounds 2 and 3 is in progress. The direct infusion of total lipids, combined with the sensitivity of the mass spectrometer operated in MRM mode, offer relatively comprehensive snapshots of lipidomes. We employed a quality control strategy to enhance precision. This chapter presents data obtained from the first round of the experiment. The data provide novel preliminary findings about the production and metabolism of oxidized membrane lipids and the involvement of LOXs and AHs in cold and freezing responses in Arabidopsis.

Materials and Methods

Overall experimental design

In this research, we utilized 23 Arabidopsis lines; each of which was given a letter label from A to X for convenient handling (Table 5.1), except for the wild-type Columbia-0 (Col-0) accession which was duplicated (A and M, treated as 2 different lines during the experiment) due to its critical role as a control. The 24 lines were grown in triplicate in 72-well plug trays (Figure 5.1

and Figure 5.2). Each tray was treated with one of the conditions described in Figure 5.3. All 17 treatments (17 trays) were repeated three times (referred to as replication rounds 1, 2, and 3). Each well of the plug tray was labeled with a number from 1 – 72. Therefore, each line was associated with three different numbers indicating its positions on the plug tray. The positions of each line were different in the three replication rounds. For example, in replication round 1, line H was grown in wells numbered 1, 15, and 38 of each of the 17 trays; in replication round 2, line H was grown in wells numbered 13, 46, and 62 (Figure 5.1). The positions of each line in a tray were randomized in a controlled manner so that there was always at least 1 plant of all 24 lines on the outside wells. Seed sowing of the 17 trays of each replication round was done on 5 consecutive days (day 1: tray 1, 2, 4, 7, 10, and 12; day 2: 3, 5, 8, and 11; day 3: 6, 9, 14, and 16; day 4: tray 13 and 17; day 5: tray 15). All handlings and treatments of each tray (watering, thinning, fertilizing, photographing, treating, and harvesting) were done according to a staggered schedule so that time-consuming steps such as thinning or harvesting could be performed by no more than 4 laboratory workers at a time, and so that no more than two trays (the maximal capacity of the freezing chamber) would require freezing treatment on the same day.

Each tray was photographed to record visible phenotypes. In parallel with lipid analysis, ion leakage measurements were performed to detect membrane damage caused by the treatments.

Arabidopsis lines

We studied 22 mutant lines (including single, double, and triple knockouts) and wild-type, i.e. accession Columbia-0 (Col-0). Each line was given a letter label from A to X for easy handling throughout the experiment, as listed in Table 5.1. Col-0 was duplicated (A and M).

All the *pPLA* knockout lines were provided by Xuemin Wang and Maoyin Li (Danforth Plant Science Center, St Louis, MO, USA). All the *lox* lines except for *lox4* were provided by Jyoti Shah (University of North Texas, Denton, TX, USA). The l*ox4* knockout line was ordered directly from Arabidopsis Biological Resource Center (ABRC). The *lox4* seeds were sown and grown for 30 days before leaves were harvested for DNA extraction. Genotype with respect to *lox4* was confirmed by PCR using forward primer GACGCGTTCGTGTCTGACT and reverse

primer GGACTCTTTCCGCCTTTGA. Seeds collected from plants confirmed to be *lox4* homozygous recessive were used as line N. The *opr3* knockout line (X) was kindly shared by Jianmin Zhou. The *opr3* knockout line (in Col-0 background with RAP-luciferase transgene inserted) was induced by EMS mutagenesis giving the G2471A base substitution which results in replacement of Trp138 by a stop codon.

Plant growth conditions

Pro-Mix "PGX" soil (Hummert International, Earth City, MO, USA) was mixed with tap water to saturation and autoclaved for 1 h and was cooled to room temperature before potting. The pots for planting were a 72-well TLC Square Plug tray (International Greenhouse Company, Danville, IL, USA), placed inside a tray with holes, then both were placed inside another tray without holes (Hummert International). To prepare for sowing, a tray was filled with 2.5 L of fertilizer solution (0.01 % Peters 20: 20: 20 (Hummert International) in tap water).

Randomized seed positions used in the three rounds of the experiment are shown in Figure 5.1. Each plant has a combined label including the tray label (e.g., F1-1, Figure 5.2) and the well number (Figure 5.1A). When sowing, a bamboo toothpick was used to place four seeds, evenly spaced, at the center of a well. After sowing, a tray was drained, covered with a propagation dome (Hummert International) and kept at 4 °C for 2 days before transfer to growth conditions (21 °C, 60 % humidity, 80 – 100 μE m^{-2} s^{-1}). On day 9 counting from the time the tray was transferred, the propagation dome was removed. On day 11, plants were thinned so that only one healthiest plant remained. Trays were watered by sub-irrigation once a week. On day 20, trays were irrigated with the 0.01 % fertilizer solution. Plants were subjected to low temperature treatments on day 28.

Cold acclimation and freezing treatment

Plants were cold acclimated and frozen using the protocol described in Chapter 3. Figure 5.3 describes the temperature regimes applied.

Sampling and lipid extraction

Two types of samples were collected from each plant (72 plants per tray): (1) leaves 5 and 6 in a 50-ml tube containing 25 ml of distilled water (Dillons Supermarket, Manhattan, KS, USA) and (2) the rest of the rosette in a 20-ml vial containing 4 ml of isopropanol with 0.01% butylated hydroxytoluene (BHT) at 75 °C. The two samples from each plant were each labeled to indicate the plant from which they were derived (for example, the two samples from plant 3 of tray F1-1 in Figure 5.2 were both labeled "F1-1-3"). The sample labels were printed on Tough Tag labels (Diversified Biotech, Dedham, MA, USA), which were used to label the 50-ml tubes and the 20-ml vials.

Harvesting was carried out on a cart carrying two heat blocks with the blocks removed to house the 20-ml vials (the vials sat in the area where the blocks normally sit). The thermal blocks were maintained at 75 °C. Other material included four 40-slot racks to hold 72 tubes containing distilled water (two racks to hold tubes before harvesting, 2 racks to hold tubes after leaves 5 and 6 had been dropped in). For trays 1, 2, 4, 6, 9, 10, 11, 12, 13, 14, 15, 16, and 17 (treatments which ended with a period at 21 °C), the rolling cart was positioned right next to the growth chamber (at room temperature). For trays 3 and 5, the cart was situated inside the cold room where the trays were treated (the heating block heaters were set at 90 °C to compensate for the cold air and still maintain the vials at 75 °C). For trays 7 and 8, the cart was positioned next to the freezing chamber in which the trays were frozen (harvesting occurred at room temperature). At the end of each of the indicated treatment periods (Figure 5.3), the leaf material from each corresponding tray was harvested simultaneously by four laboratory personnel so that the average harvesting time was less than 20 min per tray. The four personnel worked in two pairs, each pair had one "cutter" and one "dipper" who stood facing each other across the cart. The "cutter" procedure for each plant was: (1) cut the whole rosette off the roots, (2) cut leaves 5 and 6 and drop them into the gloved palm of the corresponding "dipper", and (3) drop the rest of the rosette into the corresponding pre-labeled, pre-heated 20-ml vial, cap the vial, shake the vial slightly to fully submerge the rosette, and return the vial to the heating block heaters. The "dipper" procedure for each plant included: (1) receive leaves 5 and 6 from the corresponding "cutter", (2) rinse the leaves in a beaker of distilled water, and (2) drop the leaves into the pre-labeled 50-ml tube, cap the tube, and shake the tube to completely submerge the leaves in water.

For all trays except for trays 7 and 8, the tray was set on the cart during harvesting and the two pairs of personnel sequentially harvested the plants in order from 1 to 72. For trays 7 and 8, the trays were pre-cut (before seed sowing) into blocks of 4 plants with consecutive labels (e.g., 1-4, 5-8, 9-12…). At the end of the freezing treatment, the freezing chamber continued to maintain temperature at -8 °C. The blocks of 4 plants were taken out of the freezing chamber one at a time and were quickly harvested (two plants per harvesting pair) before thawing occurred. The freezing chamber was opened and closed quickly; the temperature increased from -8 °C to -7 °C or -6 °C; the awaiting plants remained well frozen. In all cases, after the last plant of a tray was harvested, the vials were incubated at 75 °C for an additional 15 min and were allowed to cool to room temperature before being stored at -80 °C.

To begin lipid extraction, each cardboard box of 72 samples from one tray stored at -80 °C was allowed to warm to room temperature. To each vial, 12 ml of the extraction solvent (chloroform: methanol: 300 mM ammonium acetate in water, 30: 41.5: 3.5, v/v/v) were added. The vials were shaken on an orbital shaker at 100 rpm for 24 h. After being shaken, the extracted rosette from each vial was removed and put into an empty vial with the same label. The original vials with solvent were stored at -20 °C. The extracted rosettes in non-capped vials were dried first in a fume hood for 1-2 h and then in an oven at 105 °C overnight. The dried rosettes were allowed to cool to room temperature and weighed using a Mettler-Toledo AX balance (Mettler-Toledo, Greifensee, Switzerland). To eliminate electrostatic forces resulting from drying of the rosettes, the rosettes were passed through an anti-static U ionizer (Haug, Germany).

Plant phenotyping

Photos of each tray were taken at multiple times including: (1) immediately before fertilizing at 20 days old, (2) immediately before the last watering which occurred on the day before the tray was harvested (trays 1, 2, 4, 6, 9, 12, and 15) or treated (trays 3, 5, 7, 8, 10, 11, 13, 14, 16, and 17), and (3) immediately before the tray was harvested (trays 7 and 8 were not photographed immediately prior to harvesting to avoid thawing). At each time point, a tray was photographed three times with three F-stop values (f/11, f/13, and f/14), using a Nikon D40 camera with an 18-55 mm lens. Other camera parameters were: ISO 200, focal length 35-45 mm, exposure time 250

s^{-1}, built-in flash "ON". One high quality photo of each tray at each time point was chosen (total of three photos per tray) for determining the number of leaves of each plant. The cotyledons were not counted in the total number of leaves. For an emerging leaf, it was only counted if the width of the petiole was estimated to be less than half of the maximal width of the leaf.

For ion leakage measurements, when each plant was harvested, leaves number 5 and 6 (as determined by Telfer et al., 1997) were dropped into a 50-ml glass tube containing 25 ml of distilled water (purchased from Dillons Supermarket, Manhattan, KS). The tubes were tightly capped and shaken at 150 rpm for 2 h. Conductivity was measured using an electrical conductivity meter CON 510 (Oakton Instruments, Vernon Hills, IL). After the first measurement, the tubes were re-capped and incubated in a water bath at 80 - 90 °C for 2 h and were allowed to cool to room temperature so the total ion leakage could be measured. Ion leakage was the percentage of the first conductivity value in relation to the total conductivity value (second value) for each plant.

Mass spectrometry analysis

A mixture of internal standards in chloroform was included in all mass spectrometry samples for analysis (including the sample vials, the internal standard-only vials, and the quality control (QC) vials). The composition of the internal standard mixture (20 µl) added per 0.04 mg dry mass of leaf tissue is listed in Table 5.2.

A quality control (QC) stock was prepared by pooling 1 ml from samples 1-10 of all the trays of replication round 1 and 2 (a total of 34 trays). The total volume of the QC stock was 340 ml and the concentration was 0.688 mg leaf dry mass ml^{-1}. The stock was divided into 34 aliquots of 10 ml each and the aliquots were stored at -20 °C. To make mass spectrometry QC vials, a QC stock aliquot was mixed with 3.4 ml of the internal standard mix (measured with a 1-ml glass syringe) and 224.6 ml (measured with a 250-ml glass cylinder) of mass spectrometry solvent (isopropanol: chloroform: methanol: 300 mM ammonium acetate in water, 25: 30: 41.5: 3.5, v/v/v/v). After being shaken, 1.4 ml of the mixture was dispensed into each of 156 amber 2-ml vials labeled "QC1" to "QC39" (four sets). The prepared QC mass spectrometry vials were stored at -80 °C and were brought to room temperature 1 h before analysis.

To prepare the sample mass spectrometry vials, the 20-ml vials containing the extracted total lipids were brought to room temperature from -20 °C ~2 h prior to handling, one tray (72 vials) at a time. To each of the 72 2-ml amber vials (labeled "1" to "72", the tray name, for example "F1-1", was written on the rack), 20 µl of the internal standard mixture (measured with a 100-µl syringe) was added first. In sequential order from 1 to 72, a volume that contained 0.04 mg leaf dry mass from a 20-ml vial was added to the similarly labeled 2-ml amber vial; a volume of mass spectrometry solvent (isopropanol: chloroform: methanol: 300 mM ammonium acetate in water, 25: 30: 41.5: 3.5, v/v/v/v) was added to the total volume of 1.4 ml; and the amber vial was capped before the next sample was added to the next amber vial. The mass spectrometry solvent volume was measured and dispensed with a 2.5-ml dispenser (Eppendorf, Hamburg, Germany) mounted on top of the solvent bottle. Since the smallest increment of dispenser was 50 µl, the calculated mass spectrometry solvent volume was adjusted to the closest marked level of the dispenser. For example, all volumes from 1226-1275 µl were adjusted to 1250 µl and all volumes from 1276-1325 µl were adjusted to 1300 µl. In each tray, 6 internal standard-only vials were included (labeled "IS1" to "IS6"); each contained 20 µl of the internal standard mix and 1.38 ml (total of 1.4 ml) of the mass spectrometry solvent. For mass spectrometry analysis, the 72 sample vials from each tray, together with 6 "IS" vials, and 39 "QC" vials were arranged in 3 VT-54 racks.

Table 5.3 lists the positions of mass spectrometry vials in the first VT-54 rack with QC vial 1-13, IS vial 1-2, and sample vial 1-24. The second and third VT-54 rack have the same arrangement with the QC 14-26, IS 3-4, sample 25-48 for the second VT-54 rack and QC 27-39, IS 5-6, sample 49-72 for the third VT-54 rack.

Data processing and statistical analysis

Data from experimental samples were normalized to QC samples, dendrogram, and graphs were produced using the same methods in Chapter 4. T-tests were done using Excel. The Spearman's correlation coefficient ρ between lipid analytes and ion leakage were calculated using the Metaboanalyst website.

Results

Our analysis of lipid compositions and phenotypes of wild-type, AH, and LOX knockouts were designed to capture behaviors of Arabidopsis plants at critical points during a cold acclimation/freezing/thawing time course. They included early cold acclimation (1 h at 4 °C, tray 3), late cold acclimation (three days at 4 °C, tray 5), right after freezing treatment at -8 °C for 2 h with or without cold acclimation (trays 8 and 7, respectively), 1 h, 3 h, and 24 h of thawing at 21 °C after freezing treatment with cold acclimation (tray 11, 14, and 17, respectively) or without cold acclimation (tray 10, 13, and 16, respectively).

Ablation of pPLAIIγ enhances cold acclimation effect on freezing tolerance

Electrolyte leakage measurements provided a quantitative assessment of leaf damage throughout the course of low temperature exposure. As shown in Figure 5.4, ion leakage in non-acclimated Col-0 plants was at its highest level immediately after the plants were removed from the freezing chamber (74-h point). The cold acclimation effect, i.e. the increased freezing tolerance, was demonstrated by the lower ion leakage percentage of acclimated Col-0 plants at this time. In the thawing phase (75-h, 77-h, and 98-h time points), the acclimated Col-0 plants showed clear signs of recovery as the ion leakage dropped close to the level of the untreated control plants, especially at 24 h after freezing. On the other hand, the ion leakage of the non-acclimated Col-0 plants stayed high even 24 h after freezing. Differences between acclimated and non-acclimated Col-0 plants during the thawing phase were also visible as shown in Figure 5.5. At 24 h after freezing, the acclimated plants appeared normal, except for some leaf areas with visible damage. Similarly treated plants were observed to continue growing, bolting, and eventually produce seeds. On the other hand, the non-acclimated plants were shrunken and dry. Leaves of similarly treated plants were observed to turn yellow and die, but the shoots were able to make new leaves after 7 – 10 days.

To identify mutants that affect freezing response of Arabidopsis, the ion leakage percentages of the 22 lines during exposure to freezing and thawing were compared to those of Col-0. Line E (*pPLAIIγ* knockout) had lower ion leakage in cold acclimated plants during recovery compared to wild-type, especially at the 77 h time point (3 h of thawing after freezing, $p < 0.1$), as depicted

in Figure 5.4. Acclimated pPLAIIγ knockout plants were visibly less damaged than acclimated Col-0 at 3 h after freezing (77 h time point, Figure 5.5).

Freezing-induced lipid changes occur in clusters

In 35 min per sample, our MRM-based analysis was able to measure 377 lipid species. Before further data analysis, several rules were applied to ensure quality of the data. First, we eliminated lipid species with background (average intensity measured in internal-standard-only samples) higher than 40% of the averaged signals detected in all QC samples. Second, we eliminated lipids with background higher than 20% of the QC average if the majority of the chemically similar lipid analytes were eliminated by the first rule. Applying the first two rules eliminated 34 compounds. Third, we eliminated 12 more lipids that measured less than 0.1 pmol in more than 1000 experimental samples (out of 17*72 = 1224 experimental samples). Our dataset contains 331 lipid analytes, each with 1224 measurements.

Since the dataset was acquired over a long period (~ two months), variation due to instrumental performance was very likely to occur. To correct for this variation, signals of each lipid in all experimental samples were normalized to the QC samples using the same method as described in Chapter 4.

It is hypothesized that cold-acclimation, freezing and thawing affect different biochemical pathways. Each pathway, in turn, controls the biosynthesis and metabolism of multiple lipid analytes. With the assumption that metabolites affected by the same pathway will behave in the same manner as a function of cold, freezing, and thawing treatments, pathways that are affected by low temperature treatments can be identified by clustering lipids that vary together across treatments and individual plants. To identify the clusters formed in low temperature stress, we calculated a 331 x 331 distance matrix using data from 102 (17 conditions x 6 replicates) wild-type Col-0 plants of the first round of the experiment. The level of each lipid analyte in all samples was ranked (1 to 1224), and Spearman's correlation coefficient ρ was calculated for each pair of compounds. A single linkage hierarchical clustering algorithm, using the maximal ρ for each lipid analyte, was applied to generate clusters. Figure 5.6 is a dendrogram of lipids that

correlate with $\rho > 0.6$ (301 lipids). Lipids that correlate with maximal $\rho > 0.8$ form clusters labeled from A to J. Within clusters A, B, and J, 94 lipids correlate with maximal $\rho > 0.95$ forming 16 sub-clusters. For each sub-cluster, levels of 1 or 2 representative lipids of Col-0 and pPLAIIγ mutant (line E) are shown in Figure 5.7 as a function of temperature treatment.

Many known cold- and freezing-induced pathways are visible in treated Col-0 via the sub-clusters shown in Figure 5.6 and their patterns shown in Figure 5.7. The degradation of PC (sub-cluster B1, B2, and B5), PE (sub-cluster B3 and B4), MGDG (sub-cluster B6), and DGDG (sub-cluster B7, and B8), together with the formation of PA (sub-cluster A2) can be explained, at least partially, by the activation of phospholipase D (Welti et al., 2002). Also, it cannot be ruled out that PAs are synthesized from DAGs produced by phospholipase C (Testerink and Munnik, 2005). The cold acclimation effect is evident as the degradation that occurred in acclimated Col-0 plants was not as severe and the plants almost recovered to control levels by 24 h after freezing while the lipids in non-acclimated plants were largely hydrolyzed and showed no sign of recovery. Interestingly, in acclimated plants, PE with long chain fatty acids (sub-cluster B4) accumulated after the cold acclimation and maintained higher levels thoughout the freezing and thawing treatments compared to the control, instead of being degraded as in the non-acclimated plants.

Although both LPC (sub-cluster A1) and PA (sub-cluster A2) are products of membrane lipid hydrolysis, their patterns of changes in response to low temperature treatments are substantially different. While PA was induced significantly more in non-acclimated plants than in acclimated thoughout the post-freezing period, LPC was induced more in acclimated plants, especially immediately and 1 h after freezing.

The formation of TrGDG (sub-cluster A5), coupled closely with TeGDG synthesis (Figure 5.6), was more dramatic in acclimated plants than in non-acclimated plants during the thawing process. The formation of TAG (sub-cluster A3) followed a similar pattern (much more in acclimated plants than in non-acclimated plants) and TAG seemed to keep accumulating in acclimated plants even at 3 h and 24 h after freezing.

The Gal-acylation of MGDG to form acMGDG (sub-cluster 6 and sub-cluster 7) was complex to interpret as the acyl groups involved were also affected by induced oxidation. acMGDG with three non-oxidized acyl groups (most of sub-cluster A7a) was induced in both non-acclimated and acclimated plants immediately at the end of the freezing period and was induced to significantly higher levels in non-acclimated plants than in acclimated plants. Even at 24 h, when the levels in acclimated plants tended to decrease to control level, the levels in non-acclimated plants showed little reduction, making the difference even greater. Sub-cluster A7b includes mostly acMGDGs with 2 oxidized acyl groups out of the total 3 acyl groups. The overall pattern of sub-cluster A7b somewhat resembles that of sub-cluster A7a and non-acclimated plants accumulated more at 24 h into thawing. A very striking difference occurred after 1 h of thawing, when the more oxidized acMGDGs (cluster A7b) were much higher in the acclimated plants compared to the non-acclimated ones. Fully oxidized acMGDGs (sub-cluster A6) were distinctive from less oxidized acMGDG in that they were not only more induced in acclimated plants but also maintained higher levels after 1 h, 3 h, and 24 h of thawing. This pattern also helped to distinguish between possible annotations of some acMGDG. For example, acMGDG(18:4-O/36:6) and acMGDG(18:4-O/34:8-2O) have the same mass and same head-group fragment but the pattern and clustering with acMGDG(18:4-O/36:8-2O) (sub-cluster A6) suggests that the fully oxidized annotation, acMGDG(18:4-O/34:8-2O), may be the correct one for the majority of lipid detected with the relevant analytical parameters in the current experiment.

The induction pattern of ASG (sub-cluster A4) was relatively similar to that of non-oxidized acMGDG (sub-cluster A7a). ASG was induced significantly in both acclimated and non-acclimated plants as early as 1 h after freezing. Especially at 24 h post-freezing, non-acclimated plants maintained a higher level of ASG compared to acclimated ones. The changes in sterol ester synthesis in response to low temperature, on the other hand, occurred in a unique pattern: sterol esters (cluster J1) were induced during the acclimation period. Freezing temperature also induced synthesis of sterol esters; however, after 24 h of thawing, markedly higher levels of sterol esters were detected in acclimated plants, which were exposed to both cold and freezing, compared to non-acclimated plants, which were exposed only to freezing.

Lipid changes correlate with freezing-induced leaf damage

It is hypothesized that freezing- and thawing-induced changes in lipid sub-clusters play different roles in determining the ultimate fate of the plants in response to the stress. Degradation of structural lipids and synthesis of antagonistic lipids might coincide with more severe tissue damage; whereas, induction and stably high levels of healing lipids could result in recovery from stress damage. To further investigate possible roles of lipids in each sub-cluster (Figure 5.6) in plant response to freezing, the Spearman's correlation coefficient ρ between lipids and leaf damage as measure by ion leakage was calculated using data from Col-0 plants. Table 5.4 shows the average and standard deviation of all ρ values within each lipid sub-cluster. It is obvious that non-structural, freezing induced lipids (cluster A) positively correlate with leaf damage, while structural lipids (cluster B) negatively correlate with leaf ion leakage. Highest among sub-clusters that have positive ρ are A2 (PA), A7a (acMGDG with mostly non-oxidized acyl groups), and A4 (ASG). The structural lipids with lowest negative ρ values are PCs (sub-cluster B1, B5, and B2) and MGDGs (sub-cluster B6). Interestingly, among the A-cluster lipids, TAG (sub-cluster A3) express distinctively less correlation with leaf damage, suggesting different involvement in plant responses compared to its stress-induced counterparts. Similarly, the long-chain PE (sub-cluster B4) has significantly higher correlation with leaf ion leakage, compared to other presumably structural lipid classes.

Formation of OPDA-containing acMGDG is enhanced in pPLAIIγ knockout

A hypothesis which might explain why cold-acclimated line E plants (*pPLAII γ* knockout) showed better appearance (Figure 5.5) and lower ion leakage (Figure 5.4) than Col-0 plants after 3 h and 24 h of thawing is that ablation of pPLAIIγ causes alteration(s) in how lipids in sub-clusters (Figure 5.6) respond to cold-acclimation, freezing, and thawing. To test this hypothesis, autoscaled lipid levels of representative lipids of all sub-clusters of *pPLAIIγ* knockouts were compared to those of Col-0 plants throughout the temperature regime. Figure 5.7 shows comparisons of autoscaled lipid levels between Col-0 and *pPLAIIγ* knockout of all 17 sub-clusters. The majority of sub-clusters are not different between knockout and wild-type except for PC with 38 acyl carbons (sub-cluster B1, Figure 5.7i) and oxidized acMGDG (sub-cluster A6, Figure 5.7f). Since the levels of PC with 38 acyl carbons were inconsistent across untreated

plants, the differences observed are not very likely to be related to the applied temperature treatments. Sub-cluster A6, (oxidized acMGDG), on the other hand, shows consistently low levels in untreated controls. As shown in Figure 5.7f, cold-acclimated *pPLAIIγ* knockouts expressed higher levels of lipids in sub-cluster A6 (acMGDG(18:4-O/34:8-2O) and acMGDG(18:4-O/36:8-2O)) at 0 h (74^{th} h time point, $p = 0.002$), 1 h (75^{th} h time point, $p = 0.07$) and 24 h (98^{th} h time point, $p = 0.02$) of thawing after freezing compared to Col-0 plants.

Discussion

In this chapter, the analytical approach and the co-occurrence analysis developed in Chapter 4 were applied to identify lipid analytes that were similarly metabolized when Arabidopsis responded to low temperature stress. Similar to wounding response, low temperature response induced changes in levels of the majority of lipid analytes, either increasing (cluster A) or decreasing (cluster B, Figure 5.6 and Figure 5.7). Similar sub-clusters were observed in low temperature response, including acMGDG (sub-cluster A6, A7a, and A7b), ASG (sub-cluster A4), PA (sub-cluster A2), TAG (sub-cluster A3), DGDG (sub-cluster B7 and B8), MGDG (sub-cluster B6), PC (sub-cluster B5), and PE (sub-cluster B3). Some sub-clusters only formed in low temperature reponse, not in wounding response, including long-chain PC (sub-cluster B2) and long-chain PE (sub-cluster B4). This suggests that unique lipid metabolizing enzyme(s) may have been activated only in response to low temperature and not in wounding response. On the other hand, MGDG(18:4-O/16:4-O) and MGDG(18:4-O/18:4-O) did not formed a sub-cluster in low temperature response. This suggests that acyl oxidation was activated to a lesser extent in low temperature response compared to wounding response (Vu et al., 2014). This might also explain the smaller sub-cluster of fully oxidized acMGDGs with only two members, acMGDG(18:4-O/34:8-2O) and acMGDG(18:4-O/36:8-2O) induced by low temperature (sub-cluster A6).

The TrGDG formation (sub-cluster A5) was presumably catalyzed by the galactolipid: galactolipid galactosyl transferase encoded by SFR2 (Moellering et al., 2010). In this reaction, a galactose from an MGDG is transferred onto MGDG, DGDG, and TrGDG forming β-linked

DGDG, TrGDG, and TeGDG, respectively. In wounding response, the inclusion of PA(34:6) in the same sub-cluster as TrGDG(34:6) and TeGDG(34:6) suggests that DAG(34:6) released by SFR2 was converted to PA(34:6). In low temperature response, PA(34:6) was not in the TrGDG sub-cluster; instead, PA(34:6) more closely correlated with the PA sub-cluster (A2). This suggests that PA(34:6) may have been formed mostly from MGDG(34:6) hydrolysis in low temperature stress.

Co-occurrence analysis of lipid analytes in low temperature response provides biochemical insights into cold acclimation. Many sub-clusters were specifically induced more in cold-acclimated plants including LPC and LPE (sub-cluster A1), TAG (sub-cluster A3), TrGDG (sub-cluster A5, oxidized acMGDG (sub-cluster A6), long-chain PE (sub-cluster B4), and sterol esters (sub-cluster J1, Figure 5.7). Some sub-clusters were hydrolyzed to a lesser extent in cold-acclimated plants compared to non-acclimated plants: PC with 38 acyl carbons (sub-cluster B1), long-chain PC (sub-cluster B2), PE with 36 acyl carbons (sub-cluster B3), PC and PS (sub-cluster B5), MGDG (sub-cluster B6), and DGDG (sub-cluster B7 and B8, Figure 5.7). On the other hand, some sub-clusters were specifically induced more in non-acclimated plants compared to acclimated plants including PA (sub-cluster A2), ASG (sub-cluster A4), and normal-chain acMGDG (sub-cluster A7a, Figure 5.7). It is noted that while the majority of the metabolic differences between non-acclimated and acclimated plants occurred during the thawing period, fewer changes were detected during the cold acclimation period. Lipid analytes that were induced during cold acclimation include PE (sub-cluster B3 and B4) and sterol esters (sub-cluster J1, Figure 5.7).

In this chapter, co-occurrence analysis was employed to identify metabolically active lipid analytes in response to low temperature. The knowledge was utilized to focus our comparisons between knockouts and wild-types on these metabolically important lipid analytes. Cold-acclimated *pPLAIIγ* knockout plants were found to induce higher levels of OPDA-containing acMGDGs (sub-cluster A6) compared to cold-acclimated Col-0 plants during thawing (Figure 5.7f). The coincidence between higher levels of acMGDG(18:4-O/34:8-2O) and acMGDG(18:4-O/36:8-2O) and faster recovery of cold-acclimated *pPLAIIγ* knockout plants suggests a "healing" role of the concentration of OPDA in acMGDG (reported by Vu et al., 2014). pPLAIIγ may

encode an acyl hydrolase that tends to hydrolyze OPDA-containing acMGDGs specifically. pPLAIIγ was previously shown to have higher galactolipase activity than phospholipase activity in vitro (Rietz et al., 2010).

References

Bell E, Creelman RA, and Mullet JE (1995) A chloroplast lipoxygenase is required for wound-induced jasmonic acid accumulation in Arabidopsis. Proc. Natl. Acad. Sci. U. S. A. **92**, 8675-8679.

Chauvin A, Caldelari D, Wolfender JL, and Farmer EE (2013) Four 13-lipoxygenases contribute to rapid jasmonate synthesis in wounded *Arabidopsis thaliana* leaves: a role for lipoxygenase 6 in responses to long-distance wound signals. New Phytol. **197**, 566-575.

Chen M, and Thelen JJ (2013) ACYL-LIPID DESATURASE2 Is Required for Chilling and Freezing Tolerance in Arabidopsis. Plant Cell **25**, 1430-1444.

Comfurius P, and Zwaal RF (1977) The enzymatic synthesis of phosphatidylserine and purification by CM-cellulose column chromatography. Biochim. Biophys. Acta **488**, 36-42.

Degenkolbe T, Giavalisco P, Zuther E, Seiwert B, Hincha DK, and Willmitzer L (2012) Differential remodeling of the lipidome during cold acclimation in natural accessions of *Arabidopsis thaliana*. Plant J. **72**, 972-982.

Feussner, I., and Wasternack, C. (2002) The lipoxygenase pathway. Annu. Rev. Plant Biol. **53**, 275- 297.

Hamberg, M., de Leon, I.P., Rodriguez, M.J., and Castresana, C. (2005) α-Dioxygenases. Biochem. Biophys. Res. Comm. **338**, 169-174.

Ishiguro S, Kawai-Oda A, Ueda J, Nishida I, and Okada K (2001) The *DEFECTIVE IN ANTHER DEHISCIENCE* gene encodes a novel phospholipase A1 catalyzing the initial step of jasmonic acid biosynthesis, which synchronizes pollen maturation, anther dehiscence, and flower opening in Arabidopsis. Plant Cell **13**, 2191-2209.

Keunen E, Remans T, Opdenakker K, Jozefczak M, Gielen H, Guisez Y, Vangronsveld J, and Cuypers A (2013) A mutant of the *Arabidopsis thaliana* LIPOXYGENASE1 gene

shows altered signalling and oxidative stress related responses after cadmium exposure. Plant Physiol. Biochem. **63**, 272-280.

La Camera S, Balagué C, Göbel C, Geoffroy P, Legrand M, Feussner I, Roby D, and Heitz T (2009) The Arabidopsis patatin-like protein 2 (PLP2) plays an essential role in cell death execution and differentially affects biosynthesis of oxylipins and resistance to pathogens. Mol. Plant Microbe Interact. **22**, 469-481.

La Camera S, Geoffroy P, Samaha H, Ndiaye A, Rahim G, Legrand M, and Heitz T (2005) A pathogen-inducible patatin-like lipid acyl hydrolase facilitates fungal and bacterial host colonization in Arabidopsis. Plant J. **44**, 810-825.

Lee HY, Bahn SC, Shin JS, Hwang I, Back K, Doelling JH, and Ryu SB (2005) Multiple forms of secretory phospholipase A2 in plants. Prog. Lipid Res. **44**, 52-67.

Li M, Bahn SC, Fan C, Li J, Phan T, Ortiz M, Roth MR, Welti R, Jaworski J, and Wang X (2013) Patatin-Related Phospholipase pPLAIIIδ Increases Seed Oil Content with Long-Chain Fatty Acids in Arabidopsis. Plant Physiol. **162**, 39-51.

Li W, Li M, Zhang W, Welti R, and Wang X (2004) The plasma membrane-bound phospholipase Dδ enhances freezing tolerance in *Arabidopsis thaliana*. Nat. Biotechnol. **22**, 427-433.

Li W, Wang R, Li M, Li L, Wang C, Welti R, and Wang X (2008) Differential degradation of extraplastidic and plastidic lipids during freezing and post-freezing recovery in *Arabidopsis thaliana*. J. Biol. Chem. **283**, 461-468.

López MA, Vicente J, Kulasekaran S, Vellosillo T, Martínez M, Irigoyen ML, Cascón T, Bannenberg G, Hamberg M, and Castresana C (2011) Antagonistic role of 9-lipoxygenase-derived oxylipins and ethylene in the control of oxidative stress, lipid peroxidation and plant defence. Plant J. **67**, 447-458.

Matos AR, Gigon A, Laffray D, Pêtres S, Zuily-Fodil Y, and Pham-Thi AT (2008) Effects of progressive drought stress on the expression of patatin-like lipid acyl hydrolase genes in Arabidopsis leaves. Physiol. Plant. **134**, 110-120.

Moellering ER, Muthan B, and Benning C (2010) Freezing tolerance in plants requires lipid remodeling at the outer chloroplast membrane. Science **330**, 226-228.

Montillet JL, Leonhardt N, Mondy S, Tranchimand S, Rumeau D, Boudsocq M, Garcia AV, Douki T, Bigeard J, Laurière C, Chevalier A, Castresana C, and Hirt H (2013) An

abscisic acid-independent oxylipin pathway controls stomatal closure and immune defense in Arabidopsis. PLoS Biol. **11**, e1001513.

Oh IS, Park AR, Bae MS, Kwon SJ, Kim YS, Lee JE, Kang NY, Lee S, Cheong H, and Park OK (2005) Secretome analysis reveals an Arabidopsis lipase involved in defense against *Alternaria brassicicola*. Plant Cell **17**, 2832-2847.

Rietz S, Dermendjiev G, Oppermann E, Tafesse FG, Effendi Y, Holk A, Parker JE, Teige M, and Sherer GFE (2009) Roles of *Arabidopsis* Patatin-Related Phospholipases A in Root Development Are Related to Auxin Responses and Phosphate Deficiency. Mol. Plant **3**, 524-538.

Shah, J. (2005) Lipids, lipases and lipid modifying enzymes in plant disease resistance. Annu Rev. Phytopathol. **43**, 229-260.

Shah, J., and Chaturvedi, R. (2008) Lipid signals in plant-pathogen interaction**.** Annu. Plant Rev. 34, 292-333.

Telfer A, Bollman KM, and Poethig RS (1997) Phase change and the regulation of trichome distribution in *Arabidopsis thaliana*. Development **124**, 645-654.

Testerink C, and Munnik T (2005) Phosphatidic acid: a multifunctional stress signaling lipid in plants. Trends Plant Sci. **10**, 368-375.

Vu HS, Roth MR, Tamura P, Samarakoon T, Shiva S, Honey S, Lowe K, Schmelz EA, Williams TD, and Welti R (2014) Head-group acylation of monogalactosyldiacylglycerol is a common stress response, and the acyl-galactose acyl composition varies with the plant species and applied stress. Physiol. Plant., In press.

Weber, H. (2002) Fatty acid-derived signals in plants. Trends Plant Sci. **7**, 217-224.

Welti R, Li W, Li M, Sang Y, Biesiada H, Zhou HE, Rajashekar CB, Williams TD, and Wang X (2002) Profiling membrane lipids in plant stress responses. Role of phospholipase Dα in freezing-induced lipid changes in Arabidopsis. J. Biol. Chem. **277**, 31994-32002.

Figures and Tables

Figure 5.1 Seed position in trays

(A) Schematic numbering of wells within a 72-well plug tray. (B), (C), and (D) Positions of letter-coded seeds for all trays of round 1, 2, and 3, respectively.

A

1	2	3	4	5	6	7	8	9	10	11	12
13	14	15	16	17	18	19	20	21	22	23	24
25	26	27	28	29	30	31	32	33	34	35	36
37	38	39	40	41	42	43	44	45	46	47	48
49	50	51	52	53	54	55	56	57	58	59	60
61	62	63	64	65	66	67	68	69	70	71	72

B

H	V	K	G	I	T	Q	C	A	W	X	P
W	P	H	O	J	P	U	L	O	M	A	D
V	J	F	M	C	S	V	C	I	I	S	T
N	H	G	B	B	K	N	E	E	R	T	X
U	Q	R	X	W	A	K	L	G	D	F	Q
J	D	U	S	O	R	L	E	N	F	M	B

C

P	L	E	U	X	Q	G	A	B	O	N	V
H	M	B	N	D	G	L	F	I	J	B	A
K	U	Q	F	T	W	T	I	P	V	X	L
Q	C	G	D	K	V	W	X	N	H	R	E
R	O	A	U	M	S	O	E	C	P	S	J
I	H	J	D	S	R	K	F	C	T	M	W

D

M	Q	I	X	A	G	J	E	D	U	T	B
H	O	B	I	U	V	J	T	C	E	J	V
L	K	B	A	A	I	Q	E	D	M	O	P
F	X	L	R	X	W	N	N	M	F	S	C
W	U	G	G	R	P	H	T	S	K	Q	D
N	F	S	W	C	R	K	V	P	L	H	O

Figure 5.2 Example of tray and plant labeling.

Each plant is referred to by a combined label including the tray label, e.g. “F1-1”, and the well position from 1 to 72. For example, the plants shown in this figure are labeled F1-1-1 to F1-1-72.


F2-1

Figure 5.3 Cold acclimation and freezing experiment design.

Plants entered the experiment at 30-day old. The X-axis is time (h) starting from the beginning of cold acclimation treatment at 4 °C. The Y-axis is temperature (°C). Each circle marks the time and temperature when and in which the correspondingly numbered tray was harvested. The line leading to each circle represents the temperature regime applied to the tray. Red line is untreated control (C); yellow line is non-acclimated (N); and blue is acclimated (A). In words, treatments applied to each tray are: tray **1** (no treatment), tray **2** (1 h at 21 °C), tray **3** (1 h at 4 °C), tray **4** (72 h at 21 °C), tray **5** (72 h at 4 °C), tray **6** (74 h at 21 °C), tray **7** (72 h at 21 °C and 2 h at -8 °C), tray **8** (72 h at 4 °C and 2 h at -8 °C), tray **9** (75 h at 21 °C), tray **10** (72 h at 21°C, 2 h at -8 °C, and 1 h at 21 °C), tray **11** (72 h at 4 °C, 2 h at -8 °C, and 1 h at 21 °C), tray **12** (77 h at 21 °C), tray **13** (72 h at 21 °C, 2 h at -8 °C, and 3 h at 21 °C), tray **14** (72 h at 4 °C, 2 h at -8 °C, and 3 h at 21 °C), tray **15** (98 h at 21 °C), tray **16** (72 h at 21 °C, 2 h at -8 °C, and 24 h at 21 °C), tray **17** (72 h at 4 °C, 2 h at -8 °C, and 24 h at 21 °C).

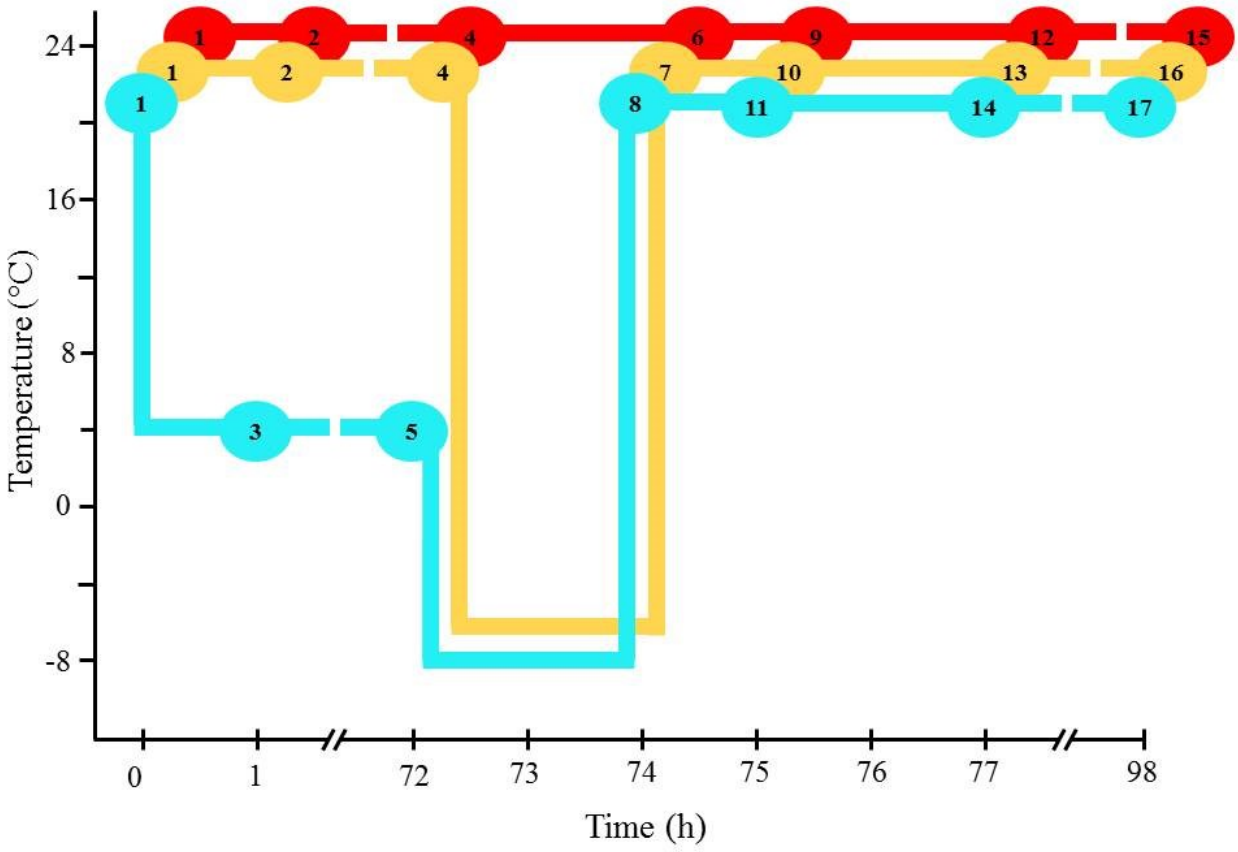

Figure 5.4 Low-temperature-induced leaf damage assessed by relative ion leakage.

The Y-axis is autoscaled level of ion leakage. The X-axis is the time course (h) of the temperature treatment (details of which are shown in Figure 5.3). At each time point, a set of six variables are shown, including untreated control (C), non-acclimated (N), and acclimated (A) of Col-0 and *pPLAIIγ* knockout (E). The box corresponding to each variable is also color-coded. The boxes summarize 6 replicates for Col-0 plants and 3 replicates for line E plants. The top and bottom of the boxes represent the 75 and 25 percentile; the bar inside the box marks the median, while the whisker is standard deviation.

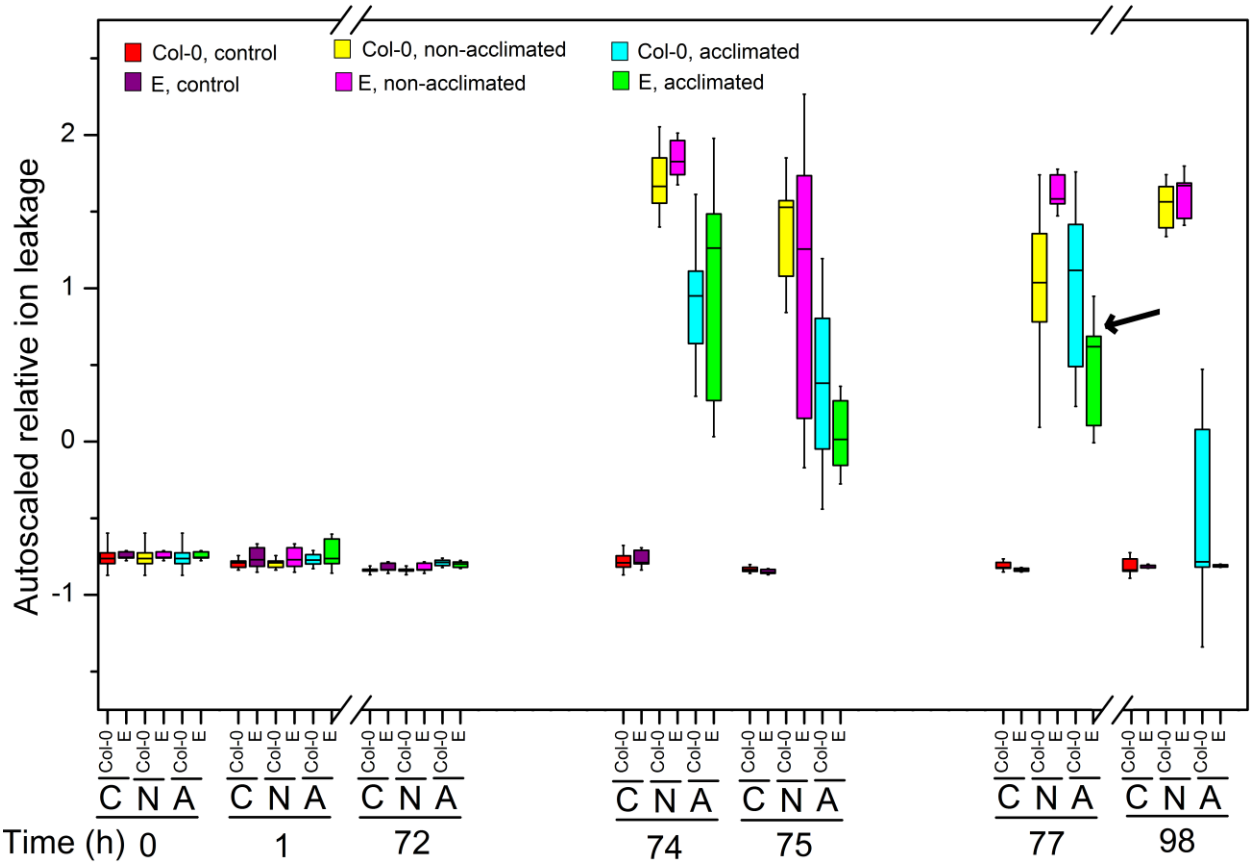

Figure 5.5 Plant appearance followed freezing treatments.

Photographs depict three wild-type plants (line A) and three line E plants (*pPLAIIγ* knockout) of untreated (control, C), non-acclimated frozen (N), and acclimated frozen (A) trays after 1 h (75th hour), 3 h (77th hour), and 24 h (98th hour) of thawing.

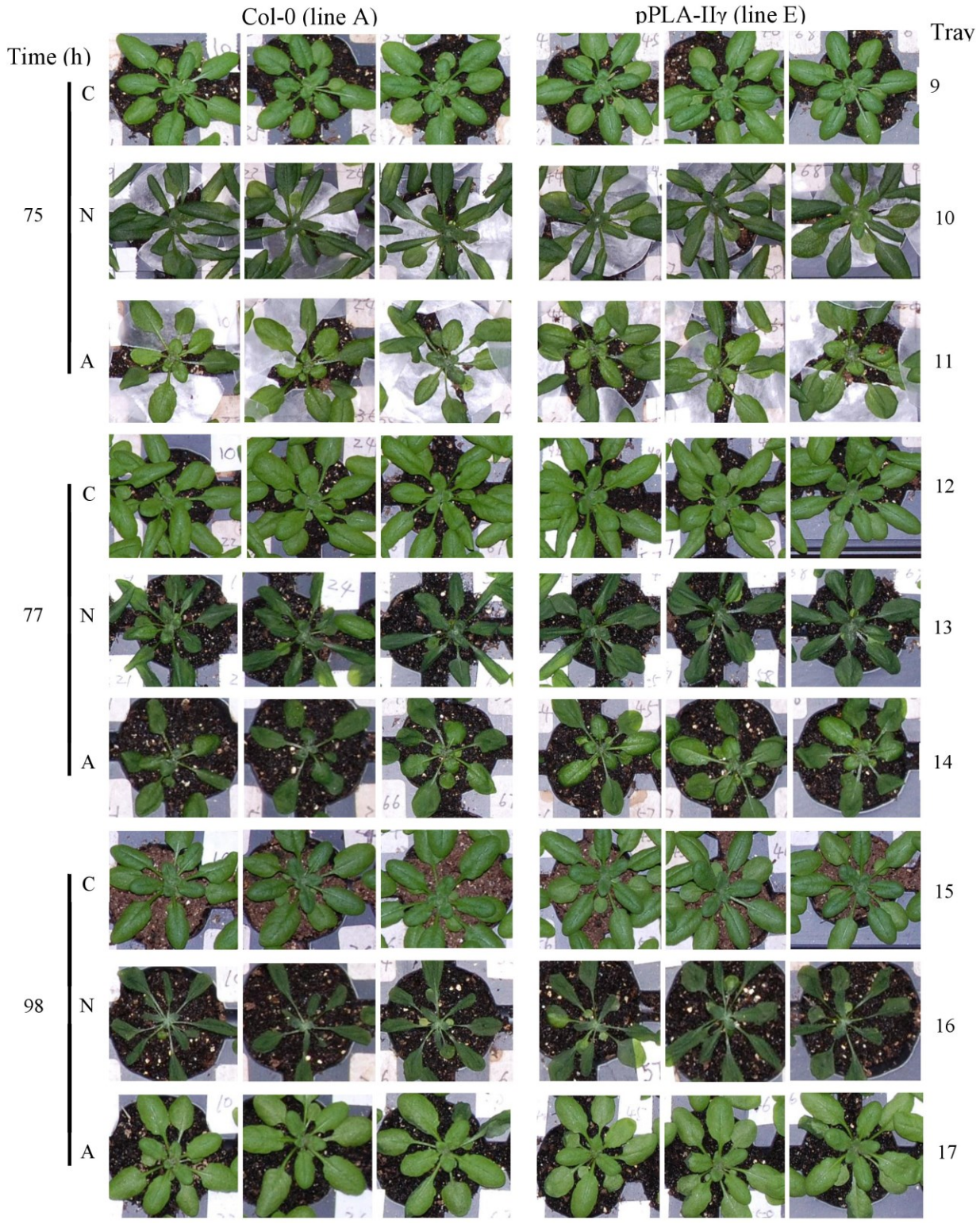
Col-0 (line A)
pPLA-IIγ (line E)
Time (h)
Tray
C
N
A
75
77
98
9
10
11
12
13
14
15
16
17

Figure 5.6 Dendrogram describing lipid co-occurrence of Col-0 plants in response to low temperature treatments.

The distance from the center to the circumference of the dendrogram represents Spearman's correlation coefficient ρ, measured by the horizontal scale in red. Only lipids with at least one $\rho > 0.6$ are shown in this dendrogram. Branches of lipids that correlate with all $\rho > 0.8$ are color-coded, labeled by a letter with the same color, from A to J, and are referred to as "clusters". Within cluster A, B, and J, branches of lipids correlate with each other with all $\rho > 0.95$ are called sub-clusters which are marked with red edges and bolded lipid names. Sub-cluster A7 is further divided into sub-cluster A7a and A7b due the difference in acyl composition. Sub-cluster A7a contains mostly acMGDG with all non-oxidized acyl groups, while sub-cluster A7b contains mostly acMGDG with two oxidized acyl groups.

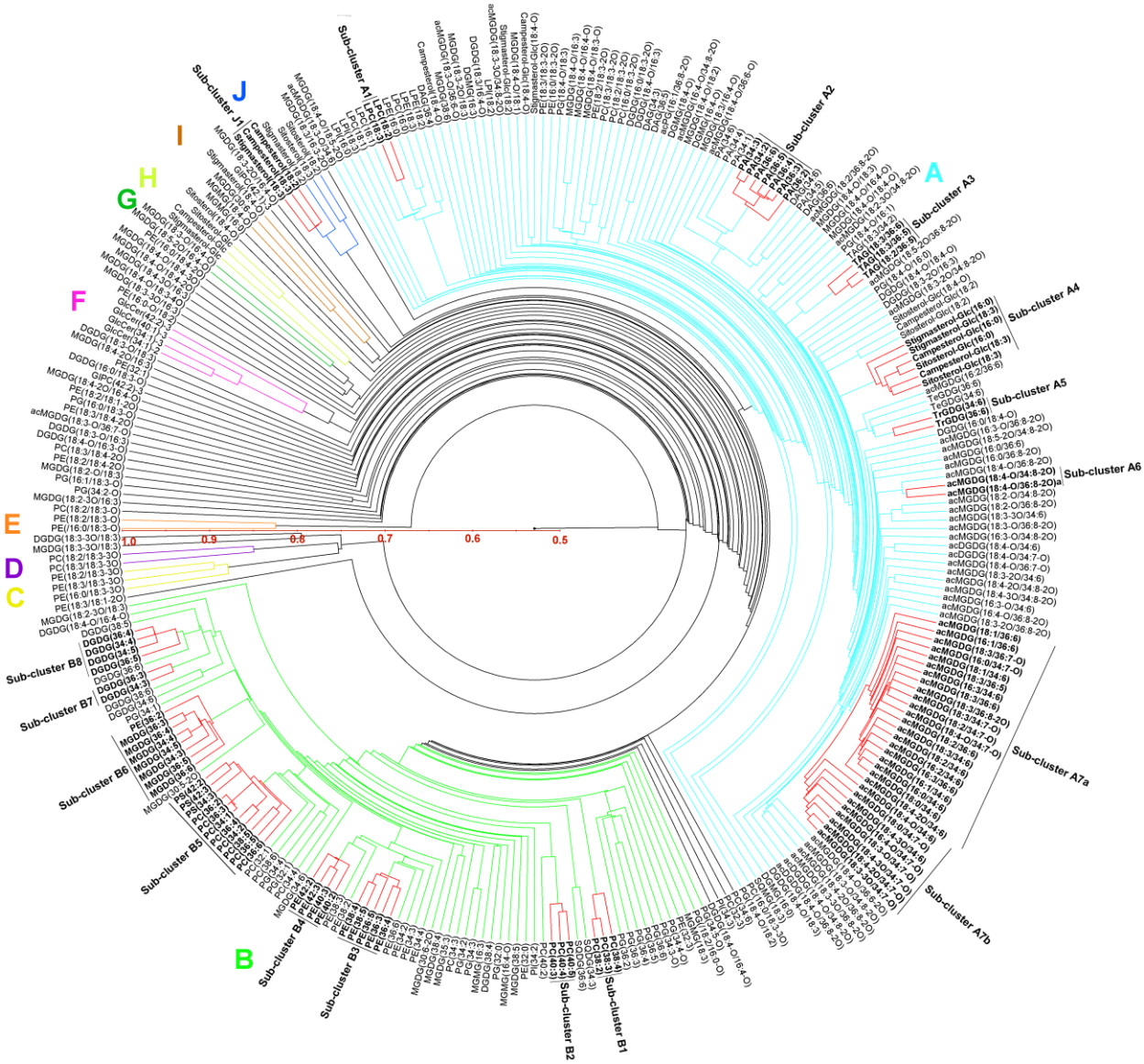
A
B
C
D
E
F
G
H
I
J
1.0
0.9
0.8
0.7
0.6
0.5
Sub-cluster A1
Sub-cluster A2
Sub-cluster A3
Sub-cluster A4
Sub-cluster A5
Sub-cluster A6
Sub-cluster A7a
Sub-cluster A7b
Sub-cluster B1
Sub-cluster B2
Sub-cluster B3
Sub-cluster B4
Sub-cluster B5
Sub-cluster B6
Sub-cluster B7
Sub-cluster B8
Sub-cluster J1

Figure 5.7 Comparisons of autoscaled lipid levels of sub-clusters between Col-0 and pPLAIIγ (line E) plants that underwent low temperature treatments., Materials and Methods). Two additional controls (last two conditions) at 22°C tested the effect of light cycle changes (time of day). Three leaves from one plant made up each sample, and five biological replicate plants were sampled for each condition.

The experimental design was influenced by previous experiments (data not shown) that demonstrated the need to minimize variation among controls and to apply treatments consistently. Variation in plant growth conditions can affect the basal levels of some oxidized lipid compounds, making comparison across multiple stress treatments difficult. Thus, an important aspect of this study was the careful limiting of variation in the control conditions; plants were grown and treated together, and care was taken to apply the stress treatments consistently. It should be noted that all treatments were sub-lethal to the plants. Arabidopsis accession Columbia is resistant to *Pst*Avr, with *Pst*Avr causing a hyper-sensitive response, which occurred within the first 12 h of inoculation. Bacterial growth in plants treated with *Pst*Avr between 12 and 24 h of infection was not significant. In contrast, Arabidopsis accession Col-0 is susceptible to *Psm*. Bacterial numbers increased 18-fold between 12 and 24 h after *Psm* infection (Figure S2.2). By 72 hour-post-inoculation (hpi), the *Psm*-inoculated leaves were chlorotic and eventually died.

For all treatments, harvested leaves were immediately extracted with solvents. To quantitatively compare the pattern of oxidized lipids in various stresses, the amount of each oxidized lipid detected in the precursor scans was normalized to the signal of an internal standard, 18:0/16:0 MGDG, and then divided by the dry mass of the extracted tissue. A normalized mass spectral signal of 1 indicates the same amount of signal produced by 1 nmol of internal standard. A single internal standard was used because of the impracticality of obtaining internal standards similar in structure to each of the oxidized lipid components. Normalizing to the signal of an internal standard corrected for any variation in response that might occur due to variable ion suppression among samples. Because the amount of mass spectral signal depends on the scan mode employed and the ability of individual compounds to undergo ionization and

fragmentation, the normalized signal can be considered only a ball-park estimate of ox-lipid level (in nmol normalized to dry mass). Normalized mass spectral signal per dry mass is an appropriate value for comparison of oxidized lipid species levels among samples and for qualitative comparison of the levels of various compounds within different samples.

Total Oxidized Lipid Accumulation as a Function of Stress

The entire ox-lipid dataset is available as Table S2.5, as individual sample values, and in Table S2.6 as averages. Total oxidized lipid levels, represented by total bar heights in Fig. 3A, were similar in all control conditions. In addition, cold acclimation at 4°C and infection with virulent pathogen *Psm* for 12 h did not produce significant changes in overall oxidized lipid amounts. Wounding produced a high level of total oxidized lipids (6.1 times the average basal signal level) within 15 min, with decreased levels seen at 45 min and a further decrease at 6 h. *Pst*Avr infection produced the highest levels of lipid oxidation (13.8 times the average basal level), but the oxidized lipids were produced much more slowly, with levels increasing between 12 and 24 h of infection. Thus, as previously shown by Andersson et al. (2006), an avirulent strain of *Pseudomonas syringae* was able to induce high levels of oxidized lipids. Although *Psm* damaged the plants severely, infection with this pathogen for 24 h caused a relatively small increase in total oxidized lipid signal (2.0 times the average basal level). Freezing also produced only a very modest accumulation of oxidized membrane lipids (1.2 times the average basal level). Per mg of dry mass, the treatment producing the highest ox-lipid mass spectral signal (*Pst*Avr infection for 24 h) produced the same amount of mass spectral signal as 4.3 nmol of internal standard (18:0/16:0 MGDG) while control samples, on the average, produced approximately the same amount of mass spectral signal as 0.5 nmol of internal standard. In comparison, on the average, the normal-chain phospholipids and galactolipids in these samples produced the same amount of mass spectral signal as 259 nmol of internal standards. The entire normal-chain lipid dataset is available as Table S2.7, as individual sample values, and in Table S2.8 as averages.

Patterns of Oxidized Lipid Accumulation as a Function of Stress

Figure 2.3 and Figure 2.4 display key aspects of the ox-lipid data. Figure 2.3 shows the oxidized lipid levels during each stress condition, emphasizing differences in amount and compositional pattern. Each color within the bars in Figure 2.3A represents the total signal from an oxidized lipid (ox-lipid) head group class. The components within each ox-lipid class are shown in Figure 2.3, panels B-G. Compositional patterns vary among stresses, with ox-MGDG and ox-DGDG predominating in wounding stress, while ox-acMGDG and ox-PG are more elevated in *Pst*Avr stress. More details of the ox-lipid changes during each stress are described in the following sections.

Figure 2.4 shows the individual signals of each oxidized lipid under each stress condition (black bar height), along with the average levels of oxidized polar lipids in the 22°C control samples (i.e., average basal levels, white bar height). Figure 2.4 indicates the changes that are statistically significant at $p < 0.05$, after correction for the False Discovery Rate (FDR). Data from control and other samples with only low levels of ox-lipids are in Figure S2.3. Among the 22°C and 4°C control samples, there were no significant differences in levels of any oxidized lipid. The mock-inoculated control samples had just slightly elevated levels of several oxidized lipid species (Figure S2.3).

Patterns of Oxidized Lipid Accumulation in Wounding

Wounding quickly induced a number of oxidized lipids (Figure 2.3 and Figure 2.4A-C). Among ox-PC and ox-PE molecular species, significant increases were observed for **4** and **5** (18:3-2O-containing PCs), which increased approximately four-fold at 15 and 45 min, respectively, after wounding, while other ox-PC and ox-PE species were unchanged. PGs, DGDGs, and MGDGs containing 18:4-O and 18:3-2O fatty acyl chains were rapidly induced. Ox-PG, ox-DGDG, and ox-MGDG species that were induced at least 30-fold, and were highest at 15 min and lowest at 6 h, included **25** (Table 2.2 for peak information), 18:4-O/16:1 PG; **26**, 18:4-O/16:0 PG; **34**,18:4-O/16:0 DGDG; **37**, 18:4-O/18:4-O DGDG; **42**, 18:3-O/18:4-O DGDG; **47**, 18:3-2O/18:4-O DGDG; **49**, 18:4-O/16:4-O MGDG; **51**, 18:4-O/18:4-O MGDG; **57**, 18:3-2O/16:4-O MGDG; and **59**, 18:3-2O/18:4-O MGDG. Galactolipid species with two oxidized acyl chains, 18:4-

O/18:4-O DGDG (**37**), 18:4-O/16:4-O MGDG (**49**), and 18:4-O/18:4-O MGDG (**51**) correspond to the formulas for arabidopsides D, A, and B, respectively. The other compounds, except **34** and **42**, were previously identified as OPDA- and/or dnOPDA-containing species (references in Table 2.2). Among the rapidly induced group, 6 h after wounding, the level of 18:4-O/16:4-O MGDG (**49**) was reduced to 15% while 18:4-O/18:4-O DGDG (**37**) was at 10% of its peak level at 15 min after wounding.

Additionally, large quantities of ox-acMGDGs were rapidly generated during wounding. Ox-acMGDG levels were more stable than levels of non-acylated ox-galactolipid species containing multiple oxidized fatty acyl chains. Between 15 min and 6 h after wounding, the level of the ox-acMGDG with the highest signal (**71**) varied less than 20%; the 6 h level was 1.1 times the 15 min level. Meanwhile, the signal of the most abundant non-acylated oxidized MGDG (**49**) at 6 h dropped to 15% of its 15 min signal. Thus, acMGDG formed a larger fraction of the total ox-lipid species at 6 h (41%) than at 15 min (16%) after wounding, because of its apparent stability in this time frame. The time course for formation of oxidized MGDGs and oxidized acMGDGs during wounding is shown in Figure S2.4A. In wounding, ox-acMGDG species corresponding to arabidopsides E (18:4-O/18:4-O/16:4-O acMGDG, major component of **71**) and G (18:4-O/18:4-O/18:4-O acMGDG, **74**) predominated among ox-acMGDGs, but 25-30% of the overall signal detected for ox-acMGDGs in wounding was due to previously undetected species. Those significantly induced include species with three oxidized acyl chains (**82** and **84**), with two oxidized acyl chains and one normal chain (**65**, **66**, **68**, **69**, **70**, **72**, **78**, **80**, and **85**), and with only one oxidized acyl chain (**61**). In wounding, the most abundant of the "minor" acylated species (behind **71** and **74** in abundance) was 18:4-O/16:4-O/16:0 acMGDG (**66**).

Patterns of Oxidized Lipid Accumulation in Bacterial Infection

Figure 2.3 and Figure 2.4D and E show ox-lipids formed upon infection with *Pst*Avr, and Figure 2.4F shows the ox-lipids formed upon infection with *Psm*. *Pst*Avr infection generated significant increases in 34 species of oxidized lipids at 12 h and in 63 species at 24 h, including some oxidized lipids in every class.

Three PC species that contain 18:3-O (**2**) and 18:3-2O (**5**, **6**) were induced significantly in *Pst*Avr infection, while PE species containing both 18:3-O and 18:3-2O (**13**, **14**, **15**, **16**, **18**) were also increased. Interestingly, 16:0/18:2-2O PE, 18:3/18:2-2O PE and 18:2/18:2-2O PE (**22**, **23**, **24**), which are present at low and similar concentrations in all other treatments and controls, *decreased* significantly at the 24 h time point of *Pst*Avr treatment as compared to the basal level.

Every detectable ox-PG also increased in *Pst*Avr infection at 24 h. ox-DGDG species containing 18:4-O (**33**-**37**) and 18:3-2O species (**43**-**47**) were increased, while none of the ox-DGDG species containing 18:3-O (**38**-**42**) were increased. Major non-acylated ox-MGDGs containing 18:4-O (OPDA) or 16:4-O (dnOPDA) (e.g., **48**-**51**) were significantly increased, along with several additional MGDG species. Twenty-six of the 27 ox-acMGDG species were significantly increased. Besides 18:4-O/18:4-O/16:4-O acMGDG (arabidopside E, major component of **71**) and 18:4-O/18:4-O/18:4-O acMGDG (arabidopside G, **74**), the species with the highest signals included 18:4-O/16:4-O coupled with 16:3, 16:0, 16:4-O, 18:3, 18:1, and 18:0 (**64**, **66**-**70**, respectively), 18:4-O/18:4-O/18:3 (**72**), and 18:3-2O/18:4-O/18:3 (**85**) acMGDGs. The time course for formation of oxidized MGDGs and oxidized acMGDGs during *Pst*Avr infection is shown in Figure S2.4B.

The non-acylated oxidized MGDGs (**49**, **51**) with the highest levels were slightly over twice as high at 24 h after *Pst*Avr infection, compared to 12 h after infection. Even so, they were only 50% and 70%, respectively, as high in *Pst*Avr infection at 24 h as at the highest level in wounding (15 min). Our observation of the prolonged presence of non-acylated oxidized MGDGs in *Pst*Avr infection was in contrast to the data of Kourtchenko et al. (2007), who found that these species dropped to basal levels by 24 h after infection with avirulent bacteria.

In comparison, the levels of **71** (includes 18:4-O/18:4-O/16:4-O; arabidopside E) and **74** (18:4-O/18:4-O/18:4-O acMGDG; arabidopside G) increased about 4-fold between 12 h and 24 h after *Pst*Avr infection. **71** was more than 7-fold higher at 24 h after *Pst*Avr infection than at the highest level in wounding. The very high induction of arabidopside E in avirulent bacterial infection is consistent with the data of Andersson et al. (2006) and Kourtchenko et al. (2007).

However, similar to their observation with **49** and **51**, Kourtchenko et al. (2007) observed that arabidopsides E and G (**71**, **74**) peaked early and decreased by 8 h post-inoculation. A potential cause of the different results may be that, in the work of Kourtchenko et al. (2007), leaf discs were punched immediately following *Pst* inoculation and were incubated in water until harvest, while in our study, leaves remained on the plants until harvest. It is possible that the continued production of oxidized membrane lipids requires the tissues to be attached.

Psm infection showed a tendency to generate oxidized complex polar lipids, but the amounts were much lower than in wounding or *Pst*Avr infection and no increases for any molecular species were significant (Figure 2.3, Figure 2.4F). This occurred even though the plants were seriously affected by *Psm* infection, and eventually the infected leaves died. The time course for formation of oxidized MGDGs and oxidized acMGDGs during *Psm* infection is shown in Figure S2.4C.

Patterns of Oxidized Lipid Accumulation in Freezing

Ox-lipid profiles of leaves of plants subjected to freezing at -8°C after cold acclimation are shown in Figure 2.3 and Figure 2.4G. Freezing induced the formation of a relatively low amount of ox- lipids. Only 18:4-O/16:4-O MGDG (**49**) was significantly increased compared to the cold-acclimated control (4°C, 84 h). This ox-galactolipid species increased 6.1-fold. Levels of acMGDGs with oxidized acyl chains during freezing were very low.

Other Stress-Associated Lipids

For comparison with ox-lipids, levels of several lipid hydrolysis products were also determined. The time courses of PA production in wounding, *Pst*Avr infection, and *Psm* infection are shown in Figure S2.4D, E, and F, respectively. Levels of lysophosphatidylcholine (LPC), lysophosphatidylethanolamine (LPE), and phosphatidic acid (PA) for the various control and stress treatments are shown in Figure S2.5. Only two treatments, PstAvr, 12 h and Freezing (-8°C, 2 h), induced significant increases in total LPC and LPE. PA was induced more than LPC

and LPE with significant accumulation at each time point in wounding, *Pst*Avr, and freezing stress. In *Pst*Avr infection, PA accumulation occurred later than did LPE and LPC. The data clearly indicate that freezing stress was much more effective in producing PA than in producing ox-lipids (Figure S2.5 compared with Figure 2.4).

Discussion

Several trends in the profiles of the lipid metabolites are apparent. First, there was a clear difference between the amount of stress induction of lipids originating in plastids, i.e. ox-PGs, ox-DGDGs, ox-MGDGs, and ox-acMGDGs, and lipids originating in the endoplasmic reticulum, i.e., ox-PCs and ox-PEs. Levels of extraplastidic ox-lipids, i.e. ox-PCs and ox-PEs, changed subtly in response to the examined stresses while plastidic oxidized lipid pools were highly responsive (Figure 2.3 and Figure 2.4). Second, the acyl species in different lipid classes differed. 18:4-O (consistent with being OPDA) and 16:4-O (dnOPDA) were found only in the plastidic lipid classes (PG, MGDG, DGDG, and acMGDG), while 18:2-O and 18:2-2O were found only in PC, PE, and PG (Table 2.2 and Tables S2.3 and S2.4). Fatty acyl chains with the formulas 18:3-O and 18:3-2O were found in all the diacyl lipid classes. acMGDG molecular species were very diverse (Table S2.4), although 18:4-O (OPDA) was very prominent. In some cases, such as with 18:2-O and 18:2-2O, the limitation on distribution is likely to be the limited distribution of the corresponding normal-chain lipids (i.e. 18:2 is rare in galactolipids), while in other cases, the distribution likely reflects the localization of key enzymes in the oxidization reactions; e.g. OPDA is not found in PC and PE because enzymes required for its formation, such as allene oxide synthase, are plastid-localized (Ferro et al., 2003; Vidi et al., 2006; Ytterberg et al., 2006). Third, particularly for the plastidic lipids, the induced pools were different compositionally than the basal lipid pools (compare Figure 2.3 and Figure 2.4 with Figure S2.3). This can also be seen in Figure 2.5, which summarizes our findings. Basal pools were rich in diacyl galactolipids with one oxidized acyl chain (Buseman et al., 2006; Figure S2.3), while induced pools were richer in ox-acMGDG and diacyl galactolipids with two oxidized acyl chains (Buseman et al., 2006; Figure 2.4). Fourth, the induced pool composition varied with time. For example, plastidic diacyl ox-lipids, as exemplified by ox-MGDG (Figure

S2.4), were formed very rapidly in wounding stress, while ox-acMGDGs were formed more slowly. The data are consistent with the conversion of ox-MGDG to ox-acMGDG by a transacylation reaction involving the transfer of an acyl chain from MGDG to the 6-position on the galactose ring of a second MGDG molecule, as demonstrated in spinach for normal-chain MGDGs by Heinz (1967b). It appears that in Arabidopsis this reaction occurs preferentially between oxidized galactolipid species, rather than among the total MGDG pool, although the data suggest that other fatty acids found in galactolipids (particularly 16:0) can be transferred. Fifth, the amount and composition of the stress-induced pool depended on the stress treatment (Figure 2.3, Figure 2.4, and Figure 2.5). Freezing induced relatively few ox-lipids, but strongly induced production of PA (Figure 2.3, Figure 2.4, and Figure 2.5; Figure S2.5). The molecular species composition of PA induced in wounding was consistent with its origin largely in PC, but the presence of small amounts of 18:3/16:3 PA in freezing and *Pst*Avr infection suggests an origin for this species in MGDG, since the 18:3/16:3 acyl combination is not found in phospholipids (Tables S2.7 and S2.8; Figure 2.5; Welti et al., 2002). This plastidic PA may be formed by phosphorylation of DAG generated from MGDG (Moellering et al., 2010). Wounding rapidly induced high levels of plastidic ox-lipids, particularly ox-MGDGs (Figure 2.3 and Figure 2.4), while in bacterial infection acMGDGs were more prominent. The fact that essentially the full complement of induced polar lipids was produced in the first 15 min after wounding may suggest that ox-lipids (and PA) are produced mainly by the short-lived activation of existing enzymes in the wounding response. This situation contrasts with that during pathogen infection in which ox-acMGDGs were very prominent and more were formed in the second 12 h after bacterial infection than in the first 12 h (Figure 2.3, Figure 2.4, Figure 2.5; Figure S2.4), suggesting either increased activation or induction of the enzyme(s) involved in ox-acMGDG formation.

In mammalian systems, specific oxidized membrane lipids have been identified as regulators of many cell types. Oxidized animal membrane lipids mediate both beneficial and detrimental functions, including inflammation, apoptosis, phenotype switching in smooth muscle cells, and innate immunity (Deigner and Hermetter, 2008; Hazen, 2008). Specific ox-PCs regulate the expression of over 1000 genes in endothelial cells (Gargalovic et al., 2006; Berliner et al., 2009),

and data suggest that oxidized phospholipids act by binding specific receptor proteins (Deigner and Hermetter, 2008).

In plants, oxidized membrane lipids may represent alterations that have occurred to prevent oxidative damage elsewhere in the cell, they may function as mediators signaling stress responses, or they may be long-term modifications that might function as stress "memory" (Wang, 2004; Andersson et al., 2006; Hisamatsu et al., 2006; Wang et al., 2006; Gális et al., 2008; Mène-Saffrané et al., 2009). Recent work by Mène-Saffrané et al. (2009) suggested that oxidized lipids are indeed involved in preventing damage elsewhere in the cell. These authors showed that non-enzymatic oxidation of trienoic fatty acyl species, correlating with malondialdehyde production, reduced lesion spread in the oxidatively stressed disease-lesion mimic, *acd2-2*. Trienoic fatty acids were implicated as reactive oxygen species (ROS) sinks that reduce ROS levels and protect against negative ROS effects in fungal infection and chronic oxidative stress responses. The notion of oxidized lipids as signals is reasonable given the well documented roles of the oxidized free fatty acids found in membrane lipids as signals via transcriptional regulation (e.g. Taki et al., 2005; Sattler et al., 2006) and the stress-specific induction of particular ox-lipids. The involvement of intact oxidized membrane lipids in signaling is also supported by their demonstrated biological activities. For example, Andersson et al. (2006) showed that 18:4/18:4-O/16:4-O MGDG (arabidopside E; major component of **71**) had greater bactericidal activity than the same molar amount of OPDA. Hisamatsu et al. (2006) showed that 18:4-O/16:4-O MGDG (arabidopside A; **49**) promoted senescence in barley leaves. However, recently, Seltmann et al. (2010) showed that levels of six arabidopsides (**35**, **37**, **49**, **51**, **71a**, **74**) were increased when plants were placed in the dark for three days or subjected to osmotic stress with sorbitol treatment, but arabidopside levels were not increased strongly by natural senescence; these authors suggest that oxidized fatty acids related to jasmonic acid may play only a secondary role in senescence.

The current data identify "ox-lipid signatures", extending the notion of the "oxylipin signature" and the working hypothesis that these signatures reflect physiological status and affect stress response (Weber et al., 1997; Kramell et al., 2000). To better understand the importance and function of oxidized membrane lipids during plant stress responses, the occurrence and timing of

specific ox-lipid species must be documented systematically. The current work is a step toward that goal. This work lays the foundation for further, ongoing work aimed at associating the formation of specific oxidized membrane lipids with the action of specific gene products and with particular stress-response phenotypes.

Conclusion

ESI MS/MS has previously been utilized as a quick and quantitative strategy for profiling oxidized membrane lipids (Buseman et al., 2006; Maeda et al., 2008, Xiao et al, 2010). In this study, we demonstrated a direct infusion ESI triple quadrupole MS method that detects oxidized membrane lipids species that include ox-PC, ox-PE, ox-PG, ox-DGDG, ox-MGDG, and ox-acMGDG, expanding the number of compounds previously characterized by Stelmach et al. (2001); Hisamatsu et al. (2003, 2005), Andersson et al. (2006), Buseman et al. (2006), Kourtchenko et al. (2007). In particular, the data indicate that the number of acMGDGs (**60**-**86** in Table 2.2) is much larger than previously described. The precursor scanning method takes 20-25 min to analyze each sample. Together with the ESI triple quadrupole MS procedure for membrane lipid profiling (Welti et al., 2002; Devaiah et al., 2006), this analysis provides a useful foundation to investigate effects of abiotic and biotic stresses on plant lipid profiles and roles of various enzymes in responses to those stresses.

Materials and Methods

Growth Conditions and Sampling for Stress Treatments

Arabidopsis thaliana accession Columbia (Col-0) seeds were sprinkled on moist soil. The soil and seeds were placed at 4°C for 48 h before moving to a growth chamber for germination. Seedlings were covered with a plastic dome until transplantation. Seven days after germinating, 2 seedlings were transplanted to each 3.5" square pot. Plants were kept in growth chamber at a temperature of 22°C, humidity of 60%, and a photoperiod of 14/10 at 100 μmol $m^{-2}s^{-1}$. Twenty-

eight days after transplanting, which corresponds to 35 days (5 weeks) post-germination, plants were ready for treatments (5 weeks old). Each treatment or control set contained three randomly mixed pots (total of six plants with five randomly chosen plants used as biological replicate samples). Three leaves from each plant (leaf numbers 6, 7 and 8) were sampled at each time point. For all samples, the leaves were cut and immediately immersed in 3 mL isopropanol with 0.01% butylated hydroxytoluene (BHT) at 75°C for 15 min. 1.5 mL chloroform and 0.6 mL water were added and samples were then stored at -20°C until analysis.

Stress Treatments

Except for the low temperature treatment, all treatments were applied on leaf numbers 6, 7 and 8, where leaf number 1 is the first true leaf (Weigel and Glazebrook, 2002). For wounding, a piece of paper tape was wrapped around the lower side of the hemostat grip so that wounding was reproducible and uniform. Each leaf was clamped perpendicular to the mid-vein in two places about 2 cm apart. Leaves were sampled at 15 min, 45 min, and 6 h after wounding. One unwounded set of plants was sampled at the same time as the 6 h-time-point set.

For bacterial treatment, suspensions of *Pseudomonas syringae* pv. *maculicola* and *Pseudomonas syringae* pv. *tomato* DC3000 expressing the *AvrRpt2* avirulence gene at 10^7 cells/mL in magnesium chloride (10 mM) were infiltrated into the abaxial surface of leaves of plants with a 1 mL syringe. The control (mock) treatment was infiltration with 10 mM magnesium chloride. Leaves were sampled 12 h and 24 h after injection. Bacterial counting was performed on additional simultaneously infiltrated plants (six for each condition), treated identically to the plants used for lipid extraction.

In the low temperature treatment, plants were cold-acclimated at 4°C for 72 h before treatment in a freezing chamber programmed so that the temperature dropped from 4°C to -2°C in 2 h (3°C/h), stayed at -2°C for 2 h, dropped to -8°C in 6 h (1°C/h), and finally stayed at -8°C for 2 h. Freezing-treated leaves were harvested after 3 h, 27 h and 84 h of cold acclimation and after 2 h at -8°C. Plants at 22°C were also harvested at each time point.

Bacterial Counts

For bacterial counting, the pathogen-inoculated leaves (6, 7 and 8) were homogenized in a total volume of 1 mL 10 mM magnesium chloride. Ten microliters each of 10^2, 10^3 and 10^4 dilutions were streaked on 1.5 % King's agar plates containing appropriate antibiotics. *Pseudomonas syringae* pv *tomato* DC3000 with avrRpt2 (*Pst*Avr, strain PV288) was streaked on plates made with rifampicin (50 μg mL^{-1}) and kanamycin (50 μg mL^{-1}). *Pseudomonas syringae* pv *maculicola* was streaked on plates made with streptomycin (100 μg mL^{-1}). Colonies were counted after incubation for 48 h in the dark at room temperature. The leaf homogenates were lyophilized, dried in an oven at 110°C, and their masses determined.

Lipid Extraction

Lipid extraction was carried out using a combination of procedures described by Bligh and Dyer (1959) and Markham et al. (2006). Briefly, each lipid extract in isopropanol with BHT, chloroform, and water (see Growth Conditions and Sampling for Stress Treatments) was transferred to a new glass tube using a Pasteur pipette, leaving the leaves in the original tube. Four mL of chloroform-methanol (2:1) was added to the leaves, samples were shaken for 30 min, and the solvent was transferred, combining it with the first extract. The addition, shaking, and transfer steps were performed totally four times. Finally 4 mL of solvent H (the organic phase of isopropanol-hexane-water (55:20:25, v/v); Markham et al., 2006) was added to the leaf material, the samples were incubated at 60°C for 15 min, and the solvent was removed and combined with the previous extracts. This step was performed four times, combining all extracts. Finally the extracted leaves were dried in an oven at 110°C, and the extracted dry leaf mass was determined. The solvent was evaporated from the extract in a CentriVap centrifugal vacuum concentrator (Labconco, Kansas City, MO), and each sample was dissolved in 1 mL chloroform. Extracts were stored at -80°C.

Tissue Mass Determination

Extracted dry leaf mass (for extracted samples) and lyophilized leaf homogenates (for bacterial counts) were weighed on a Mettler Toledo AX balance (GmbH, Greifensee, Switzerland) that provided mass data to the nearest 2 µg. To determine precision, a dried leaf sample was weighed 7 times, indicating mass of 4.095 mg with a standard deviation of 0.007 mg (0.17%). To determine accuracy, six brass weights with official masses ranging from 1 to 20 g were weighed. The balance weighed, on average, 0.17% (standard deviation 0.08%) too high. Taken together, the data indicate that weighing dried leaf tissue was not a major source of error in quantifying the compounds in the leaves.

Extracts used for QTOF and FTICR MS Analysis and Fractionation for QTOF Analysis

Crude extracts from all replicate samples of ***Pst*Avr, 24 h** or **Wounded, 15 min** treatment were combined for FTICR MS analysis. For lipid class fractionation and QTOF MS, *Arabidopsis thaliana* accession Columbia-0 plants were grown and infiltrated with *Pst*Avr for 24 h as described above. Total lipid was bulk-extracted by the combined extraction method (Bligh and Dyer, 1959; Markham et al., 2006; above). Total unfractionated lipid extract was used for QTOF analysis or fractionation. Fractionation of lipid classes was carried out as described by Buseman et al. (2006). Briefly, activated silicic acid (Unisil, Clarkson Chemical, Williamsport, PA) in chloroform was packed into a 1.5 cm diameter column (40 mL column volume). Total lipid extract from 150 mg leaf dry mass in 15 mL chloroform was applied to the column, and the column was batch-eluted in five fractions: fraction 1, 200 mL of chloroform:acetone (1:1, v/v); fraction 2, 400 mL of acetone; fraction 3, 400 mL of chloroform:methanol (19:1, v/v); fraction 4, 400 mL of chloroform:methanol (4:1, v/v); and fraction 5, 800 mL of chloroform:methanol (1:1, v/v). Each fraction was evaporated and re-dissolved in 15 mL chloroform.

Triple Quadrupole MS Analysis of Ox-lipids

Samples were prepared for mass spectral analysis by diluting a volume of each unfractionated lipid extract (in chloroform) derived from approximately 0.2 mg of leaf dry mass. An internal standard, 2.008 nmol 18:0/16:0 MGDG (a component of hydrogenated MGDG, Matreya LLC, Pleasant Gap, PA) was added to each sample, and the sample was diluted such that the final volume was 1.2 mL and the solvent composition was chloroform-methanol-300 mM ammonium acetate in water (300:665:35, v/v/v). Scans for precursors of 291.2, 293.2, 295.2 and 283.2 (for the 18:0 component of the internal standard) were carried out in negative mode, using a triple quadrupole mass spectrometer (ABI 4000, Applied Biosystems, Foster City, CA) equipped with an ESI source. The samples were directly infused at 30 µL per min. For precursor scans, the parameters were: collision gas, 2 (arbitrary units); curtain gas, 20 (arbitrary units); ion source gases 1 and 2, 45 (arbitrary units); ion spray voltage, -4500 V; source temperature, 100°C; declustering potential, -100 V; entrance potential, -10 V; collision energy, -45 V; collision cell exit potential, -20 V; and the interface heater, "on". Spectra for precursors of 291.2, 293.2 and 295.2 were acquired from 700 to 1150 *m/z* at 6 s/cycle for 65 cycles. The precursor spectrum for the internal standard (*m/z* 283.2) was acquired from 800 to 825 *m/z* at 0.5 s/cycle for 65 cycles.

A custom Analyst "add-on", supplied by Applied Biosystems and called "MultiplePeriodProcessing", was used to process and export data from Analyst to Excel. Precursor spectra generated by the triple quadrupole MS were smoothed by the software, with a smoothing option of 0.4 for previous and next point weight and 1 for current point weight, and baseline subtracted with a window width of 20 u. Peaks with intensity values lower than 50 counts per s were removed before spectra were exported as peak lists. Once exported, target *m/z* of peaks 1-86 were looked up in the appropriate precursor spectra with an *m/z* tolerance of ±0.4 from the theoretical *m/z* for the peak/compound listed in Table 2.2. Peak intensity was corrected for isotopic distribution of precursor ions minus the fragment ion (i.e. for isotopic distribution within each spectrum).

Mass spectral signals (intensities) were normalized to the signal for 2.008 nmol internal standard,18:0/16:0 MGDG, as its $[M + C_2H_3O_2]^-$ ion. 18:0/16:0 MGDG is an unnaturally occurring lipid species that was added as an internal standard to the portion of the sample being analyzed. Mass spectral signal was normalized by the following formula: (Mass spectral

intensity of each lipid molecular species x Amount of the internal standard in nmol) ÷ (Mass spectral intensity of internal standard). Thus, a signal of 1 is the same amount of signal produced by 1 nmol of internal standard, 18:0/16:0 MGDG. Finally, the data were corrected for isotopic overlap due to the fatty acyl portions (fragment ions), adjusted to account for the fraction of sample analyzed, and normalized to the sample dry mass to give the "normalized mass spectral signal per dry mass". No corrections for varying mass spectral response to the various molecular species were applied. The calculated data are appropriate for direct comparison among samples. Samples were initially analyzed as soon as extraction was complete; however, extended storage at -80°C of samples containing BHT (added at the first step of the extraction), followed by re-analysis, suggests that most ox-lipids are quite stable.

Triple Quadrupole MS Analysis of Normal-Chain Lipids

Samples were prepared for mass spectral analysis by diluting a volume of each unfractionated lipid extract (in chloroform) derived from approximately 0.2 mg of leaf dry mass. Precise amounts of internal standards, obtained and quantified as previously described (Welti et al., 2002), were added as described by Xiao et al. (2010). The sample and internal standard mixture was combined with solvents, such that the ratio of chloroform/methanol/300 mM ammonium acetate in water was 300/665/35, and the final volume was 1.2 ml. Sample introduction was as for ox-lipids. Sequential precursor and neutral loss scans of the extracts were carried out as described by Xiao et al. (2010) except that only limited *m/z* ranges around the target *m/z*s of the analytes and internal standards were scanned. The scan speed was 100 u per s. For each spectrum, 20 to 150 continuum scans were averaged in multiple channel analyzer (MCA) mode. The spectral data were smoothed and the baseline subtracted. Peaks with intensity values lower than 50 counts per s were removed, peak areas integrated, and data exported as peak lists.

LipidomeDB Data Calculation Environment (Zhou et al., 2011) was used to locate target compound peak data, deconvolute isotopes, and quantify lipids in each class in comparison to the two internal standards of that class (Brügger et al., 1997; Welti et al., 2002). Correction for chemical and/or instrumental noise was performed as previously described (Xiao et al., 2010).

Finally, the data were corrected for the fraction of the sample analyzed and normalized to the sample "dry weights" to produce data in the units nmol/mg.

QTOF MS Analysis

*Pst*Avr 24-h infection extract and fractions from its silicic acid column separation (described above) were dissolved in chloroform at a concentration of 10 mg dry tissue mass per mL. For product ion analysis, aliquots were combined with solvents (chloroform-methanol-300 mM ammonium acetate in water, v/ v/v, 300:665:35) so that the final concentrations were 0.33 to 2.5 mg leaf dry mass/mL.

Spectra were acquired on an MDS SCIEX/Applied Biosystems QStar Elite hybrid QTOF MS (Applied Biosystems), with daily calibration of the instrument using a lipid standard mixture. Samples were introduced by continuous infusion into the ESI source at a rate of 30 μL per min using the integrated Harvard syringe pump. MS/MS product ion scans were carried out in negative ionization mode, with individual fragmentation of anions of oxidized PC, PE, PG, DGDG, MGDG, and acMGDG intact lipid species that had been detected from triple quadrupole MS precursor scans. PC species were analyzed by fragmentation of $[M + C_3H_3O_2]^-$ ions in the unfractionated extract. PE and PG species were analyzed by fragmentation of $[M - H]^-$ ions in the unfractionated extract and silicic acid-separated fraction 5. MGDG and DGDG species were analyzed by fragmentation of $[M - H]^-$ and/or $[M + C_3H_3O_2]^-$ ions in the unfractionated extract and, additionally for MGDG species, silicic acid-separated fraction 2. acMGDG species were analyzed by fragmentation of $[M + C_3H_3O_2]^-$ ions in the unfractionated extract and silicic acid-separated fraction 1. Resultant acyl anion fragments allowed identification of acyl moieties in intact lipids. The ion spray voltage was set at -4.5 kV, the source temperature at 150°C, the curtain gas at 25 (arbitrary units), and the ion source gases at 20 and 30 (arbitrary units). The declustering potential was -80 V, the declustering potential 2 was -15 V, and the focusing potential was -300 V. The collision gas, nitrogen, was set at 4 (arbitrary units), and the collision energy ranged from 40 to 70 V. Data at each fragmentation mass were collected over the range of *m/z* 100 to 1150, resulting in 300 to 1800 cumulative scans during acquisition for 5 to 30 min.

Data were collected and smoothed using the Analyst QS 2.0 software. Accurate masses of the product ions were determined to ten thousandths of a mass unit.

FTICR MS Analysis

Accurate *m/z* data were collected using small *m/z* windows, which optimize sensitivity (Southam et al., 2007). Briefly, samples at a concentration of 0.014 mg dry mass per mL were analyzed using direct infusion electrospray ionization on LTQ FTICR hybrid linear quadrupole ion trap Fourier transform ion cyclotron resonance mass spectrometer (Thermo Finnigan, Bremen, Germany). The ESI source was operated in positive mode with spray voltage of 2.8 kV, a tube lens offset of 140 V and a capillary temperature of 200°C. The instrument was calibrated using an automatic routine based on a standard calibration solution containing caffeine, peptide MRFA, and Ultramark 1621 (all products of Sigma-Aldrich, St. Louis, MO). The 700 to 1200 *m/z* range was divided into multiple 30 *m/z* selected ion monitoring (SIM) intervals with 5 *m/z* overlaps at both ends. Each interval was scanned for 2 min (approximately 10 scans) using SIM MS target automated gain control value 2×10^5 of accumulated ions with a resolution R = 500,000 at *m/z* 400. FTICR mass spectra from individual scans within a mass interval were averaged using the Xcalibur 2.0 software, and peaks with average counts greater than 1000 were exported to Excel 2010.

Statistical analysis

Significance was determined at a level of $p < 0.05$, after correcting for the FDR, using Excel 2010. Comparisons were between stress samples and their controls.

Acknowledgements

The authors would like to thank Gail Ragan for helpful suggestions. We are grateful to Mark Ungerer for generously allowing us to use his freezing chamber.

References

Andersson MX, Hamberg M, Kourtchenko O, Brunnström A, McPhail KL, Gerwick WH, Göbel C, Feussner I, Ellerström M (2006) Oxylipin profiling of the hypersensitive response in *Arabidopsis thaliana*. Formation of a novel oxo-phytodienoic acid-containing galactolipid Arabidopside E. J Biol Chem **281:** 31528-31537

Berliner JA, Leitinger N, Tsimikas S (2009) The role of oxidized phospholipids in atherosclerosis. J Lipid Res **50(Supplement):** S207–S212

Bligh EG, Dyer WJ (1959) A rapid method of total lipid extraction and purification. Can J Biochem Physiol **37:** 911-917

Böttcher C, Weiler EW (2007) *cyclo*-Oxylipin-galactolipids in plants: occurrence and dynamics. Planta **226:** 629-637

Brügger B, Erben G, Sandhoff R, Wieland FT, Lehmann WD (1997) Quantitative analysis of biological membrane lipids at the low picomole level by nano-electrospray ionization tandem mass spectrometry. Proc Natl Acad Sci USA **18:** 2339-2344

Buseman CM, Tamura P, Sparks AA, Baughman EJ, Maatta S, Zhao J, Roth MR, Esch SW, Shah J, Williams TD, Welti R (2006) Wounding stimulates the accumulation of glycerolipids containing oxophytodienoic acid and dinor-oxophytodienoic acid in Arabidopsis leaves. Plant Physiol **142:** 28-39

Chehab EW, Kaspi R, Savchenko T, Rowe H, Negre-Zakharov F, Kliebenstein D, Dehesh K (2008) Distinct roles of jasmonates and aldehydes in plant-defense responses. PLoS ONE **3:** e1904

Deigner H-P, Hermetter A (2008) Oxidized phospholipids: emerging mediators in pathophysiology. Curr Opin Lipidol **19:** 289-294

Devaiah SP, Roth MR, Baughman E, Li M, Tamura P, Jeannotte R, Welti R, Wang X (2006) Quantitative profiling of polar glycerolipid species and the role of phospholipase Da1 in defining the lipid species in Arabidopsis tissues. Phytochemistry **67:** 1907-1924

Ferro M, Salvi D, Brugière S, Miras S, Kowalski S, Louwagie M, Garin J, Joyard J, Rolland N (2003) Proteomics of the chloroplast envelope membranes from *Arabidopsis thaliana*. Mol Cell Proteomics **2:** 325-345

Gális I, Gaquerel E, Panday SP, Baldwin IT (2008) Molecular mechanisms underlying plant memory in JA-mediated defence responses. Plant Cell Environ **32:** 617-627

Gargalovic PS, Imura M, Zhang B, Gharavi NM, Clark, MJ, Pagnon J, Yang WP, He A, Truong A, Patel S, Nelson SF, Horvath S, Berliner JA, Kirchgessner TG, Lusis AJ (2006) Identification of inflammatory gene modules based on variations of human endothelial cell responses to oxidized lipids. Proc Natl Acad Sci USA **103:** 12741-12746

Glauser G, Grata E, Rudaz S, Wolfender J-L (2008) High-resolution profiling of oxylipin-containing galactolipids in Arabidopsis extracts by ultraperformance liquid chromatography/time-of-flight mass spectrometry. Rapid Commun Mass Spectrom **22:** 3154–3160

Grun C, Berger S, Metther D, Mueller MJ (2007) Early accumulation of non-enzymatically synthesised oxylipins in *Arabidopsis thaliana* after infection with *Pseudomonas syringae*. Func Plant Biol **34:** 65-71

Hamberg M (1988) Biosynthesis of 12-oxo-10,15(Z)-phytodienoic acid: identification of an allene oxide cyclase. Biochem Biophys Res Comm **156:** 543-550

Hamberg M, Sanz A, Rodriguez MJ, Calvo AP, Castresana C (2003) Activation of the fatty acid α-dioxygenase pathway during bacterial infection of tobacco leaves. J Biol Chem **278:** 51796–51805

Hazen SL (2008) Oxidized phospholipids as endogenous pattern recognition ligands in innate immunity. J Biol Chem **283:** 15527–15531

Heinz E (1967a) Acylgalactosyl diglyceride from leaf homogenates. Biochim Biophys Acta **144:** 321–332

Heinz E (1967b) On the enzymatic formation of acylgalactosyl diglyceride. Biochim Biophys Acta **144:** 333–343

Heinz E, Tulloch AP (1969) Reinvestigation of the structure of acyl galactosyl diglyceride from spinach leaves. Hoppe-Seyler's Z Physiol Chem **350:** 493–498

Hisamatsu Y, Goto N, Hasegawa K, Shigemori H (2003) Arabidopsides A and B, two new oxylipins from *Arabidopsis thaliana*. Tetrahedron Lett **44:** 5553-5556

Hisamatsu Y, Goto N, Sekiguchi M, Hasegawa K, Shigemori H (2005) Oxylipins arabidopsides C and D from *Arabidopsis thaliana*. J Nat Prod **68:** 600-603

Hisamatsu Y, Goto N, Shigemori H, Hasegawa K (2006) Senescence-promoting effect of arabidopside A. Z Naturforsch [C] **61:** 363-366

Howe GA, Schilmiller AL (2002) Oxylipin metabolism in response to stress. Curr Opin Plant Biol **5:** 230-236

Imbusch R, Mueller MJ (2000) Analysis of oxidative stress and wound-inducible dinor isoprostanes F(1) (phytoprostanes F(1)) in plants. Plant Physiol **124:** 1293-1304.

Katsir L, Chung HS, Koo AJ, Howe GA (2008) Jasmonate signaling: a conserved mechanism of hormone sensing. Curr Opin Plant Biol **11:** 428-435

Kourtchenko O, Andersson MX, Hamberg M, Brunnström A, Göbel C, McPhail KL, Gerwick WH, Feussner I, Ellerström M (2007) Oxo-phytodienoic acid-containing galactolipids in Arabidopsis: Jasmonate signaling dependence. Plant Physiol **145:** 1658-1669

Kramell R, Miersch O, Atzorn R, Parthier B, Wasternack C (2000) Octadecanoid-derived alteration of gene expression and the "oxylipin signature" in stressed barley leaves. Implications for different signaling pathways. Plant Physiol **123:** 177-188

Maeda H, Sage TL, Isaac G, Welti R, DellaPenna D (2008) Tocopherols modulate extra-plastidic polyunsaturated fatty acid metabolism in *Arabidopsis* at low temperature. Plant Cell **20:** 452-470

Markham JE, Li J, Cahoon EB, Jaworski JG (2006) Separation and identification of major plant sphingolipid classes from leaves. J Biol Chem **281**: 22684-22694

Mène-Saffrané L, Dubugnon L, Chételat A, Stolz S, Gouhier-Darimont C, Farmer EE (2009) Nonenzymatic oxidation of trienoic fatty acids contributes to reactive oxygen species management in *Arabidopsis*. J Biol Chem **284:** 1702-1708

Moellering ER, Muthan B, Benning C (2010) Freezing tolerance in plants requires lipid remodeling at the outer chloroplast membrane. Science **330:** 226-228

Mueller S, Hillbert B, Dueckershoff K, Roitsch T, Krischke M, Mueller MJ, Berger S (2008) General detoxification and stress responses are mediated by oxidized lipids through TGA transcription factors in *Arabidopsis*. Plant Cell **20:** 768-785

Sattler SE, Mène-Saffrané L, Farmer EE, Krischke M, Mueller MJ, DellaPenna D (2006) Nonenzymatic lipid peroxidation reprograms gene expression and activates defense markers in Arabidopsis tocopherol-deficient mutants. Plant Cell **18:** 3706-3720

Seltmann MA, Stingl NE, Lautenschlaeger JK, Krischke M, Mueller MJ, Berger S (2010) Differential impact of lipoxygenase 2 and jasmonates on natural stress-induced senescence in Arabidopsis. Plant Physiol **152:** 1940-1950.

Southam AD, Payne TG, Cooper HJ, Arvantis TN, Viant MR (2007) Dynamic range and mass accuracy of wide-scan direct infusion nanoelectrospray Fourier transform ion cyclotron resonance mass spectrometry-based metabolomics increased by spectral stitching method. Anal Chem **79:** 4595-4602

Stelmach BA, Muller A, Hennig P, Gebhardt S, Schubert-Zsilavecz M, Weiler EW (2001) A novel class of oxylipins, *sn*1-*O*-(12-oxophytodienoyl)-*sn*2-*O*-(hexadecatrienoyl)-monogalactosyl diglyceride, from *Arabidopsis thaliana*. J Biol Chem **276:** 12832-12838

Stenzel I, Hause B, Miersch O, Kurz T, Maucher H, Weichert H, Ziegler J, Feussner I,Wasternack C (2003) Jasmonate biosynthesis and the allene oxide family of *Arabidopsis thaliana*. Plant Molec Biol **51:** 895-911

Stintzi A, Weber H, Reymond P, Browse J, Farmer EE (2001) Plant defense in the absence of jasmonic acid: the role of cyclopentenones. Proc Natl Acad Sci USA **98:** 12837-12842

Taki N, Sasaki-Sekimoto Y, Obayashi T, Kikuta A, Kobayashi K, Ainai T, Yagi K, Sakurai N, Suzuki H, Masuda T, Takamiya K, Shibata D, Kobayashi Y, Ohta H (2005) 12-oxo-phytodienoic acid triggers expression of a distinct set of genes and plays a role in wound-induced gene expression in Arabidopsis. Plant Physiol **139:** 1268-1283

Thines B, Katsir L, Melotto M, Niu Y, Mandaokar A, Liu G, Nomura K, He SY, Howe GA, Browse J (2007) JAZ repressor proteins are targets of the SCF(COI1) complex during jasmonate signalling. Nature **448:** 661-665

Thiocone A, Farmer EE, Wolfender J-É (2008) Screening for wound-induced oxylipins in Arabidopsis thaliana by differential HPLC-APCI/MS profiling of crude leaf extracts and subsequent characterization by capillary-scale NMR. Phytochem Anal **19:** 198-205

Thoma I, Loeffler C, Sinha AK, Gupta M, Krischke M, Steffan B, Roitsch T, Mueller MJ (2003) Cyclopentenone isoprostanes induced by reactive oxygen species trigger defense gene activation and phytoalexin accumulation in plants. Plant J **34:** 363-375

Vidi P-A, Kanwischer M, Baginsky S, Austin JR, Csucs G, Dörmann P, Kessler F, Bréhélin (2006) Tocopheral cyclase (VTE1) localization and vitamin E accumulation in chloroplast plastoglobule lipoprotein particles. J Biol Chem **281:** 11225-11234

Vollenweider S, Weber H, Stolz S, Chételat A, Farmer EE (2000) Fatty acid ketodienes and fatty acid ketotrienes: Michael addition acceptors that accumulate in wounded and diseased Arabidopsis leaves. Plant J **24:** 467-476

Wang X (2004) Lipid signaling. Curr Opin Plant Biol **7:** 329-336.

Wang X, Li W, Li M, Welti R (2006) Profiling lipid changes in plant response to low temperatures. Phys Plantarum **126:** 90-96

Weber H, Vick BA, Farmer EE (1997) Dinor-oxo-phytodienoic acid: a new hexadecanoid signal in the jasmonate family. Proc Natl Acad Sci USA **94:** 10473-10478

Weigel D, Glazebrook J (2002) Arabidopsis: A laboratory manual. Cold Spring Harbor Laboratory Press, New York

Welti R, Li W, Li M, Sang Y, Biesiada H, Zhou H-E, Rajashekar CB, Williams TD, Wang X (2002) Profiling membrane lipids in plant stress responses. Role of phospholipase Dα in freezing-induced lipid changes in *Arabidopsis*. J Biol Chem **277:** 31994-32002

Xiao S, Gao W, Chen Q-F, Chan S-W, Zheng S-X, Ma J, Wang M, Welti R, Chen M-L (2010) Overexpression of *Arabidopsis* acyl-CoA binding protein ACBP3 promotes starvation-induced and age-dependent leaf senescence. Plant Cell **22:** 1463-1482

Ytterberg AJ, Peltier J-B, van Wijk KJ (2006) Protein profiling of plastoglobules in chloroplasts and chromoplasts. A surprising site for differential accumulation of metabolic enzymes. Plant Physiol **140:** 984-987

Zhou Z, Marepally SR, Nune DS, Pallakollu P, Ragan G, Roth MR, Wang L, Lushington GH, Visvanathan M, Welti R (2011) LipidomeDB Data Calculation Environment: Online processing of direct-infusion mass spectral data for lipid profiles. Lipids **46:** 879-884

Figure and Tables

Figure 2.1 ESI triple quadrupole MS precursor ion spectra, acquired on extracts of leaves of Arabidopsis plants infected with *Pst*Avr for 24 h.

A and B, Pre 291.2. C, Pre 293.2. D, Pre 295.2. Pre 291.2 scan detects ox-lipids containing 18:4-O and 18:3-2O, Pre 293.2 scan detects ox-lipids containing 18:3-O and 18:2-2O, and Pre 295.2 scan detects ox-lipids containing 18:2-O. Peaks with labels in parentheses are $[M - H]^-$ adducts. Peak labels with no parentheses indicate $[M + C_2H_3O_2]^-$ adducts. Please note that intensity and *m/z* scales of the spectra differ. Panels A and B have breaks in the intensity axes. Details of peaks numbered 1-86 are shown in Table 2.2.

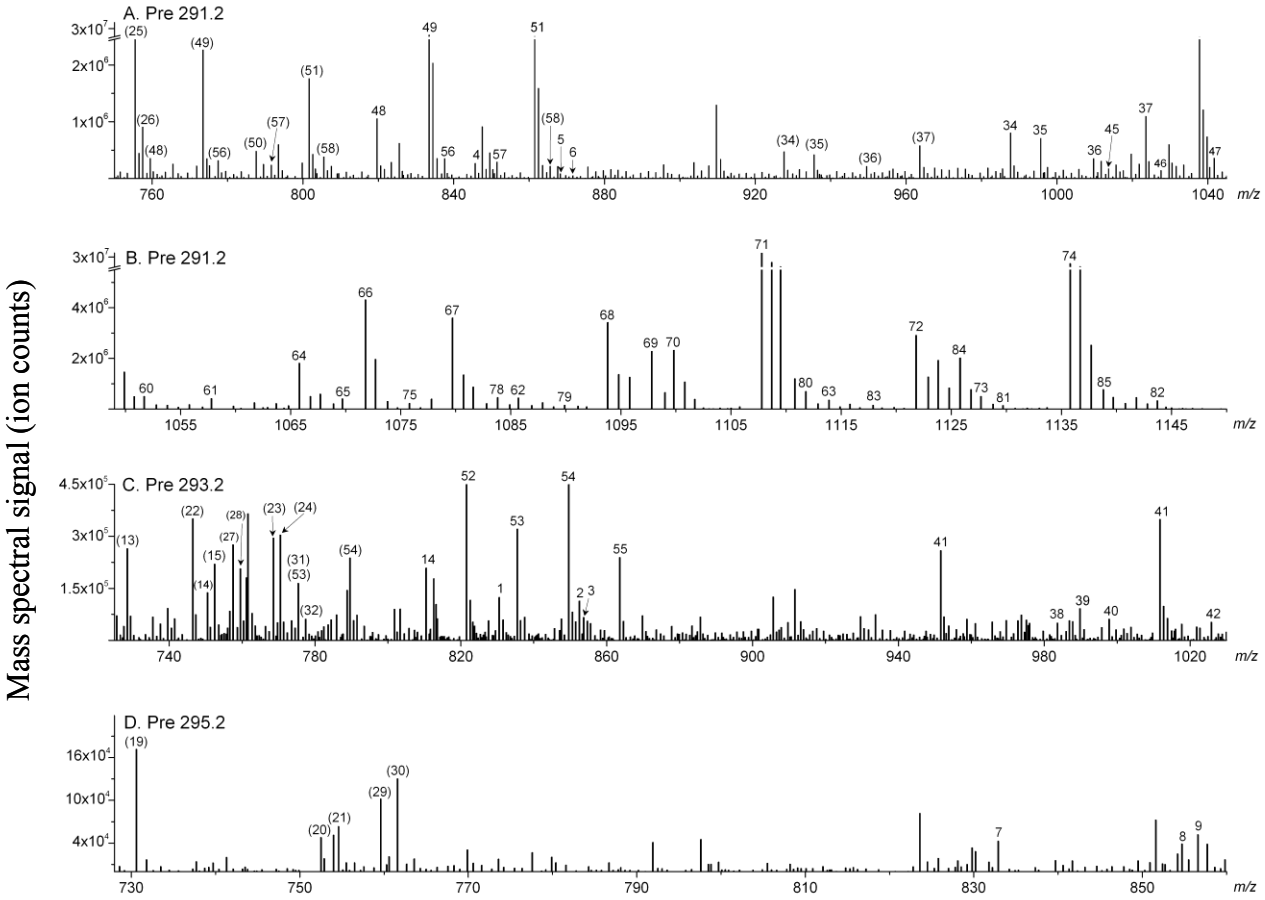

Figure 8.2 Treatments of 5 week-old wild-type Arabidopsis plants.

Each bar represents 5 plants under a single treatment, except that in the freezing treatment the plants were cold-acclimated (horizontally striped bar) at 4°C before being gradually frozen (diagonally hatched bar); see Stress Treatments in Materials and Methods. For each treatment, the white bar at the left indicates normal growth conditions, while patterned bars to the right indicate the stress conditions. The far right end of each bar indicates the harvest point. The last two samples were controls intended to identify any effects due to time of day at harvest. Total oxidized lipid signals for all samples are shown in Figure 2.3. Detailed lipid profiles of the samples indicated in bold are shown in Figure 2.4. Detailed profiles of the other samples are shown in Figure S2.3.

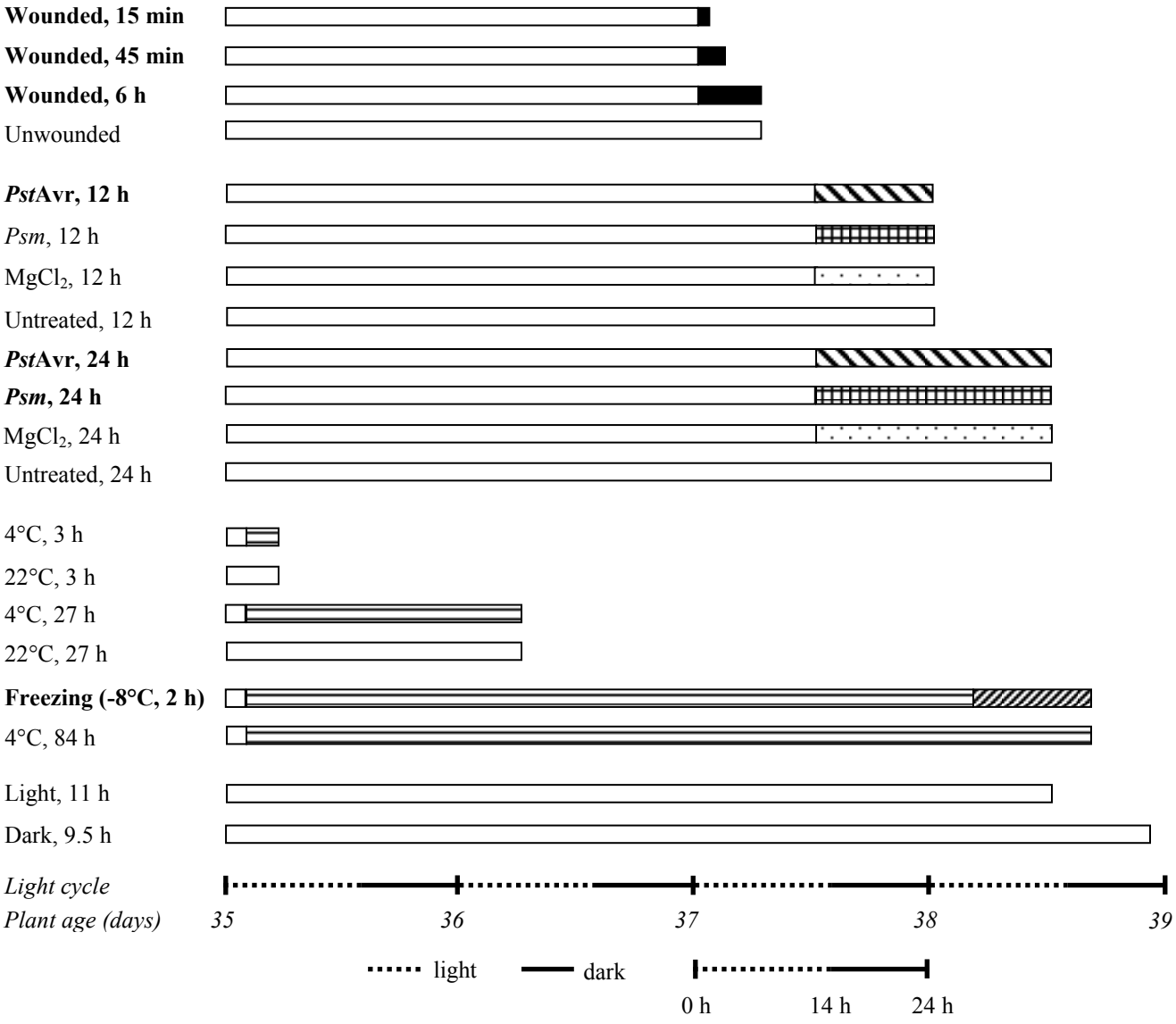

Figure 2.3 Oxidized membrane lipid levels following treatments shown in Figure 2.2.

A, Total oxidized lipids with colors indicating classes. B, ox-PC. C, ox-PE. D, ox-PG. E, ox-DGDG. F, ox-MGDG. G, ox-acMGDG. In B-G, colors indicate individual peaks detected by triple quadrupole MS precursor scanning in negative mode (Table 2.2). The size of each color-coded block represents the quantity of the ox-lipid classes (A) or of individual peaks 1–86 (B-G). Vertical axes have different scales.

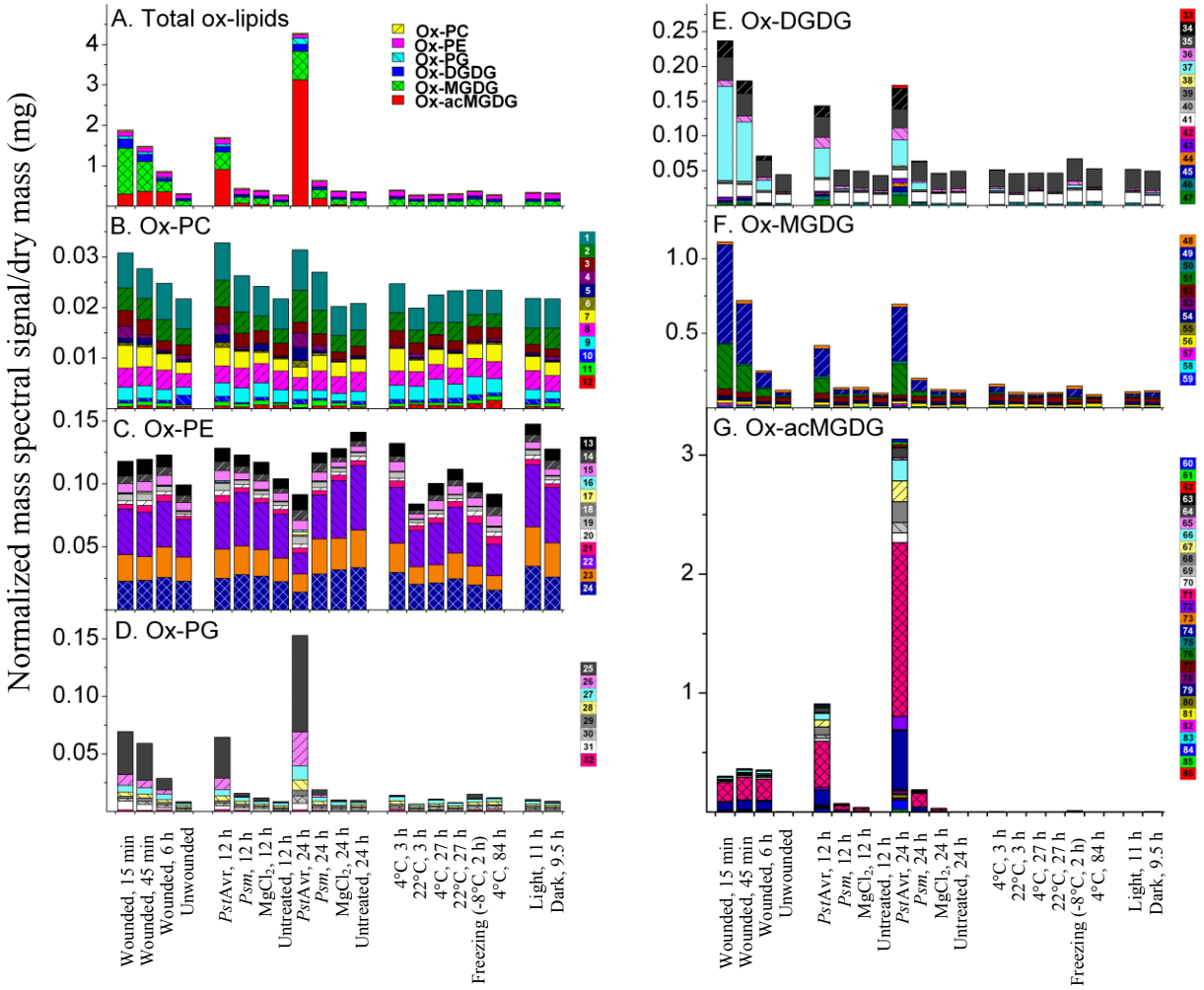

Figure 2.4 Oxidized membrane lipids under stress conditions as quantified by triple quadrupole MS precursor scanning.

A, Wounded, 15 min. B, Wounded, 45 min. C, Wounded, 6 h. D, *Pst*Avr, 12 h. E, *Pst*Avr, 24 h. F, *Psm*, 24 h. G, Freezing (-8° C, 2 h). Numbers along top *x*-axis refer to peaks/compounds in Table 2.2. In each panel, the white bars denote the basal amount as determined under the corresponding control condition: Unwounded, for A, B, and C; $MgCl_2$, 12 h, for D; $MgCl_2$, 24 h, for E and F; and 4° C, 84 h, for G. The black bars denote the amount of each ox-lipid measured in each stress treatment. Both white and black bars start at the *x*-axis. The smaller of the white and black bars is "in front" of the other bar. Increments on the vertical scales of panels A and B (below break) and C are the same; so are those on panel D and E (below break). $p < 0.05$, $n = 5$.

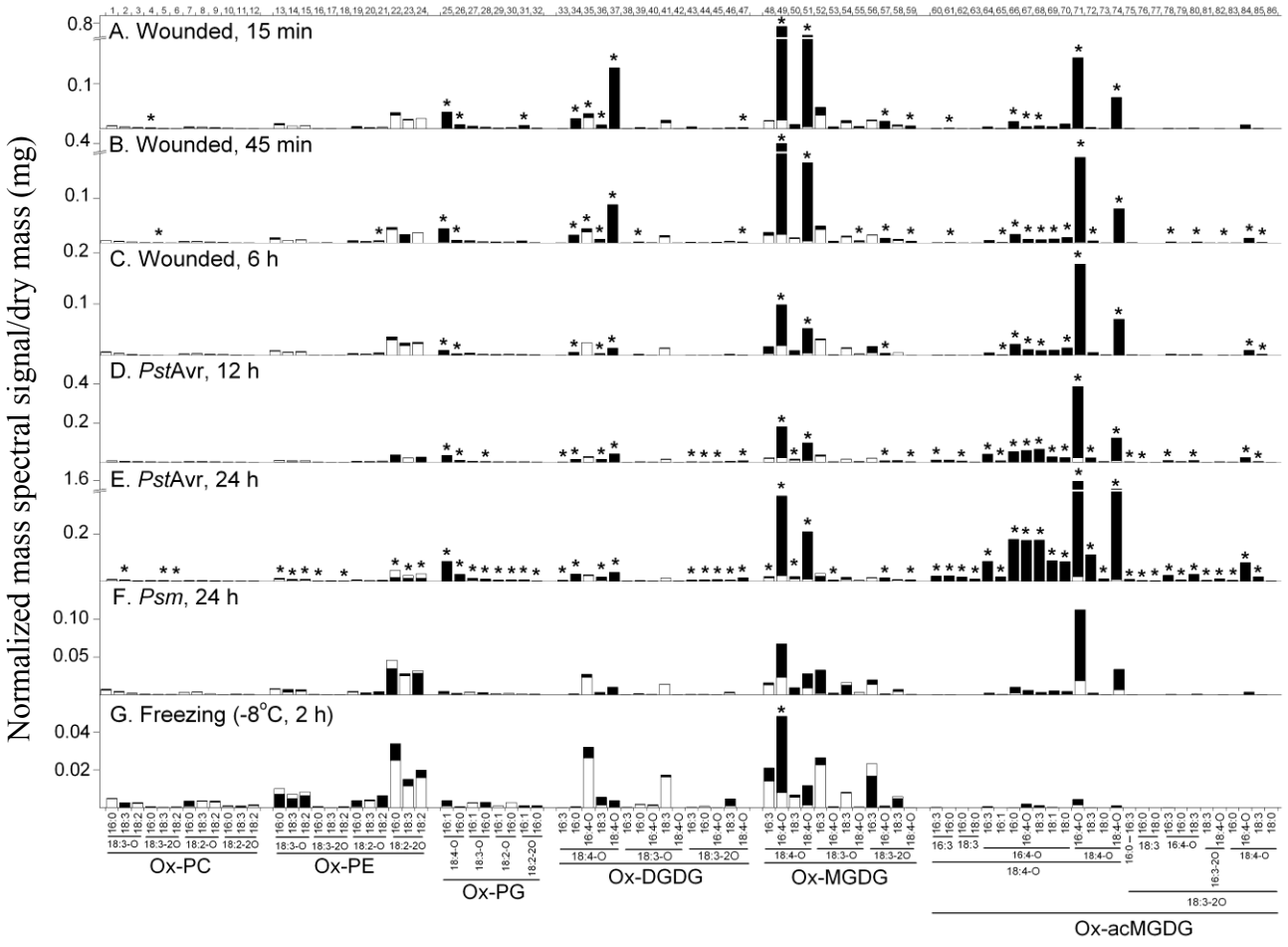

Figure 8.5 Summary of changes in ox-lipids and PA in response to stress treatments.

Each pie and each bar represent all the ox-lipids and PAs analyzed. Pie graphs show the 86 individual molecular species of ox-lipids and 12 molecular species of PA. The bars show the indicated lipid classes (see figure legend). (The colors in the bar and pie graphs are unrelated.) The area of each pie and the length of each bar for each condition represent the size of the combined ox-lipid and PA pools. The basal pool shown in this figure is an average of the pools determined for Unwounded; $MgCl_2$, 12 h; Untreated, 12 h; $MgCl_2$, 24 h; Untreated, 24 h; 4°C, 3 h; 22°C, 3 h; 4°C, 27 h; 22°C, 27 h; 4°C, 84 h; Light, 11 h; and Dark, 9.5 h (Figure 2.2).

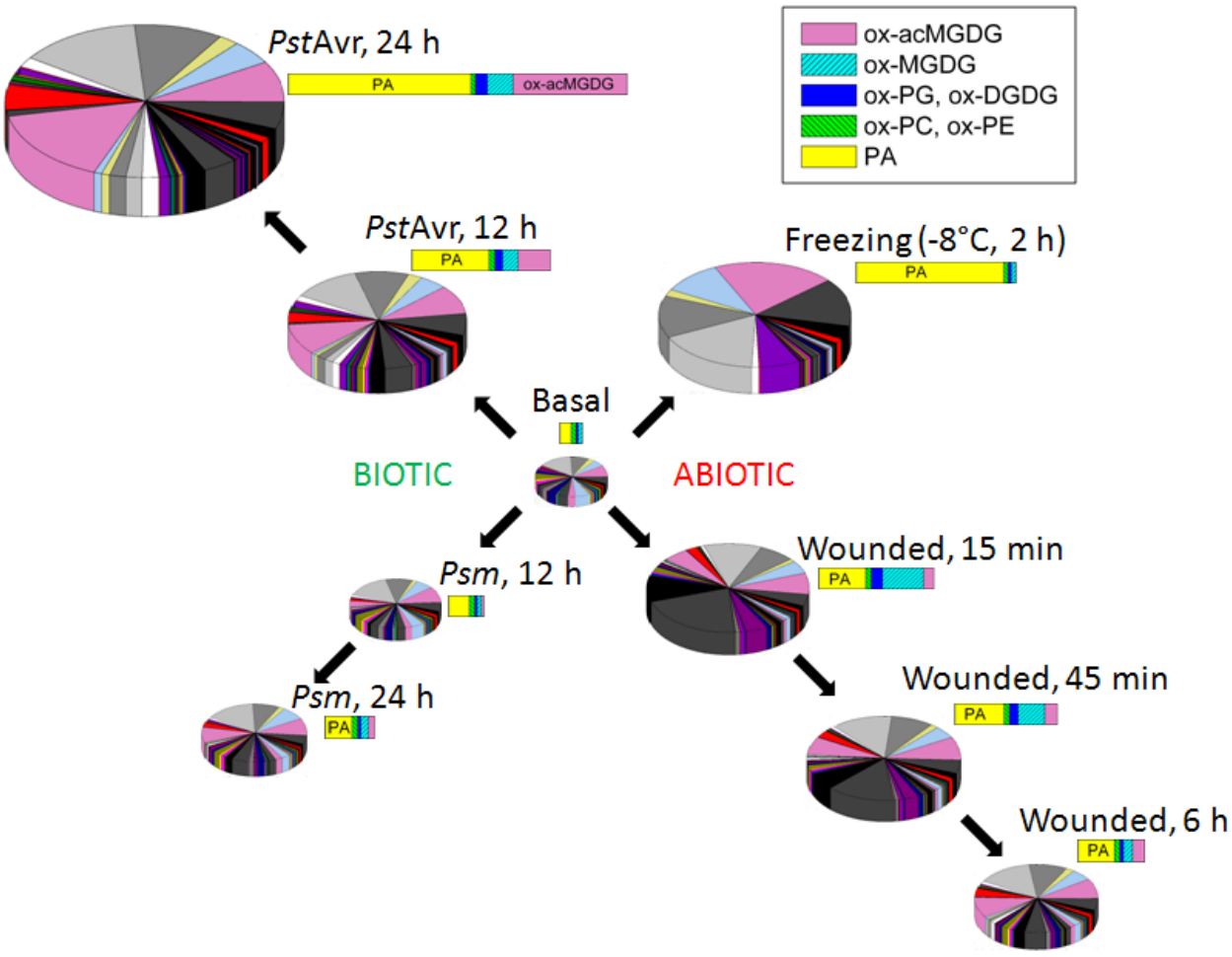

Table 2.1 Oxidized fatty acyl chains detected in extracts from leaves of *Arabidopsis thaliana* infected with *Pst*Avr for 24 h.

Figure S2.1 shows examples of possible structures and fragmentation of oxidized lipids from each class.

Triple quadrupole MS precursor scan	Chemical formula of oxidized fatty acyl anion	*m/z* of anion	Abbreviation	Examples of compounds consistent with detected formula
Acyl formulas directly scanned				
Pre 291.20	$C_{18}H_{27}O_3$	291.1966	18:4-O	OPDA, keto 18:3
Pre 293.21	$C_{18}H_{29}O_3$	293.2122	18:3-O	hydroxy 18:3, keto fatty acid
Pre 295.23	$C_{18}H_{31}O_3$	295.2279	18:2-O	hydroxy 18:2
Pre 291.20	$C_{18}H_{29}O_4$	309.2071	18:3-2O	ketol fatty acid, hydroperoxy 18:3, dihydroxy 18:3
Pre 293.21	$C_{18}H_{31}O_4$	311.2228	18:2-2O	hydroperoxy 18:2, dihydroxy 18:2
Acyl formulas identified by scanning of above anions or as a result of QTOF MS analysis				
-	$C_{16}H_{23}O_3$	263.1653	16:4-O	dnOPDA
-	$C_{16}H_{25}O_3$	265.1809	16:3-O	hydroxy 16:3
-	$C_{16}H_{25}O_4$	281.1758	16:3-2O	ketol fatty acid, hydroperoxy 16:3, dihydroxy 16:3
-	$C_{18}H_{25}O_4$	305.1758	18:5-2O	-

Table 2.2 Lipids detected by ESI MS/MS negative ion precursor ion scans, Pre 291.2, Pre 293.2, and Pre 295.2.

Tables S2.3 and S2.4 indicate the compounds detected in a simplified form.

Number[a]	M mass	M formula	Identification[b]	Detection Method[c]	Identification Evidence[d]
1	771	C42H78O9PN	18:3-O/16:0 PC	Pre 293.2, [M + $C_2H_3O_2$]$^-$	Tentative, Table S2.1
2	793	C44H76O9PN	18:3-O/18:3 PC	Pre 293.2, [M + $C_2H_3O_2$]$^-$	Table S2.1
3	795	C44H78O9PN	18:3-O/18:2 PC	Pre 293.2, [M + $C_2H_3O_2$]$^-$	Table S2.1
4	787	C42H78O10PN	18:3-2O/16:0 PC	Pre 291.2, [M + $C_2H_3O_2$]$^-$	Table S2.1
5	809	C44H76O10PN	18:3-2O/18:3 PC	Pre 291.2, [M + $C_2H_3O_2$]$^-$	Table S2.1
6	811	C44H78O10PN	18:3-2O/18:2 PC	Pre 291.2, [M + $C_2H_3O_2$]$^-$	Table S2.1
7	773	C42H80O9PN	18:2-O/16:0 PC	Pre 295.2, [M + $C_2H_3O_2$]$^-$	Table S2.1
8	795	C44H78O9PN	18:2-O/18:3 PC	Pre 295.2, [M + $_2H_3O_2$]$^-$	Table S2.1
9	797	C44H80O9PN	18:2-O/18:2 PC	Pre 295.2, [M + $C_2H_3O_2$]$^-$	Tentative, Table S2.1
10	789	C42H80O10PN	18:2-2O/16:0 PC	Pre 293.2, [M + $C_2H_3O_2$]$^-$	Table S2.1
11	811	C44H78O10PN	18:2-2O/18:3 PC	Pre 293.2, [M + $C_2H_3O_2$]$^-$	Table S2.1
12	813	C44H80O10PN	18:2-2O/18:2 PC	Pre 293.2, [M + $C_2H_3O_2$]$^-$	Tentative, Table S2.1

13	729	C39H72O9PN	18:3-O/16:0 PE	Pre 293.2, $[M - H]^-$	Table S2.1
14	751	C41H70O9PN	18:3-O/18:3 PE	Pre 293.2, $[M - H]^-$	Table S2.1
15	753	C41H72O9PN	18:3-O/18:2 PE	Pre 293.2, $[M - H]^-$	Table S2.1
16	745	C39H72O10PN	18:3-2O/16:0 PE	Pre 291.2, $[M - H]^-$	Table S2.1
17	767	C41H70O10PN	18:3-2O/18:3 PE	Pre 291.2, $[M - H]^-$	Table S2.1
18	769	C41H72O10PN	18:3-2O/18:2 PE	Pre 291.2, $[M - H]^-$	Table S2.1
19	731	C39H74O9PN	18:2-O/16:0 PE	Pre 295.2, $[M - H]^-$	Table S2.1, S2.2
20	753	C41H72O9PN	18:2-O/18:3 PE	Pre 295.2, $[M - H]^-$	Table S2.1
21	755	C41H74O9PN	18:2-O/18:2 PE	Pre 295.2, $[M - H]^-$	Table S2.1
22	747	C39H74O10PN	18:2-2O/16:0 PE	Pre 293.2, $[M - H]^-$	Table S2.1, S2.2
23	769	C41H72O10PN	18:2-2O/18:3 PE	Pre 293.2, $[M - H]^-$	Tentative, Table S2.1
24	771	C41H74O10PN	18:2-2O/18:2 PE	Pre 293.2, $[M - H]^-$	Tentative, Table S2.1
25	756	C40H69O11P	18:4-O/16:1 PG	Pre 291.2, $[M - H]^-$	Buseman et al., 2006
26	758	C40H71O11P	18:4-O/16:0 PG	Pre 291.2, $[M - H]^-$	Buseman et al., 2006
27	758	C40H71O11P	18:3-O/16:1 PG	Pre 293.2, $[M - H]^-$	Table S2.1
28	760	C40H73O11P	18:3-O/16:0 PG	Pre 293.2, $[M - H]^-$	Table S2.1
29	760	C40H73O11P	18:2-O/16:1 PG	Pre 295.2, $[M - H]^-$	Table S2.1
30	762	C40H75O11P	18:2-O/16:0 PG	Pre 295.2, $[M - H]^-$	Table S2.1
31*	776	C40H73O12P	18:2-2O/16:1 PG	Pre 293.2, $[M - H]^-$	Table S2.1
31*	776	C43H68O12	18:3-O/16:4-O MGDG	Pre 293.2, $[M - H]^-$	Table S2.1
32	778	C40H75O12P	18:2-2O/16:0 PG	Pre 293.2, $[M - H]^-$	Table S2.1
33	922	C49H78O16	18:4-O/16:3 DGDG	Pre 291.2, $[M - H]^-$	Table S2.1
34	928	C49H84O16	18:4-O/16:0 DGDG	Pre 291.2, [M +	Table S2.1

				$C_2H_3O_2]^-$	
35	936	C49H76O17	18:4-O/16:4-O DGDG	Pre 291.2, [M + $C_2H_3O_2]^-$	Hisamatsu et al., 2005
36	950	C51H82O16	18:4-O/18:3 DGDG	Pre 291.2, [M + $C_2H_3O_2]^-$	Buseman et al., 2006
37	964	C51H80O17	18:4-O/18:4-O DGDG	Pre 291.2, [M + $C_2H_3O_2]^-$	Buseman et al., 2006; Hisamatsu et al., 2005
38	924	C49H80O16	18:3-O/16:3 DGDG	Pre 293.2, [M + $C_2H_3O_2]^-$	Table S2.1
39	930	C49H86O16	18:3-O/16:0 DGDG	Pre 293.2, [M +$C_2H_3O_2]^-$	Table S2.1
40	938	C49H78O17	18:3-O/16:4-O DGDG	Pre 293.2, [M + $C_2H_3O_2]^-$	Table S2.1
41	952	C51H84O16	18:3-O/18:3 DGDG	Pre 293.2, [M + $C_2H_3O_2]^-$	Table S2.1
42	966	C51H82O17	18:3-O/18:4-O DGDG	Pre 293.2, [M + $C_2H_3O_2]^-$	Table S2.1
43	940	C49H80O17	18:3-2O/16:3 DGDG	Pre 291.2, [M + $C_2H_3O_2]^-$	Table S2.1
44	946	C49H86O17	18:3-2O/16:0 DGDG	Pre 291.2, [M - H]$^-$	Table S2.1
45'	954	C49H78O18	18:3-2O/16:4-O DGDG	Pre 291.2, [M + $C_2H_3O_2]^-$	Table S2.1
45'	954	C49H78O18	18:4-O/16:3-2O DGDG	Pre 291.2, [M + $C_2H_3O_2]^-$	Table S2.1
46	968	C51H84O17	18:3-2O/18:3 DGDG	Pre 291.2, [M + $C_2H_3O_2]^-$	Buseman et al., 2006
47	982	C51H82O18	18:3-2O/18:4-O DGDG	Pre 291.2, [M + $C_2H_3O_2]^-$	Buseman et al., 2006

48	760	C43H68O11	18:4-O/16:3 MGDG	Pre 291.2, $[M - H]^-$	Table S2.2, Buseman et al., 2006; Stelmach et al., 2001,
49	774	C43H66O12	18:4-O/16:4-O MGDG	Pre 291.2, $[M + C_2H_3O_2]^-$	Table S2.2, Buseman et al., 2006; Hisamatsu et al., 2003
50	788	C45H72O11	18:4-O/18:3 MGDG	Pre 291.2, $[M - H]^-$	Buseman et al., 2006
51	802	C45H70O12	18:4-O/18:4-O MGDG	Pre 291.2, $[M + C_2H_3O_2]^-$	Table S2.2, Buseman et al., 2006; Hisamatsu et al., 2003
52	762	C43H70O11	18:3-O/16:3 MGDG	Pre 293.2, $[M + C_2H_3O_2]^-$	Table S2.1
53	776	C43H68O12	18:3-O/16:4-O MGDG	Pre 293.2, $[M + C_2H_3O_2]^-$	Tentative, Table S2.1
54	790	C45H74O11	18:3-O/18:3 MGDG	Pre 293.2, $[M - H]^-$	Table S2.1
55	804	C45H72O12	18:3-O/18:4-O MGDG	Pre 293.2, $[M + C_2H_3O_2]^-$	Table S2.1
56	778	C43H70O12	18:3-2O/16:3 MGDG	Pre 291.2, $[M + C_2H_3O_2]^-$	Buseman et al., 2006
57	792	C43H68O13	18:3-2O/16:4-O MGDG	Pre 291.2, $[M + C_2H_3O_2]^-$	Buseman et al., 2006
58	806	C45H74O12	18:3-2O/18:3 MGDG	Pre 291.2, $[M + C_2H_3O_2]^-$	Buseman et al., 2006
59	820	C45H72O13	18:3-2O/18:4-O	Pre 291.2, [M +	Buseman et

			MGDG	$C_2H_3O_2]^-$	al., 2006
60	992	C59H92O12	18:4-O/16:3/16:3 acMGDG	Pre 291.2, [M + $C_2H_3O_2]^-$	Table S2.1, S2.2
61	998	C59H98O12	18:4-O/16:3/16:0 acMGDG	Pre 291.2, [M + $C_2H_3O_2]^-$	Table S2.1, S2.2
62	1026	C61H102O12	18:4-O/18:3/16:0 acMGDG	Pre 291.2, [M + $C_2H_3O_2]^-$	Table S2.1
63a	1054	C63H106O12	18:4-O/18:3/18:0 acMGDG	Pre 291.2, [M + $C_2H_3O_2]^-$	Table S2.1
63b	1054	C63H106O12	18:4-O/18:2/18:1 acMGDG	Pre 291.2, [M + $C_2H_3O_2]^-$	Table S2.1
64	1006	C59H90O13	18:4-O/16:4-O/16:3 acMGDG	Pre 291.2, [M + $C_2H_3O_2]^-$	Table S2.1, S2.2
65	1010	C59H94O13	18:4-O/16:4-O/16:1 acMGDG	Pre 291.2, [M + $C_2H_3O_2]^-$	Table S2.1, S2.2
66	1012	C59H96O13	18:4-O/16:4-O/16:0 acMGDG	Pre 291.2, [M + $C_2H_3O_2]^-$	Table S2.1, S2.2
67a	1020	C59H88O14	18:4-O/16:4-O/16:4-O acMGDG	Pre 291.2, [M + $C_2H_3O_2]^-$	Table S2.1, S2.2
67b	1020	C61H96O12	18:4-O/18:3/16:3 acMGDG	Pre 291.2, [M + $C_2H_3O_2]^-$	Table S2.1
68a	1034	C61H94O13	18:4-O/16:4-O/18:3 acMGDG	Pre 291.2, [M + $C_2H_3O_2]^-$	Table S2.1, S2.2
68b	1034	C61H94O13	18:4-O/18:4-O/16:3 acMGDG	Pre 291.2, [M + $C_2H_3O_2]^-$	Table S2.1, S2.2
69a	1038	C61H98O13	18:4-O/16:4-O/18:1 acMGDG	Pre 291.2, [M +$C_2H_3O_2]^-$	Table S2.1, S2.2
69b	1038	C61H98O13	18:4-O/18:4-O/16:1 acMGDG	Pre 291.2, [M +$C_2H_3O_2]^-$	Table S2.1, S2.2
70a	1040	C61H100O13	18:4-O/16:4-O/18:0	Pre 291.2, [M +	Table S2.1,

			acMGDG	$C_2H_3O_2]^-$	S2.2
70b	1040	C61H100O13	18:4-O/18:4-O/16:0 acMGDG	Pre 291.2, [M + $C_2H_3O_2]^-$	Table S2.1, S2.2
71a	1048	C61H92O14	18:4-O/18:4-O/16:4-O acMGDG	Pre 291.2, [M + $C_2H_3O_2]^-$	Table S2.1, S2.2, Andersson et al., 2006
71b	1048	C63H100O12	18:4-O/18:3/18:3 acMGDG	Pre 291.2, [M + $C_2H_3O_2]^-$	Table S2.1, S2.2
72a	1062	C63H98O13	18:4-O/18:4-O/18:3 acMGDG	Pre 291.2, [M + $C_2H_3O_2]^-$	Table S2.1, S2.2
72b	1062	C61H90O15	18:4-O/18:5-2O/16:4-O acMGDG	Pre 291.2, [M + $C_2H_3O_2]^-$	Table S2.1, S2.2
73	1068	C63H104O13	18:4-O/18:4-O/18:0 acMGDG	Pre 291.2, [M + $C_2H_3O_2]^-$	Table S2.1
74	1076	C63H96O14	18:4-O/18:4-O/18:4-O acMGDG	Pre 291.2, [M + $C_2H_3O_2]^-$	Table S2.1, S2.2, Kourtchenko et al., 2007
75	1016	C59H100O13	18:3-2O/16:0/16:3 acMGDG	Pre 291.2, [M + $C_2H_3O_2]^-$	Table S2.1
76a	1044	C61H104O13	18:3-2O/18:3/16:0 acMGDG	Pre 291.2, [M + $C_2H_3O_2]^-$	Table S2.1
76b	1044	C61H104O13	18:3-2O/18:0/16:3 acMGDG	Pre 291.2, [M + $C_2H_3O_2]^-$	Tentative, Table S2.1
77a	1072	C63H108O13	18:3-2O/18:3/18:0 acMGDG	Pre 291.2, [M + $C_2H_3O_2]^-$	Table S2.1
77b	1072	C61H100O15	18:3-2O/18:2/16:3-2O acMGDG	Pre 291.2, [M + $C_2H_3O_2]^-$	Table S2.1
77c	1072	C63H108O13	18:3-2O/18:2/18:1	Pre 291.2, [M +	Table S2.1

			acMGDG	$C_2H_3O_2]^-$	
78'	1024	C59H92O14	18:3-2O/16:4-O/16:3 acMGDG	Pre 291.2, [M + $C_2H_3O_2]^-$	Table S2.1
78'	1024	C59H92O14	18:4-O/16:3-2O/16:3 acMGDG	Pre 291.2, [M + $C_2H_3O_2]^-$	Table S2.1
79'	1030	C59H98O14	18:3-2O/16:4-O/16:0 acMGDG	Pre 291.2, [M + $C_2H_3O_2]^-$	Table S2.1, S2.2
79'	1030	C59H98O14	18:4-O/16:3-2O/16:0 acMGDG	Pre 291.2, [M + $C_2H_3O_2]^-$	Table S2.1, S2.2
80a'	1052	C61H96O14	18:3-2O/16:4-O/18:3 acMGDG	Pre 291.2, [M + $C_2H_3O_2]^-$	Table S2.1
80a'	1052	C61H96O14	18:4-O/16:3-2O/18:3 acMGDG	Pre 291.2, [M + $C_2H_3O_2]^-$	Table S2.1
80b	1052	C61H96O14	18:3-2O/18:4-O/16:3 acMGDG	Pre 291.2, [M + $C_2H_3O_2]^-$	Table S2.1
81a	1070	C61H98O15	18:3-2O/16:3-2O/18:3 acMGDG	Pre 291.2, [M + $C_2H_3O_2]^-$	Table S2.1
81b	1070	C61H98O15	18:3-2O/18:3-2O/16:3 acMGDG	Pre 291.2, [M + $C_2H_3O_2]^-$	Tentative, Table S2.1
81c	1070	C63H106O13	18:3-2O/18:2/18:2 acMGDG	Pre 291.2, [M + $C_2H_3O_2]^-$	Table S2.1
82'	1084	C61H96O16	18:3-2O/16:3-2O/18:4-O acMGDG	Pre 291.2, [M + $C_2H_3O_2]^-$	Table S2.1, S2.2
82'	1084	C61H96O16	18:3-2O/18:3-2O/16:4-O acMGDG	Pre 291.2, [M + $C_2H_3O_2]^-$	Table S2.1, S2.2
83a	1058	C61H102O14	18:3-2O/18:4-O/16:0 acMGDG	Pre 291.2, [M + $C_2H_3O_2]^-$	Table S2.1
83b	1058	C61H102O14	18:3-2O/16:4-O/18:0 acMGDG	Pre 291.2, [M + $C_2H_3O_2]^-$	Tentative, Table S2.1
84a	1066	C61H94O15	18:3-2O/18:4-	Pre 291.2, [M +	Table S2.1,

			O/16:4-O acMGDG	$C_2H_3O_2]^-$	S2.2
84b	1066	C63H102O13	18:3-2O/18:3/18:3 acMGDG	Pre 291.2, [M + $C_2H_3O_2]^-$	Table S2.1, S2.2
85	1080	C63H100O14	18:3-2O/18:4-O/18:3 acMGDG	Pre 291.2, [M + $C_2H_3O_2]^-$	Table S2.1
86	1086	C63H106O14	18:3-2O/18:4-O/18:0 acMGDG	Pre 291.2, [M + $C_2H_3O_2]^-$	Table S2.1

[a]Each number (1-86) represents a peak observed in triple quadrupole MS spectra (Figure 2.1). An asterisk (*) indicates peaks resulting from two compounds of different lipid classes with the same ion mass. A prime symbol (') indicates peaks with at least two possible identifications, where it is unclear whether the peak represents one or both compounds. Numbers followed by a, b, or c signify that accurate *m/z* analysis indicates that the peak represents multiple lipid species detected by the stated precursor scan (Tables S2.1 and S2.2).

[b]Abbreviations: acMGDG, acylated monogalactosyldiacylglycerol; DGDG, digalactosyldiacylglycerol; MGDG, monogalactosyldiacylglycerol; PC, phosphatidylcholine; PE, phosphatidylethanolamine; PG, phosphatidylglycerol.

[c]Peaks were identified in triple quadrupole MS spectra with three negative precursor scans, Pre 291.2, Pre 293.2, and Pre 295.2; each species was observed as the $[M - H]^-$ and/or $[M + C_2H_3O_2]^-$ ion.

[d]QTOF MS peak data are provided in Table S2.1. FTICR MS peak data are provided in Table S2.2. Peak identification is indicated as "Tentative" if QTOF MS *m/z* values for one acyl group (or more) were greater than 10 parts per million (ppm) from the theoretical *m/z*, and the compound was not previously identified or identified by accurate *m/z* of the intact compound in FTICR MS spectra. Previously identified peaks/compounds are marked with corresponding references.

Supplemental Data

Supplemental Data in this chapter include:

- Figure S2.1 Examples of possible structures and fragmentation of oxidized lipids from each class.
- Figure S2.2 Bacterial counts (colony forming unit (CFU) per mg of leaf dry mass) at 12 h and 24 h post-infection.
- Figure S2.3 Oxidized membrane lipid levels during various control conditions and conditions with low ox-lipid levels as quantified by triple quadrupole MS precursor scanning.
- Figure S2.4 Levels of ox-MGDG, ox-acMGDG and PA in Arabidopsis leaves during stress and control treatments.
- Figure S2.5 Levels of LPC, LPE, and PA, in Arabidopsis leaves during stress and control treatments.

Tables S2.1-S2.8 are supplied as a separate Excel file.

- Table S2.1 QTOF MS m/z data supporting compound identifications in Table 2.2. Analysis was performed on extracts from leaves of Arabidopsis thaliana infected with PstAvr for 24 h.
- Table S2.2 FTICR MS m/z data supporting compound identifications in Table 2.2. Analysis was performed on extracts from leaves of Arabidopsis thaliana infected with PstAvr for 24 h.
- Table S2.3 Simplified designation of diacyl oxidized compounds (1-59).
- Table S2.4 Simplified table of acMGDGs (60-86) identified by precursor scanning.
- Table S2.5 Levels (individual sample data) of ox-lipids during plant stress responses.
- Table S2.6 Levels (averages and standard deviations) of ox-lipids during plant stress responses.
- Table S2.7 Levels (individual sample data) of normal lipids during plant stress responses.
- Table S2.8 Levels (averages and standard deviations) of normal lipids during plant stress responses.

Figure S2.1 Examples of possible structures for anions of oxidized lipids from each class. These structures are consistent with current data, but, in fact, the acyl chain structures shown in Table 2.1 and identified with specific compounds in Table 2.2 have been identified only at the level of chemical formula. The specific structural features (e.g. presence of C=O vs. C=C double bonds vs. rings, presence of specific functional groups, positions of double bonds and functional groups, and positions of acyl chains on glycerol) have not been determined. Table 2.1 indicates some additional possibilities for acyl chain structures.

Compounds shown:

7. 18:2-O/16:0 PC, shown as the $[M + C_2H_3O_2]^-$ ion of 1-hexadecanoyl-2-(9-hydroxy-10E,12Z-octadecadienoyl)-*sn*-glycero-3-phosphocholine;

23. 18:2-2O/18:3 PE, shown as the $[M - H]^-$ ion of 1-(9-hydroperoxy-10E,12Z-octadecadienoyl)-2-(9Z,12Z,15Z-octadecatrienoyl)-*sn*-glycero-3-phosphoethanolamine;

25. 18:4-O/16:1 PG, shown as the $[M - H]^-$ ion of 1-(8-[2-(cis-pent-2'-enyl)-3-oxo-cis-cyclo-pent-4-enyl]octanoyl)-2-(3E-hexadecenoyl)-*sn*-glycero-3-phospho-(1'-*sn*-glycerol), where 8-[2-(cis-pent-2'-enyl)-3-oxo-cis-cyclo-pent-4-enyl]octanoyl is also known as 12-oxo-10,15-phytodienoyl and OPDA;

46. 18:3-2O/18:3 DGDG, shown as the $[M + C_2H_3O_2]^-$ ion of 1-(9-hydroxy-12-oxo-10E,15Z-octadecadienoyl)-2-(9Z,12Z, 15Z-octadecatrienoyl)-3-O-[α-D-galactosyl-(1→6)-O-β-D-galactosyl]-*sn*-glycerol, where 9-hydroxy-12-oxo-10E,15Z-octadecadienoyl is also known as γ-ketol;

52. 18:3-O/16:3 MGDG, shown as the $[M + C_2H_3O_2]^-$ ion of 1-(13-hydroxy-9Z,11E,15Z-octadecatrienoyl)-2-(7Z,10Z,13Z-hexadecatrienoyl)-3-O-β-D-galactosyl-*sn*-glycerol;

66. 18:4-O/16:4-O/16:0 acMGDG, shown as the $[M + C_2H_3O_2]^-$ ion of 1-(8-[2-(cis-pent-2'-enyl)-3-oxo-cis-cyclo-pent-4-enyl]octanoyl)-2-(6-[2-(cis-pent-2'-enyl)-3-oxo-cis-cyclo-pent-4-enyl]hexanoyl)-3-O-(6-O-hexadecanoyl-β-D-galactosyl)-*sn*-glycerol, where 8-[2-(cis-pent-2'-enyl)-3-oxo-cis-cyclo-pent-4-enyl]octanoyl is also known as 12-oxo-10,15-phytodienoyl and OPDA, and 6-[2-(cis-pent-2'-enyl)-3-oxo-cis-cyclo-pent-4-enyl]hexanoyl is known as dinor-oxo-phytodienoyl and dnOPDA.

OPDA = 8-[2-(cis-pent-2'-enyl)-3-oxo-cis-cyclo-pent-4-enyl]octanoic acid

dnOPDA = 6-[2-(cis-pent-2'-enyl)-3-oxo-cis-cyclo-pent-4-enyl]hexanoic acid

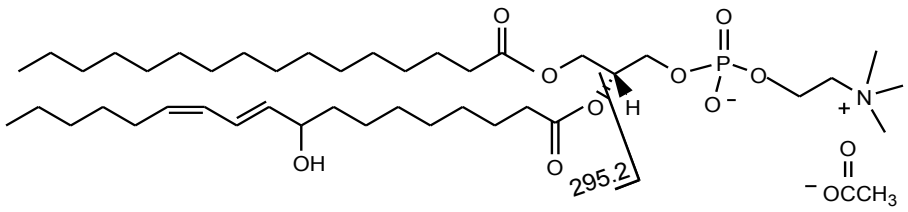

7

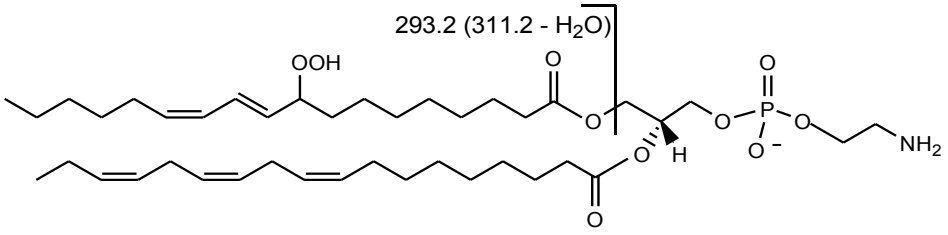

23

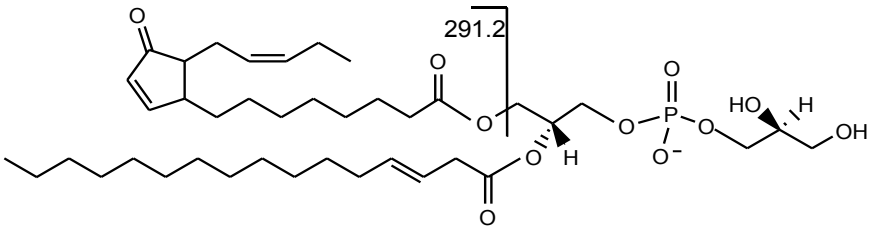

25

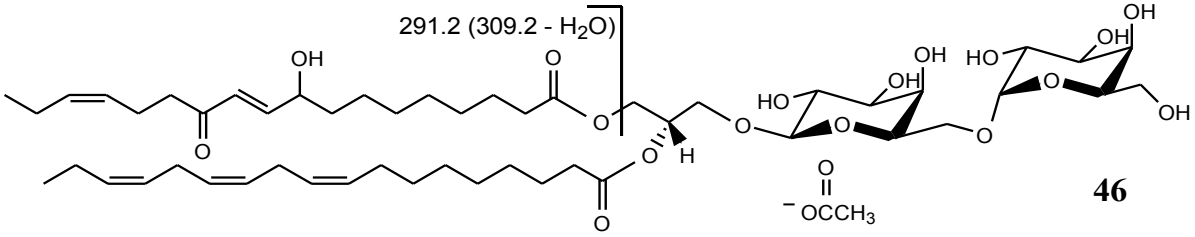

46

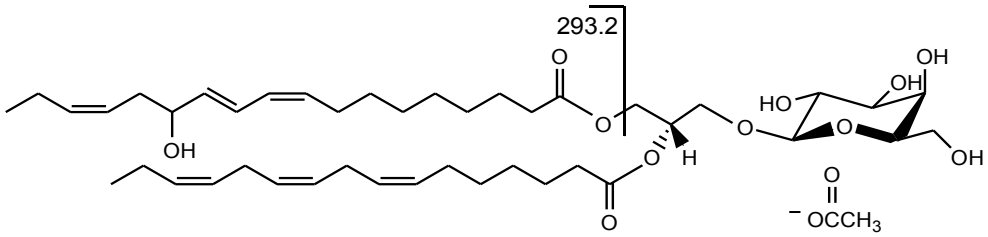

52

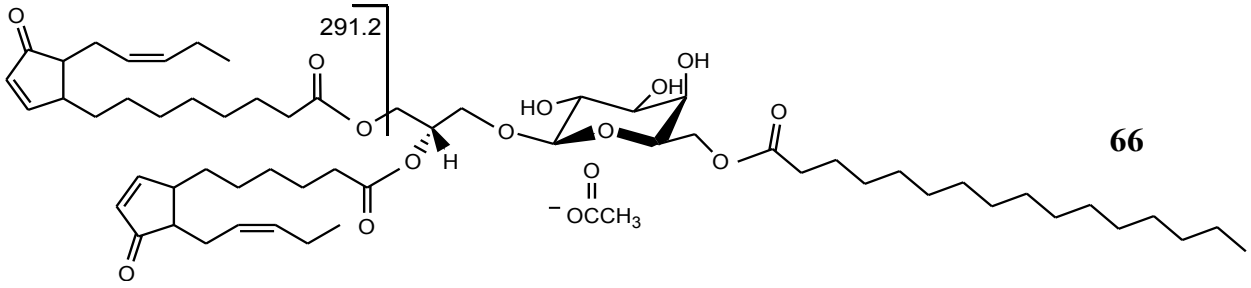

66

Figure S2.2 Bacterial counts (colony forming unit (CFU) per mg of leaf dry mass) at 12 h and 24 h post-infection.

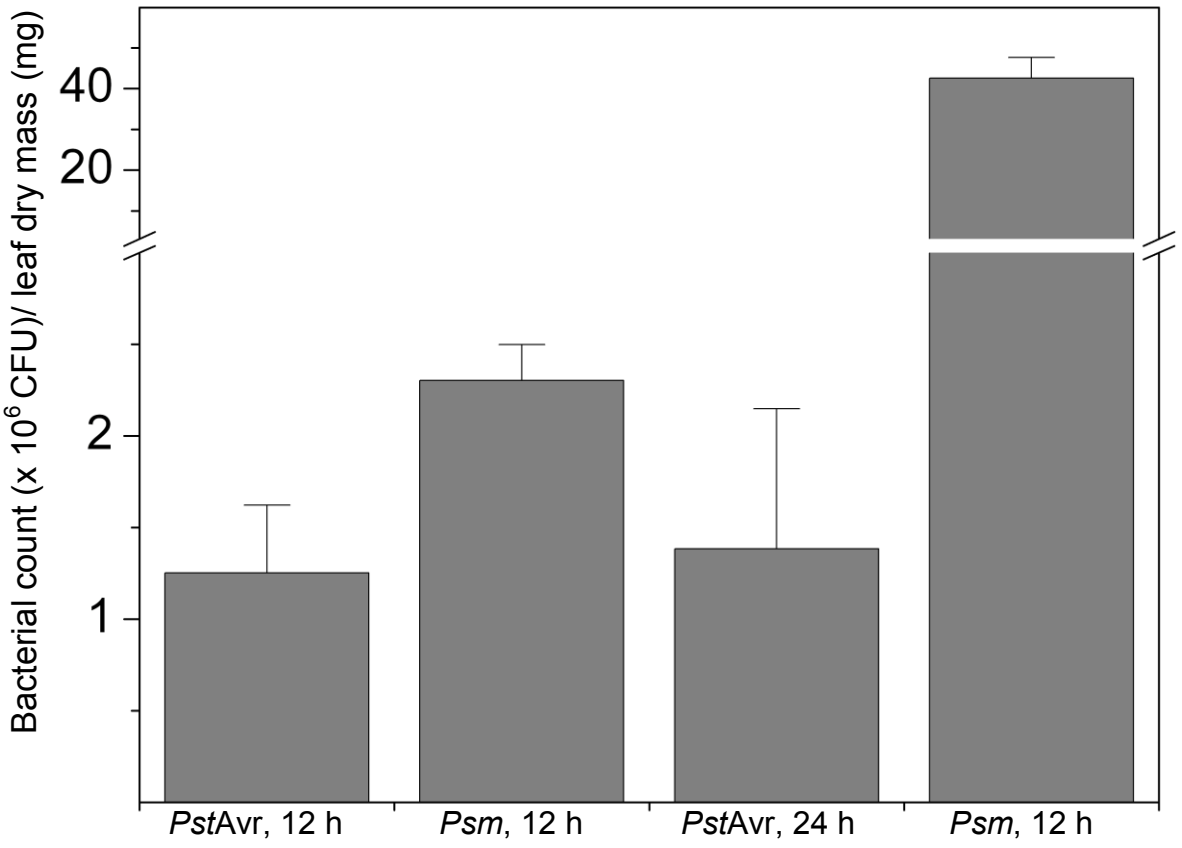

Figure S2.3 Oxidized membrane lipid levels during various control conditions and conditions with low ox-lipid levels (indicated on the panels) as quantified by triple quadrupole MS precursor scanning. Numbers along top x-axis refer to peaks/compounds in Table 2.2. Error bars indicate standard deviation.

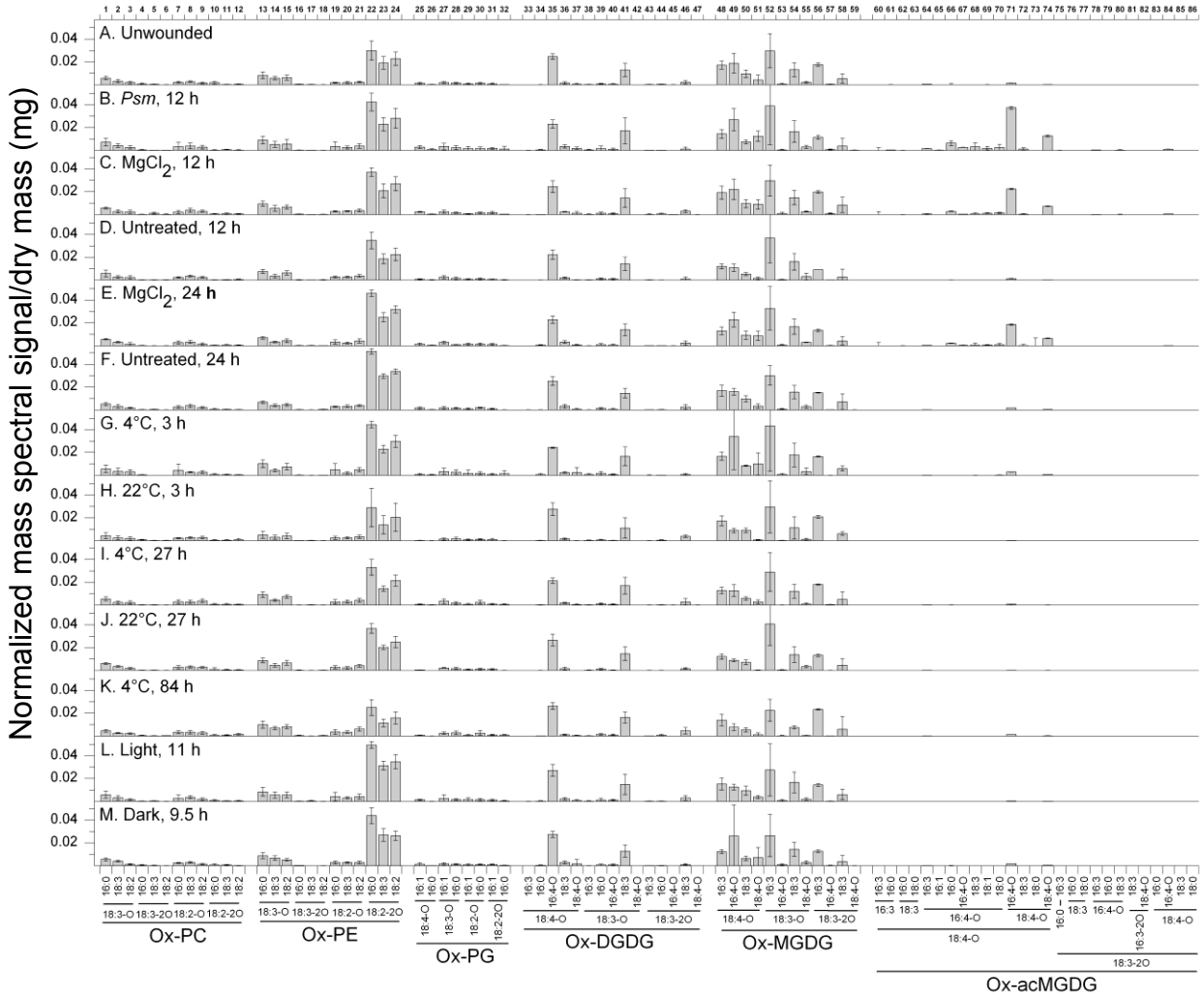

Figure S2.4 Levels of ox-MGDG, ox-acMGDG and PA in Arabidopsis leaves during stress and control treatments. Panels A, B, and C are ox-MGDG and ox-acMGDG as indicated. Panels D, E and F are PA. Error bars indicate standard deviation.

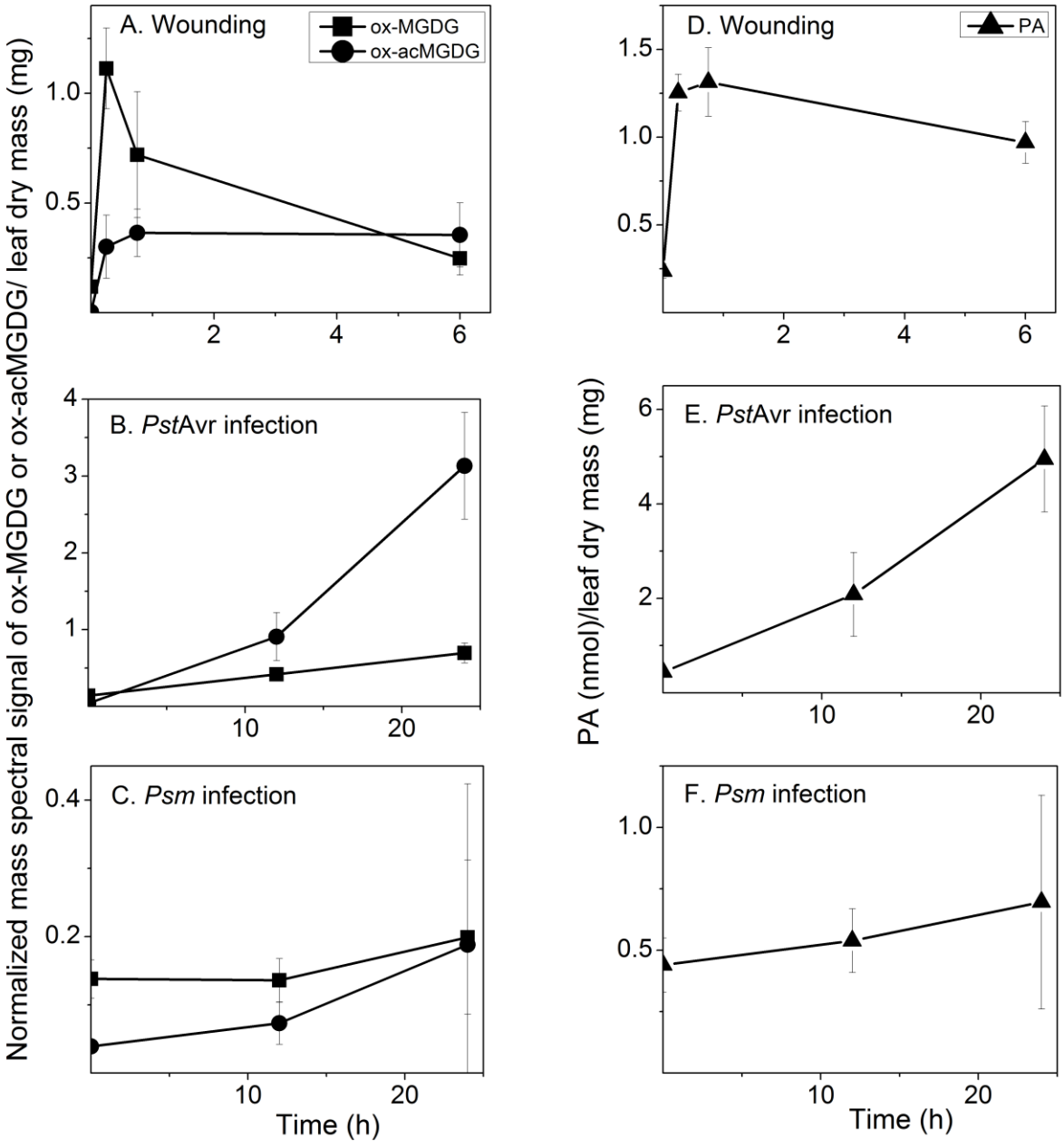

Figure S2.5 Levels of LPC, LPE, and PA, in Arabidopsis leaves during stress and control treatments. Average data used in this figure are presented in Table 2.8. Error bars indicate standard deviation. T-test was performed on 12 treatment-control pairs: **Wounded, 15 min** vs. Unwounded; **Wounded, 45 min** vs. Unwounded; **Wounded, 6 h** vs. Unwounded; ***Pst*Avr, 12 h** vs. $MgCl_2$, 12 h; ***Psm*, 12 h** vs. $MgCl_2$, 12 h; **$MgCl_2$, 12 h** vs. Untreated, 12 h; ***Pst*Avr, 24 h** vs. $MgCl_2$, 12 h; ***Psm*, 24 h** vs. $MgCl_2$, 24 h; **$MgCl_2$, 24 h** vs. Untreated, 24 h; **4°C, 3 h** vs. 22°C, 3 h; **4°C, 27 h** vs. 22°C, 27 h; **Freezing (-8°C, 2 h)** vs. 4°C, 84 h; *p < 0.05, n = 5 (except for 4°C, 3 h, n = 4).

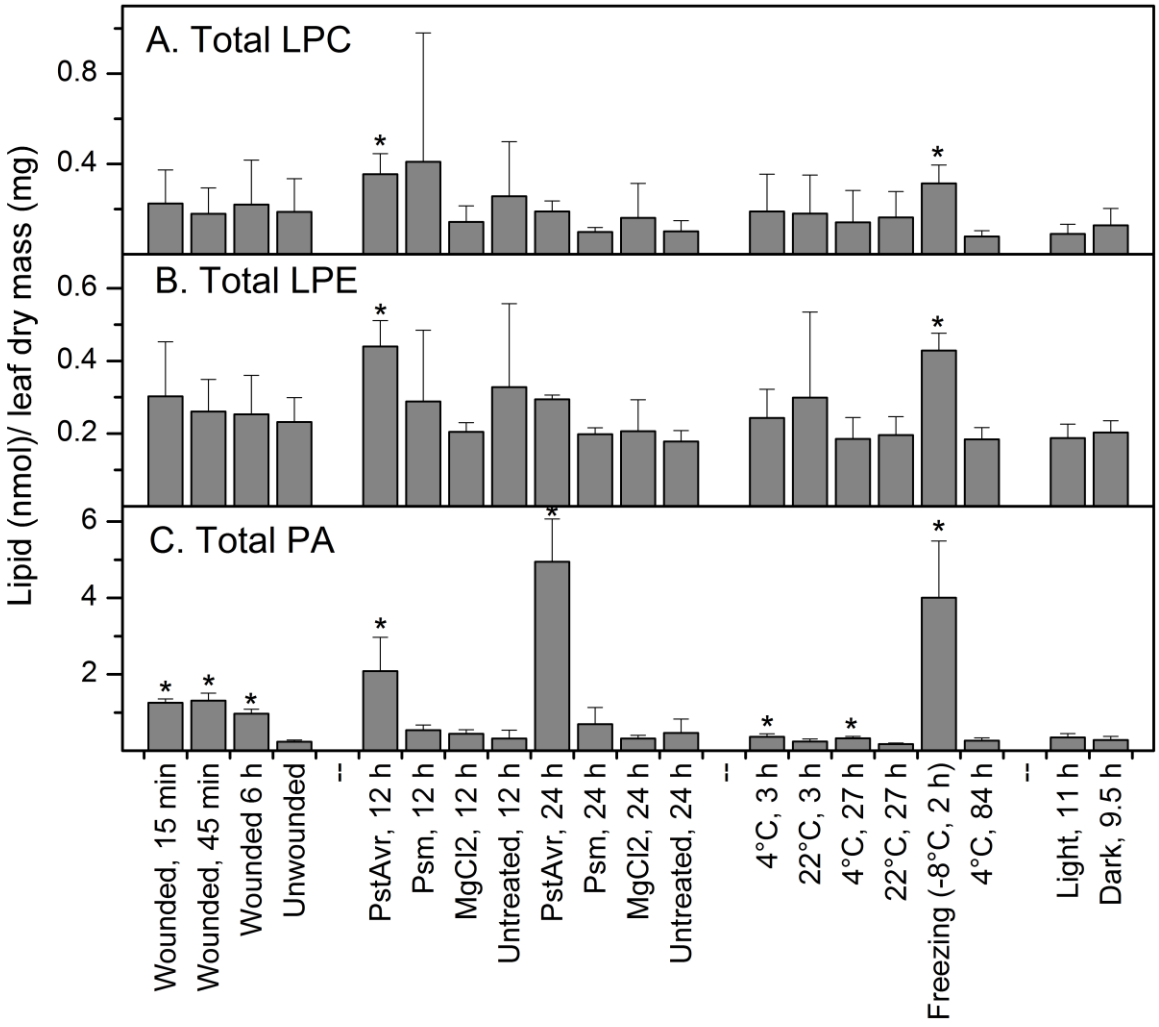

Chapter 9 - Head-group acylation of monogalactosyldiacylglycerol is a common stress response, and the acyl-galactose acyl composition varies among plant species and with applied stress

Abstract

Formation of galactose-acylated monogalactosyldiacylglycerols has been shown to be induced by leaf homogenization, mechanical wounding, avirulent bacterial infection and thawing after snap-freezing. Here, lipidomic analysis using mass spectrometry showed that galactose-acylated monogalactosyldiacylglycerols, formed in wheat (*Triticum aestivum*) and tomato (*Solanum lycopersicum*) leaves upon wounding, have acyl-galactose profiles that differ from those of wounded *Arabidopsis thaliana*, indicating that different plant species accumulate different acyl-galactose components in response to the same stress. Additionally, the composition of the acyl-galactose component of Arabidopsis acMGDG (galactose-acylated monogalactosyldiacylglycerol) depends on the stress treatment. After sub-lethal freezing treatment, acMGDG contained mainly non-oxidized fatty acids esterified to galactose, whereas mostly oxidized fatty acids accumulated on galactose after wounding or bacterial infection. Compositional data are consistent with acMGDG being formed in vivo by transacylation with fatty acids from digalactosyldiacylglycerols. Oxophytodienoic acid, an oxidized fatty acid, was more concentrated on the galactosyl ring of acylated monogalactosyldiacylglycerols than in galactolipids in general. Also, oxidized fatty acid-containing acylated monogalactosyldiacylglycerols increased cumulatively when wounded Arabidopsis leaves were wounded again. These findings suggest that, in Arabidopsis, the pool of galactose-acylated monogalactosyldiacylglycerols may serve to sequester oxidized fatty acids during stress responses.

Introduction

Membranes of plant chloroplasts contain glyco-glycerolipids with three major head groups: galactose (Gal, in monogalactosyldiacylglycerol, MGDG), digalactose (in digalactosyldiacylglycerol, DGDG) and sulfonated glucose (in sulfoquinovosyldiacylglycerol, SQDG). The Gal component of MGDG can be enzymatically modified by fatty acylation (esterification) at the 6′-hydroxyl group. Over 40 years ago, this head group acylation was characterized in spinach homogenates (Heinz, 1967a; Heinz and Tulloch, 1969). Fatty acid compositional analysis of in vitro incubation products from an ammonium sulfate-precipitated protein fraction with purified lipid substrates indicated that, when only MGDG was present, galactose-acylated MGDG (acMGDG) was formed via a dismutation reaction, i.e. 2 MGDG → acMGDG + monogalactosylmonoacylglycerol (MGMG). However, when both MGDG and DGDG were present, acMGDG was formed exclusively by transacylation from DGDG, i.e. DGDG + MGDG → acMGDG + digalactosylmonoacylglycerol (DGMG; Heinz 1967b, Heinz 1972). This early work focused on acMGDG formation in homogenized leaf tissues; however, the potential physiological role for the acylation reaction was not considered.

More recently, acMGDGs with the structure 1-(12-oxophytodienoic acid) (OPDA), 2-dinor-oxophytodienoic acid (dnOPDA), 3-(OPDA-Gal) glycerol (Arabidopside E) and acMGDG with 3 OPDA chains (Arabidopside G) were identified in Arabidopsis leaves under stress. These acMGDGs can accumulate to as much as 8% of the Arabidopsis total leaf lipid when the leaves are infected with the bacteria *Pseudomonas syringae* carrying the avirulence factor AvrRpt2 (Pst) or AvrRpm1 (Andersson et al., 2006; Kourtchenko et al., 2007). Indeed, in vitro testing indicated that Arabidopsides E and G have antimicrobial activities against the virulent bacterium *Pseudomonas syringae* DC3000 (Andersson et al., 2006) and the necrotrophic fungus *Botrytis cinerea* (Kourtchenko et al., 2007). Forty additional acMGDG molecular species (13 non-oxidized and 27 oxidized) were measured after wounding of Arabidopsis leaves (Ibrahim et al., 2011) and 27 additional acMGDGs, each with at least one oxidized fatty acid chain, were characterized as being induced significantly after wounding or avirulent bacterial infection of Arabidopsis leaves (Vu et al., 2012).

Galactolipids with cyclic oxidized acyl chains, or oxylipins, such as OPDA, esterified to glycerol are rare in plant species outside the genus *Arabidopsis* (Bottcher and Weiler, 2007). The current study adds to the evidence that, although cyclic fatty acids in membrane lipids may be restricted in occurrence, Gal acylation of MGDG is a relatively conserved process that occurs in tomato and wheat, in addition to Arabidopsis, spinach, and broad bean (Heinz, 1967b; Heinz, 1967a; Heinz and Tulloch, 1969; Heinz, 1972; Andersson et al., 2006; Kourtchenko et al., 2007; Ibrahim et al., 2011; Vu et al., 2012). MGDG Gal acylation is demonstrated to be a common response to stresses including wounding, freezing and infection with avirulent bacteria. The data show major variation in composition of the Gal-esterified acyl group, both among plant species and in response to different stresses. Furthermore, comparison of the profiles of the fatty acyl chain on the Gal of acMGDG and the fatty acyl chains of DGDG supports the notion that DGDG is the usual acyl donor for MGDG Gal acylation *in vivo*.

Materials and Methods

Plant materials

Mature wheat leaves (*Triticum aestivum* 'Thatcher') were collected from the North Agronomy Farm, Kansas State University, Manhattan, KS. Tomato plants (*Solanum lycopersicum* 'Better Boy') were purchased from Westside Market, Manhattan, KS. *Arabidopsis thaliana* accessions Columbia-0 (Col-0) and C24 were grown one plant per well in Pro-Mix 'PGX' soil (Hummert International, Earth City, MO) in 72-well plug trays (Hummert International, Earth City, MO). Trays were kept in a Conviron growth chamber under a 14/10 h light/dark cycle with 60% humidity at 21°C. Light intensity in growth chambers was maintained at 80 μmol m−2 s−1 with cool white fluorescent lights (Sylvania, Danvers, MA). Plants were fertilized twice, once when sowing and once at 20 days old, by irrigation with a 1% solution of 20-20-20 Miracle-Gro plant food (Scotts Miracle-Gro, Marysville, OH). Col-0 was harvested after 30 days and C24 after 42 days of growth.

Treatments

Arabidopsis plants were infected with bacteria (*Pseudomonas syringae*) as previously described (Vu et al., 2012). Cold acclimation was performed in a 4°C room equipped with light carts. Freezing treatment was performed in a programmable freezing chamber (Espec Corporation, Hudsonville, MI). Each tray of plants in soil was partly submerged in an ice slurry (made by adding tap water to approximately 1.5 kg of ice chips to a total volume of 4 l) to avoid supercooling during freezing treatment at −8°C for 2 h. The soil was completely in contact with the ice slurry through the irrigation holes at the bottom of the growing tray. The temperature was dropped to −8°C without gradual decreasing; at the end of the freezing treatment, plants were transferred to their growth condition (21°C, 60% humidity) and sampled after 3 and 24 h. Leaf numbers 5 and 6 were collected for ion leakage measurement (see next section), and the remaining portion of the rosette was dropped into 4 ml of 75°C isopropanol with 0.01% butylated hydroxytoluene (BHT) for lipid analysis. Leaf number is the order of leaf appearance, determined as described previously (Telfer et al., 1997). Wounding was performed by applying pressure with a hemostat across the leaf mid-vein, leaving wound marks about 6 mm apart. For the re-wounding experiment, plants were randomly assigned to one of three groups. Plants of the 'control' singly wounded group were harvested at 0 min, 5 min, 15 min, 45 min, 4 h, 24 h and 48 h after wounding. For the other two groups, a second wound was applied at the same location as the first wound either 24 or 48 h after the first wound was applied. The leaves were harvested at 0 min, 5 min, 15 min, 45 min, 4 h, 24 h and 48 h after the second wound. In the re-wounding experiment, four leaves (leaf numbers 5, 6, 7 and 8) were harvested at each time point; leaf number 5 was dropped into 2 ml of 75°C isopropanol with 0.01% BHT for lipid analysis, and leaf numbers 6, 7 and 8 were put together into a 1.5-ml tube and frozen in liquid nitrogen for phytohormone analysis by gas chromatography – mass spectrometry (MS).

Ion leakage measurement

Two leaves from each rosette were rinsed with deionized water before being dropped into a a 50-ml PYREX glass tube (Corning Inc., Corning, NY) containing 25 ml of distilled water (Dillons Supermarket, Manhattan, KS). The tubes were shaken for 2 h at 100 rpm before the first ion conductivity reading with Oakton CON 510 electrical conductivity meter (Oakton Instruments,

Vernon Hills, IL). After the first reading, the tubes were incubated at 95–100°C in a water bath for 2 h, and a second conductivity reading was taken. Relative ion leakage, as a percentage, was reported as (the first over the second conductivity reading) × 100 (%).

Lipid extraction

Modified Bligh–Dyer method (Bligh and Dyer, 1959) for polar lipid analysis

For the *Pst* and wounding experiments, three leaves were dropped into 3 ml of 75°C isopropanol containing 0.01% BHT; heating at 75°C was continued for 15 min. Chloroform (1.5 ml) and water (0.6 ml) were added, and the tube was shaken for 1 h before the solvent was transferred to another tube. For the second round of extraction, 4 ml of chloroform: methanol (2:1) was added to the leaves, followed by shaking for 30 min and combination of the solvent with the previous extract. After repeating the extraction three more times and combining the extracts, the combined extract was evaporated under a nitrogen stream and re-dissolved in 1 ml of chloroform. The extracted leaf residue was dried overnight at 105°C and the dry mass obtained by weighing.

Alternate extraction method (for polar lipid analysis)

For the freezing and re-wounding experiments, leaves were dropped into a 20-ml vial with a Teflon-lined cap containing 4 ml (2 ml in the re-wounding experiment) of 75°C isopropanol with 0.01% BHT. After 15 min at 75°C, 12 ml (6 ml in the re-wounding experiment) of extraction solvent (chloroform: methanol: 300 mM ammonium acetate in water, 30:41.5:3.5, v/v/v) were added, and the tube was shaken at room temperature for 24 h.

For gas chromatography-MS (free oxylipin analysis)

Extraction and derivatization were carried out as described previously (Schmelz et al., 2004).

Mass spectrometry

For samples extracted by the modified Bligh–Dyer method (stored in 1 ml chloroform), a volume (x μl) containing 0.2 mg leaf dry mass was diluted by adding (360 − x) μl of chloroform and 840

µl of methanol: 300 mM ammonium acetate in water (95:5, v/v). For samples extracted by the alternate method, a volume (y µl) containing 0.2 mg leaf dry mass was diluted with (1200 − y) µl of chloroform: methanol: isopropanol: 300 mM ammonium acetate in water (30:41.5:25:3.5, v/v/v/v).

Phospholipids and galactolipids with normal chains were analyzed by triple quadrupole MS using head group-specific scans and standards as described previously (Xiao et al., 2010). Precursor scans of m/z 277.2 (Pre 277.2, 18:3), m/z 291.2 (Pre 291.2, 18:4-O), m/z 293.2 (Pre 293.2, 18:3-O), m/z 295.2 (Pre 295.2, 18:2-O or 17:3-2O) and m/z 283.2 (Pre 283.2, 18:0, to detect internal standard 16:0/18:0 MGDG) were performed in negative mode as described previously (Vu et al., 2012), except that 1.505 nmol of 18:0/16:0 MGDG was used in each vial as an internal standard.

Scans for neutral loss (NL) fragments composed of Gal and a fatty acid (Table 3.1) were carried out in positive mode using an ABI 4000 triple quadrupole mass spectrometer (Applied Biosystems, Foster City, CA) with an electrospray ionization (ESI) source. To perform the NL scans listed in Table 3.1, three identical sample vials were used to provide enough volume for the analysis of each sample. To each sample vial, 0.95 nmol of di18:0 DGDG was added as an internal standard; this was detected by NL scan of m/z 341.2 (NL 341.2), with a target of m/z 966.7. The infusion flow rate was 30 µl min−1. The scan rate was 36 u s−1 for 75 cycles. Other parameters were: collision gas, 2 (arbitrary units); curtain gas, 20 (arbitrary units); ion source gases 1 and 2, 45 (arbitrary units); source temperature, 100°C; interface heater, ‘on’; ion spray voltage, 5500 V; declustering potential, 90 V; entrance potential, 10 V; collision energy, 24 V and collision cell exit potential, 23 V.

Accurate acyl mass analysis by quadrupole time-of-flight (Q-TOF) MS was performed on unfractionated lipid extracts with a Q-TOF-2 tandem mass spectrometer (Micromass Ltd., Manchester, UK), using the solvent, parameters and processing method described by Buseman et al. (2006), with a few changes. Charged precursor ions were subjected to product ion scanning in negative or positive ion mode. Precursor ions were selected by the quadrupole, tuned to transmit at 0.8 u full width at half height (i.e. monoisotopic selection). Extracts were infused into the ESI source at 20 µl min^{-1}; collision energy was 30 V.

Chemical ionization gas chromatography – MS was used to profile phytohormones of samples harvested from the re-wounding experiment following the procedure described by Schmelz et al. (2004).

Mass spectral data processing and analysis

Peak smoothing, background subtraction and peak centroiding for triple quadrupole MS data were carried out using a custom script with Applied Biosystems analyst software. After targeted peaks were identified, isotopic overlaps were calculated and subtracted from peaks within each spectrum. For NL scans, spectra were also corrected for isotopic overlaps of head group fragments. Signals of targeted peaks were normalized to the signal of the corresponding internal standard (18:0/16:0 MGDG for negative precursor scans and di18:0 DGDG for positive NL scans) and reported as normalized mass spectral signal per mg of leaf dry mass, where amount of signal produced by 1 nmol internal standard is 1 unit of signal.

To calculate the OPDA to 18:3 signal ratio in MGDGs and DGDGs in Arabidopsis, the ESI triple quadrupole MS signals were detected by scanning in negative mode for Pre 291.2 (OPDA) and Pre 277.2 (18:3). The sum of signals from MGDGs and DGDGs containing combinations of OPDA (18:4-O) with each of the five major fatty acids [16:3, 16:0, dnOPDA (16:4-O), 18:3 and OPDA] was divided by the sum of MGDGs and DGDGs containing combinations of 18:3 with each of the same five major fatty acids. To calculate the Gal-OPDA to Gal-18:3 signal ratio in acMGDGs, the sum of signals of Gal-OPDA acMGDGs [with each of the 35 diacylglycerol (DAG) combinations listed in Table S3.1], detected by scanning in positive mode for NL 453.3 (Gal-OPDA), was divided by the sum of signals of Gal-18:3 acMGDGs (with the 35 DAGs listed in Table S3.1), detected by scanning in positive mode for NL 439.3 (Gal-18:3).

Q-TOF mass spectra obtained in negative mode were mass-corrected by using, as a lock mass, the theoretical exact mass of the acyl anion of 18:3 fatty acid or OPDA, m/z 277.2173 or 291.1966, respectively. Q-TOF spectra obtained in positive mode were mass-corrected by locking on the mass of a fragment containing the glycerol backbone attached to either 18:3 fatty acid or OPDA (m/z 335.2581 or 349.2373, respectively). With the locked mass correction, the exact masses of product ions were determined to ten thousandths of a mass unit.

Results

Wound-induced acylation of the galactose of MGDG occurs in multiple plant species

acMGDGs are formed by acylation of MGDG on the carbon at the 6-position of galactose (Heinz and Tulloch, 1969). Utilizing direct infusion ESI triple quadrupole MS, acMGDG levels can be measured by NL scanning in the positive mode. Figure 3.1A depicts an acMGDG molecule, showing formation of the NL fragment, C22H43O6N (417.3 u), by collision-induced dissociation. The fragment is composed of a palmitoyl chain, 16:0 (where 16 is the number of carbons and 0 is the number of double bond equivalents, excluding the carbonyl double bond), esterified to Gal. Other NL fragments used for detection of acMGDGs are listed in Table 3.1. Each NL scan targets an acMGDG group with a common acyl-Gal component and varied DAG components. The DAG components targeted in each NL scan (Table 3.1) are listed in Table S3.1. In contrast to the previous method used by our group to detect acMGDGs by targeting fatty acyl anions (Vu et al., 2012), which did not identify the position of the detected fatty acid among the three positions in acMGDG, the current method detects the fatty acid linked to the galactose. To compare amounts of acMGDGs, signals were normalized to the signal of an internal standard, with an amount of signal equal to that of 1 nmol of the standard equal to 1. This approach allows sample-to-sample comparison of signals. More detail on the acMGDGs (as defined by DAG species in combination with each acyl-galactose species) may be viewed in Table S3.2.

Figure 3.1B shows that various plant species, from the monocot wheat to eudicots tomato and Arabidopsis, produce acMGDG in response to wounding. acMGDG is formed within 45 min after wounding with a hemostat. Fold increases of acMGDG in leaves 45 min after wounding were 3 for tomato, 18 for wheat, 20 for Arabidopsis C24 and 130 for Arabidopsis Col-0.

In acMGDG produced in response to wounding, the fatty acyl species linked to Gal varied among plant species (Figure 3.2). Figure 3.2A shows that in Arabidopsis Col-0, the most abundant Gal-linked fatty acids were 18:4-O, which has been identified as OPDA in galactolipids (Stelmach et al., 2001; Buseman et al., 2006), 16:0, 18:3-2O/20:1, 18:3 and 18:3-O (49, 19, 11, 7 and 4%, respectively, of the total acMGDG measured). Gal-linked fatty acids 18:3-2O and 20:1 have the same nominal mass and thus are not differentiated by this method. In agreement with previous analyses of *Arabidopsis thaliana* Col-0, three acMGDGs with the most abundant signals were 1-OPDA,2-dnOPDA,3-(OPDA-galactosyl) glycerol (Arabidopside E,

38% of total acMGDG signal), 1-OPDA,2-dnOPDA,3-(16:0-galactosyl) glycerol (14%) and 1,2-diOPDA,3-(OPDA-galactosyl) glycerol (7%, Arabidopside G) (Table S3.2; Andersson et al., 2006, Ibrahim et al., 2011, Kourtchenko et al., 2007, Vu et al., 2012). In Arabidopsis C24, Gal linkage of unoxidized fatty acids was more prevalent: 18:3 (32% of total acMGDG signal), 16:0 (19%), OPDA (18%), 18:2 (6%), 18:3-O (6%) and 18:3-2O/20:1 (6%) compared to Col-0 after the same wounding treatment (Figure 3.2B). While the amount of acMGDG with OPDA esterified to Gal is approximately 10-fold less in Arabidopsis C24 than in Arabidopsis Col-0, the amount of acMGDG with 18:3 esterified to Gal was slightly higher in C24 than in Col-0. Similarly, MS signals from acMGDGs in wounded tomato and wheat leaves were derived primarily from unoxidized Gal-linked fatty acids: 16:0 (40%), 18:3 (27%) and 18:2 (15%) in tomato; 18:3 (73%), 16:0 (9%) and 18:2 (6%) in wheat (Figure 3.2C–D). Scanning for NL 439.3 (18:3-containing Gal) in samples from wheat 45 min after wounding produced a massive peak at m/z 1052.8, whose signal accounted for 72% of the total acMGDG signal (Table S3.2). Accurate-mass product ion analysis of this species (acetate adduct, $[M + C_2H_3O_2]^-$, m/z 1093.8) by Q-TOF MS in the negative mode (Buseman et al., 2006, Vu et al., 2012) showed that this largest acMGDG component of wheat contained only 18:3 acyl chains, consistent with a structure of 1,2-di18:3,3-(18:3-galactosyl) glycerol (Figure S3.1). Table S3.3 shows the acyl composition (three chains) of the major acMGDG molecular species detected in Arabidopsis Col-0, tomato and wheat and the supporting accurate-mass product ion analysis.

acMGDGs accumulate following stress, including sub-lethal freezing

The total amounts of acMGDG formed under different stress treatments were determined using the NL scans indicated in Table 3.1 (Figure 3.3). As shown previously by precursor scanning for acyl anions, infection of *Arabidopsis thaliana* Col-0 with the avirulent bacteria *Pst* induced large amounts of acMGDG (Figure 3.3A; Vu et al., 2012). Wounding also induced acMGDG (Figure 3.3B). Similarly, sub-lethal freezing induced synthesis of acMGDG (Figure 3.3C). Levels of acMGDG with unoxidized fatty acyl chains had not been previously determined (Vu et al., 2012; next section). In the experiment shown in Figure 3.3C–E, Arabidopsis Col-0 plants were cold-acclimated at 4°C for 3 days or not acclimated (remained at the growth temperature of 21°C) until the freezing treatment (2 h at −8°C). Plants were returned to 21°C after freezing and sampled 3 h or 24 h later. As indicated by measurement of ion leakage at 24 h (Figure 3.3D),

non-acclimated plants sustained more damage than acclimated plants ($P < 0.001$). Figure 3.3C indicates that levels of acMGDG increased during the post-freezing period in both acclimated and non-acclimated plants, but that the levels were always higher in non-acclimated than in acclimated plants. Ion leakage measurements (Figure 3.3D) indicate that the membranes of acclimated plants were quite permeable at 3 h into the recovery period, but less so at 24 h ($P < 0.01$). In contrast, the non-acclimated plants showed greater leaf membrane damage after 24 h post freezing than at 3 h ($P < 0.05$) and much more damage at 24 h than observed in acclimated plants. Indeed, acclimated plants sustained visible damage to leaves, but the leaves were able to recover, while the damaged leaves of non-acclimated plants died, although the plant did not (see Figure S3.2). Levels of the phospholipid hydrolytic product phosphatidic acid (PA) are shown in Figure 3.3E. (Levels of other membrane lipids are shown in Table S3.4). Whereas total PA levels (Figure 3.3E) were closely correlated with leaf ion leakage (Figure 3.3D), the total acMGDG signal (Figure 3.3C) did not correlate strictly with leaf injury. Acclimated plants tended to accumulate acMGDG between 3 h and 24 h ($P < 0.1$) after freezing treatment as ion leakage dropped. Taken together, comparison of acMGDG signals in acclimated and non-acclimated plants demonstrates a link between treatment and total acMGDG accumulation, but acMGDG accumulated even during recovery.

The composition of induced acMGDGs varies among stresses

The most abundant acMGDGs in Col-0 leaves after infection of the plants by *Pst* (24 h) were those with Gal-linked fatty acids OPDA (56%), 16:0 (17%), 18:3 (10%), 18:3-2O/20:1 (6%) and 16:4-O (4%) (Figure 3.4A). The acMGDG composition, with a prevalence of OPDA and 16:0 on Gal, was similar to that formed after wounding (Figure 3.4B). The acMGDG Gal-linked acyl composition was drastically different in plants 24 h after freezing. In acclimated plants (Figure 3.4C), 18:3 (48%), 16:0 (14%), OPDA (14%), 16:3 (10%) and 18:2 (6%) were most prevalent, and in non-acclimated plants (Figure 3.4D), 18:3 (58%), 16:3 (13%), 16:0 (11%), 18:2 (7%) and OPDA (4%) were highest. Although acclimated plants accumulated approximately five-fold less acMGDG than non-acclimated plants, they accumulated approximately the same amount of OPDA-Gal acMGDG (0.48 ± 0.23 normalized MS units mg^{-1} dry mass in acclimated plants compared with 0.59 ± 0.17 units in non-acclimated plants).

Overall, the data demonstrate that during recovery from freezing, as well as during Pst infection and after wounding, significant acylation of the Gal of MGDG was induced. However, in contrast to the composition during other stresses, after freezing, the Gal-linked acyl chains were mostly unoxidized.

The proportions of 16:3, 16:0 and 18:3 in the Gal-esterified acyl chains in acMGDGs resemble proportions in DGDG

The formation of acMGDG, by a dismutation reaction when MGDG was the only substrate or by transacylation from DGDG when both MGDG and DGDG were present, has been demonstrated in in vitro experiments (Heinz, 1967b; Heinz, 1972). To define the in vivo substrate(s) for acMGDG formation, we considered the acyl compositions of Arabidopsis MGDG and DGDG. Leaf MGDG contains two major molecular species; 18:3/16:3 MGDG is present at higher levels than di18:3 MGDG. Leaf DGDG has three major molecular species: di18:3 DGDG > (16:0/18:3 DGDG + 18:3/16:0 DGDG) > 18:3/16:3 DGDG. The acyl composition of MGDG has previously been analyzed: 59% 18:3, 33% 16:3 and only 1% 16:0, whereas the acyl composition of DGDG contains 77% 18:3, 3% 16:3 and 12% 16:0 (Miquel et al., 1998). Comparing the percentages of 16:0 and 16:3 (and other acyls) esterified to the Gal of acMGDG of stressed (induced) samples to the percentages in MGDG and DGDG of untreated samples should shed light on the origin(s) of the acyl groups (Figure 3.5). The fatty acid compositions of MGDG and DGDG used in the current analysis were estimated from the percentage of each MGDG and DGDG molecular species determined by head-group scanning of untreated samples, with assignment of molecular species based on previous product ion analysis (Devaiah et al., 2006). Detailed estimation is shown in Table S3.5. The percentages of each fatty acid in MGDG and DGDG determined in this way on the untreated samples were in close agreement with the previously published data (Miquel et al., 1998). When acMGDG formation is induced by stresses in Col-0, fatty acid oxidation also occurs at various levels. Hence, for comparison of normal and head group-acylated galactolipid compositions, the contents of unoxidized fatty acids and their oxidized derivatives were summed: i.e. 16:3 and its major oxidized derivative, 16:4-O, were combined; similarly, 18:3, 18:4-O, 18:3-O and 18:3-2O were combined, as were 18:2 and 18:2-2O. The composition of the fatty acids linked to Gal in acMGDG during stress responses, reveals that the percentage of 16:0, ranging from 11 to 19%, is similar to the percentage in DGDG (11%) and

much higher than in MGDG (0.1%, Figure 3.5). While it is possible that under certain circumstances, some fatty acyl chains used to esterify Gal might come from MGDG, as suggested by the somewhat higher percentage of 16:3 and 16:4-O incorporated on the Gal of acMGDG following freezing stress (Figure 3.5E–F), the data are consistent with DGDG as the major source of the Gal-esterified fatty acids in acMGDG formed in vivo.

The oxidized fatty acyl chain OPDA is enriched on the Gal of acMGDG

To determine relative amounts of OPDA and 18:3 in MGDG, DGDG and acMGDG, ratios of MS signals for OPDA and 18:3 in MGDG and DGDG were measured using ESI triple quadrupole MS precursor scanning in negative mode, while ratios of MS signals for OPDA and 18:3 on the Gal of acMGDG were measured using NL scanning in positive mode. Levels of MGDG and DGDG detected by negative precursor scans for 18:4-O (includes OPDA), 18:3-O and 18:2-O are shown in Table S3.6. The ratios of OPDA to 18:3 signals under different treatments are shown in Table 3.2. *Pst* infection and wounding of Col-0 significantly increased the OPDA level in MGDG and DGDG ($P < 0.001$) and the OPDA/18:3 signal ratio in MGDG and DGDG ($P < 0.05$). However, the OPDA/18:3 signal ratio was several orders of magnitude higher on the Gal of acMGDG than in MGDG and DGDG under both induced and non-induced conditions. Although neither acclimated nor non-acclimated plants accumulated much OPDA in galactolipids after freezing treatment, the OPDA/18:3 signal ratio from the acyl chains on the Gal of acMGDG was significantly greater than the OPDA/18:3 signal ratio from the acyl chains esterified to the glycerols of MGDG and DGDG. Interestingly, OPDA enrichment on the Gal of induced acMGDG in cold-acclimated Col-0 plants is greater than in non-acclimated Col-0 recovering from sub-lethal freezing (Table 3.2). Taken together, the data in Table 3.2 indicate that the enrichment of OPDA on the Gal of acMGDG is roughly correlated with the availability of OPDA in MGDG and DGDG, and OPDA is concentrated in the pool of fatty acids linked to the Gal of acMGDG.

Oxidized acMGDG induction is enhanced by re-wounding

Although the existence of acMGDG has long been known, its physiological roles are still largely unclear. The fully oxidized acMGDGs Arabidopside E and Arabidopside G have been demonstrated to have anti-fungal and anti-bacterial activities in vitro (Andersson et al., 2006; Kourtchenko et al., 2007). One hypothesis about acMGDG function is that oxidized fatty acid-containing complex lipids may serve as reservoirs for precursors of oxylipin-derived phytohormones such as jasmonic acid (JA). In order to test this hypothesis, we wounded Col-0 leaves twice at the same place, with the second wound occurring either 24 or 48 h after the first. Leaves were harvested for lipid extraction at 0 min, 5 min, 15 min, 45 min, 4 h, 24 h and 48 h following each wounding event. Harvested leaves were extracted and analyzed for both complex lipids and the free phytohormones JA and OPDA. There was no enhancement by re-wounding in levels of induced total free JA and total free OPDA (Figure S3.3), indicating that the accumulation of pools of esterified oxylipins did not trigger a significantly faster or stronger response in levels of free JA or OPDA upon re-wounding.

Figure 3.6 shows levels of plastidic complex lipids MGDG, DGDG and acMGDG. Whereas free oxylipin content was not significantly higher upon re-wounding, signals from oxidized MGDG and DGDG (Figure 3.6A–C) were clearly increased by a second wounding to levels higher than by a single wounding. The second wounding did not induce major and sustained increases in signals from unoxidized acMGDG (Figure 3.6D–F). In contrast, the levels of oxidized acMGDGs (Figure 3.6G–H) were much higher during re-wounding and remained higher than the levels induced by the first wounding for up to 48 h after re-wounding.

Discussion

The present work demonstrates that acMGDGs are formed in planta across species (Figure 3.1B). Prior work established that wounding and bacterial infection induce acMGDG production in Arabidopsis (Andersson et al., 2006; Kourtchenko et al., 2007; Vu et al., 2012). Homogenization was also reported to induce MGDG acylation in spinach and broad bean leaves (Heinz 1967a, Heinz 1972). Here, we demonstrated that acMGDG is also formed in tomato and wheat in response to wounding, suggesting that Gal acylation of MGDG is a conserved response

to stress in plants. We also demonstrate that sub-lethal freezing induces acMGDG synthesis in the post-freezing period (Figure 3.3C). This was not observed in our previous study, which focused only on oxidized acMGDG and analyzed lipid levels only to the end of the freezing period (Vu et al., 2012).

The acyl composition of the acyl-Gal in acMGDG differs in different circumstances. Factors that affect the composition include the plant species, the applied stress, and, likely, other factors that affect the composition of the galactolipid pool. In general the data support the notion that in vivo formation of acMGDG occurs via transacylation from DGDG, as demonstrated previously for in vitro formation (Heinz, 1967b; Heinz, 1972). Species and accessions with more oxidized lipids in the galactolipid pool (Col-0 > C24 > other species) have more oxidized lipids in acMGDG. Stresses that induce more lipid oxidation (bacterial infection and wounding) vs those that induce less (freezing) also result in production of acMGDG with more oxidized molecular species. Wound-induced acMGDGs containing Gal-linked OPDA (Arabidopsides E and G) were not detected in *Brassica napus*, *Nicotiana tabacum*, *Pisum sativum*, *Spinacia oleracea*, *Avena sativa* and barley (Kourtchenko et al., 2007). However, we cannot rule out the possibility that acMGDG is produced in these species with unoxidized fatty acids linked to Gal, similar to the observed reaction products in wheat.

At the same time, the composition of the acyl-Gal in Arabidopsis acMGDG was determined to be more oxidized than the galactolipid acyl pool as a whole. Ibrahim et al. (2011) reported that the ratio of unoxidized acMGDG to oxidized acMGDG in Col-0 leaves harvested 30 min after wounding (regardless of the positions of oxidized fatty acids on acMGDGs) is 0.6; the detection of such a high level of oxidation agrees with our data showing that oxidized fatty acids are enriched in acMGDG. Two possible explanations for the enrichment of OPDA on the Gal of acMGDG are: (1) that an acyltransferase preferentially acylates Gal with an oxidized fatty acid compared to an unoxidized one or (2) that an oxidizing enzyme, such as a lipoxygenase, can act efficiently and directly on an unoxidized fatty acid bound to Gal. The data suggest that, as previously demonstrated in vitro, DGDG in particular is likely to be the source of acyl chains for MGDG acylation to acMGDG in vivo. To date, no protein or gene directly responsible for acylation of acMGDG has been identified. The oxidized MGDGs and DGDGs, such as

Arabidopsides A, B and D (OPDA/dnOPDA MGDG, diOPDA MGDG and diOPDA DGDG, respectively, Figure 3.6A–C) are among the most rapidly formed compounds during stress responses, and the production of acMGDG always lags behind the production of these potential substrate species. This might support the idea of preferential acylation with oxidized fatty acids. On the other hand, Nilsson et al. (2012) presented data suggesting that oxidizing enzymes can directly catalyze oxidation of membrane bound fatty acids. Interaction between a soluble lipoxygenase and a Gal-linked acyl chain might be even more likely. If an oxidizing enzyme could preferentially interact with head group-linked fatty acyl chains, this would support the second possibility.

One potential function for acMGDGs might be as a reservoir for signaling compounds. Another possibility is that acMGDGs are just signs of damage. The current work did not provide support for either of those possibilities. JA and OPDA production was not directly correlated with acMGDG levels, nor was leaf damage linked with acMGDG levels in the recovery period after freezing. An alternative notion is that the acMGDG pool serves to sequester potentially harmful fatty acids from the main membrane lipid pool. Two examples of accumulation of acMGDG during stress responses support this idea. In the period after freezing, cold-acclimated plants accumulated acMGDG as the leaves recovered and ion leakage decreased (Figure 3.3). This acMGDG in acclimated leaves was enriched in oxidized fatty acid more than the acMGDG accumulated in non-acclimated leaves which do not recover from freezing damage. The second example is accumulation of acMGDG during re-wounding (Figure 3.6). In this case, upon rewounding, levels of acMGDG with oxidized fatty acids linked to Gal appeared to increase more and to stay increased longer than other galactolipid derivatives. These examples imply that acMGDG species are relatively long-lived and may persist and increase as recovery from stress occurs.

Acknowledgements

The authors would like to thank Dr Ernst Heinz for his encouragement and helpful comments. We are grateful to Drs Xuemin Wang and Jyoti Shah for their participation in related studies. We thank Dr Mark Ungerer for use of a freezing chamber and Dr Ari Jumponen for use of a light

cart. We appreciate Dr Sunish Sehgal allowing us to harvest wheat leaves from his plantings. This work was supported by the National Science Foundation (MCB 0920663 to R. W.). Instrument acquisition at the Kansas Lipidomics Research Center was supported by National Science Foundation (EPS 0236913, DBI 0521587, DBI 1228622), Kansas Technology Enterprise Corporation, K-IDeA Networks of Biomedical Research Excellence (INBRE) of National Institutes of Health (P20RR16475) and Kansas State University. Contribution no. 13-362-J from the Kansas Agricultural Experiment Station.

References

Andersson MX, **Hamberg M**, **Kourtchenko O**, **Brunnström A**, **McPhail KL**, **Gerwick WH**, **Gobel C**, **Feussner I**, **Ellerström M** (2006) Oxylipin profiling of the hypersensitive response in Arabidopsis thaliana. Formation of a novel oxo-phytodienoic acid-containing galactolipid, arabidopside E. J Biol Chem **281**: 31528–31537

Bligh EG, **Dyer WJ** (1959) A rapid method for total lipid extraction and purification. Can J Biochem Physiol **37**: 911–917

Bottcher C, **Weiler EW** (2007) cyclo-Oxylipin-galactolipids in plants: occurrence and dynamics. Planta **226**: 629–637

Buseman CM, **Tamura P**, **Sparks AA**, **Baughman EJ**, **Maatta S**, **Zhao J**, **Roth MR**, **Esch SW**, **Shah J**, **Williams TD**, **Welti R** (2006) Wounding stimulates the accumulation of glycerolipids containing oxophytodienoic acid and dinor-oxophytodienoic acid in Arabidopsis leaves. Plant Physiol **142**: 28–39

Devaiah SP, **Roth MR**, **Baughman E**, **Li M**, **Tamura P**, **Jeannotte R**, **Welti R**, **Wang X** (2006) Quantitative profiling of polar glycerolipid species from organs of wild-type Arabidopsis and a PHOSPHOLIPASE Dα1 knockout mutant. Phytochemistry **67**: 1907–1924

Heinz E (1967a) Acylgalactosyldiglyceride from leaf homogenates. Biochim Biophys Acta **144**: 321–332

Heinz E (1967b) On the enzymatic formation of acylgalactosyldiglyceride. Biochim Biophys Acta **144**: 333–343

Heinz E (1972) Some properties of the acyl galactosyl diglyceride-forming enzyme from leaves. Z Pflanzenphysiol **69**: 359–376

Heinz E, **Tulloch AP** (1969) Reinvestigation of the structure of acyl galactosyl diglyceride from spinach leaves. Hoppe-Seyler's Z Physiol Chem **350**: 493–498

Ibrahim A, **Schutz AL**, **Galano JM**, **Herrfurth C**, **Feussner K**, **Durand T**, **Brodhun F**, **Feussner I** (2011) The Alphabet of Galactolipids in Arabidopsis thaliana. Front Plant Sci **2**: 95

Kourtchenko O, **Andersson MX**, **Hamberg M**, **Brunnström A**, **Gobel C**, **McPhail KL**, **Gerwick WH**, **Feussner I**, **Ellerström M** (2007) Oxo-phytodienoic acid-containing galactolipids in Arabidopsis: jasmonate signaling dependence. Plant Physiol **145**: 1658–1669

Miquel M, **Cassagne C**, **Browse J** (1998) A new class of Arabidopsis mutants with reduced hexadecatrienoic acid fatty acid levels. Plant Physiol **117**: 923–930

Nilsson AK, **Fahlberg P**, **Ellerström M**, **Andersson MX** (2012) Oxo-phytodienoic acid (OPDA) is formed on fatty acids esterified to galactolipids after tissue disruption in Arabidopsis thaliana. FEBS Lett **586**: 2483–2487

Schmelz EA, **Engelberth J**, **Tumlinson JH**, **Block A**, **Alborn HT** (2004) The use of vapor phase extraction in metabolic profiling of phytohormones and other metabolites. Plant J **39**: 790–808

Stelmach BA, **Muller A**, **Hennig P**, **Gebhardt S**, **Schubert-Zsilavecz M**, **Weiler EW** (2001) A novel class of oxylipins, sn1-O-(12-oxophytodienoyl)-sn2-O-(hexadecatrienoyl)-monogalactosyl Diglyceride, from Arabidopsis thaliana. J Biol Chem **276**: 12832–12838

Telfer A, **Bollman KM**, **Poethig RS** (1997) Phase change and the regulation of trichome distribution in Arabidopsis thaliana. Development **124**: 645–654

Vu HS, **Tamura P**, **Galeva NA**, **Chaturvedi R**, **Roth MR**, **Williams TD**, **Wang X**, **Shah J**, **Welti R** (2012) Direct infusion mass spectrometry of oxylipin-containing Arabidopsis membrane lipids reveals varied patterns in different stress responses. Plant Physiol **158**: 324–339

Xiao S, **Gao W**, **Chen QF**, **Chan SW**, **Zheng SX**, **Ma J**, **Wang M**, **Welti R**, **Chye ML** (2010) Overexpression of Arabidopsis acyl-CoA binding protein ACBP3 promotes starvation-induced and age-dependent leaf senescence. Plant Cell **22**: 1463–1482

Figures and Tables

Figure 3.1 acMGDG structure and occurrence upon wounding.

A) Structure of a representative acMGDG molecule, 1-18:4-O,2-16:4-O,3-(16:0-galactosyl)glycerol and the fragmentation that gives rise to the NL fragment by collision induced dissociation. A proton moves from right to left during fragmentation. B) Total acMGDG induced by wounding, measured by the 11 NL scans indicated in Table 3.1, in Arabidopsis Col-0 and C24, tomato, and wheat leaves. Units are in relation to amount of signal detected for 1 nmol of internal standard (di18:0 DGDG), which is denoted as 1. Error bars are standard deviation, n = 5. The numbers above the bars of wounded samples show the fold induction compared to corresponding unwounded samples.

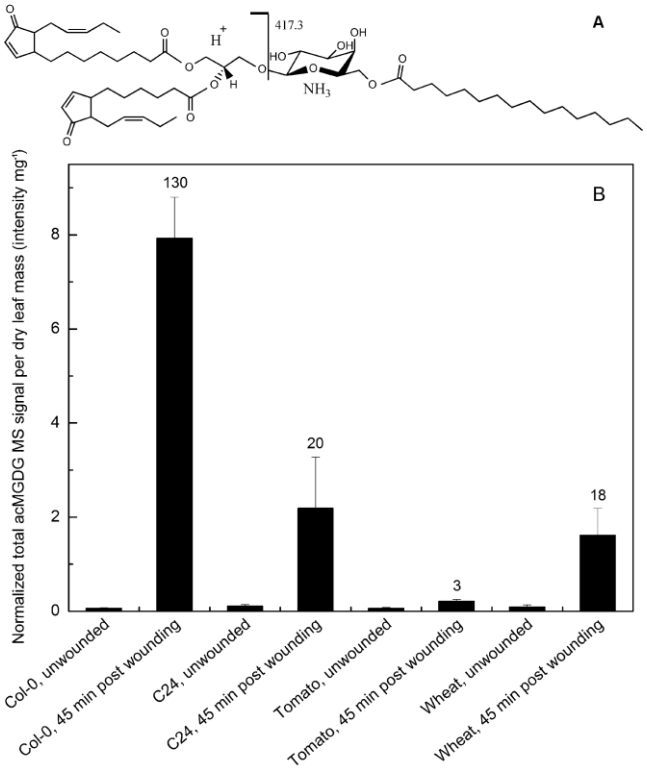

Figure 3.2 Levels of acMGDG (grouped by fatty acyl moiety on the Gal) in leaves of Arabidopsis Col-0 (A) and C24 (B), tomato (C), and wheat (D) 45 min after wounding. The y axes have different scales. Error bars are standard deviation, n = 5. The numbers above the bars show the percentage of the corresponding acMGDG group over the sum of the 11 measured acMGDG groups.

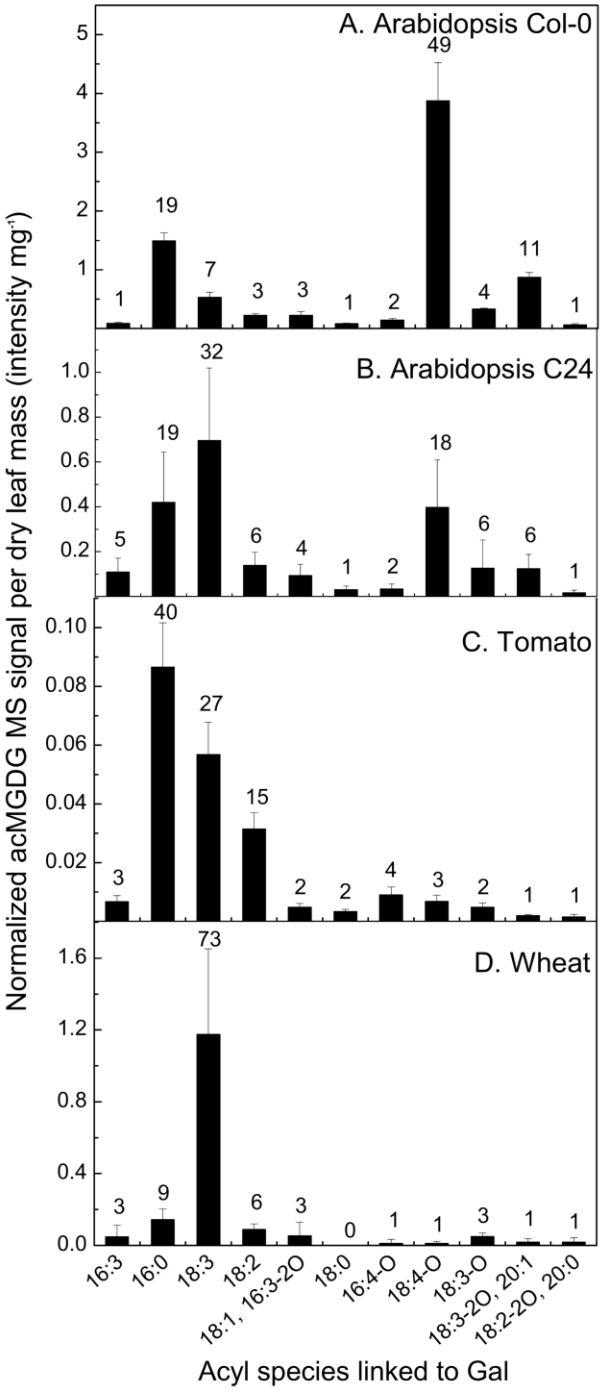

Figure 3.3 acMGDG forms in leaves of Arabidopsis Col-0 after application of different stresses, and its occurrence during freezing is not directly associated with cell membrane ion leakage.

Panels A, B, and C: acMGDG induced by Pst infection, wounding, and freezing. The y axes have different scales. Panel C shares an x-axis with Panels D and E. Panel D: Relative ion leakage (%) of acclimated and non-acclimated Arabidopsis Col-0 leaves at 3 h and 24 h after freezing treatment. Panel E: Level of total phosphatidic acid as measured by MS in acclimated and non-acclimated Arabidopsis Col-0 leaves at 3 h and 24 h after freezing treatment. Error bars are standard deviation; panels A and B: n = 5; panels C, D, and E: n = 6.

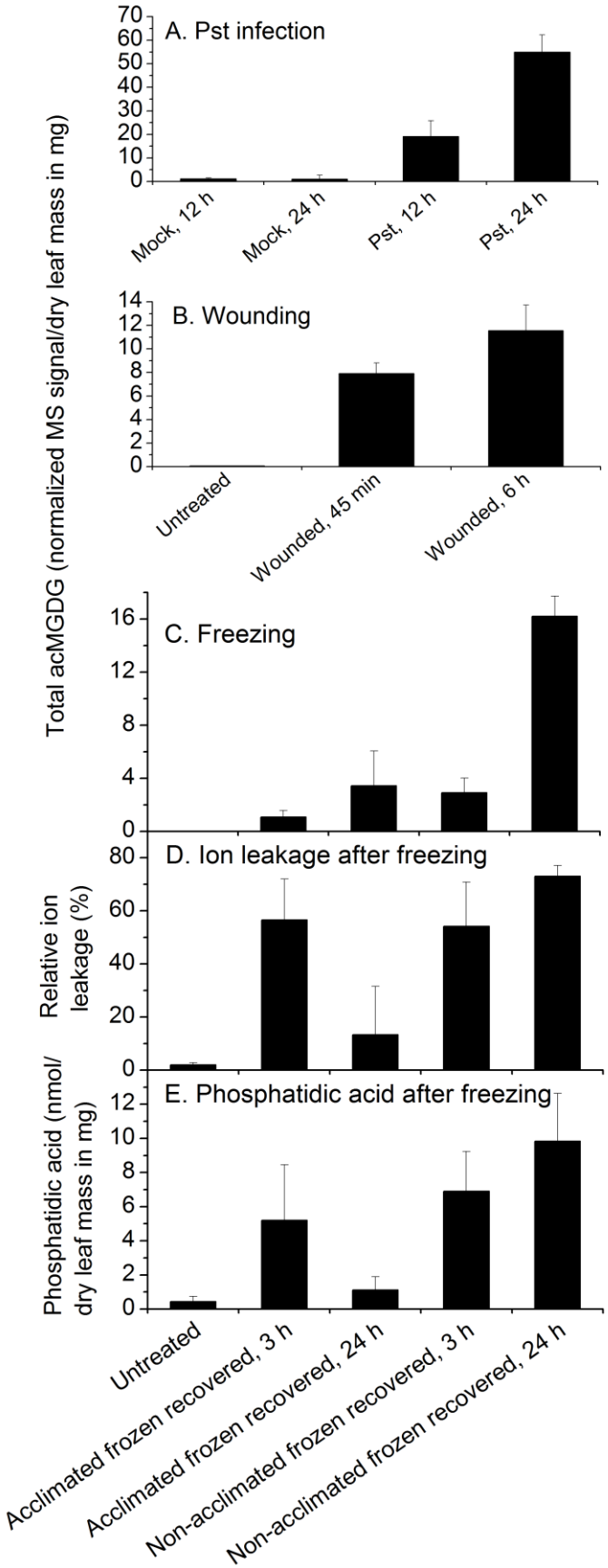
A. Pst infection
B. Wounding
C. Freezing
D. Ion leakage after freezing
E. Phosphatidic acid after freezing
Total acMGDG (normalized MS signal/dry leaf mass in mg)
Relative ion leakage (%)
Phosphatidic acid (nmol/ dry leaf mass in mg)
Mock, 12 h
Mock, 24 h
Pst, 12 h
Pst, 24 h
Untreated
Wounded, 45 min
Wounded, 6 h
Untreated
Acclimated frozen recovered, 3 h
Acclimated frozen recovered, 24 h
Non-acclimated frozen recovered, 3 h
Non-acclimated frozen recovered, 24 h

Figure 3.4 Levels of acMGDG (grouped by fatty acyl moiety on the Gal) in leaves of Arabidopsis Col-0 after application of different stresses.

Panel A: acMGDG at 24 h post Pst infection, n = 5; panel B: acMGDG at 45 min post wounding, n = 5; panel C: acMGDG of cold acclimated Col-0 plants at 24 h post freezing, n= 6; panel D: acMGDG of non-acclimated Col-0 plants at 24 h post freezing, n = 6. Y axes have different scales. Error bars are standard deviation. The numbers above the bars show the percentage of the corresponding acMGDG group over the sum of the 11 measured acMGDG groups.

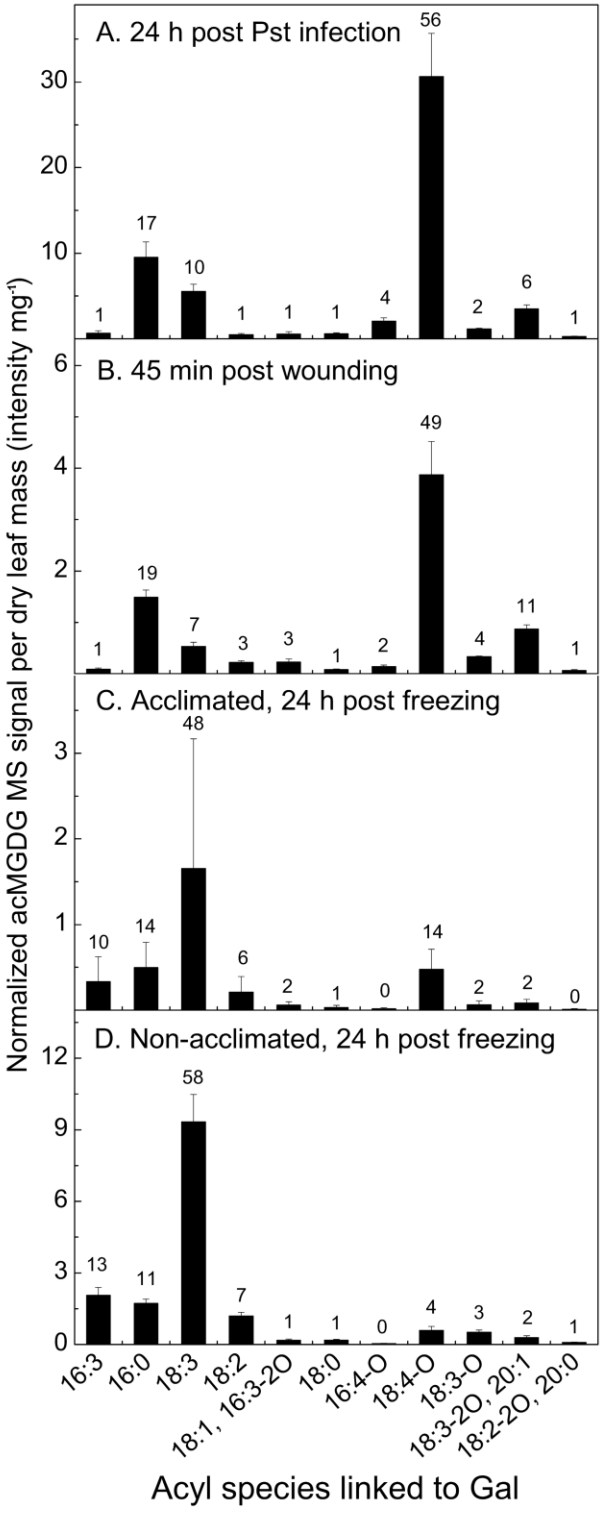
A. 24 h post Pst infection
B. 45 min post wounding
C. Acclimated, 24 h post freezing
D. Non-acclimated, 24 h post freezing
Normalized acMGDG MS signal per dry leaf mass (intensity mg-1)
Acyl species linked to Gal
16:3
16:0
18:3
18:2
18:1, 16:3-2O
18:0
16:4-O
18:4-O
18:3-O
18:3-2O, 20:1
18:2-2O, 20:0

Figure 3.5 Comparison of fatty acyl composition.

Fatty acyl composition (%) of MGDG (A) and DGDG (B) in untreated leaves and fatty acid composition of acyl-Gal in acMGDG of Col-0 plants at 24 h post Pst infection (C), n = 5; and at 45 min post wounding (D), n = 5; of cold acclimated (E) and of non-acclimated (F) Col-0 plants at 24 h post freezing, n = 6.

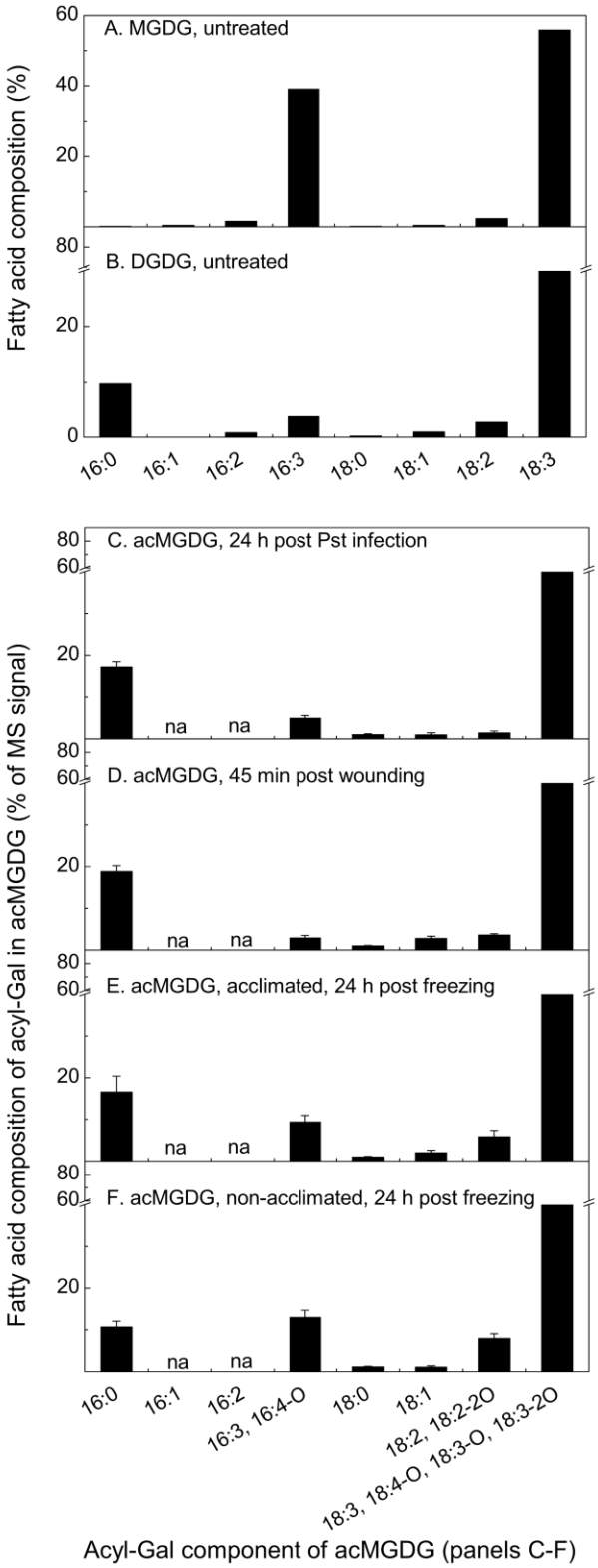
A. MGDG, untreated
B. DGDG, untreated
Fatty acid composition (%)
C. acMGDG, 24 h post Pst infection
D. acMGDG, 45 min post wounding
E. acMGDG, acclimated, 24 h post freezing
F. acMGDG, non-acclimated, 24 h post freezing
Fatty acid composition of acyl-Gal in acMGDG (% of MS signal)
na
16:0
16:1
16:2
16:3, 16:4-O
18:0
18:1
18:2, 18:2-2O
18:3, 18:4-O, 18:3-O, 18:3-2O
Acyl-Gal component of acMGDG (panels C-F)

Figure 3.6 Levels of oxidized MGDG, DGDG, and acMGDG, measured by Pre 277.2 (18:3) and Pre 291.2 (18:4-O) using direct infusion ESI triple quadrupole MS in negative mode. Levels of lipids were measured at various time points after wounding was performed at 0 h (squares). Data denoted by circles show levels of lipids after a second wounding at the 24 h time point of the first wounding, and data denoted by triangles show levels of lipids after a second wounding at the 48 h time point of the first wounding. The x-axis indicates time (h) starting from the only wounding event (squares) or final wounding event (circles and triangles). Y axes are mass spectral signal for the indicated compound, where 1 is the amount of signal detected for 1 nmol of internal standard (18:0/16:0 MGDG), The y axes have different scales. Error bars are standard deviation, n = 5.

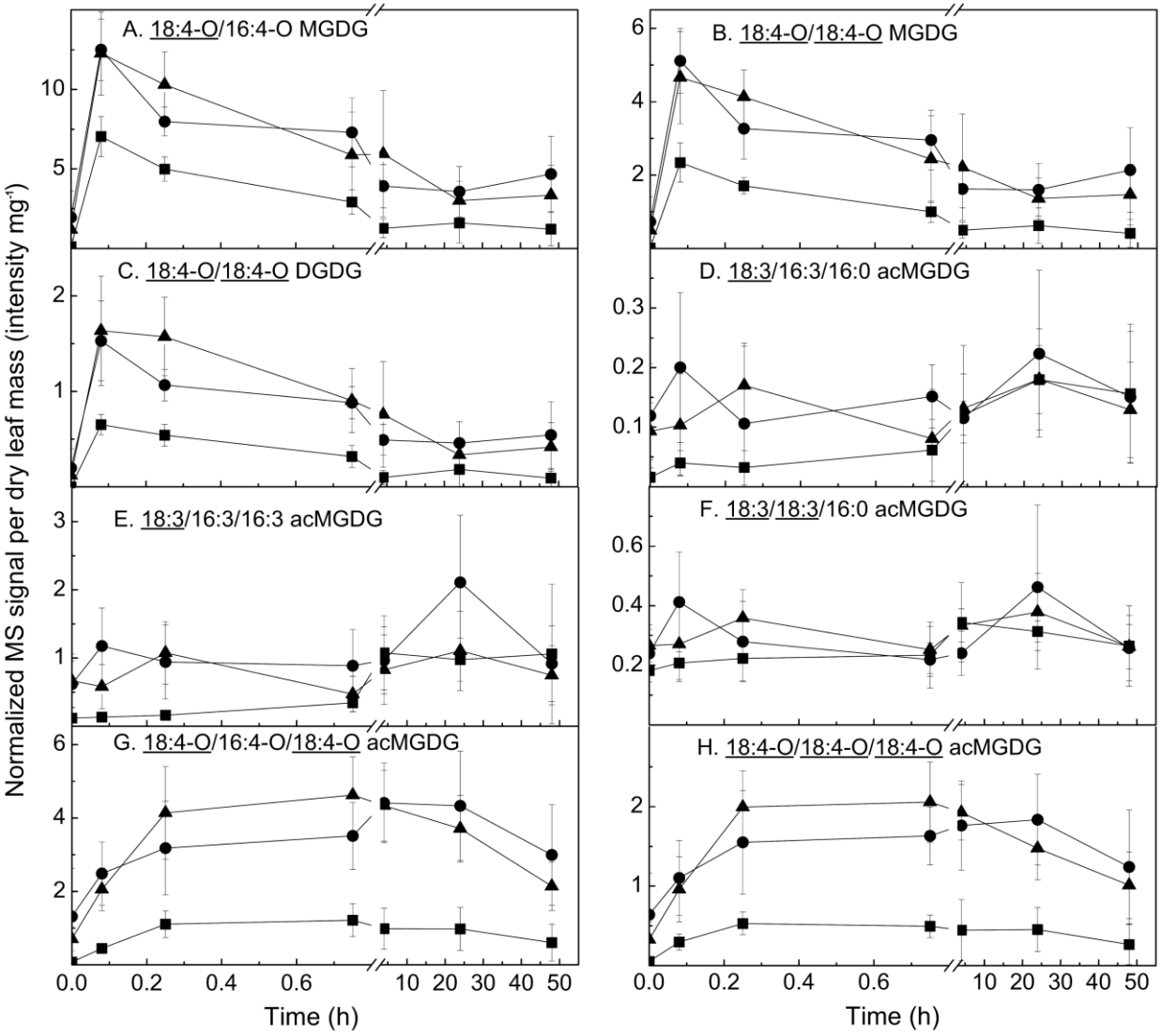

Table 3.1 NL fragments used to detect acMGDGs by ESI triple quadrupole MS in positive mode

m/z of NL fragment	Fatty acyl chain	Chemical formula of NL fragment
411.3	16:3	$C_{22}H_{37}O_6N$
417.3	16:0	$C_{22}H_{43}O_6N$
425.3	16:4-O	$C_{22}H_{35}O_7N$
439.3	18:3	$C_{24}H_{41}O_6N$
441.3	18:2	$C_{24}H_{43}O_6N$
443.3	18:1, 16:3-2O	$C_{24}H_{45}O_6N$, $C_{22}H_{37}O_7N$
445.3	18:0	$C_{24}H_{47}O_6N$
453.3	18:4-O	$C_{24}H_{39}O_7N$
455.3	18:3-O	$C_{24}H_{41}O_7N$
471.3	18:3-2O, 20:1	$C_{24}H_{41}O_8N$, $C_{26}H_{49}O_6N$
473.3	18:2-2O, 20:0	$C_{24}H_{43}O_8N$, $C_{26}H_{51}O_6N$

Table 3.2 Ratio of signals from OPDA/18:3 in galactolipids of *Arabidopsis thaliana.*

Total OPDA-containing MGDG and DGDG (normalized mass spectral signal unit per dry leaf mass), measured by scanning Pre 291.2 in negative mode (complete data in Table S3.6), are shown in the second column. Col-0 was subjected to Pst infection ("Pst, 24 h", n = 5), freezing and post-freezing at 21 °C with or without prior cold acclimation ("acclimated, 24 h" or "non-acclimated, 24 h", n = 6), and wounding ("wounded, 45 min", n = 5). C24 was also wounded and sampled after 45 min ("wounded, 45 min", n = 5). The third through fifth columns indicate the ratio of signals derived from OPDA to signals derived from 18:3 in acyl chains of MGDG, acyl chains of DGDG, or from the acyl chain on the Gal of acMGDG. Errors are standard deviation.

Treatment	**OPDA-containing MGDG and DGDG (intensity mg^{-1})**	**Ratio of OPDA/18:3 signals**		
		in MGDG	**in DGDG**	**on Gal of acMGDG**
Col-0, untreated	0.02 ± 0.01	0.0005 ± 0.0002	0.0049 ± 0.0005	5.39 ± 3.50
Col-0, Pst, 24 h	0.81 ± 0.15	0.022 ± 0.006	0.041 ± 0.010	5.82 ± 1.95
Col-0, acclimated, 24 h	0.013 ± 0.013	0.0006 ± 0.0010	0.0008 ± 0.0006	0.51 ± 0.36
Col-0, non-acclimated, 24 h	0.017 ± 0.009	0.0092 ± 0.0080	0.0080 ± 0.0070	0.063 ± 0.017
Col-0, wounded, 45 min	1.26 ± 0.23	0.0085 ± 0.0053	0.022 ± 0.011	24.1 ± 6.5
C24, untreated	0.17 ± 0.07	0.0004 ± 0.0003	0.0027 ± 0.0026	0.39 ± 0.21
C24, wounded, 45 min	0.26 ± 0.13	0.0013 ± 0.0007	0.0058 ± 0.0018	0.56 ± 0.07

Supplemental Data

Supplemental data for this chapter include:

Figure S3.1 Tentative structure of 18:3/18:3/18:3 acMGDG detected in wounded wheat leaves

Figure S3.2 Acclimated and non-acclimated *Arabidopsis thaliana* Col-0 after freezing at -8 °C for 2 h

Figure S3.3 Total free OPDA and JA after wounding and re-wounding of Col-0 plants

Tables S3.1-S3.6 are in a separate Excel file

Table S3.1 DAG fragments of acMGDG determined during NL scanning by ESI triple quadrupole mass spectrometry in positive mode using scan modes listed in Table 3.1

Table S3.2 Levels of acMGDG detected by NL scans of individual replicates (in normalized mass spectral signal unit mg-1 leaf dry mass)

Table S3.3 Accurate masses of acyl groups of acMGDG from wounded Col-0, tomato and wheat provided by Q-TOF mass spectrometry in negative mode

Table S3.4 Levels of normal chain phospholipids and galactolipids detected by triple quadrupole mass spectrometry (in nmol mg-1 leaf dry mass), performed as described in Xiao et al. (2010, supplemental data)

Table S3.5 Estimation of fatty acid composition in MGDG and DGDG

Table S3.6 Levels of 18:4-O- and 18:3-O-containing MGDG, DGDG, and phosphatidylglycerol (PG) detected by Pre scans of 291.2, 293.2 and 295.2 in negative mode, as described by Vu et al. (2012)

Figure S3.1 Tentative structure of 18:3/18:3/18:3 acMGDG detected in wounded wheat leaves.

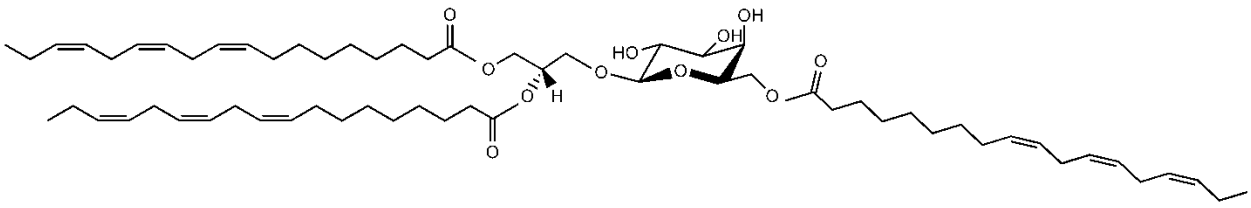

Figure S3.2 Acclimated and non-acclimated *Arabidopsis thaliana* Col-0 after freezing at -8 °C for 2 h. Numbers on the left indicate time (h) at 21 °C after freezing treatment.

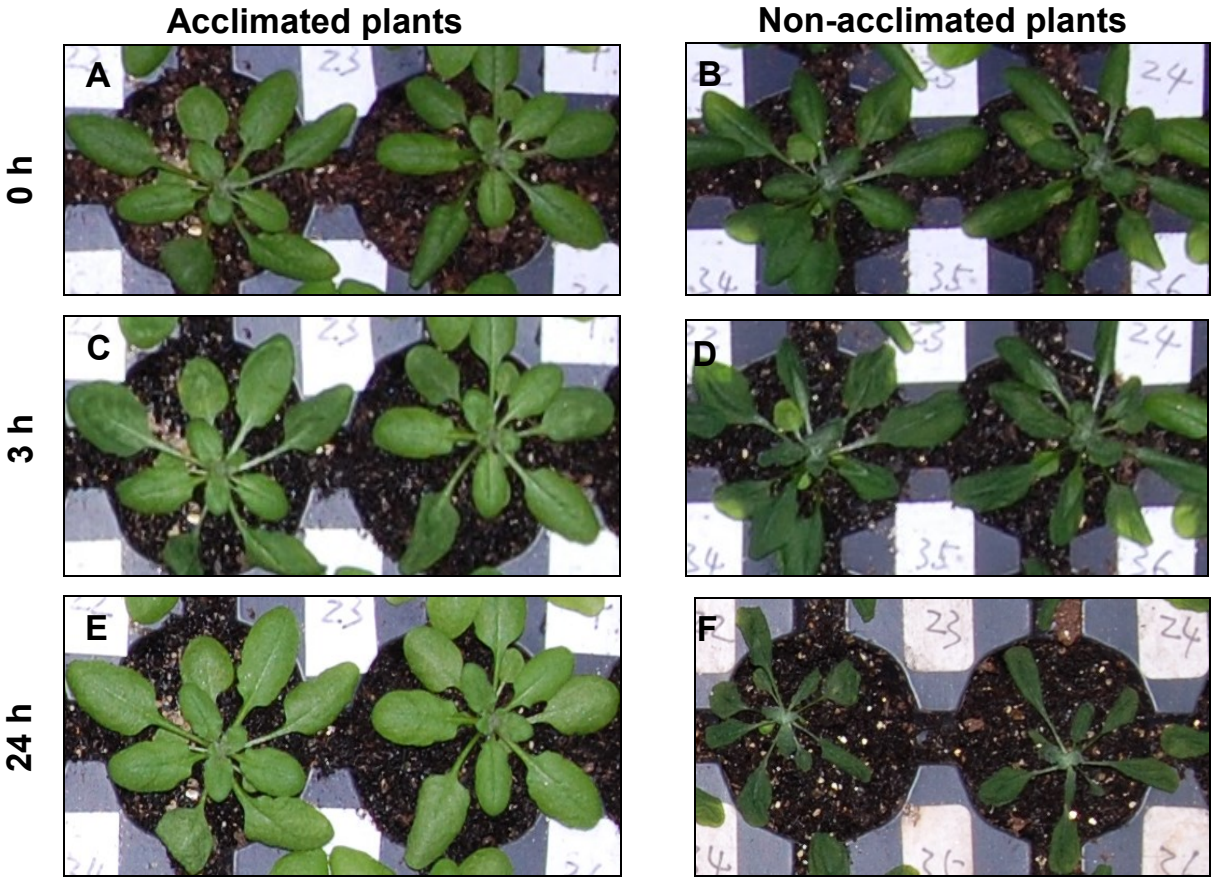

Figure S3.3 Total free OPDA and JA after wounding and re-wounding of Col-0 plants. A: total free OPDA, B: total free JA in ng/mg of leaf fresh weight. Total OPDA is sum of *cis*- and *trans*-OPDA. Total JA is sum of *cis*- and *trans*-JA.

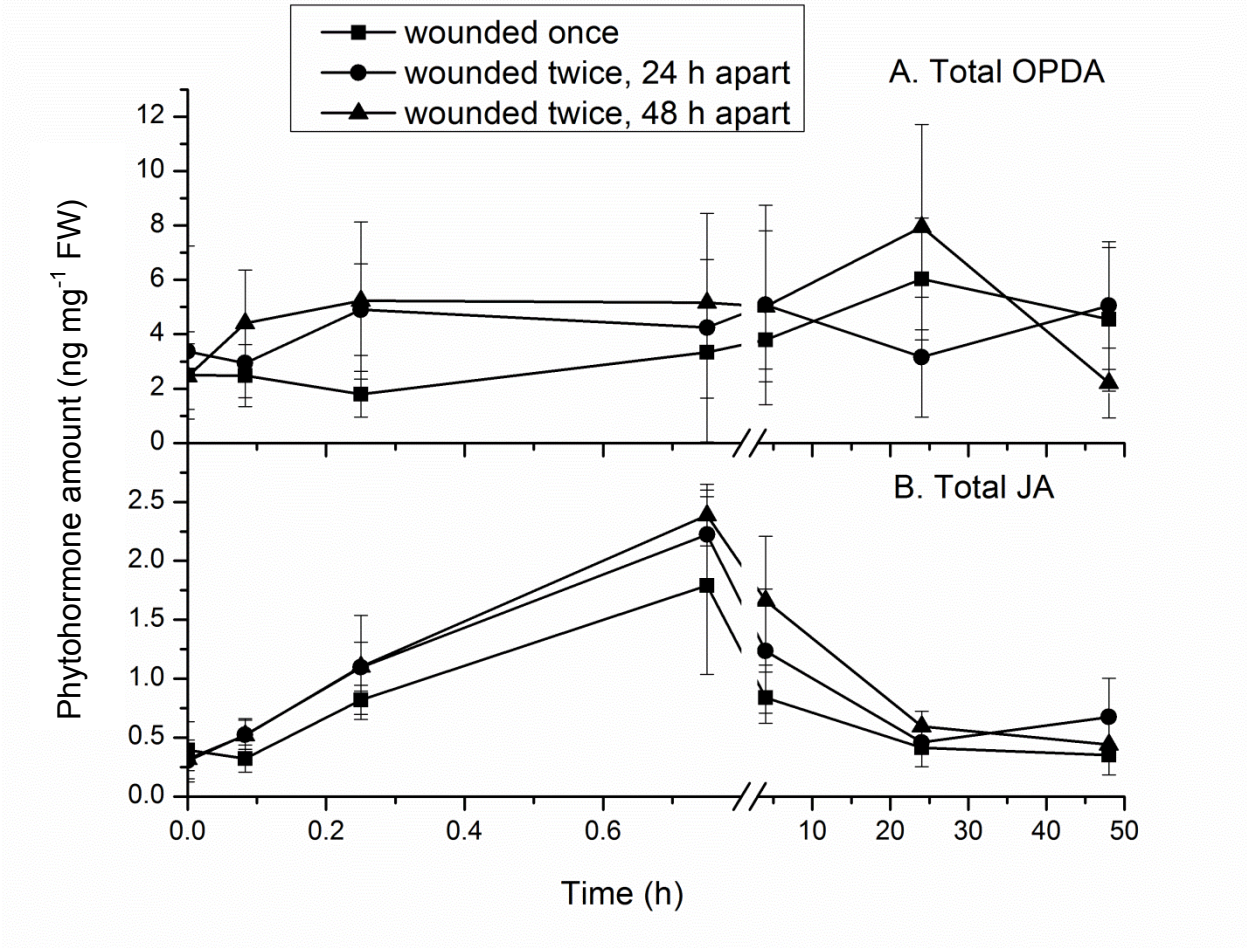

Chapter 10 - Lipid changes after leaf wounding in *Arabidopsis thaliana*: Expanded lipidomic data form the basis for lipid co-occurrence analysis

Abstract

A direct-infusion electrospray ionization triple quadrupole mass spectrometry method with multiple reaction monitoring (MRM) was employed to measure 272 lipid analytes extracted from leaves of *Arabidopsis thaliana* subjected to mechanical wounding. The lipid classes analyzed comprised galactolipids and phospholipids (including monoacyl molecular species, molecular species with oxidized acyl chains, phosphatidic acids (PAs), tri-and tetra-galactosyldiacylglycerols (TrGDGs and TeGDGs), head-group-acylated galactolipids, and head-group-acylated phosphatidylglycerol (acPG), sulfoquinovosyldiacylglycerols (SQDGs), sphingolipids, di- and tri-acylglycerols (DAGs and TAGs), and sterol derivatives. Of the 272 lipid analytes, 256 changed significantly in response to wounding. In general, levels of structural lipids decreased, whereas monoacyl molecular species, galactolipids and phosphatidylglycerols (PGs) with oxidized fatty acyl chains, PAs, TrGDGs, TeGDGs, TAGs, head-group-acylated galactolipids, acPG, and some sterol derivatives increased, many transiently. The observed changes are consistent with activation of lipid oxidizing, hydrolyzing, glycosylating, and acylating activities in the wounding response. Correlation analysis of the levels of lipid analytes across individual control and treated plants was used to construct a lipid dendrogram and to define clusters and sub-clusters of lipid analytes, each composed of a group of lipids which occurred in a coordinated manner. Current knowledge of metabolism supports the notion that observed sub-clusters comprise lipids generated by parallel metabolism or formed from sub-cluster members by a non-rate-limiting process. This work demonstrates that co-occurrence analysis, based on correlation of lipid levels among plants, is a powerful approach to defining lipids generated *in vivo* by identical or inter-twined enzymatic pathways.

Introduction

As lipid biochemists have long known, and computational biologists have recently confirmed, lipid metabolism contains more than its share of reactions catalyzed by enzymes with broad substrate selectivity, i.e., those that act on more than one substrate and produce multiple products (Carbonell et al., 2011). Indeed, knock-out or suppression of single genes has indicated that, during stress responses in plants, individual lipid-metabolizing enzymes act on multiple substrates and produce multiple products (e.g., Welti et al., 2002; Peters et al., 2010). On the other hand, application of stress to a plant activates multiple metabolic pathways. In lipid metabolism, wounding stress causes phospholipase D activation, phospholipase A activation, oxidation of fatty acids on galactolipids, and head-group acylation of monogalactosyldiacylglycerols (Narváez-Vásquez et al., 1999; Zien et al., 2001; Ryu et al., 2004; Buseman et al., 2006; Vu et al., 2014). Steuer et al. (2003) observed that individual plants under the same treatment show small biological variations in the rate and extent of activation of various metabolic pathways. Taken together, current knowledge suggests that (1) when a stress is applied, plant lipid composition will change due to activation of an array of enzymes, (2) under each treatment condition, individual plants will vary slightly in lipid composition, due to varied responses of individual pathways, and, (3) in most cases, activation of a pathway will result in simultaneous change in members of a group of lipids that represent substrates or products of the activated pathway.

Lipidomic analysis can be employed to reveal the levels of plant lipid molecular species. In the current work we have developed a direct-infusion electrospray ionization (ESI) triple-quadrupole mass spectrometry (MS) method to analyze a wide array of lipid species, with a focus on ability to analyze compositional patterns of lipids among individual plants and during stress. This approach provides good sensitivity and precision.

We predicted that lipid intermediates or products produced by the same enzyme(s) or pathway would co-occur when their metabolic pathway is activated and/or repressed in individual plants. Using tools developed for metabolomics and drawing on recent thinking about the use of metabolite level correlations to further understanding of metabolism (Camacho et al., 2005; Xia et al., 2009 and 2012; Toubiana et al., 2013), lipidomic data were analyzed to reveal lipid groups

defined by co-occurrence through stresses and among individual plants. The relationships between the revealed co-occurring groups and known plant lipid metabolism were examined.

Results

Plant wounding

To test the hypothesis described in the Introduction, we conducted a leaf-wounding experiment. Wild-type Arabidopsis (accession Columbia-0) plants were wounded with a hemostat by crimping twice across the mid-vein of three leaves. Wounded leaves were harvested 45 min and 6 h after wounding as were the leaves in the same position on unwounded control plants (n = 31 for each treatment group). Wounding at this level produces ion leakage (Figure S4.1) and an increase in expression of genes encoding enzymes involved in production of oxidized fatty acids (*ALLENE OXIDE SYNTHASE* (*AOS*) and *LIPOXYGENASE2* (*LOX2*); Figure S4.2a and b), but the leaves undergo recovery, as indicated by reduced ion leakage at 24 h (Figure S4.1). Some crimped leaf areas appear to heal, while marks remain visible in other areas at 24 h (Figure S4.3). All leaves remain green, and improvement in appearance is apparent within 24 h after wounding (Figure S4.3).

Extraction of leaves

Because our goal is to apply lipidomics in a high-throughput manner and because extraction can be a time-consuming part of lipid analysis, a streamlined extraction method was developed. After quenching of potential phospholipase D activity by immersion of leaves harvested 45 min after wounding in hot isopropanol for 15 min, a polar solvent mixture was added. After shaking for 24 h and removing the leaves, the extract was subjected to mass spectral analysis. Comparison with a modified Bligh-Dyer method (Bligh and Dyer, 1959; Welti et al., 2002) and a Bligh-Dyer type extraction, followed by additional extraction targeted at sphingolipids (Toledo et al., 1995; Markham et al., 2006), showed that the three methods each extracted similar amounts of lipid and there was only minor variation in the composition of lipids extracted by the three methods (Table 4.1 and full data set in Table S4.1).

MS analysis of lipids

To analyze stress-induced Arabidopsis leaf lipids, a direct-infusion ESI triple quadrupole MS method with MRM was developed. Each lipid analyte is defined by its mode of analysis (positive or negative), its intact ion mass/change (*m/z*), and a fragment *m/z*; an arbitrary "lipid number" corresponds to the set of parameters used in the analysis. Each analyte has been annotated, based on available information; information supporting annotations (accurate mass and LC-MS data indicating the presence of the annotated lipids in Arabidopsis thaliana tissues) is compiled in Table S4.2. Supporting quadrupole time-of-flight (QTOF) MS data not previously published are provided in Table S4.3. Abbreviations used in lipid annotations are summarized in Table 4.2, and examples of possible structures for oxidized fatty acid chains are provided in Table S4.4. MS settings for each analyte are also listed in Table S4.2. Some analytes have multiple annotations because a triple quadrupole MS, in direct infusion mode, is unable to differentiate compounds and fragments with the same nominal *m/zs*. Available data provide confidence that the vast majority of the annotations are correct, i.e., the annotation(s) indicates the major lipid(s) detected by the stated MS settings.

Infusion profiles of representative lipid analytes showed that the detected intensity varied somewhat as a function of infusion time (Figure S4.4). Some analytes, particularly negatively charged lipids including PA and phosphatidylserine (PS), were relatively retained in the loop and/or tubing, but elution of all analytes was essentially complete within 15 min of the start of infusion. To avoid variation in analyte levels due to uneven infusion, the MRM transition intensity for each analyte was acquired repeatedly throughout the entire infusion period and the intensities were averaged. Separate infusions were made for acquisition in the negative and positive modes, because initial experiments indicated that it took several seconds after mode switching for the intensity to stabilize. Infusion of a single plant extract took 35 min: a 15 min infusion in positive mode with 2.5 min of washing, followed by a 15 min infusion in negative mode with 2.5 min of washing.

Intensities were normalized to internal standards analyzed by the same method as the lipid analytes. Instrumental parameters for the internal standards are indicated in Table S4.5, and Table S4.2 indicates the internal standard(s) used for normalization of each analyte. Background

values for each lipid analyte were calculated in samples of the internal standards alone and subtracted from values in samples containing plant lipids.

The goal of the quantification was to compare levels of each lipid analyte in various plant samples, rather than to compare various lipid levels with each other. Absolute analyte levels are unreliable due to the limited number of internal standards and the variations in instrumental parameters among analytes and internal standards. In many cases, analyte intensities were normalized to intensities of standards of substantially different structure. To assure consistent data for each analyte throughout long periods of mass spectral data collection, an adaptation of the "quality control" approach suggested by Dunn et al. (2011) was employed. Representative samples from all treatments were pooled. The pooled sample, called the quality control (QC) sample, was analyzed recurrently among the experimental samples (Table S4.6). The QC analyte intensities were used to normalize the intensities in the experimental samples, as described in Experimental Procedures. Data for the lipid analytes are presented as (1) normalized intensity per mg of leaf dry mass, where a value of 1 corresponds to the same amount of intensity as derived from 1 pmol of internal standard(s) and (2) autoscaled values, produced by dividing the difference between an intensity and the mean intensity of the 93 samples by the standard deviation of the intensity of the 93 samples (Xia et al., 2009; 2012). The autoscaled values allow easy comparison of lipid levels across various samples, because all analytes can be plotted on similar scales, but do not provide information about the absolute lipid levels.

In total, the intensities of 377 MRM transitions were quantified and measurements of 272 of these lipid analytes are described here. Of these, 268 represent unique analytes, whereas four represent the same lipid measured with different instrument parameters. Each lipid analyte described in this work met the following criteria: (1) the background MRM intensity (in the internal standard-only samples) was less than 40% of the average intensity of the QC samples; and (2) the coefficient of variation, i.e., the standard deviation divided by the mean of the level of the analyte in the (identical) QC samples, was less than 20%. Coefficients of variation for individual analytes are shown in Table S4.2.

Variations in lipid analytes among individual plants and in response to wounding treatment

The full set of data for lipid analyte levels in normalized intensity per mg of leaf dry mass and as autoscaled values is provided in Tables S4.6 and S4.7. Original and autoscaled data of each lipid analyte are plotted as a function of wounding treatment (Figure S4.5). Of the 268 unique lipid analytes, 256 were significantly different in at least one of the three pairwise comparisons by ANOVA ($p < 0.01$) (Table 4.3 and Table S4.9). Tukey's post-hoc test indicates that 143 lipids were significantly different in all three pairwise comparisons and 74 lipids in comparisons between both "Wounded; 45 min" versus "Unwounded" and "Wounded; 6 h" versus "Unwounded" (Table 4.3).

The autoscaled lipid levels of individual samples are displayed as a heat map in Figure 1, and the levels of 10 lipid analytes as a function of autoscaled levels are shown in Figure 4.2. The data in Figures 4.1 and 4.2 both show that variation in lipid levels was observed in samples subjected to the same treatment, in most cases, as well as among treatments. To test the hypothesis that variation in lipid levels is due to increased or decreased activities of specific lipid pathways in individual plants and that analysis of the lipidomic data can reveal groups of lipids defined by lipid co-occurrence, correlations in the levels of the lipid analytes were determined. Spearman's correlation coefficient, ρ, was calculated for each lipid analyte with each other lipid analyte across all 93 lipid samples, including 31 samples subjected to each treatment (unwounded, wounded and harvested after 45 min, and wounded and harvested after 6 h) (Table S4.10). Spearman's correlation coefficient can range from -1 (perfect negative correlation) to 1 (perfect positive correlation) with 0 indicating no correlation.

Levels of every lipid analyte were positively correlated with the levels of at least one other lipid analyte. Of the 268 unique analytes, 264 were correlated with another lipid with a $\rho > 0.60$. By matching each lipid analyte with the one to which it was most highly correlated, a dendrogram was constructed (Figure 4.3). The dendrogram includes seven clusters of lipids, labeled A-G, corresponding to groups in which every lipid is correlated with another lipid with $\rho > 0.80$. Two of the clusters, A and C, are large, and contain 60 and 146 lipid analytes, respectively. Comparison of various correlation "cutoffs" in light of understanding of metabolism (described

in the Discussion) indicated that, within these clusters, lipids that were likely to be metabolically related were those with the highest correlation values, i.e., $\rho > 0.96$. There are 6 sub-clusters (A1-A6) in A with lipids with $\rho > 0.96$. Within C, there are 12 such sub-clusters (C1-C12).

Cluster A contains structural (i.e., membrane) lipids that are decreased as a function of wounding treatment (Figures 4.2 and S4.5, Table 4.3). These include normal chain species of DGDG, MGDG, GlcCer, GIPC, PC, PE, PG, and SQDG. Cluster B contains 3 PE species containing a normal acyl chain and 18:3-O. These analytes exhibited no change in response to wounding at 45 min but decreased at 6 h post-wounding. Cluster C contains many lipids induced by wounding. These include monoacyl lipids, including DGMGs, MGMGs, LPCs, and LPEs. Cluster C also contains head group-acylated galactolipids, acMGDG and acDGDG, as well as the only acPG species that was measured. DAG, TAG, and PA species are located in Cluster C, as are poly-galactosylated lipids, TrGDG and TeGDG. A large portion of the galactolipid analytes (acDGDG, acMGDG, DGDG, DGMG, MGDG, and MGMG) in Cluster C contains oxidized fatty acyl chains, whereas only 5 phospholipids with oxidized fatty acyl chains, i.e., PC(16:0/18:3-2O), PE(18:3/18:3-2O), PG(18:3-O/16:0), PG(18:4-O/16:0), and PG(18:4-O/16:1), fell within Cluster C. Cluster C contains several normal diacyl lipids that are likely to contain 16:3. These lipids include DAG(34:6), PA(34:6), PC(34:6), PC(32:3), and PE(32:3). Finally, Cluster C contains sterol glucosides and acyl sterol glucosides. Cluster D consists of sterol esters that change little in response to wounding. Cluster E contains two PCs with long acyl chains, PC(40:2) and PC(40:3), while Cluster F consists of 3 PEs, each with a normal-chain fatty acid and 18:3-3O. Cluster G is composed of PC(34:4) and PE(34:4).

The most highly correlated lipid analyte groups are the 18 sub-clusters, A1-A6 and C1-C12, each of which contains lipids linked by $\rho > 0.96$. Examples showing the correlation of lipid analyte levels in these clusters are provided in Figures 4.4, 4.5 and 4.6, and Figure 4.7 presents boxplots of lipid levels in response to wounding for an example lipid from each of the 18 sub-clusters. Figure 4.4 shows autoscaled values for the lipids in sub-cluster A1 (4.4a), A4 (4.4b), and A5 (4.4c) as a function of individual plant and treatment. Sub-cluster A1 includes PC(32:1) and PE(32:1), which has been identified previously as PE(16:0/16:1) (Samarakoon et al., 2012, Table S4.2). Sub-cluster A4 includes PE species (PE(34:3), PE(36:5) and PE(36:6)), which previous

analysis has shown to contain 18:3 (Welti et al., 2002; Table S4.2). Sub-cluster A5 consists of PC and PE species (PC(34:2), PE(34:2), and PE(36:4)) containing 18:2 (Welti et al., 2002; Table S4.2). Lipid analytes within the same sub-cluster vary similarly across the samples and treatments (Figure 4.4a-c). There is slightly lower co-occurrence when an analyte from each of sub-clusters A1, A4, and A5 is compared (Figure 4.4d). In addition to A1, A4, and A5, A3 is an additional PC-PE sub-cluster, which contains PC species with limited desaturation and which may contain 18:1 and/or 18:2 (Welti et al., 2002; Table S4.2). On the other hand, sub-cluster A2 consists of the incompletely desaturated MGDG species, MGDG(34:4) and MGDG(34:5), whereas A6 is comprised of completely desaturated galactolipid species, DGDG(34:6), DGDG(36:6), and MGDG(34:6). Each sub-cluster within Cluster A thus represents either a PC + PE or MGDG + DGDG group of molecular species related by acyl composition.

Figure 4.5a and 4.5b show sub-cluster C2 (PA(34:6), TeGDG(34:6), and TrGDG(34:6)) and sub-cluster C9, which includes PA(34:2), PA(34:3), PA(36:2), PA(36:3), PA(36:4), PA(36:5), and PA(36:6). The analytes within each of these sub-clusters are closely correlated, but these sub-clusters are not well correlated to each other, as illustrated by comparison of levels of PA(34:6) from sub-cluster C2 and PA(36:6) from sub-cluster C9 (Figure 4.5c). Figure 4.6a, 4.6b, and 4.6c depict the changes in sterol glucosides and acyl sterol glucosides of sub-clusters C5, C7, and C8. Again, these show a higher level of in-sub-cluster lipid co-occurence compared with inter-sub-cluster co-occurence (Figure 4.6d).

Overall, sub-clusters in Cluster C are diverse. In addition to previously mentioned sub-clusters, there is a sub-cluster (C4) composed of all four TAG species determined, a sub-cluster of Arabidopsides A and B (MGDG(18:4-O/16:4-O) and MGDG(18:4-O/18:4-O); C6), and 5 sub-clusters containing acDGDG/acMGDG. The five acDGDG/acMGDG sub-clusters (C1, C3, C10, C11, and C12) fall into two groups. Sub-clusters C1 and C3 are moderately related with the highest inter-sub-cluster ρ, ρ(C1,C3), equal to 0.91 and sub-clusters C10, C11, and C12 are closely related with the highest ρs among all 3 sub-clusters falling just short of 0.96. On the other hand, the highest ρ between any lipid in sub-clusters C1 or C3 with one in C10, C11, or C12 is 0.77. There is some potential ambiguity in annotation of the acylated galactolipid sub-clusters, which makes it difficult to fully interpret the sub-clustering. (Note that only one

annotation per lipid is shown in the dendrogram, but complete annotations including alternative interpretations are shown in Tables 4.3 and S4.2) Still, sub-cluster C3 contains some clearly normal-chain acyl species, whereas sub-clusters C10, C11, and C12 contain highly oxidized acylated galactolipids. Figure 4.7g, i, p, q, and r show examples of the patterns of lipid changes during the wounding response for a lipid from each of the 5 acylated galactolipid sub-clusters. The levels of lipids in sub-clusters C1 and C3 continued to rise between 45 min and 6 h post-wounding, while the levels of acylated galactolipids in sub-clusters C10, C11, and C12 were reduced at 6 h compared to 45 min post-wounding.

Discussion

Lipids are modular, with many different molecular species containing the same component acyl chain or head group. This modularity goes hand-in-hand with the promiscuity of lipid-metabolizing enzymes, many of which act on multiple, related substrates. Here, we show that data support the hypothesis that correlation analysis can reveal groups of lipids acted on by the same enzyme(s), using lipidomic data from control plants and plants subjected to wounding. By metabolic control analysis and computer simulation, Camacho et al. (2005) found that many cases of high correlations in the levels of different metabolites among profiles of biological replicate samples are due to control of the metabolite levels by a single enzyme. Based on current knowledge of lipid metabolism, we infer that the highly correlated sub-clusters detected here by correlation analysis ($\rho > 0.96$) may (1) consist of substrates or products of the same enzyme(s), (2) may include a lipid formed from a common starting material by a metabolic branch, and/or (3) may include a lipid formed from another member of the group by a non-rate-limiting process.

Among the sub-clusters, several are likely to be produced by parallel metabolism by the same enzyme. These include the steryl glucosides in sub-cluster C5, which are likely to have been produced by the glycosylation of sterols by UDP-Glc:sterol glycosyltransferase(s) described by DeBolt et al. (2009). It's probable that each of the acyl sterol glucoside sub-clusters (C7 and C8) was formed by parallel acylation of two sterol glucosides with the same acyl chain, although the acylating enzymes acting on sterol glucosides have not been identified. Sub-cluster C9, which

consists of PAs with fatty acids similar to extraplastidic phospholipids, may have been derived largely from the activity of phospholipases D (e.g., Zien et al., 2001; Welti et al., 2002), though it has been suggested that diacylglycerol kinase also can contribute to PA formation in stress conditions (e.g., Arisz et al., 2013). Recent data support the notion that sub-cluster C6 (Arabidopsides A and B) may have been formed by a common enzymatic pathway acting on similar, but distinct, substrates. Nilsson et al. (2012) showed that 18:4-O (oxophytodienoic acid) and 16:4-O (dinor-oxophytodienoic acid) are formed without release of the acyl chains from the galactolipid pool. It follows that the two molecular species in sub-cluster C6 would be formed from the two most abundant MGDG species, MGDG(18:3/16:3) and MGDG(18:3/18:3), by analogous pathways involving oxidation and cyclization of the esterified fatty acyl chains.

The formation of sub-cluster C2, which consists of TrGDG(34:6), TeGDG(34:6), and PA(34:6) likely involves the action of SENSITIVE TO FREEZING 2 (SFR2) (Moellering et al., 2010), a processive galactosylating enzyme that transfers a galactose from MGDGs to successively yield β-linked DGDG, TrGDG, and TeGDG from MGDG. The resulting DAG does not accumulate (Moellering et al., 2010), and while Moellering et al. (2010) provide evidence that TAG may be formed from it, the inclusion of PA(34:6) in the sub-cluster suggests that a DAG kinase may phosphorylate the DAG in a branch step. Several molecular species of TAGs are formed in response to wounding (sub-cluster C4); formation of these TAGs may involve phospholipid:diacylglycerol acyltransferase (PDAT1) (Fan et al., 2013). TAG may serve as a transient buffer for leaf acyl chains present in excess (Troncoso-Ponce et al., 2013). Unfortunately, we did not determine the level of a TAG species containing 34:6 (i.e., 18:3/16:3), which could be derived from MGDG by SFR2.

While all the sub-clusters within Cluster A are quite closely correlated, the components of the four sub-clusters containing PC and PE (A1, A3, A4, A5) and two sub-clusters of MGDG and DGDG (A2, A6) vary in their fatty acyl composition. In the plastid, DGDG is formed from MGDG by a UDP-galactose-dependent DGDG synthase (DGDGS; Kelly and Dörmann, 2002; reviewed in Li-Beisson et al., 2013). Fatty acyl chains can undergo desaturation on either MGDG or DGDG (except that FAD5 acts only on MGDG; Kunst et al., 1989). Sub-cluster A2 includes MGDG species that are not fully desaturated; their co-accumulation may indicate that

the rate of the final desaturation of MGDG acyl chains by FAD7 and/or FAD8 varied among plants and limited the rate of formation of fully desaturated species. Indeed, the level of plastidic trienoic fatty acids is regulated in stress responses and affects the ability of plants to withstand stresses, including cold and bacterial infection (Kodama et al., 1994; Routaboul et al., 2000; Yaeno et al., 2004; Chaturvedi et al., 2008). On the other hand, the occurrence of DGDG(34:6) with MGDG(34:6) in sub-cluster A6 is due to a near-constant ratio of these lipids among plants, suggesting that the conversion of MGDG to DGDG is not rate-limiting. The high correlation coefficients between PCs and PEs with the same acyl chains in sub-clusters A1 and A5 could mean either that the rate of production of acyl-identical PCs and PEs is similar and/or that enzymes involved in PC-PE (inter)conversion, perhaps through a DAG intermediate, function near equilibrium, maintaining a near-constant ratio of acyl-identical PE and PC molecular species (found together in sub-clusters). In pea leaves, PC is labeled from acetate much more rapidly than PE during a 10-min time course, suggesting that PC and PE molecular species with the same acyl chains are unlikely to be formed initially by parallel pathways (Bates et al., 2007), and that it is more likely that PC species are converted to PEs during the wounding experiment.

The modular nature and the typical action of lipid-metabolizing enzymes on multiple substrates may make complex lipids especially amenable to co-occurrence analysis as a mechanism for extending our understanding of compound relationships and metabolism. In the current analysis, acDGDGs, acPG, and many acMGDGs are a large group of lipids that has not been extensively studied. Evidence has been presented that acMGDG is formed by the reaction MGDG + DGDG → acMGDG + DGMG (Heinz, 1967; Heinz, 1972; Vu et al., 2014). The current results show that two groups of acMGDGs are formed with different kinetics. acMGDGs in sub-clusters C10, C11, and C12, most of which are rich in oxidized fatty acids, are formed rapidly (i.e., their levels are high at 45 min) and their levels drop by 6 h post-wounding (Figure 4.7p, 4.7q, 4.7r). Other acMGDGs (sub-clusters C1 and C3; Figure 4.7g, 4.7i), including all quantified molecular species unambiguously annotated as having entirely normal-chain fatty acids (acMGDG(16:0/34:6), acMGDG(16:3/34:6), acMGDG(18:2/34:6), acMGDG(18:3/34:6)), were formed more slowly, with levels considerably higher at 6 h than at 45 min. A similar phenomenon was observed previously when galactolipids containing two oxidized acyl chains accumulated much faster in response to wounding than galactolipids with a single oxidized acyl

chain (Buseman et al., 2006). Thus, the acMGDG pool reflects the diacyl species that serve as substrates for acMGDG formation; however, oxidized chains are concentrated in the acMGDG pool (Vu et al., 2014). Still, the mechanism for the rapid rise and decline in species containing two oxidized chains and the identity of the acylating enzyme(s) forming the head-group-acylated molecular species remains unknown. Additionally, the placement of a number of analytes that are not obviously structurally similar in sub-clusters C1 and C3 provides a catalyst for future reassessment of the tentative annotations.

In the current work, we have developed an MS-based analytical approach targeting a wide range of lipid molecular species. The current approach has demonstrated that levels of lipids differed among individual Arabidopsis plants, and levels of nearly all of the lipids in wild-type plants changed in response to wounding, with normal-chain "traditional" structural lipids decreasing and many other lipids increasing. The analytical precision was sufficient for a number of lipid species to be clustered based on co-occurrence among individual plants and across the stress conditions. The levels of seventy-nine percent of the lipid analytes were correlated with $\rho > 0.80$ with at least one other analyte, placing them in a lipid cluster, and 24% of the lipids were correlated with $\rho > 0.96$, placing them in a sub-cluster. While lack of high correlation can be due to either excessive analytical variation or true lack of co-occurrence, interpretation of the lipid analytical results in light of knowledge of lipid metabolism demonstrates that high positive correlation reflects metabolic relationships. At the current stage of plant lipidomic development, careful and highly replicated MS analysis can provide large amounts of information about lipid dynamics in plants under stress. The current work highlights the value of co-occurrence analysis in defining groups of metabolically-related lipids. Undoubtedly, application of co-occurrence analysis to additional lipids and to plants subjected to other perturbations will provide further metabolic insight.

Experimental procedures

Plant material, growth, and wounding treatment

Plant material and growth are described in Method S4.1. For the wounding treatment, a hemostat was used to wound leaves number 5, 6, 7 and 8 of 30-day-old plants across the mid-vein, twice

and about 6 mm apart. Leaf numbers were determined as described by Telfer et al. (1997). Leaves 6, 7, and 8 were harvested 45 min or 6 h after being wounded. For the control, leaves 6, 7, and 8 were harvested from unwounded plants. For the extraction test, fifteen plants were harvested 45 min after wounding. For the main experiment, thirty-two samples (one each from 32 plants) were collected for each of the two wounding treatments and for control plants. Each sample for lipid analysis corresponded to the three harvested leaves from one plant. In the main experiment, one sample in each treatment group (i.e., sample 23) was removed from the analysis due to technical problems; thus, n for each group is 31. The extraction test and the main experiment were performed on separate sets of plants.

Lipid extraction

In the main experiment, harvested leaves number 6, 7, and 8 were immediately dropped into 4 ml of isopropanol with 0.01% butylated hydroxytoluene (BHT) at 75°C in a 20-ml EPA vial with Teflon-lined screw-cap (Thermo Fisher Scientific, Inc., thermofisher.com). Vials were kept at 75°C for 15 min to deactivate lipid-hydrolyzing enzymes. Vials were cooled to room temperature and stored overnight at -80°C before adding 12 ml of chloroform: methanol: 300 mM ammonium acetate in water (30:41.5:3.5, v/v/v) and shaking at 100 rpm on an orbital shaker for 24 h at room temperature. Extracted leaves were transferred to a new vial and dried overnight at 105°C. The extract was stored at -80°C. Dried extracted leaves were cooled and weighed on a balance with 2 μg detection limit (Mettler Toledo, mt.com). The precision and accuracy of the balance were previously described (Vu et al., 2012). For the extraction test, 5 leaves harvested 45 min after wounding were extracted as just described (Method 1), 5 leaves were extracted as described by Welti et al. (2002; Method 2), and 5 leaves were extracted as described by Welti et al. (2002), skipping the backwash steps, followed by 4 extractions with "Solvent H" (lower phase of isopropanol/hexane/water, 55:20:25, v/v/v; Toledo et al., 1995, Markham et al., 2006; Method 3).

Lipid profiling by ESI triple quadrupole MS

To prepare analytical samples for mass spectrometry, from each sample, the volume corresponding to 0.04 mg extracted leaf dry mass was determined and that volume of sample was

transferred to a 2-ml amber vial, containing 20 µl of internal standard mix. Components of the internal standard mix are listed in Table S4.5. Isopropanol: chloroform: methanol: 300 mM ammonium acetate in water (25: 30: 41.5: 3.5, v/v/v/v) was added to make the total volume 1.4 ml. The vial was sealed with a snap-cap with a crisscross, pre-slit septum.

Quality control (QC) samples were prepared for data normalization by first pooling 300 µl of extract from samples 1-9 from each treatment (unwounded, wounded 45 min, and wounded 6 h) to make a QC stock solution. Based on the dry leaf mass of the samples used to make the combined extract, the concentration was calculated to be 0.40 mg (of leaf dry mass) ml-1 (8.1 ml total volume). To prepare working QC samples, the internal standard mixture was added and the stock was diluted, so that each working QC sample contained lipid extract corresponding to 0.04 mg combined leaf dry mass, 20 µl of the internal standard mix (as used in the other samples), and mass spectrometry solvent (isopropanol: chloroform: methanol: 300 mM ammonium acetate in water, 25: 30: 41.5: 3.5, v/v/v/v) in 1.4 ml. The QC mass spectrometry samples were labeled "QC1" to "QC39", stored at -80°C, and brought to room temperature 1 h before analysis. Analytical samples and QC samples from the main experiment were arranged in a VT 54 rack as shown in Table S4.6. For the lipid extraction test, the same analytical set-up was used.

Data were acquired with a Xevo TQ-S mass spectrometer (Waters Corporation, waters.com) equipped with an ESI source operating in direct infusion mode. Each sample was infused twice, once to acquire positive and once for negative multiple reaction monitoring (MRM) transitions. Samples were injected into a 300-µl PEEK sample loop with a 2777 autosampler (Waters Corporation). To make sure the loop was completely filled, the injection volume was set at 400 µl. The sample in the loop was infused to the mass spectrometer with an Acquity pump (Waters Corporation) controlled by an "inlet method" in MassLynx (software from Waters Corporation). Each inlet method was 17.5 min with solvents and flow rates as follows: from 0 to 11 min, methanol at 0.03 ml min-1; from 11 to 15 min, methanol at 0.09 ml min-1; from 15 to 17 min, methanol: acetic acid (9: 1, v/v) at 0.5 ml min-1; from 17 to 17.1 min, 17.1 to 17.2 min, 17.2 to 17.3 min, 17.3 to 17.4 min, and 17.4 to 17.5 min, methanol at 0.4, 0.3, 0.2, 0.1, and 0.03 ml min-1, respectively. The mass spectrometer acquired data from 0 to 15 min. The positive mode and negative mode data acquisition methods had 13 and 7 functions, respectively. Every function

acquired data on lipid analytes and internal standard components in MRM mode throughout the 15 min. Each function contained from 12 to 28 transitions which were allocated the same dwell time. In the positive mode, 130-131 scans (cycles) and, in the negative mode, 38 scans of each function were performed (Table S4.2). Parameters for each MRM transition are listed in Table S4.2 for the plant lipid analytes and in Table S4.5 for the internal standards. Other mass spectrometry parameters are indicated Method S4.4.

Samples were analyzed at the rate of 1 tray (Table S4.6) per day with a total daily analysis time of 22.75 h. Each day, a cleaned source cone was installed and an Xpertek 0.5-µm PEEK filter (P.J. Cobert Associates, Inc., cobertassociates.com) in the line between the autosampler and source was changed.

Data processing and calculation of normalized lipid intensities

"Spectrum Combine" software (a process file called SpectrumCombine_4p0p0) and a parameter file, custom-developed by Iggy Kass (Waters Corporation), was employed to process and export MassLynx data to Excel. MRM scans were combined by averaging the scans for each MRM channel within each function before export. Exported data were processed in an in-house Excel template in which the data from all samples (i.e., QC, "internal standard only", and analytical samples) were isotopically deconvoluted. The intensity per nmol of each internal standard in each sample was calculated; these values for internal standards for the same class were averaged. The deconvoluted data for each lipid were normalized to the internal standard(s) of the same lipid class (if possible) or another lipid class analyzed under similar experimental conditions (in cases where an appropriate internal standard was not available). The internal standard used for normalization of each MRM signal is indicated in Table S4.2.

Once normalized intensities were calculated, the average level of the background, as indicated by the average of the "internal standard only" samples from that tray, was subtracted from every other sample in the tray. An adaptation of the method of Dunn et al. (2011) was used to assure that the data could be compared throughout extended acquisition periods. The values for the first 5 QC samples in each set of analytes (Table S4.6) were eliminated, due to potential instrument

instability when the instrument is first started after installation of a cleaned cone. To correct for any drift during acquisition of each tray's data, a trend line was constructed of the intensity data for each lipid in the remaining 8 identical QC samples as a function of vial position number in the tray. Each lipid intensity in each analytical sample was multiplied by the average of that lipid's level in the QC samples on that tray divided by the level of the lipid on the QC trend line at the sample's vial position. To correct for any variability across different trays (days), the trend-corrected value of each lipid in each sample was multiplied by the average of the QC values for that lipid from the entire acquisition process divided by the average of that lipid's level in the QC samples on the sample's own tray. After calculation of the lipid levels in each sample, the values were divided by the dry mass of the sample analyzed (0.04 mg).

The lipid values are normalized intensity per mg leaf dry mass, where a value of 1 is the intensity of 1 pmol of internal standard. Because the internal standards were not uniformly well-matched to the lipids analyzed (some differ in class; many differ substantially in m/z), the absolute values of the analytes provide only a rough guide to absolute amount of each lipid.

Statistical analysis and figure and table production

Auto-scaling and analysis of variance (ANOVA) with Tukey's post hoc tests were performed (Table S4.9), and the heat map (Figure 4.1), correlation table (Table S4.10), and Figure S4.5 were produced using utilities at the Metaboanalyst website (metabolanalyst.ca; Xia et al., 2009 and 2012). Autoscaling allows easy comparison of patterns of the levels of different lipids across samples. The autoscaled value of a lipid in a sample is equal to: [(the original value of the lipid in the sample) – (the average value for that lipid among all samples)] divided by (the standard deviation for that lipid among all samples). Figures 4.2, 4.4, 4.5, 4.6, and 4.7 were produced using Origin 8.5 (OriginLab Corporation, originlab.com). Clustering was performed using Cluster 3.0 (Eisen et al., 1997). The output was imported to Dendroscope (Huson et al., 2007; Huson and Scornavacca, 2012) to produce the dendrogram, which was modified in color.

Acknowledgements

The authors thank Iggy Kass of Waters Corporation for writing the program to export data from MassLynx, and Samantha Elledge, Laura Welti, Cong Tuan Son Van, and Haibao Tang for help in production of the figures. This material is based upon work supported by the National Science Foundation under Collaborative Research Grant Nos. MCB-0920663 (to RW and GG), MCB-0920600 (to XW), and MCB-0920681 (to JS). The mass spectrometers used in the analyses were acquired with NSF funding under Grant Nos. DBI-1228622, DBI 0521587, and EPS 0236913. Contribution no. 14-244-J from the Kansas Agricultural Experiment Station.

References

Arisz SA, van Wijk R, Roels W, Zhu JK, Haring MA and Munnik T (2013) Rapid phosphatidic acid accumulation in response to low temperature stress in Arabidopsis is generated through diacylglycerol kinase. Front Plant Sci. 4, 1. doi: 10.3389/fpls.2013.00001

Bates PD, Ohlrogge JB and Pollard M (2007) Incorporation of newly synthesized fatty acids into cytosolic glycerolipids in pea leaves occurs via acyl editing. J. Biol. Chem. **282**, 31206-31216.

Bligh EG and Dyer WJ (1959) A rapid method of total lipid extraction and purification. Can. J. Biochem. Physiol. **37**, 911-917.

Buseman CM, Tamura P, Sparks AA, Baughman EJ, Maatta S, Zhao J, Roth MR, Esch SW, Shah J, Williams TD and Welti R (2006) Wounding stimulates the accumulation of glycerolipids containing oxophytodienoic acid and dinor-oxophytodienoic acid in Arabidopsis leaves. Plant Physiol. **142**, 28-39.

Camacho D, Fuente A and Mendes P (2005) The origin of correlations in metabolomics data. Metabolomics **1**, 53-63.

Carbonell P, Lecointre G and Faulon J-L (2011) Origins of specificity and promiscuity in metabolic networks. J. Biol. Chem. **286**, 43994-44004.

Chaturvedi R, Krothapalli K, Makandar R, Nandi A, Sparks AA, Roth MR, Welti R and Shah J (2008) Plastid omega3-fatty acid desaturase-dependent accumulation of a systemic acquired resistance inducing activity in petiole exudates of Arabidopsis thaliana is independent of jasmonic acid. Plant J. **54**, 106-117.

DeBolt S, Scheible WR, Schrick K, Auer M, Beisson F, Bischoff V, Bouvier-Navé P, Carroll A, Hematy K, Li Y, Milne J, Nair M, Schaller H, Zemla M and Somerville C (2009) Mutations in UDP-Glucose:sterol glucosyltransferase in Arabidopsis cause transparent testa phenotype and suberization defect in seeds. Plant Physiol. **151**, 78-87.

Dunn WB, Broadhurst D, Begley P, Zelena E, Francis-McIntyre S, Anderson N, Brown M, Knowles JD, Halsall A, Haselden JN, Nicholls AW, Wilson ID, Kell DB, Goodacre R and Human Serum Metabolome (HUSERMET) Consortium. (2011) Procedures for large-scale metabolic profiling of serum and plasma using gas chromatography and liquid chromatography coupled to mass spectrometry. Nat. Protoc. **6**, 1060-1083.

Eisen MB, Spellman PT, Brown PO and Botstein D (1997) Cluster analysis and display of genome-wide expression patterns. Proc. Natl. Acad. Sci. USA **95**, 14863-14868.

Fan J, Yan C and Xu C (2013) Phospholipid:diacylglycerol acyltransferase-mediated triacylglycerol biosynthesis is crucial for protection against fatty acid-induced cell death in growing tissues of Arabidopsis. Plant J. **76**, 930-942.

Heinz E. (1967) On the enzymatic formation of acyl galactosyldiglyceride. Biochim. Biophys. Acta **144**, 333–343.

Heinz E. (1972) Some properties of the acyl galactosyl diglyceride-forming enzyme from leaves. Z. Pflanzenphysiol. **69**, 359–376.

Huson DH and Scornavacca C (2012) Dendroscope 3: An interactive tool for rooted phylogenetic trees and networks. Syst. Biol. **61**, 1061-1067.

Huson DH, Richter DC, Rausch C, Dezulian T, Franz M and Rupp R (2007) Dendroscope: An interactive viewer for large phylogenetic trees. BMC Bioinformatics. **8**, 460.

Kelly AA, and Dörmann P (2002) DGD2, an Arabidopsis gene encoding a UDP-galactose-dependent digalactosyldiacylglycerol synthase is expressed during growth under phosphate-limiting conditions. J. Biol. Chem. **277**, 1166–1173.

Kodama H, Hamada T, Horiguchi G, Nishimura M and Iba K (1994) Genetic enhancement of cold tolerance by expression of a gene for chloroplast [omega]-3 fatty acid desaturase in transgenic tobacco. Plant Physiol. **105**, 601-605.

Kunst L, Browse J and Somerville C (1989) A mutant of Arabidopsis deficient in desaturation of palmitic acid in leaf lipids. Plant Physiol. **90**, 943-947.

Markham JE, Li J, Cahoon EB and Jaworski JG (2006) Separation and identification of major plant sphingolipid classes from leaves. J. Biol. Chem. **281**, 22684-22694.

Moellering ER, Muthan B and Benning C (2010) Freezing tolerance in plants requires lipid remodeling at the outer chloroplast membrane. Science **330**, 226-228.

Narváez-Vásquez J, Florin-Christensen J and Ryan CA (1999) Positional specificity of a phospholipase A activity induced by wounding, systemin, and oligosaccharide elicitors in tomato leaves. Plant Cell **11**, 2249-2260.

Nilsson AK, Fahlberg P, Ellerström M and Andersson MX (2012) Oxo-phytodienoic acid (OPDA) is formed on fatty acids esterified to galactolipids after tissue disruption in Arabidopsis thaliana. FEBS Lett. **586**, 2483-2487.

Peters C, Li M, Narasimhan R, Roth M, Welti R and Wang X (2010) Non-specific phospholipase C NPC4 promotes response to abscisic acid and tolerance to hyperosmotic stress in Arabidopsis. Plant Cell **22**, 2642-2659.

Routaboul JM, Fischer SF and Browse J (2000) Trienoic fatty acids are required to maintain chloroplast function at low temperatures. Plant Physiol. **124**, 1697-1705.

Ryu SB (2004) Phospholipid-derived signaling mediated by phospholipase A in plants. Trends Plant Sci. **9**, 229-235.

Steuer R, Kurths J, Fiehn O and Weckwerth W (2003) Observing and interpreting correlations in metabolomics networks. Bioinformatics **19**, 1019-1026.

Telfer A, Bollman KM and Poething RS (1997) Phase change and the regulation of trichome distribution in Arabidopsis thaliana. Development **124**, 645-654.

Toledo MS, Suzuki E, Straus AH and Takahashi, HK (1995) Glycolipids from Paracoccidioides brasiliensis. Isolation of a galactofuranose-containing glycolipid reactive with sera of patients with paracoccidioidomycosis. J. Med. Vet. Mycol. **33**, 247-251.

Toubiana D, Fernie AR, Nikoloski Z and Fait A (2013) Network analysis: tackling complex data to study plant metabolism. Trends Biotechnol. **31**, 29-36.

Troncoso-Ponce MA, Cao X, Yang Z and Ohlrogge JB (2013) Lipid turnover during senescence. Plant Sci. 205-206, 13-19.

Vu HS, Tamura P, Galeva NA, Chaturvedi R, Williams TD, Wang X, Shah J and Welti R (2012) Direct infusion mass spectrometry of oxylipin-containing Arabidopsis thaliana

membrane lipids reveals varied patterns in different stress responses. Plant Physiol. **158**, 324-339.

Vu HS, Roth MR, Tamura P, Samarakoon T, Shiva S., Honey S, Lowe K, Schmelz EA, Williams TD and Welti R (2014) Head-group acylation of monogalactosyldiacylglycerol is a common stress response, and the acyl-galactose acyl composition varies with the plant species and applied stress. Physiol Plant. In press.

Welti R, Li W, Li M, Sang Y, Biesiada H, Zhou H-E, Rajashekar CB, Williams TD and Wang X (2002) Profiling membrane lipids in plant stress responses. Role of phospholipase Dα in freezing-induced lipid changes in Arabidopsis. J. Biol. Chem. **277**, 31994-32002.

Xia J, Psychogios N, Young N and Wishart DS (2009) MetaboAnalyst: a web server for metabolomic data analysis and interpretation. Nucl. Acids Res. **37**, W652-660.

Xia J, Mandal R, Sinelnikov I, Broadhurst D and Wishart DS (2012) MetaboAnalyst 2.0 - a comprehensive server for metabolomic data analysis. Nucl. Acids Res. **40**, W127-133.

Yaeno T, Matsuda O and Iba K (2004) Role of chloroplast trienoic fatty acids in plant disease defense responses. Plant J. **40**, 931-941.

Zien CA, Wang C, Wang X and Welti R (2001). In-vivo substrates and the contribution of the common phospholipase D, PLDa, to wound-induced metabolism of lipids in Arabidopsis. Biochim. Biophys. Acta **1530**, 236-248.

Figures and Tables

Figure 4.1 Heatmap of autoscaled lipid levels determined by MS analysis.

272 analytes are shown in 93 samples. Each sample represents one plant under control (unwounded) or wounding treatment (n = 31 for each treatment).

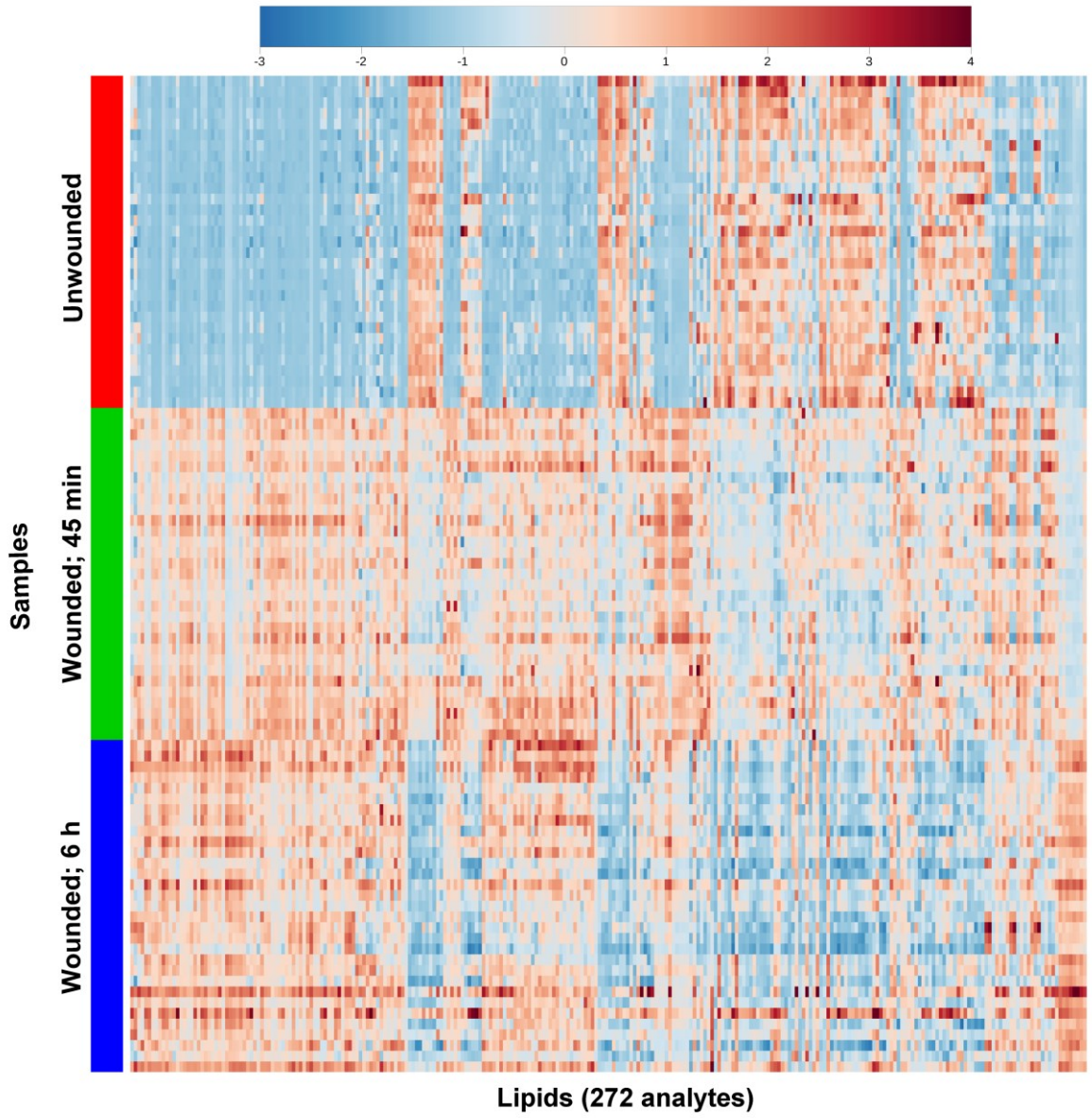

Figure 4.2 Autoscaled levels of representative lipid analytes in individual plants.
Each sample represents one plant under control (unwounded) or wounding treatment (n = 31 for each treatment). Connections between points were included to make it easier to visualize the variations in lipid levels across samples.

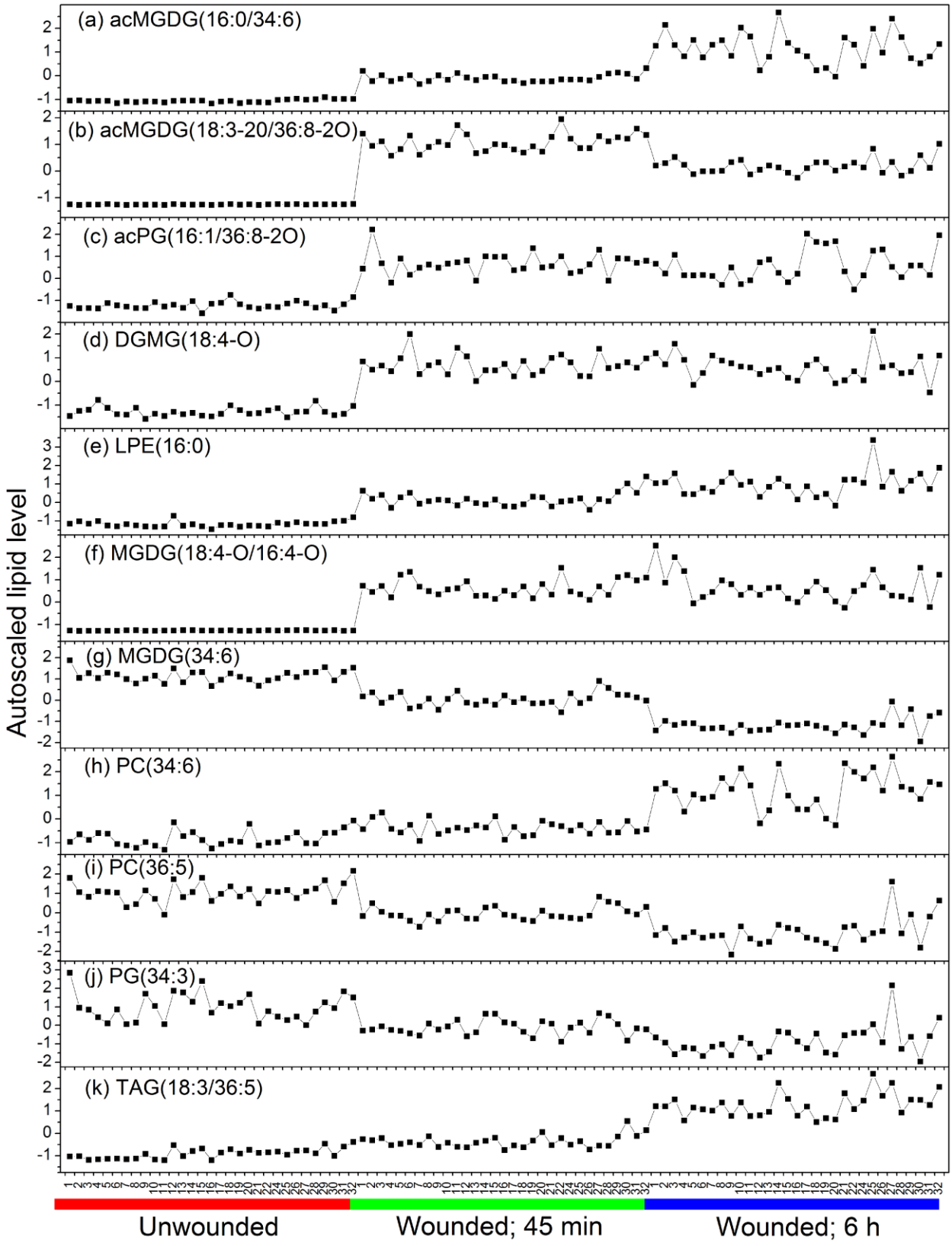
(a) acMGDG(16:0/34:6)
(b) acMGDG(18:3-20/36:8-2O)
(c) acPG(16:1/36:8-2O)
(d) DGMG(18:4-O)
(e) LPE(16:0)
(f) MGDG(18:4-O/16:4-O)
(g) MGDG(34:6)
(h) PC(34:6)
(i) PC(36:5)
(j) PG(34:3)
(k) TAG(18:3/36:5)
Autoscaled lipid level
Unwounded
Wounded; 45 min
Wounded; 6 h

Figure 4.3 Lipid dendrogram.

272 lipid analytes were clustered using a single-linkage hierarchical algorithm based on Spearman's correlation coefficient, ρ (Table S4.10). The center of the dendrogram is at ρ = 0.305. There is a scale break from ρ = 0.340 to ρ = 0.590. Eight analytes were excluded from the dendrogram due to their low level of correlation with other analytes (maximal ρ < 0.6) or because they were repeat measurements of included lipids. A single annotation is provided for each analyte; additional potential annotations are indicated in Table 4.3. Seven clusters with ρ > 0.8 are indicated by letters and colors: A (blue), B (orange), C (green), D (lavender), E (aqua), F (pink), and G (rust). Six sub-clusters of ρ > 0.96 within cluster A and twelve sub-clusters of ρ > 0.96 within cluster C are indicated as A1-A6 and C1-C12. The sub-cluster lines are red, and the lipid annotations within sub-clusters are bold.

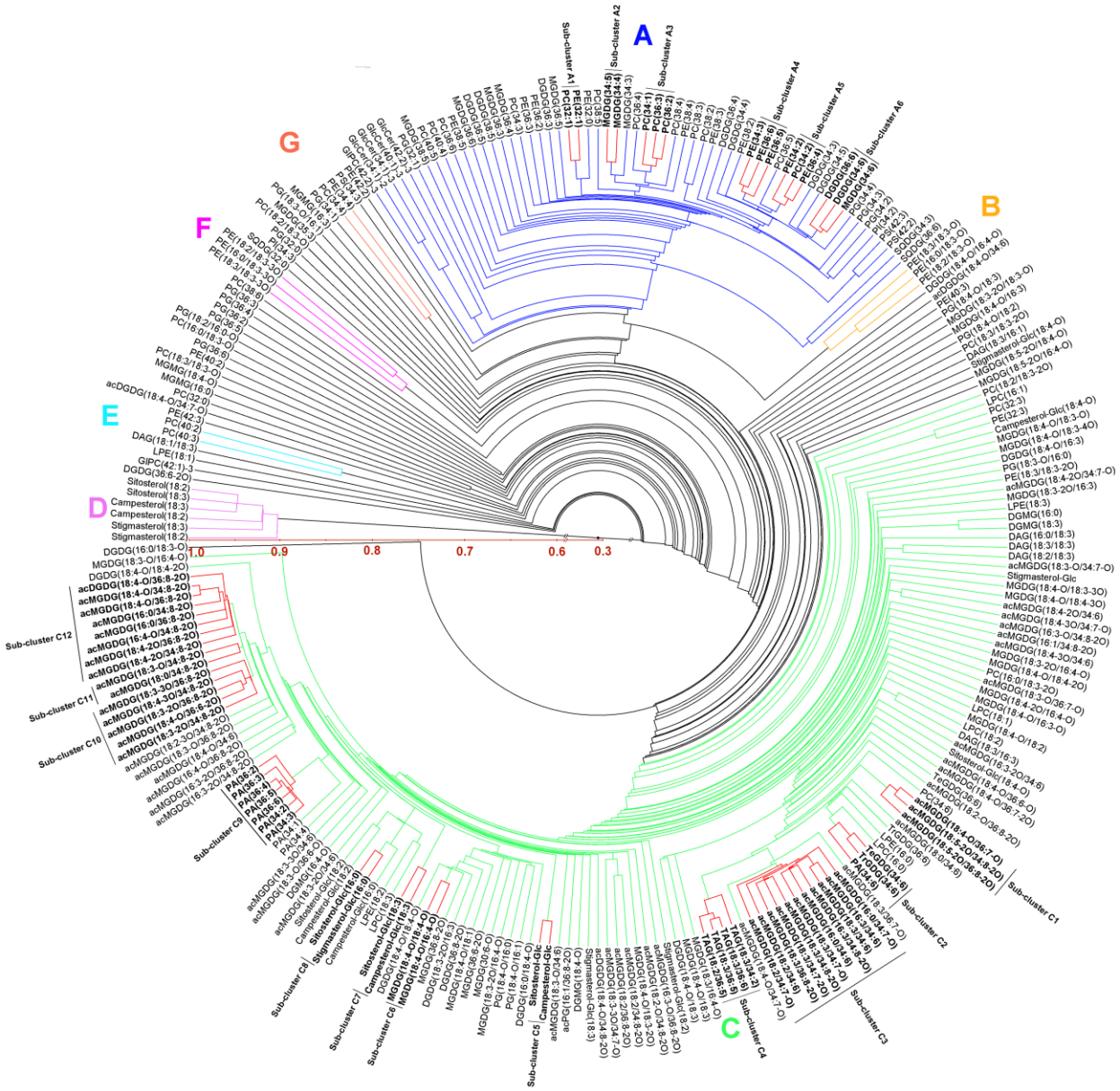

Figure 4.4 Autoscaled levels of representative lipid analytes in sub-clusters A1, A4, and A5. Points represent individual plants subjected to control or wounding treatment as indicated. Panels a, b, and c represent the three clusters, and panel d shows lipid levels for one lipid from each cluster. Text or insets show Spearman's correlation coefficient for pairs of lipids within the clusters (a, b, and c) and for representative pairs of lipids in different clusters (d).

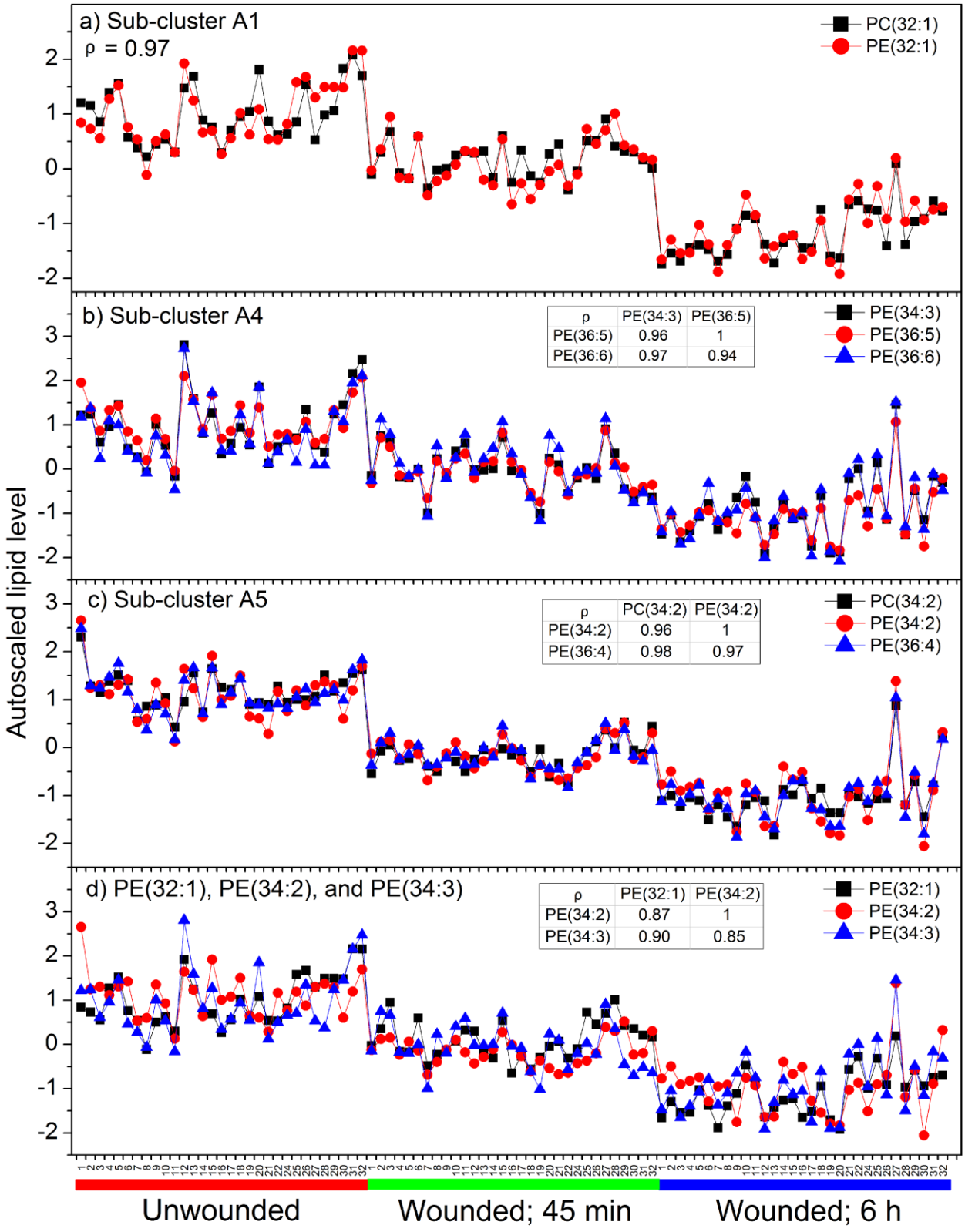
a) Sub-cluster A1
ρ = 0.97
PC(32:1)
PE(32:1)
b) Sub-cluster A4
ρ | PE(34:3) | PE(36:5)
PE(36:5) | 0.96 | 1
PE(36:6) | 0.97 | 0.94
PE(34:3)
PE(36:5)
PE(36:6)
c) Sub-cluster A5
ρ | PC(34:2) | PE(34:2)
PE(34:2) | 0.96 | 1
PE(36:4) | 0.98 | 0.97
PC(34:2)
PE(34:2)
PE(36:4)
d) PE(32:1), PE(34:2), and PE(34:3)
ρ | PE(32:1) | PE(34:2)
PE(34:2) | 0.87 | 1
PE(34:3) | 0.90 | 0.85
PE(32:1)
PE(34:2)
PE(34:3)
Autoscaled lipid level
Unwounded
Wounded; 45 min
Wounded; 6 h

Figure 4.5 Autoscaled levels of representative lipid analytes in sub-clusters C2 and C9. Points represent individual plants subjected to control or wounding treatment as indicated. Panels a and b represent the two clusters, and panel c shows lipid levels for one lipid from each cluster. Text or insets show Spearman's correlation coefficient for pairs of lipids within the clusters (a and b) and for representative pairs of lipids in different clusters (c).

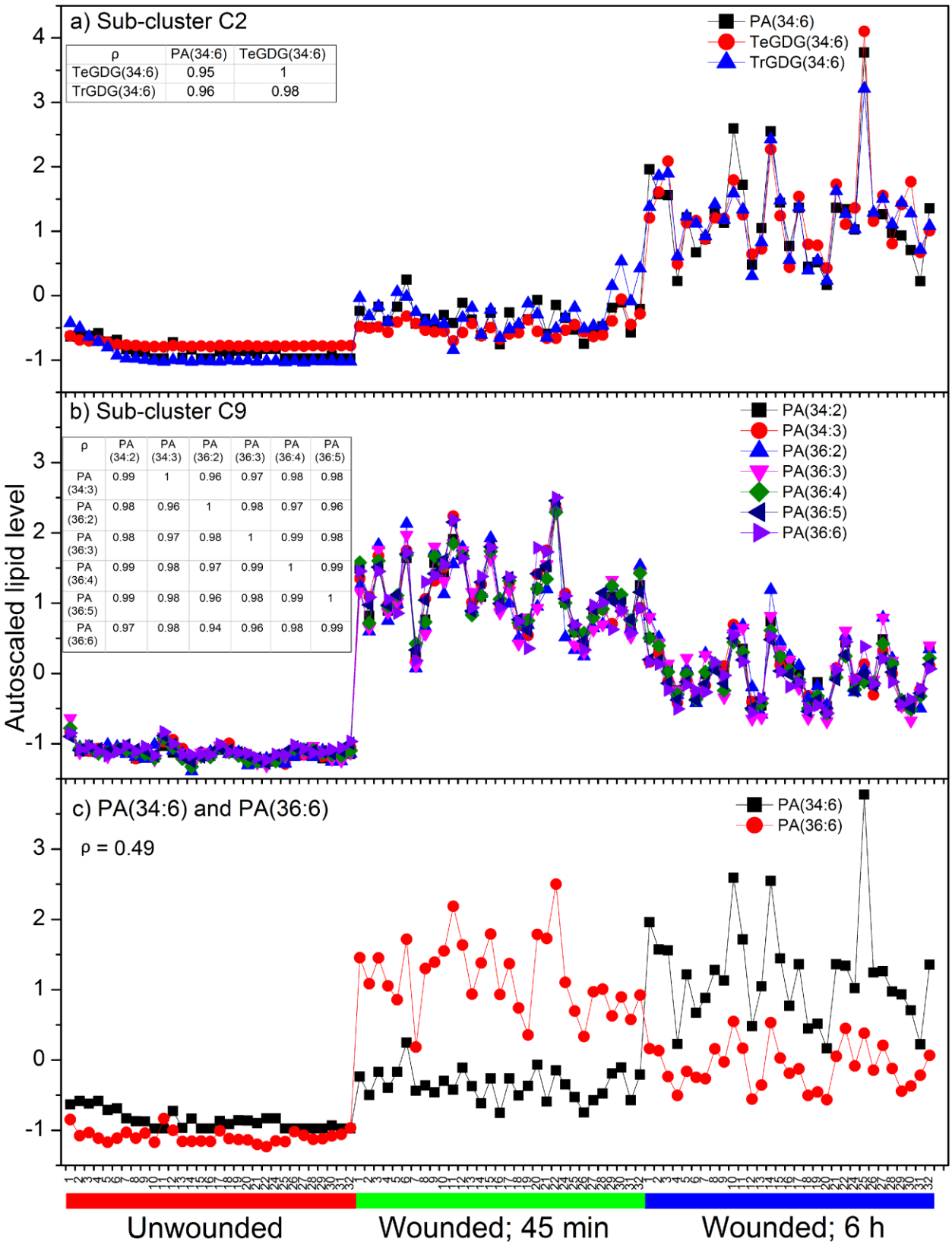
a) Sub-cluster C2
ρ | PA(34:6) | TeGDG(34:6)
TeGDG(34:6) | 0.95 | 1
TrGDG(34:6) | 0.96 | 0.98
PA(34:6)
TeGDG(34:6)
TrGDG(34:6)
b) Sub-cluster C9
ρ | PA (34:2) | PA (34:3) | PA (36:2) | PA (36:3) | PA (36:4) | PA (36:5)
PA (34:3) | 0.99 | 1 | 0.96 | 0.97 | 0.98 | 0.98
PA (36:2) | 0.98 | 0.96 | 1 | 0.98 | 0.97 | 0.96
PA (36:3) | 0.98 | 0.97 | 0.98 | 1 | 0.99 | 0.98
PA (36:4) | 0.99 | 0.98 | 0.97 | 0.99 | 1 | 0.99
PA (36:5) | 0.99 | 0.98 | 0.96 | 0.98 | 0.99 | 1
PA (36:6) | 0.97 | 0.98 | 0.94 | 0.96 | 0.98 | 0.99
PA(34:2)
PA(34:3)
PA(36:2)
PA(36:3)
PA(36:4)
PA(36:5)
PA(36:6)
Autoscaled lipid level
c) PA(34:6) and PA(36:6)
ρ = 0.49
PA(34:6)
PA(36:6)
Unwounded
Wounded; 45 min
Wounded; 6 h

Figure 4.6 Autoscaled levels of representative lipid analytes in sub-clusters C5, C7, and C8. Points represent individual plants subjected to control or wounding treatment as indicated. Panels a, b, and c represent the three clusters, and panel d shows lipid levels for one lipid from each cluster. Text or insets show Spearman's correlation coefficient for pairs of lipids within the clusters (a, b, and c) and for representative pairs of lipids in different clusters (d).

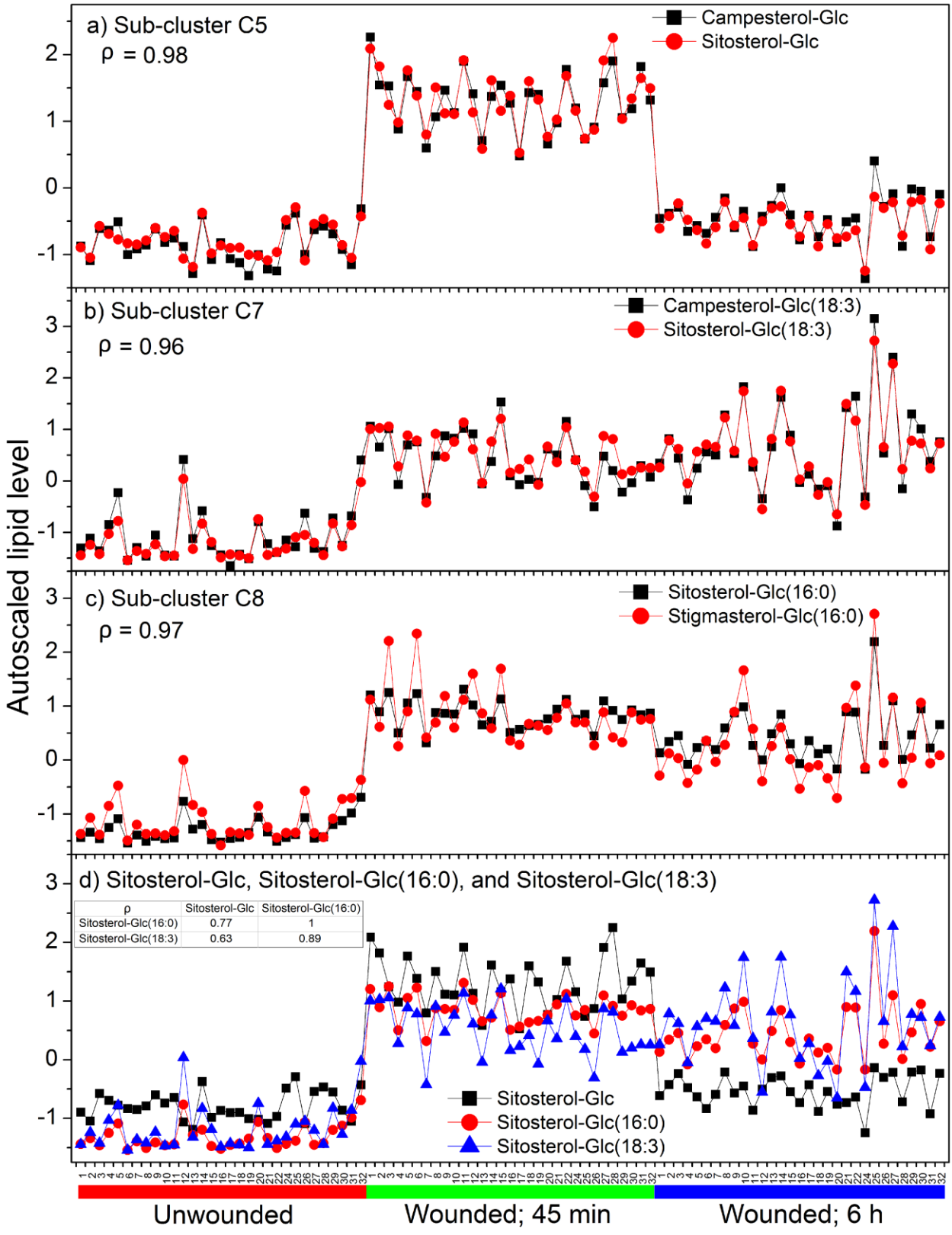
a) Sub-cluster C5
ρ = 0.98
Campesterol-Glc
Sitosterol-Glc
b) Sub-cluster C7
ρ = 0.96
Campesterol-Glc(18:3)
Sitosterol-Glc(18:3)
c) Sub-cluster C8
ρ = 0.97
Sitosterol-Glc(16:0)
Stigmasterol-Glc(16:0)
d) Sitosterol-Glc, Sitosterol-Glc(16:0), and Sitosterol-Glc(18:3)
ρ | Sitosterol-Glc | Sitosterol-Glc(16:0)
Sitosterol-Glc(16:0) | 0.77 | 1
Sitosterol-Glc(18:3) | 0.63 | 0.89
Sitosterol-Glc
Sitosterol-Glc(16:0)
Sitosterol-Glc(18:3)
Autoscaled lipid level
Unwounded
Wounded; 45 min
Wounded; 6 h

Figure 4.7 Autoscaled levels of a representative lipid from each sub-cluster.

The box depicts the middle 50% of the autoscaled values. The line within the box represents the median and the error bars represent standard deviation. n = 31 for each treatment.

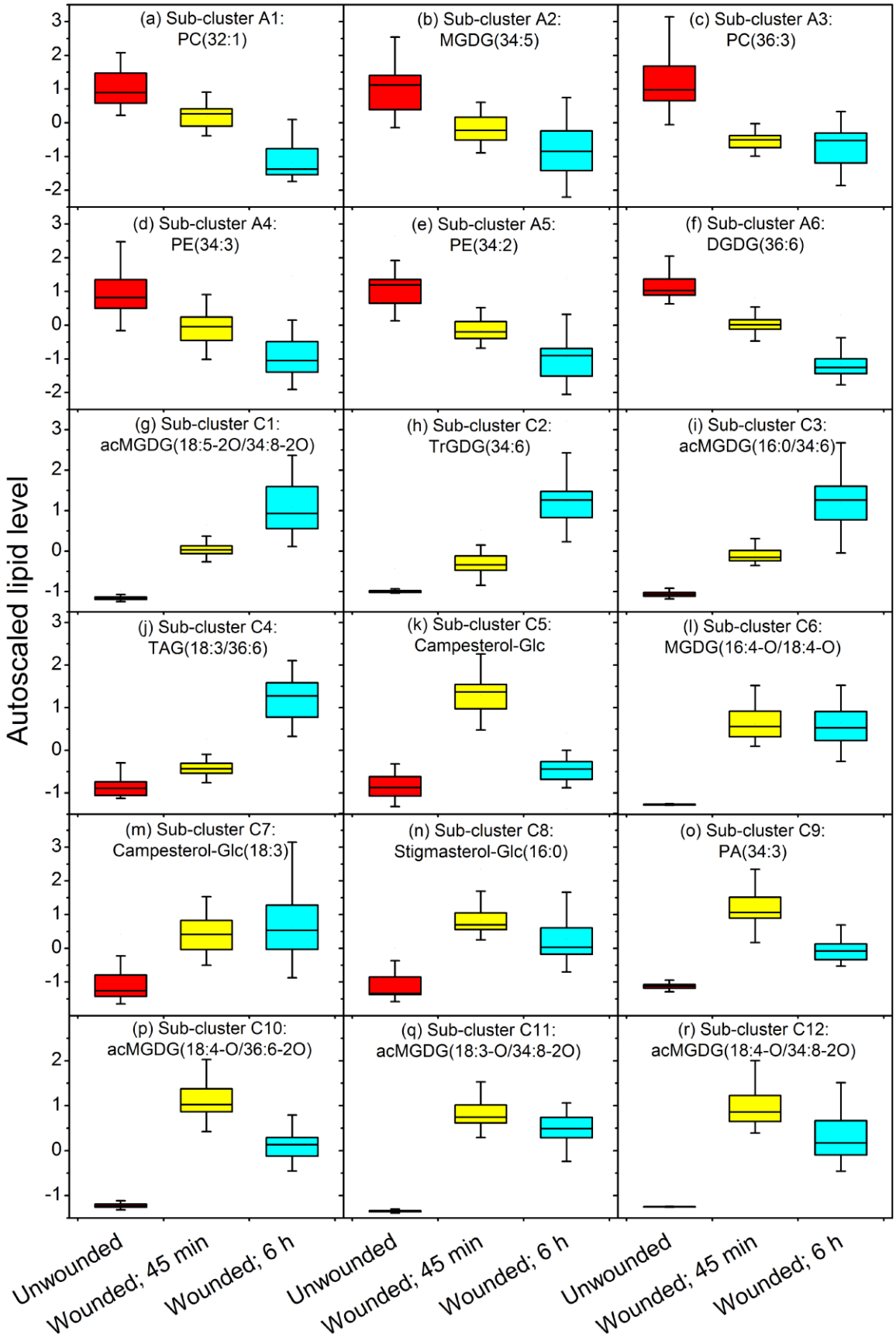
Autoscaled lipid level
(a) Sub-cluster A1: PC(32:1)
(b) Sub-cluster A2: MGDG(34:5)
(c) Sub-cluster A3: PC(36:3)
(d) Sub-cluster A4: PE(34:3)
(e) Sub-cluster A5: PE(34:2)
(f) Sub-cluster A6: DGDG(36:6)
(g) Sub-cluster C1: acMGDG(18:5-2O/34:8-2O)
(h) Sub-cluster C2: TrGDG(34:6)
(i) Sub-cluster C3: acMGDG(16:0/34:6)
(j) Sub-cluster C4: TAG(18:3/36:6)
(k) Sub-cluster C5: Campesterol-Glc
(l) Sub-cluster C6: MGDG(16:4-O/18:4-O)
(m) Sub-cluster C7: Campesterol-Glc(18:3)
(n) Sub-cluster C8: Stigmasterol-Glc(16:0)
(o) Sub-cluster C9: PA(34:3)
(p) Sub-cluster C10: acMGDG(18:4-O/36:6-2O)
(q) Sub-cluster C11: acMGDG(18:3-O/34:8-2O)
(r) Sub-cluster C12: acMGDG(18:4-O/34:8-2O)
Unwounded
Wounded; 45 min
Wounded; 6 h
Unwounded
Wounded; 45 min
Wounded; 6 h
Unwounded
Wounded; 45 min
Wounded; 6 h

Table 4.1 Characteristics of three lipid extraction methods.

Method 1 is the single-step extraction method used for the main experiment in the current work. Method 2 is a modification of the Bligh and Dyer (1959) method (Welti et al., 2002). Method 3 includes Method 2, omitting backwashes, followed by additional extraction with solvent containing isopropanol, hexane, and water (Toledo et al., 1995; Markham et al., 2006). "Intensity normalized to internal standards per dry mass" indicates the total amount of mass spectral signal detected by each method in all lipid classes in comparison to internal standards added at the time of mass spectral analysis (post-extraction). "Percent of total intensity" indicates the intensity detected in each class by each method. Abbreviations are indicated in Table 4.2.

	Composition of extracts from Arabidopsis 45 min after wounding (Intensity normalized to internal standards per dry mass (units · mg^{-1}))		
	Extraction method 1 (Single-step)	Extraction method 2	Extraction method 3
Total intensity	634334 ± 12830	609413 ± 31828	604970 ± 57144
	Percent of total intensity		
Lipid class	Extraction method 1 (Single-step)	Extraction method 2	Extraction method 3
acDGDG	0.0070 ± 0.0029	0.0060 ± 0.0008	0.0069 ± 0.0010
acMGDG	2.33 ± 0.22	2.42 ± 0.23	2.82 ± 0.41
acPG	0.0023 ± 0.0005	0.0017 ± 0.0004	0.0024 ± 0.0007
DAG	0.0064 ± 0.0006	0.0079 ± 0.0010	0.0090 ± 0.0009
DGDG	11.80 ± 0.45	11.35 ± 0.33	9.75 ± 0.70
DGMG	0.0403 ± 0.0036	0.0372 ± 0.0238	0.0184 ± 0.0023
GIPC	0.0086 ± 0.0016	0.0072 ± 0.0027	0.0278 ± 0.0015
GlcCer	2.70 ± 0.13	2.16 ± 0.09	1.96 ± 0.12
LPC	0.0560 ± 0.0208	0.3235 ± 0.4332	0.0482 ± 0.0111
LPE	0.0372 ± 0.0086	0.0513 ± 0.0374	0.0251 ± 0.0040
MGDG	66.22 ± 1.08	68.15 ± 1.20	70.32 ± 1.24

MGMG	0.0745 ± 0.0031	0.0201 ± 0.0056	0.0206 ± 0.0026
PA	0.297 ± 0.039	0.484 ± 0.045	0.505 ± 0.033
PC	4.21 ± 0.33	4.46 ± 0.366	3.84 ± 0.31
PE	2.19 ± 0.03	2.23 ± 0.10	2.20 ± 0.16
PG	4.92 ± 0.18	5.10 ± 0.17	5.19 ± 0.26
PI	1.12 ± 0.03	1.18 ± 0.02	1.17 ± 0.05
PS	0.0482 ± 0.0015	0.0508 ± 0.0017	0.0476 ± 0.0020
SQDG	0.297 ± 0.020	0.313 ± 0.007	0.302 ± 0.020
Sterol derivatives	3.60 ± 0.46	1.61 ± 0.06	1.72 ± 0.06
TAG	0.0114 ± 0.0005	0.0131 ± 0.0037	0.0122 ± 0.0006
TeGDG	0.0010 ± 0.0003	0.0010 ± 0.0001	0.0012 ± 0.0001
TrGDG	0.0169 ± 0.0016	0.0175 ± 0.0017	0.0167 ± 0.0032

Table 4.2 Lipid name abbreviations

Lipid group	Example abbreviation	Abbreviation explanation
Monoacyl glycerophospholipids		
digalactosylmonoacylglycerol	DGMG(18:3)	(Acyl carbons: acyl carbon-carbon double bonds[a])
lysophosphatidylcholine	LPC(16:0)	
lysophosphatidylethanolamine	LPE(16:0)	
monogalactosylmonoacylglycerol	MGMG(18:3)	
Polar diacyl glycerolipids		
phosphatidic acid	PA(34:3)	(Total acyl carbons: total carbon-carbon double bonds)
phosphatidylcholine	PC(32:0)	
phosphatidylethanolamine	PE(36:2)	
phosphatidylglycerol	PG(34:1)	
phosphatidylinositol	PI(38:4)	
phosphatidylserine	PS(36:5)	
digalactosyldiacylglycerol	DGDG(36:6)	
monogalactosyldiacylglycerol	MGDG(34:6)	
sulfoquinovosyldiacylglycerol	SQDG(34:3)	
tetragalactosyldiacylglycerol	TeGDG(34:6)	
trigalactosyldiacylglycerol	TrGDG(34:6)	
Head-group-acylated polar glycerolipids		
acylated digalactosyldiacylglycerol	acDGDG(18:4-O/36:8-2O)	(Head-group acyl carbons: head-group acyl carbon-carbon double bonds/total *sn-1,2* acyl carbons: total *sn-1,2* carbon-carbon double bonds)

acylated monogalactosyldiacylglycerol	acMGDG(16:0/34:6)	
acylated phosphatidylglycerol	acPG(16:1/36:8-2O)	(Acyl carbons: carbon-carbon double bonds for one acyl chain/total acyl carbons: total carbon-carbon double bonds for the other two acyl chains combined)
Neutral glycerolipids		
triacylglycerol	TAG(18:3/36:6)	(Acyl carbons: carbon-carbon double bonds for one acyl chain/total acyl carbons: total carbon-carbon double bonds for the other two acyl chains combined)
diacylglycerol	DAG(16:0/18:3)	(Acyl carbons: carbon-carbon double bonds for one acyl chain/acyl carbons: carbon-carbon double bonds for the other acyl chain)
Polar diacyl lipids measured in negative mode		
DGDG, MGDG, PC, PE, PG	PC(16:0/18:3-O)	(Acyl carbons: carbon-carbon double bonds for one acyl chain/acyl carbons: carbon-carbon double bonds for the other acyl chain)[b]
Sphingolipids		
glycosylinositolphosphoceramide	GIPC(42:2)-3	(Carbons: carbon-carbon double bonds of sphingoid base + fatty amide)-number of hydroxyl groups in base plus acyl chain

glycosylceramide	GlcCer(42:2)-3	
Sterol derivatives		
acylated sterol glucoside	Sitosterol-Glc(18:3)	(Acyl carbons: acyl carbon-carbon double bonds)
sterol ester	Campesterol(18:3)	
sterol glucoside	Sitosterol-Glc	---

[a]"Double bonds" can also indicate double bond equivalents, such as rings. "Extra" oxygen atoms in acyl chains are indicated by a "-O"; for example, oxophytodienoic acid is 18:4-O to indicate 4 double bond equivalents and 1 "extra" oxygen atom.

[b]Note: *sn*-1 and *sn*-2 positions of acyl chains on the glycerol were not determined.

Table 4.3 ANOVA and post-hoc test results.

One-way ANOVA was performed to compare the levels of the lipids among the three treatments. If a significant difference ($p < 0.01$) was detected for a lipid, a Tukey post-hoc test was performed to identify the differing treatments. Significantly different lipids were marked "up" if the lipid was higher at 45 min after wounding than in unwounded plants, at 6 h than in unwounded plants, or at 6 h than at 45 min. "Down" indicates significant changes in the opposite direction. Comparisons that are not significantly different are marked "-". The "Cluster/Sub-cluster" column shows the cluster/sub-cluster name for each lipid in a labeled unit in the dendrogram (Figure 4.3).

Lipid Name	**Wounded; 45 min vs Unwounded**	**Wounded; 6 h vs Unwounded**	**Wounded, 6 h vs Wounded; 45 min**	**Cluster/Sub-cluster**
acDGDG(18:4-O/34:6)	up	up	-	not in a cluster[f]
acDGDG(18:4-O/34:7-O)	-	up	-	not in a cluster[f]
acDGDG(18:4-O/34:8-2O) or acDGDG(18:4-O/36:6)	up	up	-	C
acDGDG(18:4-O/36:8-2O)	up	up	-	C12
acMGDG(16:0/34:6)	up	up	up	C3
acMGDG(16:0/34:7-O)	up	up	up	C3
acMGDG(16:0/34:8-2O) or acMGDG(16:0/36:6)	up	up	-	C12
acMGDG(16:0/36:8-2O)	up	up	-	C12
acMGDG(16:1/34:8-2O) or acMGDG(16:1/36:6)	up	up	up	C
acMGDG(16:3/34:6)	up	up	up	C3
acMGDG(16:3/34:8-2O) or acMGDG(16:3/36:6)	up	up	up	C3
acMGDG(16:3-O/34:8-2O) or acMGDG(16:3-O/36:6)	up	up	-	C
acMGDG(16:3-O/36:8-2O)	up	up	-	C

acMGDG(16:3-2O/34:6) or acMGDG(18:1/34:6)	up	up	up	C
acMGDG(16:3-2O/34:8-2O) or acMGDG(16:3-2O/36:6) or acMGDG(18:1/34:8-2O) or acMGDG(18:1/36:6)	up	up	down	C
acMGDG(16:3-2O/36:8-2O) or acMGDG(18:1/36:8-2O)	up	up	down	C
acMGDG(16:4-O/34:8-2O) or acMGDG(16:4-O/36:6)	up	up	down	C12
acMGDG(16:4-O/36:8-2O)	up	up	down	C
acMGDG(18:0/34:6)	up	up	up	C
acMGDG(18:0/34:8-2O) or acMGDG(18:0/36:6)	up	up	down	C11
acMGDG(18:2/34:6)	up	up	up	C3
acMGDG(18:2/34:7-O)	up	up	up	C3
acMGDG(18:2/34:8-2O) or acMGDG(18:2/36:6)	up	up	-	C
acMGDG(18:2/36:8-2O)	up	up	down	C
acMGDG(18:2-O/34:8-2O) or acMGDG(18:2-O/36:6)	up	up	-	C
acMGDG(18:2-O/36:8-2O)	up	up	up	C
acMGDG(18:2-3O/34:8-2O) or acMGDG(18:2-3O/36:6)	up	up	down	C
acMGDG(18:3/34:6)	up	up	up	C3
acMGDG(18:3/34:7-O)	up	up	up	C3
acMGDG(18:3/34:7-2O) or acMGDG(18:3/36:5)	up	up	up	C3
acMGDG(18:3/34:8-2O) or acMGDG(18:3/36:6)	up	up	up	C3
acMGDG(18:3/36:7-O)	up	up	up	C

acMGDG(18:3/36:8-2O)	up	up	up	C3
acMGDG(18:3-O/34:6)	up	up	-	C
acMGDG(18:3-O/34:7-O)	up	up	up	C
acMGDG(18:3-O/34:8-2O) or acMGDG(18:3-O/36:6)	up	up	down	C11
acMGDG(18:3-O/36:6-O)	up	up	down	C
acMGDG(18:3-O/36:7-O)	up	up	up	C
acMGDG(18:3-O/36:8-2O)	up	up	-	C
acMGDG(18:3-2O/34:6)	up	up	-	C
acMGDG(18:3-2O/34:8-2O) or acMGDG(18:3-2O/36:6)	up	up	down	C10
acMGDG(18:3-2O/36:8-2O)	up	up	down	C10
acMGDG(18:3-3O/34:6)	up	up	down	C
acMGDG(18:3-3O/34:7-O)	up	up	down	C
acMGDG(18:3-3O/36:8-2O)	up	up	down	C10
acMGDG(18:4-O/34:6)	up	up	down	C
acMGDG(18:4-O/34:7-O)	up	up	up	C
Arabidopside E: acMGDG(18:4-O/34:8-2O) or acMGDG(18:4-O/36:6)	up	up	down	C12
acMGDG(18:4-O/36:6-O)	up	up	up	C
acMGDG(18:4-O/36:6-2O)	up	up	down	C10
acMGDG(18:4-O/36:7-2O) (alternative fragmentation)	up	up	up	C
acMGDG(18:4-O/36:7-O)	up	up	up	C1
[a]Arabidopside G: acMGDG(18:4-O/36:8-2O)	up	up	down	C12
[a]Arabidopside G: acMGDG(18:4-O/36:8-2O) (alternative fragmentation)	up	up	down	not in dendrogram[a]
acMGDG(18:4-2O/34:6)	up	up	-	C

acMGDG(18:4-2O/34:7-O)	up	up	up	C
acMGDG(18:4-2O/34:8-2O) or acMGDG(18:4-2O/36:6)	up	up	down	C12
acMGDG(18:4-2O/36:8-2O)	up	up	-	C12
acMGDG(18:4-3O/34:6)	up	up	-	C
acMGDG(18:4-3O/34:7-O)	up	up	-	C
acMGDG(18:4-3O/34:8-2O) or acMGDG(18:4-3O/36:6)	up	up	down	C10
acMGDG(18:5-2O/34:8-2O) or acMGDG(18:5-2O/36:6)	up	up	up	C1
acMGDG(18:5-2O/36:8-2O)	up	up	up	C1
acPG(16:1/36:8-2O)	up	up	-	C
DAG(34:3)	up	up	-	C
DAG(34:4)	up	up	-	not in a cluster[f]
DAG(34:6)	up	up	up	C
DAG(36:4)	-	-	up	not in a cluster[f]
DAG(36:5)	up	up	-	C
DAG(36:6)	up	up	-	C
DGDG(16:0/18:3-2O)	up	-	down	not in dendrogram[e]
DGDG(16:0/18:3-O)	up	up	-	not in a cluster[f]
DGDG(16:0/18:4-O)	up	up	-	C
DGDG(18:3-2O/16:3)	up	up	down	C
DGDG(18:4-O/16:3)	up	up	-	C
Arabidopside C: DGDG(18:4-O/16:4-O)	up	up	-	not in a cluster[f]
DGDG(18:4-O/18:3)	up	up	up	C
Arabidopside D: DGDG(18:4-O/18:4-O)	up	up	-	C
DGDG(18:4-O/18:4-2O) or DGDG(18:4-O/20:2)	up	up	down	C
DGDG(34:3)	down	down	down	A

DGDG(34:4)	down	down	down	A
DGDG(34:5)	down	down	down	A
DGDG(34:6)	down	down	down	A6
DGDG(36:3)	down	down	down	A
DGDG(36:4)	down	down	down	A
DGDG(36:5)	down	down	-	A
DGDG(36:6)	down	down	down	A6
DGDG(36:6-2O) or DGDG(38:4)	-	-	-	not in a cluster[f]
DGDG(36:8-2O) or DGDG(38:6)	up	up	down	C
DGDG(38:5) or DGDG(36:7-2O)	down	down	-	A
DGMG(16:0)	up	up	down	C
DGMG(16:4-O)	up	up	-	C
DGMG(18:3)	up	up	down	C
DGMG(18:4-O)	up	up	-	C
GIPC(42:1)-3	down	down	-	not in a cluster[f]
GIPC(42:2)-3	down	down	-	A
GlcCer(34:1)-2	-	down	down	A
GlcCer(34:1)-3	-	-	-	A
GlcCer(40:1)-3	-	-	-	A
GlcCer(42:2)-3	-	down	down	A
LPC(16:0)	up	up	up	C
LPC(16:1)	up	up	-	C
LPC(18:1)	up	up	up	C
LPC(18:2)	up	up	-	C
LPC(18:3)	up	up	down	C
LPE(16:0)	up	up	up	C
LPE(18:1)	up	-	-	not in a cluster[f]
LPE(18:2)	up	up	down	C
LPE(18:3)	up	up	down	C

MGDG(18:3/16:4-O)	up	up	up	C
MGDG(18:3-O/16:4-O)	up	up	-	C
MGDG(18:3-2O/16:3)	up	up	-	C
MGDG(18:3-2O/16:4-O) or MGDG(20:1/16:4-O) (16:4-O as fragment)	up	up	-	C
MGDG(18:3-2O/16:4-O) (18:4-O as fragment)	up	up	-	C
MGDG(18:3-2O/18:3-O)	up	up	down	not in a cluster[f]
MGDG(18:4-O/16:3)	up	up	-	not in a cluster[f]
MGDG(18:4-O/16:3-O)	up	up	up	C
[b]Arabidopside A: MGDG(18:4-O/16:4-O) (16:4-O as fragment)	up	up	-	C6
[b]Arabidopside A: MGDG(18:4-O/16:4-O) (18:4-O as fragment)	up	up	-	not in dendrogram[b]
MGDG(18:4-O/18:1) or MGDG(18:4-O/16:3-2O)	up	up	-	C
MGDG(18:4-O/18:2)	up	up	up	C
MGDG(18:4-O/18:3)	up	up	up	C
MGDG(18:4-O/18:3-O)	up	up	-	C
MGDG(18:4-O/18:3-2O) or MGDG(18:4-O/20:3)	up	up	-	C
MGDG(18:4-O/18:3-3O)	up	up	-	C
MGDG(18:4-O/18:3-4O)	up	up	-	C
Arabidopside B: MGDG(18:4-O/18:4-O)	up	up	-	C6
MGDG(18:4-O/18:4-2O)	up	up	-	C
MGDG(18:4-O/18:4-3O)	up	up	down	C
MGDG(18:4-2O/16:4-O) or MGDG(20:2/16:4-O)	up	up	up	C

MGDG(18:5-2O/16:4-O) or MGDG(20:3/16:4-O)	up	up	up	not in a cluster[f]
MGDG(18:5-2O/18:4-O) or MGDG(20:3/18:4-O)	up	up	-	not in a cluster[f]
MGDG(30:6-O)	up	up	down	C
MGDG(34:3)	down	down	down	A
MGDG(34:4)	down	down	down	A2
MGDG(34:5)	down	down	down	A2
MGDG(34:6)	down	down	down	A6
MGDG(35:3)	up	-	down	not in a cluster[f]
MGDG(36:3)	down	down	-	A
MGDG(36:4) or MGDG(34:6-2O)	down	down	-	A
MGDG(36:5) or MGDG(34:7-2O)	down	down	down	A
MGDG(36:6) or MGDG(34:8-2O)	down	down	down	A
MGDG(36:6-2O) or MGDG(38:4)	up	up	down	C
MGDG(36:8-2O) or MGDG(38:6)	up	up	-	C
MGDG(38:5) or MGDG(36:7-2O)	down	down	down	A
MGMG(16:0)	up	-	-	not in a cluster[f]
MGMG(16:3)	-	-	-	not in a cluster[f]
MGMG(18:3)	-	-	down	not in dendrogram[e]
MGMG(18:4-O)	up	-	-	not in a cluster[f]
PA(34:1)	up	up	down	C
PA(34:2)	up	up	down	C9
PA(34:3)	up	up	down	C9
PA(34:4)	up	up	-	C
PA(34:6)	up	up	up	C2
PA(36:2)	up	up	down	C9
PA(36:3)	up	up	down	C9

PA(36:4)	up	up	down	C9
PA(36:5)	up	up	down	C9
PA(36:6)	up	up	down	C9
PC(16:0/18:3-O)	-	down	down	not in a cluster[f]
PC(16:0/18:3-2O)	up	up	-	C
PC(18:2/18:3-O)	-	down	down	not in a cluster[f]
PC(18:2/18:3-2O)	up	up	down	C
PC(18:3/18:3-O)	-	down	down	not in a cluster[f]
PC(18:3/18:3-2O)	up	up	down	not in a cluster[f]
PC(32:0)	-	-	-	not in a cluster[f]
PC(32:1)	down	down	down	A1
PC(32:3)	-	up	up	C
PC(34:1)	down	down	-	A3
PC(34:2)	down	down	down	A5
PC(34:3)	down	down	down	A
PC(34:4)	down	down	-	G
PC(34:6)	up	up	up	C
PC(36:2)	down	down	-	A3
PC(36:3)	down	down	-	A3
PC(36:4)	down	down	-	A
PC(36:5)	down	down	down	A
PC(36:6)	-	down	down	A
PC(38:2)	down	down	down	A
PC(38:3)	down	down	down	A
PC(38:4)	down	down	down	A
PC(38:5)	down	down	down	A
PC(38:6)	-	-	-	not in a cluster[f]
PC(40:2)	down	-	up	E
PC(40:3)	down	-	up	E
PC(40:4)	down	down	-	A
PC(40:5)	down	down	-	A

PE(16:0/18:3-O)	-	down	down	B
PE(16:0/18:3-2O)	-	-	down	not in dendrogram[e]
PE(16:0/18:3-3O)	up	up	up	F
PE(18:2/18:3-O)	-	down	down	B
PE(18:2/18:3-2O)	up	down	down	not in dendrogram[e]
PE(18:2/18:3-3O)	-	up	up	F
PE(18:3/18:3-O)	-	down	down	B
PE(18:3/18:3-2O)	up	up	down	C
PE(18:3/18:3-3O)	-	up	up	F
PE(32:0)	down	down	down	A
PE(32:1)	down	down	down	A1
PE(32:3)	-	up	up	C
PE(34:2)	down	down	down	A5
PE(34:3)	down	down	down	A4
PE(34:4)	down	-	-	G
PE(36:2)	down	down	-	A
PE(36:3)	down	down	-	A
PE(36:4)	down	down	down	A5
PE(36:5)	down	down	down	A4
PE(36:6)	down	down	down	A4
PE(38:2)	down	down	down	A
PE(38:3)	down	down	down	A
PE(38:4)	down	down	down	A
PE(38:5)	down	down	-	A
PE(40:2)	down	-	up	not in a cluster[f]
PE(40:3)	-	up	up	not in a cluster[f]
PE(42:2)	down	down	-	not in a cluster[f]
[c]PE(42:3) (measured in positive mode)	down	down	down	not in a cluster[f]
[c]PE(42:3) (measured in negative mode)	-	-	-	not in dendrogram[c]

PG(18:3-O/16:0)	up	up	up	C
PG(18:3-O/16:1)	up	up	-	not in a cluster[f]
PG(18:2/16:0-O)	down	down	down	not in a cluster[f]
PG(18:4-O/16:0)	up	up	down	C
PG(18:4-O/16:1)	up	up	down	C
PG(18:4-O/18:2)	up	up	down	not in a cluster[f]
PG(18:4-O/18:3)	up	up	down	not in a cluster[f]
PG(32:0)	-	-	-	not in a cluster[f]
PG(32:1)	-	down	down	A
PG(34:1)	down	down	-	not in a cluster[f]
PG(34:2)	down	down	down	A
PG(34:3)	down	down	down	A
PG(34:4)	down	down	down	A
PG(36:2)	-	-	down	not in a cluster[f]
PG(36:3)	-	down	-	not in a cluster[f]
PG(36:4)	-	down	-	not in a cluster[f]
PG(36:5)	-	-	-	not in a cluster[f]
PG(36:6)	-	-	-	not in a cluster[f]
PI(34:2)	down	down	down	A
[d]PI(34:3) (measured in positive mode)	-	down	-	not in a cluster[f]
[d]PI(34:3) (measured in negative mode)	-	-	-	not in dendrogram[d]
PS(34:3)	down	down	-	not in a cluster[f]
PS(42:2)	down	down	down	A
PS(42:3)	down	down	down	A
SQDG(32:0)	up	down	down	not in a cluster[f]
SQDG(34:3)	down	down	down	A
SQDG(36:6)	-	down	down	A
Campesterol(18:2)	-	-	-	D
Campesterol(18:3)	-	-	up	D

Campesterol-Glc	up	up	down	C5
Campesterol-Glc(16:0)	up	up	-	C
Campesterol-Glc(18:2)	up	up	down	C
Campesterol-Glc(18:3)	up	up	-	C7
Campesterol-Glc(18:4-O)	up	up	-	C
Sitosterol(18:2)	-	-	-	D
Sitosterol(18:3)	-	-	up	D
Sitosterol-Glc	up	up	down	C5
Sitosterol-Glc(16:0)	up	up	down	C8
Sitosterol-Glc(18:2)	up	up	down	C
Sitosterol-Glc(18:3)	up	up	-	C7
Sitosterol-Glc(18:4-O)	up	up	up	C
Stigmasterol(18:2)	-	-	up	D
Stigmasterol(18:3)	down	-	up	D
Stigmasterol-Glc	up	-	down	C
Stigmasterol-Glc(16:0)	up	up	down	C8
Stigmasterol-Glc(18:2)	up	-	down	C
Stigmasterol-Glc(18:3)	up	up	-	C
Stigmasterol-Glc(18:4-O)	up	up	-	not in a cluster[f]
TAG(18:2/36:5)	up	up	up	C4
TAG(18:3/34:2)	up	up	up	C4
TAG(18:3/36:5)	up	up	up	C4
TAG(18:3/36:6)	up	up	up	C4
TeGDG(34:6)	-	up	up	C2
TeGDG(36:6)	-	up	up	C
TrGDG(34:6)	up	up	up	C2
TrGDG(36:6)	up	up	up	C

[a] and [b] Indicates lipid measured twice in the same mode by different fragmentation events. For each, the second measurement was not included in the dendrogram.

[c] and [d] Indicate lipid measured once by a fragmentation event in the positive and once by a fragmentation event in negative mode. For each, the second measurement (in negative mode) had poor sensitivity

compared to the positive measurement and was not included in the dendrogram.

[e] Not in dendrogram due to $\rho < 0.6$.

[f] Not in a cluster due to $\rho < 0.8$, but still in dendrogram, because $\rho > 0.6$.

Supplemental Data

Supplemental data for this chapter include:

Figure S4.1 Ion leakage of Arabidopsis Col-0 control (unwounded) and wounded plants.

Figure S4.2 Expression of *ALLENE OXIDE SYNTHASE* (*AOS*) and *LIPOXYGENASE2* (*LOX2*) as quantified by qRT-PCR.

Figure S4.3 Leaf appearance before and after wounding.

Figure S4.4 Infusion profiles of representative lipids, as a function of time.

Figure S4.5 Levels of lipids as a function of wounding treatment. (This figure is supplied in a separate PDF file)

Tables S4.1-S4.10 are in a separate Excel file

Table S4.1 Comparison of three extraction methods**.**

Table S4.2 Lipids analyzed with their experimental parameters and evidence for their identification.

Table S4.3 Accurate masses of acyl groups of acMGDG from wounded *Arabidopsis thaliana* (Col-0) by Q-TOF mass spectrometry.

Table S4.4 Oxidized fatty acyl species relevant to this work.

Table S4.5 Internal standards employed in lipid profiling.

Table S4.6 Arrangement of samples in mass spectral lipid profiling in 4 mass spectrometry sample trays.

Table S4.7 Lipid amounts (normalized intensity per mg of leaf dry mass)

Table S4.8 Autoscaled lipid profiling data.

Table S4.9 One-way ANOVA and Tukey's post-hoc test results.

Table S4.10 Correlation among amounts of lipids across plant samples.

Methods S4.1 Plant material and growth

Method S4.2 Ion leakage measurement

Method S4.3 Quantification of gene expression by Real-Time-PCR

Method S4.4 Instrument parameters for analyses on the XevoTS-Q mass spectrometer

Method S4.5 Dendrogram file format conversion

Appendix S4.1 References cited in Supporting Information

Figure S4.1 Ion leakage of Arabidopsis Col-0 control (unwounded) and wounded plants.
*Student's t-test indicated a significant difference from unwounded leaves; $p < 0.001$, $n = 10$.

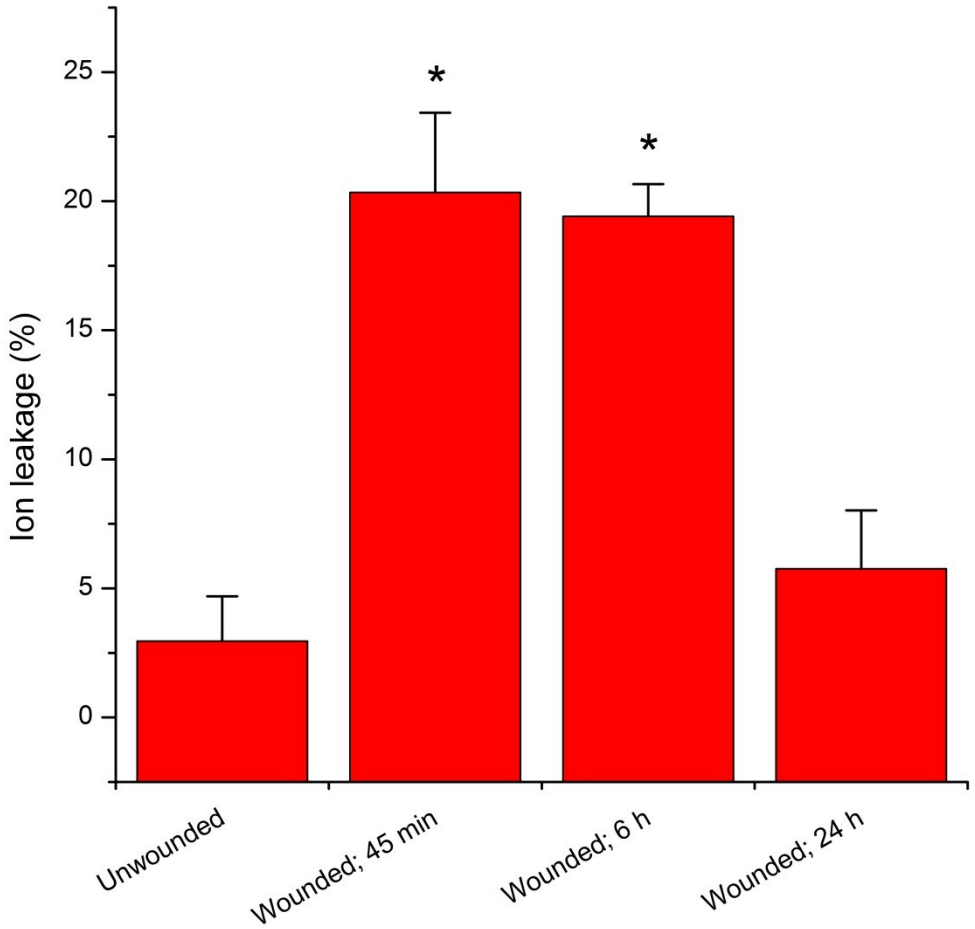

Figure S4.2 Expression of *ALLENE OXIDE SYNTHASE* (*AOS*) and *LIPOXYGENASE2* (*LOX2*) as quantified by qRT-PCR. The levels of *AOS* and *LOX2* expression were normalized to that of a constitutive control gene, *EF1α*. Six unwounded plants and 6 wounded plants were sampled. The Q test for discordant data (Shoemaker et al., 1974) was applied, resulting in removal of one datum in the unwounded *AOS* data set and one datum in the *LOX2* wounded data set. The data indicate that *AOS* expression was 3.9-fold greater and *LOX2* expression was 7.3-fold greater in leaf 6 of wounded plants, compared to leaf 6 of unwounded plants.
*The p-value for the comparison of unwounded and wounded plant gene expression was < 0.001 for both genes by Student's t-test.

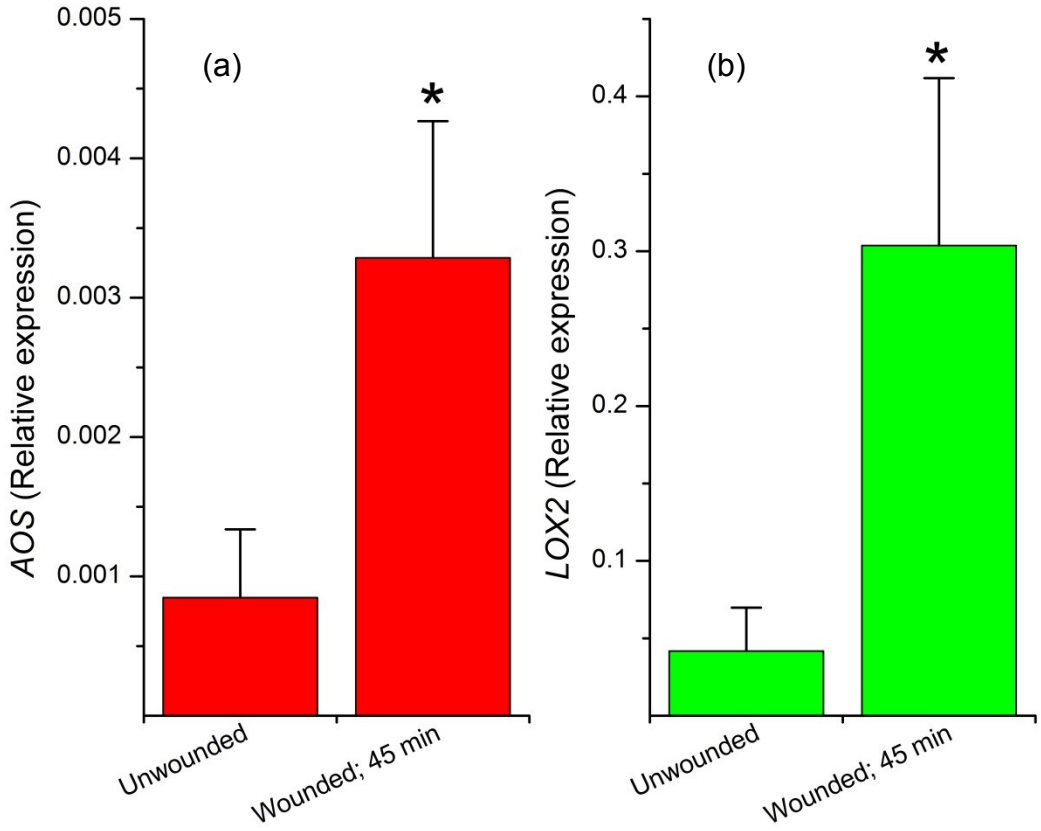

Figure S4.3 Leaf appearance before and after wounding. Plants were 4-week old.

Figure S4.4 Infusion profiles of representative lipids, as a function of time. The vertical axis is relative intensity (%). The horizontal axis is time (min) from 0 to 15 min. Following lipid names are the polarity of the mass spectrometer (positive/negative), the intact ion *m/z*>fragment *m/z*, and the maximum intensity (i.e., the intensity of 100%). The samples were directly infused from a 300 µl loop. The initial period of no intensity represents the time it took for the sample to reach the mass spectrometer. The sample solvent was isopropanol: chloroform: methanol: 300 mM ammonium acetate in water (25: 30: 41.5: 3.5, v/v/v/v). From 0 to 11 min, the sample was pushed through the loop with methanol at 30 µl min^{-1} and, from 11 to 15 min, with methanol at 90 µl min^{-1}. In positive mode each lipid was scanned 130 or 131 times, and in negative mode each lipid was scanned 38 times, during the 15 min of data acquisition.

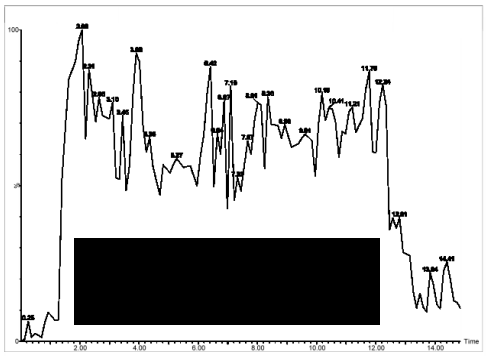
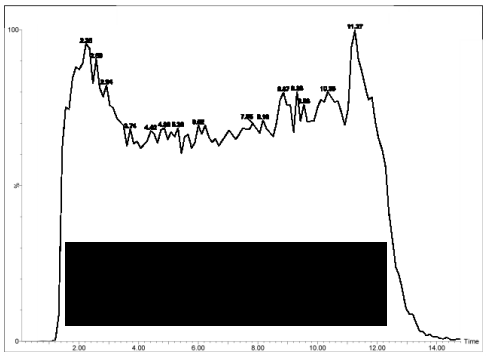
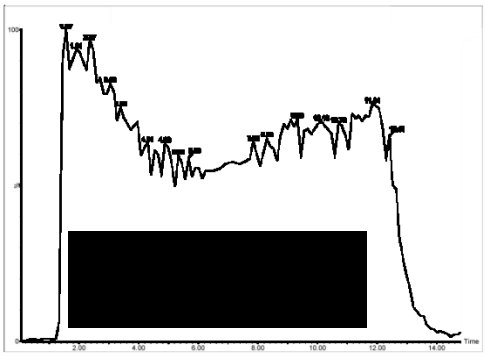
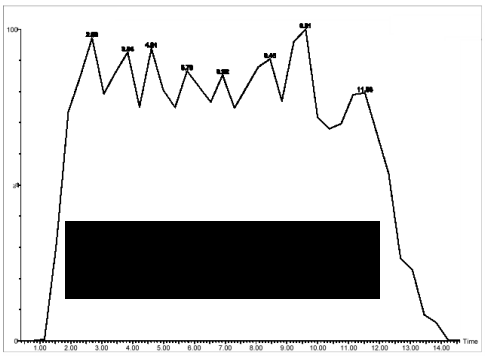
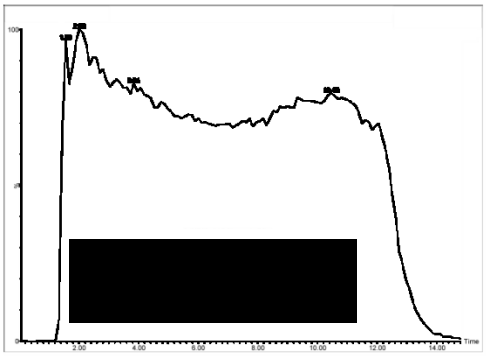
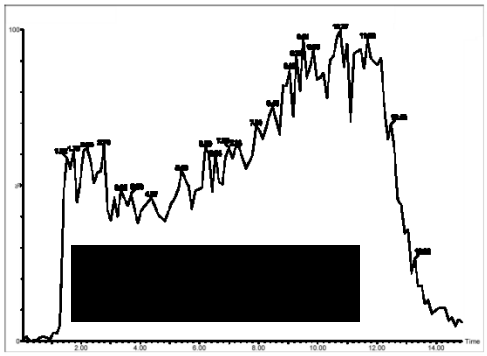
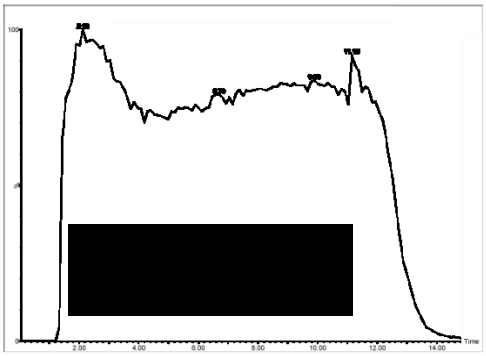
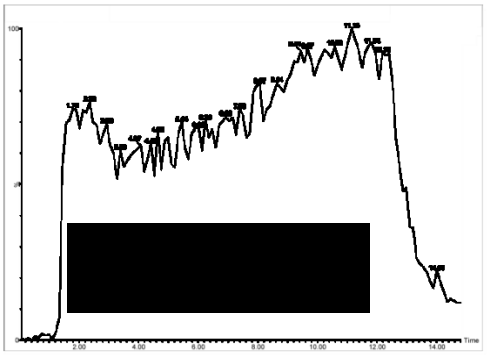

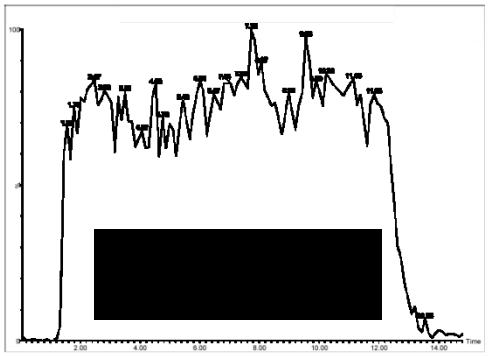

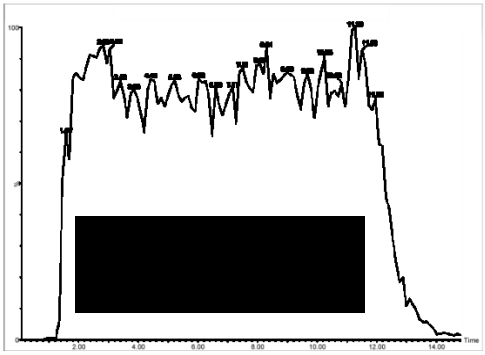

Methods S4.1 Plant material and growth

Arabidopsis thaliana accession Columbia-0 (Col-0) seeds were soaked in tap water at 4°C for 2 days before being sown at 4 seeds per well in 72-well plug trays (International Green House Company, Danville, IL, USA) filled with loosely packed, water-saturated, autoclaved, and cooled Pro-Mix "PGX" soil (Hummert International, Springfield, MO, USA). Trays were placed in a growth chamber under a 14/10 h light/dark cycle at 21°C with 60% humidity. Light intensity was maintained at 80 μmol m^{-2} sec^{-1} with cool white fluorescent lights. Trays were covered with propagation domes for the first 7 days to maintain high humidity. Trays were watered once per week. On day 12 after sowing, plants were reduced to one plant per well. On day 19, trays were fertilized with 0.01% Miracle-Gro 20-20-20 (Scotts Miracle-Gro Co., Marysville, OH, USA).

Method S4.2 Ion leakage measurement

Ion leakage was measured as described previously (Vu et al., 2014). Briefly, leaves were harvested at 45 min, 6 h, and 24 h after wounding, rinsed with distilled water, and shaken in a test tube containing 25 ml of distilled water at 100 rpm for 2 h before the conductivity of the solution was measured. The solution was then heated to and maintained at 95-100°C for 2 h to fully release the leaves' ions. After cooling to room temperature, a second conductivity measurement was taken. The ion leakage (%) was calculated as the first measurement over the second measurement x 100.

Method S4.3 Quantification of gene expression by real-time-PCR

Total RNA was extracted from wounded and unwounded leaf samples by the acid guanidinium thiocyanate-phenol-chloroform extraction method according to Chomczynski and Sachhi (1987). DNA contamination in isolated RNA samples was removed by treatment with RNase-free DNase

(Ambion, lifetechnologies.com), and RNA was spectrophotometrically quantified at 260 nm. DNA-free total RNA (2 μg) from each sample was used for cDNA synthesis. The first-strand cDNA synthesis was performed with Oligo (dT) primer using M-MLV Reverse Transcriptase (Promega, promega.com) according to the manufacturer's instructions. Individual real-time PCR reactions contained 5 μL of the SYBR Green PCR master mix (Applied Biosystems, *appliedbiosystems.com*), 2 μL of cDNA, 0.3 μL of 10 μM forward and reverse primers, and 2.4 μL of distilled water on an Eco qPCR system (Illumina, illumina.com) using the following amplification protocol: 10 min polymerase activation and denaturation at 95°C, and 40 cycles of 95°C for 10 sec, 60°C for 30 sec, and 72°C for 30 sec. This was followed by denaturation to confirm a single PCR product. Melt curves were obtained by slow heating at 0.5°C sec^{-1}, from 55°C to 95°C while continuously monitoring the fluorescence signal. A negative control without a cDNA template and a positive control with a known cDNA template were run to evaluate the overall specificity. The levels of *AOS* (At5g42650) and *LOX2* (At3g45140) expression was normalized to that of a constitutive control gene *EF1α* (At5g60390) by subtracting the cycle threshold value of control *EF1α* from the cycle threshold value of *AOS* and *LOX2*. The *EF1α*-F (5′- accaagattgacaggcgttc-3′) and *EF1α*-R (5′- tgcaacagtctgcctcatgt -3′), *AOS*-F (5'-ccctttttccgatttctctcc-3') and *AOS*-R (5'-acggtagcctccggttagtt-3'), and *LOX2*-F (5′-ggtctcgatgacattgctga-3′) and *LOX2*-R (5′-aggcatctcaaactcgcact-3′) gene-specific primers were used for PCR amplification of *EF1α*, *AOS*, and *LOX2*, respectively. Expression was measured in leaf 6 of 4-week-old wild-type (Col-0) Arabidopsis, either unwounded or subjected to wounding on leaves 5, 6, and 7.

Method S4.4 Instrument parameters for analyses on the XevoTS-Q mass spectrometer

The global settings for all analyses on the Xevo TS-Q mass spectrometer were: capillary voltage, ±2.8 kV; source offset voltage, ±30.0 V; cone voltage, ±40.0 V; source temperature, 150°C; desolvation temperature, 250°C; cone gas flow, 150 L h^{-1}; desolvation gas flow, 650 L h^{-1}; collision gas flow, 0.1 mL min^{-1}; nebulizer gas pressure, 7 bar; low mass 1 and 2 resolution, 2.5; high mass 1 and 2 resolution, 14.5; ion energy 1 and 2, 1.0. Interchannel delay (ICD) was 0.006-0.012 sec in positive mode and 0.100 sec in negative mode. Interscan delay (ISD) was 0.020 sec in positive mode and 0.100 sec in negative mode.

Method S4.5 Dendrogram file format conversion

Clustering results produced by Cluster 3.0 (Eisen et al., 1997) (.gtr and .cdt files) were converted to NEWICK format (.nwk) using a Python script written by Haibao Tang (J. Craig Venter Institute, Rockville, MD, USA). The script can be obtained from the following link: https://github.com/tanghaibao/treecut/blob/master/scripts/eisen_to_newick.py.

Appendix S4.1 References cited in Suppplemental data

Andersson MX, Hamberg M, Kourtchenko O, Brunnström A, McPhail KL, Gerwick WH, Goebel C, Feussner I and Ellerström M (2006) Oxylipin profiling of the hypersensitive response in *Arabidopsis thaliana*. Formation of a novel oxo-phytodienoic acid-containing galactolipid Arabidopside E. J. Biol. Chem. 281, 31528-31537.

Burgos A, Szymanski J, Seiwert B, Degenkolbe T, Hannah MA, Giavalisco P and Willmitzer L (2011) Analysis of short-term changes in the *Arabidopsis thaliana* glycerolipidome in response to temperature and light. The Plant Journal 66, 656–666.

Buseman CM, Tamura P, Sparks AA, Baughman EJ, Maatta S, Zhao J, Roth MR, Esch SW, Shah J, Williams TD and Welti R (2006) Wounding stimulates the accumulation of

glycerolipids containing oxophytodienoic acid and dinor-oxophytodienoic acid in Arabidopsis leaves. Plant Physiol. 142, 28-39.

Chomczynski P and Sachhi N (1987) Single-step method of RNA isolation by acid guanidinium thiocyanate-phenol-chloroform extraction. Anal. Biochem. 162, 156-159.

Devaiah SP, Roth MR, Baugham E, Li M, Tamura P, Jeannotte R, Welti R and Wang XM (2006) Quantitative profiling of polar glycerolipid species and the role of phospholipase Dα1 in defining the lipid species in Arabidopsis tissues. Phytochemistry 67, 1907-1924.

Eisen MB, Spellman PT, Brown PO and Botstein D (1997) Cluster analysis and display of genome-wide expression patterns. Proc. Natl. Acad. Sci. USA 95, 14863-14868.

Esch, S.W., Tamura, P., Sparks, A.A., Roth, M.R., Devaiah, S.P., Heinz, E., Wang, X., Williams TD and Welti R (2007) Rapid characterization of fatty acyl composition of complex lipids by collision-induced dissociation time-of-flight mass spectrometry. J. Lipid. Res. 48, 235-241.

Glauser G, Grata E, Rudaz S and Wolfender JL (2008) High-resolution profiling of oxylipin containing galactolipids in Arabidopsis extracts by ultraperformance liquid chromatography/time-of-flight mass spectrometry. Rapid Commun. Mass Spectrom. 22, 3154-3160.

Grun G, Berger S, Matthes D and Mueller MJ (2007) Early accumulation of non-enzymatically synthesized oxylipins in *Arabidopsis thaliana* after infection with *Pseudomonas syringae*. Funct. Plant Biol. 34**,** 65-71.

Hisamatsu Y, Goto N, Hasegawa K and Shigemori H (2003) Arabidopsides A and B, two new oxylipins from *Arabidopsis thaliana*. Tetrahedron Lett. 44, 5553-5556.

Hisamatsu Y, Goto N, Sekiguchi M, Hasegawa K and Shigemori H (2005) Oxylipins arabidopsides C and D from *Arabidopsis thaliana*. J. Nat. Prod. 68, 600-603.

Hsu F-F, Turk J, Williams TD and Welti R (2007) Electrospray ionization multiple stage quadrupole ion-trap and tandem quadrupole mass spectrometric studies on phosphatidylglycerol from Arabidopsis leaves. J. Am. So.c Mass Spectrom. 18, 783-90.

Ibrahim A, Schütz AL, Galano JM, Herrfurth C, Feussner K, Durand T, Brodhun F and Feussner I (2011) The alphabet of galactolipids in *Arabidopsis thaliana*. Front Plant Sci. DOI: 10.3389/fpls.2011.00095.

Kourtchenko O, Andersson MX, Hamberg M, Brunnström A, Goebel C, McPhail KL, Gerwick WH, Feussner I and Ellerström M (2007) Oxo-phytodienoic acid containing galactolipids in Arabidopsis: Jasmonate signaling dependence. Plant Physiol. 145, 1658-1669.

Li M, Baughman E, Roth MR, Han X, Welti R, and Wang X (2014) Quantitative profiling and pattern analysis of triacylglycerol species in Arabidopsis seeds by electrospray ionization mass spectrometry. Plant J. 77, 160-172.

Maeda H, Sage TL, Isaac G, Welti R and DellaPenna D (2008) Tocopherols modulate extra-plastidic polyunsaturated fatty acid metabolism in *Arabidopsis* at low temperature. Plant Cell 20, 452-470.

Markham JE and Jaworski JG (2007) Rapid measurement of sphingolipids from Arabidopsis thaliana by reversed-phase high-performance liquid chromatography coupled to electrospray ionization tandem mass spectrometry. Rapid Commun. Mass Spectrom. 21, 1304-1314.

Okazaki Y, Shimojima M, Sawada Y, Toyooka K, Narisawa T, Mochida K, Tanaka H, Matsuda F, Hirai A, Hirai MY, Ohta H and Saito K (2009) A chloroplastic UDP-glucose pyrophosphorylase from Arabidopsis is the committed enzyme for the first step of sulfolipid biosynthesis. Plant Cell 21, 892-909.

Peters C, Li M, Narasimhan R, Roth MR, Welti R and Wang X (2010) Nonspecific phospholipase C NPC4 promotes responses to abscisic acid and tolerance to hyperosmotic stress in Arapidopsis. Plant Cell 22, 2642-2659.

Samarakoon T, Shiva S, Lowe K, Tamura P, Roth MR and Welti R (2012) Arabidopsis thaliana membrane lipid molecular species and their mass spectral analysis. In *High throughput phenotyping in plants, Methods in Molecular Biology*. Ed., J. Normanly. Humana Press, New York, NY. 918, 179-268.

Schrick K, Shiva S, Arpin J, Delimont N, Isaac G, Tamura P and Welti R (2012) Steryl glucoside and acyl steryl glucoside analysis of Arabidopsis seeds by electrospray ionization tandem mass spectrometry. Lipids 47, 185-193.

Shigemori H, Nakajyo H, Hisamatsu Y, Sekiguchi M, Goto N and Hasegawa K (2006) Arabidopside F, a new oxylipin from *Arabidopsis thaliana*. Heterocycles 69, 295-301.

Shoemaker JP, Garland CW and Steinfeld JI (1974) "Experiments in Physical Chemistry", McGraw-Hill, Inc., pp. 34-39.

Stelmach BA, Mueller A, Hennig P, Gebhardt S, Schubert-Zsilavecz M and Weiler EW (2001) A novel class of oxylipins, sn1-O-(12-oxophytodienoyl)-sn2-O-(hexadecatrienoyl)-monogalactosyl diglyceride, from *Arabidopsis thaliana*. J. Biol. Chem 276, 12832-12838.

Vu HS, Tamura P, Galeva NA, Chaturvedi R, Williams TD, Wang X, Shah J and Welti R (2012) Direct infusion mass spectrometry of oxylipin-containing Arabidopsis thaliana membrane lipids reveals varied patterns in different stress responses. Plant Physiol. 158, 324-339.

Vu HS, Roth MR, Tamura P, Samarakoon T, Shiva S, Honey S, Lowe K, Schmelz EA, Williams TD and Welti R (2014) Head-group acylation of monogalactosyldiacylglycerol is a common stress response, and the acyl-galactose acyl composition varies with the plant species and applied stress. Physiol Plant. In press.

Welti R, Li W, Li M, Sang Y, Biesiada H, Zhou H, Rajashekar CB, Williams TD and Wang X (2002) Profiling membrane lipids in plant stress responses. Role of phospholipase Dα in freezing-induced lipid changes in Arabidopsis. J. Biol. Chem. 277, 31994-32002.

Welti R, Wang X and Williams TD (2003) Electrospray ionization tandem mass spectrometry scan modes for plant chloroplast lipids. Anal. Biochem. 314, 149-152.

Wewer V, Dombrink I, Vom Dorp K and Dörmann P (2011) Quantification of sterol lipids in plants by quadrupole time-of-flight mass spectrometry. J. Lipid Res. 52, 1039–1054.

Xiao S, Gao W, Chen Q, Chan S, Zheng S, Ma J, Wang M, Welti, R and Chye M-L. (2010) Overexpression of Arabidopsis acyl-CoA binding protein ACBP3 promotes starvation-induced and age-dependent leaf senescence. Plant Cell 22, 1463-1482

Yang W, Zheng Y, Bahn SC, Pan X, Li M, Vu HS, Roth MR, Scheu B, Welti R, Hong Y and Wang X (2011) The patatin-containing phospholipase A pPLAIIα modulates oxylipin formation and water loss in Arabidopsis thaliana. Mol. Plant 5, 452-460.

Zoeller M, Stingl N, Krischke M, Fekete A, Waller F, Berger S and Mueller MJ (2012) Lipid profiling of the Arabidopsis hypersensitive response reveals specific lipid peroxidation and fragmentation processes: biogenesis of pimelic and azelaic acid. Plant Physiol. 160, 365-378.

Chapter 11 - Roles of lipoxygenases and lipases in Arabidopsis in response to freezing

Abstract

The analytical approach developed in Chapter 4 was used to measure 331 lipids extracted from Arabidopsis exposed to cold acclimation, freezing and thawing. The data from wild-type plants were used to construct a dendrogram depicting clusters and sub-clusters of lipids that have similar patterns in response to treatments. The levels of these lipids were compared between the wild-type and 22 lines with knockout mutations in oxophytodienoic reductase, lipoxygenase and acyl hydrolase genes. Preliminary analysis of the data suggests that an increased formation of oxophytodienoic-acid-containing acylated monogalactosyldiacylglycerols (Arabidopsides E and G) during tissue thawing of cold-acclimated, frozen *pPLAIIγ* knockout coincided with a better recovery compared to wild-type.

Introduction

Lipoxygenases (LOXs) initiate lipid oxidation under various stresses. The enzymatic lipid oxidation catalyzed either by 9-LOXs or 13-LOXs produces either 9- or 13-hydroperoxy fatty acids, which are the precursors of many oxylipins. In Arabidopsis, the 9-LOX pathway, which includes LOX1 and LOX5, has been shown to have an antagonistic interaction with the ethylene pathway in the control of oxidative stress and modulation of bacterial defense (López et al., 2011). LOX1 was demonstrated to be essential in stomatal closing in response to bacterial infection (Montillet et al., 2013) and to be involved in Arabidopsis early response to cadmium exposure (Keunen et al., 2013). All four Arabidopsis 13-LOXs, LOX2, LOX3, LOX4, and LOX6 were shown to contribute to jasmonate synthesis in wounded leaves (Chauvin et al., 2013). Chauvin et al. (2013) also showed that LOX6 was the only 13-LOX necessary for the initiation of early jasmonate synthesis in systemic leaves. In an earlier study, LOX2 was shown to be required for wound-induced accumulation of jasmonic acid (Bell et al., 1995). These results suggest that the involvements of individual LOX genes in plant responses to different stresses are

different. Although LOX-derived products are induced by many abiotic and biotic stresses (Feussner and Wasternack, 2002; Weber, 2002; Hamberg et al., 2005; Shah, 2005; and Shah and Chaturvedi, 2008), the potential roles of each LOX gene in biosynthesis of oxidized lipids under plant stress conditions are understudied. Therefore, analyses of LOX mutants are critical to define specific roles of each LOX gene in the formation of stress-induced oxidized membrane lipids.

Acyl hydrolases (AHs) affect plant stress responses and might be involved in metabolism of oxidized membrane lipids. The Arabidopsis genome has many gene families tentatively encoding acyl hydrolase such as DEFECTIVE IN ANTHER DEHISENCE 1 (DAD-1)-like proteins (Ishiguro et al., 2001), secreted phospholipase A2 (Lee et al., 2005), GDSL lipases (Oh et al., 2005), and patatin-like proteins (PLP) (La Camera et al., 2005). PLP2 is involved in cell death execution, oxylipin synthesis, and pathogen resistance (La Camera et al., 2009). In a research on gene expression response to stresses, out of six PLPs: At4g37070, At2g26560, At4g37050, At2g39220, At3g54950 and At3g63200 (PLP1, PLP2, PLP3, PLP6, PLP7, and PLP9, respectively) only PLP2, PLP3, and PLP7 were induced by drought and PLP2 was further demonstrated to be induced in wounding and have AH activity *in vitro* (Matos et al., 2008). PLP1, PLP3, and PLP5 were demonstrated to have different roles in root response to phosphate deprivation (Rietz et al., 2010). It is clear that the PLPs play important roles in plant stress responses and are possibly involved in membrane lipid metabolism. However, very little is know about their substrates, products, and especially functions of each PLP under stress conditions. Although many phospholipases have been demonstrated to activate and play important roles in plant responses to cold and freezing (Welti et al., 2002; Li et al., 2004; Li et al., 2008), the roles of PLP in low temperature stress are still poorly studied (Li et al., 2013). Therefore, it is important to study PLP mutants to define their roles in stress-induced metabolism of oxidized membrane lipids.

Improving plant freezing tolerance has great agricultural significance. Naturally, some plants, including Arabidopsis, can increase their freezing tolerance after a period of exposure to low, non-freezing temperature; this is termed cold acclimation. Changes in lipid composition during cold acclimation are very important among the molecular strategies that help plants increase their

freezing tolerance. ACYL-LIPID DESATURASE 2 (ADS2) was shown to desaturate esterified 16:0 at low temperature, and this was shown to be important for freezing tolerance (Chen and Thelen, 2013). The accumulation of triacylglycerols during the acclimation period was reported to be a distinguishing factor between Arabidopsis ecotypes with different freezing tolerance (Degenkolbe et al., 2012). A distinct, acclimation-independent freezing tolerating mechanism is the converting of monogalactosyldiacylglycerol to oligogalactosyldiaclyglycerol by SENSITIVE TO FREEZING 2 (SFR2), a constitutively expressed protein (Moellering et al., 2010). Thus, cold acclimation and ultimately freezing tolerance involve diverse lipid compositional changes. To better understand the changes and their bases, a systematic approach is needed to study mechanisms underlying plant freezing tolerance.

In this research, we applied the high throughput lipidomics strategy developed in Chapter 4 to study Arabidopsis oxophytodienoic reductase, LOX and AH knockout mutants responding to cold acclimation and freezing. Six wild-type control plants and three plants of each knockout line were grown in a tray. Each tray was exposed to a unique temperature treatment. Afterward, the plants were harvested for both leaf damage assesment by ion leakage and lipid analysis. The whole treatment was repeated three times. Analysis of the first round is complete and analysis of rounds 2 and 3 is in progress. The direct infusion of total lipids, combined with the sensitivity of the mass spectrometer operated in MRM mode, offer relatively comprehensive snapshots of lipidomes. We employed a quality control strategy to enhance precision. This chapter presents data obtained from the first round of the experiment. The data provide novel preliminary findings about the production and metabolism of oxidized membrane lipids and the involvement of LOXs and AHs in cold and freezing responses in Arabidopsis.

Materials and Methods

Overall experimental design

In this research, we utilized 23 Arabidopsis lines; each of which was given a letter label from A to X for convenient handling (Table 5.1), except for the wild-type Columbia-0 (Col-0) accession which was duplicated (A and M, treated as 2 different lines during the experiment) due to its critical role as a control. The 24 lines were grown in triplicate in 72-well plug trays (Figure 5.1

and Figure 5.2). Each tray was treated with one of the conditions described in Figure 5.3. All 17 treatments (17 trays) were repeated three times (referred to as replication rounds 1, 2, and 3). Each well of the plug tray was labeled with a number from 1 – 72. Therefore, each line was associated with three different numbers indicating its positions on the plug tray. The positions of each line were different in the three replication rounds. For example, in replication round 1, line H was grown in wells numbered 1, 15, and 38 of each of the 17 trays; in replication round 2, line H was grown in wells numbered 13, 46, and 62 (Figure 5.1). The positions of each line in a tray were randomized in a controlled manner so that there was always at least 1 plant of all 24 lines on the outside wells. Seed sowing of the 17 trays of each replication round was done on 5 consecutive days (day 1: tray 1, 2, 4, 7, 10, and 12; day 2: 3, 5, 8, and 11; day 3: 6, 9, 14, and 16; day 4: tray 13 and 17; day 5: tray 15). All handlings and treatments of each tray (watering, thinning, fertilizing, photographing, treating, and harvesting) were done according to a staggered schedule so that time-consuming steps such as thinning or harvesting could be performed by no more than 4 laboratory workers at a time, and so that no more than two trays (the maximal capacity of the freezing chamber) would require freezing treatment on the same day.

Each tray was photographed to record visible phenotypes. In parallel with lipid analysis, ion leakage measurements were performed to detect membrane damage caused by the treatments.

Arabidopsis lines

We studied 22 mutant lines (including single, double, and triple knockouts) and wild-type, i.e. accession Columbia-0 (Col-0). Each line was given a letter label from A to X for easy handling throughout the experiment, as listed in Table 5.1. Col-0 was duplicated (A and M).

All the *pPLA* knockout lines were provided by Xuemin Wang and Maoyin Li (Danforth Plant Science Center, St Louis, MO, USA). All the *lox* lines except for *lox4* were provided by Jyoti Shah (University of North Texas, Denton, TX, USA). The l*ox4* knockout line was ordered directly from Arabidopsis Biological Resource Center (ABRC). The *lox4* seeds were sown and grown for 30 days before leaves were harvested for DNA extraction. Genotype with respect to *lox4* was confirmed by PCR using forward primer GACGCGTTCGTGTCTGACT and reverse

primer GGACTCTTTCCGCCTTTGA. Seeds collected from plants confirmed to be *lox4* homozygous recessive were used as line N. The *opr3* knockout line (X) was kindly shared by Jianmin Zhou. The *opr3* knockout line (in Col-0 background with RAP-luciferase transgene inserted) was induced by EMS mutagenesis giving the G2471A base substitution which results in replacement of Trp138 by a stop codon.

Plant growth conditions

Pro-Mix "PGX" soil (Hummert International, Earth City, MO, USA) was mixed with tap water to saturation and autoclaved for 1 h and was cooled to room temperature before potting. The pots for planting were a 72-well TLC Square Plug tray (International Greenhouse Company, Danville, IL, USA), placed inside a tray with holes, then both were placed inside another tray without holes (Hummert International). To prepare for sowing, a tray was filled with 2.5 L of fertilizer solution (0.01 % Peters 20: 20: 20 (Hummert International) in tap water).

Randomized seed positions used in the three rounds of the experiment are shown in Figure 5.1. Each plant has a combined label including the tray label (e.g., F1-1, Figure 5.2) and the well number (Figure 5.1A). When sowing, a bamboo toothpick was used to place four seeds, evenly spaced, at the center of a well. After sowing, a tray was drained, covered with a propagation dome (Hummert International) and kept at 4 °C for 2 days before transfer to growth conditions (21 °C, 60 % humidity, 80 – 100 $\mu E\ m^{-2}\ s^{-1}$). On day 9 counting from the time the tray was transferred, the propagation dome was removed. On day 11, plants were thinned so that only one healthiest plant remained. Trays were watered by sub-irrigation once a week. On day 20, trays were irrigated with the 0.01 % fertilizer solution. Plants were subjected to low temperature treatments on day 28.

Cold acclimation and freezing treatment

Plants were cold acclimated and frozen using the protocol described in Chapter 3. Figure 5.3 describes the temperature regimes applied.

Sampling and lipid extraction

Two types of samples were collected from each plant (72 plants per tray): (1) leaves 5 and 6 in a 50-ml tube containing 25 ml of distilled water (Dillons Supermarket, Manhattan, KS, USA) and (2) the rest of the rosette in a 20-ml vial containing 4 ml of isopropanol with 0.01% butylated hydroxytoluene (BHT) at 75 °C. The two samples from each plant were each labeled to indicate the plant from which they were derived (for example, the two samples from plant 3 of tray F1-1 in Figure 5.2 were both labeled "F1-1-3"). The sample labels were printed on Tough Tag labels (Diversified Biotech, Dedham, MA, USA), which were used to label the 50-ml tubes and the 20-ml vials.

Harvesting was carried out on a cart carrying two heat blocks with the blocks removed to house the 20-ml vials (the vials sat in the area where the blocks normally sit). The thermal blocks were maintained at 75 °C. Other material included four 40-slot racks to hold 72 tubes containing distilled water (two racks to hold tubes before harvesting, 2 racks to hold tubes after leaves 5 and 6 had been dropped in). For trays 1, 2, 4, 6, 9, 10, 11, 12, 13, 14, 15, 16, and 17 (treatments which ended with a period at 21 °C), the rolling cart was positioned right next to the growth chamber (at room temperature). For trays 3 and 5, the cart was situated inside the cold room where the trays were treated (the heating block heaters were set at 90 °C to compensate for the cold air and still maintain the vials at 75 °C). For trays 7 and 8, the cart was positioned next to the freezing chamber in which the trays were frozen (harvesting occurred at room temperature). At the end of each of the indicated treatment periods (Figure 5.3), the leaf material from each corresponding tray was harvested simultaneously by four laboratory personnel so that the average harvesting time was less than 20 min per tray. The four personnel worked in two pairs, each pair had one "cutter" and one "dipper" who stood facing each other across the cart. The "cutter" procedure for each plant was: (1) cut the whole rosette off the roots, (2) cut leaves 5 and 6 and drop them into the gloved palm of the corresponding "dipper", and (3) drop the rest of the rosette into the corresponding pre-labeled, pre-heated 20-ml vial, cap the vial, shake the vial slightly to fully submerge the rosette, and return the vial to the heating block heaters. The "dipper" procedure for each plant included: (1) receive leaves 5 and 6 from the corresponding "cutter", (2) rinse the leaves in a beaker of distilled water, and (2) drop the leaves into the pre-labeled 50-ml tube, cap the tube, and shake the tube to completely submerge the leaves in water.

For all trays except for trays 7 and 8, the tray was set on the cart during harvesting and the two pairs of personnel sequentially harvested the plants in order from 1 to 72. For trays 7 and 8, the trays were pre-cut (before seed sowing) into blocks of 4 plants with consecutive labels (e.g., 1-4, 5-8, 9-12…). At the end of the freezing treatment, the freezing chamber continued to maintain temperature at -8 °C. The blocks of 4 plants were taken out of the freezing chamber one at a time and were quickly harvested (two plants per harvesting pair) before thawing occurred. The freezing chamber was opened and closed quickly; the temperature increased from -8 °C to -7 °C or -6 °C; the awaiting plants remained well frozen. In all cases, after the last plant of a tray was harvested, the vials were incubated at 75 °C for an additional 15 min and were allowed to cool to room temperature before being stored at -80 °C.

To begin lipid extraction, each cardboard box of 72 samples from one tray stored at -80 °C was allowed to warm to room temperature. To each vial, 12 ml of the extraction solvent (chloroform: methanol: 300 mM ammonium acetate in water, 30: 41.5: 3.5, v/v/v) were added. The vials were shaken on an orbital shaker at 100 rpm for 24 h. After being shaken, the extracted rosette from each vial was removed and put into an empty vial with the same label. The original vials with solvent were stored at -20 °C. The extracted rosettes in non-capped vials were dried first in a fume hood for 1-2 h and then in an oven at 105 °C overnight. The dried rosettes were allowed to cool to room temperature and weighed using a Mettler-Toledo AX balance (Mettler-Toledo, Greifensee, Switzerland). To eliminate electrostatic forces resulting from drying of the rosettes, the rosettes were passed through an anti-static U ionizer (Haug, Germany).

Plant phenotyping

Photos of each tray were taken at multiple times including: (1) immediately before fertilizing at 20 days old, (2) immediately before the last watering which occurred on the day before the tray was harvested (trays 1, 2, 4, 6, 9, 12, and 15) or treated (trays 3, 5, 7, 8, 10, 11, 13, 14, 16, and 17), and (3) immediately before the tray was harvested (trays 7 and 8 were not photographed immediately prior to harvesting to avoid thawing). At each time point, a tray was photographed three times with three F-stop values (f/11, f/13, and f/14), using a Nikon D40 camera with an 18-55 mm lens. Other camera parameters were: ISO 200, focal length 35-45 mm, exposure time 250

s^{-1}, built-in flash "ON". One high quality photo of each tray at each time point was chosen (total of three photos per tray) for determining the number of leaves of each plant. The cotyledons were not counted in the total number of leaves. For an emerging leaf, it was only counted if the width of the petiole was estimated to be less than half of the maximal width of the leaf.

For ion leakage measurements, when each plant was harvested, leaves number 5 and 6 (as determined by Telfer et al., 1997) were dropped into a 50-ml glass tube containing 25 ml of distilled water (purchased from Dillons Supermarket, Manhattan, KS). The tubes were tightly capped and shaken at 150 rpm for 2 h. Conductivity was measured using an electrical conductivity meter CON 510 (Oakton Instruments, Vernon Hills, IL). After the first measurement, the tubes were re-capped and incubated in a water bath at 80 - 90 °C for 2 h and were allowed to cool to room temperature so the total ion leakage could be measured. Ion leakage was the percentage of the first conductivity value in relation to the total conductivity value (second value) for each plant.

Mass spectrometry analysis

A mixture of internal standards in chloroform was included in all mass spectrometry samples for analysis (including the sample vials, the internal standard-only vials, and the quality control (QC) vials). The composition of the internal standard mixture (20 µl) added per 0.04 mg dry mass of leaf tissue is listed in Table 5.2.

A quality control (QC) stock was prepared by pooling 1 ml from samples 1-10 of all the trays of replication round 1 and 2 (a total of 34 trays). The total volume of the QC stock was 340 ml and the concentration was 0.688 mg leaf dry mass ml^{-1}. The stock was divided into 34 aliquots of 10 ml each and the aliquots were stored at -20 °C. To make mass spectrometry QC vials, a QC stock aliquot was mixed with 3.4 ml of the internal standard mix (measured with a 1-ml glass syringe) and 224.6 ml (measured with a 250-ml glass cylinder) of mass spectrometry solvent (isopropanol: chloroform: methanol: 300 mM ammonium acetate in water, 25: 30: 41.5: 3.5, v/v/v/v). After being shaken, 1.4 ml of the mixture was dispensed into each of 156 amber 2-ml vials labeled "QC1" to "QC39" (four sets). The prepared QC mass spectrometry vials were stored at -80 °C and were brought to room temperature 1 h before analysis.

To prepare the sample mass spectrometry vials, the 20-ml vials containing the extracted total lipids were brought to room temperature from -20 °C ~2 h prior to handling, one tray (72 vials) at a time. To each of the 72 2-ml amber vials (labeled "1" to "72", the tray name, for example "F1-1", was written on the rack), 20 µl of the internal standard mixture (measured with a 100-µl syringe) was added first. In sequential order from 1 to 72, a volume that contained 0.04 mg leaf dry mass from a 20-ml vial was added to the similarly labeled 2-ml amber vial; a volume of mass spectrometry solvent (isopropanol: chloroform: methanol: 300 mM ammonium acetate in water, 25: 30: 41.5: 3.5, v/v/v/v) was added to the total volume of 1.4 ml; and the amber vial was capped before the next sample was added to the next amber vial. The mass spectrometry solvent volume was measured and dispensed with a 2.5-ml dispenser (Eppendorf, Hamburg, Germany) mounted on top of the solvent bottle. Since the smallest increment of dispenser was 50 µl, the calculated mass spectrometry solvent volume was adjusted to the closest marked level of the dispenser. For example, all volumes from 1226-1275 µl were adjusted to 1250 µl and all volumes from 1276-1325 µl were adjusted to 1300 µl. In each tray, 6 internal standard-only vials were included (labeled "IS1" to "IS6"); each contained 20 µl of the internal standard mix and 1.38 ml (total of 1.4 ml) of the mass spectrometry solvent. For mass spectrometry analysis, the 72 sample vials from each tray, together with 6 "IS" vials, and 39 "QC" vials were arranged in 3 VT-54 racks.

Table 5.3 lists the positions of mass spectrometry vials in the first VT-54 rack with QC vial 1-13, IS vial 1-2, and sample vial 1-24. The second and third VT-54 rack have the same arrangement with the QC 14-26, IS 3-4, sample 25-48 for the second VT-54 rack and QC 27-39, IS 5-6, sample 49-72 for the third VT-54 rack.

Data processing and statistical analysis

Data from experimental samples were normalized to QC samples, dendrogram, and graphs were produced using the same methods in Chapter 4. T-tests were done using Excel. The Spearman's correlation coefficient ρ between lipid analytes and ion leakage were calculated using the Metaboanalyst website.

Results

Our analysis of lipid compositions and phenotypes of wild-type, AH, and LOX knockouts were designed to capture behaviors of Arabidopsis plants at critical points during a cold acclimation/freezing/thawing time course. They included early cold acclimation (1 h at 4 °C, tray 3), late cold acclimation (three days at 4 °C, tray 5), right after freezing treatment at -8 °C for 2 h with or without cold acclimation (trays 8 and 7, respectively), 1 h, 3 h, and 24 h of thawing at 21 °C after freezing treatment with cold acclimation (tray 11, 14, and 17, respectively) or without cold acclimation (tray 10, 13, and 16, respectively).

Ablation of pPLAIIγ enhances cold acclimation effect on freezing tolerance

Electrolyte leakage measurements provided a quantitative assessment of leaf damage throughout the course of low temperature exposure. As shown in Figure 5.4, ion leakage in non-acclimated Col-0 plants was at its highest level immediately after the plants were removed from the freezing chamber (74-h point). The cold acclimation effect, i.e. the increased freezing tolerance, was demonstrated by the lower ion leakage percentage of acclimated Col-0 plants at this time. In the thawing phase (75-h, 77-h, and 98-h time points), the acclimated Col-0 plants showed clear signs of recovery as the ion leakage dropped close to the level of the untreated control plants, especially at 24 h after freezing. On the other hand, the ion leakage of the non-acclimated Col-0 plants stayed high even 24 h after freezing. Differences between acclimated and non-acclimated Col-0 plants during the thawing phase were also visible as shown in Figure 5.5. At 24 h after freezing, the acclimated plants appeared normal, except for some leaf areas with visible damage. Similarly treated plants were observed to continue growing, bolting, and eventually produce seeds. On the other hand, the non-acclimated plants were shrunken and dry. Leaves of similarly treated plants were observed to turn yellow and die, but the shoots were able to make new leaves after 7 – 10 days.

To identify mutants that affect freezing response of Arabidopsis, the ion leakage percentages of the 22 lines during exposure to freezing and thawing were compared to those of Col-0. Line E (*pPLAIIγ* knockout) had lower ion leakage in cold acclimated plants during recovery compared to wild-type, especially at the 77 h time point (3 h of thawing after freezing, $p < 0.1$), as depicted

in Figure 5.4. Acclimated pPLAIIγ knockout plants were visibly less damaged than acclimated Col-0 at 3 h after freezing (77 h time point, Figure 5.5).

Freezing-induced lipid changes occur in clusters

In 35 min per sample, our MRM-based analysis was able to measure 377 lipid species. Before further data analysis, several rules were applied to ensure quality of the data. First, we eliminated lipid species with background (average intensity measured in internal-standard-only samples) higher than 40% of the averaged signals detected in all QC samples. Second, we eliminated lipids with background higher than 20% of the QC average if the majority of the chemically similar lipid analytes were eliminated by the first rule. Applying the first two rules eliminated 34 compounds. Third, we eliminated 12 more lipids that measured less than 0.1 pmol in more than 1000 experimental samples (out of 17*72 = 1224 experimental samples). Our dataset contains 331 lipid analytes, each with 1224 measurements.

Since the dataset was acquired over a long period (~ two months), variation due to instrumental performance was very likely to occur. To correct for this variation, signals of each lipid in all experimental samples were normalized to the QC samples using the same method as described in Chapter 4.

It is hypothesized that cold-acclimation, freezing and thawing affect different biochemical pathways. Each pathway, in turn, controls the biosynthesis and metabolism of multiple lipid analytes. With the assumption that metabolites affected by the same pathway will behave in the same manner as a function of cold, freezing, and thawing treatments, pathways that are affected by low temperature treatments can be identified by clustering lipids that vary together across treatments and individual plants. To identify the clusters formed in low temperature stress, we calculated a 331 x 331 distance matrix using data from 102 (17 conditions x 6 replicates) wild-type Col-0 plants of the first round of the experiment. The level of each lipid analyte in all samples was ranked (1 to 1224), and Spearman's correlation coefficient ρ was calculated for each pair of compounds. A single linkage hierarchical clustering algorithm, using the maximal ρ for each lipid analyte, was applied to generate clusters. Figure 5.6 is a dendrogram of lipids that

correlate with $\rho > 0.6$ (301 lipids). Lipids that correlate with maximal $\rho > 0.8$ form clusters labeled from A to J. Within clusters A, B, and J, 94 lipids correlate with maximal $\rho > 0.95$ forming 16 sub-clusters. For each sub-cluster, levels of 1 or 2 representative lipids of Col-0 and pPLAIIγ mutant (line E) are shown in Figure 5.7 as a function of temperature treatment.

Many known cold- and freezing-induced pathways are visible in treated Col-0 via the sub-clusters shown in Figure 5.6 and their patterns shown in Figure 5.7. The degradation of PC (sub-cluster B1, B2, and B5), PE (sub-cluster B3 and B4), MGDG (sub-cluster B6), and DGDG (sub-cluster B7, and B8), together with the formation of PA (sub-cluster A2) can be explained, at least partially, by the activation of phospholipase D (Welti et al., 2002). Also, it cannot be ruled out that PAs are synthesized from DAGs produced by phospholipase C (Testerink and Munnik, 2005). The cold acclimation effect is evident as the degradation that occurred in acclimated Col-0 plants was not as severe and the plants almost recovered to control levels by 24 h after freezing while the lipids in non-acclimated plants were largely hydrolyzed and showed no sign of recovery. Interestingly, in acclimated plants, PE with long chain fatty acids (sub-cluster B4) accumulated after the cold acclimation and maintained higher levels thoughout the freezing and thawing treatments compared to the control, instead of being degraded as in the non-acclimated plants.

Although both LPC (sub-cluster A1) and PA (sub-cluster A2) are products of membrane lipid hydrolysis, their patterns of changes in response to low temperature treatments are substantially different. While PA was induced significantly more in non-acclimated plants than in acclimated thoughout the post-freezing period, LPC was induced more in acclimated plants, especially immediately and 1 h after freezing.

The formation of TrGDG (sub-cluster A5), coupled closely with TeGDG synthesis (Figure 5.6), was more dramatic in acclimated plants than in non-acclimated plants during the thawing process. The formation of TAG (sub-cluster A3) followed a similar pattern (much more in acclimated plants than in non-acclimated plants) and TAG seemed to keep accumulating in acclimated plants even at 3 h and 24 h after freezing.

The Gal-acylation of MGDG to form acMGDG (sub-cluster 6 and sub-cluster 7) was complex to interpret as the acyl groups involved were also affected by induced oxidation. acMGDG with three non-oxidized acyl groups (most of sub-cluster A7a) was induced in both non-acclimated and acclimated plants immediately at the end of the freezing period and was induced to significantly higher levels in non-acclimated plants than in acclimated plants. Even at 24 h, when the levels in acclimated plants tended to decrease to control level, the levels in non-acclimated plants showed little reduction, making the difference even greater. Sub-cluster A7b includes mostly acMGDGs with 2 oxidized acyl groups out of the total 3 acyl groups. The overall pattern of sub-cluster A7b somewhat resembles that of sub-cluster A7a and non-acclimated plants accumulated more at 24 h into thawing. A very striking difference occurred after 1 h of thawing, when the more oxidized acMGDGs (cluster A7b) were much higher in the acclimated plants compared to the non-acclimated ones. Fully oxidized acMGDGs (sub-cluster A6) were distinctive from less oxidized acMGDG in that they were not only more induced in acclimated plants but also maintained higher levels after 1 h, 3 h, and 24 h of thawing. This pattern also helped to distinguish between possible annotations of some acMGDG. For example, acMGDG(18:4-O/36:6) and acMGDG(18:4-O/34:8-2O) have the same mass and same head-group fragment but the pattern and clustering with acMGDG(18:4-O/36:8-2O) (sub-cluster A6) suggests that the fully oxidized annotation, acMGDG(18:4-O/34:8-2O), may be the correct one for the majority of lipid detected with the relevant analytical parameters in the current experiment.

The induction pattern of ASG (sub-cluster A4) was relatively similar to that of non-oxidized acMGDG (sub-cluster A7a). ASG was induced significantly in both acclimated and non-acclimated plants as early as 1 h after freezing. Especially at 24 h post-freezing, non-acclimated plants maintained a higher level of ASG compared to acclimated ones. The changes in sterol ester synthesis in response to low temperature, on the other hand, occurred in a unique pattern: sterol esters (cluster J1) were induced during the acclimation period. Freezing temperature also induced synthesis of sterol esters; however, after 24 h of thawing, markedly higher levels of sterol esters were detected in acclimated plants, which were exposed to both cold and freezing, compared to non-acclimated plants, which were exposed only to freezing.

Lipid changes correlate with freezing-induced leaf damage

It is hypothesized that freezing- and thawing-induced changes in lipid sub-clusters play different roles in determining the ultimate fate of the plants in response to the stress. Degradation of structural lipids and synthesis of antagonistic lipids might coincide with more severe tissue damage; whereas, induction and stably high levels of healing lipids could result in recovery from stress damage. To further investigate possible roles of lipids in each sub-cluster (Figure 5.6) in plant response to freezing, the Spearman's correlation coefficient ρ between lipids and leaf damage as measure by ion leakage was calculated using data from Col-0 plants. Table 5.4 shows the average and standard deviation of all ρ values within each lipid sub-cluster. It is obvious that non-structural, freezing induced lipids (cluster A) positively correlate with leaf damage, while structural lipids (cluster B) negatively correlate with leaf ion leakage. Highest among sub-clusters that have positive ρ are A2 (PA), A7a (acMGDG with mostly non-oxidized acyl groups), and A4 (ASG). The structural lipids with lowest negative ρ values are PCs (sub-cluster B1, B5, and B2) and MGDGs (sub-cluster B6). Interestingly, among the A-cluster lipids, TAG (sub-cluster A3) express distinctively less correlation with leaf damage, suggesting different involvement in plant responses compared to its stress-induced counterparts. Similarly, the long-chain PE (sub-cluster B4) has significantly higher correlation with leaf ion leakage, compared to other presumably structural lipid classes.

Formation of OPDA-containing acMGDG is enhanced in pPLAIIγ knockout

A hypothesis which might explain why cold-acclimated line E plants (*pPLAII γ* knockout) showed better appearance (Figure 5.5) and lower ion leakage (Figure 5.4) than Col-0 plants after 3 h and 24 h of thawing is that ablation of pPLAIIγ causes alteration(s) in how lipids in sub-clusters (Figure 5.6) respond to cold-acclimation, freezing, and thawing. To test this hypothesis, autoscaled lipid levels of representative lipids of all sub-clusters of *pPLAIIγ* knockouts were compared to those of Col-0 plants throughout the temperature regime. Figure 5.7 shows comparisons of autoscaled lipid levels between Col-0 and *pPLAIIγ* knockout of all 17 sub-clusters. The majority of sub-clusters are not different between knockout and wild-type except for PC with 38 acyl carbons (sub-cluster B1, Figure 5.7i) and oxidized acMGDG (sub-cluster A6, Figure 5.7f). Since the levels of PC with 38 acyl carbons were inconsistent across untreated

plants, the differences observed are not very likely to be related to the applied temperature treatments. Sub-cluster A6, (oxidized acMGDG), on the other hand, shows consistently low levels in untreated controls. As shown in Figure 5.7f, cold-acclimated *pPLAIIγ* knockouts expressed higher levels of lipids in sub-cluster A6 (acMGDG(18:4-O/34:8-2O) and acMGDG(18:4-O/36:8-2O)) at 0 h (74^{th} h time point, $p = 0.002$), 1 h (75^{th} h time point, $p = 0.07$) and 24 h (98^{th} h time point, $p = 0.02$) of thawing after freezing compared to Col-0 plants.

Discussion

In this chapter, the analytical approach and the co-occurrence analysis developed in Chapter 4 were applied to identify lipid analytes that were similarly metabolized when Arabidopsis responded to low temperature stress. Similar to wounding response, low temperature response induced changes in levels of the majority of lipid analytes, either increasing (cluster A) or decreasing (cluster B, Figure 5.6 and Figure 5.7). Similar sub-clusters were observed in low temperature response, including acMGDG (sub-cluster A6, A7a, and A7b), ASG (sub-cluster A4), PA (sub-cluster A2), TAG (sub-cluster A3), DGDG (sub-cluster B7 and B8), MGDG (sub-cluster B6), PC (sub-cluster B5), and PE (sub-cluster B3). Some sub-clusters only formed in low temperature reponse, not in wounding response, including long-chain PC (sub-cluster B2) and long-chain PE (sub-cluster B4). This suggests that unique lipid metabolizing enzyme(s) may have been activated only in response to low temperature and not in wounding response. On the other hand, MGDG(18:4-O/16:4-O) and MGDG(18:4-O/18:4-O) did not formed a sub-cluster in low temperature response. This suggests that acyl oxidation was activated to a lesser extent in low temperature response compared to wounding response (Vu et al., 2014). This might also explain the smaller sub-cluster of fully oxidized acMGDGs with only two members, acMGDG(18:4-O/34:8-2O) and acMGDG(18:4-O/36:8-2O) induced by low temperature (sub-cluster A6).

The TrGDG formation (sub-cluster A5) was presumably catalyzed by the galactolipid: galactolipid galactosyl transferase encoded by SFR2 (Moellering et al., 2010). In this reaction, a galactose from an MGDG is transferred onto MGDG, DGDG, and TrGDG forming β-linked

DGDG, TrGDG, and TeGDG, respectively. In wounding response, the inclusion of PA(34:6) in the same sub-cluster as TrGDG(34:6) and TeGDG(34:6) suggests that DAG(34:6) released by SFR2 was converted to PA(34:6). In low temperature response, PA(34:6) was not in the TrGDG sub-cluster; instead, PA(34:6) more closely correlated with the PA sub-cluster (A2). This suggests that PA(34:6) may have been formed mostly from MGDG(34:6) hydrolysis in low temperature stress.

Co-occurrence analysis of lipid analytes in low temperature response provides biochemical insights into cold acclimation. Many sub-clusters were specifically induced more in cold-acclimated plants including LPC and LPE (sub-cluster A1), TAG (sub-cluster A3), TrGDG (sub-cluster A5, oxidized acMGDG (sub-cluster A6), long-chain PE (sub-cluster B4), and sterol esters (sub-cluster J1, Figure 5.7). Some sub-clusters were hydrolyzed to a lesser extent in cold-acclimated plants compared to non-acclimated plants: PC with 38 acyl carbons (sub-cluster B1), long-chain PC (sub-cluster B2), PE with 36 acyl carbons (sub-cluster B3), PC and PS (sub-cluster B5), MGDG (sub-cluster B6), and DGDG (sub-cluster B7 and B8, Figure 5.7). On the other hand, some sub-clusters were specifically induced more in non-acclimated plants compared to acclimated plants including PA (sub-cluster A2), ASG (sub-cluster A4), and normal-chain acMGDG (sub-cluster A7a, Figure 5.7). It is noted that while the majority of the metabolic differences between non-acclimated and acclimated plants occurred during the thawing period, fewer changes were detected during the cold acclimation period. Lipid analytes that were induced during cold acclimation include PE (sub-cluster B3 and B4) and sterol esters (sub-cluster J1, Figure 5.7).

In this chapter, co-occurrence analysis was employed to identify metabolically active lipid analytes in response to low temperature. The knowledge was utilized to focus our comparisons between knockouts and wild-types on these metabolically important lipid analytes. Cold-acclimated *pPLAIIγ* knockout plants were found to induce higher levels of OPDA-containing acMGDGs (sub-cluster A6) compared to cold-acclimated Col-0 plants during thawing (Figure 5.7f). The coincidence between higher levels of acMGDG(18:4-O/34:8-2O) and acMGDG(18:4-O/36:8-2O) and faster recovery of cold-acclimated *pPLAIIγ* knockout plants suggests a "healing" role of the concentration of OPDA in acMGDG (reported by Vu et al., 2014). pPLAIIγ may

encode an acyl hydrolase that tends to hydrolyze OPDA-containing acMGDGs specifically. pPLAIIγ was previously shown to have higher galactolipase activity than phospholipase activity in vitro (Rietz et al., 2010).

References

Bell E, Creelman RA, and Mullet JE (1995) A chloroplast lipoxygenase is required for wound-induced jasmonic acid accumulation in Arabidopsis. Proc. Natl. Acad. Sci. U. S. A. **92**, 8675-8679.

Chauvin A, Caldelari D, Wolfender JL, and Farmer EE (2013) Four 13-lipoxygenases contribute to rapid jasmonate synthesis in wounded *Arabidopsis thaliana* leaves: a role for lipoxygenase 6 in responses to long-distance wound signals. New Phytol. **197**, 566-575.

Chen M, and Thelen JJ (2013) ACYL-LIPID DESATURASE2 Is Required for Chilling and Freezing Tolerance in Arabidopsis. Plant Cell **25**, 1430-1444.

Comfurius P, and Zwaal RF (1977) The enzymatic synthesis of phosphatidylserine and purification by CM-cellulose column chromatography. Biochim. Biophys. Acta **488**, 36-42.

Degenkolbe T, Giavalisco P, Zuther E, Seiwert B, Hincha DK, and Willmitzer L (2012) Differential remodeling of the lipidome during cold acclimation in natural accessions of *Arabidopsis thaliana*. Plant J. **72**, 972-982.

Feussner, I., and Wasternack, C. (2002) The lipoxygenase pathway. Annu. Rev. Plant Biol. **53**, 275- 297.

Hamberg, M., de Leon, I.P., Rodriguez, M.J., and Castresana, C. (2005) α-Dioxygenases. Biochem. Biophys. Res. Comm. **338**, 169-174.

Ishiguro S, Kawai-Oda A, Ueda J, Nishida I, and Okada K (2001) The *DEFECTIVE IN ANTHER DEHISCIENCE* gene encodes a novel phospholipase A1 catalyzing the initial step of jasmonic acid biosynthesis, which synchronizes pollen maturation, anther dehiscence, and flower opening in Arabidopsis. Plant Cell **13**, 2191-2209.

Keunen E, Remans T, Opdenakker K, Jozefczak M, Gielen H, Guisez Y, Vangronsveld J, and Cuypers A (2013) A mutant of the *Arabidopsis thaliana* LIPOXYGENASE1 gene

shows altered signalling and oxidative stress related responses after cadmium exposure. Plant Physiol. Biochem. **63**, 272-280.

La Camera S, Balagué C, Göbel C, Geoffroy P, Legrand M, Feussner I, Roby D, and Heitz T (2009) The Arabidopsis patatin-like protein 2 (PLP2) plays an essential role in cell death execution and differentially affects biosynthesis of oxylipins and resistance to pathogens. Mol. Plant Microbe Interact. **22**, 469-481.

La Camera S, Geoffroy P, Samaha H, Ndiaye A, Rahim G, Legrand M, and Heitz T (2005) A pathogen-inducible patatin-like lipid acyl hydrolase facilitates fungal and bacterial host colonization in Arabidopsis. Plant J. **44**, 810-825.

Lee HY, Bahn SC, Shin JS, Hwang I, Back K, Doelling JH, and Ryu SB (2005) Multiple forms of secretory phospholipase A2 in plants. Prog. Lipid Res. **44**, 52-67.

Li M, Bahn SC, Fan C, Li J, Phan T, Ortiz M, Roth MR, Welti R, Jaworski J, and Wang X (2013) Patatin-Related Phospholipase pPLAIIIδ Increases Seed Oil Content with Long-Chain Fatty Acids in Arabidopsis. Plant Physiol. **162**, 39-51.

Li W, Li M, Zhang W, Welti R, and Wang X (2004) The plasma membrane-bound phospholipase Dδ enhances freezing tolerance in *Arabidopsis thaliana*. Nat. Biotechnol. **22**, 427-433.

Li W, Wang R, Li M, Li L, Wang C, Welti R, and Wang X (2008) Differential degradation of extraplastidic and plastidic lipids during freezing and post-freezing recovery in *Arabidopsis thaliana*. J. Biol. Chem. **283**, 461-468.

López MA, Vicente J, Kulasekaran S, Vellosillo T, Martínez M, Irigoyen ML, Cascón T, Bannenberg G, Hamberg M, and Castresana C (2011) Antagonistic role of 9-lipoxygenase-derived oxylipins and ethylene in the control of oxidative stress, lipid peroxidation and plant defence. Plant J. **67**, 447-458.

Matos AR, Gigon A, Laffray D, Pêtres S, Zuily-Fodil Y, and Pham-Thi AT (2008) Effects of progressive drought stress on the expression of patatin-like lipid acyl hydrolase genes in Arabidopsis leaves. Physiol. Plant. **134**, 110-120.

Moellering ER, Muthan B, and Benning C (2010) Freezing tolerance in plants requires lipid remodeling at the outer chloroplast membrane. Science **330**, 226-228.

Montillet JL, Leonhardt N, Mondy S, Tranchimand S, Rumeau D, Boudsocq M, Garcia AV, Douki T, Bigeard J, Laurière C, Chevalier A, Castresana C, and Hirt H (2013) An

abscisic acid-independent oxylipin pathway controls stomatal closure and immune defense in Arabidopsis. PLoS Biol. **11**, e1001513.

Oh IS, Park AR, Bae MS, Kwon SJ, Kim YS, Lee JE, Kang NY, Lee S, Cheong H, and Park OK (2005) Secretome analysis reveals an Arabidopsis lipase involved in defense against *Alternaria brassicicola*. Plant Cell **17**, 2832-2847.

Rietz S, Dermendjiev G, Oppermann E, Tafesse FG, Effendi Y, Holk A, Parker JE, Teige M, and Sherer GFE (2009) Roles of *Arabidopsis* Patatin-Related Phospholipases A in Root Development Are Related to Auxin Responses and Phosphate Deficiency. Mol. Plant **3**, 524-538.

Shah, J. (2005) Lipids, lipases and lipid modifying enzymes in plant disease resistance. Annu Rev. Phytopathol. **43**, 229-260.

Shah, J., and Chaturvedi, R. (2008) Lipid signals in plant-pathogen interaction**.** Annu. Plant Rev. 34, 292-333.

Telfer A, Bollman KM, and Poethig RS (1997) Phase change and the regulation of trichome distribution in *Arabidopsis thaliana*. Development **124**, 645-654.

Testerink C, and Munnik T (2005) Phosphatidic acid: a multifunctional stress signaling lipid in plants. Trends Plant Sci. **10**, 368-375.

Vu HS, Roth MR, Tamura P, Samarakoon T, Shiva S, Honey S, Lowe K, Schmelz EA, Williams TD, and Welti R (2014) Head-group acylation of monogalactosyldiacylglycerol is a common stress response, and the acyl-galactose acyl composition varies with the plant species and applied stress. Physiol. Plant., In press.

Weber, H. (2002) Fatty acid-derived signals in plants. Trends Plant Sci. **7**, 217-224.

Welti R, Li W, Li M, Sang Y, Biesiada H, Zhou HE, Rajashekar CB, Williams TD, and Wang X (2002) Profiling membrane lipids in plant stress responses. Role of phospholipase Dα in freezing-induced lipid changes in Arabidopsis. J. Biol. Chem. **277**, 31994-32002.

Figures and Tables

Figure 5.1 Seed position in trays

(A) Schematic numbering of wells within a 72-well plug tray. (B), (C), and (D) Positions of letter-coded seeds for all trays of round 1, 2, and 3, respectively.

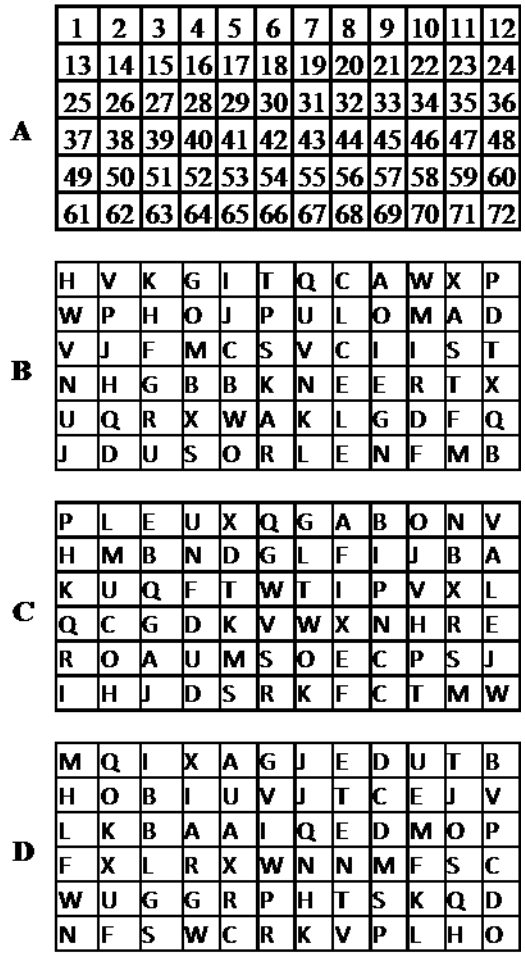

Figure 5.2 Example of tray and plant labeling.

Each plant is referred to by a combined label including the tray label, e.g. “F1-1”, and the well position from 1 to 72. For example, the plants shown in this figure are labeled F1-1-1 to F1-1-72.

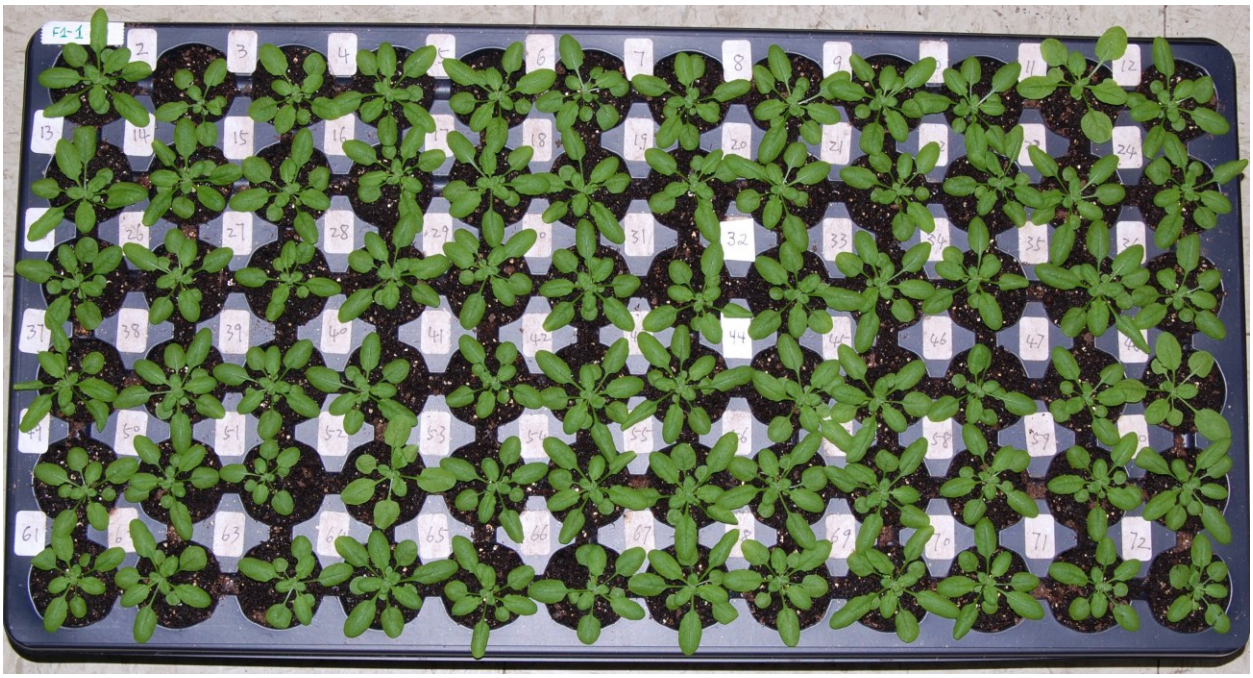
F2-1

Figure 5.3 Cold acclimation and freezing experiment design.

Plants entered the experiment at 30-day old. The X-axis is time (h) starting from the beginning of cold acclimation treatment at 4 °C. The Y-axis is temperature (°C). Each circle marks the time and temperature when and in which the correspondingly numbered tray was harvested. The line leading to each circle represents the temperature regime applied to the tray. Red line is untreated control (C); yellow line is non-acclimated (N); and blue is acclimated (A). In words, treatments applied to each tray are: tray **1** (no treatment), tray **2** (1 h at 21 °C), tray **3** (1 h at 4 °C), tray **4** (72 h at 21 °C), tray **5** (72 h at 4 °C), tray **6** (74 h at 21 °C), tray **7** (72 h at 21 °C and 2 h at -8 °C), tray **8** (72 h at 4 °C and 2 h at -8 °C), tray **9** (75 h at 21 °C), tray **10** (72 h at 21°C, 2 h at -8 °C, and 1 h at 21 °C), tray **11** (72 h at 4 °C, 2 h at -8 °C, and 1 h at 21 °C), tray **12** (77 h at 21 °C), tray **13** (72 h at 21 °C, 2 h at -8 °C, and 3 h at 21 °C), tray **14** (72 h at 4 °C, 2 h at -8 °C, and 3 h at 21 °C), tray **15** (98 h at 21 °C), tray **16** (72 h at 21 °C, 2 h at -8 °C, and 24 h at 21 °C), tray **17** (72 h at 4 °C, 2 h at -8 °C, and 24 h at 21 °C).

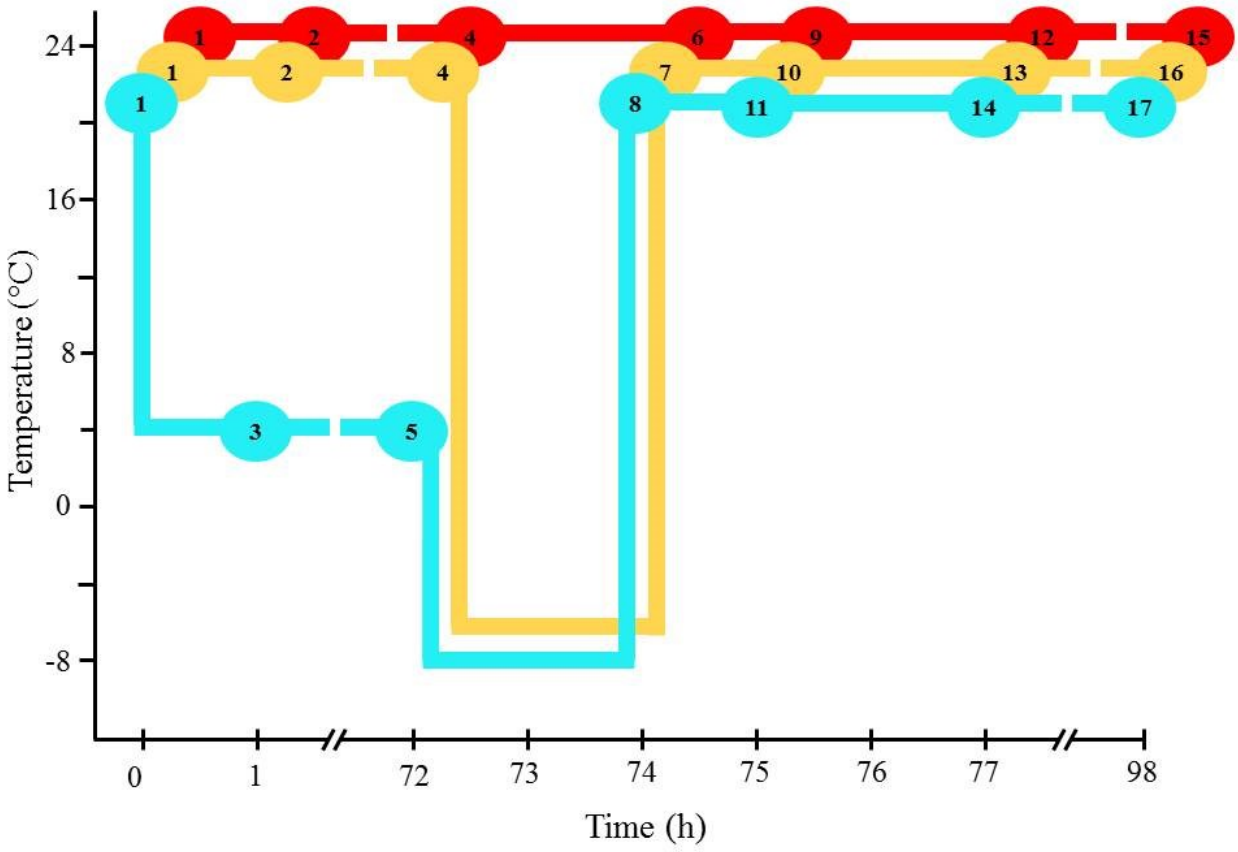

Figure 5.4 Low-temperature-induced leaf damage assessed by relative ion leakage.

The Y-axis is autoscaled level of ion leakage. The X-axis is the time course (h) of the temperature treatment (details of which are shown in Figure 5.3). At each time point, a set of six variables are shown, including untreated control (C), non-acclimated (N), and acclimated (A) of Col-0 and *pPLAIIγ* knockout (E). The box corresponding to each variable is also color-coded. The boxes summarize 6 replicates for Col-0 plants and 3 replicates for line E plants. The top and bottom of the boxes represent the 75 and 25 percentile; the bar inside the box marks the median, while the whisker is standard deviation.

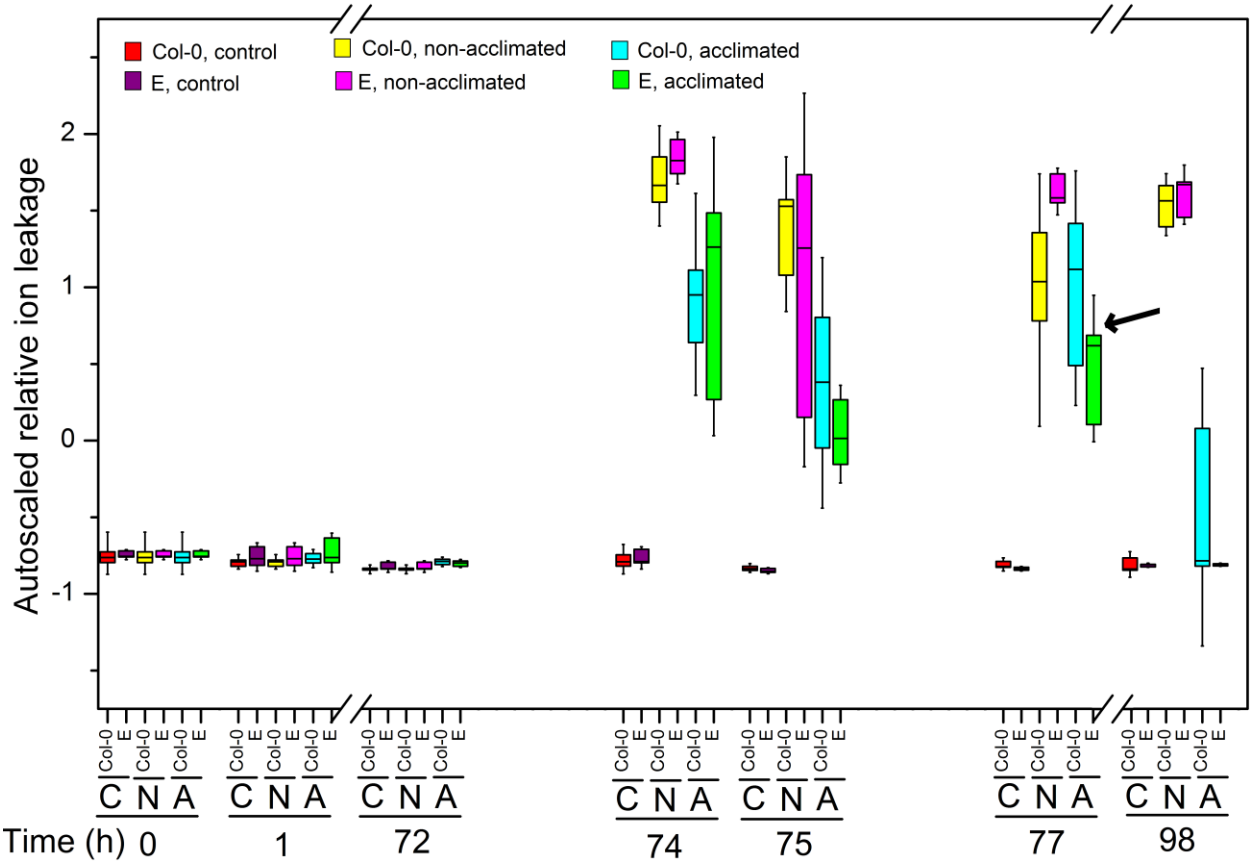

Figure 5.5 Plant appearance followed freezing treatments.

Photographs depict three wild-type plants (line A) and three line E plants (*pPLAIIγ* knockout) of untreated (control, C), non-acclimated frozen (N), and acclimated frozen (A) trays after 1 h (75th hour), 3 h (77th hour), and 24 h (98th hour) of thawing.

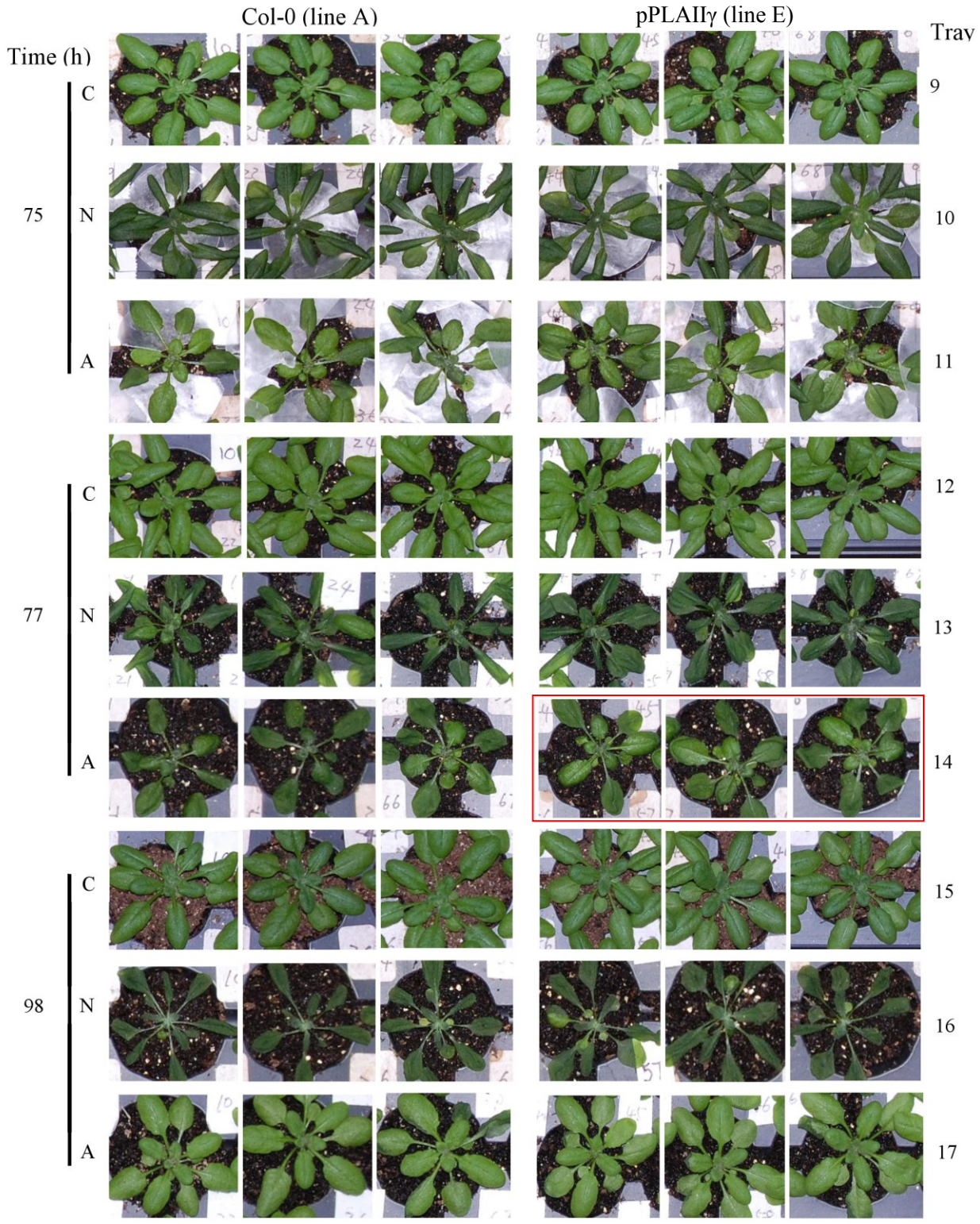
Col-0 (line A)
pPLAIIγ (line E)
Time (h)
Tray
75
77
98
C
N
A
9
10
11
12
13
14
15
16
17

Figure 5.6 Dendrogram describing lipid co-occurrence of Col-0 plants in response to low temperature treatments.

The distance from the center to the circumference of the dendrogram represents Spearman's correlation coefficient ρ, measured by the horizontal scale in red. Only lipids with at least one $\rho > 0.6$ are shown in this dendrogram. Branches of lipids that correlate with all $\rho > 0.8$ are color-coded, labeled by a letter with the same color, from A to J, and are referred to as "clusters". Within cluster A, B, and J, branches of lipids correlate with each other with all $\rho > 0.95$ are called sub-clusters which are marked with red edges and bolded lipid names. Sub-cluster A7 is further divided into sub-cluster A7a and A7b due the difference in acyl composition. Sub-cluster A7a contains mostly acMGDG with all non-oxidized acyl groups, while sub-cluster A7b contains mostly acMGDG with two oxidized acyl groups.

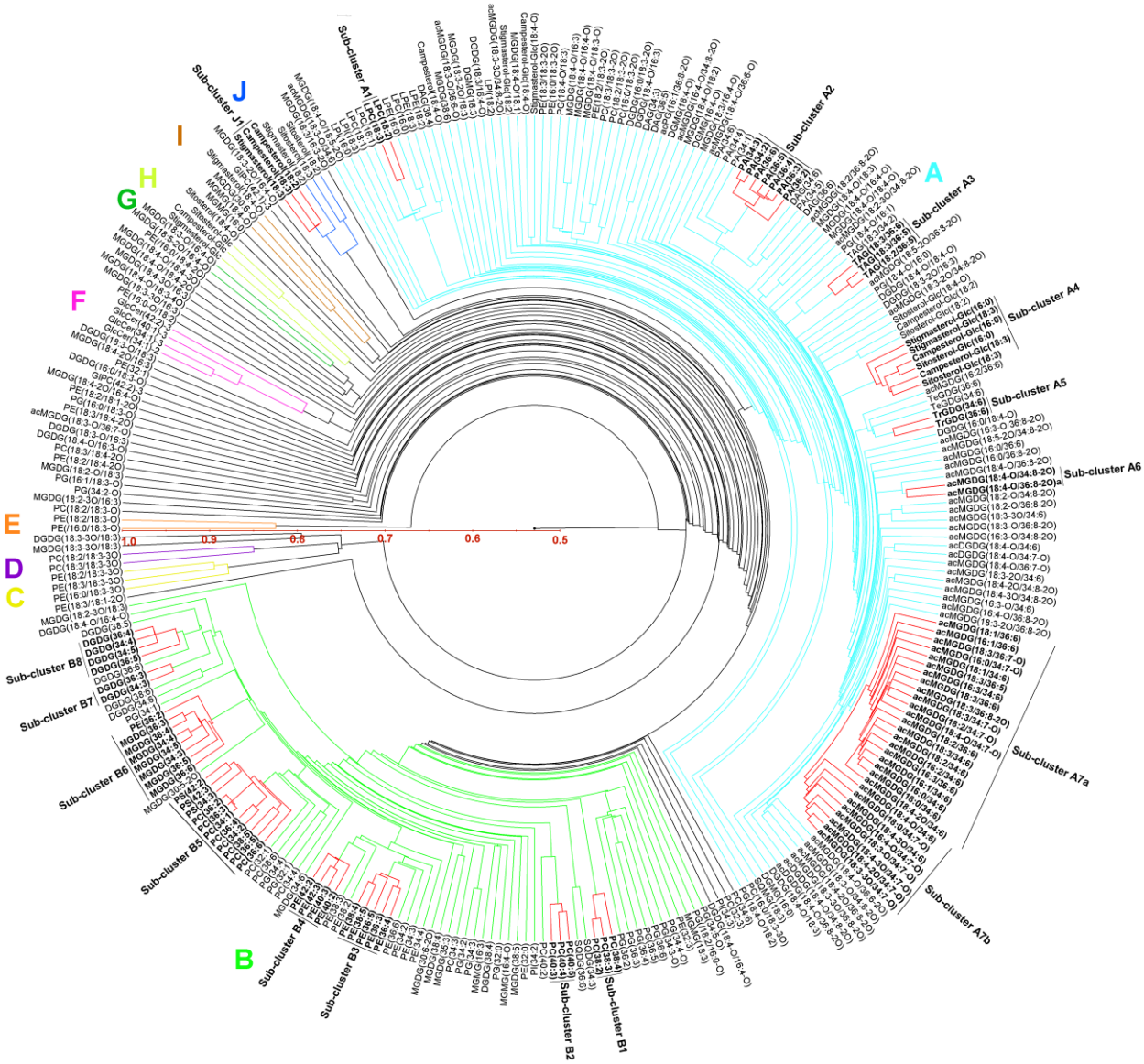
A
B
C
D
E
F
G
H
I
J
1.0
0.9
0.8
0.7
0.6
0.5
Sub-cluster A1
Sub-cluster A2
Sub-cluster A3
Sub-cluster A4
Sub-cluster A5
Sub-cluster A6
Sub-cluster A7a
Sub-cluster A7b
Sub-cluster B1
Sub-cluster B2
Sub-cluster B3
Sub-cluster B4
Sub-cluster B5
Sub-cluster B6
Sub-cluster B7
Sub-cluster B8
Sub-cluster J1

Figure 5.7 Comparisons of autoscaled lipid levels of sub-clusters between Col-0 and pPLAIIγ (line E) plants that underwent low temperature treatments.

The Y axis represents autoscaled lipid levels. The X axis displays the time course (h) of the low temperature treatments. At each time point, six combinations of plant line and treatment are presented: untreated control (C) for Col-0 and line E (pPLAIIγ), non-acclimated (N) Col-0 and line E, and acclimated (A) Col-0 and line E. Each Col-0 treatment has 6 replicates and each E treatment has 3 replicates, which are summarized by a color-coded box. The top and bottom of the box indicate the 75 and 25 percentile. The horizontal bar inside the box indicates the median value and the whisker is standard deviation. This figure has 17 panels from (a) to (q).

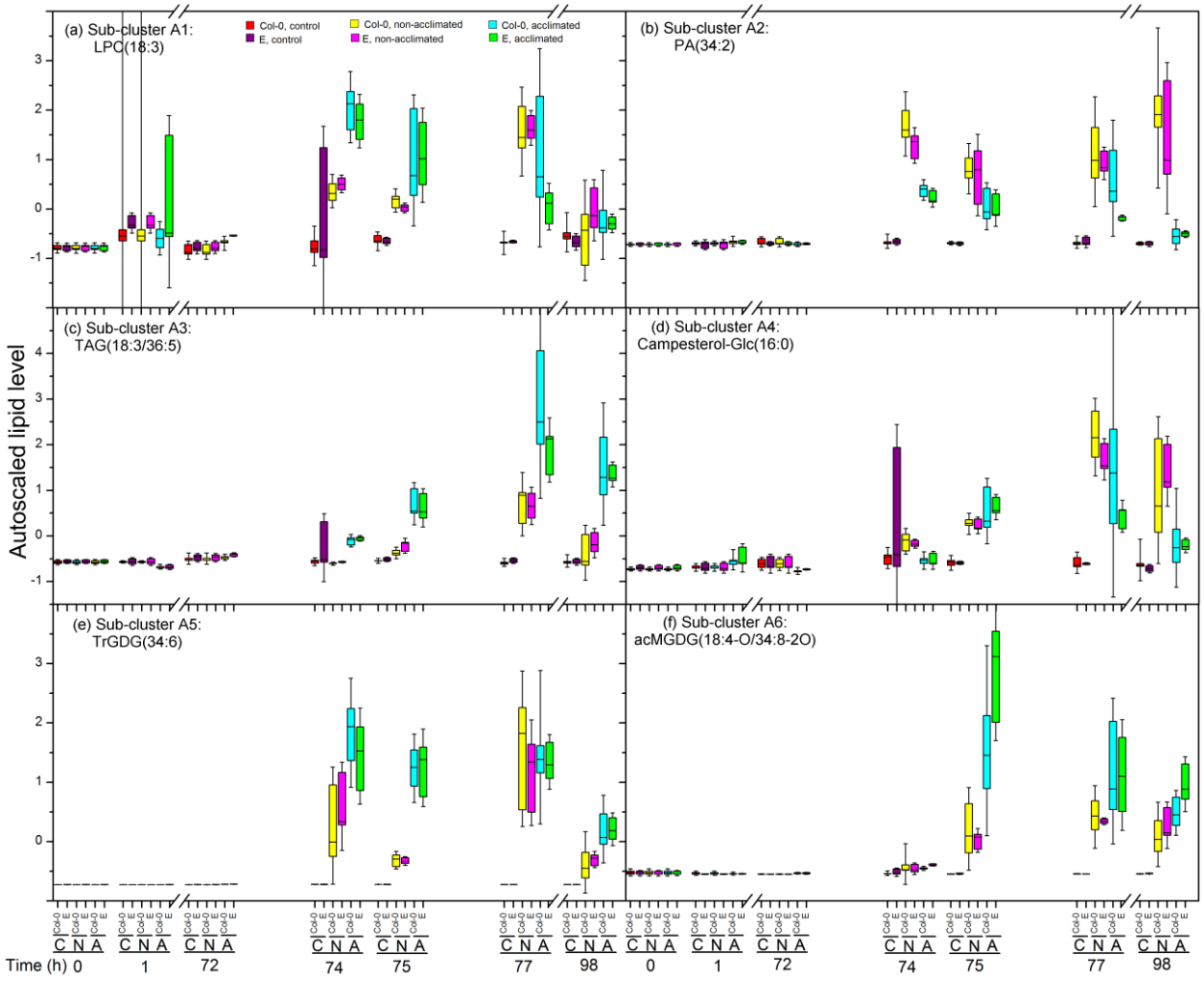

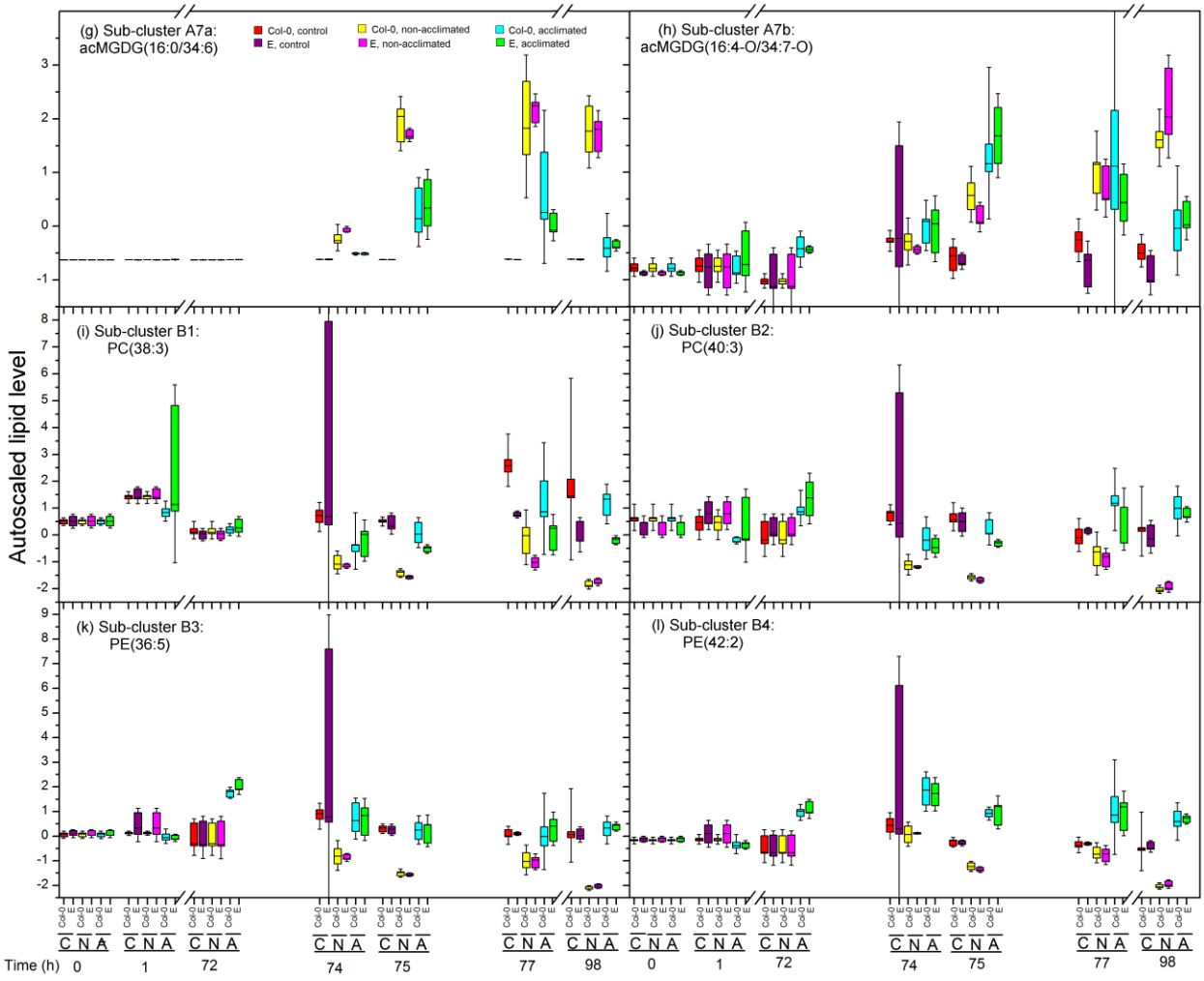
(g) Sub-cluster A7a:
acMGDG(16:0/34:6)
Col-0, control
E, control
Col-0, non-acclimated
E, non-acclimated
Col-0, acclimated
E, acclimated
(h) Sub-cluster A7b:
acMGDG(16:4-O/34:7-O)
(i) Sub-cluster B1:
PC(38:3)
(j) Sub-cluster B2:
PC(40:3)
(k) Sub-cluster B3:
PE(36:5)
(l) Sub-cluster B4:
PE(42:2)
Autoscaled lipid level
C N A
Time (h) 0 1 72 74 75 77 98

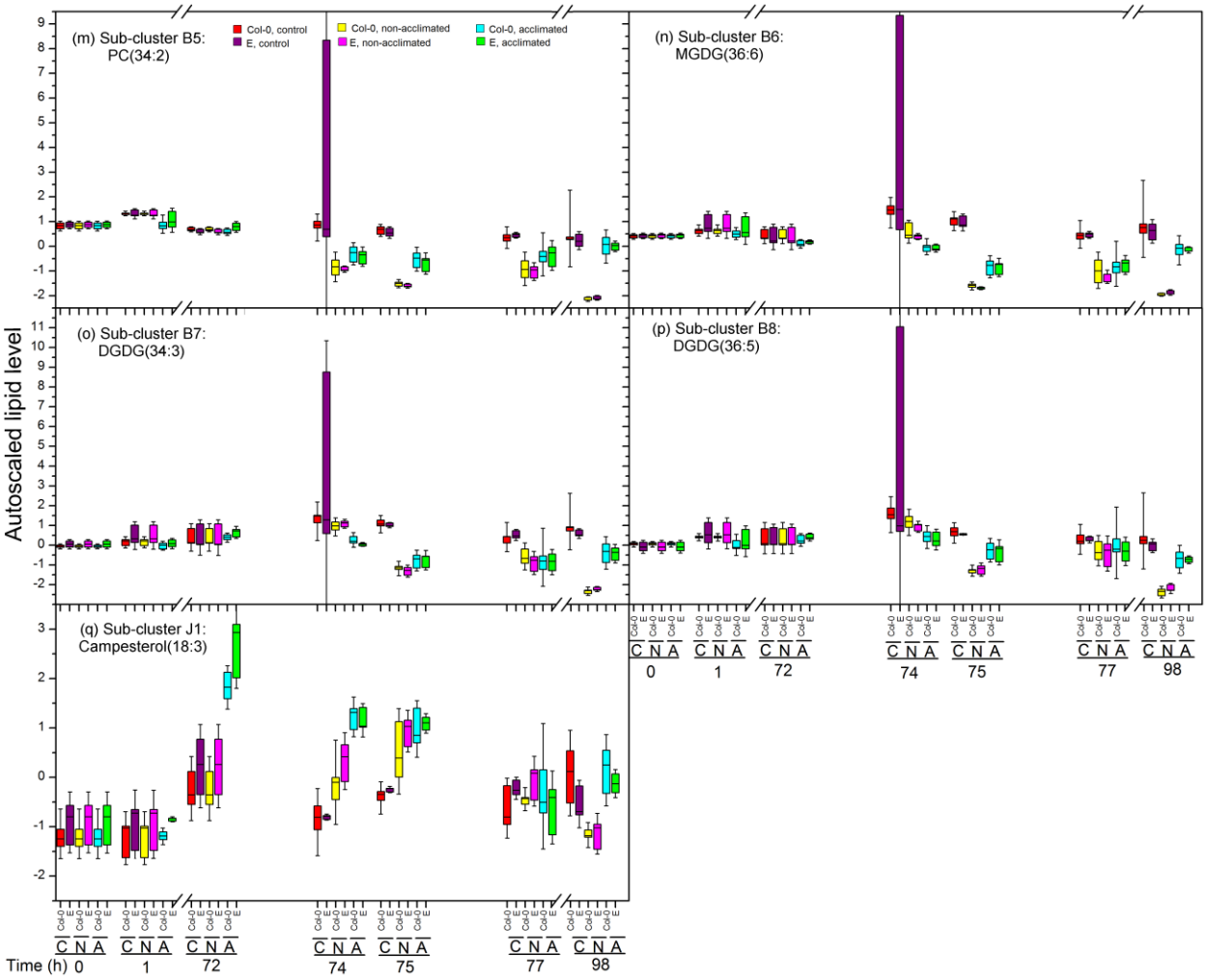
(m) Sub-cluster B5: PC(34:2)
(n) Sub-cluster B6: MGDG(36:6)
(o) Sub-cluster B7: DGDG(34:3)
(p) Sub-cluster B8: DGDG(36:5)
(q) Sub-cluster J1: Campesterol(18:3)
Col-0, control
E, control
Col-0, non-acclimated
E, non-acclimated
Col-0, acclimated
E, acclimated
Autoscaled lipid level
Time (h)
C N A
0
1
72
74
75
77
98

Table 5.1 List of Arabidopsis lines used in the experiment.

Letter label	Genotype	Knockout line number	Enzyme encoded
A	Columbia-0		
B	At1g61850	Salk_087152	pPLAI
C	At1g61850 x At2g26560		pPLAI x pPLAIIα
D	At1g61850 x At3g54950		pPLAI x pPLAIIIβ
E	At4g37070	Salk_039679	pPLAIIγ
F	At2g26560	Salk_059119	pPLAIIα
G	At2g26560 x At3g54950		pPLAIIα x pPLAIIIβ
H	At4g37050	Salk_142351	pPLAIIβ
I	At4g37060	Salk_090933	pPLAIIδ
J	At4g37060 x At3g54950		pPLAIIδ x pPLAIIIβ
K	At2g39220	Salk_040363	pPLAIIIα
L	At3g54950	Salk_057212	pPLAIIIβ
M	Columbia-0		
N	At3g54950 x At4g29800 x At3g63200		pPLAIIIβ x pPLAIIIγ x pPLAIIIδ
O	At3g54950 x At3g63200		pPLAIIIβ x pPLAIIIδ
P	At4g29800	Salk_088404	pPLAIIIγ
Q	At3g63200	Salk_029470	pPLAIIIδ
R	At1g55020	SALK_059431	LOX1
S	At5g43590	Salk_080154	pPLAIIε
T	At1g55020 x At3g22400	SALK_059431 x SALK_044826	LOX1 X LOX5
U	At1g72520	SALK-138527	LOX4
V	At3g22400	SALK_044826	LOX5
W	At1g67560	SALK_138907	LOX6
X	opr3	(*see text*)	OPR3

Table 5.2 Internal standards used in lipid profiling.

The amounts shown are in 20 µl of chloroform.

Internal standards	Internal standards with individual acyl chains specified	Amount added (nmol) per 0.04 mg dry mass of leaf tissue	Origin
DGDG(34:0)	DGDG(18:0/16:0)	0.359	Purchased from Matreya LLC (Pleasant Gap, PA, USA)
DGDG(36:0)	DGDG(18:0/18:0)	0.947	Matreya
LPC(13:0)	LPC(13:0)	0.12	Purchased from Avanti Polar Lipids, Inc., (Alabaster, AL, USA)
LPC(19:0)	LPC(19:0)	0.12	Avanti
LPE(14:0)	LPE(14:0)	0.06	Avanti
LPE(18:0)	LPE(18:0)	0.06	Avanti
MGDG(34:0)	MGDG(18:0/16:0)	1.505	Matreya
MGDG(36:0)	MGDG(18:0/18:0)	1.302	Matreya
PA(28:0)	PA(14:0/14:0)	0.06	Avanti
PA(40:0)	PA(diphytanoyl) [i.e., PA(20:0/20:0)]	0.06	Avanti
PC(24:0)	PC(12:0/12:0)	0.12	Avanti
PC(48:2)	PC(24:1/24:1)	0.12	Avanti
PE(24:0)	PE(12:0/12:0)	0.06	Avanti
PE(46:0)	PE(23:0/23:0)	0.06	Synthesized from PC(23:0/23:0) (Avanti) by transphosphatidation (Comfurius and Zwaal, 1977)
PG(28:0)	PG(14:0/14:0)	0.06	Avanti
PS(28:0)	PS(14:0/14:0)	0.04	Avanti
PS(40:0)	PS(diphytanoyl) [i.e., PS(20:0/20:0)]	0.04	Avanti
TAG(51:3)	TAG(17:1/17:1/17:1)	0.308	Purchased from Nu-Chek Prep, Inc. (Elysian, MN, USA)
MGDG(34:0)	MGDG(18:0/16:0)	listed above	Matreya
MGDG(36:0)	MGDG(18:0/18:0)	listed above	Matreya
MGDG(34:0)	MGDG(18:0/16:0)	listed above	Matreya
MGDG(36:0)	MGDG(18:0/18:0)	listed above	Matreya

Table 5.3 Positions of sample vials on a mass spectrometry sample tray.

"QC" is quality control sample. "IS" is internal standard-only sample. The order shown here is for plants 1 to 24 of plant tray F1-1. Two more sample trays, in which the samples will be from F1-1-25 to F1-1-48, and F1-1-49 to F1-1-72, with similar arrangement, are utilized to analyze plant tray F1-1.

Slot number	Sample name	Internal standard mix (µl)	Amount of leaf dry mass (mg)
1	QC1	20	0.04
2	QC2	20	0.04
3	QC3	20	0.04
4	QC4	20	0.04
5	QC5	20	0.04
6	QC6	20	0.04
7	F1-1-1	20	0.04
8	F1-1-2	20	0.04
9	F1-1-3	20	0.04
10	IS1	20	0
11	QC7	20	0.04
12	F1-1-4	20	0.04
13	F1-1-5	20	0.04
14	F1-1-6	20	0.04
15	QC8	20	0.04
16	F1-1-7	20	0.04
17	F1-1-8	20	0.04
18	F1-1-9	20	0.04
19	F1-1-10	20	0.04
20	QC9	20	0.04
21	F1-1-11	20	0.04
22	F1-1-12	20	0.04
23	F1-1-13	20	0.04
24	F1-1-14	20	0.04
25	QC10	20	0.04

26	F1-1-15	20	0.04
27	F1-1-16	20	0.04
28	F1-1-17	20	0.04
29	F1-1-18	20	0.04
30	IS2	20	0
31	QC11	20	0.04
32	F1-1-19	20	0.04
33	F1-1-20	20	0.04
34	F1-1-21	20	0.04
35	QC12	20	0.04
36	F1-1-22	20	0.04
37	F1-1-23	20	0.04
38	F1-1-24	20	0.04
39	QC13	20	0.04

Table 5.4 Correlation of lipids in sub-clusters with leaf damage as quantified by ion leakage.

Spearman's correlation coefficient ρ of each lipid with leaf ion leakage was calculated using the Metaboanalyst website and was averaged for each sub-cluster shown in Figure 5.6

Sub-cluster	Lipid class	Spearman's correlation coefficient ρ with leaf ion leakage
A1	LPC	0.61 ± 0.03
A2	PA	0.78 ± 0.02
A3	TAG	0.32 ± 0.04
A4	ASG	0.68 ± 0.07
A5	TrGDG	0.62 ± 0.02
A6	acMGDG (with three oxidized acyl groups)	0.69 ± 0.01
A7a	acMGDG (with mostly non-oxidized acyl groups)	0.72 ± 0.02
A7b	acMGDG(with mostly 2 oxidized acyl groups)	0.68 ± 0.03
B1	PC	-0.6 ± 0.05
B2	PC	-0.5 ± 0.05
B3	PE	-0.46 ± 0.1
B4	PE	-0.03 ± 0.07
B5	PC, PS	-0.66 ± 0.07
B6	MGDG, PE	-0.59 ± 0.04
B7	DGDG	-0.48 ± 0.03
B8	DGDG	-0.26 ± 0.04
J1	Sterol ester	0.08 ± 0.11

Chapter 12 - Conclusions and future directions

Conclusions

Chapter 2 and Chapter 3 present evidence supporting the hypothesis that Arabidopsis induces different lipidomes in response to different stress agents. In response to avirulent bacteria and wounding, both acyl oxidation and head-group acylation were significantly induced and the abundant plastidic lipid, MGDG, was acylated with both normal-chain and oxidized fatty acids. Freezing stress, on the other hand, primarily induced head-group acylation but not acyl oxidation, leading to high levels of normal-chain acMGDG, as well as PA, in low temperature response.

Chapter 4 utilizes co-occurrence analysis to study the metabolic modularity of lipids in response to wounding. The analytical approach and data analysis strategies employed in Chapter 4 successfully detected known lipid metabolizing pathways via the identities and changing patterns of lipid analytes in sub-clusters (Figure 4.3). The same approach was applied to study Arabidopsis response to low temperature stress and successfully identified many metabolic modules that were specifically induced by cold acclimation.

The knowledge provided by co-occurrence analysis was utilized in a LOX and AH knockout study which hints at the function of pPLAIIγ as an acyl hydrolase specifically acting on oxidized acMGDG. The concentration of OPDA in acMGDG (Chapter 3) and the faster freezing recovery of acclimated *pPLAIIγ* knockout, which expressed higher levels of OPDA-containing acMGDG, compared to Col-0 (Chapter 5) suggest that oxidized acMGDG may serve as a sequestering pool for harmful oxidized fatty acids.

Future directions

Arabidopsis responding to biotic stresses, such as bacterial and fungal infection, has been shown to massively alter lipid metabolism (Andersson et al., 2006; Kourtchenko et al., 2007; Vu et al., 2012). Application of co-occurrence analysis in studying response to biotic stresses promises novel and interesting findings.

Head-group acylation of membrane lipids under stress conditions is evolutionarily conserved (Heinz, 1972; Vu et al., 2014). Many classes of membrane lipids can be acylated at the polar head-group including MGDG, DGDG, PG, and PE (Heinz, 1972; Andersson et al., 2006; Kourtchenko et al., 2007; Ibrahim et al., 2011; Kilaru et al., 2012; Vu et al., 2012; Vu et al., 2014). Furthermore, head-group acylation occurred in response to various stresses including avirulent bacterial infection, wounding, and freezing (Andersson et al., 2006; Kourtchenko et al., 2007; Ibrahim et al., 2011; Vu et al., 2012; Vu et al., 2014). Chapters 3 and 5 suggest that acMGDG might serve as a sequestering pool for harmful oxidized fatty acids. However, the accumulation of normal-chain acMGDG in wounded wheat, wounded Arabidopsis C24, and non-acclimated Arabidopsis suggests that acMGDG may also play other roles in stress responses. In order to study the functions of both oxidized and normal-chain acMGDGs, the identity of the acylating enzyme(s) needs to be determined.

Instead of utilizing the knowledge provided by co-occurrence analysis of wild-type Arabidopsis lipidome in response to stress as a guide to study mutant lines as in Chapter 5, co-occurrence analysis can be applied directly to datasets obtained from knockout plants in response to a stress. This would provide more comprehensive views of the simultaneous effects of mutation and stress on Arabidopsis lipidomes. However, since software needed for lipid co-occurrence analysis, namely Cluster 3.0 and Dendroscope, were not specifically designed to handle lipid data, especially lipid names, further optimization is needed to improve usage of co-occurrence analysis.

References

Andersson MX, Hamberg M, Kourtchenko O, Brunnström A, McPhail KL, Gerwick WH, Göbel C, Feussner I, and Ellerström M (2006) Oxylipin profiling of the hypersensitive response in *Arabidopsis thaliana*. Formation of a novel oxo-phytodienoic acid-containing galactolipid, arabidopside E. J. Biol. Chem. **281**, 31528-31537.

Heinz E (1972) Some properties of the acyl galactosyl diglyceride-forming enzyme from leaves. Zeitschrift fur Pflanzenphysiologie **69**, 359-360-376.

Ibrahim A, Schötz AL, Galano JM, Herrfurth C, Feussner K, Durand T, Brodhun F, and Feussner I (2011) The Alphabet of Galactolipids in *Arabidopsis thaliana*. Front. Plant. Sci. **2**, 95.

Kilaru A, Tamura P, Isaac G, Welti R, Venables BJ, Seier E, and Chapman KD (2012) Lipidomic analysis of N-acylphosphatidylethanolamine molecular species in Arabidopsis suggests feedback regulation by N-acylethanolamines. Planta **236**, 809-824.

Kourtchenko O, Andersson MX, Hamberg M, Brunnström A, Göbel C, McPhail KL, Gerwick WH, Feussner I, and Ellerström M (2007) Oxo-phytodienoic acid-containing galactolipids in Arabidopsis: jasmonate signaling dependence. Plant Physiol. **145**, 1658-1669.

Vu HS, Roth MR, Tamura P, Samarakoon T, Shiva S, Honey S, Lowe K, Schmelz EA, Williams TD, and Welti R (2014) Head-group acylation of monogalactosyldiacylglycerol is a common stress response, and the acyl-galactose acyl composition varies with the plant species and applied stress. Physiol. Plant., In press.

Vu HS, Tamura P, Galeva NA, Chaturvedi R, Roth MR, Williams TD, Wang X, Shah J, and Welti R (2012) Direct infusion mass spectrometry of oxylipin-containing Arabidopsis membrane lipids reveals varied patterns in different stress responses. Plant Physiol. **158**, 324-339.

Appendix A – Permission to release copyrighted material

In

CHAPTER 2

Direct infusion mass spectrometry of oxylipin-containing Arabidopsis membrane lipids reveals varied patterns in different stress responses

Vu HS, Tamura P, Galeva NA, Chaturvedi R, Williams TD, Wang X, Shah J and Welti R

(2012) Plant Physiol. **158**, 324-339.

In

CHAPTER 3

Head-group acylation of monogalactosyldiacylglycerol is a common stress response, and the acyl-galactose acyl composition varies among plant species and with applied stress

Vu HS, Roth MR, Tamura P, Samarakoon T, Shiva S., Honey S, Lowe K, Schmelz EA, Williams TD and Welti R (2014) Physiol Plant. In press.